Shining a Light on Forensic Anthropology:

The Use of Alternative Light Sources to Detect Skeletal Remains Underwater.

By

Catherine Anne Maidment

A thesis submitted in partial fulfilment for the requirements for the degree of Doctor of Philosophy at the University of Central Lancashire.

Volume 1 of 2

August 2023

STUDENT DECLARATION

Concurrent registration

I declare that while registered as a candidate for the research degree, I have not been a registered candidate or enrolled student for another award of the University or other academic or professional institution.

Material submitted for another award

I declare that no material contained in the thesis has been used in any other submission for an academic award and is solely my own work.

Collaboration

I declare that this research project was not part of a collaboration.

Signature of Candidate:

C. A. Maidment

Type of Award: Doctor of Philosophy

School: Natural Sciences

ABSTRACT

Aquatic searches for human remains are time consuming and expensive, focused on locating intact cadavers rather than bone. Once a body becomes skeletonised it is more vulnerable to the destructive mechanics of currents and tides, leading to fragmentation, dispersal, and modification of the bone surface. This makes locating and identifying bone even more challenging. Alternative light sources (ALS) are a crime scene staple, routinely used to locate body fluids such as semen and saliva, by stimulating the natural autofluorescence of proteins. This process is non-contact, and non-destructive, used to reveal latent evidence and facilitate documentation and recovery. Bone also produces fluorescence when exposed to ALS, which is thought to be primarily due to the highly collagenous organic content.

This research united current strands of osseous ALS research by implementing a unique methodology combining thermogravimetric analysis (TGA) to quantify bone collagen, and a bespoke C++ computer program: The Osteo-Fluorescence Calculator (OFC) to quantify bone fluorescence, which enabled deeper interpretation of the collagen-fluorescence relationship, the taphonomic impact on bone autofluorescence, and its use in terrestrial and underwater crime scenes, not previously reported in literature.

Key results indicated that collagen is most likely the primary contributor to bone autofluorescence, and that the larger the collagen volume the greater the observed fluorescence intensity when photographed with blue light (450 nm) and orange filter in a terrestrial ($p = .000$) and underwater contexts ($p = .000$). However, differentiation and control studies suggest that bone colour, texture, and morphology may also influence fluorescence emissions, but differentiation between bone and other non-bone items is possible due to variable fluorescence intensities, including in an underwater context. Hot water was identified as a suitable preparation technique for bone undergoing ALS analysis, as it produced homogenous fluorescence, similar to pre-macerated values ($p = .012$), with limited collagen degradation ($p = .023$), whereas biological washing powder was destructive to bone collagen content ($p = .000$) and produced exaggerated and inconsistent fluorescence ($p = .180$).

Taphonomic studies confirmed that bone autofluorescence can be produced in terrestrial (p= .000) and submerged tap water environments (p= .000) when using blue light (450 nm) and an orange filter. Although underwater fluorescence levels were reduced compared to terrestrial findings, submersion in tap and seawater for 6-months led to a dramatic increase in bone fluorescence intensity (p= .000) and a minor reduction in collagen content (p= .000), which would aid dark, underwater searches. Comparatively, saltwater was no more destructive to porcine bone collagen than tap water, after submersion for 6-months (p= .000), indicating that ALS can be used to search for bone for at least 6-months after skeletonization.

Overall, this research demonstrated that effective ALS examination has the potential to help simplify search methodologies, reduce costs, speed up recovery, and triage findings, with implications for missing persons cases, crime scene investigation and archaeological contexts.

TABLE OF CONTENTS

STUDENT DECLARATION i
ABSTRACT ii
TABLE OF CONTENTS iv
DEDICATION AND ACKNOWLEDGEMENTS 1
LIST OF FIGURES AND TABLES 2
FIGURES 2
TABLES 20
LIST OF ABBREVIATIONS 26
1.0 - INTRODUCTION 28
1.4 – ALS AND BONE FLUORESCENCE 39
2.0 - AIMS OF RESEARCH 46
3.0 – ORIGINAL CONTRIBUTION TO RESEARCH AND FORENSIC SCIENCE 51
3.1 – CONTRIBUTION TO RESEARCH 51
3.2 – CONTRIBUTION TO FORENSIC SCIENCE 53
4.0 - THESIS STRUCTURE 55
5.0 – AQUATIC SEARCH STRATEGIES FOR HUMAN REMAINS 56
6.0 – CRIME SCENE DOCUMENTATION AND PHOTOGRAPHY 71
7.0 - THE ROLE OF FLUORESCENCE IN CRIME SCENE INVESTIGATIONS 79
7.1 - LIGHT 79
7.2 - FLUORESCENCE 84
7.3 – FLUORESCENCE TERMINOLOGY 87
8.0 – BONE FLUORESCENCE 99
8.1 – OTHER WAVELENGTH AND FILTER COMBINATIONS 102
9.0 - BONE COMPOSITION AND TAPHONOMY 119
9.1 – COLLAGEN 119
9.3 – AMINO ACIDS 122
10.0 – ETHICAL CONSIDERATIONS AND APPROVAL 134
11.0 - METHODOLOGY 137
11.3 – COMPUTERISED FLUORESCENCE QUANTIFICATION 144
11.4 – THE OSTEO-FLUORESCENCE CALCULATOR (OFC) 147
12.0 – QUANTIFICATION OF COLLAGEN 154
SECTION A: BONE PREPARATION AND PHOTOGRAPHY REFINEMENT 161
13.0 – SECTION A, QUESTION 1: MACERATION PILOT STUDY 162

13.1.3 - AQUEOUS MACERATION 166
13.1.5 - ENZYMATIC 173
13.2 - MATERIALS 177
13.3 - METHOD 178
13.3.1 – COLLAGEN QUANTIFICATION 181
13.3.2 – PHOTOGRAPHY 182
13.3.3 – FLUORESCENCE ANALYSIS 184
13.3.4 – STATISTICAL ANALYSIS 185
14.0 – MACERATION PILOT STUDY RESULTS 186
14.1.1 – COLLAGEN QUANTIFICATION AND BONE MASS 187
14.1.2 - FLUORESCENCE 190
14.1.3 – STATISTICAL ANALYSIS 193
14.2 – BIOLOGICAL WASHING POWDER 195
14.2.1 – COLLAGEN QUANTIFICATION AND BONE MASS 196
14.2.2 – FLUORESCENCE ANALYSIS 199
14.2.3 – STATISTICAL ANALYSIS 202
14.3 – ENZYMATIC MACERATION 204
14.3.1 - COLLAGEN 204
14.3.2 - FLUORESCENCE 206
14.3.3 – STATISTICAL ANALYSIS 210
14.5 – MACERATION PILOT STUDY CONCLUSIONS 220
15.0 - SECTION A, QUESTIONS 2-5: PHOTOGRAPHY REFINEMENT METHODOLOGY 221
15.1 – MATERIALS 223
16.0: SECTION A, QUESTION 2: COLLAGEN AND FLUORESCENCE DISTRIBUTION 225
16.1 – METHOD 225
16.2 – RESULTS AND DISCUSSION 226
17.0: SECTION A, QUESTION 3: BACKGROUNDS AND POSITIONING 229
17.2 – RESULTS AND DISCUSSION 230
18.0: SECTION A, QUESTIONS 4 & 5: PHOTOGRAPHY REFINEMENT 233
18.1 – TERRESTRIAL PHOTOGRAPHY REFINEMENT 233
18.2 – OPTIMAL PHOTOGRAPHY DISTANCE 237
18.3 – SUBMERGED PHOTOGRAPHY REFINEMENT 239
19.0 - SECTION A: SUMMARY 244
SECTION B: THE APPLICATION OF ALS TO DETECT BONE 246
20.0 - CORE METHODOLOGY 250
20.1.2 – EQUIPMENT 251
20.2 – METHOD 253

20.2.1 – MACERATION 253
21.0 - SECTION B, QUESTION 1: TERRESTRIAL AND UNDERWATER BONE FLUORESCENCE 256
21.3 – RESULTS AND DISCUSSION 259
21.3.1 – FLUORESCENCE 259
21.3.5 – HAMMERHEAD: BONE DIMENSIONS 288
21.4 – COLLAGEN ANALYSIS 296
21.5 – STATISTICAL ANALYSIS 299
21.5.2 – BONE DIMENSIONS 304
21.5.3 – COLLAGEN 310
21.5.3a - CRIME-LITE 2 COMPARISONS 310
22.0 - SECTION B, QUESTION 2: THE COLLAGEN-FLUORESCENCE RELATIONSHIP 314
22.2 – RESEARCH QUESTION SPECIFIC METHOD 315
22.2.3 - FLUORESCENCE 315
22.3 – RESULTS AND DISCUSSION 315
22.3.1 - BONE DIMENSIONS 318
22.3.3 - SPSS STATISTICS 331
22.4 – CONCLUSIONS 335
23.0 - SECTION B, QUESTION 3: DIFFERENTIATION AND CONTROLS 337
23.1 - QUESTION 3A: NON-BONE CONTROLS 337
23.2 - QUESTION 3A: NON-BONE CONTROLS RESULTS 343
23.2.1 - QUANTITATIVE ANALYSIS 352
23.2.2 - VISUAL EVALUATION 357
23.2.3 - ORGANIC AND INORGANIC COMPARISONS 371
24.0 - SECTION B, QUESTION 3B: PORCINE COLLAGEN POWDER 376
24.1 - RESEARCH QUESTION SPECIFIC METHOD 376
24.1.2 – METHOD 377
24.1.2a - PHOTOGRAPHY 377
24.1.2b - FLUORESCENCE 377
24.2 - RESULTS AND DISCUSSION 378
25.0 - SECTION B, QUESTION 3C DEMINERALISED AND DEPROTEINISED PORCINE BONE 383
25.1 - DEMINERALISED BONE 383
25.1.1 - MATERIALS 383
25.1.2 - METHOD 384
25.2 - DEPROTEINISED BONE 387
25.2.1 - MATERIALS AND METHOD 387
25.3 - CALCINED BONE ASH 389
25.3.1 - MATERIALS AND METHOD 389

25.3.2 - STATISTICAL ANALYSIS 390
25.4 - RESULTS AND DISCUSSION 391
25.4.2 - DEPROTEINISED BONE 395
25.4.3 - CALCINED BONE ASH 400
25.4.4 - FLUORESCENCE SCALE 404
25.5 - CONCLUSIONS 412
26.0 - SECTION B, QUESTION 4 414
26.1 - MATERIALS 414
26.2 - METHOD 415
26.2.3 - STATISTICAL ANALYSIS 420
26.3 - RESULTS AND DISCUSSION 421
26.3.1 - WATER ANALYSIS 422
26.3.2 - BONE CHANGES 428
26.3.3 - FLUORESENCE 442
26.3.4 - COLLAGEN 454
26.3.5 - STATISTICAL ANALYSIS 458
26.4: CONCLUSIONS 470
27.0 - SECTION B: SUMMARY 473
28.0 – THESIS DISCUSSION AND FUTURE WORK 475
29.0 – FINAL CONCLUSIONS AND RECOMMENDATIONS 479
30.0 – APPENDICES 482
31.0 - REFERENCES 483

DEDICATION AND ACKNOWLEDGEMENTS

This Ph.D. thesis is dedicated to:

Russell Arthur Maidment, who always cared.

and

Kathleen Olive Denton, who was always there.

RIP

I would like to acknowledge colleagues across the University of Huddersfield and the University of Central Lancashire for their support and guidance throughout the development of this PhD project. I would especially like to thank my PhD supervisors Anna Williams and Jennifer Jones for their support, encouragement, and sheer belief throughout my supervision, as well as the amazing teaching and research opportunities that they made available to me.

I would also like to thank my wonderful fellow PhD-ers, Gabi Mroz, Ibu Olowe, Mike Parsons, and most of all Caley Mein, who stuck by me to the bitter end and would not let me quit, despite how many times I asked.

I would love to thank my partner Liam MacDonald for his technical expertise in the creation of the OFC software, without your hard work and unwavering support I would not have achieved any of this.

I would also like to thank James Rooney, from the University of Huddersfield, who was forever cheerful and helpful whenever the TGA refused to work.

LIST OF FIGURES AND TABLES

FIGURES

Figure 1: Diagrams of two of the most common underwater search techniques employed by forensic diving teams A) Sweep, B) Pier-walk or parallel search technique [56] *58*

Figure 2: Illustration demonstrating how side scan sonar is deployed when searching aquatic contexts for human remains [82] *64*

Figure 3: Side scan sonar output successfully identifying a submerged body in Lake Underhill, Orlando, Florida [82] *68*

Figure 4: Side scan sonar output highlighting the body in Lake Lawne, Orlando, Florida, partially obscured by placement within a depression on the lake floor. *68*

Figure 5: Enhanced side scan sonar output highlighting the body in Lake Lawne, Orlando, Florida, and demonstrating the uneven lake floor. *68*

Figure 6: Diagram illustrating how light interacts with the basic DSLR camera configuration [211] *72*

Figure 7: Structure of a standard DSLR camera compared to a mirrorless digital camera [213] *73*

Figure 8: The exposure triangle [217] *74*

Figure 9: Diagram of the electromagnetic spectrum [207] *79*

Figure 10: Wavelength energy levels based on the position in the electromagnetic spectrum [245] *80*

Figure 11: Sequence of underwater wavelength absorption and scattering at different depths in a marine context (Edited by Catherine Maidment, 2023) [255] *82*

Figure 12: Diagram of Stoke's Shift [124] *84*

Figure 13: The colour wheel: illustrating that the optimal colour of barrier filter for fluorescence visualisation is opposite on the colour wheel to the colour of the incident wavelength [243] *86*

Figure 14: Demonstration of how an orange filter filters blue wavelengths of light to reveal fluorescence (Edited by Catherine Maidment) [124] *86*

Figure 15: Diagram of how blue ALS wavelengths stimulate autofluorescence, which can then be consequently viewed using orange coloured goggles or photographed using an orange barrier filter fitted to the camera lens. [262] *87*

Figures 16: Examples of body fluids deposited on a cotton substrate and stimulated by blue light (450nm) and viewed with an orange filter. A) Blood under natural light, B) Blood under ALS, C) Semen under natural light, D) Semen under ALS, E) Saliva under natural light, F) Saliva under ALS [120]..... 92

Figure 17: Example of GSR A) appearance to the naked eye, B) 440 nm with orange filter (Edited by Catherine Maidment, 2023) 95

Figure 18: 'Yellow' haematoma enhanced with violet ALS (400-430 nm), photographed with a yellow filter [287]..... 96

Figure 19: The 'molten lava' appearance of bone due to partial burning, stimulated using the YAG laser [143] 103

Figure 20: A) A humerus photographed under normal light conditions. B) The same humerus photographed using UV, showing how the brown area and white border emitting white light blue/white fluorescence, and the burned areas not responding to the ALS [307]..... 105

Figure 21: Photograph of the distal epiphysis of a human femur demonstrating bleaching of the cortical bone and leaching of fat (arrow) due to prolonged submersion in a marine environment [106] 114

Figure 22: Burnt floor tile that resembles human skull, recovered from the remains of a burned building during a bush fire in Victoria, Southeast Australia, 2009 [311]..... 116

Figure 23: Melted glue fragment, recovered from the remains of a burned building during a bush fire in Victoria, Southeast Australia, 2009, which resembled a human tooth [311]..... 116

Figure 24: Diagram of bone composition [323]..... 119

Figure 25: Manually defleshed porcine phalange photographed under natural light..... 122

Figure 26: The same manually defleshed porcine phalange seen in fig. 25 but photographed using blue light (450nm) coupled with an orange barrier filter, demonstrating strong bone autofluorescence. 122

Figure 27: A line graph from Swaraldahab and Christensen (2016) [146] comparing the level of fluorescence intensity between four temporal groups of bones, with the largest spread in fluorescence values noted in the oldest ancient specimens. 129

Figure 28: Fluorescence image of a fluorescing porcine rib, converted to grayscale using the Averaged equation 141

Figure 29: Original image of a fluorescing porcine rib (450nm, orange filter) 141

Figure 30: Fluorescence image of a fluorescing porcine rib, converted to grayscale using the weighted Luminosity equation *141*

Figure 31: Fluorescence comparison of human bones burned at 700°C (left), and at 900°C (right) when stimulated 420-470 nm, demonstrating a shift in colour from green to red/brown [158] (Edited by Catherine Maidment, 2023) *144*

Figure 32: Screenshot of the default ImageJ toolbar..... *145*

Figure 33: Flowchart describing the user experience when processing fluorescence photographs using the OFC. *148*

Figure 34: Selecting the grid specifications. *149*

Figure 35: Selecting input and output folders. *150*

Figure 36: Selecting a save location and saving the settings. *150*

Figure 37: Save settings on screen message..... *151*

Figure 38: Text to indicate the progress of fluorescence image processing. *152*

Figure 39: Successful processing of fluorescence images, selection of output folder to view result *152*

Figure 40: Selection of an example processed fluorescence image. *153*

Figure 41: Example of OFC output..... *153*

Figure 42: TGA of collagen demonstrating phases of thermal alteration [460] Edited by Catherine Maidment 2023..... *158*

Figure 43: A) Lateral view of a human ulna before exposure to Dermestid beetles, and B) after 30 days exposure C) The red square highlights the prescence of two circular lesions located at the lateral, proximal epiphysis, and D) a cross section of the same lesions via CBCT, illustrating the internal destruction of the trabecular and cortical bone. [479] (Edited by Catherine Maidment, 2023) *165*

Figure 44: Human radius A) before B) after exposure to Dermestid beetles, showing extensive destruction to the proximal ephiysis and trabecular bone, including thinning of the cortical layer. C) Demonstrates Londitudinal CBCT section of the cortical thinning and drilling of the medullary cavity for pupation chambers (red arrows) [479], (Edited by Catherine Maidment, 2023)..... *166*

Figure 45: The appearance of porcine phalange after 2 months submersion in room temperature 30% peroxide solution, [491] (Edited by Catherine Maidment, 2023)..... *170*

Figure 46: Anterior and posterior images demonstrating macroscopic bleaching changes present on a porcine humerus (Sus scrofa domesticus) simmered for 1 hour in 25% peroxide [489] (Edited by Catherine Maidment, 2023) *170*

Figure 47: A) SEM photomicrograph demonstrating typical result following microwave maceration (×37 magnification) B) SEM photomicrograph illustrating the typical surface changes associated with manual maceration (×37 magnification). C) SEM photomicrograph showing the extensive cortical flaking and destruction of the natural morphology and texture resulting from sodium hypochlorite maceration (×15 magnification) [156] *171*

Figure 48: Ratio of ribs used in the maceration pilot study based on anatomical region *177*

Figure 49: Slow cooker used to perform hot water maceration (80°C) *178*

Figure 50: Equipment configuration used during the washing powder and enzymatic maceration techniques. A) Stockpot on hot plate, B) Example of porcine ribs in maceration solution. *179*

Figure 51:The central anterior aspect of a porcine rib where collagen scraping for TG analysis were obtained *181*

Figure 52: Equipment configuration for fluorescence photography *183*

Figure 53: Example of photographs taken per porcine rib (Sus Scrofa Domesticus) sample A) Natural light with scale, B) Natural light, in situ with polystyrene spheres, C) Fluorescence photograph consisting of blue light 450nm with orange camera filter. *183*

Figure 54: A final grayscale image of a porcine rib (Sus scrofa domesticus) processed using the OFC. ... *185*

Figure 55: Final appearance of porcine ribs (Sus scrofa domesticus) after hot water maceration (approx. 80°C), ribs 1-5 ..... *187*

Figure 56: Final appearance of porcine ribs (Sus scrofa domesticus) after hot water maceration (approx. 80°C), ribs 6-10 ..... *187*

Figure 57: Changes in bone mass of ten porcine ribs (Sus scrofa domesticus) macerated in hot water (approx. 80°C) *189*

Figure 58: Changes in calculated bone collagen of ten porcine ribs (Sus scrofa domesticus) macerated in hot water (approx. 80°C) *189*

Figure 59: Changes in average fluorescence of 10 porcine ribs (Sus scrofa domesticus) macerated in hot water (approx. 80°C) *192*

Figure 60: Results of Wilcoxon signed-rank test, comparing fresh and macerated fluorescence values of ten porcine ribs (Sus scrofa domesticus) subjected to hot water maceration (approx. 80°C) 193

Figure 61: Results of paired-samples t-test analysis, comparing the changes in bone mass, calculated collagen content, and average fluorescence, of the ten ribs subjected to hot water maceration (approx. 80°C) 194

Figure 62: Final appearance of porcine ribs (Sus scrofa domesticus) post biological washing powder maceration (approx. 50°C), ribs 1 – 5 195

Figure 63: Final appearance of porcine ribs (Sus scrofa domesticus) post biological washing powder maceration (approx. 50°C), ribs 6 - 10 195

Figure 64: Surface changes exhibited by rib 2 after being macerated in the washing powder solution (approx. 50°C) 196

Figure 65: Surface changes exhibited by rib 6 after being macerated in the washing powder solution (approx. 50°C) 196

Figure 66: Surface changes exhibited by rib 8 after being macerated in the washing powder solution (approx. 50°C) 196

Figure 67: Changes in mass of ten porcine ribs (Sus scrofa domesticus) macerated in biological washing powder (approx. 50°C) 198

Figure 68: Changes in collagen content of the ten porcine ribs (Sus scrofa domesticus) macerated in biological washing powder (approx. 50°C) 198

Figure 69: Changes in average fluorescence of the ten porcine ribs (Sus scrofa domesticus) macerated in biological washing powder (approx. 50°C) 201

Figure 70: Results of paired-samples t-test analysis, comparing the changes in bone mass, calculated collagen content, and average fluorescence, of the ten ribs subjected to biological washing powder maceration (approx. 50°C) 202

Figure 71: Results of Wilcoxon signed-rank test, comparing fresh and macerated fluorescence values of ten porcine ribs (Sus scrofa domesticus) subjected to biological washing powder maceration (approx. 50°C) 203

Figure 72: Final appearance of porcine ribs (Sus scrofa domesticus) post enzymatic maceration (approx. 55°C), ribs 1 - 5 204

Figure 73: Final appearance of porcine ribs (Sus scrofa domesticus) post enzymatic maceration (approx. 55°C, ribs 6 -10 ..... *204*

Figure 74: Changes in bone mass of ten porcine ribs (Sus scrofa domesticus) subjected to enzymatic maceration (approx. 55°C) *206*

Figure 75: Changes in collagen content of ten porcine ribs (Sus scrofa domesticus) subjected to enzymatic maceration (approx. 55°C) *206*

Figure 76: Changes in average fluorescence of the ten porcine ribs (Sus scrofa domesticus) subjected to enzymatic maceration (approx. 55°C) *209*

Figure 77: Post maceration appearance of ribs 1-3 subjected to enzymatic maceration (approx. 55°C), dark staining present at the neck of the ribs (red circles). *210*

Figure 78: Results of paired-samples t-test analysis, comparing the changes in bone mass, calculated collagen content, and average fluorescence, of the 10 ribs subjected to enzymatic maceration (approx. 55°C) *211*

Figure 79: Results of Wilcoxon signed-rank test, comparing fresh and macerated fluorescence values of 10 porcine ribs (Sus scrofa domesticus) subjected to enzymatic maceration (approx. 50°C) *211*

Figure 80: Foster and Freeman Ltd™ Crime-lite 2 ALS *224*

Figure 81: FoxFury Ltd. Hammerhead ALS *224*

Figure 82: Vertebral, central, and sternal regions of a porcine rib (Sus scrofa domesticus) *225*

Figure 83: Improved equipment configuration for fluorescence photography *235*

Figure 84: Diagram illustrating the dimensions of the polystyrene insert used during fluorescence photography. *236*

Figure 85: Photograph of the polystyrene insert used during fluorescence photography. *236*

Figure 86: Terrestrial photograph of fresh porcine rib (Sus scrofa domesticus) using the Hammerhead ALS and yellow filter *239*

Figure 87: Submerged photograph of macerated porcine rib (Sus scrofa domesticus) using the Hammerhead ALS and yellow filter. *239*

Figure 88: Equipment configuration for underwater fluorescence photography *240*

Figure 89: Diagram of equipment configuration for terrestrial fluorescence photography *252*

Figure 90: Diagram of equipment configuration for submerged fluorescence photography *253*

Figure 91: Water hardness classification for Huddersfield, as reported by Yorkshire Water [496] 257

Figure 92: Comparison of average terrestrial fluorescence values of porcine ribs photographed with the Crime-lite 2 and the orange filter at 0.6, 0.4 and 1/3s exposure times. 267

Figure 93: Comparison of average underwater fluorescence values of porcine ribs photographed with the Crime-lite 2 and the orange filter at 0.6, 0.4 and 1/3s exposure times. 267

Figure 94: Comparison of average terrestrial fluorescence values of porcine ribs photographed with the Crime-lite 2 and the yellow filter at 0.6, 0.4 and 1/3s exposure times. 268

Figure 95: Comparison of average underwater fluorescence values of porcine ribs photographed with the Crime-lite 2 and the yellow filter at 0.6, 0.4 and 1/3s exposure times. 268

Figure 96: Comparison of average terrestrial and underwater fluorescence values of porcine ribs photographed with the Crime-lite 2 and the orange filter at 0.6s exposure time 269

Figure 97: Comparison of average terrestrial and underwater fluorescence values of porcine ribs photographed with the Crime-lite 2 and the yellow filter at 0.6s exposure time 269

Figure 98: Comparison of average terrestrial and underwater fluorescence values of porcine ribs photographed with the Crime-lite 2 and the orange filter at 0.4s exposure time. 270

Figure 99: Comparison of average terrestrial and underwater fluorescence values of porcine ribs photographed with the Crime-lite 2 and the yellow filter at 0.4s exposure time. 270

Figure 100: Comparison of average terrestrial and underwater fluorescence values of porcine ribs photographed with the Crime-lite 2 and the orange filter at 1/3s exposure time. 271

Figure 101: Comparison of average terrestrial and underwater fluorescence values of porcine ribs photographed with the Crime-lite 2 and the yellow filter at 1/3s exposure time. 271

Figure 102: Graphical representation showing the general compositional differences between trabecular (spongy) bone and cortical (compact) bone. 273

Figure 103: Porcine rib 23 photographed terrestrially using the Crime-lite 2 with the orange filter at 0.6s exposure time 274

Figure 104: Porcine rib 23 photographed terrestrially using the Crime-lite 2 with the orange filter at 1/3s exposure time. 274

Figure 105: Porcine rib 20 photographed using the Crime-lite 2 with the orange filter at 0.6s exposure time. 275

Figure 106: Porcine rib 20 photographed using the Crime-lite 2 with the yellow filter at 0.6s exposure time. 275

Figure 107: Porcine rib 23 photographed underwater using the Crime-lite 2 with the orange filter at 0.6s exposure time. 276

Figure 108: Porcine rib 23 photographed underwater using the Crime-lite 2 with the yellow filter at 0.6s exposure time. 276

Figure 109: Comparison of average underwater fluorescence values compared with the measured width of the 29 porcine bones. Photographed using the Crime-lite 2, orange filter, and 0.4s exposure time. ... 279

Figure 110: Photograph of the Crime-lite 2 single LED (diameter 23 mm) 280

Figure 111: Photograph of the Hammerhead light source illustrating the two LEDs (diameter 18 mm each) 280

Figure 112: Comparison of average terrestrial fluorescence values of porcine ribs photographed with the Hammerhead and the orange filter at 0.6, 0.4 and 1/3s exposure times. 282

Figure 113: Comparison of average underwater fluorescence values of porcine ribs photographed with the Hammerhead and the orange filter at 0.6, 0.4 and 1/3s exposure times. 282

Figure 114: Comparison of average terrestrial and underwater fluorescence values of porcine ribs photographed with the Hammerhead and the orange filter at 0.6s exposure time. 283

Figure 115: Comparison of average terrestrial and underwater fluorescence values of porcine ribs photographed with the Hammerhead and the orange filter at 0.4s exposure time. 283

Figure 116: Comparison of average terrestrial and underwater fluorescence values of porcine ribs photographed with the Hammerhead and the orange filter at 1/3s exposure time. 284

Figure 117: Comparison between bone width and terrestrial fluorescence taken with the orange filter, 0.6s 290

Figure 118: Comparison between bone width and underwater fluorescence taken with the orange filter, 0.6s 290

Figure 119: Comparison between bone width and terrestrial fluorescence taken with the orange filter, 0.4s 291

Figure 120: Comparison between bone width and underwater fluorescence taken with the orange filter, 0.4s 291

Figure 121: Comparison between bone width and terrestrial fluorescence taken with the orange filter, 1/3s 292

Figure 122: Comparison between bone width and underwater fluorescence taken with the orange filter, 1/3s 292

Figure 123: Comparison between bone length and terrestrial fluorescence taken with the orange filter, 0.6s 293

Figure 124: Comparison between bone length and underwater fluorescence taken with the orange filter, 0.6s 293

Figure 125: Comparison between bone length and terrestrial fluorescence taken with the orange filter, 0.4s 294

Figure 126: Comparison between bone length and underwater fluorescence taken with the orange filter, 0.4s 294

Figure 127: Comparison between bone length and terrestrial fluorescence taken with the orange filter, 1/3s 295

Figure 128: Comparison between bone length and underwater fluorescence taken with the orange filter, 1/3s 295

Figure 129: Comparison between the calculated collagen content and mass of the porcine bones (Sus scrofa domesticus)..... 298

Figure 130: T-test comparisons of the average terrestrial fluorescence results of the porcine bones (Sus scrofa domesticus) photographed using the Crime-lite 2 with the orange filter at 0.6s, 0.4s and 1/3s... 299

Figure 131: Result of Wilcoxon signed rank test comparing the average fluorescence values of the terrestrial photographs taken at 0.6s and 0.4s exposure times using the yellow filter 300

Figure 132: Result of Wilcoxon signed rank test comparing the average fluorescence values of the terrestrial photographs taken at 0.6s and 1/3s exposure times using the yellow filter..... 300

Figure 133: Result of Wilcoxon signed rank test comparing the average fluorescence values of the terrestrial photographs taken at 0.4s and 1/3s exposure times using the yellow filter 300

Figure 134: Result of Wilcoxon signed rank test comparing the average fluorescence values of the terrestrial photographs taken using the orange and yellow filters at 0.6s exposure time. 301

Figure 135: Result of Wilcoxon signed rank test comparing the average fluorescence values of the terrestrial photographs taken using the orange and yellow filters at 0.4s exposure time. 301

Figure 136: Result of Wilcoxon signed rank test comparing the average fluorescence values of the terrestrial photographs taken using the orange and yellow filters at 1/3s exposure time. 301

Figure 137: Result of Wilcoxon signed rank test comparing the average fluorescence values of the underwater photographs taken using the orange filter at 0.6s and 0.4s exposure times 302

Figure 138: Result of Wilcoxon signed rank test comparing the average fluorescence values of the underwater photographs taken using the orange filter at 0.6s and 1/3s exposure times. 302

Figure 139: Result of Wilcoxon signed rank test comparing the average fluorescence values of the underwater photographs taken using the orange filter at 0.4s and 1/3s exposure times. 302

Figure 140: Result of Wilcoxon signed rank test comparing the average fluorescence values of the underwater photographs taken using the yellow filter at 0.4s and 0.6s exposure times. 302

Figure 141: Result of Wilcoxon signed rank test comparing the average fluorescence values of the underwater photographs taken using the yellow filter at 0.6s and 1/3s exposure times. 303

Figure 142: Result of Wilcoxon signed rank test comparing the average fluorescence values of the underwater photographs taken using the yellow filter at 0.4s and 1/3s exposure times 303

Figure 143: Result of Wilcoxon signed rank test comparing the average fluorescence values of the underwater photographs taken using the yellow and orange filters at 0.6s exposure time. 304

Figure 144: Result of Wilcoxon signed rank test comparing the average fluorescence values of the underwater photographs taken using the yellow and orange filters at 0.4s exposure time 304

Figure 145: Result of Wilcoxon signed rank test comparing the average fluorescence values of the underwater photographs taken using the yellow and orange filters at 1/3s exposure time 304

Figure 146: Result of Wilcoxon ranked sign test comparing the average terrestrial fluorescence values produced using the Hammerhead light source, and bone mass. 305

Figure 147: Result of Wilcoxon signed rank test comparing the average terrestrial fluorescence values produced using the Hammerhead light source, and bone width. 305

Figure 148: Result of Wilcoxon signed rank test comparing the average terrestrial fluorescence values produced using the Hammerhead light source, and bone anterior-posterior. 306

Figure 149: Result of Wilcoxon signed rank test comparing the average terrestrial fluorescence values produced using the Hammerhead light source, and bone length. 306

Figure 150: Result of Wilcoxon signed rank test comparing the average terrestrial fluorescence values produced using the Crime-lite 2, and bone mass. 308

Figure 151: Result of Wilcoxon signed rank test comparing the average terrestrial fluorescence values produced using the Crime-lite 2, and bone width. 308

Figure 152: Result of Wilcoxon signed rank test comparing the average terrestrial fluorescence values produced using the Crime-lite 2, and bone anterior-posterior 308

Figure 153: Result of Wilcoxon signed rank test comparing the average terrestrial fluorescence values produced using the Crime-lite 2, and bone length. 308

Figure 154: Result of Wilcoxon signed rank test comparing the average underwater fluorescence values produced using the Crime-lite 2, and bone mass. 309

Figure 155: Result of Wilcoxon signed rank test comparing the average underwater fluorescence values produced using the Crime-lite 2, and bone width. 309

Figure 156: Result of Wilcoxon signed rank test comparing the average underwater fluorescence values produced using the Crime-lite 2, and bone anterior-posterior. 309

Figure 157: Result of Wilcoxon signed rank test comparing the average underwater fluorescence values produced using the Crime-lite 2, and bone length. 309

Figure 158: Result of Wilcoxon signed rank test comparing the calculated bone collagen content and bone mass. 310

Figure 159: Result of Wilcoxon signed rank test comparing the calculated bone collagen content and bone width. 310

Figure 160: Result of Wilcoxon signed rank test comparing the calculated bone collagen content and bone anterior-posterior. 311

Figure 161: Result of Wilcoxon signed rank test comparing the calculated bone collagen content and bone length. 311

Figure 162: Comparison between calculated bone collagen level and bone mass 318

Figure 163: Comparison between bone width and terrestrial autofluorescence, photographed with the orange filter at 0.6s 322

Figure 164: Comparison of between bone length and terrestrial autofluorescence, photographed with the orange filter at 0.6s *322*

Figure 165: Comparison of calculated bone collagen and average terrestrial autofluorescence, photographed with the orange filter. A potentially erroneous result (rib 15) is circled in red. *324*

Figure 166: Comparison of calculated bone collagen and average terrestrial autofluorescence, photographed with the orange filter, and 0.6s exposure time. *325*

Figure 167: Comparison of calculated bone collagen and average terrestrial autofluorescence, photographed with the orange filter, and 0.4s exposure time. *325*

Figure 168: Comparison of calculated bone collagen and average terrestrial autofluorescence, photographed with the orange filter, and 1/3s exposure time. *325*

Figure 169: Comparison of all terrestrial fluorescence data points (all exposure times and all ROIs) compared with the calculated collagen content for each porcine bone (sus scrofa domesticus). *326*

Figure 170: Comparison of calculated bone collagen and average underwater autofluorescence, photographed with the orange filter, and 0.6s exposure time. *327*

Figure 171: Comparison of calculated bone collagen and average underwater autofluorescence, photographed with the orange filter, and 0.4s exposure time. *327*

Figure 172: Comparison of calculated bone collagen and average underwater autofluorescence, photographed with the orange filter, and 1/3s exposure time. *327*

Figure 173: Comparison of all submerged fluorescence data points (all exposure times and all ROIs) compared with the calculated collagen content for each porcine bone (sus scrofa domesticus). *328*

Figure 174: Example thermogram from porcine rib 2 demonstrating buoyancy artefact (circled in red) *330*

Figure 175: T-test comparisons of the average terrestrial fluorescence results of the porcine bones (Sus scrofa domesticus), photographed at 0.6s exposure time, compared to the calculated collagen content. *332*

Figure 176: T-test comparisons of the average terrestrial fluorescence results of the porcine bones (Sus scrofa domesticus), photographed at 0.4s exposure time, compared to the calculated collagen content. *332*

Figure 177: T-test comparisons of the average terrestrial fluorescence results of the porcine bones (Sus scrofa domesticus), photographed at 1/3s exposure time, compared to the calculated collagen content. 332

Figure 178: Result of the Wilcoxon signed rank test comparing the average underwater fluorescence results of the porcine bones (Sus scrofa domesticus), photographed at 0.6s exposure time, compared to the calculated collagen content. 333

Figure 179: Result of the Wilcoxon signed rank test comparing the average underwater fluorescence results of the porcine bones (Sus scrofa domesticus), photographed at 0.4s exposure time, compared to the calculated collagen content. 333

Figure 180: Result of the Wilcoxon signed rank test comparing the average underwater fluorescence results of the porcine bones (Sus scrofa domesticus), photographed at 1/3s exposure time, compared to the calculated collagen content. 333

Figure 181: Average terrestrial fluorescence level of each non-bone control (arranged from highest fluorescence level to the lowest), photographed using the Hammerhead ALS and orange filter at 1/3s 353

Figure 182: Average underwater fluorescence level of each non-bone control (arranged from highest fluorescence level to the lowest), photographed using the Hammerhead ALS and orange filter at 1/3s. 353

Figure 183: Comparison of average underwater and terrestrial fluorescence level of each non-bone control, photographed using the Hammerhead ALS and orange filter at 1/3s. 354

Figure 184: Comparison of average terrestrial fluorescence level of each non-bone control, photographed using the Hammerhead ALS and Crime-lite 2, coupled with the orange filter at 1/3s. 356

Figure 185: Comparison of average terrestrial fluorescence level of each non-bone control, photographed using Crime-lite 2, and the orange and yellow filters at 1/3s. 357

Figure 186: Terrestrial fluorescence of the cockle shell produced using the Crime-lite 2 and orange filter at 1/13s exposure time. 363

Figure 187: Terrestrial fluorescence of the cockle shell produced using the Hammerhead ALS and orange filter at 1.3s exposure time. 363

Figure 188: Blue mussel shell (natural light) 364

Figure 189: Shield limpet (natural light) 364

Figure 190: Comparison of terrestrial fluorescence levels of the seven shell specimens, produced using the Hammerhead light, orange filter, and 1/3s exposure time. 365

Figure 191: Visual comparison of the six sea glass specimens, photographed under natural light 368

Figure 192: Visual comparison of terrestrial fluorescence of the six sea glass specimens, photographed using the Crime-lite 2, orange filter, and 1/3s exposure time. 368

Figure 193: Visual comparison of terrestrial fluorescence of the six sea glass specimens, photographed using the Crime-lite 2, yellow filter, and 1/3s exposure time. 368

Figure 194: Visual comparison of terrestrial fluorescence of the six sea glass specimens, photographed using the Hammerhead ALS, orange filter, and 1/3s exposure time. 368

Figure 195: Visual comparison of submerged fluorescence of the six sea glass specimens, photographed using the Hammerhead ALS, orange filter, and 1/3s exposure time. 368

Figure 196: Comparison of terrestrial fluorescence levels of the six sea glass specimens, produced using the Hammerhead light, orange filter, and 1/3s exposure time. 369

Figure 197: Average terrestrial fluorescence results of the eight control items in table 43, as produced by the Hammerhead ALS and orange filter, the Crime-lite 2 and orange filter, and the Crime-lite 2 with yellow filter, all captured at 1/3s exposure time (sorted according to the Hammerhead values). 373

Figure 198: Porcine collagen powder embedded in epoxy resin to form a collagen control block. 376

Figure 199: Epoxy resin only control block. 376

Figure 200: Comparison of terrestrial and underwater average fluorescence levels of the porcine collagen powder and epoxy resin only control blocks. 379

Figure 201: Square epoxy resin only control block, photographed under natural light. 381

Figure 202: Terrestrial fluorescence of the square epoxy resin only control block, photographed with the Hammerhead ALS, orange filter, and 1/3s exposure time. 381

Figure 203: Submerged fluorescence of the square epoxy resin only control block, photographed with the Hammerhead ALS, orange filter, and 1/3s exposure time. 381

Figure 204: Dremel™ 3000 130 W Rotary Multi Tool, fitted with a diamond edge circular blade 383

Figure 205: The six sections of porcine rib (Sus scrofa domesticus) prior to demineralisation. 383

Figure 206: Diagram of the demineralising bone equipment configuration 385

Figure 207: Photograph of the demineralising bone equipment configuration 385

Figure 208: Appearance of the manually defleshed porcine ribs (Sus scrofa domesticus) prior to burning, photographed under natural light. *387*

Figure 209: Methane gas powered roll top BillyOh.com 3 burner hooded domestic BBQ *388*

Figure 210: Photograph showing the porcine ribs (Sus scrofa domesticus) in-situ in the BBQ. *388*

Figure 211: Calcined bone ash photographed under natural light. *390*

Figure 212: Calcined bone ash embedded in epoxy resin, photographed under natural light. *390*

Figure 213: Comparison of average calculated terrestrial and aquatic fluorescence results for the six demineralised porcine bone (Sus scrofa domesticus) sections. Photographed with the Hammerhead light, orange filter, and 1/3s exposure time. *393*

Figure 214: calculated average fluorescence values for each burned porcine rib. *397*

Figure 215: Average terrestrial fluorescence values of all examined control specimens (except deproteinised bone 2), produced using the Hammerhead light source, orange filter, and photographed at 1/3s exposure time. *408*

Figure 216: Average submerged fluorescence values of all applicable control specimens, produced using the Hammerhead light source, orange filter, and photographed at 1/3s exposure time. *409*

Figure 217: Terrestrial fluorescence scale *410*

Figure 218: Underwater fluorescence scale *411*

Figure 219: External view of the black plastic boxes used to house the submerged porcine bone specimens (Sus scrofa domesticus). *417*

Figure 220: Internal view of the black plastic boxes used to house the submerged porcine bone specimens (Sus scrofa domesticus). *417*

Figure 221: Internal view of plastic boxes with porcine ribs in-situ (Sus scrofa domesticus) and filled with water. *417*

Figure 222: Position of boxes in the outside environment *417*

Figure 223: Position of boxes covered with tarpaulin sheet. *417*

Figure 224: Diagram of the equipment configuration for the aquatic taphonomy salinity experiment .. *418*

Figure 225: Measured changes in pH in the tap water and saltwater contexts over the 6-month period (reading taken at each 2-month interval) *426*

Figure 226: Measured changes in total dissolved solids (TDS) in the tap water and saltwater contexts over the 6-month period (reading taken at each 2-month interval) 426

Figure 227: Measured changes in conductivity in the tap water and saltwater contexts over the 6-month period (reading taken at each 2-month interval) 427

Figure 228: Measured changes in turbidity in the tap water and saltwater contexts over the 6-month period (reading taken at each 2-month interval) 427

Figure 229: Photographs of the porcine ribs (Sus scrofa domesticus), taken in natural light, after submersion in tap water for 2 months, exhibiting a pinkish grey/brown pigmentation. 429

Figure 230: Photographs of the porcine ribs (Sus scrofa domesticus), taken in natural light, after submersion in saltwater for 2 months, exhibiting yellow/orange discolouration and yellow greasy deposits on the bone surface..... 429

Figure 231: White, crystalline deposit at the butchered epiphyses and dark pink pigmentation, seen in the porcine ribs (Sus scrofa domesticus) that had been submerged in saltwater for 4 months. 431

Figure 232: White deposit and visual increase in porosity noted in the shorter, wider porcine ribs (Sus scrofa domesticus) that had been submerged in saltwater for 4 months. 431

Figure 233: Photographs of the tap water porcine bones (Sus scrofa domesticus) after submersion for 4 months, exhibiting a pale pink discolouration with yellowing across the diaphysis. Some surface damage and increased porosity (red circle). 432

Figure 234: Photographs of the tap water porcine bones (Sus scrofa domesticus) after submersion for 4 months, exhibiting a pale pink discolouration with yellowing across the diaphysis. Possible evidence of microbial tunnelling (red circle)..... 432

Figure 235: Diffuse pink/red discolouration graduating to a darker reddish/brown towards the epiphyses in the porcine ribs (Sus scrofa domesticus), submerged in tap water for 6 months. 433

Figure 236: Appearance of two example porcine ribs (Sus scrofa domesticus) displaying yellow pigmentation and a thick layer of greasy/fatty surface deposits, after submersion in saltwater for 6 months. 434

Figure 237: White surface deposits seen at the butchered epiphyses of two porcine ribs (Sus scrofa domesticus), after submersion in saltwater for 6 months. 434

Figure 238: Average changes in terrestrial fluorescence of the 18 porcine ribs (Sus scrofa domesticus), seen at each submersion interval. *450*

Figure 239: Average changes in underwater fluorescence of the 18 porcine ribs (Sus scrofa domesticus), seen at each submersion interval. *450*

Figure 240: Differences in average terrestrial bone fluorescence observed in porcine bone (Sus scrofa domesticus) that had been submerged in tap water for 2-, 4-, and 6-month durations. *452*

Figure 241: Differences in average terrestrial bone fluorescence observed in porcine bone (Sus scrofa domesticus) that had been submerged in saltwater for 2-, 4-, and 6-month durations. *452*

Figure 242: Differences in average underwater bone fluorescence observed in porcine bone (Sus scrofa domesticus) that had been submerged in tap water for 2-, 4-, and 6-month durations. *453*

Figure 243: Differences in average underwater bone fluorescence observed in porcine bone (Sus scrofa domesticus) that had been submerged in saltwater for 2-, 4-, and 6-month durations. *453*

Figure 244: Differences in calculated collagen content in porcine bones (Sus scrofa domesticus) that had been submerged in tap water for 2-, 4-, and 6-month durations. *457*

Figure 245: Differences in calculated collagen content in porcine bones (Sus scrofa domesticus) that had been submerged in saltwater for 2-, 4-, and 6-month durations. *457*

Figure 246: Results of the independent samples median test comparing the day 0 data from the 2-month data group. *459*

Figure 247: Results of the independent samples median test comparing the 2-month post-submersion data from the 2-month data group. *460*

Figure 248: Result of the Kruskal Wallis test for day 0 data for the 2-month dataset, grouped according to terrestrial fluorescence *460*

Figure 249: Result of the Kruskal Wallis test for the 2-month data for the 2-month dataset, grouped according to terrestrial fluorescence. *460*

Figure 250: Result of the Wilcoxon Signed Ranks tests comparing day 0 measurements to the 2-month fluorescence, collagen, and bone dimension values. *464*

Figure 251: Result of the Wilcoxon Signed Ranks tests comparing day 0 measurements to the 6-month values. *464*

Figure 252: Results of the independent samples median test comparing the day 0 data from the 6-month data group. *465*

Figure 253: Results of the independent samples median test comparing the 6-month post-submersion data from the 6-month data group. *465*

Figure 254: Result of the Kruskal Wallis test for day 0 data, for the 6-month dataset, grouped according to terrestrial fluorescence *466*

Figure 255: Result of the Kruskal Wallis test for 6-month data for the 6-month dataset, grouped according to terrestrial fluorescence *466*

Figure 256: Result of the Wilcoxon Signed Ranks tests comparing salt and tap water fluorescence values in the 2-month and 6-month temporal groups. *469*

Figure 257: Result of the Wilcoxon Signed Ranks tests comparing salt and tap water fluorescence values of the 2-month and 6-month temporal groups, to the respective calculated collagen values. *469*

TABLES

Table 1: Stages of aquatic decomposition [26] *30*

Table 2: Summary of photographic results for the orange, yellow, and red filters produced during the MSc study. *101*

Table 3: Example of the luminosity equation used to convert coloured images to grayscale. *140*

Table 4: Bone quality scoring and descriptions used to score the final maceration results (adapted from Steadman et al, 2005) [149]. *180*

Table 5: Final maceration duration for sample set and each maceration technique. *186*

Table 6: Results of collagen quantification of ten porcine ribs (Sus scrofa domesticus) subjected to hot water maceration (approx. 80°C), including summary of changes in mass and collagen content. *188*

Table 7: Summary of photographic results of 10 porcine ribs (Sus Scrofa Domesticus) before and after hot water maceration (approx. 80°C) *190*

Table 8: Average fluorescence values for porcine ribs (Sus scrofa domesticus) subject to hot water maceration (approx. 80°C), alongside calculated fluorescence and percentage change *192*

Table 9: Results of collagen quantification of ten porcine ribs (Sus scrofa domesticus) subjected to maceration with biological washing powder (approx. 50°C), including summary of changes in mass and collagen content. *197*

Table 10: Summary of photographic results of ten porcine ribs (Sus scrofa domesticus) before and after maceration with biological washing powder (approx. 50°C) *199*

Table 11: Average fluorescence values for ten porcine ribs (Sus scrofa domesticus) subject to biological washing powder maceration (approx. 50°C), alongside calculated fluorescence and percentage change *201*

Table 12: Results of collagen quantification for the ten porcine ribs (Sus scrofa domesticus) subjected to enzymatic maceration (approx. 55°C) *205*

Table 13: Summary of photographic results of ten porcine ribs (Sus scrofa domesticus) before and after enzymatic maceration (approx. 55°C) *207*

Table 14: Average fluorescence values for porcine ribs (Sus scrofa domesticus) subject to enzymatic maceration (approx. 55°C), alongside calculated fluorescence and percentage change *208*

Table 15: Comparison of the average bone mass, fluorescence, collagen content, and bone scores for all three maceration techniques *214*

Table 16: Comparison of intraindividual variation of pre and post maceration average fluorescence values, for each maceration dataset *217*

Table 17: The distribution of porcine ribs (Sus scrofa domesticus) per research question, including the preparation method used. *223*

Table 18: Summary of fluorescence results of anatomical regions of macerated porcine ribs (Sus scrofa domesticus); central (A), vertebral (B), sternal (C). *226*

Table 19: Fluorescence and collagen results of central, vertebral, and sternal aspects of macerated porcine ribs (Sus scrofa domesticus), where (A) refers to the central/diaphysis, (B) refers to the vertebral end, and (C) refers to the sternal end. *227*

Table 20: Average fluorescence and calculated collagen content calculated for each anatomical region based on the three examined porcine ribs (Sus scrofa domesticus) *227*

Table 21: A summary of the photographic results for positioning methodology testing *231*

Table 22: A summary of the photographic results for background testing *232*

Table 23: Summarised results of terrestrial photographs taken at 14, 18, 22cm with the Hammerhead ALS and orange filter *238*

Table 24: Summarised fluorescence results of submerged macerated porcine rib (Sus scrofa domesticus) photographed using refined camera settings, Hammerhead light, and orange filter. *241*

Table 25: Summarised fluorescence results of submerged macerated porcine rib (Sus scrofa domesticus) photographed using Crime-lite 2 covered with plastic bag, in conjunction with orange and yellow barrier filters. *242*

Table 26: Summarised fluorescence results of submerged macerated porcine rib (Sus scrofa domesticus) photographed using Crime-lite 2 without the plastic bag, in conjunction with orange and yellow barrier filters. *243*

Table 27: Distribution of porcine ribs (Sus scrofa domesticus) per research question and corresponding preparation method *250*

Table 28: Summary of all photographic fluorescence results for rib 1 stimulated using the Crime-lite 2 with the orange and yellow filters in terrestrial and underwater setting respectively, as well as the Hammerhead light coupled with the orange filter in terrestrial and underwater contexts. 262

Table 29: Summary of average changes in averaged fluorescence levels of porcine bone when photographed with ALS and the appropriate orange and/or yellow filters in terrestrial and underwater contexts. 264

Table 30: Summary of average bone mass, length, width and anterior to posterior measurements of the photographed porcine bones (excluding rib 17) 277

Table 31: Summary of average fluorescence of the photographed porcine bones (excluding rib 17) in terrestrial and underwater contexts, using the Hammerhead ALS, orange filter, and the three exposure times: 0.6s, 0.4s, and 1/3s. 281

Table 32: Calculated collagen content for the thirty porcine bones used in the terrestrial compared to underwater fluorescence dataset. 296

Table 33: Average dimensions for the 54 porcine ribs (sus scrofa domesticus) used during section B, research question 2; examining the collagen-fluorescence relationship. 314

Table 34: average collagen, mass, and fluorescence data collected from the 54 porcine ribs (Sus scrofa domesticus), at each exposure time, and during both deposition contexts. 316

Table 35: Summarised terrestrial and submerged photographic fluorescence results for porcine ribs 1 and 16 (Sus scrofa domesticus), generated using the Hammerhead ALS coupled with the orange filter, across each exposure time (0.6s, 0.4s, 1/3s) 317

Table 36: Average bone dimensions of the fresh porcine ribs (Sus scrofa domesticus) (n=30), examined in section B, question 1 320

Table 37: Average bone dimensions of the macerated porcine ribs (Sus scrofa domesticus) (n=54), examined in section B, question 2 320

Table 38: Twenty-seven naturally occurring non-bone items recovered from terrestrial and aquatic environments, alongside provenance data, descriptions, and dimensions. 339

Table 39: Average fluorescence results for the 27 non-bone items recovered from terrestrial and aquatic environments, tabulated according to context and filter used. 344

Table 40: Summarised photographic fluorescence results for all 27 non-bone control items, including all filters, contexts, and ALS devices 345

Table 41: Visual comparison of fluorescence levels of ceramic fragments 1 and 3, produced using the Crime-lite 2 at 1/3s exposure time with the orange and yellow filters. 358

Table 42: Visual comparison of fluorescence levels of the cockle and queen scallop shells, produced using both light sources and all photography configurations. 361

Table 43: Visual comparison of terrestrial fluorescence levels of four organic and four inorganic non-bone control samples, photographed using the Hammerhead light source, orange filter, 1/3s exposure time. 372

Table 44: Colour comparison of the four stone specimens from the non-bone control dataset, photographed under natural light. 374

Table 45: Visual table summarising the photographic fluorescence results of the porcine collagen powder and epoxy resin control blocks, photographed using the Hammerhead light in terrestrial and aquatic settings, with the orange filter at 1/3s exposure time. 378

Table 46: Dimensions of the six portions of porcine rib (Sus scrofa domesticus). 384

Table 47: Dimensions of the fresh porcine ribs (Sus scrofa domesticus) prior to burning. 387

Table 48: Photographic fluorescence results of the six demineralised bone samples photographed using the Hammerhead ALS, orange filter, at 1/3s exposure time, in terrestrial and submerged contexts. 391

Table 49: Average calculated terrestrial and aquatic fluorescence results, standard deviation, and range, for the six demineralised porcine bone (Sus scrofa domesticus) sections. Photographed with the Hammerhead light, orange filter, and 1/3s exposure time. 392

Table 50: Comparison of terrestrial and aquatic average fluorescence values of the demineralised porcine bone segments (sus scrofa domesticus), and the fresh and macerated porcine bone datasets from section B, research questions 1 & 2. Photographed using the Hammerhead ALS, orange filter, and 1/3s exposure time. 395

Table 51: Summarised fluorescence results of the deproteinised porcine ribs (Sus scrofa domesticus), photographed using the Hammerhead ALS, orange filter, and 1/3s exposure time in a terrestrial context. 396

Table 52: Recorded intervals and burning temperatures. 397

Table 53: Calculated average fluorescence values for each burned porcine rib, photographed using the Hammerhead ALS, orange filter, and 1/3s exposure time in a terrestrial context. 397

Table 54: Comparison of terrestrial average fluorescence values of the deproteinised porcine bones (sus scrofa domesticus), six demineralised porcine bone segments, and the fresh and macerated porcine bone terrestrial datasets from section B, research questions 1 & 2. Photographed using the Hammerhead ALS, orange filter, and 1/3s exposure time in a terrestrial context. 399

Table 55: Example of the photographic fluorescence results of the bone ash control, photographed using the Hammerhead ALS, orange filter, and 1/3s exposure time in a terrestrial context. 400

Table 56: Calculated average fluorescence values for each burned porcine rib, photographed using the Hammerhead ALS, orange filter, and 1/3s exposure time in a terrestrial context. 401

Table 57: Overview of the bone derived control samples discussed in research question section B, question 3a-c, alongside an example of a manually defleshed fresh porcine bone (sus scrofa domesticus), obtained using the 450 nm Hammerhead light source, orange filter, and 1/3s exposure time in terrestrial and tap water contexts. 403

Table 58: Average dimensions for the 54 porcine ribs (sus scrofa domesticus) used during section B, research question 4: the impact of salinity. 414

Table 59: Photographs of all 54 porcine ribs (Sus scrofa domesticus) before and after maceration, with labels attached. 416

Table 60: Quantified collagen levels of the six porcine ribs (Sus scrofa domesticus), pre and post hot water maceration (80°C), including the calculated reductions. 421

Table 61: Visual changes observed in each aquatic context and the applicable interval. 422

Table 62: Water chemistry measurements recorded at each interval, and the calculated changes observed overtime. 423

Table 63: Photographic summary of the post-submersion appearance for each set of porcine ribs (Sus scrofa domesticus) retrieved at each submersion interval and deposition context, photographed under natural light. 428

Table 64: Changes in mass, length, width and anterior-posterior for all porcine bones (Sus scrofa domesticus) across each submersion interval, including the calculated percentage change for each

measurement. Data for the tap water specimens is contained in the top half and the saltwater data in the lower half. 437

Table 65: Average recorded temperature data for each interval and ambient temperature for the duration of the submerged salinity experiment. 441

Table 66: Summarised photographic fluorescence results for the 2-month tap water specimens. 443

Table 67: Summarised photographic fluorescence results for the 2-month saltwater specimens. 444

Table 68: Summarised photographic fluorescence results for the 4-month tap water specimens. 445

Table 69: Summarised photographic fluorescence results for the 4-month saltwater specimens. 446

Table 70: Summarised photographic fluorescence results for the 6-month tap water specimens. 447

Table 71: Summarised photographic fluorescence results for the 6-month saltwater specimens. 448

Table 72: Calculated average differences in emitted florescence in porcine ribs (Sus scrofa domesticus) after each submersion interval, when photographed using the Hammerhead ALS, orange filter, at 1/3s exposure time, in terrestrial and aquatic contexts. 450

Table 73: Comparison of calculated average differences in emitted florescence in porcine ribs (Sus scrofa domesticus) after each submersion interval, and across each aquatic context. Photographed using the Hammerhead ALS, orange filter, at 1/3s exposure time. 451

Table 74: Changes in calculated collagen levels for the porcine ribs (Sus scrofa domesticus) submerged in the tap water and saltwater contexts for 2-months. 455

Table 75: Changes in calculated collagen levels for the porcine ribs (Sus scrofa domesticus) submerged in the tap water and saltwater contexts for 4-months. 455

Table 76: Changes in calculated collagen levels for the porcine ribs (Sus scrofa domesticus) submerged in the tap water and saltwater contexts for 6-months. 456

LIST OF ABBREVIATIONS

(Alphabetical order)

AIU = arbitrary intensity units

ALS = Alternative light source

A/P = Anterior-posterior measurement

App = Application

DSC = Differential Scanning Calorimetry

DNA = Deoxyribonucleic acid

FTIR = Fourier-transform infrared spectroscopy

HTA = Human Tissue Authority

HTF = Human Taphonomy Facility

IR = Infra-red

LED = Light emitting diode

Max. = Maximum

Min. = Minimum

NIR = Near infra-red

NTU = Nephelometric turbidity units

OFC = Osteo-Fluorescence Calculator

PMI = Post-mortem interval

PMSI = Post-mortem submersion interval

%N = Percentage of nitrogen

RGB = Red, green, blue

ROI = Region of Interest

ROV = Remotely operated vehicle

SEM = Scanning electron microscope

S.D. = Standard Deviation

TDS = Total dissolved solids

TGA = Thermogravimetric Analysis

UAV = Unmanned aerial vehicle

UV = Ultraviolet

UV-VIS = Ultraviolet-Visible spectrum

VOC = Volatile organic compound

YAG = Yttrium Aluminium Garnet

1.0 - INTRODUCTION

With over 70% of the Earth's surface consisting of water [1] it is inevitable that human remains will be found in aquatic contexts [1, 2]. The UK alone has approximately 40,000 lakes [3], 12,429 km of coastline [4] and 200,000 km of watercourses [5], and in 2018 recorded approximately 585 water-related deaths including suicides, accidental deaths and deaths related to suspected criminal activity [6]. Recent high-profile water-related cases include the disappearance of the Titan deep sea submarine, where five people were killed when the vessel imploded during a diving expedition to see the wreckage of the Titanic and in the UK [7], the death of Nicola Bulley, who is thought to have fallen into the River Wyre in St Michael's, Lancashire when walking her dog [8]. From a global perspective, in 2015 the World Health Organisation created initiatives to promote water safety and reduce drownings [9], as their research cites approximately 372,000 deaths worldwide annually [9]. However, this data does not include more extraordinary events such as mass disasters - which often include high numbers of casualties - such as the 2011 tsunami in Japan where approximately 19,000 people died [10] and the disappearance of the 2014 Malaysia airlines flight 370 air disaster, presumed to have crashed into the Indian Ocean carrying 239 passengers [11].

Terrestrial search strategies for missing people and human remains are well established with detection dogs [12], aerial searches [13], and crime scene search patterns routinely used [14]. Additional information gained from external sources such as CCTV, eyewitnesses, and digital evidence support these investigations by helping to build a timeline and reconstruct the events surrounding the death [15]. Buried human remains have also been the subject of extensive research, encompassing archaeological and forensic topics such as detecting clandestine and mass graves [13, 16] , investigating the influence of soil composition on decomposition rates and preservation [17, 18], and assessing the effectiveness of different geophysical techniques [19], all of which can be used to coordinate excavation efforts [20].

However, body deposition in water complicates recovery efforts [21]. Not only does water physically conceal a body, but due to its highly dynamic nature and variability [22], human remains can be transported great distances, making them extremely difficult to

find even if the location of where the person entered the water is known [23, 24]. The destructive properties of water also pose a risk to the integrity of the body, the potential forensic evidence it may carry, as well as a risk to investigators who need to navigate the scene [23, 25-27]. This ever-changing environment coupled with complex decomposition processes, severely limits the timescales in which searches can be conducted successfully [1]. As a result, strategies are often based on case experience, force specific training, and general guidance publications [28-30] such as: *Guidance on the Management, Recording and Investigation of Missing Persons* (2005) [31], *Practice Advice on Search Management and Procedures* (2006) [32] and the *Grampian Police missing persons guidelines* (2007) [33]. However, these publications focus primarily on living people and feature extensive chapters on the psychology of missing persons, efficient search management, and correct reporting procedure.

Out of these three publications, *The Grampian Police missing persons guidelines* (2007) [33] provides the most detailed discussion of missing persons in water although it comprises of brief 'rules of thumb' and tips rather than scientific recommendations. However, it does emphasise that the speed of the water is integral when estimating the mobility of a submerged body [33], which has been explored in scientific literature. Algorithms to plot the trajectory of bodies focus on the speed, depth, and directionality of water to estimate the original deposition point and extrapolate potential resurfacing timescales and locations [2, 34-38]. However, a range of intrinsic and extrinsic factors influence the accuracy and reliability of these estimations; rainfall prior and during submersion, body mass, clothing layers, geographical location, context topography, time of year, and the manner of entering the water will need to be taken into consideration [36]. Marine environments are particularly problematic due to tidal currents and whether the person entered the water from the shoreline or at sea as this can drastically alter a body's journey [24]. Prediction models can calculate current patterns based on tides, wind, water temperatures, and salinity, and have been used to estimate the drift of human bodies at sea [37]. Examples include the Portuguese Coastal Operational Modelling System (PCOMS) and Lagrangian drift model, which map sections of coastal current allowing investigators to estimate body displacement [24, 37]. However, results can be vague leading to very broad search areas [37]. Furthermore, forensic research in the UK is conducted using pigs rather than humans as the use of human subjects for

forensic research is not currently governed by the Human Tissue Authority (HTA) [39]. As a result, many of these calculations are derived from international studies, or individual case work, meaning that sample data is low and the results not necessarily applicable to UK waterways [2, 36, 37, 40].

These issues are further exacerbated by the complex decomposition process experienced by submerged bodies, which differs significantly from the more predictable decomposition occurring in bodies on land [41, 42]. In terrestrial depositions, it is generally accepted that there are approximately five stages of human decomposition described as fresh, bloat, active, advanced, and skeletonisation [43-45]. The sequence and progression of these stages is dictated by extrinsic and intrinsic factors such as temperature, access for insects, clothing or coverings, wounds or trauma, and geographical location [46-49]. In aquatic contexts, decomposition is estimated to be two to three times slower [40], significantly due to the generally cooler temperatures compared to terrestrial decomposition [50]. Cadavers will exhibit similar features and stages to terrestrial decomposition, but the manifestation and duration will be different [36, 50], due to lower oxygen levels limiting bacterial growth, submerged portions of the body being less accessible to insects, and movement by water currents and tides increasing the chances of disarticulation and mechanical decomposition [26, 40]. There are also post-mortem changes which are more likely to appear in aqueous contexts such as adiopocere [51], but also additional decomposition phases of floating and sinking [36, 52]. The commonly reported stages of aquatic decomposition can be seen in table 1 below.

Table 1: Stages of aquatic decomposition [26]

Stage	Characteristics
1. Fresh submerged	Fresh; sunken remains
2. Early floating	Bloated; floating remains
3. Early floating decay	Minor decay; disarticulation of soft tissue
4. Advanced floating decay	Major decay; skeletal exposure
5. Sunken remains	Remains sink; bones

Although these stages report an immediate sinking of human remains, an initial floating phase is also possible [53], normally the result of residual air trapped in the deceased's lungs when entering the water [26, 54]. If the individual was alive upon submersion and subsequently succumbed to drowning, then water may have entered the lungs and stomach, displaced the air, and consequently weighed the body down, leading to sinking [55]. Depending on the depth and flow of the water this initial sinking can assist searching investigators as the body is less likely to move far from the deposition point and decomposition will have slowed further as the limiting effects of cold water temperatures, limited oxygen, and no access for insects increases at greater depths [50]. Typically, this means that the body will remain whole for longer and therefore more detectable to search methods. However according to the Grampian guidelines (2007), after approximately 28 days, the body will resurface once decomposition has progressed and the body has become bloated [33]. Bloating in a body is due to a build-up of abdominal gases produced by continual intestinal bacterial propagation no longer regulated by a living host [45]. This activity produces gas which increases buoyancy, which eventually overcomes the mass of the individual, bringing them to the surface [26, 55]. For a time, this also can make the body easier to detect with basic visual search tactics such as walking the embankments and using search boats being the most effective, particularly if the body becomes snagged on nearby vegetation. However, it is highly dependent on the condition of the body and the nature of the aquatic environment itself [56]. Bodies submerged during the warmer months or in warmer water temperatures are thought to resurface quicker compared to those deposited during colder contexts [55, 57], most likely due to the more favourable temperatures for bacterial proliferation [36, 58], but bodies that are subjected to greater depths will take longer to resurface or may not resurface at all due to increased pressure acting on the body [53, 54] and colder aquatic temperatures slowing the decomposition rate [36, 50].

Although the Grampian guidelines (2007) [33] state that salinity does not influence the resurfacing rate of bodies, literature suggests that decomposition is expedited in freshwater contexts compared to marine environments due to lower salinity and higher bacterial communities [42, 59]. Substrates containing high salinity levels are known to slow decomposition by retarding bacterial growth [60] particularly when coupled with

the more constant, lower aquatic temperatures [61, 62]. Other research suggests that clothing may also promote buoyancy of a body due to trapping air between clothing layers [63-65], but the extent of this effect will be influenced by the composition of the clothing layers [64] and how the material behaves when wet [26]. For example natural fibres are absorbent and therefore can reduce buoyancy more than synthetic materials [26, 66] whilst also encouraging adiopocere formation [66]. Close fitting clothing or additional wrappings would be restrictive therefore reducing the capacity for air pockets and the development of bloat [1, 49, 67]. Other intrinsic factors such as body composition have also been considered, with some research suggesting that bodies with a higher body fat percentage have a tendency to float [53] but additional variables such as layers of clothing worn, and age of the decedent would can also influence buoyancy [68]. Bodies inflicted with trauma prior to submersion are less likely to float [54], especially if that damage is sustained to the abdominal cavity allowing gases to vent, and an influx of water. Although gases can accumulate elsewhere in the body such as face and genitals, it is to a much lesser extent compared to the much larger abdominal cavity [45].

Similarly, although the Grampian guidelines (2007) estimate body resurfacing from bloat within 28 days, this guidance does not consider the huge variety of waterways within the UK, ranging from canals, lakes, lochs, estuaries, rivers, and streams, as well as coastline [69]. Each of these contexts vary in width, depth, tides, and currents [70], and exhibit different chemical composition, temperature, and biodiversity [69, 71]. In casework published in literature, authors report a great variation in the presentation and persistence of bloat [72]. For example, Petrik et al (2013), identified bloat characteristics in bodies recovered between 14 and 45 days after death, from a freshwater environment in British Columbia [27], citing greater degradation in the bodies recovered water sources with a current or flow, compared those from still or standing water [27]. Conversely, Palazzo et al (2021) identified bloating characteristics in bodies from 5 days recovered from the Northern Adriatic Sea.

Despite the increased visibility of a floating body, once it has resurfaced it can in fact become more challenging for search teams to locate as the increased buoyancy makes the body much more mobile and when propelled by strong winds or currents can travel

much further away from the deposition site [38, 59]. Consequently, most aquatic search strategies are aimed at finding the body in the earliest stages of decomposition, either immediately after submersion or just as the body has resurfaced, where movement through the water is minimal and the body is still intact [68].

1.1 – CURRENT SEARCH STRATEGIES

The recovery of submerged human remains is a complex and time-consuming process, with investigators needing to overcome highly variable terrain, complex water dynamics, limited visibility, and adverse weather conditions [73]. Even in shallow water, there is the possibility of hidden or unusual currents or sunken debris that may not be obvious from external examination but can pose a risk to diving teams and trap a submerged body [74]. Therefore, highly trained specialist police diver teams [23, 75] are needed to carry out the search but often require support from experts trained in additional geophysical technologies [10], such as side scan sonar [75, 76], and water penetrating radar (WPR) [77, 78], or more traditional methods such as detection dogs [14], to narrow search areas and highlight targets of interest . Diving teams are restricted to short bursts of manual investigation due to the dangerous search environments [79, 80] but these additional search techniques allow searches to be carried out for longer, at greater depths, and across more unfavourable terrain. Each geophysical technique will be discussed in more detail in chapter 5.4, but in general they offer a non-invasive approach and work by transmitting pulses of sound waves or electromagnetic energy through a substrate, with the echo detected by an accompanying receiver [23, 81]. Voids or anomalies within these echo signals suggest the presence of an object, which depending on size, shape, and expert interpretation, may suggest the presence of a body [81, 82]. This encourages targeted investigations by the diving teams which saves time and reduces the duration needed in the water [83].

Consequently, a whole body is much easier to detect than body parts or skeletal remains due to the larger size producing better contrast with the surrounding environment [75]. Detection dogs are trained to detect the chemical emissions from a body during the decomposition process, known as volatile organic compounds (VOCs) [84]. Although more often used in terrestrial body recovery, detection dogs can be taken on boats across an area of still water to scent VOCs of submerged bodies [85]. However, not all

methods are suitable for all aquatic conditions and although less time consuming for investigators, the results need to be interpreted by experts [82]. For example, WPR is not effective in salt water environments due to high conductivity of salt ions impeding the distance that the sound waves can travel [83]. Detection dogs struggle to detect VOCs in locations with strong currents as the constant movement disperses the scent [86], and bodies in very advanced stages of decomposition exhibit much lower VOC concentration [87]. The results of side scan sonar can be difficult to interpret particularly when imaging a crowded aquatic landscape where multiple objects are within close proximity, overlapping, or of a similar size [88]. For example, a body surrounded by dense vegetation, or submerged within a container such as a suitcase or bag can create confusing shadows and/or completely obscure points of interest, consequently requiring deeper interpretation or repeated scans [82]. Dismembered body parts and child bodies are much more difficult to differentiate, due to their smaller size, especially if body parts have been deposited in insolation away from the main trunk of the body [82]. Scattered body parts create further challenges for search teams as each body part can move independently through the water and travel at different rates, making the movements difficult to predict, widening the search area, and subsequently requiring longer searches [89]. Body parts also have a greater surface area to volume ratio compared to whole bodies which increases their exposure to the taphonomic environment and access for scavenger communities [90], which accelerate decomposition through consumption of the tissues [26]. Extensive dismemberment would also reduce the possibility of bloat occurring if the torso has already been compromised.

Consequently, how bodies behave in water is not fully understood [57, 65], and the huge range of influencing factors make predicting a body's movement, as well as the rate of decomposition, difficult to assess [29, 36]. Much of the data that does exist is derived from case studies or drawn from professional experience [57, 65], which can be useful in immediate tactical strategizing, but it's not always supported by research. The window of opportunity to find bodies in these early stages can be short and is largely unpredictable [68], and search strategies are more limited compared to terrestrial investigations [82]. Once the post-mortem interval increases, and a body passes the bloat stage, the chances of successfully recovering a whole body diminishes [65] as

continued exposure to the taphonomic environment takes its toll [53].

1.2 – SUBMERGED SKELETAL REMAINS

The bloat stage ends once the body loses structural integrity through the bacterial breakdown of the soft tissues, or through trauma inflicted by environmental obstacles or scavenger activity perforating the body cavities [91]. This rupture releases the built-up gases, resulting in the body sinking once again [26]. After the body sinks, it becomes much more difficult to locate as it may have travelled far from the original deposition point and is no longer visible from the surface [53]. As decomposition progresses there is also a reduction in physical size due to putrefaction degradation, consumption of the tissue by bacteria and scavengers, and mechanical destruction by environmental influences such as wind, rain, and contact with the terrain [26, 92]. With advancing decomposition and destruction of soft tissue there is an increasing likelihood of fragmentation and disarticulation of the body, as the tissue depletes, bone becomes exposed, and joints eventually weaken [93]. Disarticulation of a body is thought to occur in a predictable sequence but is dictated by body position, deposition environment, and clothing [93, 94].

Tissue depletion and bone exposure in a floating body occurs quickest in areas where the soft tissue is thinnest, such as the skull, hands, and lower legs, with disarticulation of skeletal elements following the same general sequence [54]. Research suggests that bodies tend to float in a prone position due to the relative density of the human limbs compared to the head and trunk, with the appendages and head hanging down [55], rendering them more vulnerable to water movements and abrasion from the ocean floor or riverbed. The small bones of the hands, wrists, feet, and ankles separate from the body first, along with the mandible and cranium [1, 26]. This is followed by the long bones of the long arms and legs, then the upper limbs [22], and finally the separation of the spinal column and pelvis [90]. However, strong currents and tides, or interaction with rugged aquatic landscapes will accelerate disarticulation, through mechanical disruption, whereas a still environment would be less destructive [53]. As on land, consumption of the body by scavengers will also accelerate decomposition and disarticulation, whereas submersion in an acidic environment may promote adiopocere formation in residual tissues and thus prevent disarticulation [94, 95]. Individual skeletal

elements separated from the main body are often not searched for or recovered, especially in deep, open water such as the ocean [22] Consequently, bones are often only found opportunistically once they wash ashore [53], often in partially articulated clusters or in isolation [29, 30, 92]. Overall, there are no specific methodologies focused on finding skeletal remains. The extended submersion interval leaves little to no scent for detection dogs to detect [12] and the physical size of target is drastically reduced due to disarticulation, damage, and dispersal of the skeleton [96] making remains less visible/recognisable to geophysical imaging techniques [22, 88, 91, 97]. Dispersal of remains further complicates identification as bones become dissociated from the main assemblage. This is further compounded by police officers conducting searches, who are not routinely trained in human osteology and therefore may be unfamiliar with skeletal material and the drastic morphological changes that bone can undergo whilst submerged [75, 98].

1.3 – TAPHONOMY OF SKELETAL REMAINS

Taphonomic alterations to bone manifest both macroscopically and microscopically and are dictated by the deposition environment [92]. The most common alterations are changes to surface colour [99]. In terrestrial contexts, discolouration arises from prolonged contact with soil, and can be expedited in acidic environments [100], due to corrosive action making bones more porous [101]. Tannins from adherent topsoil or humus can give bones the typical medium brown colouration [30, 99], but the mineral content of soil influences more diffuse colour staining [102]. For example, sustained manganese exposure produces brown to black colour changes, whereas high levels of copper typically create a greenish yellow appearance [99], and high levels of iron leads to ferrous deposits and reddish pigmentation [102]. Discolouration due to metallic deposits may also pose an issue for ALS analysis, as iron and copper particles possess autofluorescence capabilities [103, 104], and could potentially amplify fluorescence yields. However, this has yet to be explored in literature within this context.

Surface deposition creates localised patches of differential staining in accordance with the bone surfaces in contact with the soil [99], while burial leads to more widespread staining throughout the assemblage [102]. Bones in aquatic contexts also experience colour changes due to soil [105] particularly in still bodies of water where bones may be

resting on the bottom, or impaction of silt, sediment, and mud due to tumbling from waves and currents [54]. Algae growth which accumulates on the exposed surface of bones in damp, but sunlit environments can create a greenish appearance [105, 106] whereas in drier, more exposed environments bleaching is more likely to occur, lightening the bone to a paler, white exterior [107]. Terrestrial deposition bleaching is a result of photodegradation from sustained exposure to ultraviolet radiation emitted by the sun [108]. This manifests differentially across the skeletal assemblage due to partial burial/coverings and body positioning, with only the exposed surfaces becoming bleached [102]. However extended submersion in a marine environment can also lead to bleaching [92], resulting from the breakdown of the organic content from bone and the deposition of salt crystals, producing a chalky appearance [30, 106]. This marine bleaching occurs in a much more uniform distribution as complete submersion enables access to all bone surfaces [30, 106].

Other surface changes such as erosion, pitting, rounding, and widowing of the foramina occur in aquatic contexts [30] where the bones are exposed to the repetitive motion of the water and any suspended precipitates such as sand or grit, and abrasive action against the sea or riverbed [1, 106, 109]. This leads to thinning of the normally robust cortical bone and exposure of the delicate trabecular spongy bone underneath [30], leaving it vulnerable to microbial infiltration and subsequent microscopic degradation of the collagen and mineral components [92]. Ultimately, this makes the bones more fragile and difficult to identify as this erosive action can reshape or completely obliterate vital skeletal landmarks which are also required for post-recovery osteological analysis [30, 109]. Fracturing, splintering and fragmentation of skeletal elements can also occur, including possible separation of the epiphyses and breakage of protuberances [30, 106], also negatively affecting the ability to identify individual bones [110]. This variability in taphonomic alterations, as well as target size, is a possible contributing factor to the lack of search strategies tailored to skeletal remains and later PMI timescales. Consequently, a preliminary identification technique such ALS, that could highlight bones in varying states of preservation would be of great benefit to investigations.

As bones become free from the main assemblage dispersal throughout the environment becomes likely [107]. In surface depositions exposed bones may be displaced from the

original deposition site by scavengers [111], with some American studies showing vultures and coyotes moving bones miles [112, 113]. Bones may also become displaced due to construction work or farming, exposing clandestine graves or archaeological settlements [114]. Extensive flooding can also displace skeletal remains by washing away large amounts of soil carrying remains into nearby rivers and outlets [53, 57]. Submerged bones can become scattered and displaced due to tides, currents, and scavengers with individual bones travelling through water at varying rates [90, 115]. Irregular and heavier bones such as the pelvic innominates or femora generally travel only short distances due to their greater density, complex topography, and size, [113, 115] with greater likelihood of becoming obstructed by terrain. More regular, lighter, more cylindrical bones such as ulnae, or small elements like the phalanges and vertebrae have a higher trabecular to cortical bone ratio making them less dense and more buoyant, and therefore able to move much greater distances [57, 90, 115].

As well as obscuring the morphological features of bones, changes to the shape, colour, and texture can make bone resemble other environmental items such as wood, stone, or shell, making differentiation especially challenging [22]. Similarly, human remains may become co-mingled or confused with other debris or faunal bone, further complicating the identification and differentiation processes [22]. As mentioned previously forensic anthropologists are generally not involved in the initial search for human remains and are typically only contacted once suspected bone has been recovered by the police search teams, with identification often conducted using photographs [107, 116]. This can be problematic as without osteological training it is possible that there are many bones that are not being recovered at the scene, particularly if they have been subjected to extended post-mortem interval where taphonomic alterations and fragmentation have occurred, and therefore could be mistaken for other environmental debris. In addition to this, due to the difficult methodologies associated with recovering submerged skeletal remains, once a few bones have been recovered, investigations may not continue as proof of death has been established and the likelihood of finding other bones is slim [106]. This decision can be distressing for the families of the deceased who will be waiting for information regarding the fate of their loved one, but also potentially negative implications for ongoing police investigations, as it can make identifying the individual more difficult, and reduce

opportunities for forensic evidence retrieval. Consequently, there is great call for a simple and cost-effective solution to assist investigators in advanced death investigations, to boost the number of bones found without adding additional health safety risks for the diving teams. Alternative light sources (ALS) may provide the answer.

1.4 – ALS AND BONE FLUORESCENCE

ALS is a common crime scene investigation tool already routinely used at crime scenes and in the laboratory to locate trace evidence such as fingerprints [98], gunshot residue (GSR) [117] and fibres [118], as well as organic body fluids such as semen and blood [119-121], which produce particularly strong results. This is due to the natural fluorophore composition of proteins within these substances, which produce fluorescence when stimulated by selected wavelengths of light [122]. Semen is documented to be most responsive using short wavelengths, approximately 450 nm [119]. Exposure to ALS leads to absorption of light photons which creates molecular excitation within the target substance and rapid emission of longer light wavelengths [120]. These longer wavelengths are fluorescence [123] and can be observed when viewed through a complementary coloured camera filter or eyewear [124]. This naturally enhances the contrast between the subject and its background thus making latent evidence more visible [125]. The technique is non-destructive and produces an immediate response with no lingering effects [126], thus preserving the integrity of the evidence whilst still allowing it to be easily documented [127]. Similarly, the protein-rich collagen component of bone also emits fluorescence when exposed to ALS [128-131], however there has been little research specifically directed at understanding the mechanisms behind this interaction in an osseous context.

The few pilot studies published in the current literature are predominantly feasibility studies, investigating the practical aspects of ALS examination of bone including optimal wavelength and coloured filter combination, and light position when in the laboratory [132, 133]. Miranda et al (2017) examined tooth and bone fragments using an array of coloured filters (red, orange, and yellow) in conjunction with blue light (455 nm) and concluded that an orange filter coupled with blue light was the most successful combination for visualizing bone fluorescence [132]. Green et al (2019) also investigated

orange, yellow, and red coloured filters when using 415 nm, 450 nm, 505 nm and 530 nm ALS wavelengths, and the light source positioned at 30 cm, 100 cm, 300 cm and 500 cm standardised distances from the specimen [133]. They also reported that brightest fluorescence levels were achieved when using blue light and the orange filter, with the light source standardised at 30 cm. However, fluorescence was still observable when the light was positioned at 100 cm [133].

These conclusions are supported by previous MSc research conducted by Maidment, 2017 [134] where 17 porcine bones (*Sus scrofa domesticus*) were photographed terrestrially using 450 nm blue light and five different coloured filters; red (654 nm), yellow (476 nm), orange (576 nm), green (532 nm) and blue (450 nm). The orange filter was the most successful producing strong fluorescence with distinct contrast between the background and the bone. Phase 2 of this MSc research included photographing porcine humeri submerged in 30 L of different types of water: fresh, sea, and canal. In this instance, the yellow filter produced the best results when the bone was photographed in the freshwater context.

Christensen et al (2014) [135] also examined bone in an aquatic context, with a study focused on viability of using ALS to look for bone in a marine environment. In their article they suggested that short wavelengths of light, particularly blue light, operate well underwater due to longer wavelengths such as red and yellow light being absorbed when operating at greater depths [135]. During their investigations they concluded that the yellow filter worked best when visualising bone fluorescence and that differentiation could be made between bone and other common aquatic debris such as shells, wood, sea glass, and seaweed which did not fluoresce when exposed to blue light, and instead appeared black. However, blue light is also greatly scattered in an aquatic context, which is why the sea appears blue [136], consequently may limit how much light can penetrate the water.

A terrestrial field study focused on locating macerated porcine bones, and porcine teeth, in a wooded area in Florida, USA, using blue light (450 nm) and an orange filter was particularly successful. Authors concluded that using ALS in conjunction with traditional CSI line search techniques would significantly increase the number of bones being located [137]. Although it was noted that some vegetation in the terrain also produced

small levels of fluorescence, the search volunteers looking for the bones had no problems differentiating between bone and the deposition environment, despite no previous familiarity with bone identification [137]. However operational parameters, such as the distance between the specimen and the light source, and the projection distance, were not evaluated. However, it was noted that due to interference from ambient light, ALS searches are best carried out at night. In a marine environment, Christensen et al (2014) observed bone fluorescence up to 10-15 feet during night-time dives, but with lesser success in shallower water during the day, when the sunlight was able to penetrate the surface, diluting the fluorescence results [135].

The other major avenue of bone fluorescence research focuses on locating burned bone at fire scenes and how thermal destruction influences the fluorescence levels seen [16-18]. Current studies investigate how varying temperatures and incremental timescales can alter the appearance and structure of bone, making it difficult to recognise within a fire damaged context. As ALS is non-destructive it can be used to help differentiate bone from other debris by examining target items in-situ without disturbing the potentially fragile remains, which have been weakened from the fire exposure. Heating bone drastically alters its molecular structure leading to distinctive colour changes, surface alterations such as charring, delamination and fracturing [138], and other gross morphological modifications such as shrinking, warping, and fragmentation [139]. This can make identification challenging as the morphological landmarks required to identify bone may be obscured, altered, or destroyed [139], rendering it difficult to distinguish from surrounding debris. It is understood that measurement of these characteristics can help investigators estimate the temperature and duration of a fire, as individual components of bone burn away in a predictable sequence [138, 140].

Literature reports that structural changes to bone start to occur once temperatures reach approximately 100°C, with destruction and eventual elimination of the organic component between 400°C and 600°C [141]. This is referred to as calcination and is characterised by greyish-white, bluish, bone colour and extremely brittle, lightweight consistency, as all that remains is the compromised mineral aspect [138]. As collagen comprises approximately 90% of the organic component of bone [101, 139], calcined bone will no longer respond to ALS stimulation as the proteinaceous collagen has been

destroyed [142]. A range of ALS light sources has been investigated in burned bone studies, including green light (532 nm), UV (approximately 350 nm) and blue light, with varying levels of success [131, 143]. Gallant (2013) utilised green light coupled with an orange filter and observed a 'molten lava' type appearance resulting from differential burning, highlighting areas of exposed bone amongst patches of charring [143]. However, as with many other bone fluorescence studies, subjective visual scoring was used to quantify results and it was subsequently determined that these findings may not be discerning enough to aid fire investigators. Gallant (2013) also noted that although UV light did stimulate some fluorescence in the bone samples, it was weaker compared to the YAG green light and bone could not be differentiated from the surrounding fire scene debris [143]. Other studies have discussed how the colour of the emitted fluorescence as well as the intensity could be an indicator of lower fire temperatures, which could also be informative when interpreting archaeological remains [130], but that charring also blocks bone autofluorescence. However, like many of the other bone fluorescence publications, the focus of investigation was on the application of ALS, and although it was suggested that bone collagen was responsible, no quantitative analysis was conducted. UV light has also been used as a screening tool to assess bone preservation when selecting samples for isotope analysis as the organic aspect naturally decomposes over time [92].

Osseous material is vulnerable to underwater degradation due to its porous texture making it susceptible to ion exchange [9, 80]. More specifically, prolonged submersion in a marine environment can lead to salt ions infiltrating the bone through its pores [9], leading to dissolution of the mineral content, and leaching of the organic material [81] as the solubility of collagen is increased [69, 80]. This gives bone an overall bleached appearance [9, 81, 82] sometimes accompanied by chalky deposits on the bone surface [81]. However, due to the difficulties surrounding implementation of aquatic taphonomic studies, there is little understanding regarding the timescales of these changes [9], as conclusions have been drawn from retrospective casework rather than experimentation [81, 83, 84], making it difficult to isolate the active variables. However, results from the MSc study conducted by this author [134] suggest that high salinity may be destructive to bone collagen. Twelve manually defleshed porcine humeri (*Sus scrofa domesticus*) were immersed in 3 water types: sea, fresh and canal, over a 21-day period,

and the collagen content quantified using thermogravimetric analysis at 7-day intervals. The temperature, pH, conductivity, total dissolved solids (TDS) and turbidity of each water type was also analysed. Strong statistically significant relationships between submersion interval and collagen loss in the sea water (R = 0.962, P = 0.019) and canal water (R = 0.925, P = 0.038) were found. There were also statistically significant relationships found between conductivity and collagen loss in the canal water (R = 0.901, P = 0.050) and fresh water (R = 0.999, P = 0. 000) [134]. This suggests that the observed collagen losses may be attributed to increased salinity. However, as the water was collected from natural sources, and the sample size was small, there were too many variables for these determinations to be conclusive. Although not reflected in the results of the MSc pilot study, literature states that high pH levels can accelerate collagen degradation in submerged bone through weakening of the bonds between collagen and hydroxyapatite [95, 144]. Environments with abundant water and oxygen, prompt microbial infiltration of bone collagen , which is expedited by bone damage or fragmentation, providing further access points for microorganisms leading to further degradation of the bone [144].

Conversely, other papers discuss how the protective structural composite of hydroxyapatite and collagen in bone helps to impede degradation [89], particularly from microbial infiltration [101], so that dissolution of the mineral aspect is required before the collagen content can be accessed [145]. Aquatic decomposition is generally slower compared to decomposition on land [93], due to the usually lower water temperatures and anaerobic conditions, particularly at greater depths, which inhibit bacterial growth and scavenger activity [128]. Similarly, although salt water is eventually detrimental to collagen content, decomposition is thought to be further slowed in marine environments compared to fresh water [145] due to the higher salt content also inhibiting microbial activity [60, 145] .Consequently, there are no definitive timescales for survival of bone collagen underwater. Although Swaraldahab and Christensen (2016) did discount fluorescence in buried human remains over 200 years old [146], they acknowledged that fluorescence would be expected in recent remains i.e. those found in timescales consistent with forensic guidelines i.e., up to 100 years old [123], but there has been no comparable research conducted in submerged osseous material.

As a result, our understanding of bone fluorescence in both terrestrial and underwater contexts is very limited, and there is conflicting information regarding optimal methodology. Although current researchers are generally agreed that blue light approximately 450 nm is the most suitable, the correct camera filter is suggested to be either orange or yellow, and only one paper discussing bone fluorescence in an aquatic context has been published to date [135]. Consequently, orange, and yellow filters were used during this PhD thesis, and preliminary pilot tests were completed to help ascertain the most suitable filter for the terrestrial and underwater contexts.

Although collagen is referenced as being the most likely source of bone fluorescence there have been no published attempts at collagen quantification, with only a few studies quantifying the fluorescence output and others relying on descriptive personal interpretation. If fluorescence quantification is conducted, it is usually calculated using generic and easily accessible image analysis software such as Image J or Adobe Photoshop [132, 142, 147, 148], with publications only reporting the numerical results and often lacking supporting photographs to demonstrate their findings [135, 146]. Consequently, this can make it difficult to interpret the success of these research projects as well as truly replicate the methodologies described.

Another significant issue is the use of maceration to prepare bones used for experimentation. Maceration is a long-standing anthropological technique used to clean bone of residual tissue to facilitate easy examination and storage [149]. There is a wide range of techniques documented in literature, for example mechanical cleaning through power washing or exposure to scavenging insects, chemical methods including submersion in acids, bleach, or concentrated enzymes, and heating techniques such as microwaving and boiling [149-151]. The most common method used in anthropology is submerging bones in hot water, often with biological detergent to accelerate the breakdown of tissues [152]. There is no standardisation across the discipline, as methods are usually conducted according to institutional guidelines formed from personal experience [153, 154]. This leads to variation in temperature, detergent volume and brand, and submersion interval, and therefore variation in results [150].

It is well documented that maceration can also be detrimental to bone, as high temperatures are thought to denature collagen, destroy DNA, and destabilise bone

structure [155]. Aggressive chemical maceration from biological detergents, bleaching, and acid exposure can lead to increased bone fragility [151] resulting from corrosion of cortical bone and surface damage such as cracking, fraying, and splintering [156]. In many of the articles previously mentioned examining bone ALS analysis some form of maceration has been used to prepare the bones such as drying, temperature treatments, and warm water maceration [132, 133, 135, 137]. However, details of the methodologies used were not disclosed and the possible influence of this maceration on the final observed bone fluorescence was not addressed. This means the conclusions drawn from these results may not be truly representative which potentially undermines the validity of the currently reported theories and methodologies, as well as any subsequently developed research. More research is required to truly understand the relationship between bone collagen and observed fluorescence, as well as to investigate the impact of intrinsic and extrinsic factors on the crucial collagen component, including the influence of maceration. This PhD research uses a unique methodology of bespoke computer software and TGA to measure both collagen and bone fluorescence to fully explore the proposed collagen-fluorescence relationship, the influence of maceration, and investigate the impact of the deposition context. In doing so, it will enable accurate evaluation of the suitability of ALS for underwater investigation and inform the creation of impactful and informative forensic guidelines to assist search teams in the field. This multifaceted piece of research has implications for a range of circumstances concerning human skeletal remains including crime scenes, shipwrecks, archaeological contexts, and mass disasters by helping to manage expectations, maximise bone recovery, triage findings, and potentially reduce the possibility of misidentifications.

2.0 - AIMS OF RESEARCH

The overall purpose of this PhD project is to investigate the viability of ALS to search for bone in both terrestrial and submerged environments, with the aim of developing operational guidelines for crime scene use. It focuses on unifying current strands of research and introducing a unique combination of bespoke quantification for both collagen and fluorescence to fill the gaps in knowledge surrounding the hypothesised collagen-fluorescence relationship and discuss the impact of the taphonomic environment. To facilitate this, research was divided into two sections. Section A focuses on the preparation of bone for ALS analysis including the possible use of maceration and development of photography protocols. These results informed the experimental design for section B. Section B centres on the application of the ALS methodology in terrestrial and underwater contexts. Experimentation focused on exploring the hypothesised collagen-fluorescence relationship of fresh and macerated porcine bone (*Sus scrofa domesticus*), examining the impact of a saltwater environment on bone collagen and fluorescence, the potential differentiation between bone and other common non-bone environmental items from aquatic and terrestrial contexts, and the fluorescence of demineralised and deproteinised bone. The research questions for each of these sections are outlined below.

Section A: Bone preparation and photography refinement

Question 1: Is maceration a suitable preparation technique for bone intended for laboratory ALS analysis? Examining the effect of three common maceration techniques: hot water maceration (approx. 80°C), warm water with biological washing powder (50°C) and enzymatic maceration using lipase and protease (55°C), on bone collagen and fluorescence levels.

Question 2: Does the intensity of bone fluorescence in porcine ribs vary between the vertebral, diaphysis, and sternal regions of the bone, when photographed in a terrestrial context using blue light (450 nm) and an orange camera filter?

Question 3: What material provides the most effective contrast during osteological fluorescence photography between play sand, polystyrene sheet, polystyrene spheres, white card (200gsm), black card (220gsm), clear plastic box, and black plastic box, when photographing porcine bone in a terrestrial context, using blue light (450 nm) and orange camera filter.

Question 4: What is the optimal exposure time, f-stop and ISO level required to visualise bone fluorescence when photographing porcine bone (*Sus scrofa domesticus*) in a terrestrial setting using blue light (approximately 450 nm) and orange and yellow filters?

Question 5: What is the optimal distance from the sample to the light source when photographing porcine bone (*Sus scrofa domesticus*) using the Crime-lite 2 and the FoxFury Hammerhead devices, in combination with orange and yellow filters in terrestrial and tap water contexts?

Section B: The application of ALS to detect bone

Question 1: Is there a statistical difference in observed bone fluorescence of fresh porcine bone (*Sus scrofa domesticus*) between terrestrial and tap water contexts? A comparison of terrestrial and underwater fluorescence levels of 30 macerated porcine ribs (*Sus scrofa domesticus*). photographed using blue light (approximately 450 nm) and orange and yellow filters.

Question 2: Is there a correlation between the amount of collagen content in bone and the level of bone fluorescence seen when photographed using blue light (approximately 450 nm) and orange and yellow filters? A statistical comparison of fluorescence and collagen levels of 54 macerated porcine ribs (*Sus scrofa domesticus*).

Question 3a: Is it possible to distinguish between porcine bone (*Sus scrofa domesticus*) and other 27 non-bone control items when photographed using blue light

(approximately 450 nm) and orange and yellow filters, in terrestrial and tap water contexts?

Question 3b: To what extent does pure porcine collagen powder fluoresce when exposed to ALS? Quantifying the fluorescence levels of pure porcine collagen powder photographed using blue light (approximately 450 nm) and orange and yellow filters, in terrestrial and tap water contexts

Question 3c: Will demineralised and deproteinised porcine bone (*Sus scrofa domesticus*) fluoresce when photographed using blue light (approximately 450 nm) and orange and yellow filters in terrestrial and tap water contexts?

Question 4: Is high water salinity destructive to bone collagen and subsequent fluorescence over time? Comparison of changes in bone fluorescence and collagen content of 54 macerated porcine ribs (*Sus scrofa domesticus*) submerged in tap water and simulated sea water, at 2-month intervals over a 6-month period, photographed using blue light (approximately 450 nm) and orange and yellow filters.

Based on these research questions eight hypotheses were formulated:

1. Hypothesis: Alternative light sources can be used to preliminarily identify bone in terrestrial and underwater environments using blue light (450-470 nm) when photographed with an orange camera filter

   Null hypothesis: Alternative light sources cannot be used to preliminarily identify bone in terrestrial and underwater environments using blue light (450-470 nm) when photographed with an orange camera filter

2. Hypothesis: Porcine bone (*Sus scrofa domesticus*) produces fluorescence in both terrestrial and underwater environments when exposed to blue light (450-470 nm) and viewed with a coloured filter.

   Null hypothesis: Porcine bone (*Sus scrofa domesticus*) does not produce fluorescence in terrestrial and underwater environments when exposed to blue light

(450-470 nm) and viewed with a coloured filter.

3. Hypothesis: There is a correlation between the amount of bone collagen in porcine bone (*Sus scrofa domesticus*) and the levels of fluorescence seen when exposed to blue light (450-470 nm) and photographed with an orange camera filter.

   Null hypothesis: There is no correlation between the amount of bone collagen in porcine bone (*Sus scrofa domesticus*) and the levels of fluorescence seen when exposed to blue light (450-470 nm) and photographed with an orange camera filter.

4. Hypothesis: When using blue light (450-470 nm) and a camera fitted with an orange or yellow camera filter it is possible to differentiate between bone and other environmental items within terrestrial and underwater contexts

   Null hypothesis: When using blue light (450-470 nm) and a camera fitted with an orange or yellow camera filter it is not possible to differentiate between bone and other environmental items within terrestrial and underwater contexts.

5. Hypothesis: Environmental items produce different levels of fluorescence compared to porcine bone (*Sus scrofa domesticus*) when exposed to blue light (450-470 nm) and photographed with an orange camera filter.

   Null hypothesis: Environmental items do not produce different levels of fluorescence compared to porcine bone (*Sus scrofa domesticus*) when exposed to blue light (450-470 nm) and photographed with an orange camera filter.

6. Hypothesis: Exposure times need to be adjusted when photographing macerated porcine bone compared to fresh porcine bone when exposed to blue light (450-470 nm) and photographed with an orange camera filter.

   Null hypothesis: Exposure times do not need to be adjusted when photographing macerated porcine bone compared to fresh porcine bone when exposed to blue light

(450-470 nm) and photographed with an orange camera filter.

7. Hypothesis: Macerated bone produces higher fluorescence levels compared to fresh bone due to removal of residual tissue when exposed to blue light (450-470 nm) and photographed with an orange camera filter.

   Null hypothesis: Macerated bone does not produce higher fluorescence levels compared to fresh bone when removed of residual tissue and exposed to blue light (450-470 nm) and photographed with an orange camera filter.

8. Hypothesis: High water salinity is not destructive to porcine bone collagen when submerged for 6 months, which leads to a reduction in observed fluorescence levels when using blue light (450 -470 nm) and photographed with an orange camera filter.

   Null hypothesis: High water salinity is destructive to porcine bone collagen when submerged for 6 months, which leads to a reduction in observed fluorescence levels when using blue light (450 -470 nm) and photographed with an orange camera filter.

3.0 – ORIGINAL CONTRIBUTION TO RESEARCH AND FORENSIC SCIENCE

3.1 – CONTRIBUTION TO RESEARCH

This PhD thesis introduces a novel application for forensic ALS technology, by focusing on the use of fluorescence to detect bone underwater. This includes the implementation of a unique and innovative research methodology comprised of bespoke C++ fluorescence quantification software; the Osteo-Fluorescence calculator (OFC), combined with Thermogravimetric analysis (TGA) for collagen quantification. This holistic approach has not previously been performed in literature, although some papers have explored the potential of bone fluorescence, most publications focus on terrestrial studies, burned bone, and/or microscopic analysis of bone sections, to calculate the preservation status and subsequent suitability for downstream analyses such as DNA extraction or stable isotope analysis.

Quantification of fluorescence intensity is not often conducted in literature as accurately measuring fluorescence emissions can be complex. The overall conversion of light is known as luminescence, and fluorescence refers to the emitted light that recedes quickly after initial excitation [157]. These types of emission wavelengths have a short decay time and are superseded by long-decay phosphorescence, which persists for slightly longer post stimulation [157, 158]. The difference in decay time is less than second, therefore is it not usually possible to differentiate between the two types of emissions easily [158]. Consequently, when fluorescence is measured, it focuses on the presence or absence of light emissions, spectral shift is emissions, or the overall intensity, which are measured using default features of commercially available software [148, 158].

Only a few papers in literature have explored the use of ALS in terrestrial and underwater contexts, and there has never been a comparison of terrestrial and submerged fluorescence. Therefore, it is currently unclear how the deposition context may influence bone fluorescence visualisation, and whether adaptations in methodology are required to ensure fluorescence production. There is also no consistency regarding the coloured filter and photographic parameters for documenting

bone fluorescence, even across similar deposition contexts, and other than temporal degradation of collagen, there has been no research into the effects of the taphonomic environment on bone collagen and emitted fluorescence. Without this foundational knowledge it is difficult to interpret whether ALS is a feasible tool for osteological crime scene searches, and it makes evaluating the results of current publications more challenging. Therefore, this PhD includes original methodology and experimentation beginning aimed at understanding the fundamental relationship between bone collagen and autofluorescence, by including a section of research dedicated to examining photographic protocols in both terrestrial and underwater contexts.

Additional experimentation includes examination of prolonged submersion of porcine bone in simulated seawater and tap water bone (*Sus scrofa domesticus*), to investigate how the aquatic taphonomic environment may influence bone collagen and fluorescence. This data helps to inform the development of methodological recommendations for use of ALS detection of bone in the field. The inclusion of bone and non-bone controls supported interpretations of the observed fluorescence results, in both terrestrial and submerged contexts, as well as evaluating potential discrimination between bone from other common materials found at excavations and crime scene investigations, research that has not been conducted previously.

Finally, many studies published in literature utilise macerated bone, but no research has been conducted into how maceration may have influenced the observed bone fluorescence, and subsequent interpretations regarding the significance of published results. As a result, a pilot study was conducted to investigate the impact of maceration of bone collagen and fluorescence.

3.2 – CONTRIBUTION TO FORENSIC SCIENCE

Providing a deeper understanding of the mechanisms behind bone fluorescence production and subsequent fluorescence emissions, ultimately provides greater insight into how this technique could be implemented in real world forensic scenarios. This technique offers the possibility of repurposing a known methodology for non-destructive, non-contact, preliminary identification of bone at the crime scene. It is proposed that this would be beneficial to crime scene investigators, who usually do not have any osteological training, particularly when examining bone that has been exposed to the taphonomic environment for extended timescales and therefore may have lost the skeletal landmarks that would normally facilitate identification.

Successful stimulation of bone fluorescence is thought to increase the visibility of bone, which would therefore enable simple and fast triage of potential osseous material. This capability would benefit forensic science by assisting investigators to maximise the number of bones collected from the scene, subsequently increasing the volume of potential forensic evidence as well as the number of bones to create a fuller osteological profile. Most significantly, this data would not only assist with the identification of the deceased, but also contribute to the reconstruction of events surrounding the death and enable the return of more of a person to the bereaved family.

Specifically, the successful application of ALS in aquatic contexts, would provide investigators with a valuable identification tool to support the diminished toolkit currently available, as most search strategies, and professional guidance, are focused on locating whole cadavers or rescuing living people. There are currently no search techniques specifically tailored to extended post-mortem intervals (PMI) and locating skeletal remains. Bones are often found in isolation or partially articulated sections, with smaller bones transported away from the primary assemblage by tides, currents, and scavengers. Traditional diver implemented searches can be painstaking and time-consuming, with divers operating in potential treacherous conditions with low visibility.

By investigating the collagen-fluorescence relationship, the taphonomic alteration to bone, and the photography parameters for bone fluorescence, this PhD aimed to make a direct contribution to the understanding of aquatic and terrestrial bone fluorescence, and the development of guidance for the use of ALS for bone recovery in the field. Bone

fluorescence offers the capability to perform broad searches; to help find more bones that previously may not have been recovered, and consequently speed up searches, which presents the opportunity to save money, time, and resources. The OFC has the potential to provide a unique, portable fluorescence quantification tool, to aid investigators decision-making at the scene, and triage items for anthropological analysis.

As well as forensic science applications, this type of non-destructive technique could be beneficial for locating bone at mass disasters sites and during archaeological excavations, including being able to distinguish bone from other debris such as stone, ceramic, and foliage.

4.0 - THESIS STRUCTURE

Chapters 5.0 through 10.0 are an evaluation of the current literature, relevant to the use of ALS technology to search for skeletal remains, including current search strategies employed to search for missing individuals in terrestrial environments, including discussion of some of the key published guidelines presently available to police constabularies. The chapter then moves on to discuss the common search techniques used to locate submerged human remains, predominantly whole cadavers, and highlighting the limited tactics directed at skeletal remains. The consequent chapters focus on crime scene documentation and photography, and how ALS is currently used by investigators during forensic examination. Further chapters describe the composition of mammalian bone, including collagen content and the possible sources of bone fluorescence, followed by how bone can be altered by the taphonomic environment. Critique of relevant publications is included throughout, to systematically discuss how ALS could be applied to osseous material, and the subsequent gaps in current knowledge this PhD endeavoured to investigate. More specifically, chapter 11.0 provides an outline of the technical rationale alongside explanation of the key quantification components developed and used during this PhD project: the Osteo-Fluorescence Calculator (OFC), and thermogravimetric analysis (TGA).

Research questions were addressed in two sections; section A, consisting of five questions, focused on maceration preparation of porcine bone and development of a core methodology, and section B, composed of four research questions, examined the collagen-fluorescence relationship and the use of bone fluorescence in forensic examination. Each research question is addressed separately, including method, results, discussion, and summary and conclusions, with a brief summary at the end of the section. These points of discussion were then used to inform the final thesis discussion, and subsequent conclusions. The final thesis discussion evaluates how the results of this PhD study answer the proposed hypotheses and the subsequent implications for forensic search strategies for skeletal remains.

5.0 – AQUATIC SEARCH STRATEGIES FOR HUMAN REMAINS

Searching for missing people and human remains is a complex and multidisciplinary endeavour, requiring collation of data from a variety of different sources to build a picture of an individual's last movements [159]. Terrestrial search strategies are well established, with human remains detection dogs, aerial searches, infrared imaging, and crime scene tactics such as line, spiral, or grid routinely employed [160]. Additional data from CCTV and eyewitnesses as well as digital resources including social media, GPS, banking transactions, and mobile phone data can support investigations by reconstructing a timeline of events [14]. Surface deposited and buried human remains have been the subject of extensive research, encompassing archaeological and forensic topics such as detecting clandestine and mass graves [19], investigating the influence of soil composition and scavengers on decomposition rates [84, 161, 162], and assessing the effectiveness of different geophysical techniques [163, 164], all of which can be used to coordinate recovery efforts [164]. However, there is a deficit in knowledge regarding submerged human remains. Not only does water physically conceal a body , but due to its highly dynamic nature and variability [23], human remains submerged in water can be transported great distances and subjected to extreme taphonomic alteration due to currents, waters, and aquatic scavenging [38, 51, 65]. This ever-changing environment, coupled with complex decomposition processes, severely limits the timescales in which searches can be conducted successfully [56].

Current strategies for searching aquatic contexts are limited [67], and are usually adapted from terrestrial methodologies, primarily focus on locating whole cadavers or living missing persons, facilitated by the large target size producing sufficient contrast with the environment [159]. Strategies are often based on professional experience, force specific training, and general guidance from publications such as: *Guidance on the Management, Recording and Investigation of Missing Persons* (2005) [31], *Practice Advice on Search Management and Procedures* (2006) [32] and the *Grampian Police missing persons guidelines* (2007) [33]. However, as mentioned in chapter 1.0, these publications focus predominantly on living people and feature extensive chapters on the psychology of missing persons, efficient search management, and correct reporting

procedure. These publications are marketed as practice advice for current officers, and the Grampian guidelines is the only one of the three publications to have data directly drawn from research, which included the retrospective analysis of 3,000 missing person cases [33].

According to the *Practice Advice on Search Management and Procedures* (2006), aquatic searches of inland waterways such as rivers, begins with a visual search to identify bodies that may be floating, entangled in nearby vegetation, caught on obstructions, or washed ashore [32]. The dimensions of the waterway will then be used to dictate whether searches are carried out by boat, on foot, or both, taking into account the topography of the surrounding foliage and landscape [38]. Determinations of when and where the person entered the water, and the flow rate of currents and tides will be calculated to estimate the speed of the water and subsequent movements of the body [37, 38]. This data will then enable investigators to establish the likely limits of the search area and put in place physical or visual barriers. Visual barriers consist of search personnel positioned at specified observation points along the water's edge to monitor the water as it passes through, consequently raising the alarm if the body reaches that point [165]. Physical barriers can be placed directly in the water, to block further movement of the body if it reaches that point [32]. Types of physical barriers can include netting, inflatable tubing, or human barrier of personnel stationed at intervals across the width of the water [91]. The appropriate type of barrier will be selected based on the composition of the waterway such as depth, width, and flow rate, as well the expertise of the personnel in attendance, and the dimensions of the subject being searched for [91]. Individuals deployed directly into the water to conduct searches require extensive health and safety training and expertise in aquatic searches, consequently police diving units are required [32, 79].

5.1 – DIVING TEAMS

Specialist police diver teams are the frontline of aquatic searches [23, 74, 82], conducting fingertip searches to search for evidence such as weapons, mobile phones, and victim's belongings, as well as human remains [91, 166]. As with terrestrial crime scene investigation, there are a number of different search patterns that can be implemented, depending on the dimensions and orientation of the target body of water [21, 167].

Common methodologies include ‘line search’ where multiple boats or personnel are positioned in a line across the width of the water and move in formation up the waterway, very similar to the terrestrial line search [21]. ‘Creeping line ahead search’ is used when resources are limited, and an individual boat or diver conducts a search in continuous parallel lines, much like the approach used in a terrestrial grid search [168]. Adaptations of the ‘Creeping line ahead’ strategy are the ‘sweep’; (fig. 1a) where a diver moves in either a decreasing or increasing arcing motion whilst tethered to a tender on a shoreline, and the ‘pier-walk or parallel search technique’ (fig. 1b); where the diver swims in a more uniform sweeping motion and can be directed and followed by the tender who is located on an adjacent surface such as a pier [56]. The ‘circular search’ is comparable to the spiral terrestrial search, and is used in more open relatively shallow water, where there is no shoreline for the tender to be located [168]. Instead, the tender is situated in a boat and the diver searches in a circular motion emanating from the boat, but changes direction after each completed circle to avoid disorientation and repeated searches of the same area [168]. However, the most common technique conducted by divers is a line search which is commonly deployed in rivers and canals. Here a line is extended from one side of a river to another and the diver searches along this line [168]. In addition to searching an entire scene, ‘snag position search’ can be employed to investigate specific areas of interest where a body may have been obstructed or trapped [56, 168].

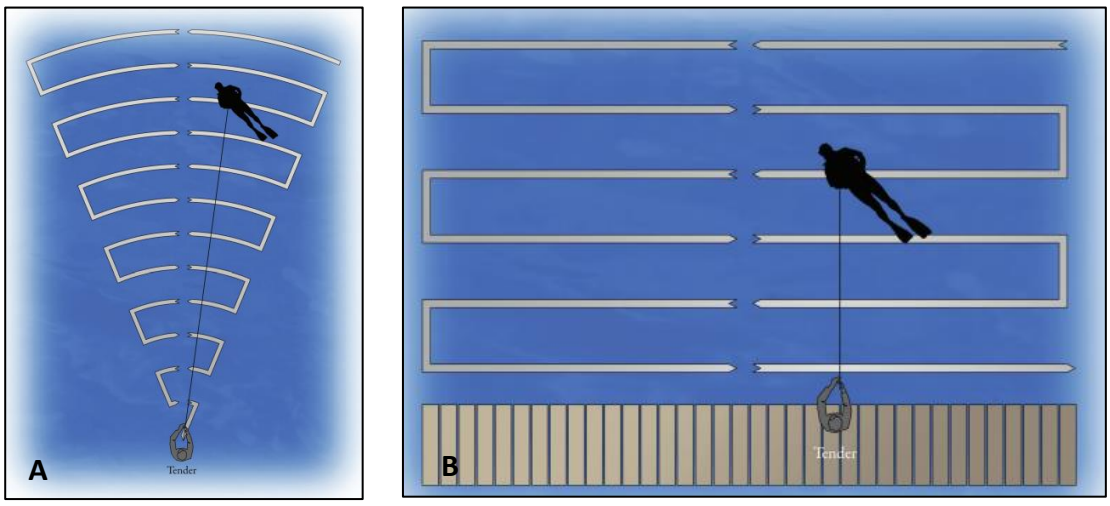

Figure 1: Diagrams of two of the most common underwater search techniques employed by forensic diving teams A) Sweep, B) Pier-walk or parallel search technique [56]

However, water conditions can be treacherous, with strong currents, complex topography, and varying water clarity limiting visibility and movement [82, 91]. Consequently, divers are usually restricted to short intervals of submersion, up to 20-30 mins, and limited depths to ensure their safety [56]. Implementation of additional search techniques enables searches to be carried out for longer, at greater depths, and across a variety of terrains, whilst reducing the need for extensive manual investigation, or draining bodies of water which can be costly and have a detrimental impact on the environment [74, 82].

5.2 – DETECTION DOGS

Detection dogs are used to detect the chemical emissions from a body during decomposition, known as volatile organic compounds (VOCs) [169]. They are trained using decomposing human and/or animal tissue, hair, or clothing, [85] and either bark, sit, or point to indicate a positive finding at a crime scene [169]. Normally used in terrestrial body recovery, detection dogs can also be positioned on boats or walked along the edges of bodies of water to detect the presence of decomposition VOCs [159]. Issues arise when the water is fast flowing or less favourable weather conditions such as high winds and heavy rain, which disperse scents and wash away decomposition products [85]. Similarly, dense vegetation, compacted and deep burial, tight body coverings, and extended PMI, inhibit VOC emissions, reducing the concentration of VOC compounds for the dogs to detect [170]. Furthermore, conflicting decomposition scents from local wildlife or stagnating water can make isolating the target scent much more difficult and may lead to misidentifications or false positives [86].

Typically, human remains dogs are not as effective at locating skeletal remains as whole bodies [171, 172]. Once decomposition has reached the skeletal stage, there is a drastic reduction in soft tissue and decomposition products, due to advanced putrefaction, consumption by insects and scavengers, and environmental destruction [171]. Consequently, decomposition is radically slowed and there is fundamental reduction in VOC emissions, which can fall below the limit of detection for human remains dogs and cannot compete with other scents within the search context [86, 169].

5.3 – REMOTE DETECTION METHODS

UAV (unmanned aerial vehicles) or drones [173], can be used to remotely search for human remains in aquatic contexts by providing a much higher vantage point to document the scene [174]. Drones require limited resources and therefore can be deployed quickly, providing preliminary documentation of a scene even before full deployment of diving teams [79, 174]. When coupled with a camera, drones can search the scene prior to diving teams entering the water [175], providing investigators with aerial images of the terrain, potential access routes, and any likely hazards such as a debris, crevices, or sharp rocks, that would pose a risk to recovery teams and evidence collection [56]. These images enable fuller reconstruction of the crime scene and preparation of search strategies [176], but may also provide valuable detail for interpretating any trauma evidence found on the recovered remains, and the likely path the body took whilst moving through the water [79].

Aerial images can provide much wider documentation of the overall scene [177], and alternative perspective of dense vegetation such as reeds, grass, and shrubland where a body may be embedded or obscured which may not be viewable from the ground [79, 159]. Similarly, drones provide a convenient method of searching waterways that may not be accessible by boat or foot [177], and live streaming/recording enables continuous monitoring of changeable search conditions promoting proactive decision making [174]. If the water is relatively clear, drone photography can be used to remotely document human remains in situ [178], which is usually not possible with manual search methods with documentation and preservation of evidence only beginning once the body is retrieved [179].

Limitations arise when needing to fly drones in restricted airspaces, requiring government permissions or forgoing the flight [180]. Successful flights would also be dependent on optimal weather conditions and the specifications of the individual drone, i.e., strong winds and rain would prevent the drone from taking off or would destabilise the drone in the air [176]. The power, velocity, size, and weight of the drone vary across models and would need to be taken into consideration before deployment [181]. For example, if the potential search area is very large, a more powerful drone may be required to maximise flight duration, whereas a more compact scene such as a canal

with houses on each side could require a smaller unit to minimise sound and prevent damage to any nearby structures. However, drone selection would also have financial implications, with more sophisticated models generally generating higher upfront costs and longer flight times requiring extended labour expenses [168]. Reflections from the water can distort images or block photography altogether, and tree coverage, or buildings in the search area can obstruct the drones' flight path and impede imaging attempts [174, 182]. Despite being relatively simple to deploy, drones still require a trained expert to execute a safe and effective search, as well as knowledge and experience to identify items of interest, especially when interpreting high altitude images or associated technologies such as infrared or hyperspectral outputs [83].

In surface depositions, residual heat from life will quickly dissipate as algor mortis (cooling of the body) proceeds, at approximately 1°C per hour, until body temperature reaches equilibrium with the ambient temperature [45]. This process is expedited by external factors such as wind and rain, and diurnal fluctuations [128]. However, as decomposition advances through the fresh and bloat stages, reaching active decay, there will be a sharp increase in cadaveric temperature due to fervent maggot activity [183] and decomposition of surrounding vegetation caused by leaching decomposition products [79]. This can be identified using thermal imaging and hence facilitate retrieval of the body [184, 185]. Hyperspectral imaging is a repurposed agricultural tool which identifies changes in plant vitality by analysing the reflected light from photosynthetic compounds (chlorophyll) and leaf structure and is predominantly used for remote detection of clandestine burials [186].

However, thermal, and hyperspectral imaging are less effective when searching for bodies in aquatic contexts [79]. Imaging would only be restricted to the surface of the water; therefore, fully submerged bodies would not be detected [79]. In floating bodies, low water temperatures accelerate the post-mortem cooling of the body [55, 160], and waves and currents wash away maggot activity [187, 188]. The lower temperatures slow decomposition, and the physical barrier of the water, alongside reduced oxygen levels, impedes bacterial proliferation and insect colonisation [50]. Therefore, submerged bodies do not usually exhibit the increased body temperature usually observed in surface depositions, and any temperature changes that may occur can be obscured by

tight clothing or wrappings [50]. Consequently, this methodology is not to be beneficial when searching for submerged skeletal remains, due to the likely deeper submersion depths, and the advanced stage of decomposition.

An articulated skeleton or differentially decomposed body may be easier to identify from drone imagery, particularly in shallow or still water [178]. However, as PMI increases, the chances of fragmentation, dispersal and taphonomic modification also increases, [90] and dry skeletal remains will eventually reach temperature equilibrium with the deposition environment. It is documented that finding whole skeletal assemblages in aquatic contexts is uncommon, and that it is more likely that individual skeletal elements will be found incidentally once they wash ashore [53]. Consequently, drone imaging would struggle to capture images of individual bones in water or in surface depositions, as a result of their small size and taphonomic alterations, which make them difficult to distinguish from the environment [189].

Remote operate vehicles (ROVs) can be used to search for human remains underwater [88, 93] Sometimes referred to as underwater drones or hydrographic drones in literature, ROVs are more frequently used to conduct geological survey of the seabed to monitor ecological habitats and environmental changes [190]. They are also used to maintain and repair offshore infrastructure and instruments used in the gas and oil industries [191]. In archaeological contexts ROVs equipped with GPS, side-scan sonar, and other imaging equipment, can document submerged archaeological sites and retrieve artefacts, such as at the Comacchio Lagoon in Italy [192] and famously the Titanic wreckage [80].

ROVs enable investigation of waterways considered too hazardous for dive units such as those with limited visibility or those at great depths which would also require sustained submersion [80]. In forensic contexts, ROVs can be used to document and retrieve evidence items such as weapons, and document human remains in-situ [93]. During standard underwater investigations occasionally some evidence items are not retrieved due to hazardous water conditions, therefore ROVs offer the possibility of at least documenting the items, if not recovering them, thus helping to maximise evidential contributions to an investigation [82]. For example, in Indonesia, ROVs were successfully used to locate bodies and motorcycles that had been aboard an overloaded vessel and

sank to a depth of 1,500 feet (450 m) in June 2018 [193]. Although underwater ROVs would not be able to directly recover bodies, accurate identification of human remains in-situ contributes to the reconstruction of events and preparation of search strategies [93]. In theory it may be possible for ROVs to recover individual skeletal elements, but there would be a risk of causing additional trauma or breakage as the bones would be additionally fragile from taphonomic degradation. Moreover, the successful deployment of underwater ROVs will be dependent on the composition of the sea, lake, or riverbed, as softer or loose sediment may lead to reduced traction, embedding, and the disturbance of particles reducing visibility or covering nearby evidence items. A cluttered or rocky topography would be obstructive to the ROVs movements and hinder searches [191].

The use of drones at crime scenes is a developing methodology, and as such currently lacks established protocols and validation [177]. Moreover, the image quality produced from ROVs is often not of a high enough standard for detailed scientific analysis [190]. Similarly, not all constabularies have access to drones or ROVs as they can be expensive to procure and maintain and would require a trained operator [194]. Consequently, additional experts are often contracted to assist with investigations, but geophysical techniques have a more established precedent in aquatic crime scene searches [88]. Geophysical techniques are usually non-invasive and rely on the transmission and detection of sound waves or electromagnetic energy through a substrate [67]. Voids or anomalies within reflected transmission signals indicate the presence of an object, which depending on size, shape, and expert interpretation, can suggest the presence of a body [67]. This encourages targeted investigations by diving teams saving time and reducing the duration needed in the water [81]. Consequently, a whole body is much easier to detect than body parts or skeletal remains due to the larger size producing better contrast with the surrounding environment [67].

5.4 – GEOPHYSICAL TECHNIQUES

Side-scan sonar is one of the most popular search techniques used in forensic investigations to locate human remains, and utilises sound propagation to highlight objects of interest [88]. Pulses of sound at a known frequency are emitted from a transmitter (referred to as a towfish) immersed in the water, suspended from a boat, at

a right angle to the boats path [76]. When the projected sound waves reach an object, the sound waves are reflected and subsequently detected by a hydrophone receiver, as shown in figure 2 [195]. The intensity of these returning frequencies is digitally interpreted by an onboard computer and converted into a visual output [82]. The resolution of the final image is determined by the frequency of the emitted (and therefore reflected) soundwaves. Shorter frequencies produce greater resolution and increased clarity, enabling clearer distinction between objects in close vicinity [82, 195]. However longer frequencies enable greater penetration and therefore a longer field of view, with less 'noise' evident in the final output [76]. Consequently, emission frequency is selected based on the topography of the aquatic landscape but is best suited to bodies of water with a more varied geological profile so that the sound waves can be reflected [195].

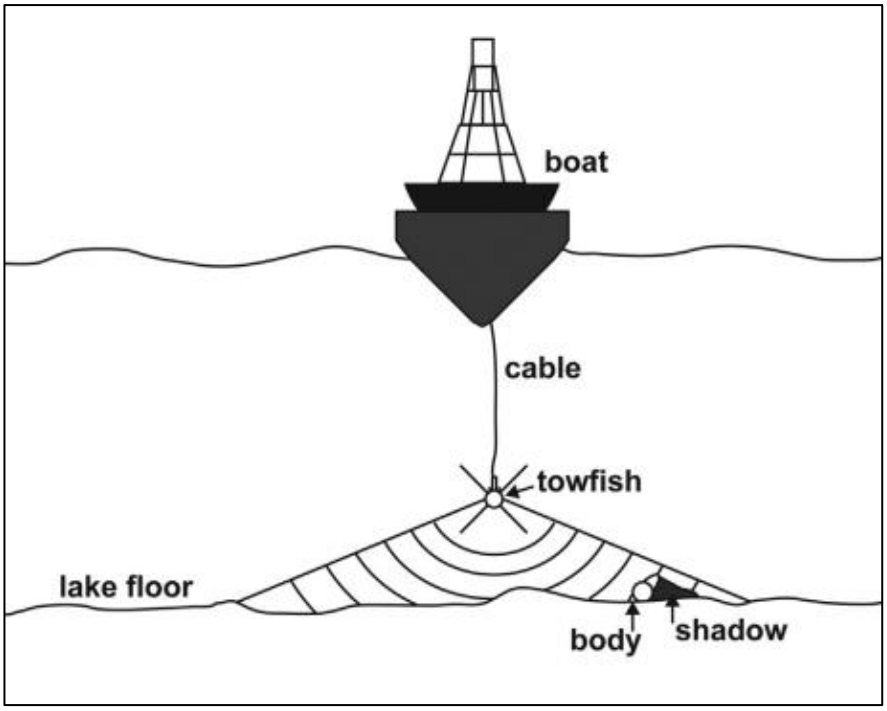

Figure 2: Illustration demonstrating how side scan sonar is deployed when searching aquatic contexts for human remains [82]

Side-scan sonar is not affected by the composition of the water and is a valuable tool in water with low visibility or when searching for human remains at night [82]. It is not influenced by salinity and can be used in many water types including fresh, salt, and

brackish water [88]. However, it is not as suited to shallow or deep water, due to the need to deploy the sensor beneath the boat, and the relatively short penetration distance of sound waves [82, 88]. Furthermore, softer sediments can absorb the sound waves rather than reflecting them [83]. These issues are magnified when attempting to image a crowded aquatic landscape where there are multiple, overlapping, or similar sized objects [88]. Consequently side-scan sonar is not suited for skeletal recovery, as individual bones would most likely be too small to discern from the background on the final scans. Larger skeletal elements such as the skull and os coxae may be easier to locate but smaller bones such as phalanges or vertebrae would most likely still be missed, leading to incomplete recovery, and curtailed osteological evaluation. However, handheld sonar devices give divers more autonomy when in the water [96], enabling targeted examination of areas of interest or individual items, even in low visibility [82]. This is particularly advantageous in stretches of water where a boat is unable to manoeuvre and therefore cannot conduct a full scan [56].

Ground penetrating radar (GPR) is another technique routinely used in archaeological, forensic, and geological contexts to examine the composition of soil stratigraphy, and to locate buried evidence and graves [82, 159, 196]. When used in water it is often referred to as water penetrating radar (WPR) although it is the same technology [197]. WPR works in a similar way to sonar but uses an antenna to transmit short pulses of electromagnetic waves through the water which are then refracted, reflected, and scattered upon interaction with an object, leading to changes in velocity [83]. These reflected signals are subsequently detected by a receiver and converted into a cross-sectional image known as a reflection profile [78]. The changes in velocity are a result of differences in energy exchange when the electromagnetic waves pass through contrasting materials, for example when passing through soil compared to a decomposing body [82]. These differences in composition can then be seen on the reflection profile and consequently highlight potential search sites.

Some advantages of WPR are that it not only detects objects within the water, but it can penetrate the bottom surface of the body of water, revealing buried objects [81, 88], which could possibly highlight human remains buried by sediment and silt. WPR can also penetrate vegetation, which would be obstructive to other techniques such as side-scan

sonar, divers, or ROVs [82]. Ruffell (2006) describes a forensic case of a speedboat colliding with a jet ski, leading to severing of the jet ski rider's leg and subsequent sinking of the vessel. WPR was successfully used to locate the jet ski and the severed limb allowing the reconstruction of events and prosecution of the speedboat owner [77].

However, WPR is not effective in water with high salinity and brackish environments, due to high conductivity and the presence of suspended particulates limiting the distance that the electromagnetic waves can travel and causing backscatter of light [83, 198]. These types of environments can also create strong reverberations known as 'ringing' which mask the true electromagnetic signals and impedes interpretation [77, 197]. Transmission of the electromagnetic waves can also be disrupted by strong currents and waves as well as high winds moving the antennas or boat or snagging the antenna lines [83]. Furthermore, any metal presence in the structure of the boat would also cause inference with the WPR signals, therefore rubber dinghies are usually used to conduct WPR investigations [197]. Consequently, it is unlikely that individual skeletal elements would produce a signal strong enough to be differentiated from any background readings, particularly in a highly populated or complex underwater context.

All the methods discussed in this chapter only detect the presence of an anomaly or object, and do not necessarily provide detail about the nature of that item. Therefore, repeated dives and scans of the same area may be required if multiple objects are detected, as they will each require manual investigation by accompanying dive teams. This fact is especially true for sonar and radar methodologies where the primary output is a digitised graphical representation of the overall scene, and when the background environment is complex or crowded [82, 88].

Figures 3-5 below are examples of side scan sonar outputs from two American case studies, as reported by Schultz et al (2013) [82]. Figure 3 shows a submerged body found in Lake Underhill, Orlando, Florida, where investigators were dispatched shortly after a boating accident. The lake had a mean depth of 4.27 m with a maximum depth of 8.84 m and the scans were carried out at night when the diving teams were unable to enter the water. The body was successfully detected using a frequency of 1800 kHz and is clearly identifiable as a human body in the final image. This search was facilitated by the bottom of the lake being predominantly flat, comprised of silt and sand, and free from

obstructions. In contrast, figures 4 and 5 are images of Lake Lawne, Orlando, Florida, located approximately 7.5 miles (direct) from Lake Underhill [199]. Lake Lawne is shallow with an average depth of 1.83 m and a maximum depth of 7.32 m, but the depth rapidly fluctuates throughout the day. In this case, an individual went missing after falling from a jet ski. Challenges were encountered due to the undulating lakebed, punctuated with numerous holes and crevices, meaning continual adjustment to towfish to accommodate the varying depths, whilst ensuring sufficient clearance. These depth adjustments led to corresponding adjustments made to the image to ensure accurate visualisation [82]. In this case the body was partially lying within a depression on the lake floor, and therefore was not immediately identifiable due to complex shadows obscuring the body shape. Additional sonar scans at a higher resolution were conducted to reveal more of the body and consequently help direct divers to the site. However, interpretation of the image was still difficult due to the more complex topography of the lakebed, which can be seen in figure 3. These difficulties highlight some of the limitations associated with this technique and therefore why it may not be sensitive enough to search for skeletal remains, particularly dispersed, isolated skeletal elements.

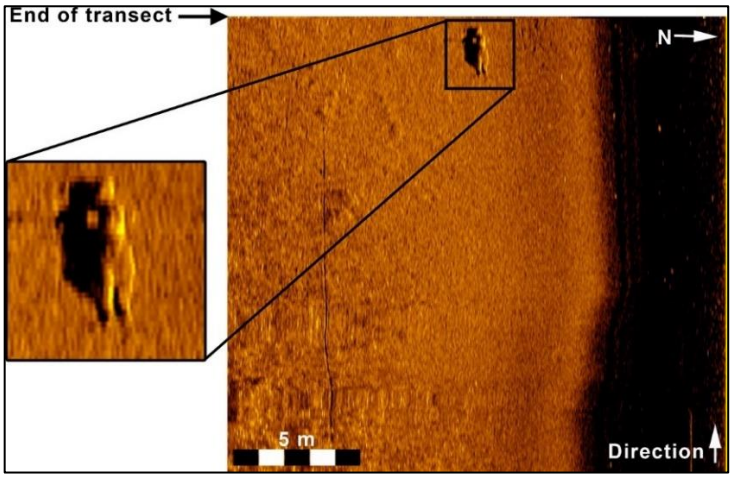

Figure 3: Side scan sonar output successfully identifying a submerged body in Lake Underhill, Orlando, Florida [82]

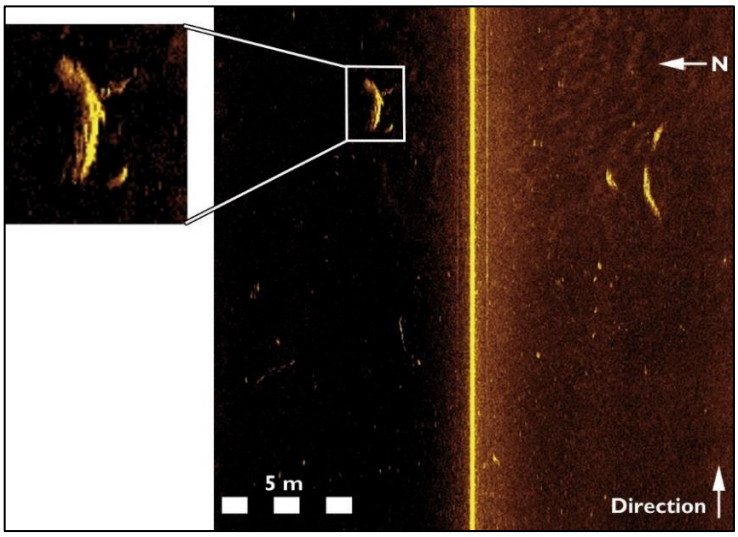

Figure 4: Side scan sonar output highlighting the body in Lake Lawne, Orlando, Florida, partially obscured by placement within a depression on the lake floor.

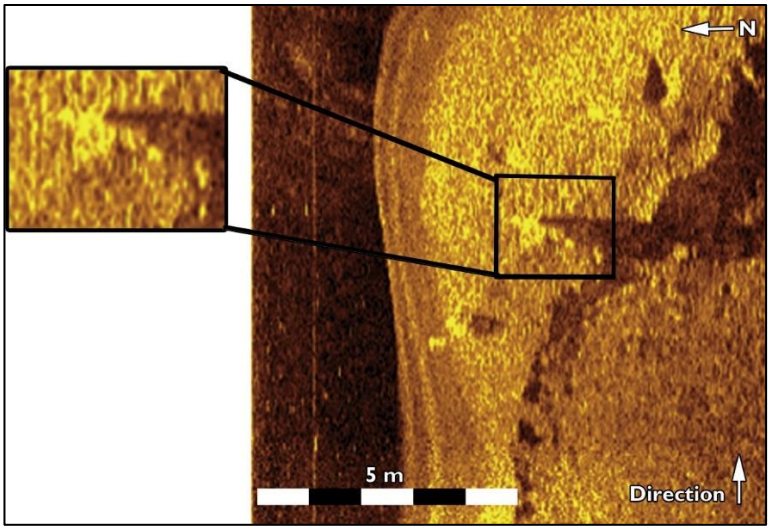

Figure 5: Enhanced side scan sonar output highlighting the body in Lake Lawne, Orlando, Florida, and demonstrating the uneven lake floor.

Consequently, most geophysical imaging techniques can be expensive, requiring specialist devices, additional expertise, and transportation to move sizeable equipment to and from the scene [78, 82, 83, 88]. Although these techniques offer the potential to speed up searches, cover larger search areas, and direct targeted search strategies [78, 82, 83, 88], if the environmental conditions are not optimum or a technique is selected inappropriately or used incorrectly, then this can have detrimental effects on the investigation, potentially wasting time and money.

Furthermore, there are no specific methodologies focused on finding skeletal remains. The extended submersion interval leaves little to no scent for detection dogs to detect [12] and the physical size of target is drastically reduced due to disarticulation, damage, and dispersal of the skeleton [96], making remains less visible to geophysical imaging techniques [22, 88, 91, 97]. This is compounded by police officers and divers conducting searches, who are not routinely trained in human osteology and therefore may be unfamiliar with skeletal material and the drastic morphological changes that bone can undergo whilst submerged [75, 98].

Furthermore, this highlights the potential for the use of submersible ALS to assist divers at aquatic crime scenes. ALS would be handheld and therefore would be comparable to the handheld sonars that are currently used. However, investigators would also be familiar with ALS from terrestrial crime scene searches and therefore it would be a simple transition to underwater use. Unlike sonar, ALS would also assist with the identification of osseous material as well as the detection, providing a preliminary indicator of whether a material is bone based on the degree of fluorescence emitted. This identification would include potential differentiation from other underwater debris and would not require the divers to have any osteological expertise. As with the other detection methods discussed, ALS would be a supplementary technique, providing another tool for divers to use at the scene rather than replacing existing strategies.

However, as with many areas of aquatic forensics, research into the use of ALS to search for bones underwater is limited, with current publications lacking quantitative analysis [135]. More specifically, there is no published research directly discussing the impact of the aquatic environment of bone fluorescence, or how the collagen-relationship may be affected by prolonged submersion. As a result, this PhD research includes specific result

questions focused on the comparative and quantitative analysis of porcine bone in terrestrial and aquatic environments, with the aim of assessing the potential of ALS examination for underwater detection of bone.

6.0 – CRIME SCENE DOCUMENTATION AND PHOTOGRAPHY

Accurate search and recovery of forensic evidence is vital for successful crime scene investigation [14] and how that evidence is documented and secured will ultimately dictate future analyses and whether that evidence can be used in court [200]. Alongside recording techniques such as scene sketches and notes [118], crime scene photography is the primary tool used to capture the crime scene in its original state, and forms part of standard forensic practice universally accepted by the criminal justice system [201, 202]. Photography is considered one the most efficient and objective means of creating a permanent record of the crime scene as well as individual items of interest [202], mitigating subjectivity and helping to alleviate investigator bias [203, 204]. Photographs also support the chain of custody by allowing dynamic documentation of the scene as items are moved or recovered for analysis [205] and providing a visual record for any retrospective analysis by law enforcement and future discussion in court [206]. The use of photographs also reduces the need to bring physical exhibits to the courtroom, reducing the risk of contamination and breakage of often fragile forensic evidence [207], and enables convenient viewing of evidence that would otherwise be unavailable such as vehicles or biological material including victim injuries and blood stains [204, 208].

6.1- CAMERAS

'Point-and-shoot' cameras are the most accessible type of digital camera as they utilise auto focus and built in flash to optimise photography parameters on behalf of the user [203]. However, point-and-shoot cameras usually lack the ability to manually adjust photography parameters, are not very powerful and do not always have a screen, which consequently render them unsuitable for crime scene investigation, particularly for underwater photography [204]. A common camera used in forensic photography is the digital single lens reflex camera (DSLR) [203, 209] which uses mirrors to assist with the real time viewing of the subject to facilitate photograph composition, as well as the enhanced functionality to control all photography parameters [206]. In DSLR cameras, reflected light bouncing off the subject enters the camera through the aperture, as shown in figure 6 below [207]. Prior to pushing the shutter release this light will hit a mirror known as the 'reflex mirror' which is positioned at a 45-degree angle [206]. The

light is then reflected up into a further series of 5 mirrors, referred to as a pentaprism/pentamirror, which then projects the light through the viewfinder [207]. This sequence of mirrors allows the subject of the photograph to be viewed in its correct orientation as we would view it. Without this structure the image would appear inverted [210]. Upon depression of the shutter button, the reflex mirror lifts to allow the light to hit the image sensor which digitally captures the image and stores the data onto a memory card [203]. Images can be taken in quick succession, with large capacity memory cards enabling storage and transportation of hundreds of images, recording individual digital date/time signatures, contributing to contemporaneous documentation [207].

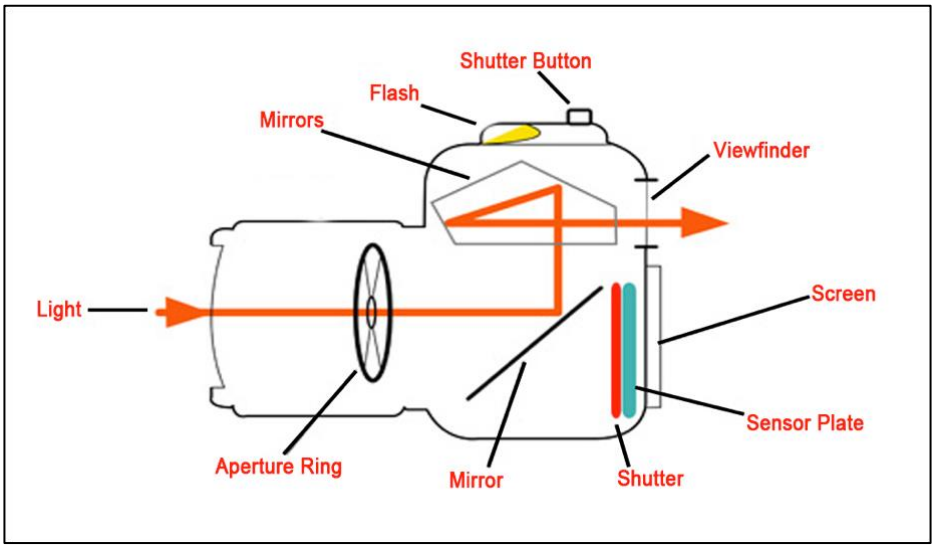

Figure 6: Diagram illustrating how light interacts with the basic DSLR camera configuration [211]

DSLR cameras have been considered the standard camera of choice for forensic investigations for many years [203, 204, 207], but with advances in digital technology mirrorless digital cameras are now becoming popular [204]. Mirrorless cameras offer the same control over image capture as a DSLR, but they do not contain mirrors, as shown in the comparison image figure 7 below. Instead, the inverted image is corrected digitally by the camera whilst still allowing for real-time viewing of the subject [212]. Mirrorless cameras are therefore smaller and lighter compared to DSLRs, making them easier to manoeuvre and store [204]. They are often cheaper, as they contain fewer components, and contain a simpler structure more in common with a point-and-shoot style camera

[204, 212]. However, due to a higher power consumption caused by the digital image correction, mirrorless cameras can lose their charge faster compared to a DSLR [212].

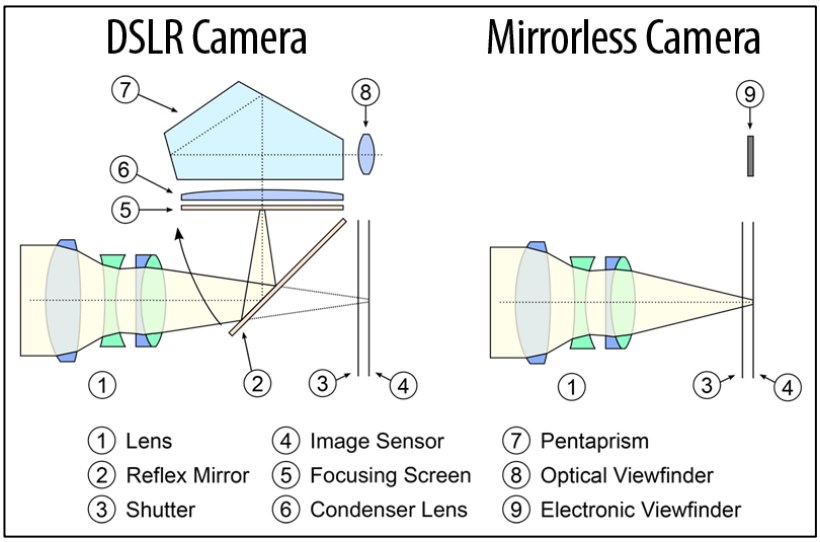

Figure 7: Structure of a standard DSLR camera compared to a mirrorless digital camera [213]

A DSLR camera would be the optimal choice for this PhD project, as they are the most used camera at crime scenes [202]. However, due to the funding constraints of this PhD research and physical difficulties encountered trying to locate an affordable unwater housing for a DSLR, a mirrorless camera was seen as a suitable compromise as they offer many of the same benefits of a DSLR but in a more accessible format. After much consideration, a mirrorless Sony™ A6000 was selected for use in this thesis due to the smaller size, cost, and weight. However, most importantly, the mirrorless Sony™ A6000 enabled manual setting of the photographic settings, therefore still allowing for investigation into a possible method for bone fluorescence documentation.

Successful forensic image capture relies on tailoring the camera settings, as well as camera positioning, ambient lighting, and the use of zoom lenses, to subject in question [203], to ensure accurate documentation with an appropriate level of detail depending on future analysis [214]. For example, fingerprint and footwear impressions are usually photographed at a ratio of 1:1 [202] and at a perpendicular angle [206] to ensure accurate representation of the mark's characteristics for future matching of the print, often conducted through direct visual comparison and physical overlays [215]. To

achieve this specificity, the camera settings controlling the 3 aspects of exposure also known as the 'exposure triangle' [207] as shown in figure 7 below; the F number, shutter speed, and ISO, need to be adjusted [216]. These settings regulate the level of light entering the camera which ultimately contributes to the clarity of the image produced [203].

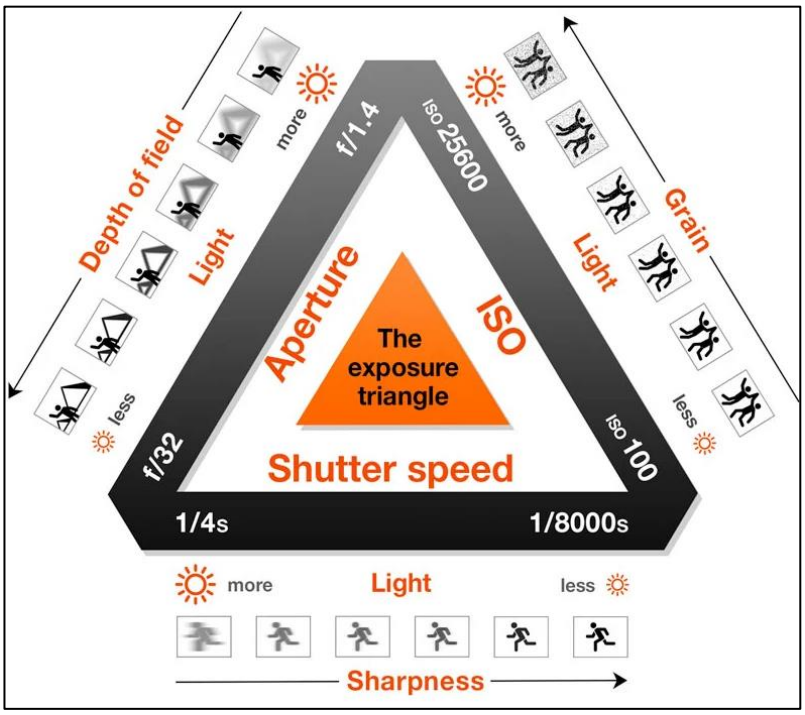

Figure 8: The exposure triangle [217]

Aperture size is selected using f-stops or f numbers and controls the amount of light directed onto the camera sensor [206]. The term aperture refers to the physical opening created by a set of overlapping metal blades often referred to as the diaphragm or aperture ring [212] as shown in figure 6. The f-stop dictates the size of this opening [203], and the higher the f-stop number the smaller the size of the aperture and less light hitting the sensor, which consequently leads to a darker image [207]. Every time the f-stop is increased the amount of light is halved and vice versa, when reducing the f number by one increment the amount of light exposed to the sensor is doubled [203]. Aperture size also impacts the depth of field [125].

Depth of field is the term used to describe the area of focus within an image [212]. A short depth of field would produce a narrow area of focus often meaning the main subject of the photograph would be in sharp focus whereas the surrounding background

would be blurry [214]. This is useful when photographing individual objects or portraits where detail is paramount such as a weapon or an injury [204]. A deep depth of field would lead to a much larger area of focus meaning more of the image is in sharp focus [125]. Consequently, a deep depth of field is more suited to landscape style shots, such as documenting the overall crime scene or entrance and exit routes [208]. The greater the higher f-stop number, the smaller the aperture and the deeper the depth of field [125].

The exposure time, also referred to as the shutter speed, dictates how much light hits the sensor by controlling how long the shutter remains open once the shutter release button has been pressed [209]. The shutter speed is measured in seconds, therefore the longer the duration the longer the sensor is exposed to light [202].

Unlike shutter speed and aperture size, ISO does not control the amount of light hitting the sensor in any capacity [204], rather it is a camera setting used to balance shadows and highlights within a photograph [212]. Often reported as an acronym for International Standards Organisation [209], ISO is a term that has been retained from film photography and was used to categorise how sensitive a particular film type was to light [209]. The more sensitive the film, the lower the allocated ISO number [212]. In modern digital photography ISO is also discussed as describing how sensitive the sensor is to light but this isn't strictly accurate as this would be determined by the number of megapixels [214]. ISO is in fact a digital function used by the camera to lighten or darken an image and can be useful when helping to select aperture or shutter speed [207].

As with aperture and shutter speed, altering the ISO will also affect other aspects of the image [203]. In film photography, using films with great sensitivity to light ran the risk of grain, where the metallic crystals contained within the film could be seen in the final developed photograph producing a random speckled effect [218]. Digital images experience noise rather than grain [219], which is defined as random variation in brightness in some pixels within the image due to increasing the ISO brightness [204]. This can make an image look blurry even though it was originally sharp [212]. Another advantage of moving away from film photography is the elimination of grain, although digital images can experience noise, the ISO can be adjusted at the scene and another image taken. Whereas once an ISO of film was selected, all the images would be taken

using that one roll and the presence of grain would not be evident until after the images developed, consequently impacting all images from that film [218].

6.2 – OTHER DIGITAL METHODS

In addition to basic still photography, crime scene photographers now have a whole range of techniques and technologies at their disposal, which is growing with time, including major developments in digital capture and 3D modelling [178, 220, 221]. Photogrammetry, using handheld scanners to capture 3D images of objects, has been a long-established technique in forensic anthropology to catalogue skeletal collections and visualise individual osteological landmarks or points of interest [222-225]. It has been used in forensic pathology to document injuries and identifying features of deceased individuals to supplement post-mortem examinations [226].

However, there has recently been a resurgence of its use at crime scenes due to the growing popularity of using technology to speed up scene documentation [207], with newer more large-scale methodologies such as terrestrial 3D laser scanning [227] and UAV drones [177]. This is primarily due to the ability to capture large, complex scenes using vast clouds of digital data points for computational interpretation and reassembling enabling the objective capture of whole scenes or areas of focus [220, 228]. When used correctly, these techniques create little disruption to the scene itself by limiting the amount of personnel on site and can help investigators plan access routes, highlight areas of interest, and subsequently organise search strategies [208, 223].

These techniques can also provide a tangible, more immersive graphical representation of the crime scene to facilitate discussion in court [221], even providing an interactive 3D reconstruction that allows the jury to ‘walk’ the crime scene [208, 221]. It is thought this may have a direct beneficial impact on criminal cases as it allows broader observation and measurement of data points, more relatable visualisation of the crime scene, and spatial documentation of exhibits, as well as sensitive reproduction of forensic exhibits which otherwise might be too confronting or distressing for members of the jury [208, 220, 225, 229]. However, these technologies can be expensive, and do not always capture the finer details of a scene, particularly if it densely populated with exhibits [223, 229]. Handheld photogrammetry is very effective at capturing intricate

detail of individual exhibits or isolated areas of interest [223, 230] but to create a full 3D image, multiple images of all sides of the object need to be completed which can be very time consuming [228, 229].

Not all scenes are suitable for this type of imaging such as underwater scenarios or compact indoor environments [229]. The use of traditional still image photography is a simpler technique, with established operating procedures and training courses [202], and provides investigators with the autonomy to pinpoint items of interest based on professional experience, all whilst moving freely across the crime scene [203, 204]. Some scanning technologies need to operate from a fixed position and therefore multiple deployments may be required to ensure documentation of all angles, depending on the capabilities of the model [208].

Missing potential evidence or miscalculating the placement of items has significant detrimental impact on forensic interpretation as this data is vital for reconstructing the crime [203], and any subsequent revisions of testimony could possibly undermine confidence in the presented evidence and the technique itself. For example, at mass disasters scenes such as an air crash, the positioning of debris or even human remains can inform investigators about the cause, mode, or intensity of the disaster, including where individuals may have been sitting, the location of any explosions or defects in the plane, and ultimately if it was accidental or suspicious [205]. Although scanning technologies could be efficient at capturing the overall crash site, still photography and investigator expertise would be needed to identify and document key exhibits and human remains [231, 232].

Supplementary techniques can be used alongside still photography to amplify or enhance forensic detail and assist documentation [178]. For example, footwear impressions should be photographed in situ [216], but it is best practice to also create a mould of the impression (if found in a suitable substrate e.g., mud or sand) to be photographed later, or to create an inked impression for subsequent comparison photography [205]. Similarly, fingerprint powder is commonly used to enhance the ridge detail left behind by individuals handling items at a crime scene [233]. Fingerprint powders are available in a range of colours and compositions designed for an array of surfaces and contexts [234] and adhere to the secretions of sweat and oil produced by

the pores on human hands and feet [235], which are deposited during handling or interacting with objects or surfaces [235]. Similarly, superglue fuming can expose latent finger marks left on glossy materials [236, 237], and Ninhydrin reagent can be employed to expose fingerprints left on porous surfaces such as paper [238], producing a purple positive reaction which can be accelerated when heated [239]. All these techniques rely on chemical reactions to make the latent evidence more visible by enhancing the contrast between the subject and the deposition surface. As a result, these procedures are destructive and once applied can irreversibly alter the integrity and morphology of the prints [235, 237, 239]. A non-destructive alternative would be to use light to illuminate and enhance areas of interest prior to more permanent retrieval.

7.0 - THE ROLE OF FLUORESCENCE IN CRIME SCENE INVESTIGATIONS

7.1- LIGHT

Light has always played an integral role in forensic examinations [212], where manipulation of the wavelength, angle, and intensity can be used to locate potential forensic evidence, enable documentation, or form part of the forensic analysis [212, 240-242]. The visible spectrum (400 – 750nm) is the part of the electromagnetic spectrum that is what we refer to as 'light', as shown in figure 9 below, between ultraviolet and infrared light [157].

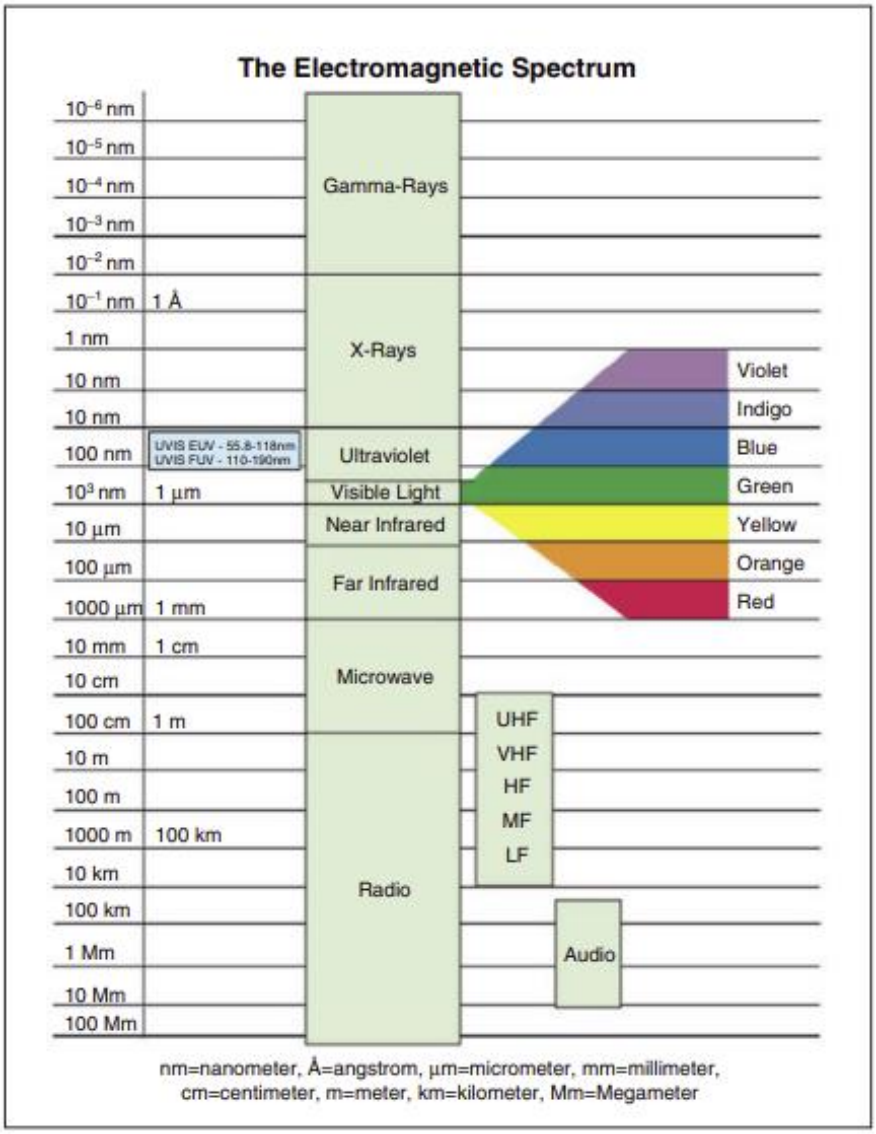

Figure 9: Diagram of the electromagnetic spectrum [207]

Electromagnetic radiation travels in waves and can be measured based on their length from crest to crest (m) and their frequency (Hertz), which ultimately determines the level of energy the wave transmits [124]. The longer the wavelength, the lower the frequency and the lower the energy; a common example of lower frequency wavelengths is radio waves [178]. Conversely, gamma rays and x-rays are examples of much shorter wavelengths with a higher frequency and produce much greater levels of energy [178, 243]. Visible light is the only aspect of the electromagnetic spectrum that is visible to the human eye and encompasses wavelengths between 400–700 nm as shown in fig. 10 below [157]. Ultraviolet wavelengths are shorter at approximately 200-375 nm and infrared are towards the longer end of the spectrum at approximately 700-900 nm [244].

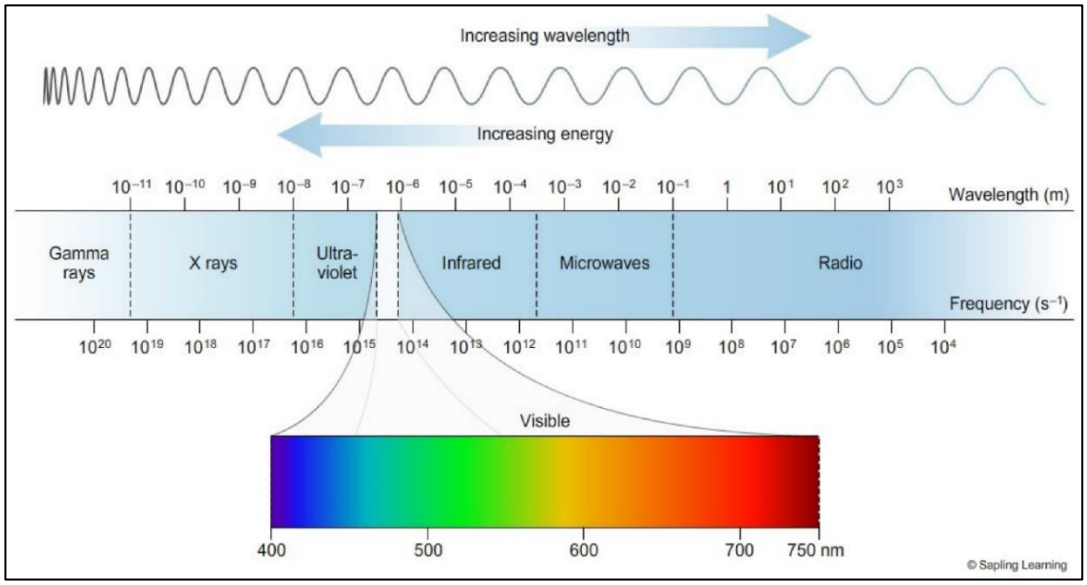

Figure 10: Wavelength energy levels based on the position in the electromagnetic spectrum [245]

When light interacts with a surface, it can either be absorbed, reflected, transmitted, or converted [246]. White light such as sunlight contains all the wavelengths of the visible spectrum and what the human eye perceives as colour is a result of light hitting an object and some wavelengths of light being reflected whilst others are absorbed [247]. An object will be observed as white if all wavelengths are reflected, whereas an object will appear as black if all wavelengths are absorbed [202]. Most objects will both reflect and absorb some wavelengths producing a range of colours, for example an object will

appear orange if all colours are absorbed other than wavelengths of approximately 600 nm which are reflected [202, 247].

Basic light techniques such as a camera flash and general torch light are fundamental at crime scenes for preliminary illumination and evidence documentation [73]. However, colouration, texture, and structure of examined surfaces as well as the properties and volume of any deposited evidence, will impact the search and recovery process [248, 249]. For example, darker surfaces can make some evidence such as blood more difficult to see [246] and transparent substances such as semen or saliva may allow the deposition surface to show through, also impeding observation [250]. Wet deposits can be more reflective as well as change in colour and texture as they dry [249].

Drying rates may be influenced by the composition of the deposition surface e.g., an absorbent textile surface may retain fluids for longer compared to a hard surface with no absorbance [120]. Changing the angle and orientation of the light source can help when searching for evidence at the crime scene and when examining individual exhibits [178]. Using an oblique angle rather than shining a light directly onto a surface can create greater levels of contrast and shadow whilst avoiding direct reflection [178, 215], therefore making latent evidence stand out from the background substrate [202]. This is particularly helpful when looking for small items of evidence such as fibres and hairs [251]. It can also aid observation of textured or three-dimensional surfaces such as footwear impressions [178].

Transmission of light occurs when light passes through another material, such glass or water [243]. Movement through a material can cause a decrease in energy levels as the light stimulates excitation of the surrounding molecules as it passes through and can lead to a change in wavelength [252]. This process can also lead to bending and scattering of the light through diffraction or refraction [251], and these principles underline the basic concept of light filtration [243]. Water is much heavier and optically denser than air [168] meaning that it contains a higher number of particles per litre [253]. Consequently, water exhibits a higher refractive index, meaning that light is slowed to a greater extent, with a much greater angle of deviation from the initial angle of incidence [254].

As depth increases many of the wavelengths from white light will be absorbed and scattered. Red and violet wavelengths are usually absorbed first whereas the blue and

green wavelengths experience scattering for much greater depths which is why most submerged objects appear blue or green [255]. Figure 11 below illustrates the different depths that the wavelengths of visible light are absorbed in an ocean environment.

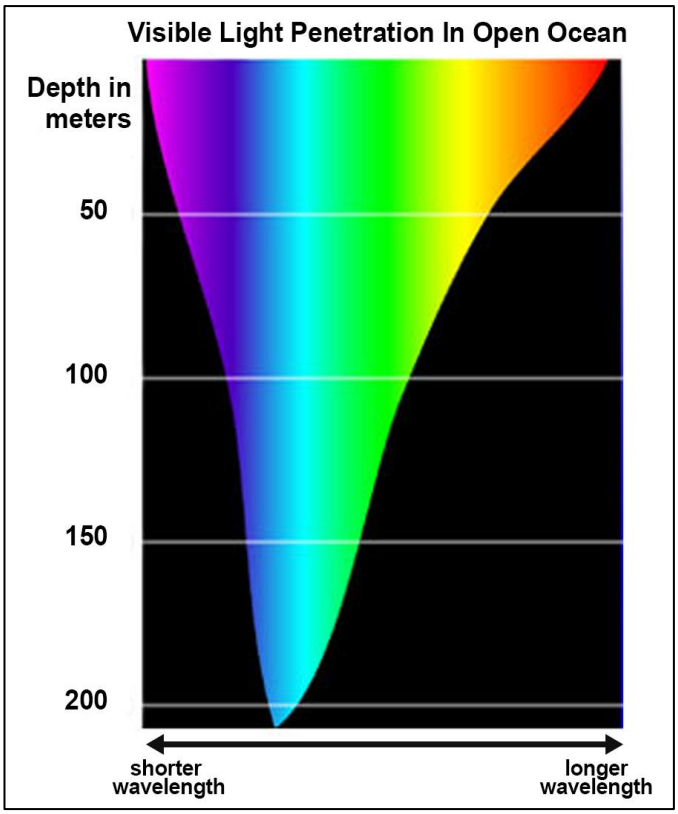

Figure 11: Sequence of underwater wavelength absorption and scattering at different depths in a marine context (Edited by Catherine Maidment, 2023) [255]

This persistence of blue light at greater depths provides potential support for the use of ALS in deeper aquatic contexts [135], particularly as many papers cite blue wavelengths as the most successful for stimulating bone fluorescence [132, 133, 135, 146, 148, 256]. The extent of this research is discussed in greater detail later in section 8.0. However, as underwater osteological ALS research is still in the early stages, most published research discusses laboratory experimentation, including short stimulation distances [131-133]. However, there is still inconsistency in the reported findings regarding the source of bone fluorescence and the subsequent stimulation parameters. Consequently, this PhD research also focuses on the fundamentals of ALS examination of bone, but with the aim

of informing future fieldwork experimentation, such as deeper submersion and longer stimulation distances which will influence the spectral shift in wavelengths.

Conversion of light occurs when excitation leads to the eventual emission of light of a different wavelength [202]. Absorption of photons by a natural fluorophore, leads to an elevation in electron energy levels, and an overall higher energy state [122]. This stimulation is followed by relaxation processes, through which the molecule dissipates excess energy [257]. This complex mechanism of energy exchange is influenced by the medium (such as different solvents or matrices) in which the fluorescence process occurs [257]. For example, in a rigid crystalline matrix compared to a more flexible environment, a phosphorescent molecule may undergo intersystem crossing at different rates, influencing the efficiency of relaxation processes and, consequently, the emission characteristics of the molecule [258].

A fluorophore is a term used to describe a chemical compound that can emit light upon molecular excitation from light energy [122, 146, 257] and the term autofluorescence describes the naturally generated fluorescence emitted by a substance without chemical enhancement [130]. In ALS examination the emitted wavelengths of light are usually longer in wavelength [252], and the conversion from short to long wavelength is referred to as the Stokes shift (fig. 12) [178], in reference to Sir George Stokes, who also introduced the term ‘fluorescence’ when describing the properties of fluorite minerals in 1853 [259].

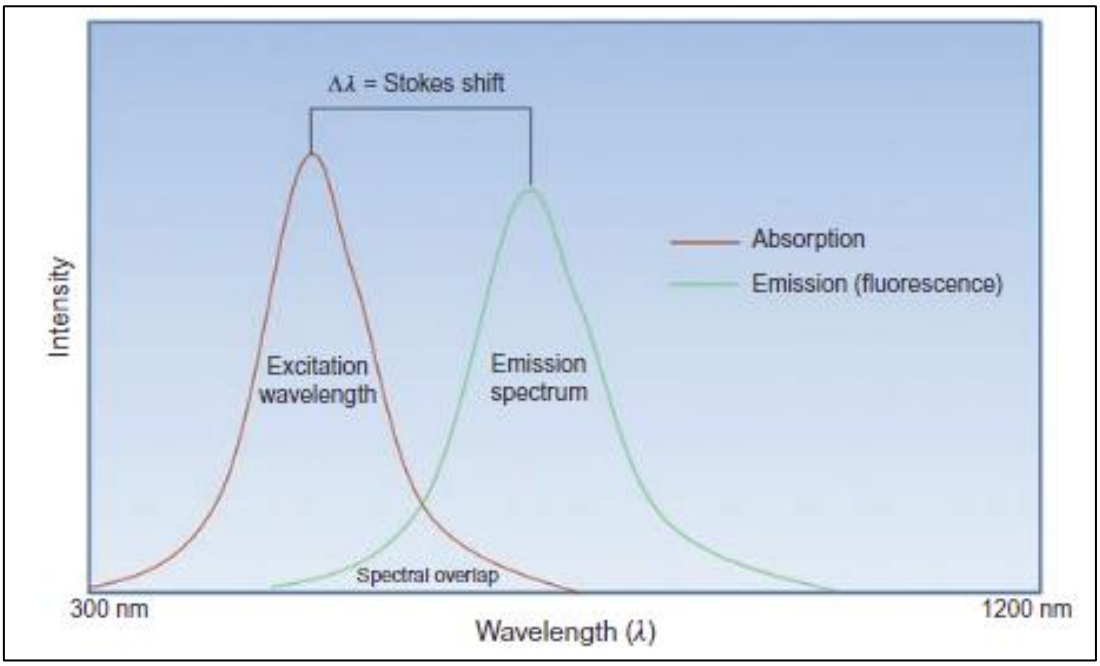

Figure 12: Diagram of Stoke's Shift [124]

7.2- FLUORESCENCE

When viewed with the appropriate coloured filter these longer wavelengths are observed as fluorescence, with the subject appearing to glow [252]. This fluorescence naturally enhances the contrast between the subject and its background, making latent evidence more visible [125, 252]. To observe the fluorescence, a coloured filter, either attached to the camera lens or worn as glasses, is required to selectively modify the spectrum of light reaching the camera sensor, isolating target fluorescent wavelengths and filtering out extraneous scattering and the original excitation [219, 260].

Long pass filters operate by selectively permitting the transmission of longer wavelengths of light while absorbing/obstructing shorter wavelengths [137]. Barrier filters suppress specific wavelengths of light while allowing others to pass through [125] enabling targeted wavelength management [261]. Bandpass filters are also discussed, and usually this type of filter is designed to let through a specific bandwidth of light for example, approximately 400–450 nm would be the bandwidth for blue light [212]. However, these terms are often used interchangeably in the literature, therefore, to avoid confusion, throughout this PhD barrier filters were used for all experimentation to ensure accurate quantification of fluorescence.

In accordance with colour theory, the most appropriate colour for a barrier filter is usually the opposite colour of the wavelength of the excitation light, as seen on the colour wheel (fig. 13) [243]. For example, when using blue light an orange filter is required to block excess blue wavelengths and only let through the orange fluorescence light [252]. Figure 14 illustrates how an orange barrier filter filters blue excitation light but allows visualisation of the orange-coloured fluorescence emissions. Figure 15 demonstrates the overall process from how a substance is stimulated through to how it is subsequently viewed and/or photographed.

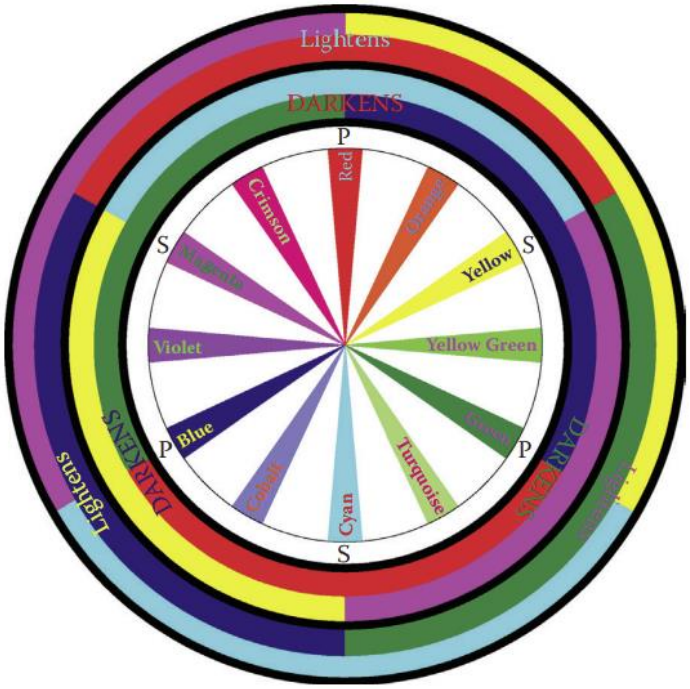

Figure 13: The colour wheel: illustrating that the optimal colour of barrier filter for fluorescence visualisation is opposite on the colour wheel to the colour of the incident wavelength [243]

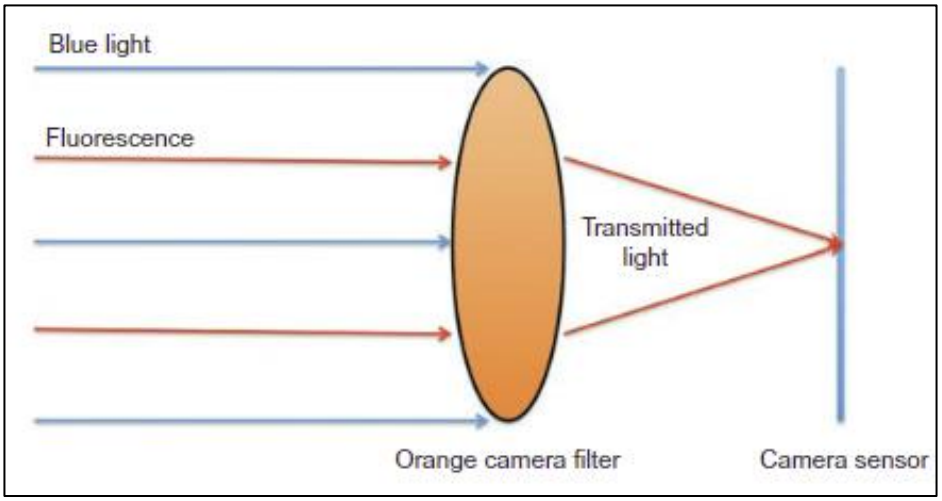

Figure 14: Demonstration of how an orange filter filters blue wavelengths of light to reveal fluorescence (Edited by Catherine Maidment) [124]

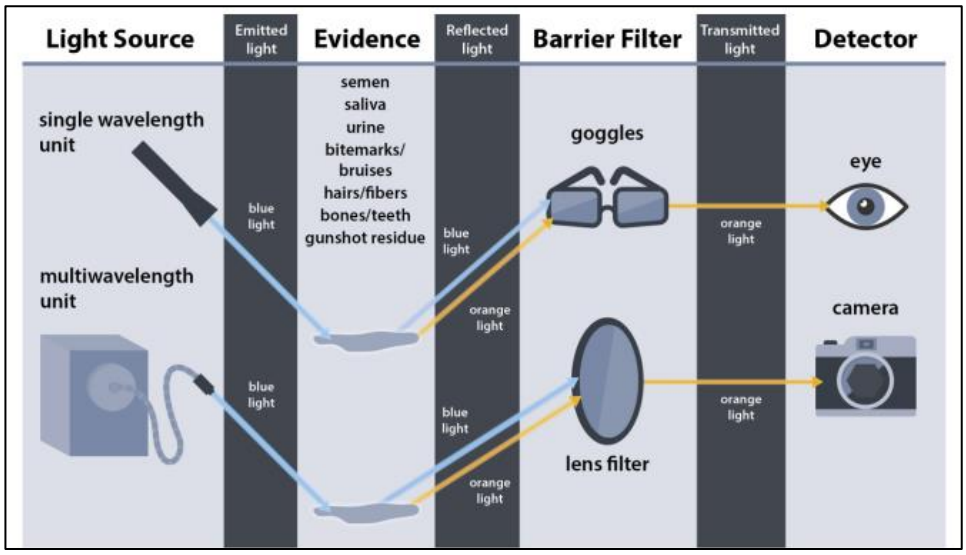

Figure 15: Diagram of how blue ALS wavelengths stimulate autofluorescence, which can then be consequently viewed using orange coloured goggles or photographed using an orange barrier filter fitted to the camera lens. [262]

7.3 – FLUORESCENCE TERMINOLOGY

A significant problem with current literature regarding the phenomenon of fluorescence is the lack of consistent terminology. The terminology varies across literature, as terms such as luminescence, fluorescence, photoluminescence, and phosphorescence are erroneously used interchangeably [252]. Miller & Marin (2015) explain that the overall conversion of light is known as luminescence, and that fluorescence refers to emitted light that recedes quickly after initial excitation, whereas phosphorescence applies to light that persists after stimulation [202]. This explanation is also supported by Marin & Buszka (2013) [124], and the term 'fluorescence' has been used in this context extensively across forensic ALS based literature, covering a range of topics including body fluids, injuries, and bone [120, 126, 135, 137, 263].

Lennard and Stoilovic (2004) also agree with this discrimination but go further to specify that fluorescence and phosphorescence are derivatives of specifically photoluminescence rather than luminescence, as luminescence is an umbrella term incorporating light production from many different stimuli [264]. This includes, thermoluminescence, where heat is the catalyst for light emission, bioluminescence, where light is produced by biological processes, and chemiluminescence, where light is a product of a chemical reaction [252]. This distinction is reflected in some published research such as Stoilovic, (1991) who quantified photoluminescence of semen stains

[265]. Lennard and Stoilovic (2004) maintain that the distinction between fluorescence and phosphorescence is based on persistence, with fluorescence only occurring during direct excitation whereas phosphorescence is prolonged light emission [264].

On the contrary, in 2017 Krap et al use the umbrella term 'luminescence' to describe light produced by burned bone under ALS stimulation, stating that 'luminescence can be distinguished if the excitation light is filtered out by a long pass filter' and that the difference between fluorescence and phosphorescence emissions in radiation is differences in decay time [131]. In 2021, Krap et al, go further to specify photoluminescence to describe emitted light from burned bone, in their paper focused on differentiation between fluorescence combined with short-decay phosphorescence, in comparison to long-decay phosphorescence [142]. They state that the decay range for fluorescence is nanoseconds whereas it is microseconds and longer for phosphorescence. However, it is unclear from the method how the authors were able to discriminate between phosphorescence and fluorescence emissions during their experimentation, particularly as a 'presence or absence' visual scoring system was used for quantification, without any measurement of persistence.

During photography, Krap et al (2021) reportedly used positive and negative controls for comparison and to help identify positive fluorescence levels, the definition of positive phosphorescence was not divulged. It could be the case that the authors classified all emitted light as phosphorescence, as they also stated that short-decay phosphorescence (and therefore fluorescence) cannot be visibly observed, unlike long-decay phosphorescence. However, this discrimination was not clearly stated. Similarly, in a more recent study by Schariatmadary et al (2023) the term 'luminescence' was also used to describe observed light waves from burned bone and stated that fluorescence and phosphorescence cannot be easily differentiated during ALS stimulation. Although the authors spend time defining the term photoluminescence, the umbrella term luminescence is instead used to describe their results [158].

Irrespective of these points, Krap et al (2021) reported that long-decay phosphorescence was absent in all human bone samples processed in temperatures up to 400°C [142]. Consequently, the debate regarding terminology may not be wholly relevant to this PhD project, as most bones examined here were fresh or hot water macerated (80°C

maximum). Moreover, throughout this PhD experimentation, emitted light was photographed at the point of excitation, and included all light emissions. Arguably photoluminescence may be a more specific term as it would accurately describe the origins of the emitted light [124]. However, the larger consensus within current literature is that fluorescence is the accepted term for the immediate emissions of light produced during short wave ALS stimulation, including when examining bone, with overall short lifetimes [132, 135, 137, 266]. Consequently, to ensure comparative discussion with literature, this PhD thesis uses the term fluorescence, to mean all emitted light produced during ALS stimulation.

There are also several instances in literature where IR and UV fluorescence are used as general adjectives for alternative light wavelengths, including wavelengths within the visible spectrum. This can be confusing, and is not accurate, as IR specifically denotes the near infrared wavelengths of the electromagnetic spectrum (700-900 nm) and UV refers to the ultraviolet bands (200-375 nm) [202]. This distinction is important as the amount of radiation associated with these different sections of the spectrum is very different, and subsequently will impact analyses and crime scene conduct. Therefore, whenever UV or infrared are specifically discussed in this thesis, these terms will be used in direct reference to the appropriate bandwidths. Successful fluorescence production and subsequent documentation is also dependent on the type of light source used as well as the camera configuration.

7.4 – ALS AND FLUORESCENCE PHOTOGRAPHY

Alternative light sources have become a fundamental tool for forensic analysis, used in laboratory examination and in the field [212]. These devices can emit a chosen narrow wavelength of light rather than the full spectrum white light [178]. ALS equipment is usually easily transportable and ranges from single or multi-LED handheld torches designed for targeted areas of interest, up to more powerful lasers and lamps which can be used to illuminate broader stretches of terrain [204, 212]. Wavelengths generally range from 200 to 1200 nm [267]. Common features include robust outer casings, long battery life, and a reliable, calibrated beam intensity to ensure continuous light emission at the designated wavelength [262]. Power level and distribution of the light varies between models [212], with some being described as ‘tuneable’ i.e., capable of variable

wavelengths using filters or different bulbs to maximise its use at the crime scene [208, 268].

Due to their portability, ALS can provide a simple and convenient screening tool when searching wider scenes as well as focused examination of areas of interest or individual exhibits [267]. This flexibility can help to inform the construction of search strategies regarding examination, collection, or further analysis such as sequence of presumptive testing or fingerprint examination [252]. The application of individual wavelengths also enables users to tailor searches towards specific evidence types that may be particularly pertinent to the ongoing investigation such as body fluids when examining a sexual assault, or gunshot residue when investigating a firearms offence. These factors also make ALS a suitable candidate to aid searching for skeletal remains, providing the ability to search large scale, open crime scenes such as potential grave sites, archaeological excavations, aquatic depositions, or disaster scenes, as well as triage for individual elements or bone fragments [137].

Routine crime scene fluorescence photography is a relatively modern technological development. Prior to the widespread use of digital cameras, fluorescence photography was expensive and time consuming, requiring specialised high sensitivity film and the taking of many photographs to guarantee a usable fluorescence image [219] [124]. This meant that fluorescence photography was not often carried out. Similarly, in the early days of digital photography, camera sensors were not always sensitive enough to detect the light wavelengths of fluorescence so images could end up over or underexposed [124]. Over time digital cameras have improved in specifications, including larger, more sensitive sensors capable of producing more detailed and higher quality images [219]. General recommendations outlined in crime scene photography texts include the use of manual settings to maximise fluorescence documentation, including longer exposure times to combat the dark photography conditions and maximise fluorescence exposure [125]. The removal of any UV filters where applicable, is recommended to ensure full fluorescence detection and tripods are advised to minimise blurring during the longer exposure times [252]

ALS examination of autofluorescent objects is non-destructive and produces an immediate response with no lingering effects, as the fluorescence disperses once the

light source is removed, if there is no phosphorescence [34]. This is in comparison to the previously discussed Ninhydrin reagent used to enhance fingerprints which permanently alters the appearance of the examined print, or similarly when using products such as Luminol®, Flourescein® and Bluestar® to enhance blood stains [269]. These chemicals do create a transient fluorescence effect but due to the liquid application these products can dilute blood stains [270], altering morphological features, and resulting in possible negative ramifications for blood pattern analysis [271].

Stimulating autofluorescence using ALS not only preserves the integrity and structure of the evidence but also facilitates documentation [212]; factors which are integral to effective crime scene analysis and forensic anthropological investigations [272-274]. More specifically, forensic anthropology techniques used to produce an anthropological profile generally concentrate on the morphological characteristics and the physical condition of the bones [110, 274]. Therefore, carrying out any destructive analyses which would alter these structures could inhibit identification of individual skeletal elements, potentially obscure trauma/pathology, or completely remove forensic evidence [110]. Ultimately, this could jeopardise victim identification, by limiting the number of bones and data available for constructing the osteological profile [110]. Research suggests that it is the proteins found in seminal fluid and other body fluids that are thought to respond to light stimulation [120]. Short wave light approximately 400-500 nm is most frequently used when searching for biological material [120, 275, 276], and as approximately 50% of bone composition is protein (90% of which is collagen) [130], therefore ALS provides a potentially novel approach for searching for skeletal remains.

7.5 – OVERVIEW OF CURRENT ALS RESEARCH

Much of the ALS research in the literature centres on the detection of body fluids such as semen, blood, and saliva [120, 263, 265, 275]. Numerous studies have been published on the identification and persistence of blood and semen across varying deposition surfaces and fabric compositions, after washing, and on skin, observed using a range of forensic light sources and wavelengths [120, 246, 265, 271]. These studies have helped to enhance understanding of blood pattern formation, recovery timescales, and the evolving morphology of stains during drying [127, 249]. In its natural state, blood

typically responds to light between 300-900 nm with the greatest absorption seen at approximately 410 nm [246]. However, blood absorbs light rather than converts to fluorescence [178], and therefore produces a dark appearance when viewed with coloured filters creating contrast with the substrate [246], helping investigators discern between stains at the crime scene. Fluorescent enhancement of blood stains involves additional chemical reagent such as Luminol®, Flourescein® or Bluestar® [205]. This chemical enhancement of stains is an example of chemiluminescence [205, 212] as the chemical reagents are responding to excitation rather than the blood itself [212].

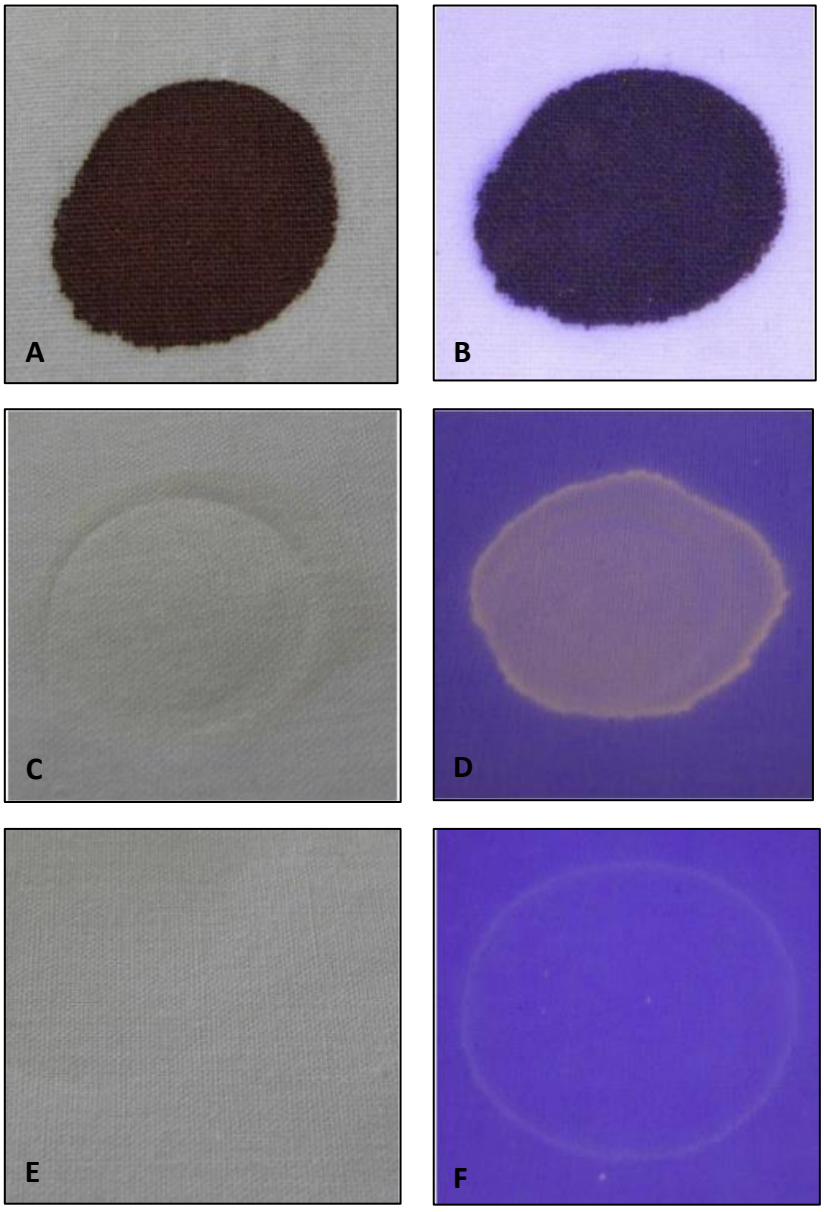

Figures 16: Examples of body fluids deposited on a cotton substrate and stimulated by blue light (450nm) and viewed with an orange filter. A) Blood under natural light, B) Blood under ALS, C) Semen under natural light, D) Semen under ALS, E) Saliva under natural light, F) Saliva under ALS [120]

Semen is naturally autofluorescent and generally responds to wavelengths between 300-480 nm [265] but fresh stains most strongly to blue light at approximately 420-450 nm and viewed with an orange filter [250, 275]. As with blood, the main influencing factor inhibiting successful fluorescence visualisation is the deposition surface. Wawryk & Odell (2002) examined fluorescence retention of semen deposits on the skin of human forearms in comparison to cloth [126]. They reported that the semen samples left on skin exhibited much fainter fluorescence compared to the cloth swatches, and in less than half of the participants only some fluorescence was detectable the following day [126]. In a similar study, Tay et al (2021) noted that more absorbent fabrics such as bed linen and mattress lining absorbed the semen sample and drastically altered its appearance, creating a ring of bright fluorescence with a void in the centre, rather than homogeneously across the entire stain, also known as the coffee stain effect. This distinct morphology led to lower observable fluorescence levels, which overall could make the stains more difficult to see at crime scenes [250].

Examinations into enhancement of saliva traces are often run concurrently with investigations into blood and semen, mostly looking into differentiation between the different biological stains, as many body fluids typically respond to broad wavelengths between 300-480 nm [277]. Saliva stains are especially difficult to discern as once dry they become practically colourless [278] but visualisation can be achieved when stains are stimulated by wavelengths of between 450-470 nm [127, 250]. However, the colour and texture of the deposition substrate will influence the absorption rate and level of contrast of the saliva deposit, subsequently impacting the intensity of observable fluorescence [278]. Other biological fluids include sweat and tears, with confirmed autofluorescence detected using 254 nm and 410 nm wavelengths [248] particularly on exhibits such as clothing and bedding [276].

Other notable research, with direct applications to the use of ALS at crime scenes, focuses on combining ALS with 360° High Dynamic Range (HDR) cameras to rapidly screen crime scenes for body fluids, enabling initial documentation of the scene as well as potential stains [127]. During a simulated crime scene, Sheppard et al (2017) found that the ALS camera system was able to detect semen stains as small as 5 µl on white cotton swatches using blue light (455 nm) and a yellow filter up to 300 cm from the

camera. Saliva stains were also detected using the ALS camera system, but fluorescence was much fainter and therefore required larger volumes of sample. As with all body fluid research, the deposition substrate led to the greatest variability in results [127]. Darker substrates limited the amount of detectable fluorescence, as well as porous fabrics absorbing the semen and saliva and reducing fluorescence levels, supporting results seen by Tay et al (2021) [250]. The colour of some substrates, specifically yellow cardboard, emitted background fluorescence and masked the fluorescence of the saliva samples, making them more difficult to detect [127, 250].

7.6 – ALS DETECTION OF OTHER LATENT EVIDENCE

Aside from biological evidence, other studies have focused on trace evidence such as gunshot residue (GSR), hair, and fibres [251, 264]. Although initial sweeps for crime scene textile fibres can be conducted using white light at oblique angles [273], ALS technology can be used to target specific-coloured fibres and to search more uneven surfaces which would cast obstructive shadows [208, 264]. Autofluorescence of textile fibres is usually the result of optical brighteners used to whiten garments when washing [246, 249, 279], fluorescent pigments or dyes used for colouration, or inherent natural fluorescence if the fibre is of animal or polymer origin [259]. UV light and blue light (approximately 450 nm) are the most effective for stimulating fluorescence in textile fibres, however prolonged exposure can degrade pigments [264]. UV light can be used to search for hair at crime scenes, with dyed or bleached hair producing higher intensities [178]. Viner et al (2014), was able to detect singeing to feathers and fur as a result of power line electrocution using ALS wavelengths of 450 nm, 485 nm, 530 nm, and 570 nm, viewed with red filter glasses, with the strongest fluorescence observed at 570 nm [280].

Gunshot residue is a composite of organic and inorganic elements primarily unburned and partially burned gunpowder particles, metallic fragments, primer residues, and lubricants which are expelled from a firearm when a shot is discharged and deposited on surrounding surfaces [281]. Due to their small size (0.5 to 5.0 µm in diameter) particulates are difficult to see, especially on darker skin or clothing [282] and are transient in nature so can be easily washed away or transferred [283]. Therefore, a non-contact and non-destructive technique such as ALS enables identification, measurement,

and documentation of GSR particulates, prior to confirmatory chemical testing, without disturbing the evidence [282, 283]. Using wavelengths of approximately 430-495 nm in combination with orange barrier filters [117, 124, 282], detecting the presence of GSR can help link possible perpetrators to the shooting [242, 281], and interpretation of distribution patterns can provide information regarding shooter and victim placement [282]. An example of how the appearance of GDR can be enhanced with ALS can be seen in figure 17 a-b below.

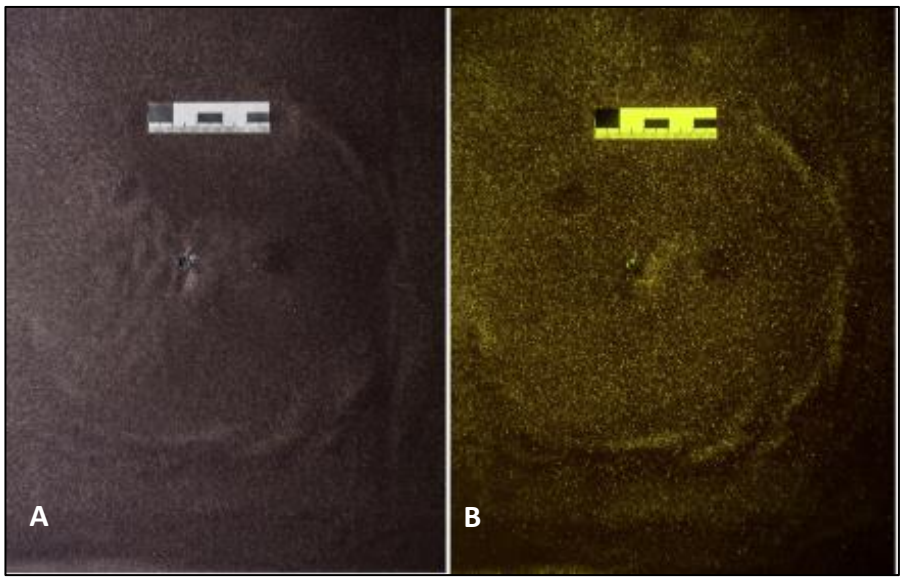

Figure 17: Example of GSR A) appearance to the naked eye, B) 440 nm with orange filter (Edited by Catherine Maidment, 2023)

Schulz et al (2007) used a tuneable forensic light source the Spex Mini-CrimeScope MCS 400 to identify epidermal particles amongst contaminants such as sand, fibres, and soil as well as those deposited on a range of surfaces including wood, stone, metals, and textiles. They established that ALS was able to effectively cut search times in half, using excitation wavelengths between 390 and 475 nm, but noted that the wavelength needed to be varied according to deposition substrate, and to minimise any erroneous background fluorescence [268]. Bite marks, bruising and injuries have also been widely investigated on deceased and living skin [251, 284, 285]. In living tissues, bruising is a result of blood pooling in the interstitial spaces typically in the dermal layer of skin at the injury site [124], which can cause visible discolouration and inflammation [286]. However, the age of the bruise and the amount of force applied during its creation will influence its discernibility and persistence [285].

Figure 18: 'Yellow' haematoma enhanced with violet ALS (400-430 nm), photographed with a yellow filter [287]

Consequently, bruises are not always evident at the point of examination, but ALS can be used to detect and enhance injuries even in the deeper layers of skin and up to months after initial development [285], as demonstrated by figure 18. Haemoglobin, and its metabolite bilirubin, absorb light and when stimulated by ALS producing a dark, non-fluorescent appearance, much like blood stains at a crime scene [287]. UV light approximately 365 nm can superficially penetrate the epidermis [288], revealing surface injuries [289]. However, due to the damaging effects of high intensity UV radiation on skin [287], longer wavelengths are preferred including blue bandwidths [290] and infra-red [291], which can penetrate deeper into skin layers revealing bruising that may be healing or just not visible under natural light [124].

Longer wavelengths are more appropriate for individuals with dark skin tones as melanin also absorbs UV light and therefore can confound injury perception [290]. Scafide et al (2022) found that 415 nm and 450 nm wavelengths, viewed with a yellow filter, produced the most consistent results, enhancing bruises (produced 1-21 hours previously) across six different skin colour categories: very light, light, intermediate, tan, brown, and dark [290]. Holbrook and Jackson (2013) were able to identify strangulation marks in 90% of

172 living strangulation victims who had no external visible marks using 415–515 nm and multiple-coloured glasses, with orange being the most successful [292]. Exploitation of this phenomenon facilitates forensic documentation by increasing the contrast and visibility of the injury in comparison to the non-traumatised skin, allowing the injury to be measured and compared to reference impressions to help reconstruct the events surrounding an assault [292].

ALS excitation can also be used to enhance latent fingerprints [235] and investigate fraudulent documents [293]. Much of the research on the stimulation of fingerprints concentrates on prints that have been pre-treated with cyanoacrylate (superglue) and/or fluorescent dyes and powders [234, 294] and are therefore an example of chemiluminescence methods rather than autofluorescence [212]. Cyanoacrylate is a standard method of fingerprint recovery from non-porous evidence items and ALS enhancement is used as a non-destructive supplement to enhance ridge detail for documentation and further analysis [237]. Historically fluorescent powders have been used for more complex surfaces where greater visibility is required to contrast with multiple substrates colours or textures [235].

Literature also suggests that short UV light (200–300 nm) can stimulate autofluorescence in finger marks [219, 295], originating from sweat and secretions, as well as other extrinsic contaminants [296]. Overall, the level of fluorophores in untreated fingerprints is generally very low [124] which leads to variable success with ALS stimulation, and hence the need for additional powders and treatments [234, 297]. These issues are exacerbated as fingerprints age, leading to drying and further lowering fluorescence levels [295].

Despite this, some papers have examined the excitation of latent prints without chemical additives. Bond (2015) compared the clarity of fingerprints left on thermal paper at room temperature examined using white light, blue light (450 nm) and varying intensities of UV LED torches (peak 365 nm) [298]. The clearest and most complete prints were observed using the UV torch whereas the prints examined with blue light lacked finer ridge details [298]. Due to the very low levels of fluorescence produced by latent finger marks, shortwave UV laser stimulation (200–300 nm) and reflected UV imaging are often the more successful routes for boosting visibility [295].

However, a high intensity UV argon laser, a precise angle of excitation, specialist camera, and an optimal visualisation context are required to ensure the highest chances of success, which makes these methods challenging to perform at crime scenes [299]. Even with the ideal environment it can be a time-consuming process of trial and error to successfully generate a viable fingerprint, with results varying hugely [300]. Consequently, UV laser excitation is better suited to laboratory examination where time pressure, equipment availability, and working environment are less restrictive [300]. As with all shortwave UV light sources, safety is a key consideration, as prolonged exposure can be destructive to DNA, and therefore targeted and sequential analysis is required when choosing UV light [295, 301].

Bandwidths of 385–548 nm have also been used for detecting and recording alterations to documents in forensic cases, such as watermarks, erasures, and differentiation between inks [293]. Coloured filters help to enhance contrast and can screen out target ink pigments to reveal others underneath, such as blue filter to filter out blue ink to expose the original black ink beneath [293]. Senior et al (2012) cite a broad range of wavelengths between 200 to 700 nm when using UV–Vis spectroscopy to characterise and date ball point pen inks [302]. Similarly, Houlgrave et al (2011), used 583 and 549 nm light coupled with red and orange glasses respectively to scrutinise the separation results of ball point pen inks by thin-layer chromatography (TLC). It was reported that ALS examination provided a higher level of discrimination between the inks by emphasising the more subtle bands and revealing latent components that were not visible under white light [303]. As with fingerprint examination, ALS examination of documentation is generally reserved for laboratory analysis where individual exhibits can be analysed, and where pre-treatments such as TLC or additional equipment such as UV-Vis can be used [293].

Consequently, there is a precedent for the use of alternative light sources in forensic science, and the ongoing need for a simple non-destructive screening tools to aid crime scene assessment. This broad range of research demonstrates the versatility of ALS and how it is applicable to a range of current forensic applications. Although applying ALS to skeletal remains could be a logical progression, current research into ALS analysis of bone is scant. However, some initial studies have yielded encouraging preliminary results.

8.0 – BONE FLUORESCENCE

As bone ALS research is an emerging discipline, most research has been conducted under laboratory conditions utilising bones from existing skeleton collections and has usually been designed as feasibility studies to test methodological variables such as wavelength, filter, and ALS model [132, 133, 135]. For example, Green et al (2019) conducted a series of experiments aiming to optimise the parameters for ALS examination of bone, including investigating the most effective wavelength and filter combination for discriminating porcine bone from non-bone objects such as rocks and sand [133]. They determined that bone fluorescence could be detected up 100 cm from the specimen, although fluorescence emitted by previously 'heat-treated' bone became fainter at 30 cm which could have implications for examining bone that has been exposed to environments with high heat [133]. This result contrasted with the fluorescence levels of frozen and non-treated bone samples which maintain consistent fluorescence levels up to 30 cm. The methodology indicated that the heat-treated bone may have been boiled but no explicit technical details were reported [133], and as there was only one example of each bone condition, it is difficult to confidently say whether the boiling influenced the level of visible fluorescence, or if it were possibly the result of natural variation across the dataset.

Green et al (2019) went on report that 450 nm coupled with an orange filter was optimum when viewing bone fluorescence [133], which is in keeping with parameters of other biological materials such as blood, and semen [120] as well as in other bone fluorescence studies [132]. In their study, Miranda et al (2017) examined tooth and bone fragments using an array of colour filters in conjunction with blue light (455 nm). They also concluded that an orange filter coupled with blue light was the most successful combination for visualizing bone fluorescence [132]. Although the specimens used in both studies were macerated, the results corroborated previous MSc research conducted by Maidment (2017), investigating the optimal filter combination for fresh, manually defleshed porcine bone [134]. After photographing the porcine bones in a laboratory environment with blue light (450 nm) combined with orange, yellow, red, green, and blue camera filters, the results showed that the orange and yellow filters were

the most successful when viewing bone fluorescence, due to the high level of observable fluorescence combined with defined contrast with the background substrate, which was visible across a variety of bone types. It was also noted that bone composition, morphology, and size may also play a role in bone fluorescence production, as unexpectedly, smaller bones such as metatarsals produced much higher fluorescence results compared to the bone larger specimens [134]. A summary of these photographic fluorescence results can be seen in table 2. Although this factor was not explored during this PhD thesis, as the same bone type was used throughout the experimentation to ensure standardisation, further research is required, and it will be taken into consideration for future work.

Table 2: Summary of photographic results for the orange, yellow, and red filters produced during the MSc study.

Filter	Filter			
	Natural	Orange	Yellow	Red
(Os Coxa) Acetabulum		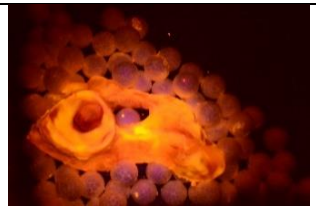		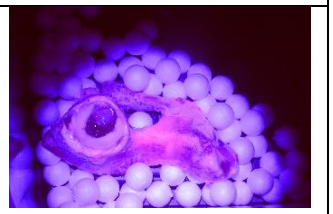
Metatarsal		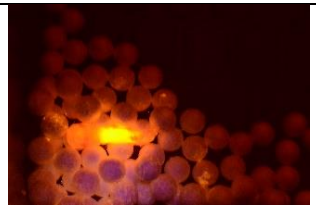	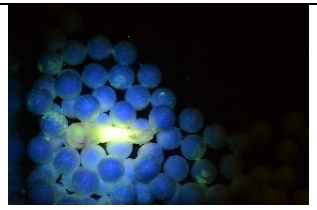	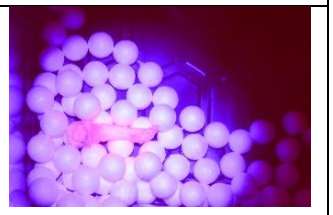
Humerus		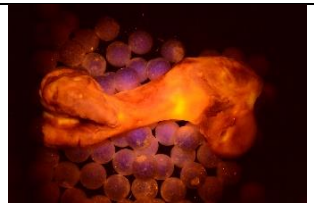	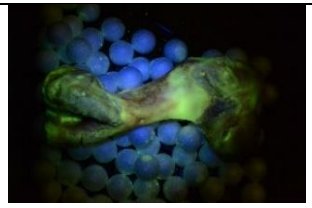	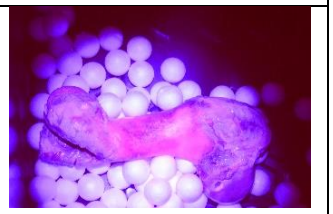

8.1 – OTHER WAVELENGTH AND FILTER COMBINATIONS

Although blue wavelengths are the most reported in bone fluorescence literature, no specific wavelength has been cited consistently across literature [137]. This is most likely due to the use of different ALS models during experimentation, the purchase of which is influenced by institution budgets, the location of light source manufacturers, and product familiarity [266]. Similarly, although orange and yellow filters have frequently been reported as the most successful at visualising bone fluorescence, other coloured filters, such as red filters, have also been explored.

Prior to conducting their study into the estimation of PMI using human femoral bone sections (known PMIs of 1 - 49 years), Sterzik et al (2016) trialled a range of wavelengths: 415, 440, 460, 490, 550, and 570 nm in combination with orange, yellow and dark red barrier filters. They concluded that the most intense fluorescence result was seen when using 490 nm (light blue/green) with a dark red filter and subsequently used this configuration throughout their study [148]. However, this selection was based on subjective observation rather than quantitative analysis. Similarly, Capasso et al (2015) examined sections of macerated archaeological human femora to investigate the relationship between bone composition and autofluorescence as well as time since death (TSD), using confocal microscopy at 488 nm (blue/green light) combined with a 543 nm filter [122]. Whereas, Krap et al (2017) conducted an extensive systematic comparison of five different forensic light sources with eleven filter combinations to examine the fluorescent properties of cremated bone, including 350 to 380 nm (UV, peak at 365 nm), 400 to 430 nm (violet, peak at 410 nm), 420 to 470 nm (blue, peak at 445 nm), 445 to 510 nm (blue/green, peak at 475 nm) and 480 to 560 nm (green, peak at 520 nm), across varying temperatures, burning durations, and heating substrates (adipose or air) [131]. They concluded that the blue ALS with a wavelength of 420 to 470 nm, in combination with a yellow filter, produced the best results over the full range of temperatures and durations, asserting that ALS is a viable technique when recovering cremated bone from fire scenes and can provide insight into post-mortem and peri-mortem burning events. These conclusions are supported by more recent research by Schariatmadary et al (2023) who identified a spectral shift in bone fluorescence as a direct result of burning temperature [158].

Gallant 2013 also investigated burned bone but utilised a YAG (Yttrium Aluminium Garnet) green laser light source (532 nm) coupled with an orange filter to examine 20 semi-fleshed fresh porcine bones of different types including scapulae, humeri, and whole fleshed pig heads, burned in a simulated house fire [143]. A UV light source (350 nm) was also used for comparison. Excitation with the YAG laser produced a characteristic 'molten lava' appearance (shown in figure 19), resulting from differential burning of bone and flesh, highlighting areas of exposed bone amongst patches of charring. Although the UV light did stimulate some fluorescence in the bone samples, it was comparatively weaker than the YAG green light, rendering the bone samples indistinguishable from the surrounding fire scene debris. The YAG laser was described as producing intense levels of fluorescence and creating variable fluorescence levels compared to other items at the scene [143].

Figure 19: The 'molten lava' appearance of bone due to partial burning, stimulated using the YAG laser [143]

Although Gallant's (2013) trials with UV light were unsuccessful, historically UV fluorescence of bone has been a prominent avenue of research, predominantly within archaeological studies, including burned bone, as it is frequently encountered during

excavations [130]. Several studies state that stimulation of bone with UV light creates a distinctive blue, whitish-blue, or green autofluorescence [130, 304, 305], and that monitoring changes in colour and intensity can be used to estimate post-mortem interval and assess bone preservation, with the ultimate aim of discriminating between modern and archaeological bones and highlighting samples best suited for further analysis [148, 304]. Hoke et al (2013) suggested that there was a correlation between the colour of the autofluorescence produced and PMI, stating that yellow fluorescence is more abundant in older bone samples, and was only observed within their dataset in bone samples over 90 years old [123]. Older studies proposed that homogenous blue fluorescence was indicative of fresh or more modern specimens up to 100 years old, whereas inconsistent and decreased fluorescence levels were indicative of compromised bone integrity associated with antiquity and/or taphonomic degradation, with complete loss of fluorescence in specimens between 500-800 years old [306]. Hoke et al (2011) refute this theory, as they observed blue fluorescence in bone samples over thousands of years old, as well as in compromised bone samples, concluding that UV fluorescence offers a non-destructive screening alternative to histological examination, particularly for well-preserved archaeological bone samples [304].

In a case study conducted by Sheirs et al (2015), a 360 nm UV light source was used to examine burned skeletonised human remains retrieved from a construction site. They viewed the subsequent fluorescence with standard safety glasses coated with ‘anti-UV coating’ and photographed the results. The authors observed characteristic differential fluorescence across the bones, where non-fluorescent charred areas of bone were bordered by areas of yellow/orange fluorescence, attributed to accelerated loss in organic content due to fire exposure. This produced a clear distinction with the typical blue fluorescence exhibited by the unburned bone [307], as shown in images 20 a-b below.

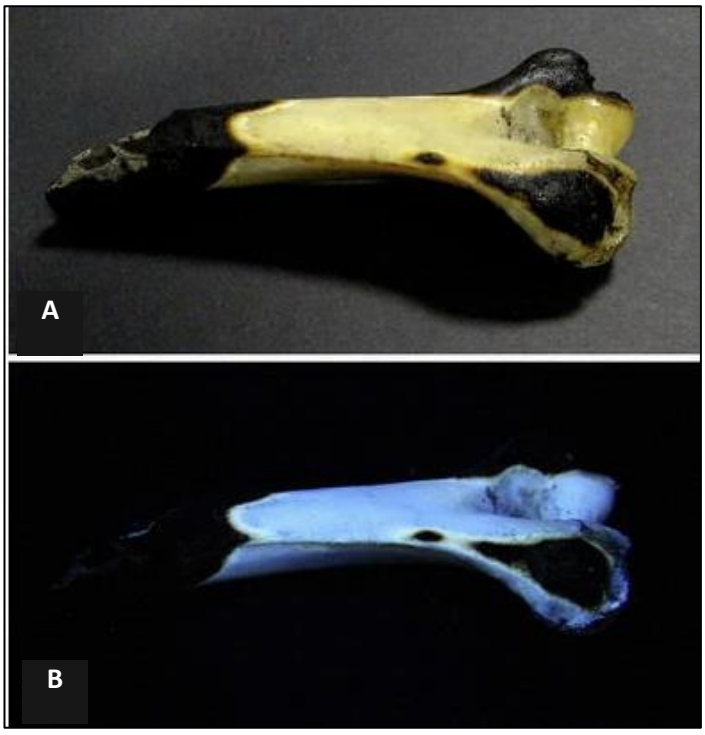

Figure 20: A) A humerus photographed under normal light conditions. B) The same humerus photographed using UV, showing how the brown area and white border emitting white light blue/white fluorescence, and the burned areas not responding to the ALS [307]

They surmised that UV light would be beneficial for determining the burn patterns of burnt remains, including potentially how the body was positioned at the time of burning, as well as discerning between bone alterations caused by burning rather than environmental or taphonomic origin. They went on to echo the same advantages as previous papers with regards to the technique's simplicity and easy implementation at crime scenes but did state that their results were not in full support of other studies due to differences in observed fluorescence colour [307]. However, they concluded that these differences may be the result of inter-observer interpretation, as well as differences in UV wavelength, and the use of different burning temperatures. Consequently, it is suggested that a quantitative approach would help to reduce these challenges and facilitate more informed interpretations. Subjective and qualitative assessment of bone autofluorescence is recurrent in literature [135, 143, 266, 304, 307], therefore a major facet of this PhD thesis was the development of a bespoke quantitative computer program to measure observed fluorescence; the Osteo-Fluorescence calculator (OFC), the specifics of which are discussed in chapters 11.0, and 13.3.3.

Ultimately the selection of an effective filter is dependent on the specific wavelength of the light source in use, as well as the ALS's individual specifications [212]. The use of many different models of ALS, and subsequently different wavelengths, described throughout research may go some way to explaining why there is such inconsistency regarding recommendations for optimum wavelength and filter to visualise bone fluorescence. Similarly, the purpose of the ALS examination is also influential. Although UV light has successfully been used to stimulate fluorescence of bone sections within a laboratory, the aim of these studies was to understand the events surrounding the deposition of the bones; such as burning conditions [142, 307] the preservation, and the PMI [123], as well as distinguishing between archaeological and modern specimens [304] rather than detecting the presence of bone. Therefore, although the results of these studies are informative and contribute to the greater understanding of bone fluorescence, many utilised expensive high-powered microscopes and other non-portable equipment which cannot and would not be used in the field, and therefore are not fully translatable to this PhD project.

On the other hand, when UV light was used in an attempt to identify bone at a simulated crime scene, as reported by Gallant (2013), the fluorescence produced was considered not strong enough to facilitate identification [143]. In their study, Krap et al (2021) also acknowledged that blue light provided greater bone fluorescence intensity compared to UV light, but the blue light was visible and the requirement for coloured glasses and filters impeded examination, particularly in comparison to the non-visible UV light [142]. However, the distance between the specimen and the light source was not stipulated in Krap et al's study, but seemingly standardised for both light sources. The excitation environment was described as a closed box with a hole for observation and a hole for the insertion of the light sources. Therefore, it could be suggested that the weaker and non-visible UV light would naturally be better suited to a small, enclosed space, in comparison to the intense visible blue light, which could be visually overpowering. As each light source has individual specifications and capabilities it may have been beneficial to adapt the distance from the specimen for each light source, and therefore make a more objective comparison with the light sources performing optimally. This would have ensured the most representative results. Throughout this PhD thesis, two different blue light sources were used individually and compared, but preliminary

method refinement tests were carried out to ensure that the distance from the specimen, light source and camera were optimised for each light source.

As mentioned previously, Green et al (2019) concluded in their study that bone fluorescence stimulated by blue light was visible up to 100cm [133], therefore blue light is arguably better suited to a more open environment, where there is greater distance between the user and the items under observation, such as in the field at crime scenes, archaeological excavations, and mass disasters etc. More specifically, the more intense fluorescence makes blue light a better candidate for bone identification and screening, as the higher intensity could create greater contrast with the deposition context, increasing visibility to searching investigators. The use of ALS equipment and associated filters would probably be adopted readily by forensic investigators as they already routinely use this technology to search for latent evidence such as body fluids [126, 308]. Furthermore, due to the shorter wavelength UV light transmits higher levels of radiation energy compared to the longer wavelengths of blue light and therefore can be more damaging to human eyes and skin [178]. This poses a larger risk at crime scenes as the wavelengths are not visible, which may lead to inadvertent exposure if multiple team members are in attendance and unaware of its use and intensity [264].

Historically, UV light sources were used at crime scenes to locate latent evidence such as fibres and hair but only after the recovery of biological evidence [207] as UV light is known to damage biological samples such as semen and saliva, including degradation of DNA, which would be detrimental to downstream analysis [250]. Although there have been no publications directly studying the effect of UV ALS examination on bone structure in this context, the photodegradation effects of solar UV rays in skeletal remains is well known, with prolonged exposure producing a bleached appearance in exposed skeletal surfaces [30, 146]. No such effects have been discussed in conjunction with blue wavelengths, which further supports its use in crime scene contexts. This sentiment is reflected in the few published field studies using ALS to find bone in terrestrial and underwater environments, which concentrate on the use of blue light approximately 400-450 nm.

8.2 – FIELD STUDIES IN BONE FLUORESCENCE

In a study conducted by Harte et al (2020), six simulated clandestine graves were populated with examples of common trace evidence including small porcine bone fragments (10mm^3 and 5mm^3) hair, cloth, and lead [137]. Three graves were excavated in daylight and three graves were excavated in darkened conditions (under a tent) using only blue ALS (455 nm) and an orange filter. As the study was focused on archaeological applications of ALS, excavations were completed by three archaeologists of differing experience levels, excavating one gravesite with ALS and one in daylight each. Some challenges were reported due to unfamiliarity with excavating graves in the dark and the addition ALS equipment, but results showed bone fragments were more than twice as likely to be found using the ALS device compared to standard daylight excavation [137].

However, in total, fewer items of trace evidence were recovered during the ALS excavations compared to the daylight sites, as items that did not fluoresce, such as lead, were not detected due to the darkened conditions. Ostensibly, this infers that the ALS searches were not as effective as standard daylight excavation, but realistically it emphasises that ALS is a supplementary tool to assist investigators, rather than to replace existing search strategies, and suggests that ALS can be used successfully to detect skeletal remains. Although this study provided insightful empirical data to help understand the recovery rates of trace evidence it isn't entirely reflective of how ALS would be used in the field.

On the other hand, Brown and Christensen (2018) devised a study exploring the use of ALS to search for bone in a surface deposition scenario. ALS (450 nm with orange filter) was used to search for 48 randomly distributed porcine bone in a designated area of woodland in the grounds of George Mason University, Virginia, USA [266]. Groups of two untrained volunteers with no anthropological or law enforcement experience were deployed to find bone using either standard line search during the day, ALS only search conducted at night, or a combined methodology of line search during the day followed by an ALS examination at night. As participants were unfamiliar with bone morphology, line search procedure, and bone fluorescence, a brief explanation and demonstration was also provided prior to commencement. Results showed that the use of ALS on average significantly boosted the number of bones found by the volunteers. Only 40% of

bones were recovered during the daytime line search, which rose to 69% of bones recovered during ALS searches. When combined, the daylight line search followed by ALS examination at night led to the highest number of bones being found, totalling on average 78% [266].

These results support the theory that blue ALS is particularly suited to crime scene screening, and when combined with established search strategies can be effective at locating bone. The use of untrained volunteers was also informative, as the expectation would be that police officers and crime scene investigators, who are generally unfamiliar with bone morphology, would most likely be the end users of this technique. Conversely, the archaeologist with the least amount of experience in Harte et al's study (2020) struggled the most to find the trace evidence, comparatively finding the fewest elements, as well as underestimating the depth of the grave cut [137]. On reflection, the use of ALS at a dark grave site is arguably a much more advanced scenario in comparison to searching a stretch of woodland, requiring more specialist skills and stratigraphic knowledge. Therefore, it is understandable that an individual with relatively limited excavation experience would be substantially hindered in this context.

It is noted that bones used by Brown and Christensen (2018) were deposited on the surface and not buried as in Harte et al (2020), and therefore were relatively unobscured, aiding ALS identification [266]. Moreover, any adherent soil or vegetation would most likely reduce observed fluorescence levels blocking the light from interacting with the bone, an issue that would be more apparent in a burial environment. Brown and Christensen (2020) however did state that despite some instances of low-level fluorescence from environmental debris (leaves and flora), the volunteers had no issues discerning the bone specimens [266]. This may have been facilitated by using pre-processed bones, prepared using warm water maceration. The influence of maceration will be discussed in more detail in chapter 13.0 and is the focus of a pilot study within this PhD due to its frequent use in bone fluorescence research. Brown and Christensen acknowledged that further experiments using non-processed bone conducted at different times of the year with different weather conditions would provide a more comprehensive picture of the effectiveness of ALS searches [266]. Harte et al (2020), also used defleshed bone samples but did not detail how this was achieved [137].

In addition to terrestrial contexts, a single aquatic preliminary field investigation has been conducted to date. Christensen et al (2014) tested the use of ALS underwater firstly in a freshwater lake and then a deep marine environment using a 450 nm wavelength coupled with a yellow filter. They commented that bone was detectable in both environments, but fluorescence observation was easier in the deep marine environment due to darker working conditions which meant less interference from ambient light [135]. They also stated that shortwave light is particularly beneficial for underwater scenarios, as longer wavelengths are absorbed more readily underwater, as previously mentioned in chapter 7.0. In theory, the use of shorter wavelengths of light could allow investigators to search for bones for longer and at greater depths, which could assist with the investigation and recovery of skeletal remains from archaeological shipwrecks, or maritime and aircraft disasters [135].

To date, this study by Christensen et al (2014) is the only underwater ALS study focused on bone, and as it is a pilot study it is significantly focused on feasibility testing, primarily whether aquatic ALS analysis is possible, and the parameters of the Rofin PoliLight-Flare® light source [135]. Although the study was successful in demonstrating that underwater bone fluorescence was attainable, there is no justification of why a yellow filter was chosen over other colours, when orange has been used in the past, and only qualitative, subjective observations of bone fluorescence were conducted. Consequently, there is also no quantitative indication of how the water environment may impact the level of fluorescence seen, other than how greater levels of darkness improved fluorescence visibility, particularly in comparison to terrestrial bone fluorescence. A selection of human and non-human bones was included in the study, but it is unclear how these bones were obtained or prepared for examination, whether they were fresh or archaeological, or specifically which samples were used for underwater testing. As only one light source was used, it is difficult to know whether the results seen in the study would be replicable between different light sources, particularly as no photographs were included in this study.

As a result, the main aim of this PhD research was to examine the use of alternative light sources to detect skeletal remains underwater. Research questions were constructed to address some of the points highlighted by Christensen et al's (2014) study. More

specifically, to determine whether aquatic bone fluorescence can be produced with different forensic light sources in conjunction with orange and yellow barrier filters, as both have proven successful in terrestrial contexts [131, 132, 146, 256].

A comparison between aquatic and terrestrial bone fluorescence was also undertaken using both fresh and macerated bone, to see if there were any observable differences in the intensity of the fluorescence emissions. Fluorescence emissions are generally weaker compared to the original excitation wave, as energy is consumed during molecular excitation within the sample and subsequent re-emission [309]. As water is denser than air, and refracts light [168], energy would also be depleted as it passes through the water before and after interacting with the bone. Therefore, it is possible that fluorescence signals could be impeded in submerged contexts, leading to lower observed fluorescence levels. However, reducing the temperature of a substance is known to increase fluorescence intensity [124]. Water temperatures are often much lower and more stable than terrestrial contexts, particularly at greater depths, such as in a marine environment [22], and therefore may boost observable fluorescence. Implementation of a bespoke software program (the OFC) was used to quantify terrestrial and submerged bone fluorescence in an attempt to eliminate subjective observation. Differentiation between bone and non-bone items has also been a recurrent theme in bone fluorescence literature and presents a major consideration when proposing this technique for use at crime scenes.

8.3 – DIFFERENTIATION

Many materials also possess autofluorescence properties and will naturally fluoresce when exposed to ALS, such as common household lubricants, cleaning products, food items, and cosmetics [310], and as previously discussed in chapter 7.4; fibres, GSR, body fluids, and hair can all be stimulated by wavelengths within the blue light spectrum [120, 137, 283]. Similarly, some surfaces on which the target material is deposited can also produce fluorescence, for example some textiles may fluoresce if washed with detergents containing optical brighteners [279] and background colouration can make some fluorescence difficult to see [127, 250]. This additional fluorescence is referred to as a false positive [267] and has been reported by multiple authors when assessing body

fluids such as semen and saliva when using ALS, as many different types of body fluids respond to the same broad excitation range [127, 250].

However, the liquid nature of biological fluids means that morphologically they will appear similar, especially under ALS fluorescence, where characteristics such as colour and texture may not be as obvious [308]. Similarly, fluids can be absorbed or dried out, depending on the deposition surface, and physically form a low, almost 2D profile when in-situ, particularly if low in volume or transparent. Conversely, bones are 3D and opaque, and even smaller fragments would likely stand out against a flat substrate therefore it could be argued that false positives could be less problematic when detecting osseous material. However, the taphonomic environment can drastically alter the appearance of bone [54, 102, 106, 108] and although basic observations based on the physical attributes of the fluorescing materials would assist with triaging and identification, further research is necessary.

Whole bone is inherently much easier to identify due to the size, shape, texture, and the presence of osteological landmarks, particularly on larger or more recognisable bones such as os coxae, long bones, or skulls. However, the skeletonisation of human remains is usually a long process occurring over an extended post-mortem interval [28]. Therefore, skeletal remains will be interacting with the deposition environment for sustained durations which inevitably leads to changes in bone appearance and integrity [89]. Drastic changes to bone appearance can alter or eliminate osteological characteristics, making bone resemble other items such as wood or stone [53]. Disarticulation, fragmentation, bleaching, colour changes, increased porosity, and fractures are common examples of taphonomic bone modifications which significantly alter the appearance of bone and may lead to bones being disregarded or missed during recovery operations [89, 102]. More complex scenarios such as mass disasters, aquatic depositions, and criminal cases can further exacerbate issues with identification, through comingling of skeletal remains with other individuals, faunal bones and environmental debris, as well as additional trauma through burning, dismemberment, and crushing [311], and context specific alterations such as the erosive windowing and rounding of osteological features associated with movement through water [109].

Bones in aquatic contexts experience a range of specific taphonomic alterations including colour changes due to soil impaction from lying in still bodies of water, or through tumbling from waves and currents [54, 102, 106]. Algae growth on the exposed surface of bones in damp, but sunlit environments can create a distinct greenish appearance whereas extended submersion in a marine environment can lead to bleaching, resulting from the breakdown and leaching of the organic content and the deposition of salt crystals, producing a chalky white appearance [53] as shown in figure 21. Marine bleaching manifests uniformly as complete submersion enables access to all bone surfaces [106], while differential bleaching across the skeletal assemblage is seen in terrestrial deposition contexts due to the UV photodegradation only damaging the exposed surfaces [106, 108]. Erosion, pitting, rounding, and widowing of the foramina occur in aquatic contexts where bones are exposed to the repetitive motion of waves and currents combined with any suspended precipitates such as sand or silt, submerged or floating detritus, and abrasive action against the sea or riverbed [90, 109]. This leads to thinning of the cortical bone and exposure of the trabecular bone underneath creating a spongey appearance [106]. Fracturing, splintering and breakage of skeletal elements can also occur alongside possible separation of the epiphyses and breakage of protuberances, processes, and tuberosities [53], all of which would normally assist investigators with bone recognition and identification [107, 116].

Figure 21: Photograph of the distal epiphysis of a human femur demonstrating bleaching of the cortical bone and leaching of fat (arrow) due to prolonged submersion in a marine environment [106]

Dispersal of osseous material is also a common occurrence in cases of skeletonised remains. Submerged bones can become scattered and displaced due to tides, currents, and scavengers with individual bones travelling through water at varying rates [90]. Irregular and heavier bones such as the pelvic innominates or femora generally travel only short distances due to their greater density, complex topography, and size, as there is greater likelihood of them becoming obstructed by terrain [29, 57, 90, 115]. More regular, lighter, more cylindrical bones such as humeri, or small elements like the phalanges have a higher trabecular to cortical bone ratio, making them less dense and more buoyant, and therefore able to move much greater distances [29, 57, 90, 115] . Subsequently, bones are often found in insolation and often opportunistically once they wash ashore [90, 109]. In surface depositions exposed bones may be displaced from the original deposition site by scavengers, with some American research showing vultures, wolves, coyotes, and rodents moving bones many metres from the original assemblage during the consumption of tissues or taking bones back to their nests and dens [112, 113]. Whole buried skeletons may also become displaced due to construction work or farming, exposing clandestine graves or archaeological settlements, and extensive flooding may wash bones into rivers and outlets [57, 114]. Scavenger activity can also leave traumatic changes on the bone surface modifying skeletal landmarks, obscuring pathologies or injuries, and overall compromising bone integrity [111].

Consequently, it is likely that when searching for bones at crime scenes, the osseous material encountered could be incomplete, damaged, and potentially unrecognisable as bone. This theory is iterated in the studies conducted by Brown and Christensen's (2018) and Harte et al's (2020), who omitted whole bones from their ALS bone fluorescence field studies in favour of smaller bone fragments and less obvious skeletal elements such as phalanges, to better represent disarticulated skeletal assemblages encountered in real life scenarios [137, 266]. In general, forensic anthropologists do not routinely attend crime scenes, often only becoming involved once potential skeletal remains have been identified [1]. Consequently, the initial responsibility of locating possible bones falls on the investigating crime scene officers, who are not routinely trained in osteological examination and identification. Therefore, an easy-to-use screening method, such as ALS technology, poses substantial benefit to search teams, to help distinguish between bone and other deposition debris.

As demonstrated by the archaeologists and volunteers in Brown and Christensen's (2018) and Harte et al's (2020) studies, ALS would require little training to successfully locate bone, particularly for crime scene investigators who already use ALS as part of routine examination for body fluids and latent evidence [137, 266]. What's more, as the blue wavelengths of light are non-destructive, unlike UV light, use of ALS would eliminate the risk of damaging any potential evidence or damaging an already compromised bone [312], as well as reducing the risk to the user [287]. As a result, many of the bone fluorescence studies focused on ALS as an on-site screening tool, have included a differentiation element to assess whether bone can be distinguished from other materials [133, 135, 256].

Through a series of laboratory experiments using archival human bone and teeth, and case studies, Craig and Vezaro (1998) verified that skeletal material could easily be differentiated from surrounding samples of rock, as bones and teeth exhibit fluorescence 20–50 times stronger than that of rocks in their sample [256]. Wavelengths of between 380-540 nm coupled with orange glasses provided the most successful results [256]. The technique proved particularly useful when examining skeletal remains of a new-born infant who had reportedly died during birth and was buried shortly after. The infant remains were exhumed two years later, and using ALS, investigators were able to identify

the bone fragments whilst sifting through the soil in the laboratory. The non-destructive and non-invasive technique allowed conservative handling of the fragile skeletal remains [256].

As previously mentioned, Green et al (2019) also conducted differentiation studies comparing the terrestrial fluorescence results of rocks, sand, dog tooth enamel, dog tooth root, and various bones including human clavicle, dog ulna, and porcine epiphysis with soil, frozen porcine bone, boiled porcine bone and bone dust. Brightness results were compared using ImageJ software, with results indicating that 450 nm light in combination with an orange filter allowed the best discrimination between bone and non-bone objects, with rock exhibiting the least amount of brightness and the boiled pig bone emitting the most, although exact values are unclear [133].

Identification of burned and cremated skeletal remains is especially difficult as many different materials when burnt can imitate the appearance of bone [313]. For example, during investigations into the 2009 bushfires in Victoria, Australia, burnt floor tiles mimicked the appearance of cranial fragments and burnt glue fragments could be mistaken for dentition, as shown in figures 22-23 below [311].

Figure 22: Burnt floor tile that resembles human skull, recovered from the remains of a burned building during a bush fire in Victoria, Southeast Australia, 2009 [311]

Figure 23: Melted glue fragment, recovered from the remains of a burned building during a bush fire in Victoria, Southeast Australia, 2009, which resembled a human tooth [311]

Similarly, Ramsthaler et al (2013), in their publication regarding recovery of badly burnt skeletal remains, stated that, in their personal experience, the heavy soot deposits and intermingling of bone fragments with fire scene debris led to osseous material being missed frequently at fire scenes [314]. They also expressed that several false positives were caused by items that were not bone when using ALS technology, so therefore it should be used with caution [314]. However, the paper did not provide detail regarding what wavelengths were used and what the non-bone items were, therefore it is difficult to interpret whether optimal wavelengths were used. This contrasts with Gallant et al (2013) who noticed variable levels of fluorescence during their simulated fire scene, leading to the potential for differentiation between bone and adjacent objects, specifically a blanket [143].

In addition to underwater testing, Christensen et al's (2014) study also reported the possibility of differentiation between human and non-human bone and other debris such as stones, shells, and coral in a terrestrial laboratory environment [135]. Using ultraviolet, 450, and 530 nm wavelengths, in combination with a range of coloured filters in red, orange, and yellow, they compared the fluorescence of 32 non-bone items comprising of shells, coral, rocks and beach glass, with 8 human bone samples, 6 non-human bone samples, and 2 non-human tooth samples. They concluded that bone and teeth could easily be distinguished from the non-bone items when using 450 nm with a yellow filter as non-fluorescent items appeared dark or black, whereas bone and tooth fluorescence were observed as bright yellow to orange. The differences in fluorescence were hypothesised to be due to varying collagen content across the samples [135]. This result promises the potential for differentiation but as no quantification of the fluorescence or collagen was conducted and no images were provided it is difficult to truly assess these results.

Unfortunately, the number of non-bone items used in each study was relatively few, with many of the reported results based on subjective visual assessment by one individual rather than quantification [133, 135, 256]. Although Green et al (2019) did carry out quantification based on a methodology by Miranda et al (2017), there were no figures reported in the final article, so it is difficult to fully appreciate the range of fluorescence values witnessed and consequently the degree of possible differentiation [132, 133].

However, cumulatively the results of these studies do indicate that differentiation between bone and other items is possible but requires further research. Therefore, additional research questions in this PhD concentrated on quantifying the relationship between the organic component of bone and the level of fluorescence seen, including the creation of negative and positive controls derived from bone, and comparisons with other common non-bone items. Addressing these research themes is vital to understanding the aetiology of bone fluorescence, producing foundational data that can better inform interpretations regarding the use of ALS for real world applications, and shaping a potential operational methodology. Although true differentiation would be conducted microscopically [315, 316] or through elemental analysis and/or histological examination of the bone microstructure [317-319], the ability to preliminarily triage potential bone at the scene could help to speed up crime scene searches, reduce misidentifications, and maximise the number of bones recovered. Overall, this ALS technique could help to save time, money, and resources, and potentially help to recover more of a missing person so that they can be returned to their family.

However, the preservation of the examined bones, as well as the composition of the deposition environment, will influence the intensity of observed fluorescence levels. Therefore, it is integral to understand bone composition to firstly interpret the origins of osseous autofluorescence and then subsequently explore how extrinsic influences may lead to bone alterations and influence fluorescence emissions. Without this knowledge it would be impossible to fully determine if ALS could be used successfully in real world forensic scenarios.

9.0 - BONE COMPOSITION AND TAPHONOMY

Bone is a dynamic and highly organised connective tissue [320] comprising of a unique 3-dimensional multiscale microstructure [320, 321] adapted to provide flexibility, strength, and support [322]. Microscopically, this intricate composition is referred to as the bone matrix [129], and in mammalian and human bone is a composite of three main components; water, inorganic hydroxyapatite, and a protein rich organic aspect comprising primarily of collagen [131]. Structurally the hydroxyapatite crystals provide the robustness and stability [323] and are interspersed between large bundles of collagen fibrils which provide flexibility [313]. Figure 24 below illustrates the intricate composition of the bone matrix in mammalian bone.

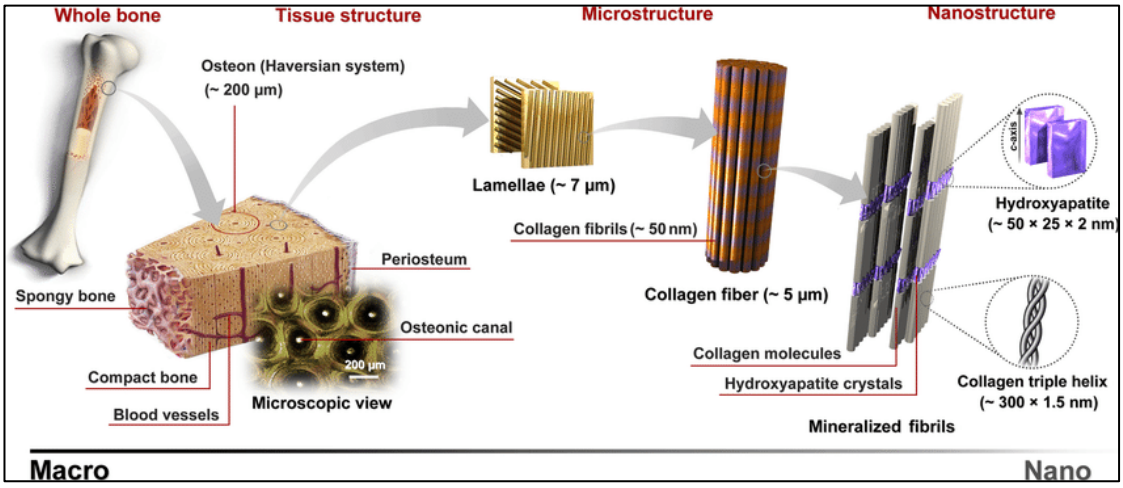

Figure 24: Diagram of bone composition [323]

9.1 – COLLAGEN

Collagen is considered the most abundant protein in the natural world [324] and constitutes one third of proteins within the human body [321]. However, there are thought to be up to 20 [325, 326] genetically distinct types of collagens resulting from the varying configuration of molecular cross-linking of amino acids throughout its triple helical structure [326, 327]. Consequently, each collagen type has structural specificity and individual biochemical properties for focussed functionality [326]. Types I, II, III, IV, and V are the most researched [328], as types I to III constitute between 80-90% of all collagens within the human body [326]. In bone, type I collagen constitutes

approximately 80-90% of this organic component [320, 321] and it is also found in tendons, ligaments, and skin due to its more elastic capabilities [328]. Conversely, type II is more robust and is largely confined to cartilages to provide shock absorption at the joints [327]. Types III to V are more specialised, with type III often found with type I in elastic muscular tissues such as arteries [329], and types IV and V localised to basement membranes [330]. The molecular composition and the general distribution of collagen can also vary by species and tissue type [328], and play a significant role in healing, disease, and aging [328, 331, 332].

As a result, there has been extensive research about collagen in a wide range of disciplines such as regenerative medicine and bioengineering [326], as well as archaeology and forensic science [333]. However, most significantly it has also been acknowledged as one of the most important tissue components for natural fluorescence [328] as many papers cite the complex amino acid cross-linking as the potential source [321, 327, 328, 334]. Several studies have specifically identified aromatic amino acids such as phenylalanine, tryptophan, and tyrosine as receptive to short wave UV light [132, 328, 335] and are classified as natural fluorophores. A natural fluorophore is a substance that is capable of emitting light when excited by an external source of radiation energy such as a forensic light source [122]. In body fluid research, tryptophan is thought to be the main fluorophore responsible for autofluorescence in saliva, whereas in semen it is thought to be the flavoprotein riboflavin [250]. However, the origin of the natural fluorescence of bone is still unclear.

9.2 – THE ORIGIN OF BONE FLUORESCENCE

The relationship between bone composition and autofluorescence is poorly understood with several conflicting theories reported in literature. There are four main theories surrounding the source of bone fluorescence a) the organic component, most likely the collagen content, (b) stimulation of amino acid fluorophores, (c) absorption of antibiotics, specifically tetracycline, and (d) the mineral aspect of bone.

Prentice (1965, 1967) stated that bone autofluorescence is primarily due to collagen content rather than any incidental absorption of other substances, but also suggests that fluorescence intensity is dictated by osteon maturation, inferring that the older the

osteon the greater the intensity of observable fluorescence when microscopically examined with UV light (peak 360 nm) [129, 336]. Prentice goes on to say that bone samples taken from younger individuals, where there is an abundance of new osteons, showed poor levels of autofluorescence compared to bone samples from older individuals where advanced mineralisation had occurred. Superficially, this would suggest, that intrinsic fluorescence is linked to the mineral aspect of bone, but after demineralisation with EDTA, the level of autofluorescence remained unchanged, which suggests that intrinsic fluorescence is not associated with the mineral aspect of the bone. These results are reflected in a more contemporary study conducted by Capasso et al (2015).

Capasso et al (2015) [122] compared the autofluorescence of modern and archaeological bone sections using confocal laser scanning microscopy (excitation wavelength 488 nm). Homogeneous bone autofluorescence was noted in untreated bone sections, with a dramatic increase in absolute fluorescence frequency from 39.93 AIU (arbitrary intensity units) to 1659.53 AIU, once demineralised with EDTA. Conversely, bone sections digested with bacterial collagenase suffered a drastic reduction in autofluorescence intensity (which was also restricted to the walls of the lacunae and canalicular system) from 39.3 to 19.33 AIU [122]. These results support the hypothesis that the organic component is responsible for the autofluorescence of bone.

Drzazga et al (2011) investigated the spectroscopic intensity of bone fluorescence in femora and mandibles of new-born rats. They established that fluorescence intensity increased with age (7 to 28 days) and postulated that the increase was the result of additional non-collagenous proteins active during bone development [337]. However non-collagenous proteins are thought to only constitute a maximum 5% of bone volume [338], and therefore it seems unlikely that this small volume would be the primary source boosting fluorescence. Initially the findings from these studies are at odds with the most recounted hypothesis in literature, that collagen is likely responsible for autofluorescence, particularly as juvenile skeletons are generally thought to contain much higher levels of collagen compared to adult skeletons, as mineralisation increases with biological age [334, 339]. However, in early bone development, bones begin as a cartilaginous framework made from hyaline cartilage where upon osteoblasts deposit

osteoid which mineralises into new bone, a process known as ossification [339]. There are three different types of cartilage in the human body, hyaline cartilage, fibrocartilage, and elastic cartilage, but crucially hyaline cartilage, which makes up most of the collagen in the body [340], is made from type II collagen rather the type I found in bone [341]. As mineralisation occurs over time, the concentration of type I collagen will increase as the bone grows, which could explain the higher levels of fluorescence observed by Prentice (1965, 1967) [129, 336] and Drzazga et al (2011) in adult skeletons rather than juvenile [337]. This hypothesis is further supported by Maidment (2017) [134] where retained articular cartilage on manually defleshed porcine bones was seen to retard ALS stimulation (450 nm), as shown in figures 25 and 26 below.

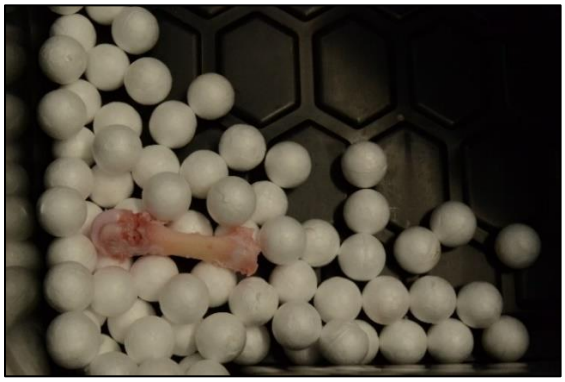

Figure 25: Manually defleshed porcine phalange photographed under natural light.

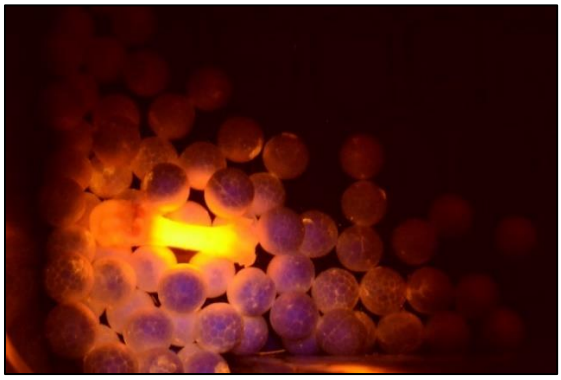

Figure 26: The same manually defleshed porcine phalange seen in fig. 25 but photographed using blue light (450nm) coupled with an orange barrier filter, demonstrating strong bone autofluorescence.

9.3 – AMINO ACIDS

Many other studies across a range of disciplines including biomedical science, forensic science, and archaeology have specifically identified the organic component of bone as the source of bone autofluorescence [142, 342, 343]. Swaraldahab and Christensen (2016) also suggest that the organic component of bone, specifically collagen, is the likely source of bone fluorescence, but also name two common amino acids: tryptophan and tyrosine as the natural fluorophores possibly responsible [146]. This theory has since been echoed in research conducted by Harte et al, (2020) Ren et al, (2008), and Via & Jerele (2023) who stated that residues of fluorescent aromatic amino acid rings tryptophan, tyrosine, and phenylalanine are responsible for bone autofluorescence [137, 344, 345].

Tryptophan, tyrosine, and phenylalanine, are amino acids known to have autofluorescence properties and can be found in a variety of substances, including body fluids such as saliva [250]. Phenylalanine is a precursor to tyrosine, which eventually metabolises into neurotransmitters including adrenaline, noradrenaline, and dopamine, which help regulate mood and neurological function [346]. It is classified as an essential amino acid, meaning the human body does not naturally produce it and therefore it needs to be acquired through diet [347]. However, phenylalanine is not routinely found in type 1 bone collagen or bone and is considered to only contribute a negligible amount to the intrinsic fluorescence of proteins due to low absorptivity [348] therefore it is unlikely to be responsible for bone fluorescence.

In bone, amino acids tryptophan and tyrosine are instrumental in the homeostatic regulation of bone osteogenesis and resorption [347, 349]. Phosphorylation of tyrosine residues moderates the production of osteoclasts to maintain healthy levels of bone resorption [350]. Tryptophan is the catabolic precursor to several vital bioactive metabolites including melatonin, serotonin, niacin, and kynurenine, which are fundamental in the regulation of the body's immune system, circadian rhythm, and neurotransmitters [351]. More specifically, the constituents of the tryptophan to kynurenine catabolic pathway are influential in the cellular differentiation of mesenchymal stem cells into osteogenic osteoblasts, required for bone growth and remodelling [352]. In their study investigating the UV fluorescence of new-born rats, Drzazga et al (2011) reported an increase in UV fluorescence emission intensity which they attributed to an increase in tryptophan residues as the rats aged [337].

Jamme et al (2013) describe how the level of tyrosine and tryptophan is dependent on bone microstructure, with osteocytes presenting a higher tyrosine to tryptophan ratio compared to the bone matrix [353]. They go on to state that they believe no other tissue type presents with a higher tyrosine fluorescence level than bone, but also simultaneously remark that tryptophan is thought to exhibit the highest levels of fluorescence compared to other natural fluorophores [353]. Tryptophan is also classed an essential amino acid, whereas tyrosine is nonessential and is produced endogenously [354]. This difference in aetiology may account for the localisation of the two amino acids within bone histology. Tryptophan is found in higher concentrations within the bone

matrix as it is absorbed through diet [351], and tyrosine is concentrated within osteocytes, directly contributing to bone remodelling [350]. Although tryptophan contributes to the development of osteoblasts and deposition of new bone, it is also a fundamental component of many other molecular interactions [352].

However, other authors suggest that tyrosine could be the primary amino acid responsible for autofluorescence in type 1 collagen, as although tryptophan is prolific in the natural world, and presents in low quantities in the bone matrix [355], it is not found in type 1 collagen [356]. Shen et al (2018) investigated the autofluorescence characteristics of tyrosine in type 1 collagen derived from bovine Achilles tendons. They reported that collagenase cleavage of type 1 collagen molecules resulted in increased UV fluorescence output due to exposure of additional tyrosine residues [357].

However, it is known that collagen composition varies between species and tissue type, as demonstrated by the disparities between cartilage and bone collagen [358]. More specifically, tendon usually contains two variations of the pyridinoline cross-linking, stemming from lysine aldehydes and hydroxylysine aldehydes [101]. However, the ratio of each type of cross-link is dependent on the anatomical functionality of the tissue [359]. For example, rat tail tendons only contain allysine cross-links, whereas Achilles tendon is predominantly hydroxyallysine [360]. Bone collagen cross-links are also predominantly hydroxyallysine [360], but as Shen et al (2018) only investigated bovine tendon, this comparison is more suggestive rather than truly translatable to human bone [357].

Type 1 collagen in bone exhibits unique cross-linking of tyrosine and another amino acid pyridinoline (also known as hydroxylysyl pyridinoline), which is also thought to possess some autofluorescence properties [359]. In medicine, pyridinoline residues in urine are an indicator for bone metastasis from urinary cancer primaries, such as prostate and bladder [361]. Pyridinoline is found in both type 1 collagen in bone and type 2 collagen in hyaline cartilage, but the positioning and quantity of cross-linking, and subsequent molecular structure, varies between the two. More specifically the concentration of pyridinoline cross-links in hyaline cartilage is much higher than bone [359], and the number of mature pyridinoline cross-links in bone is relatively low and thought to decrease with mineralisation [362]. Consequently, this indicates that pyridinoline may

not be responsible for bone autofluorescence, as other research suggests that mature mineralised bone produces higher levels of fluorescence [129, 336, 337]. Furthermore, despite all four of these amino acids being stimulated by an overlapping range of UV wavelengths, literature also reports individual optimal excitation wavelengths. Pyridinoline is considered to have a primary excitation wavelength within the near UV spectrum [363], typically up to 200 nm; tryptophan has a recognised excitation spectrum of 250-300 nm, and phenylalanine and tyrosine are reported to respond to the far UV range 300-400 nm [348]. However, these wavelengths do not correspond with the reported 450 nm blue light discussed in crime scene research in relation to body fluids and bone.

9.4 – BONE COLLAGEN AND THE DEPOSITION ENVIRONMENT

In studies investigating the degradation of bone, it is suggested that fluorescence may decline over time due to denaturation of the organic content and reorganisation of the mineral aspect [146, 364, 365]. Swaraldahab & Christensen's 2016 study comparing fluorescence (490 nm) of human and porcine bone of different antiquity, stated that fluorescence should not be expected in remains over 200 years old [146]. Similarly, Sterzik et al (2016) demonstrated that fluorescence intensity of human femoral bone sections decreased over time (max. PMI up to 49 years) and speculated that the reduction in fluorescence intensity was related to degradation of bone collagen [148], although the collagen was not quantified. Hoke et al (2013) correlated a spectral shift from blue to yellow/brown bone fluorescence when stimulated with UV light, in line with increasing PMI, with a considerable increase in yellow fluorescence observed in specimens over 1000 years old [123]. They also suggested that the loss of collagen and modification of the mineral phase contributed to the alteration in fluorescence [123]. However, they were unable to establish a relationship between PMI and fluorescence intensity, and they also did not measure the collagen content [123].

The variation in the fluorescence findings by Sterzik et al, (2016) [148] and Swaraldahab & Christensen (2016) [146] may also be explained by the presence of fluorescence quenchers present in the burial contexts. Hoke et al (2011) suggests that metal ions present in soil can interact with the crystalline calcium phosphate minerals, leading to reorganisation of the collagen fibres. This change in composition leads to a reduction in

fluorescence functionality and no longer responds to ALS stimulation [304]. However, the metal ions can also inhibit bacterial collagenases and therefore preserve bone microstructure [366] leading to a conflicting presentation of well-preserved but non-fluorescent bone [304].

Swaraldahab & Christensen (2016) go on to say that the deposition context and taphonomic influences will alter the rate and mechanism of collagen degradation [146]. In each of the three studies discussed in the paragraph above, most bones were retrieved from inhumations from varying geographical locations. The 28 bone samples used by Sterzik et al, (2016) were collected from six different cemeteries which exhibited four different soil profiles, which would have differentially influenced osseous preservation. This may provide some explanation as to why greater diversity in fluorescence intensity was noted in the samples with longer PMIs [148]. The intwined nature of bone collagen and apatite directly contributes to the persistence of bone in burial contexts [367, 368]. The presence of collagen can provide a defence against increases in mineral crystallinity, and similarly the hydroxyapatite can provide a physical barrier against bacterial infiltration and hydrolysis [369], which are thought to be the two primary drivers of collagen degradation [101].

Generally, more acidic, well-aerated, moist soils are shown to promote decomposition, whereas more alkaline, close textured, waterlogged soils can inhibit the rate of decomposition and possibly lead to preservation of some tissues if adiopocere forms [30, 368]. Highly conductive soils comprised of largely sand or gravel experience recurrent cycles of flooding with fresh water, leading to accelerated dissolution of bone mineral [365]. Buried remains are most at risk from microscopic diagenetic changes led by microbial tunnelling from environmental bacteria [370] as well as bacteria originating from the body [371, 372]. These cellular changes are exacerbated by repeated freeze/thaw or wet/dry cycles in uncovered burial environments, where the fluctuations in moisture and temperature can erode the mineral aspect and weaken the collagen fibrils [101].

In surface depositions, continuous exposure to direct sunlight will result in a bleached appearance of osseous material, as well as drying the bone surface and leading to cracking, splitting, and fraying, and degradation of the bone structure [108]. Osseous

material is also considered more vulnerable to underwater degradation due to its natural susceptibility to ion exchange [22, 106]. More specifically, prolonged submersion in a marine environment can lead to salt ions infiltrating the bone through its pores [106], leading to dissolution of the mineral content and increased collagen solubility [54], resulting in leaching of organic material . Consequently, the bone develops an overall bleached appearance [22, 54, 106] sometimes accompanied by chalky deposits on the bone surface [106]. However, due to the difficulties surrounding implementation of aquatic taphonomic studies, there is little understanding regarding the timescales of these changes [101, 105, 106, 373], as conclusions have been drawn from retrospective casework rather than experimentation [81, 83, 84], making it difficult to isolate the active variables.

Results of an MSc study by Maidment (2017) [134] suggests that salinity may be destructive to bone collagen. This study consisted of 12 manually defleshed pig humeri (*Sus scrofa domesticus*) immersed in 3 water types: sea, fresh and canal, over a 21-day period. At 7-day intervals, a humerus was removed, the amount of collagen quantified using thermogravimetric analysis (TGA), and the respective water chemistry analysed, including temperature, pH, conductivity, total dissolved solids (TDS) and turbidity. Statistical analysis demonstrated strong significant relationships between interval and collagen loss in the sea water ($R = 0.962$, $P = 0.019$) and canal water ($R = 0.925$, $P = 0.038$), as well as conductivity and collagen loss in the canal water ($R = 0.901$, $P = 0.050$) and fresh water ($R = 0.999$, $P = 0.000$), thus suggesting that the collagen changes could be linked to salinity. Literature states that high pH levels can also accelerate collagen degradation in submerged bone through weakening of the bonds between collagen and hydroxyapatite [144]. Environments with abundant water and oxygen, prompt microbial infiltration of bone collagen [374, 375] which is expedited by bone damage or fragmentation, providing further access points for microorganisms [376].

Conversely, other papers discuss how the protective structural composition of hydroxyapatite and collagen in bone helps to impede degradation, particularly from microbial infiltration [376, 377], requiring dissolution of the mineral aspect before the collagen content can be accessed [378]. Furthermore, aquatic decomposition is generally slower than decomposition on land [40], due to the usually lower water

temperatures and anaerobic conditions [62], particularly at greater depths [26, 61, 62]; which inhibit bacterial growth and scavenger activity [26]. Similarly, although salt water is eventually detrimental to collagen content, decomposition is further slowed in marine environments compared to fresh water due to the higher salt content also inhibiting microbial activity [60, 95, 188]. In a study by Pfretzschner (2004), they found that after one year of submersion, a human bone with an average diameter of 1 cm, only loses approximately 5–15% of its collagen and can remain in the early stages of bone diagenesis for between 50 to 500 years [375]. Consequently, there are no definitive timescales for survival of bone collagen underwater.

However, in their temporal study, Swaraldahab & Christensen (2016) used bones from the Terry Collection and other human skeletal collections, alongside 'fresh and 'semi-recent' porcine bones, to investigate the effect of time on bone fluorescence [146]. The human bones obtained from the skeletal collections had been macerated, prior to storage [379], as this is common practice in archival collections [152]. Swaraldahab & Christensen (2016) also stated that the semi-recent porcine bone group had been warm water macerated as part of a previous study, but the exact procedure was not disclosed. It appears that the fresh porcine group were the only samples that were not macerated. Maceration can be damaging to bone structures, particularly when using high heat or abrasive chemicals [149, 152, 156]. As the full maceration methods were not disclosed, and it is possible different maceration methods were used for the archaeological and porcine samples (due to being macerated at different times and institutions), it is difficult to judge the influence of maceration on the study's results. However, this variation in preparation methods may account for the greater spread of fluorescence values noted in the archaeological and macerated bone samples, as shown in figure 27, in conjunction with temporal degradation suggested by the authors. Furthermore, the fresh and semi-recent specimens were porcine in origin whereas the historical and ancient sample groups were human, so variation in species bone and collagen composition may have also introduced some inconsistency.

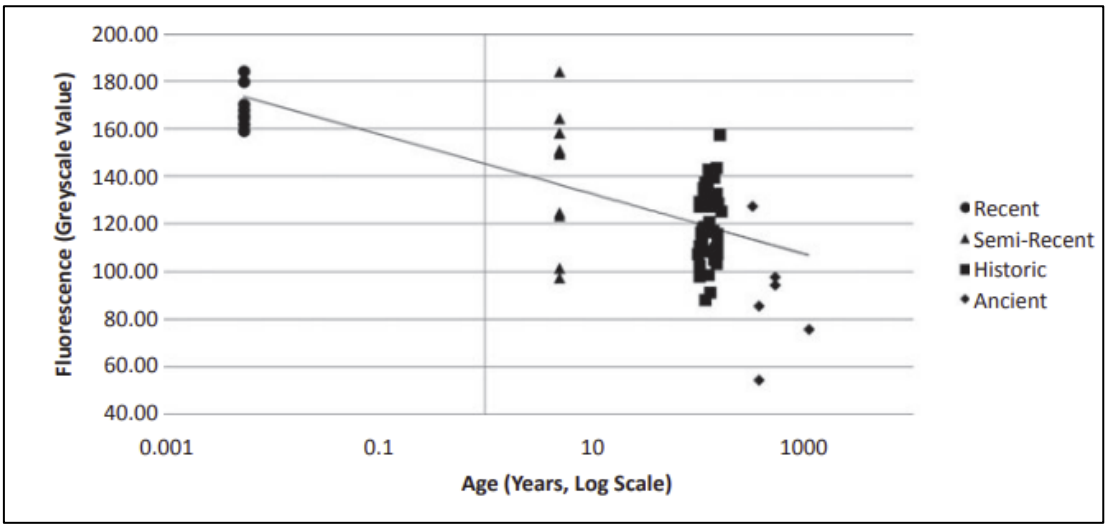

Figure 27: A line graph from Swaraldahab and Christensen (2016) [146] comparing the level of fluorescence intensity between four temporal groups of bones, with the largest spread in fluorescence values noted in the oldest ancient specimens.

Sterzik et al (2016) mentioned that most of the bones used in their study showed signs of adipocere when they were excavated. Traditionally adipocere is thought to preserve bone during decomposition [148], so would not have been destructive to bone structures so would not account for the variation in bone fluorescence noted in the samples over 30 years old. However, they did highlight that one sample which was 'very much affected by adipocere' showed very high levels of fluorescence. This result is especially relevant, as other authors have suggested that bacterial infiltration may be the source of bone autofluorescence, and as adipocere is driven by anaerobic bacterial action, this contributes to this theory.

9.5 – TETRACYCLINE BONE FLUORESCENCE

Several papers examining the fluorescence of archaeological skeletal remains propose that absorption of bacteria from diet or the deposition context may be the cause of human skeletal autofluorescence [122]. Specifically, the antibiotic compound tetracycline has been discussed by several authors examining the fluorescence properties of archaeological skeletal remains. When examining a Sudanese Nubian skeletal population (350–550 CE), Bassett et al, (1980) suggested that the consumption of ale and/or grain contaminated by streptomyces bacteria led to build of osseous tetracycline fluorescence [380]. Hummert & Gerven (1982) also reported the presence

of tetracycline labelling in skeletons excavated from cemeteries in Kulubnarti, Nubia dating between 550 and 1450 CE, including differential tetracycline labelling, where three rings of fluorescent bone was seen within an individual osteon [381]. This layered pattern of fluorescence has also been observed by Cook et al (1989) when examining skeletal remains from the Dakhleh Oasis, Egypt dating from the Roman Period (CE 400-500), as well as evidence of tetracycline labelling in tooth enamel [382]. This distinctive layering of fluorescence, confined to cellular structures rather than diffuse across the bone, is indicative of exogenous acquisition of tetracycline rather than environmental absorption or inherent autofluorescence, as it mirrors the bone remodelling cycle of deposition, mineralisation, and resorption [343].

Conversely, Piepenbrink et al (1983) [383] inferred that Bassett et al (1980) may be mistaken in their interpretation of the tetracycline fluorescence and suggested that the concentric osteon fluorescence may be the results of bacterial infiltration from the deposition environment, as some microorganisms excrete tetracycline like fluorophores and do not always leave tunnelling evidence on bone microstructures [343]. However, the evidence of differential osteon fluorescence is incompatible with this theory [382]. Furthermore, Capasso et al (2015), investigated the autofluorescence properties of human femora and specifically sampled skeletons from Italian archaeological sites and ossuaries, which had been radiocarbon dated, to ensure they were not exposed to any possible sources of natural antibiotics. The authors observed homogenous fluorescence, indicative of bone autofluorescence, across the bone section when samples were exposed to an excitation wavelength of 488 nm [122].

Tetracycline has a natural affinity for calcium and its intense fluorescence response to ALS means that it is frequently used in medicine to label bone undergoing surgery [345, 347]. However, in a comparative study conducted by Ristow et al (2020) comparing the autofluorescence and tetracycline induced fluorescence of necrotic porcine mandibles, they found very little difference in the manifestation of tetracycline induced fluorescence compared to natural bone autofluorescence. They proposed that rather than being the direct cause of bone fluorescence, tetracycline exposure may just boost the already present natural autofluorescence [384]. Overall, repeated exposure to tetracycline was required to permanently alter the fluorescent properties of bone. Ristow et al (2020)

implemented 20 weeks of tetracycline injections to ensure its assimilation into porcine bone, and the tetracycline fluorescence found in the archaeological skeletons has been attributed to repeated consumption of tetracycline, both deliberately and incidentally [380, 382, 384].

9.6 – MINERAL CONTENT

Necrosis (tissue death) occurs when the blood supply to the tissue is compromised. In bone this disrupts the normal homeostasis of bone remodelling, leading to the collapse of bone microstructure [385]. In a study conducted by Al-Ghaithi et al (2021) comparing healthy and necrotic human femoral heads using Raman spectroscopy, they noticed an increase in carbonate to phosphate ratio indicative of changes in bone crystallinity, and a reduced collagen cross-linking ratio, demonstrating disruption to the collagen cross-links [386]. As necrotic bone does not fluorescence, this may be evidence that bone autofluorescence is in part linked to the mineral aspect of bone. This is supported by a study conducted by Lambrecht & Mallol (2020).

Whilst investigating the autofluorescence of experimentally heated bovine bone, Lambrecht & Mallol (2020) hypothesized that bone samples heated between 100-200°C formed new molecules, similar in composition to tetracycline, via thermal degradation of the organic matrix [130]. These new molecules would attach to the mineral aspect of the bone and consequently acted as fluorophores. They claim that this change in state led to a spectral shift in fluorescence emissions from 510 to 527 nm, with a secondary emission seen at 545 nm, when excited with blue light (400–440 nm).

Gonzalez et al (2018) discuss a similar shift in fluorescence emission when heating synthetic carbonated hydroxyapatite, which can be considered an analogue for bone mineral [387]. They observed changes to the carbonate and hydroxide content which they argue led to a rearrangement of the crystal structure and a subsequent shift in fluorescence emission from 510 to about 540 nm [387]. Lambrecht & Mallol (2020) go on to say that the unheated and calcined (700°C) bone samples in their study exhibited ‘near-identical’ autofluorescence which they propose supports the hypothesis that, when stimulated with blue light (400–440 nm), the mineral content is the primary source of bone autofluorescence [130]. This is because literature explains that the organic

component of bone is thought to be completely removed by heat at approximately 500-600°C [141], which would indicate that the remaining bone material was mineral only.

However, no quantification of either the organic or mineral content was conducted by Lambrecht & Mallol (2020), other than observing changes in mass, and identifying the presence of hydroxyapatite using Raman spectroscopy [130]. Therefore, the theorised structural changes reported in the study are not supported by data. Similarly, fluorescence intensity was not measured quantitatively, and instead was produced by subjective visual observation and the selection of the exposure time used to capture the fluorescence. Therefore, it is difficult to interpret the reported changes in fluorescence accurately as these observations could be influenced by intraobserver bias.

Furthermore, multiple articles have reported that calcined bone does not fluorescence when exposed to ALS, due to the thermal destruction of the organic component of bone and reorganisation of the mineral aspect, which is why the ALS technique has been considered for identifying burned bone at fire scenes [131, 142, 143, 158, 307, 388] even using the same spectrum of wavelengths as Lambrecht & Mallol (2020) [130]. Therefore, it seems unlikely that the mineral content is the primary source of bone autofluorescence, but it is reasonable to suggest that it may contribute, possibly through its molecular interactions with the organic component of bone.

It is apparent from literature that there is still great debate regarding the origins of bone autofluorescence. Although the collagenous aspect of bone seems to be regarded as the main contributor, the molecular composition and relationship between the organic and inorganic aspects of bone may also influence fluorescence intensity. It could be that the autofluorescence of bone is more nuanced than currently reported, possibly dictated by orientation of the collagen cross-links rather than just the presence of collagen or individual amino acids. Many papers make broad generalisations regarding amino acids and bone composition that perpetuates potentially misleading conclusions making interpretations of the current research challenging. Similarly, most of the current literature has focused on the cross sections of bones stimulated by wavelengths within the UV spectrum and subsequently analysed using microscopic analytical techniques. Consequently, much of the research is not fully applicable to fieldwork or crime scene scenarios, creating a significant deficit in the understanding of how bone fluorescence

may be utilised outside of the laboratory. Furthermore, the lack of objective quantification in the current research means the relationship between bone fluorescence and bone composition has not been sufficiently explored, and much of the theory regarding bone autofluorescence is derived from persistent assumptions rather than empirical data.

10.0 – ETHICAL CONSIDERATIONS AND APPROVAL

Historically, animal proxies have been used throughout scientific research to model human response to emerging therapies, procedures, and medications, as well as facilitate anatomical learning and development [389]. In forensic taphonomy, animal cadavers are frequently used to investigate the process of decomposition and help decipher how intrinsic and extrinsic variables may influence its progression [390, 391]. This knowledge can then be applied to forensic scenarios by informing interpretations at crime scenes and estimating the post-mortem interval [39, 392].

Taphonomic studies using human cadavers are primarily restricted to human taphonomy facilities (HTF) [39, 393]. New facilities are being constructed all over the world [394] and help to build on the knowledge gained from previous animal studies by using donated human cadavers to replicate ongoing forensic casework or to conduct original research projects, enabling empirical measurement of decomposition changes specific to the climate and geography of the host environment [154, 395]. HTFs are currently operating in Australia, The Netherlands, and the USA, but have not yet been constructed in the UK [39, 396, 397]. The Human Tissue Authority (HTA) governs the use, retention, and disposal of human tissue in the UK via the application of the Human Tissue Act 2004 [398]. Currently, HTA legislation does not specifically discuss or regulate the use of human tissue for forensic research, therefore taphonomic and forensic experimentation is still performed using animal analogues which is governed by local institution ethical guidelines and protocols [398].

Animal analogues offer many benefits to forensic research, as population attributes and origins can be more readily controlled, with shared commonality such as breed, diet, age, and size, whereas humans exhibit greater variation due to lifestyle, heritage, and global mobility [39, 393]. Amassing a sufficient population of human cadavers is much more difficult compared to purchasing animal carcasses, due to variability in donation timescales as well as the acceptance criteria defined by receiving facilities [395]. Consequently, human datasets used in research are usually less homogeneous compared to animal groups as the bodies exhibit different times since death, as well as much greater inter-individual differences such as age, sex, body mass, and cause of

death. Admissions at HTFs can be infrequent and sporadic therefore researchers cannot usually afford to be selective or wait for specific characteristics [399]. This variation can make interpretations challenging and possibly undermine results when attempting to make direct comparisons within the group [390], but conversely it is much more representative of true forensic scenarios[393]. Access to animal products is less regulated compared to human tissue, and generally cheaper to procure, and simpler to store, with known, accurate times of death easily obtainable due to group euthanasia conducted in the meat and pet food industries [390]. Subsequently, animal proxies allow isolation of individual variables of interest [393] and can facilitate more robust statistical analysis with greater standardisation, as sample sizes can be larger and biologically more consistent [395, 399].

A range of different animal proxies have been used in forensic science literature, often selected based on availability and cost, examples include rabbits, deer, sheep, and mice, but pigs are by far the most common [391, 394, 395, 400]. Pigs are considered the standard proxy for forensic science as they are thought to best model human physiology and anatomy [389]. More specifically, pigs are relatively hairless, exhibit a similar fat-to-muscle ratio, tissue density, and internal anatomy compared to humans, as well as partake in an omnivorous diet and have an endogenous microbiome [390]. Anthropologically, mammalian bone, including pigs, demonstrates the same types of histological features as human bone, with bones performing similar mechanical roles within the body during life [401]. Consequently, an array of studies has been published which have effectively contributed to the understanding of human decomposition and the factors that may affect it [394]. This includes studies exploring decomposition of hanging bodies, the succession of carrion insects, decomposition of dismembered bodies, characterisation of volatile organic compounds, and the use of geophysical techniques to locate clandestine buried remains [402].

However, some research suggests that there are some major biological differences between pigs and humans which limit how effectively porcine research can emulate human decomposition [389]. Between 2012 and 2015 Connor et al (2018) compared the decomposition trajectory of 22 human remains and 17 pig cadavers at the Forensic Investigation Research Station in western Colorado [390]. They noted a significant

divergence in the rate and presentation of decomposition between the human and pig cadavers, concluding that anatomical differences, such as digestive tract composition, and potentially presence of diabetes within the human sample may have influence decomposition progression [390]. Similarly, Dautartas et al (2019) reported differential rates of decomposition when comparing, pig, rabbit, and human cadavers at University of Tennessee's Anthropology Research Facility, highlighting that on average pig and rabbit cadavers decomposed much faster compared to human remains with greater levels of inter-individual variation noted in the human group [391].

Consequently, it is acknowledged that human bones would be the optimal material for experimentation in this PhD project, in order to produce the most representative results and maximum relatability to forensic contexts. However, as this research is being conducted in the UK, porcine bone has been selected as the best available proxy due to the universally accepted physiological similarities outlined above, straightforward accessibility enabling larger and more homogenous sample population, and to ensure compliance with HTA legislation. As research into the use of alternative light sources to locate bone is still in its early stages, it would be advantageous to limit influencing factors and inter-individual variability to help ascertain the foundational knowledge to better understand the mechanisms surrounding bone fluorescence which can then be built upon in future research.

This research project was approved by the University of Central Lancashire Animal Welfare and Ethics Review Body (AWERB), reference number: RE/21/06, and received Research Programme Approval (RPA) by the School of Natural Sciences, University of Central Lancashire. All porcine bones purchased for this project were originally destined for human consumption and therefore were not killed specifically for this project. Any potential influence of using porcine bone rather than human osseous material will be addressed during the discussion sections of this thesis and will be taken into consideration when determining pathways for future work.

11.0 - METHODOLOGY

This PhD research consisted of two sections. Section A: Bone preparation and photography refinement, and Section B: The application of ALS to detect bone. Experimental methodologies are discussed during each section, and respective research questions, but quantifying bone collagen content and the intensity of subsequent emitted bone fluorescence, formed the foundations for all experimental design.

11.1 – QUANTIFICATION OF BONE FLUORESCENCE

As the use of ALS to detect bone is a novel application, many studies have focused on feasibility studies and often use subjective, visual methods for detecting bone fluorescence and changes in fluorescence emissions. Digital photographs are the major experimental output for research focused on whole or fragmented bone, as significant physical space is required to accommodate the light sources alongside the samples [131-133]. The use of whole and fragmented bone as opposed to bone sections is vital to better replicate how bone would be found in real world scenarios, such as crimes scenes, archaeological excavations etc., and consequently to produce data that is directly applicable to the technique's intended end users. However, this has led to some complications when quantifying bone autofluorescence.

Gallant (2013) only conducted on scene observations of simulated fires when assessing the use of the YAG light for fire scenes [143]. Harte et al (2020) [137], Brown & Christensen (2018) [266], Christensen et al (2014) [135], and Craig & Vezaro (1998) [256] all concentrated on the practical applications of ALS in the field and did not conduct any quantification of the fluorescence seen, but rather measured the recovery rate of bones and trace evidence. Miranda et al (2017) [132], Green et al (2019) [133], Swaraldahab & Christensen (2016) [146], and Sterzik et al, (2016, 2018) [147, 148] did include methods for fluorescence quantification, using computer software to analyse the RGB values of photographs. Commercial software including ImageJ and Photoshop are frequently used for fluorescence image analysis due to their precedent in current literature, ease of access, and general familiarity [132, 146, 147]. Although different computer programs were used, both ImageJ and Photoshop quantify fluorescence based on image

brightness derived from the ratio of RGB values of pixels [132, 147, 202].

11.2 – RGB AND GRAYSCALE

In digital technology, all monitors, cameras, and screens display visual data using tiny points of light called pixels [403]. The density, arrangement, proximity, and saturation of pixels is what forms images and consequently conveys information to the user [404]. The greater number of pixels within an image, the higher the image resolution and consequently the more detail that can be seen [202]. All colours within a digital image are formed based on the ratio of red, green, and blue [405]. Consequently, each individual pixel has 3 associated colour channels determining the intensity of red, green, and blue [405, 406]. Each value ranges from 0 to 255, where 255 represents a colour expressed in its full intensity, and 0 demonstrating no representation of that colour [407]. The ratio of these values within the pixel dictates the overall colour observed by the user, for example if the following ratio is applied R = 255, G = 0, B = 0, the pixel would present as pure red [405]. Swaraldahab & Christensen (2016) used ImageJ to quantify bone fluorescence from digital photographs [146]. This process involved standardising the size of the photograph to 300 x 300 pixels before using the *Averaged* grayscale equation below to convert the RGB data from colour to grayscale:

(Value of **red** + Value of **green** + Value of **blue**) /3

Equation 1: Averaged RGB equation [146]

This equation is applied to each pixel within the photograph which uses the ratio of red, green, and blue to convert to a value between 0 and 255, where 0 is equivalent to pure black and 255 is equivalent to pure white [408]. This value is applied to all three channels, and therefore each pixel is assigned one value, changing the image from colour to grayscale [406]. Miranda et al (2017) and Green et al (2019) used a very similar method but firstly used photoshop to reduce their photographs to 100 × 100-pixel regions of interest (ROI) to eliminate the inclusion of any background imagery [132, 133]. The photographs were then converted to grayscale using ImageJ. The specific grayscale equation was not disclosed in the article, but the default grayscale algorithm used by ImageJ is the same one described by Swaraldahab & Christensen (2016), and as Miranda et al (2016) references Swaraldahab & Christensen (2016) in their article, it is reasonable

to assume that the same algorithm was followed [132, 146]. The final grayscale value is representative of the brightness intensity of that pixel [409], and therefore represents the intensity of the fluorescence. When this equation is applied to a specified region of interest or across the whole bone sample, it offers a potential method for quantification of bone fluorescence.

In literature, several authors using this method to analyse bone fluorescence refer specifically to the use of 8-bit grayscale [132]. The term 8-bit refers to the pixel depth of the image, which is in essence how much data is used to encode each of the three channels that make up the colour of the pixel [405]. A 'bit' is the smallest unit of data used by computers, and a 'byte' comprises of 8 bits [408]. Grayscale images are usually stored in 8-bit format as it is generally accepted that there is a maximum of 256 (0-255 inclusive) possible shades of grey [408]. Some software offers the capability of generating higher density grayscale images such as 16-bit and 24-bit, but this leads to multiple bytes of information per channel, and consequently would return grayscale values in excess of 16,000,000. Trying to compare values of this magnitude would not be informative and would make interpretation challenging. In computing, grayscale images are generally only used in the simpler 8-bit format [409].

A limitation of this form of fluorescence quantification is the use of the *Averaged* equation to convert the fluorescence images to grayscale, as averaging the RGB values does not consider the complexity of the image or the viewer [404]. This issue is perpetuated in literature due to a reliance of software automation and oversights in previous research. For example, Harbeck et al (2011) used Photoshop to examine the colour of fluorescence emitted by burned bovine tibiae and described the tonal value as being optimised automatically by the software, but do discuss what this means or what affect it have had on the results [410]. As previously mentioned, Miranda et al (2016), Swaraldahab & Christensen (2016), and Green et al (2019) used the same *Averaged* RGB equation, as their research was developed based on each other's methodologies [132, 133, 146].

The human eye is naturally more sensitive to red and green light and less sensitive to blue wavelengths [404, 407]. This divergence is not reflected in quantification results when only averaging the three RGB values and does not account for the light and shade

within an image. Usually, images converted to grayscale using the *Averaged* equation will appear darker in comparison to other grayscale images [411]. This is detrimental to experimental fluorescence results as it is not truly reflective of the fluorescence levels seen, and subsequently may distort interpretations. The use of a weighted RGB equation is favoured in computing as it better represents how the human eye perceives colour [404]. There are several different weighted equations for grayscale conversion, but many focus on optimising computer vision [405], such as *Lightness*, *Decolorize*, and *Luster* equations [407]. However, the most popular is the *Luminosity* method, which is considered standard for image processing software including MATLAB and GIMP [412, 413]. This equation puts greater emphasis on the contributions of green and red to better replicate how the human eye sees colour, as shown in the equation below:

$$(0.299 \times R) + (0.587 \times G) + (0.114 \times B)$$

Equation 2: Luminosity weighted RGB equation [407]

Table 3 demonstrates how this weighted grayscale equation converts the RGB colour values to grayscale and figures 28-30 provide a comparison of how the same image of a fluorescing porcine rib appears when converted to grayscale using the *Averaged* equation and the *Luminosity* method. A clear distinction in brightness level can be observed between the two grayscale images, with the *Luminosity* method providing a level of brightness which is more representative of brightness levels in the original fluorescence image.

Table 3: Example of the luminosity equation used to convert coloured images to grayscale.

Image	Red	Green	Blue	Output
Coloured image	233	125	47	
(0.299*R) + (0.587*G) + (0.114*B) = (0.299*233) + (0.587*125) + (0.114*47)				
Grayscale	148.4	148.4	148.4	

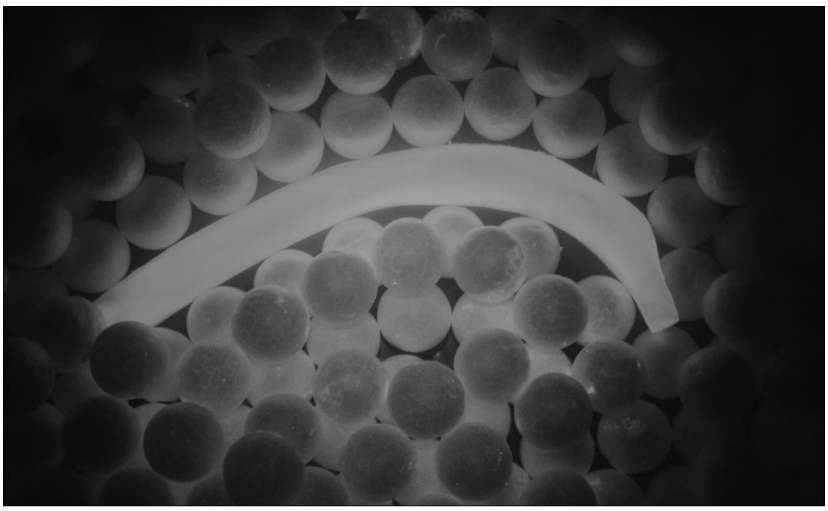

Figure 28: Fluorescence image of a fluorescing porcine rib, converted to grayscale using the Averaged equation

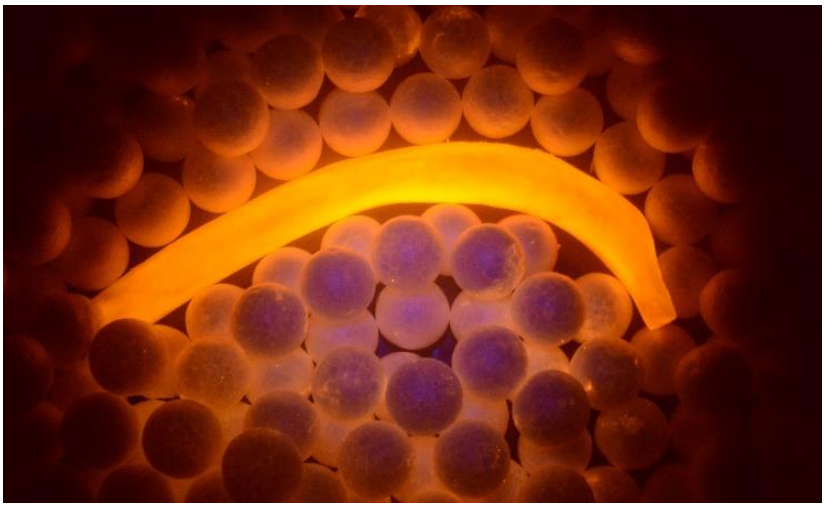

Figure 29: Original image of a fluorescing porcine rib (450nm, orange filter)

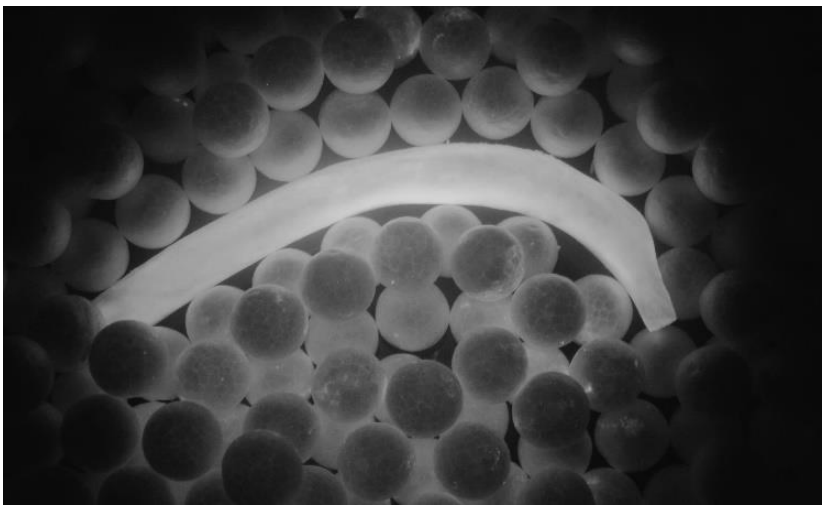

Figure 30: Fluorescence image of a fluorescing porcine rib, converted to grayscale using the weighted Luminosity equation

Other authors have focused on quantifying the intensity of individual RGB colour spaces of fluorescence images, in accordance with the predicted fluorescence colour output, such as UV stimulated bone fluorescence emissions, which are consistently reported as blue [148, 158] . However, although software such as ImageJ and Photoshop enable separation and individual quantification of RGB colour spaces, this approach is not entirely representative of the fluorescence seen. It is often assumed that pixels that appear as blue may only be represented in the blue colour channel. However, although blue items will predominantly contribute to the blue channel, it is very likely it will also differentially contribute to the red and green as well, as digital images use a combination of only three colours to create all possible colours within an image, including tonal gradation and brightness [414]. Consequently, it is very unlikely that any blue pixels will only be pure blue.

During their UV bone studies, Sterzik et al, (2016, 2018) attempted to account for this composite colour ratio by using the eye dropper function in Photoshop [147, 148]. The eyedropper tool was used to select a pixel within the image considered positive for blue fluorescence, and then that RGB ratio was used to calibrate the subsequent quantification, i.e., quantifying the number of pixels within the image that only had a ratio of red 0, green 186, blue 203. They included a tolerance of 75, but it is not clear which channel the tolerance was applied to. Even with the tolerance of 75, this approach would not account for all the unique RGB combinations that encode for blue.

Furthermore, as the calibration for blue fluorescence was produced using one bone sample, this ratio will not account for the natural variation in bone composition, and subsequently fluorescence levels, across the dataset, particularly as the calibration colour was selected based on subjective observer selection. However, most significantly, prior to quantifying the level of blue fluorescence, each image was adjusted using the "auto levels" feature to optimise the images for visual assessment. Similarly, as in Harbeck et al (2011), this auto adjustment will artificially moderate the brightness and intensity levels and therefore potentially distort successive analyses, and potentially produce misleading results [147, 148].

Schariatmadary et al (2023) used ImageJ to quantify the spectral shift in bone fluorescence as a function of burn temperature, by measuring the percentage of each

RGB colour space in fluorescence photographs [158]. ImageJ allows easy segmentation of the RGB values by producing a histogram of each colour contribution. This method provides a general overview of the changes in colour intensity of the fluorescence exhibited by bones burned at different temperatures, stimulated by blue light (420-470 nm), and photographed with a yellow filter. The most notable conclusion was the major shift from green to red fluorescence recorded between 700-900°C (fig. 31 below).

This method enabled objective and quantitative colorimetric comparison of the spectral shift in bone fluorescence, but the overall fluorescence intensity throughout all burning stages was only measured visually. Inferences were made to the fact that changes in bone composition, primarily collagen, were responsible for the differences in fluorescence, but no quantification of collagen was conducted. Therefore, although this data does contribute to the understanding of how bone structure is influenced during burning, it does not contribute to understanding regarding the collagen-fluorescence relationship. Similarly, although individual quantification of each colour space provides a more comprehensive overview of the colour of the fluorescence, it may still not be truly representative due to how colours are encoded in digital images [404, 414]. In the context of this PhD project, the intensity of the fluorescence was the focus of measurement rather than colour, as the interpretation of colour is subjective, and its saturation can be influenced by intrinsic and extrinsic factors as demonstrated by Schariatmadary et al, (2023) [158], Sterzik et al, (2016, 2018) [147, 148], and Hoke (2011) [304].

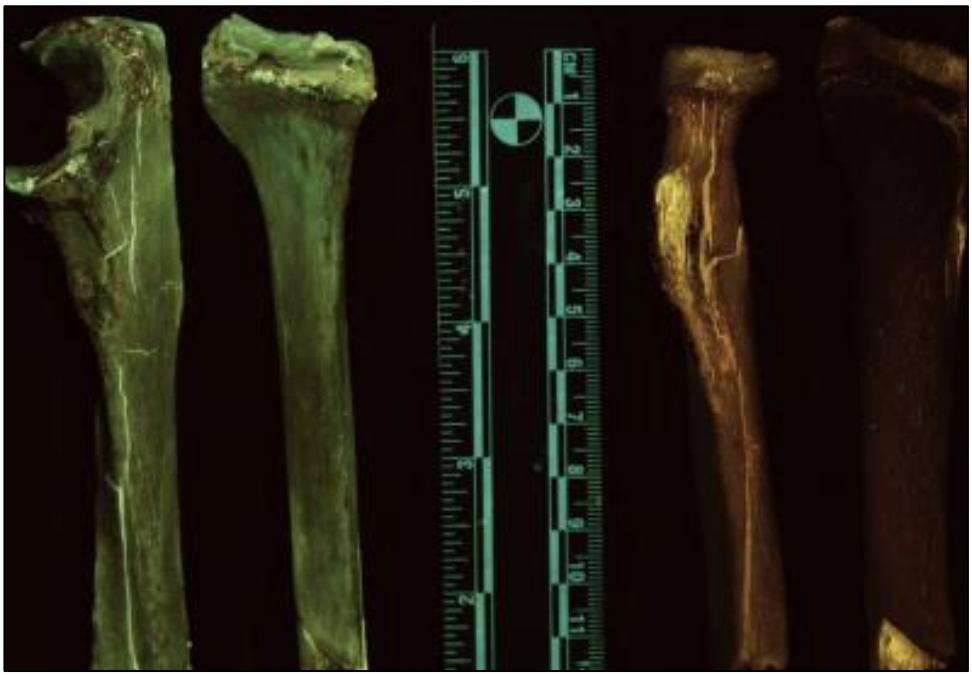

Figure 31: Fluorescence comparison of human bones burned at 700°C (left), and at 900°C (right) when stimulated 420-470 nm, demonstrating a shift in colour from green to red/brown [158] (Edited by Catherine Maidment, 2023)

11.3 – COMPUTERISED FLUORESCENCE QUANTIFICATION

ImageJ and Photoshop are used frequently in forensic and biomedical literature [415, 416], but this sustained use is linked to inherited practice and precedence in literature, and arguably not necessarily suitability for the task. ImageJ is opensource and free to use [417], making it highly accessible [418, 419]. It can be adapted to the user's needs with the use of macros and plug-ins to extend functionality [417, 418]. There is currently a huge array of plug-ins available, and as ImageJ development is community driven rather than by an individual software developer, more plug-ins are created all the time [416, 419]. The ability to highly customise ImageJ functionality is desirable [417] but due to the large volume of plug-ins, (currently approximately 417) [420], it can be challenging to identify the plug-ins required, particularly if several different analyses are required and therefore several different plug-ins need to be downloaded . Similarly, as the plug-ins and macros were developed for specific studies or tasks [416], there may not always be a suitable plug-in available and macro/plug-in creation requires a degree of programming proficiency and familiarity with technological terminology [420]. ImageJ was developed for a scientific audience, with a basic user interface (figure 32) and limited instructional documentation which restricts accessibility [421]. This is in

comparison to Adobe Photoshop, which is considered a leading brand in photo editing software and is not marketed as an analytical program [422].

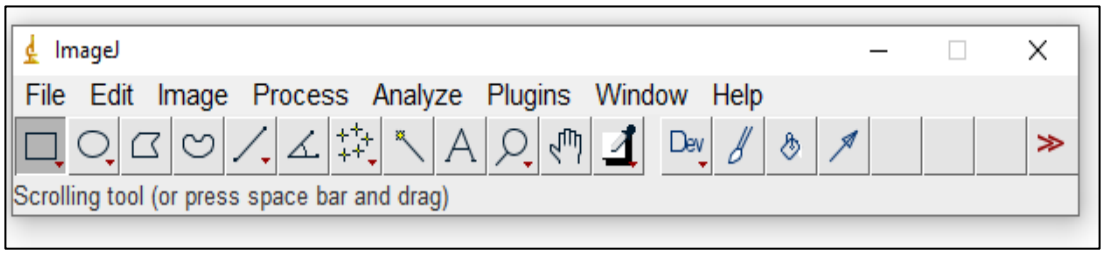

Figure 32: Screenshot of the default ImageJ toolbar

The use of Photoshop in scientific literature is prolific, including within forensic science [120, 415, 423, 424]. Photoshop requires an annual subscription, which can be bought as an individual, business, or educational institute [422]. At the time of writing, prices range from £353.88 for an individual subscription, or £120 per year per student for a department up to 100 students, although additional features and cloud apps require separate purchase [422].

Although it has many features in common with ImageJ, Photoshop's primary focus is design, and creative manipulation of images and video [422]. Photoshop is not opensource and therefore it cannot be edited to meet service needs [422]. However, its interface is arguably more user friendly compared to ImageJ but requires a more powerful computer to run efficiently. As Photoshop and other Adobe products are commonplace in educational institutions and in workplaces, users may already have some familiarity with its interface, terminology, and features, but as the program is not specifically designed for scientific image analysis, novel repurposing of individual features can be required to produce the desired results, such as the use of the eyedropper tool by Sterzik et al (2016, 2018) [147, 148].

Currently neither program is created to be used at crime scenes. ImageJ in not available as a mobile app and it is not compatible with Android or Apple operating systems due to being written in Java programming language. Adobe offers an express version of Photoshop for use on mobile devices, but it is specifically designed for aesthetic purposes for 'making quick, powerful, and easy photo edits' [422]. As each program has

its limitations, other authors have opted to create bespoke software to analyse their fluorescence results.

Barreiro et al (2022) investigated fluorescence during their study into differentiation of bone and non-bone objects at fire scenes [388]. They developed an automated computer program in MATLAB 2021a (MathWorks®, MA, USA) which splits the RGB channels of each image into the respective colours and then produced a new image based on the calculated difference between the green and blue values. Using a "luminescence threshold" (that was not divulged), pixels exhibiting fluorescence were selected and a mean fluorescence value was calculated. The "integrated density" for each image was also calculated by dividing the mean fluorescence value by the number of fluorescence pixels identified. The program processed full images rather than selecting regions of interest.

It was not stated why this program was used rather than commercial software, but the authors did mention that the program automated the analysis process which therefore negated any intervention from the user. In contrast to the other research papers previously discussed, there was no mention of automatic levelling of the RGB values, or the addition of corrective factors, indicating that the fluorescence was analysed in its original state. However, it is unclear why the RGB channels were split, and a composite image created based on the difference in the blue and green values.

However, the authors used a threshold to determine which pixels would be classified as fluorescing, much like Sterzik et al (2016, 2018) [147, 148], but it was not disclosed what this value was or how it was determined. The computer program also processed the whole image, which could be beneficial as it allows fluorescence quantification of the whole bone, inclusive of morphology and size. However, it could also be detrimental, as the background material the bones were photographed on was not disclosed, and if it met the threshold for fluorescence classification it could be included erroneously. There was no discussion of any steps taken to ensure that this was not the case.

To this author's knowledge, Barreiro et al's (2022) program is currently the only bespoke piece of software created to calculate bone fluorescence [388]. Although commercial software is accessible and has been used in previous research, it possesses limitations regarding ease of use and specificity to bone fluorescence. Microscopic and

spectroscopy quantification techniques can provide detailed quantification of fluorescence emission wavelengths, but general emission intensity has only been investigated sporadically. Furthermore, microscopic techniques require significant bone preparation to facilitate examination including destructive alteration such as sectioning and staining. Therefore, microscopic fluorescence techniques are not applicable for bone identification at crime scenes. Consequently, there is an opportunity for the development of a simple to use computer program tailored towards quantifying bone fluorescence analysis, and which can be used to identify bone in the laboratory and at crime scenes.

11.4 – THE OSTEO-FLUORESCENCE CALCULATOR (OFC)

As a result, this PhD project uses a bespoke C++ computer program: the Osteo-Fluorescence Calculator (OFC), to quantify bone fluorescence in photographs taken of whole porcine ribs, stimulated with blue light (450 nm), and visualised with orange and yellow barrier filters. A bespoke program was chosen to enable full control of the fluorescence quantification, by implementing the weighted RGB *Luminosity* equation to comprehensively analyse the fluorescence intensity whilst rejecting the use of any automated normalisation tools to ensure the observed fluorescence is analysed in its original state. Measuring brightness rather than individual RGB colour spaces ensures that all fluorescence emissions are included in the intensity calculations, and implementing a grid functionality enables selection of regions of interest (ROI) for simple, fast, and replicable quantification. Due to its simple programming, the OFC can be ported to mobile devices for on scene examination. Full details of the OFC's technical specifications and how the program works can be found in the materials and method chapter 13.3.3. However, figure 33 conveys the overall fluorescence image processing pathway, and figures 34-41 illustrate the user interface of the OFC, alongside a step-by-step example of how a user would process a bone fluorescence image.

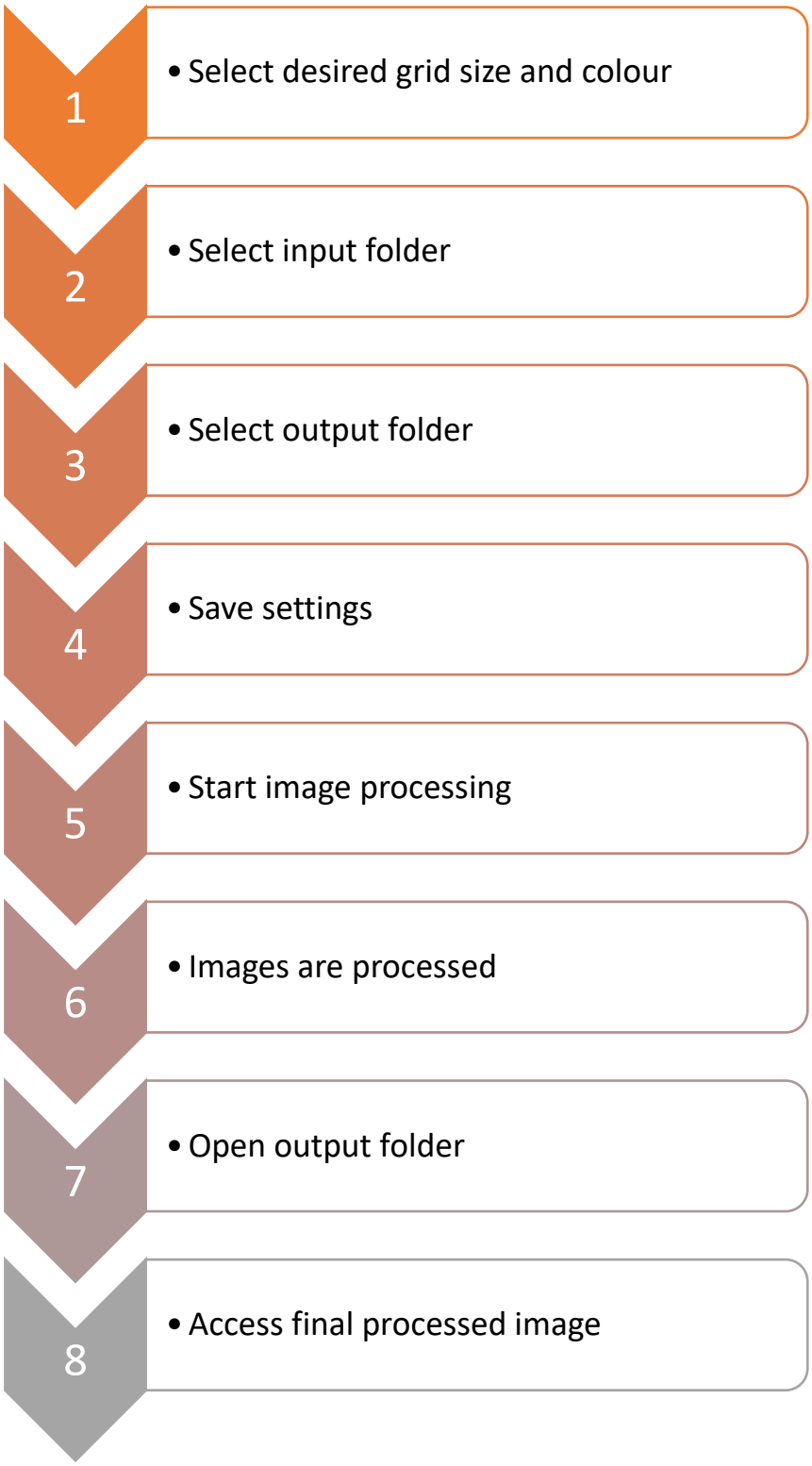

Figure 33: Flowchart describing the user experience when processing fluorescence photographs using the OFC.

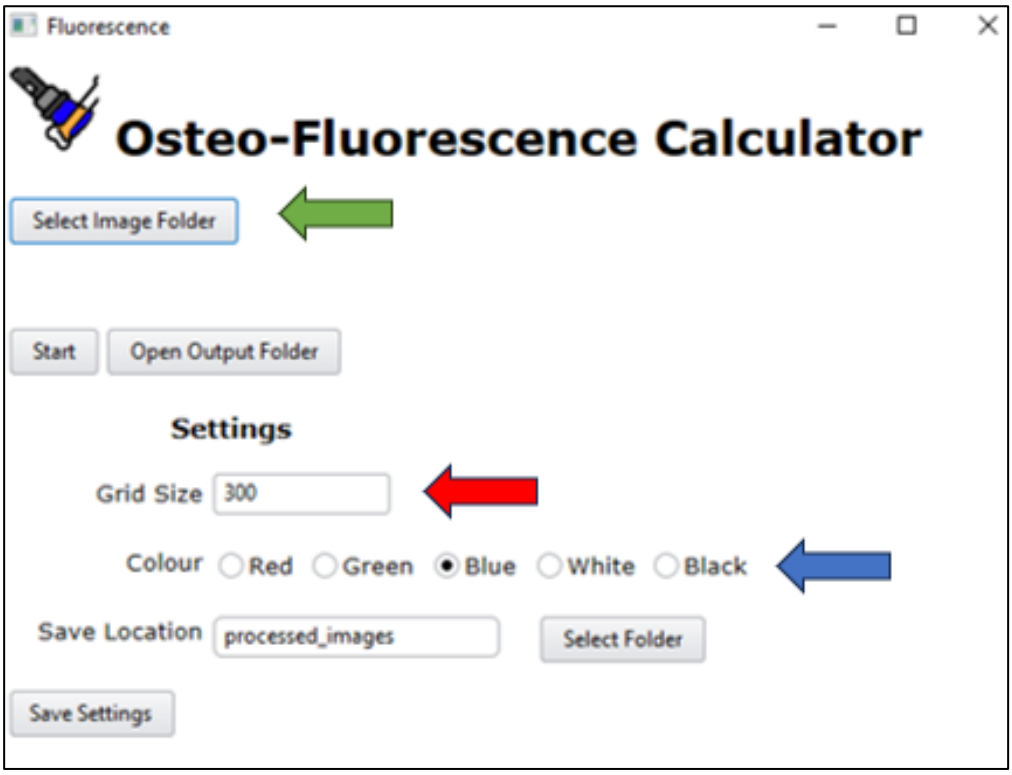

Figure 34: Selecting the grid specifications.

Step 1: Figure 34 above, illustrates the homepage for the user interface of the OFC. Here the user can input the desired grid size in pixels (red arrow), to tailor the size of the ROIs, and select the colour of the grid (blue arrow) to assist with visibility of the fluorescence values. In this example the grid size has been selected as 300 x 300 pixels, and the grid colour set to blue.

Step 2: Once a grid size and colour has been selected, the process would begin by clicking the 'Select Image Folder' button (green arrow, fig. 34). This will enable the user to browse the folders on their computer and select the folder containing the images that they wished to be processed i.e., the input folder (fig. 35). All images in a folder can be processed automatically therefore helping to speed up processing times.

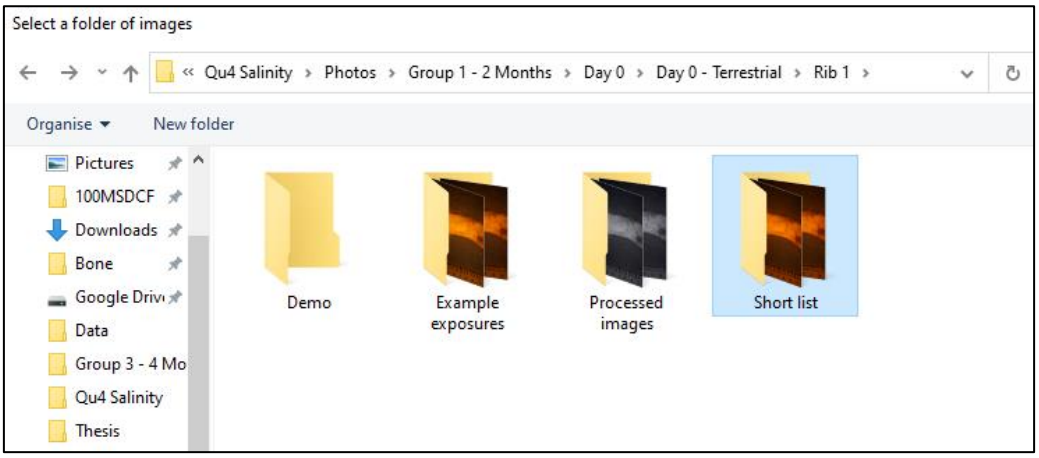

Figure 35: Selecting input and output folders.

Step 3: Once an input folder of images has been selected, the user will select a save location. The save location will be the destination folder for the final computed images i.e., the output folder. In this example, the 'Short list' folder was selected as the input folder and the 'Demo' folder was selected as the output folder (fig. 35).

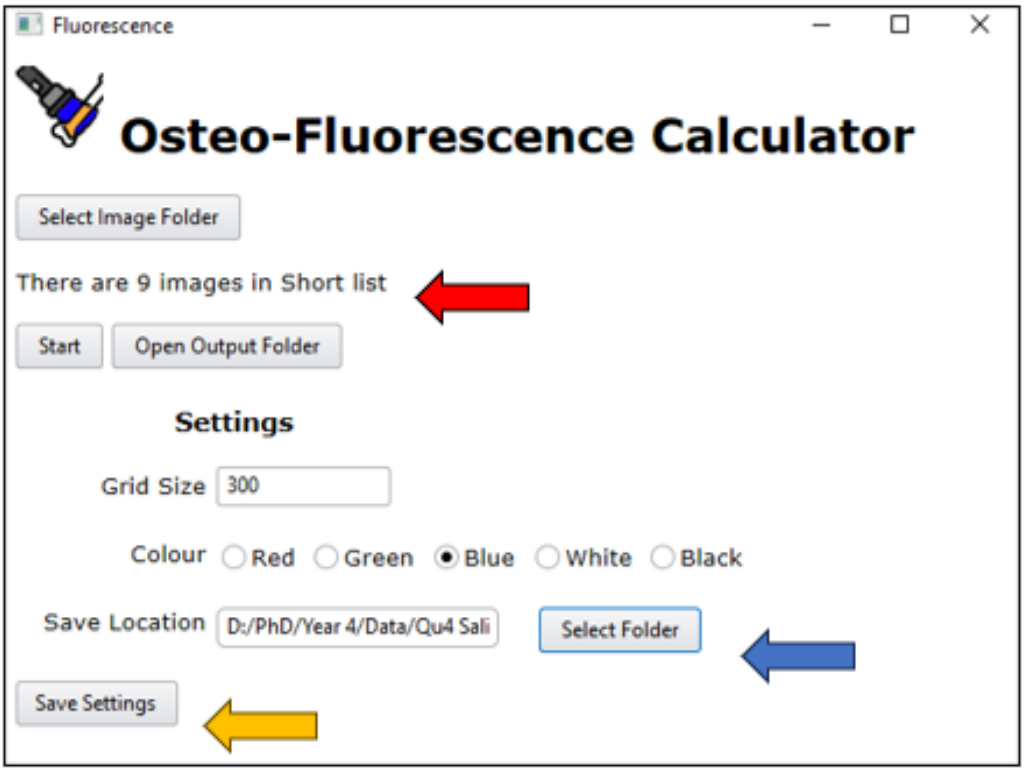

Figure 36: Selecting a save location and saving the settings.

Step 4: After both folders have been selected the home screen will update to display how many photographs are in the input folder (red arrow), and the save location will update to read the file location of the desired output folder (blue arrow). The user will need to select the 'Save Settings' button at the bottom of the page (yellow arrow), and a message will appear on screen to communicate that the settings were saved (fig. 37).

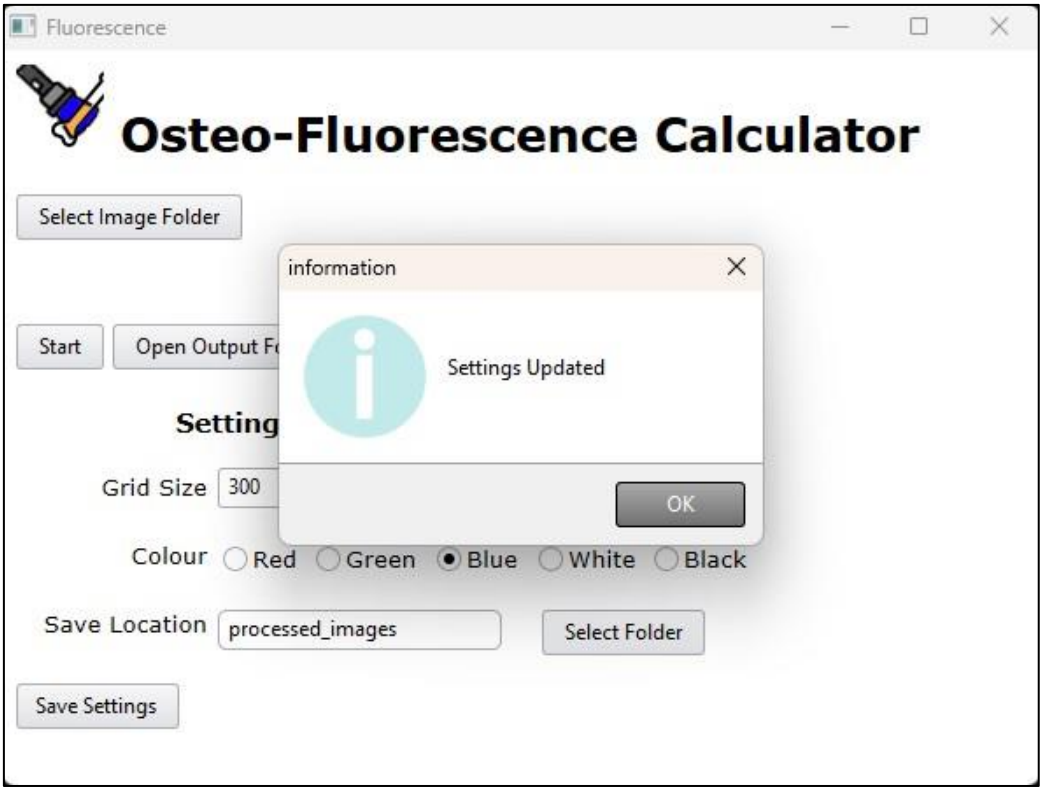

Figure 37: Save settings on screen message.

Step 5: During processing, the number of processed images (red arrow) will steadily increase as each image is processed (fig. 38), giving the user an indication of progress. This message will then change to 'Successfully processed X images' once complete, as shown in figure 39 below (red arrow).

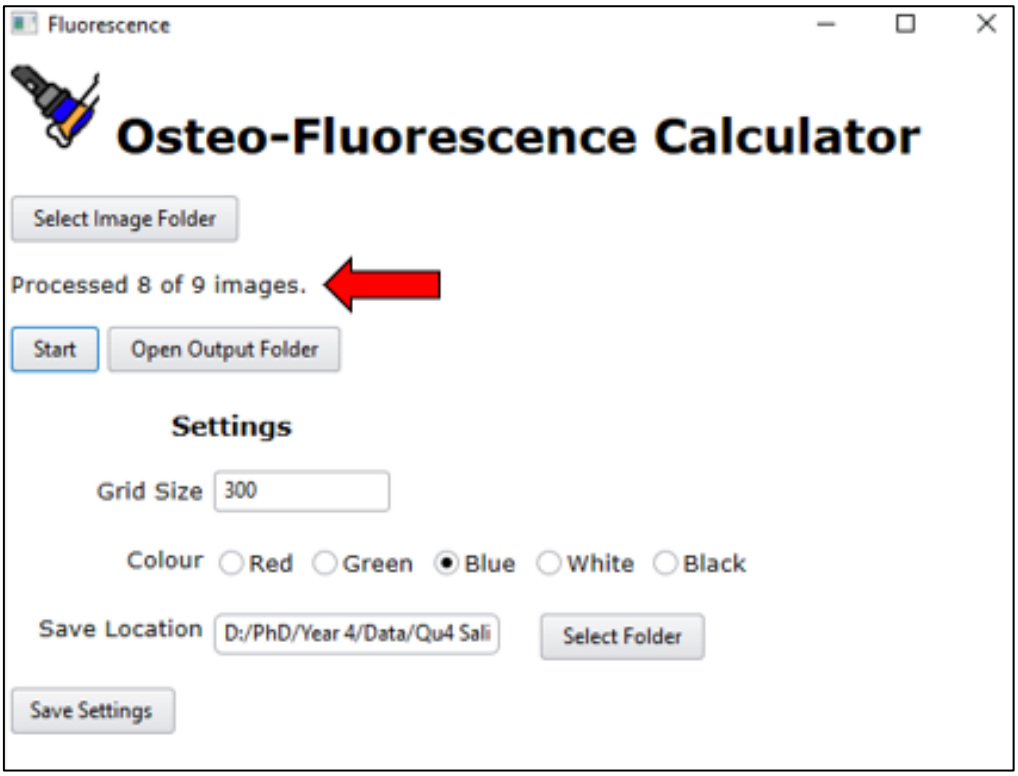

Figure 38: Text to indicate the progress of fluorescence image processing.

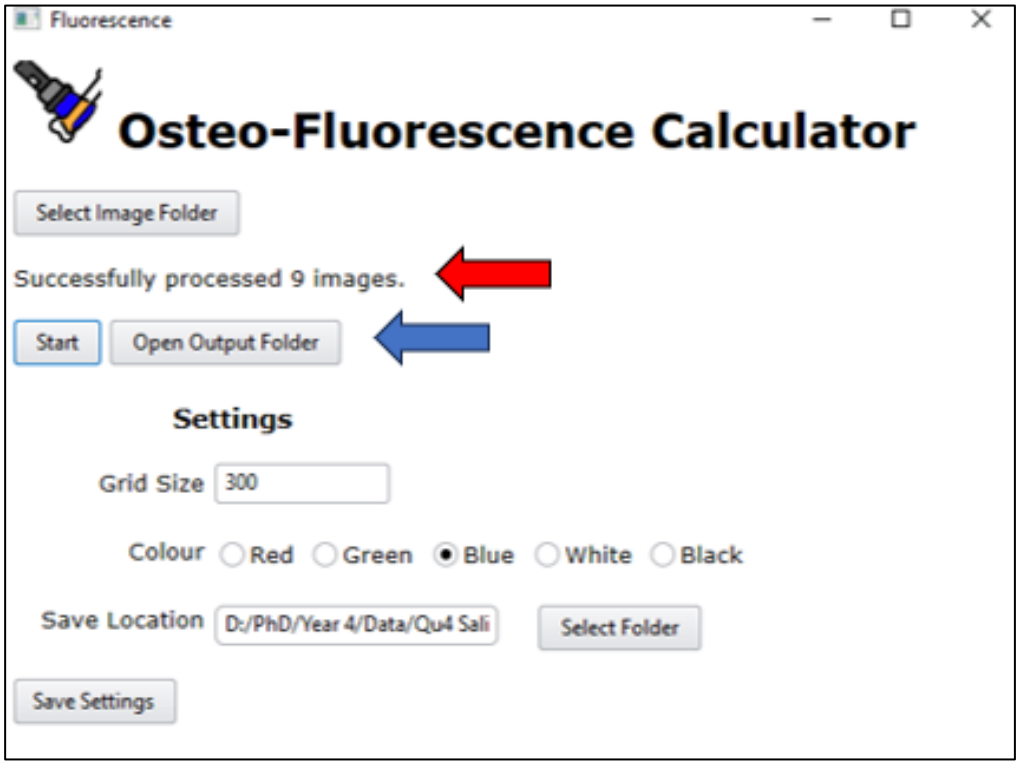

Figure 39: Successful processing of fluorescence images, selection of output folder to view result

Step 6: Once processing is complete, the user can select the 'Open Output Folder' button (blue arrow, fig. 39), and this will open up the designated output

folder selected previously, as shown in figure 39 (blue arrow). All the processed images are now available and can be opened to inspect the fluorescence result.

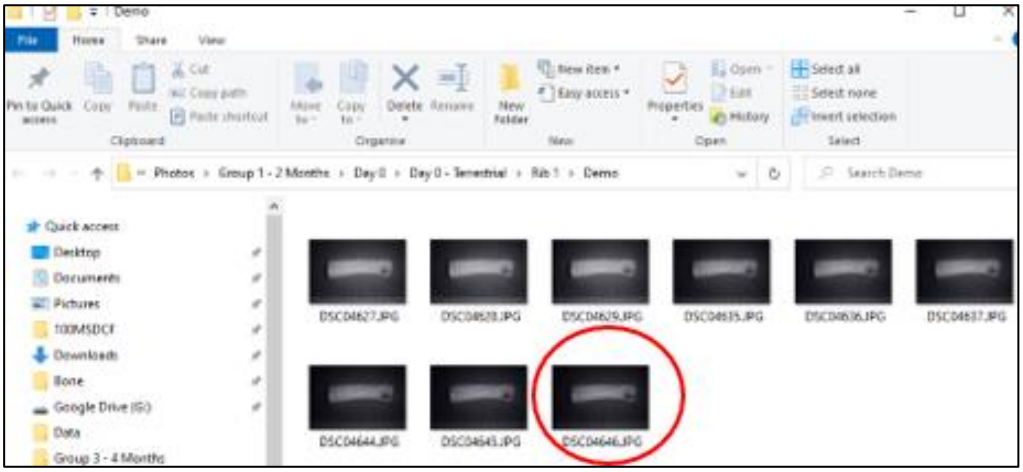

Figure 40: Selection of an example processed fluorescence image.

Step 7: In this example, the final image labelled DSC4646.JPG (red circle, fig. 40), is shown in figure 41 below, to illustrate the final image appearance.

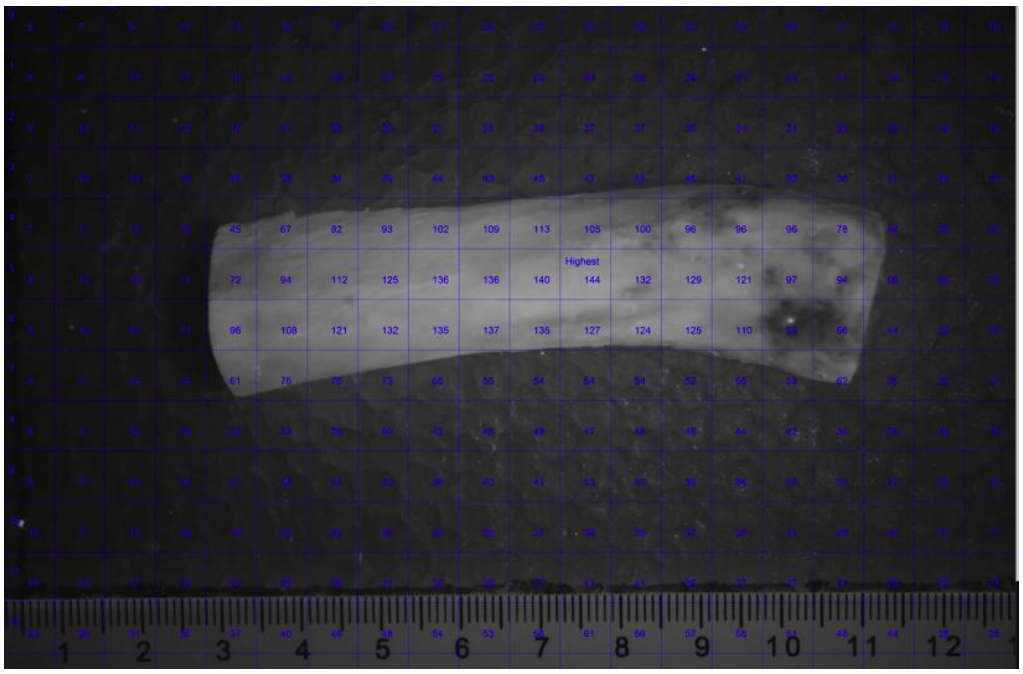

Figure 41: Example of OFC output

Analysis of the current literature highlighted the need for accurate quantification of both bone fluorescence and composition to better understand the source of bone autofluorescence. As a result, this PhD thesis focused on the fluorescence of bone collagen, as most published research suggests that the organic component contributes the most to bone autofluorescence.

12.0 – QUANTIFICATION OF COLLAGEN

Current literature has discussed the significance of collagen in the role of bone fluorescence, but very little direct analysis has been conducted. This is possibly due to many techniques being destructive in nature and therefore researchers can be limited when using archaeological human osteological collections. Furthermore, analytical techniques can be expensive, time consuming, and require significant laboratory space, consumables, and specialised equipment [425]. As previously discussed, there have been a few studies analysing the histological distribution of bone fluorescence and determining the presence and absence of bone fluorescence after deproteinization and demineralisation [304, 336]. Lambrecht & Mallol (2020) used Raman spectroscopy to detect the presence of hydroxyapatite but not collagen [130], and Harbeck et al (2011) did measure collagen during isotopic analysis but did not quantify fluorescence [410].

Consequently, the collagen-fluorescence relationship is poorly understood with no direct comparison made between collagen content and fluorescence output. However, collagen quantification techniques are well documented, with a range of destructive and non-destructive techniques detailed in literature. Fourier Transform Infrared Spectroscopy (FTIR) and Raman spectroscopy offer a non-destructive method to estimate bone composition [319, 338], and more thermal methods such as Differential Scanning Calorimetry (DSC) [426] and Thermogravimetric Analysis (TGA) [141, 427] have been used extensively in material sciences as well archaeological research but are destructive in nature. Chemical extraction of collagen is also destructive but is particularly popular in literature as it is a prominent component of isotopic analysis [338].

12.1 – STABLE ISOTOPE ANALYSIS

Stable isotope analysis is common practice in archaeological research investigating dietary and migration patterns of ancient populations [428-430] as well as forensic science [431]. It is a highly sensitive method that can provide detailed data regarding the ratio of carbon, nitrogen, and strontium isotopes in bone samples [432]. The collagen content of bones needs to be extracted to carry out isotopic analysis [433], and

this is commonly accomplished through gelatinisation of ground bone powder or chunks [434, 435]. The total collagen yield is calculated based on the mass of the gelatinised collagen in comparison to the total weight of the bone sample [434, 436]. Specific methods for gelatinisation vary across literature but commonly incorporate a multistep process of hydrochloric acid demineralisation, and several days incubation in sodium hydroxide or chloroform to remove lipids and humic acids [433, 434, 437]. This process can also be followed by various filtration steps to purify the gelatinised collagen by removing protein contaminants, before finally being freeze-dried [438].

Isotope quantification is subsequently conducted using mass spectrometry [439]. Consequently, it is time consuming and can often be expensive as it requires complex equipment and acquisition of specific standards [431]. The quality and purity of collagen is prioritised during collagen extraction to ensure informative isotopic results [436]. However, purity and quality of collagen are not a priority in this PhD project, particularly as there are no downstream analyses to perform. At this early stage in bone fluorescence research, where there are conflicting theories regarding the source of bone fluorescence, it is essential to start with foundational studies before graduating to more targeted and detailed investigations. However, fluorescence photography was the primary mode of fluorescence data capture for this PhD project, and as such the gelatinisation techniques were adapted to assist with the creation of the negative controls, discussed in chapter 25.0.

12.2 – FOURIER-TRANSFORM SPECTROSCOPY (FTIR)

In the literature, Fourier-transform infrared spectroscopy (FITR) has been used extensively to study diagenetic and thermal alterations to the mineral phase of bone by measuring the size and volume of apatite crystals and estimating the carbonate and calcium phosphate content [440]. As well as analysing the inorganic aspect of bone, FTIR is routinely used as a pre-screening tool for radiocarbon dating and isotopic analysis to assess the purity of collagen, estimate bone preservation, and calculate potential collagen yield [438]. FTIR is a vibrational spectroscopic technique, which produces an infrared spectrum through identification of a compound's functional groups by measuring the differential radiation absorption of molecular bonds stimulated by a laser [441]. FITR offers a rapid, and relatively inexpensive option compared to other

methodologies, and requires minimal sample for testing [442]. Samples destined for FTIR analysis also require minimal preparation but are usually ground and sometimes filtered prior to analysis [441]. However, literature highlights that irregularity in sample preparation and consequently particle size, can introduce measurement inconsistencies and therefore reduce replicability [443]. As FTIR is primarily used as a screening tool, the results are presented as an estimation of collagen content rather than a direct quantification. As the major aim of this PhD study is to quantify fluorescence, FTIR would not be suitable at this time as true quantification is required to assess the collagen-fluorescence relationship. As most samples used in this project were fresh or moist in consistency, this would introduce difficulties with regards to grinding, potentially requiring drying which would take additional time and laboratory space. Grinding of samples was avoided in other studies, as it was thought the friction and heat produced could alter the mineral, organic, and water content of the bone [323].

12.3- SPECTROSCOPY

Raman and near infra-red (NIR) spectroscopy are further examples of vibrational spectroscopy techniques that feature heavily in the analysis of archaeological bone, and are championed for their non-destructive nature, meaning they are used when preservation of fragile and historically significant artefacts is paramount [425, 444]. Raman spectroscopy has been validated for determining the presence, abundance, and quality of collagen in human and faunal osseous material, and NIR offers similar claims, in addition to rapid sample processing [367]. In recent years simplified, portable Raman spectrometers and handheld NIR spectroscopes have been developed to facilitate swift on-site analysis, although they tend to be less powerful than their laboratory counterparts [338, 445]. Despite these advantages, spectroscopy methods are considered semi-quantitative, and only provide a superficial measurement of bone composition, with a penetration depth ranging from microns to millimetres, and so they detect the presence and quality of the collagen rather than the quantity [367]. Therefore, FTIR does not offer sufficient quantification capability required for this PhD project.

Measuring the percentage of nitrogen (%N) within bone samples can also provide an indication of protein content, as nitrogen in bone is solely derived from the protein

aspect [443] and has been used to estimate bone preservation as well as for basic PMI estimation [446]. As with FTIR, this method is rapid and requires very little preparation and sample volume [443]. However, this technique does not differentiate between the potential protein sources of nitrogen i.e., whether it is collagen, non-collagenous proteins, or contaminants from the environment [447]. Although reported as one of the most accurate screening tools for collagen preservation [443], %N technique was only able to correctly predict whether a bone sample was suitable for radiocarbon dating in 84% of 200 bones analysed.

Consequently, the %N technique lacks the required sensitivity needed for this PhD study. Measuring the carbon to nitrogen ratio (C:N) has been described as a more accurate method for determining the presence of type I collagen, in comparison to measuring either component individually [448]. The typical C:N ratio for bone is reportedly 2.8-3.6 [338], whereas degraded collagen, bacterial excretions, and other bone proteins are thought to exhibit C:N ratios outside of this range, which allows for a more discriminating collagen analysis [436]. However, C:N ratio quantification is only suited to well-preserved bone specimens [338], and does not quantify degraded type I collagen sequences, therefore the results of this analysis would not be entirely representative of the total type I collagen content within the bone. Collagen content is especially difficult to detect in poorly preserved bones [449] and as part of the aim of this PhD project is to investigate the preservation of submerged bone, a more comprehensive technique is required.

12.4 – THERMAL METHODS

Thermal methods have been used to measure bone composition in several studies across archaeological and forensic literature, including determination of species and dating of skeletal remains [450, 451]. TGA involves the stable burning of a sample at scaled temperatures and durations [452], where the mass of the sample is continuously measured to monitor structural changes [453]. This provides quantitative data about the organic and inorganic composition of bone which is visualised through steps or peaks on a graph[454]. This graph is referred to as a thermogram [141] and interpretation of these peaks is based on an understanding of the structural composition of bone, as different components burn off in a predictable sequence . Extensive literature shows that during

incineration, bone undergoes four key phases [453]. Phase 1 is attributed to moisture loss [452] with complete removal thought to occur between 50 – 260˚C [455], phase 2 is the pyrolysis of the organic component resulting in calcination at around 200 - 400˚C [138, 456], with complete removal by 600˚C [457]. Alterations of the mineral hydroxyapatite denote phase 3, with production of additional carbonates and significant increase in size of the hydroxyapatite crystals at approximately 500 - 700˚C [458]. Finally, phase 4 occurs at approximately 800˚C and is characterised by the breakdown of the overall bone matrix resulting in amalgamation of remaining components, loss of structure, and shrinkage [459]. Figure 42 below illustrates the TGA process of collagen and a hydroxyapatite collagen composite illustrating the approximate TGA phases seen in bone [460]. Each red rectangle represents an individual phase which is annotated accordingly.

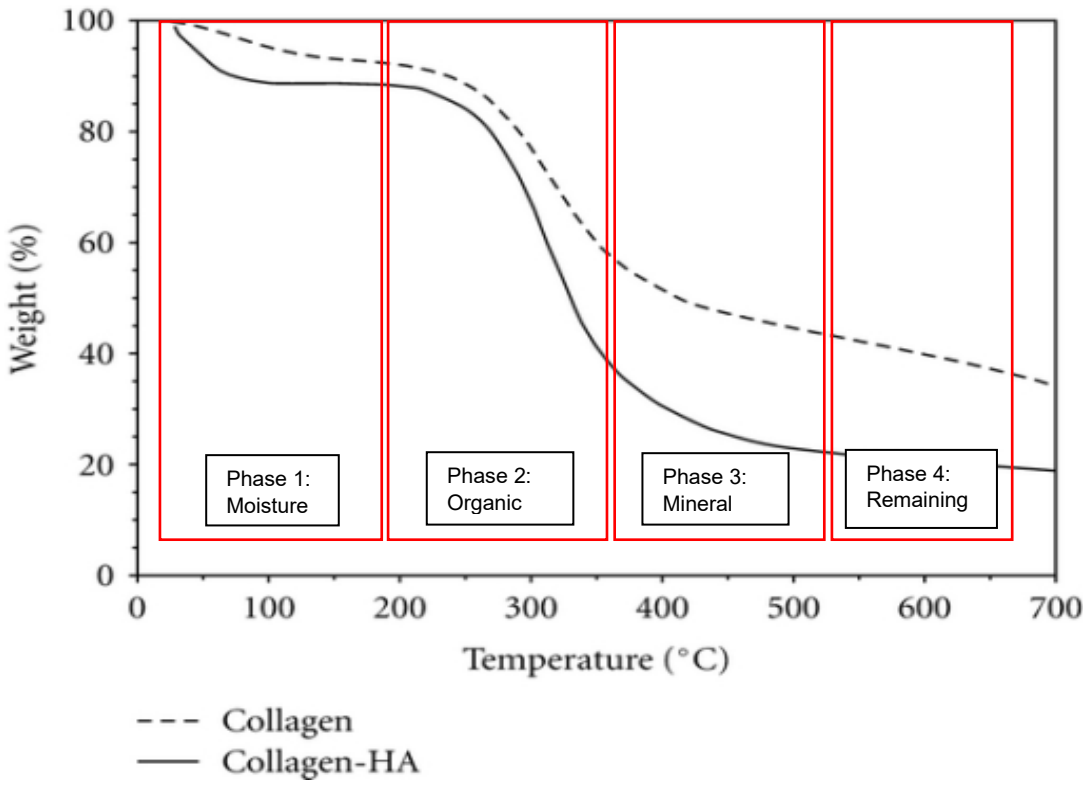

Figure 42: TGA of collagen demonstrating phases of thermal alteration [460] Edited by Catherine Maidment 2023

Differential scanning calorimetry is another thermal technique used to characterise compounds through thermal denaturation [426, 461]. Due to its triple helix configuration of interdependent collagen fibrils and apatite crystals, bone produces

specific and predictable thermal transitions, as demonstrated by Nielson-Marsh et al (2000) when they investigated the heat-induced degradation of bone collagen [368]. These thermal transitions have been found to be influenced by bone composition i.e., the proportion of mineral, collagen, and water, which in turn are affected by intrinsic variation due to age of the individual, antiquity of the skeletal remains, and pathological modifications [462]. This data can assist with understanding the maturation and mineralisation of skeletal tissue, as well as taphonomic alterations such as fossilisation [323, 462]. However, porcine bone has been shown to possess significantly more water than human or bovine bone which may influence the progression and results of DSC analysis [141, 323, 458], which is reiterated by Kubisz & Mielcarek (2005), who state that water volume directly affects the denaturation temperature of bone collagen [457]. Lower water content usually results in an increase in denaturation temperature, whereas higher water levels would lead to a lower temperature [457].

The presence of additional moisture is less of an issue in TGA quantification as quantification focuses on changes in mass. TGA also provides a clear measure of organic content of bone and therefore would make a simpler quantification strategy. This is supported by previous success using TGA during past MSc work completed by this author, as discussed in section 8. Although thermal methods are destructive, they require a relatively small sample volume and minimal sample preparation. They also produce definitive quantitative results even from compromised bone, such as incinerated, weathered, or historic bone [141]. Therefore, TGA was a suitable analysis to use to quantify collagen from the submerged skeletal remains during this PhD project. Although thermal techniques have been used within anthropological studies, to this author's knowledge TGA quantification has only been used briefly in the context of bone fluorescence analysis, by Harbeck et al (2011) where it was used to measure the mineral aspect of bone rather than organic component [410].

Consequently, this PhD project presents a novel methodology combining bespoke fluorescence quantification software; the OFC, together with TGA to measure bone collagen, enabling direct exploration of the hypothesised collagen-fluorescence relationship, and influencing taphonomic agents, to fill the gap in current research. However, as previously discussed in section 8, many of the bone fluorescence studies

published in literature use macerated bone specimens. Other authors suggest that the high temperatures and abrasive chemicals often used in maceration techniques can be detrimental to bone structure and subsequently the collagen content. In each of these studies the impact of maceration on the collagen content and bone fluorescence was not addressed, therefore it is not known whether the reported fluorescence results are representative of natural bone fluorescence or whether they are a product of the maceration treatment. Without this knowledge it is difficult to accurately interpret data currently published in literature, and therefore plan an accurate methodology for this research project. As a result, an exploration into the impact of maceration was also required to establish what impact maceration may have on the bone composition and answering the first research question of this PhD project by determining whether maceration was a suitable preparation technique for bone undergoing ALS analysis.

SECTION A:

BONE PREPARATION AND PHOTOGRAPHY REFINEMENT

Section A of this PhD thesis includes a maceration pilot study to explore maceration as a potential preparation method for bone intended for ALS analysis, and additional methodological refinement studies exploring the photography protocol, and aiming to answer the following research questions:

Question 1: Is maceration a suitable preparation technique for bone intended for laboratory ALS analysis? Examining the effect of 3 common maceration techniques: hot water maceration (approx. 80°C), warm water with biological washing powder (50°C) and enzymatic maceration using lipase and protease (55°C), on bone collagen and fluorescence levels

Question 2: Does the intensity of bone fluorescence in porcine ribs vary between the vertebral, diaphysis, and sternal regions of the bone, when photographed in a terrestrial context using blue light (450 nm) and an orange camera filter?

Question 3: What material provides the most effective contrast during osteological fluorescence photography between play sand, polystyrene sheet, polystyrene spheres, white card (200gsm), black card (220gsm), clear plastic box, and black plastic box, when photographing porcine bone in a terrestrial context, using blue light (450 nm) and orange camera filter.

Question 4: What is the optimal exposure time, f-stop and ISO level required to visualise bone fluorescence when photographing porcine bone (*Sus scrofa domesticus*) in a terrestrial setting using blue light (approximately 450 nm) and orange and yellow filters?

Question 5: What is the optimal distance from the sample to the light source when photographing porcine bone (*Sus scrofa domesticus*) using the Crime-lite 2 and the FoxFury Hammerhead devices, in combination with orange and yellow filters in terrestrial and tap water contexts?

Each question is addressed sequentially, followed by a final discussion for the whole section.

13.0 – SECTION A, QUESTION 1:

MACERATION PILOT STUDY

Is maceration a suitable preparation technique for bone intended for laboratory ALS analysis? Examining the effect of 3 common maceration techniques: hot water maceration (approx. 80°C), warm water with biological washing powder (50°C) and enzymatic maceration using lipase and protease (55°C), on bone collagen and fluorescence levels.

13.1 - CURRENT RESEARCH INTO MACERATION TECHNIQUES

Maceration is a common procedure regularly used in forensic anthropology to prepare skeletal remains for examination [149], usually involving the application of water, heat, chemicals, or insects to remove residual tissue from bone [156, 463]. Successful removal of soft tissues exposes the key morphological landmarks and skeletal structures required to estimate the osteological profile [156] and assist with identification and ultimately leaving clean, dry bone for further analysis and eventual storage [464, 465]. A plethora of techniques have been explored in literature, as methodologies are frequently born from inherited institutional practice or derived from casework experience [150, 466]. The rising popularity of molecular and genetic analysis of skeletal remains has led to re-evaluation of traditional maceration methods [152, 155]. Differing processing times and possible detrimental side effects to bone integrity can jeopardise further analyses such as DNA extraction, trauma identification, or proteomic quantification [149, 152, 155], as well as altering the integral skeletal features required for estimating the osteological profile. Consequently, methodology parameters vary greatly [153], and the creation and selection of techniques is also dictated by departmental resources such as equipment availability, laboratory space, financial costs, health and safety considerations, and the overall purpose of the maceration such as forensic examination or museum display [467-469]. Techniques can be broadly categorised into approximately six types based on the mechanism of tissue removal including: physical, bacterial, chemical, enzymatic, invertebrate, and cooking [149]. There is no definitive maceration method suitable for all types of bone with each method bringing its own successes and limitations [153, 156].

13.1.1- NATURAL MACERATION

Natural maceration is where skeletal remains are left to naturally decompose in a controlled environment such as a laboratory or left exposed to the elements in an open context such as a taphonomy facility [470]. Objectively it is considered one of the best approaches to maceration as it is driven by natural decomposition, forgoing the use of additional aids such as heat or chemicals which may cause damaging side effects [149]. However, natural maceration is time consuming, particularly in countries with colder climates, with clean, dry remains taking anywhere from weeks to months to achieve [149]. In addition to this, prolonged exposure to the deposition environment will eventually induce taphonomic changes within bone structures, instigated by environmental influences such as soil composition including pore size, pH, and moisture levels, or weathering modifications resulting from the sun, rain, and wind [22].

Taphonomic alteration can be evidenced microscopically by the presence of bacterial tunnelling, increased porosity, and destruction of histological characteristics, and macroscopic manifestations include bleaching, cracking, fractures, and erosion of cortical bone [471]. Bone exposure will also occur differentially across a body due to anatomical variation and body positioning [28], meaning the duration of taphonomic exposure for each skeletal element will also vary. Even within individual elements, regions of bone with complex skeletal morphology or denser tissue coverage will most likely retain material for longer compared to simpler structures. For example, the pelvis comprises multiple bones which exhibit numerous points of articulation with the spine and femora, including dense muscle, cartilage, and ligaments located posteriorly and laterally needed to maintain upright posture, and facilitate movement [116].

In a body left to decompose naturally in a supine position, the anterior aspects of the pubic symphyses are often quickly exposed due to thinner tissue density, but the posterior muscle and connective tissues are much more robust and protected beneath the body [17, 28]. This means the pelvis is often one of the last skeletal elements to disarticulate as these tissues take longer to decompose, keeping the pelvic bones together for longer. In hot and dry contexts, muscle and connective tissue are also more likely to mummify due to high ambient temperatures, low humidity, and low moisture content with the tissue [45, 472]. Dismembered limbs decomposing separate from the

main trunk are also more likely to mummify due to the smaller surface area to volume ratio, and the lower concentrations of adipose tissue than those of a whole body [473]. Similarly due to the separation from the main trunk of the body, and therefore the primary site of bacteria, individual body parts generally decompose slower compared to a whole body [473]. Consequently, it can be difficult to naturally macerate individual skeletal elements without controlling the deposition context. As a result, natural maceration methods lack standardisation, with limited reproducibility due to changeable ambient conditions, and require significant laboratory or outside space to process the specimens. A variety of maceration techniques have been published in scientific literature aiming to speed up the removal of soft tissue whilst limiting damage to the bones.

13.1.2 – PHYSICAL AND INVERTEBRATE MACERATION

Simple physical maceration using scalpels, knives and other tools offers an easy and cost-effective approach to accelerating bone cleaning [474], but total removal of tissue is virtually impossible and substantial osteology knowledge is required to ensure accurate and safe disarticulation and flesh removal without marking underlying bony structures [150, 474]. Couse and Conner (2015) discuss the possibility of power washing using pressurised water jets to dislodge and remove soft tissues from mountain lion skulls. This technique was found to be effective but required a large area to conduct the process safely, as well as a means of collecting the tissue fragments that were sprayed from the skull. The highly pressurised water was also able to dislodge teeth and damage thin or weakened bone including sites exhibiting trauma or pathological modification [150]. Therefore, this technique was deemed unsuitable for forensic casework.

The use of invertebrates is a well-established methodology in museum contexts [475, 476], expediting results whilst still mirroring natural decomposition processes. Invertebrate maceration uses necrophagous invertebrates, which consume the decomposed flesh from skeletal remains [477]. The most commonly used species is Dermestid beetles (*Coleoptera dermestidae*) [466, 475, 478]. This method is in keeping with natural maceration as these types of beetles will generally attend bodies in the advanced stages of decomposition [475] and are particularly helpful in removing tissue that is difficult to reach with scalpels or knives [151]. However, acquisition, cultivation,

and maintenance of Dermestid beetle (*Coleoptera dermestidae*) colonies is time consuming, requiring significant laboratory space and specialist housing due to their ability to bore through many materials [477]. Similarly, if left unattended Dermestid beetles will also consume bone once soft tissue is unavailable [466] and may resort to building pupation chambers in the cortical bone [479]. This behaviour creates destructive scavenging evidence on the bone's surface [479] and throughout the medullary cavity, as illustrated in figures 43 and 44. Offele et al (2007), recorded similar destructive changes when using Dermestid beetles to macerate dental tissues, including increased translucency of tooth roots, which is usually an indicator of advanced age, and therefore could lead to overestimations [466, 480].

The presence of additional bone modifications is especially problematic for forensic investigations, as it can confound morphological interpretations and subsequently impact victim identification or the reconstruction of events. Additionally, as Dermestid beetles attend in the later stages of decomposition, they prefer desiccated soft tissue, which limits the scope of this maceration technique [149]

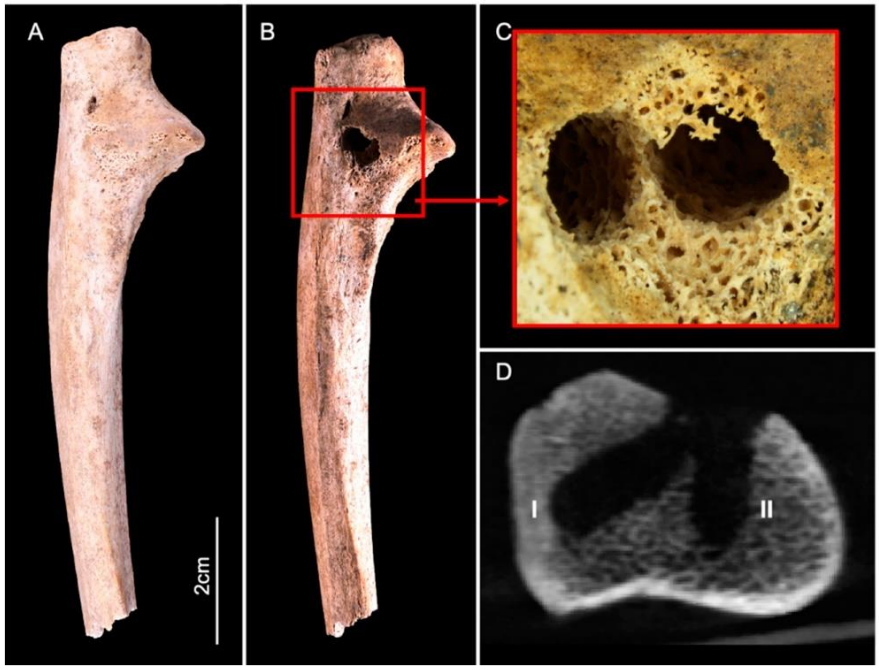

Figure 43: A) Lateral view of a human ulna before exposure to Dermestid beetles, and B) after 30 days exposure C) The red square highlights the prescence of two circular lesions located at the lateral, proximal epiphysis, and D) a cross section of the same lesions via CBCT, illustrating the internal destruction of the trabecular and cortical bone. [479] (Edited by Catherine Maidment, 2023)

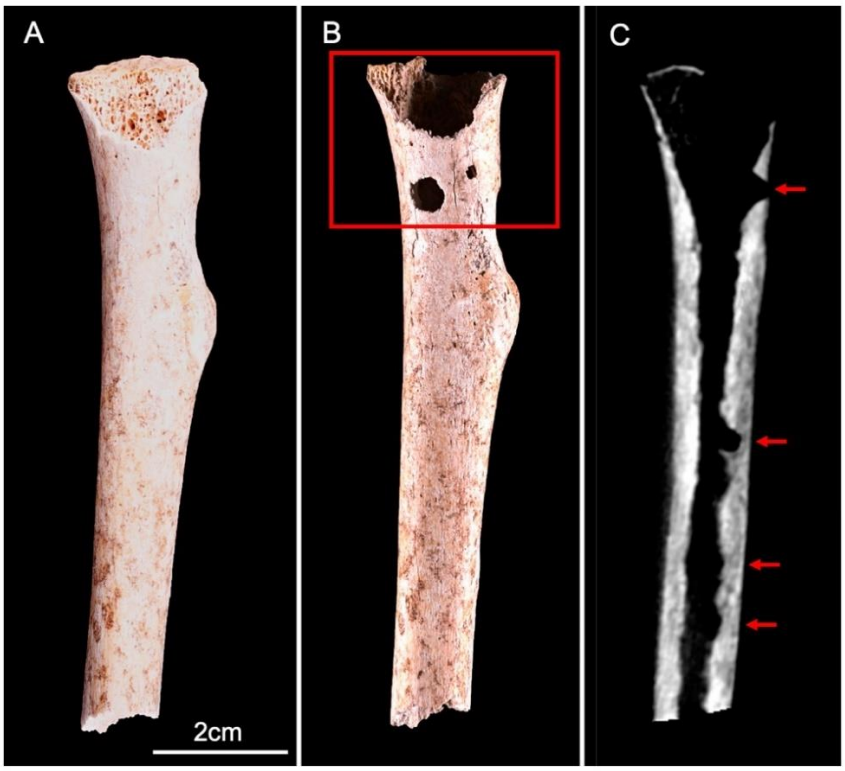

Figure 44: Human radius A) before B) after exposure to Dermestid beetles, showing extensive destruction to the proximal ephiysis and trabecular bone, including thinning of the cortical layer. C) Demonstrates Londitudinal CBCT section of the cortical thinning and drilling of the medullary cavity for pupation chambers (red arrows) [479], (Edited by Catherine Maidment, 2023)

13.1.3- AQUEOUS MACERATION

Historically, aqueous maceration methodologies have been particularly popular within the anthropology community [49, 470]. Submersion in cold or room temperature water is considered the most natural and gentlest approach to aquatic maceration and is often used in museums where time pressures are not as urgent compared to forensic science [467]. This technique is simple, cost effective, and minimises detrimental effects from high temperatures [477], particularly if conducted in an enclosed, temperature-controlled environment such as a laboratory, as it mitigates extreme diurnal and seasonal temperature variations. However, as with terrestrial natural maceration, it is a very slow process, and can typically require months to complete, depending on the size of the subject [470]. In fact, deposition in water usually slows decomposition due to lower ambient temperatures and oxygen levels compared to terrestrial contexts, slowing bacterial proliferation [26]. The water also presents a physical barrier to insects and scavengers, diminishing mechanical decomposition, but also protecting the bone

from consumption damage [26, 481]. However, a high moisture content coupled with an acidic pH level can lead to the formation of adiopocere [45, 482], which would also inhibit decomposition [482]. Similarly, although prolonged submersion will soften tissues, it is usually necessary for the flesh to be manually removed post-submersion, using scalpels and tweezers [470] which further extends the processing time, need for laboratory space, and requires further considerations for the disposal of both contamination water and soft tissue [51]. Due to the extended timescales associated with cold water maceration additional reagents or increased temperatures are typically used to improve effectiveness and speed up reactions [149, 465, 477] .

Higher water temperatures, approximately 37°C and above, boost microbial activity and accelerate the breakdown of tissues [149]. However very high temperatures such as boiling will denature bacteria and enzymes [483] and instead macerate through rapid destruction of tissues [484]. There is a well-established precedent of hot and boiling maceration techniques published in scientific literature [151]. Prolonged boiling is often conducted over several days and is a common method when macerating full skeletons. Many of the human taphonomy facilities around the world employ a method of extended hot or boiling water maceration and historically, the renowned Hamann-Todd and Terry skeletal collection was boiled for approximately 72hrs [379]. However, aggressive heating can also lead to the weakening of periodontal ligaments leading to loss of teeth, which would hinder attempts to identify the individual [156]. Extended boiling can also be highly damaging to bone leading to cracking, splitting, and bleaching due to the loss of collagen through leaching [485] destruction of histological characteristics and molecular material which may be needed for further examination such as DNA or proteomic biomolecules [152, 154, 464].

Gent et al (2023) found that high temperature maceration (up to 87 ˚C) with liquid detergent, was highly damaging to the biomolecular integrity of bovine bones, destroying essential protein markers, and consequently eliminating the possibility of proteomic PMI estimation [152]. In 2004, Arismendi et al (2004) investigated the impact of common maceration techniques on DNA yields from human rib bones including simmering in Arm & Hammer® washing powder, boiling in water alone, and simmering in ALCONOX® powdered detergent, each for a duration of 1.5 hours [486]. They

suggested that neither of the chemicals used in the study were detrimental to DNA extraction and replication, but boiling temperatures and longer durations should be avoided [486]. Similarly, Steadman et al (2006) suggests that hot (90°C) and boiling water (100°C) techniques were effective maceration techniques only when used acutely, as high DNA yields can still be obtained [149], whereas Lee et al (2010) found that treatments exceeding 90°C accelerated DNA degradation, producing poor bone quality in human femora and tibiae samples, with a low success rate for DNA replication [155]. Boiling water alone does not fully remove fats or tissue particularly if located at points of articulation where bone morphology is complex [467] therefore it's common for methodologies to include additional aids such as liquid and powdered detergents to hasten tissue removal as well as chemicals for bleaching, degreasing, and dehydrating to amplify up results [155].

13.1.4 - WASHING POWDER, DETERGENTS, AND BLEACH

The use of biological washing powder and liquid detergent in aqueous maceration is extremely common due to being cheap, simple, easy to carry out, easily taught to others, and fewer potential health and safety concerns [474, 483]. Washing powder contains a mixture of enzymes and detergents making it very effective at removing tissue, grease, and any discolouration from bone [153, 477, 483]. Accompanying heat can promote bacterial action and activate chemical reactions to accelerate maceration and produce aesthetically pleasing results [149]. Compared to traditional manual defleshing techniques or the use of only water, macerating bones in a heated detergent solution reduces the maceration timescales to hours or days rather than weeks or months [151]. This shortened duration is more favourable for forensic investigations where time is limited and the trajectory of ongoing investigations will be dictated by the results of osteological examinations, such as the identification of the deceased, or possible cause of death [474]. However, commercial washing powders and detergents can alter the cortical surface of bone, altering the essential landmarks and often leading to a chalky appearance figure 45 [149]. The quantity and concentration of the ingredients contained in commercial washing powders, including enzymes and additional ingredients such as bleaching additives, vary between brands and are considered proprietary knowledge, therefore precise quantities are usually not obtainable [465]. This creates further

difficulties when assessing the suitability of a product for maceration and fuels the use of inherited techniques to ensure reproducibility, although reformulation of products and reagents over time could also cause inconsistencies.

Bleaching chemicals such as hydrogen peroxide or sodium hypochlorite are used to deflesh, degrease, whiten, and sterilise bone [470, 487]. As a strong alkali, bleach oxidises proteins leading to the quick breakdown of soft tissues [470] and producing an aesthetically pleasing white colouration to bone, as shown in figure 46 [487-489]. Consequently, bleaching was popular in the curation of museum collections, but it's use has now become infrequent due to heightened awareness of the damage it can cause to bone structures and underlying molecular compounds, and consequently not used for forensic casework [477]. When used in isolation, and when combined with washing powder and/or boiling water, bleach can compromise the cortical structure of bone, making it brittle, and leading to splitting and fraying [149, 487]. Prolonged exposure causes extensive surface damage as demonstrated in figure 47, and destruction of bone microstructure [467] including thinning of bone layers [151], smoothing of skeletal morphology and trauma characteristics, and erosion of histological features [156, 467].

Potassium hydroxide is another heavy alkaline solution known to effectively macerate and degrease bone, but it also causes surface cracks and shrinkage due to rapid desiccation and dehydration [467] and is known to dissolve bone if left for too long [490], and is therefore often avoided. In the papers that examine the retention of osteological DNA during maceration it was found that submersion in bleach solutions was the most deleterious to DNA yields and purity, when comparing multiple maceration techniques including washing powder/detergent preparations, microwaving, and boiling [149, 155, 484].

Figure 45: The appearance of porcine phalange after 2 months submersion in room temperature 30% peroxide solution, [491] (Edited by Catherine Maidment, 2023)

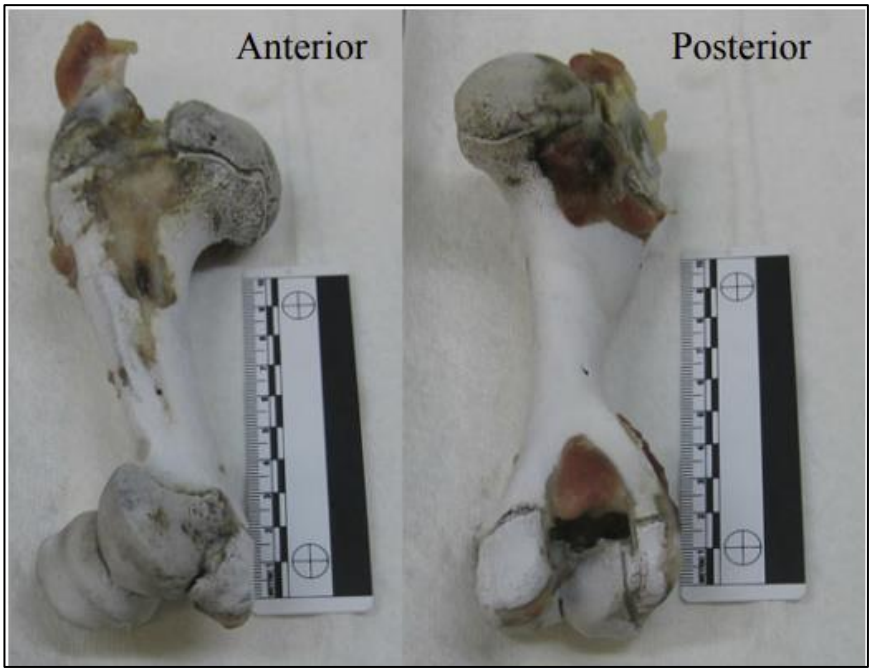

Figure 46: Anterior and posterior images demonstrating macroscopic bleaching changes present on a porcine humerus (Sus scrofa domesticus) simmered for 1 hour in 25% peroxide [489] (Edited by Catherine Maidment, 2023)

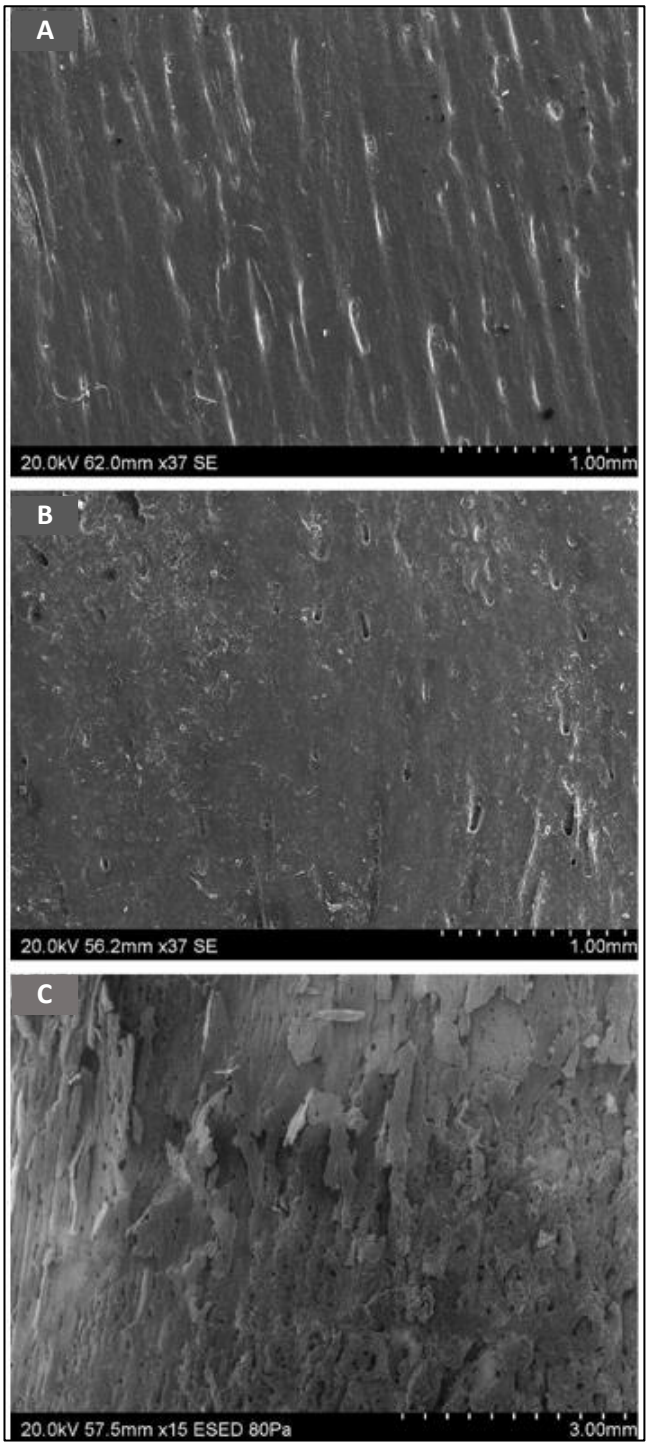

Figure 47: A) SEM photomicrograph demonstrating typical result following microwave maceration (×37 magnification) B) SEM photomicrograph illustrating the typical surface changes associated with manual maceration (×37 magnification). C) SEM photomicrograph showing the extensive cortical flaking and destruction of the natural morphology and texture resulting from sodium hypochlorite maceration (×15 magnification) [156]

However, Mann and Berryman (2012) assert that household bleaching is a viable method for defleshing skeletal remains if carefully monitored and conducted in short bursts, such as 15–20 mins, and they highlighted the need to thoroughly rinse the bones with water to halt any further chemical reactions [470]. Specifically, they suggest bleach maceration can assist investigators when interpreting cartilaginous trauma as the bleach does not dissolve the cartilage, or when examining small, delicate bones not pertinent to DNA analysis or victim identification but still valuable for forensic investigation, such as the hyoid and nasal turbinates [470].

Conversely Steadman et al (2006) found that soaking porcine ribs in 10% bleach solution (sodium hypochlorite) was the most destructive technique out of the eleven procedures tested, producing an inconsistent chalky appearance with increased porosity at the sternal ends and flaking cortices [149]. However, the minimum submersion interval used for this technique was 12 days with a maximum of 70 days, with loose soft tissue being removed by hand whenever the solution was changed. This prolonged duration and gradual increase in bone exposure will have contributed to the significant bone damage reported.

Most anthropological techniques rely on the interpretation of bone morphology and calculations of skeletal metrics to create estimations regarding sex, age, and stature [110]. For example, the shape of the mental eminence and the degree of the mandibular angle are scrutinised when estimating sex, whereas measuring the length of long bones is vital for stature calculations [110]. Ultimately, the results of these examinations could contribute to the inclusion or exclusion of possible identities when making comparisons to missing persons records, and therefore influence the trajectory of the investigation. Similarly, any alteration to the dimensions of trauma such as cut marks including the width, kerf floor, or striation/tooth marks would have an impact when attempting to match suspected weapons [156], and subsequently influence the allocation of downstream analyses such as DNA or fingerprint analysis. This would not only have implications for the cost of a case but possibly lead to misinterpretations and misdirection of the police enquiries.

13.1.5- ENZYMATIC

Targeted chemical maceration using chosen enzymes in controlled quantities has been cited in literature as a faster and gentler alternative to washing powder and bleaching, requiring lower temperatures and shorter durations, ensuring the retention of bone structure and morphological features [465, 492, 493]. The inclusion of targeted enzymes such as proteases to breakdown proteins and lipases to dissolve lipids can reduce the inclusion of additional destructive additives, and allow more stringent control over quantities used, reducing the risk of corrosion to cortical bone and the bone matrix [465]. However, some authors suggest that enzymes can be unpredictable and difficult to handle [151], and are more expensive than other techniques, whilst requiring more specialist storage and more complex risk assessment [474, 477]. Papain, pancreatin, trypsin and pepsin have all been explored in literature as they mirror enzymes used in commercial washing powders and/or common digestive enzymes [149, 156].

King and Birch (2015) found that pancreatin maceration conducted at 35°C produced inconsistent results in porcine ribs, noting damage to the cortical surface through flaking and alteration to inflicted stab wounds [156]. Yin et 2010 found that although room temperature trypsin maceration did not increase porosity in macerated lamb femora, there was a reduction in bone hardness yield most likely due to weakening of the collagen fibres, which was not seen in samples macerated in room temperature water alone [493]. However, other studies report more positive results, such as Simonsen et al (2011), who examined the maceration of whole mice and rats using a formulation of liquid protease and lipase in water heated to 55°C ± 5°C. They reported that a whole rat was successfully macerated in 3 hours and whole mice took as little as 1 hour and exhibited comparable skeletal surface changes seen in the warm water maceration control specimens, which took 4-7 days [465].

Uhre et al (2015) examined changes in cut marks and DNA quality in macerated sections of human ribs using washing powder in boiling water and a liquid protease and lipase solution at 55°C ± 5°C. It was concluded that although both techniques effectively macerated the specimens, the enzymatic solution was faster and gentler, macerating the rib sections in 3 hours rather than 24 hours. The cut marks on the ribs subjected to washing powder maceration exhibited a high level of fraying and breakage, with

decreased tool mark detail compared to the those macerated in the enzyme solution [492].

As noted in each of these studies, enzymatic preparations typically require lower temperatures to ensure optimal lytic action without denaturation [487]. This is particularly beneficial for skeletal remains as historically it was thought that the highly reactive hydroxyapatite [324] and the more vulnerable organic content of bone could become irreversibly altered or destroyed when exposed to high temperatures [324, 464]. However other studies have hypothesised that destructive thermal alterations to bone may not occur until temperatures reach over 100°C [138], and more specifically that shorter durations of heat exposure may still be acceptable [149], whereas 'overcooking' should be avoided [155, 470]. This is illustrated by the success seen in microwaving methodologies such as Steadman et al (2006) and King and Birch (2015), where bursts of heat were successfully used to macerate porcine ribs and were reportedly the most efficient and gentle approach when compared to other traditional aqueous methods [149, 156]. These conclusions were also echoed in further findings by Uhre et al (2015), who noticed only minor surface changes to cut marks inflicted on human ribs which were boiled for a short duration, with no evidence of molecular change [492].

13.1.6 – MACERATION AND BONE FLUORESCENCE

However, there are no studies directly evaluating the impact of maceration on bone fluorescence produced via ALS. The limited published literature focuses on the applications of bone ALS or photography optimisation, with most studies examining fluorescence of burned bone and how thermal destruction of the proteinaceous organic content leads to a decrease in fluorescence [158, 307]. Other studies concentrate on methodological development such as wavelength and filter combination [132], distance from ALS to specimen [133], and influence of time and the deposition environment [146]. In most cases the bone samples used in these studies have been prepared for examination; described as dried, heat treated, or macerated with warm water [132, 133, 135] but with no discussion into the details of the defleshing techniques used, and whether this may have influenced the fluorescence seen [132, 133, 135, 266]. As

discussed in the paragraphs above, the use of prolonged high heat is known to have detrimental effects on bone structure, which could damage the organic content [149].

As the organic component of bone is thought to be responsible for bone fluorescence, any damage, specifically to the collagen aspect, could negatively influence fluorescence levels. In addition to this, some washing powders also contain fluorescence additives and optical brighteners, in addition to bleach, which are intended to make white clothing appear whiter [279]. The inclusion of these additives could also be problematic for ALS analysis, as it's possible these fluorescent chemicals may also respond to ALS stimulation potentially causing artificial inconsistencies in the observed fluorescence output, a problem which has been seen in body fluid recovery where clothing has been washed [246, 249]

ALS analysis of bone is the most responsive when the bone is free from residual tissue and cartilage, as retained tissue creates a physical barrier between the light source and the bone, preventing molecular excitation [134]. In previous MSc work conducted by this author examining the bone fluorescence of 17 porcine bones of different types, residual cartilage and connective tissue retained at the epiphyses of bones during manual defleshing did not fluorescence when exposed to blue light approximately 450 nm [134]. Although cartilage also contains collagen it is type I rather than type II, as discussed in section 9.0 [341], which contains fewer aromatic rings [494, 495] and therefore also does not respond to the light source. Consequently, maceration is a much-needed step when preparing bone for ALS analysis, particularly in a laboratory environment.

Although it is very unlikely macerated bones would be found at a crime scene, an extended post-mortem interval will naturally lead to the decomposition of soft tissues, culminating in skeletal remains. Current search strategies concentrate on the early post-mortem period, as discussed in chapter 5.0, with no current techniques specifically aimed at locating skeletal remains. Therefore, it is vital to investigate the basic relationship between bone fluorescence and ALS, so that more contextual understanding can then be extrapolated. Without further investigation into the influence of maceration, it is difficult to accurately interpret any currently published osteological ALS results, and consequently determine whether this is a viable search

methodology. These challenges are further exacerbated by the lack of standardisation in maceration techniques used in these studies and omission of the precise methodology used [132, 133, 135, 266]. These factors present problematic ramifications for the validity of any future work that may have been based on these findings. Therefore, to build a greater understanding of the mechanisms surrounding bone fluorescence production, and to inform further experimentation within this PhD project, a suitable maceration technique needs to be found.

As a result, three popular maceration techniques were examined in a pilot study to answer research question one. Methods were developed from literature and informed by common anthropology practice, with a focus on exploring the influence of temperature and the maceration substrate on bone integrity, collagen content, and subsequent autofluorescence. Method one was hot water maceration, conducted at 80°C to evaluate the impact of high temperature, method two was a biological washing powder solution heated to 50°C so not to denature the enzymes, and to restrict the influencing factor to the washing powder. The third method was a targeted enzymatic approach adapted from Steadman et al (2006) and Uhre et al (2015) [149, 492], consisting of 20 ml of protease and 20 ml of lipase in 1 L of tap water heated to an optimised temperature of 55°C. Further detail for each methodology can be seen in the method chapter 13.3. All methods required limited laboratory space and equipment, and could be performed in accordance with forensic timescales [151].

13.2- MATERIALS

Thirty porcine ribs (*Sus scrofa domesticus*) were obtained fresh from a local butcher based in Huddersfield. The ribs were purchased as individual ribs rather than racks to ensure there was natural variability within the sample. The ribs were manually defleshed using a PM40 scalpel to remove any large portions of flesh and help standardise the amount of residual tissue across all specimens. Manual defleshing was completed in small batches of five ribs to limit any degradation, with each rib taking approximately five minutes to deflesh. Once defleshed the ribs were kept frozen at -18°C until use and defrosted overnight in the refrigerator (2°C) the night before. After manual defleshing, the average mass of the porcine ribs used in this pilot study was 18.34 g. To aid discussion regarding the influence of bone composition on the success of the different maceration techniques, each rib was categorised based on identifiable osteological landmarks, to ascertain the most likely anatomical region of the rib. Figure 48 below details the number of vertebral, sternal, and diaphysis rib sections used in this pilot study. All ribs were randomly allocated to each maceration technique.

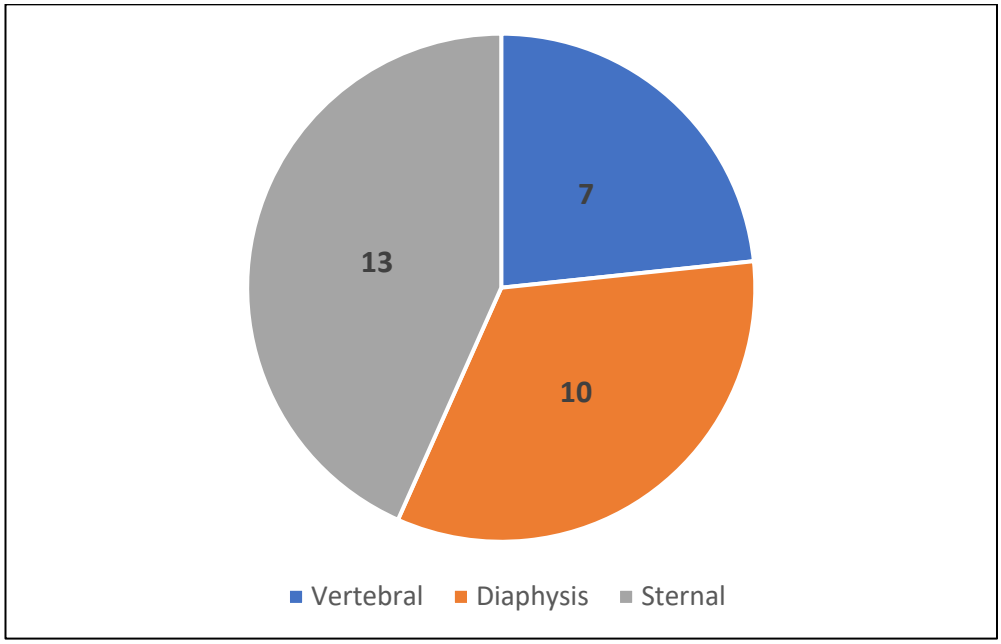

Figure 48: Ratio of ribs used in the maceration pilot study based on anatomical region

13.3- METHOD

Three common maceration methods were explored during this pilot study. Ten porcine ribs per technique were macerated in two individual sessions of five ribs. This was to prevent overcrowding within the maceration containers and to ensure even exposure to the reagents used. For all techniques the ribs were initially observed every 30 mins until nearing completion when the intervals were reduced to 15 mins, 10 mins and then 5 mins to ensure maximum maceration but to prevent overcooking.

1. Hot water maceration

Two sessions of five porcine ribs (*Sus scrofa domesticus*) were submerged in 1 L of tap water within a Morphy Richards™ 48709 stainless steel 3.5 L slow cooker set to high (fig. 49). A slow cooker was used as it is considered common practice throughout biological anthropology as it is cheap, convenient, and more gradual compared to boiling. Once the water had reached the desired temperature (80°C), recorded using a digital thermometer, the ribs were added to the slow cooker.

Figure 49: Slow cooker used to perform hot water maceration (80°C)

2. Washing powder and warm water maceration

For each session, five porcine ribs (*Sus scrofa domesticus*) were macerated in a 6.2 L stainless-steel stockpot containing 50 ml of Surf biological washing powder dissolved in 1 L of tap water (total volume 1.05 L) heated to 50°C using a Velp Scientifica AREX digital CerAlTop™ hot plate. The temperature was measured using a digital thermometer. The washing powder was added to the water once it had reached 50°C, stirred to ensure even distribution, and then the ribs were added.

3. Enzyme maceration

For each session, five porcine ribs (*Sus scrofa domesticus*) were macerated in a solution comprising of 20 ml Novozymes Savinase® liquid protease and 20ml Novozymes Lipex® liquid lipase in 1 L of tap water (1.04 L total volume). Both enzymes were obtained from the National Centre for Biotechnology Education, University of Reading, and were produced by submerged fermentation of a genetically modified microorganism followed by a purification process. This solution was heated to 55°C in a 6.2 L stainless-steel stockpot, using a Velp Scientifica AREX digital CerAlTop™ hot plate, positioned in a fume cupboard to limit inhalation exposure. The temperature was measured using a digital thermometer. Once the water reached 55°C the enzymes were added and the solution stirred to ensure even distribution, the five ribs were then introduced to solution. Figure 50 illustrates the stockpot and hotplate equipment set up, including submersion of the bones.

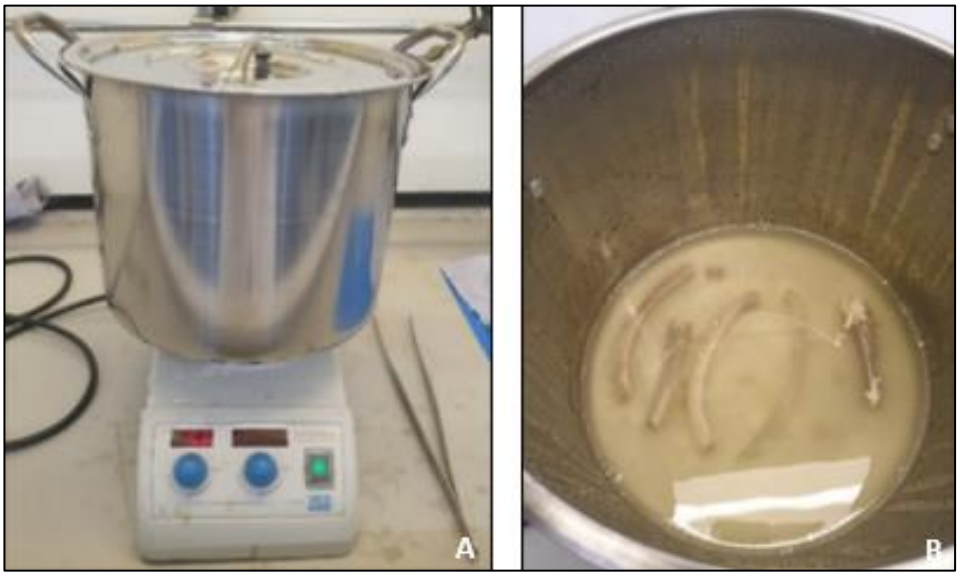

Figure 50: Equipment configuration used during the washing powder and enzymatic maceration techniques. A) Stockpot on hot plate, B) Example of porcine ribs in maceration solution.

Throughout maceration, the lids of the slow cooker and stockpot were kept closed to help maintain temperature and to limit evaporation. For all the techniques, maceration was considered complete once all grease was removed from the bones, and any remaining tissue could be lifted off easily. After the maceration was complete, the duration was recorded, and the ribs were removed from the solutions. The ribs were

then rinsed with cold deionised water for 5 mins to halt any further changes and photographed under natural light, to record any surface modifications. The samples were then left to dry overnight at room temperature (18˚C) and fluorescence photography was conducted the following day. Maceration duration was not standardised across the three methodologies to prevent bone changes occurring due to overprocessing. Final maceration durations for each technique can be seen in the results chapter 14.0.

A basic visual scoring system to quantify the surface changes of the macerated bones was conducted by adapting Steadman et al (2005) study examining the effects of chemical and heat maceration on the recovery of osseous DNA. Despite being subjective in nature, the implementation of a scoring system enabled comparative measurement of surface texture modifications. In their study, Steadman et al (2005) examined the ease of flesh removal, soft tissue texture, and the odour of each examined maceration technique in addition to bone quality. However, the primary objective of this pilot study is to establish whether maceration may be modifying bone composition and subsequently impacting fluorescence output. Therefore, only the scoring system related to bone quality was relevant. The descriptive parameters of the scoring system can be seen in table 4 below: but in brief, a number between one and five is assigned based on the observed physical changes in bone texture, such as porosity, erosion, and flexibility, with a score of one indicating the poorest preservation and five the most preserved.

Table 4: Bone quality scoring and descriptions used to score the final maceration results (adapted from Steadman et al, 2005) [149].

Score	Description
1	Brittle, fragile, easily broken
2	No cortical erosion but bone is lighter in weight and porous
3	Softer, more pliable than normal bone but no cortical damage
4	Cortex eroding and/or flaking but bone will not easily fracture
5	Strong, normal bone texture and quality

13.3.1 – COLLAGEN QUANTIFICATION

Thermogravimetric analysis (TGA) was used to quantify the collagen content of the porcine ribs. Bone samples were scraped from the central anterior surface of each rib (fig. 51 below) onto a clean piece of filter paper using a size 10 scalpel, before being transferred to individual 2 ml plastic tubes. The scrapings were frozen (-18°C) to limit bacterial growth and defrosted overnight in the refrigerator (2°C) before processing. For each sample, 5mg of bone scrapings was processed in an alumina crucible (70µl) in a Nitrogen atmosphere using a Mettler Toledo TGA machine at a flow rate of 50 ml per minute. Each sample ran for 75 mins with an insertion temperature of 25°C increasing 10°C per minute to a final temperature of 800°C. Interpretation and analysis concentrated on phase 2 of the resulting profile i.e., the organic content (as discussed in chapter 12.4), so that collagen levels could then be calculated. This was conducted using tangential equations produced through the integrated Star analysis TGA software to measure the thermogram curves and therefore quantify the changes in mass. Collagen content of the bones was calculated as 90% of the organic peak measured by TGA, as this represents the typical collagen content discussed in literature [130].

Figure 51:The central anterior aspect of a porcine rib where collagen scraping for TG analysis were obtained

13.3.2 – PHOTOGRAPHY

A Nikon D3100 Digital Single Lens Reflex (DSLR) camera fitted with an AF-S Nikkor 18-55mm lens was used in conjunction with a Calumet tripod. The default UV filter was removed from the camera and automatic photography settings were used to maximise fluorescence exposure and capture. The distance from the camera to the specimen was set at 25 cm with a camera zoom of 40 mm to ensure full coverage of the specimen whilst limiting background interference.

During photography, the specimens were housed in a 32 L black box by Really Useful Storage Ltd and a 1.6 x 2.1 m sheet of black photography cloth was placed over the camera and box to block out the natural light (figure 51). The ALS was a Crime-lite 2 by Foster and Freeman Ltd™ which consists of single LED that produces a narrow beam of blue light at 420 – 470 nm with a peak of 450 nm. For each photograph, the Crime-lite 2 was positioned directly adjacent to the camera to ensure a constant distance from the specimen (25 cm). Each specimen was firstly photographed under natural light with a scale and then in situ within the black box with 300 white 10 mm polystyrene spheres. These spheres were used to act as a control, to enhance contrast, and to reduce reflections from the black plastic box, as this had proven helpful in other papers [132] and previous MSc work [134]. The specimens were then photographed using the Crime-lite 2 with an orange barrier filter attached to the camera lens. The full photography set up is illustrated in figure 52 below, and figure 53 A-C demonstrates examples of photographs taken per sample.

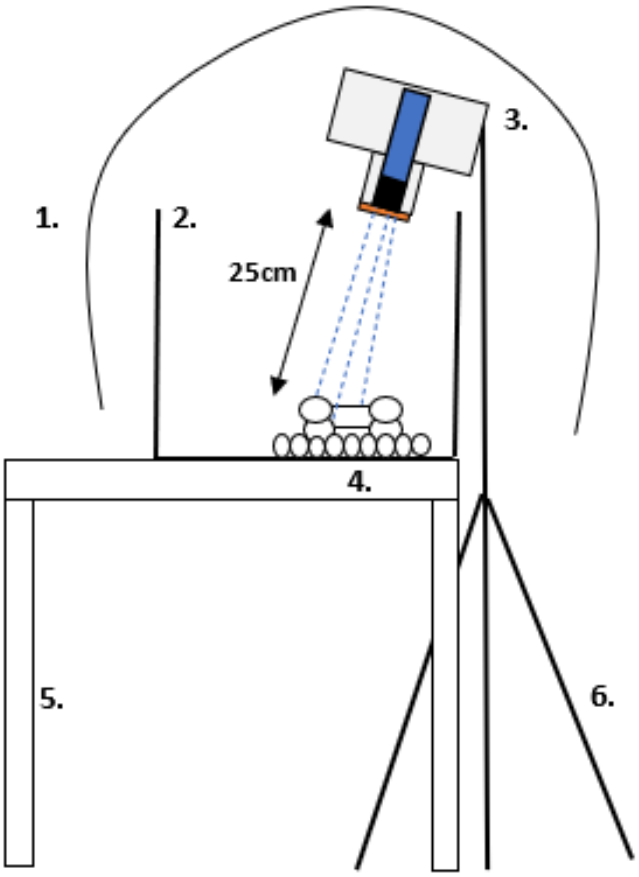

1. Photography cloth
2. Black box
3. Camera with coloured filter, and Crime-Lite 2
4. Polystyrene spheres
5. Table
6. Tripod

Figure 52: Equipment configuration for fluorescence photography

Figure 53: Example of photographs taken per porcine rib (Sus Scrofa Domesticus) sample A) Natural light with scale, B) Natural light, in situ with polystyrene spheres, C) Fluorescence photograph consisting of blue light 450nm with orange camera filter.

13.3.3 – FLUORESCENCE ANALYSIS

To quantify bone fluorescence, a bespoke C++ computer program: the "Osteo-Fluorescence Calculator" (OFC) was designed by this author and created by software engineer Liam MacDonald. As discussed in section 11.3, commonly used software such as ImageJ and Photoshop have been used in current literature primarily due to free access and/or previous familiarity [147], but are designed for broad image analysis. The OFC speeds up and simplifies the computation of multiple photographs, resulting in faster computing output as well as an overall more transparent and easily reproducible process. It also allows implementation of features specifically designed for this project, such as a grid to select regions of interest, which can be difficult to perform effectively in ImageJ or Photoshop.

After each photography session, all photographs were transferred from the SD memory card to a desktop computer and processed using the OFC. Each 6000 x 4000 jpeg image was converted to grayscale using the *Luminosity* equation as discussed in section 11.3. The image was then overlain with a 300 x 300-pixel grid, with each square labelled with the calculated fluorescence and coordinates to allow selection of regions of interest (ROI). Three adjacent grid squares located on the central anterior aspect of each rib were selected as ROIs, due to the most exposed bone being present, the light distribution being the most consistent, and the same anatomical location the bone scrapings were obtained for collagen analysis. Three photographs for each specimen were used to calculate an overall average fluorescence. All fluorescence data and corresponding grid coordinates of ROIs were collated in an excel spreadsheet for statistical analysis. Figure 54 is an example output of the OFC program and a transcript of the C++ source code can be seen in appendix 1. The final fluorescence value is a computer-generated figure representing pixel intensity, which ranges from 0 (pure black) to 255 (pure white), as such there are no units associated with this number [408].

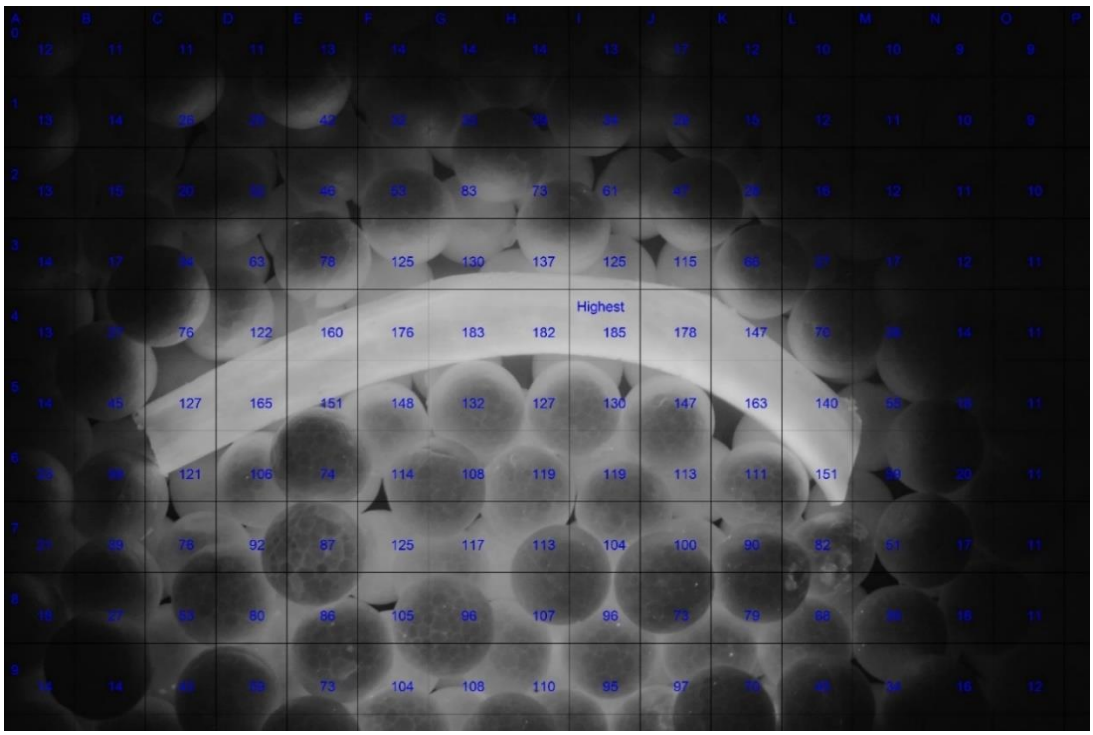

Figure 54: A final grayscale image of a porcine rib (Sus scrofa domesticus) processed using the OFC.

13.3.4 – STATISTICAL ANALYSIS

All statistical analysis was conducted using IBM™ SPSS Statistics v23 software and Microsoft Excel spreadsheets using a combination of paired student t-tests and bar graphs to interpret potential relationships and correlations seen. More specifically, analyses focused on examining any changes in observed bone fluorescence, calculated collagen volume, and bone mass that may have occurred due to maceration. Comparative analysis between the three techniques was also conducted to evaluate whether any of the maceration methods was a suitable preparation technique for bone destined for ALS analysis.

14.0 – MACERATION PILOT STUDY RESULTS

The final maceration durations for each maceration technique and individual maceration session can be seen in the table 5 below:

Table 5: Final maceration duration for sample set and each maceration technique.

Maceration technique	Maceration duration (mins)	
	Specimens 1-5	Specimens 6-10
Hot water (80°C)	175	173
Bio. washing powder (50°C)	205	210
Enzymatic (55°C)	75	62

For simplicity, the results of each maceration technique will be discussed in turn, followed by an overarching discussion and conclusion.

14.1 – HOT WATER MACERATION

This technique took a maximum of 2 hours and 55 minutes to complete. All ribs exhibited a uniform creamy grey-beige colouration and were clean of all residual tissue. There was no evidence of increased porosity, erosion, flaking, or fractures, although some slightly drier surface patches were noted on the anterior surface of ribs 1-3. The bones felt robust, with no evidence of structural modification. Figures 55 and 56 demonstrate the final surface texture of all ten ribs photographed under natural light. Overall, this led to a bone quality score of 5 for all ten ribs, and consequently an average score of 5, indicating the highest level of bone quality. Bone quality scores for all ribs for each maceration technique are tabulated in appendix 2.

Figure 55: Final appearance of porcine ribs (Sus scrofa domesticus) after hot water maceration (approx. 80°C), ribs 1-5

Figure 56: Final appearance of porcine ribs (Sus scrofa domesticus) after hot water maceration (approx. 80°C), ribs 6-10

14.1.1 – COLLAGEN QUANTIFICATION AND BONE MASS

Table 6 below summarises the results of the collagen quantification for the hot water maceration obtained using TGA, alongside a summary of the calculated changes in bone mass and collagen content. On average the porcine ribs experienced a 2.91 g (14.7%, s.d.= 0.38) loss of bone mass ranging from 1.64 g up to 4.55 g, when macerated in hot water (80°C) as illustrated in figure 57. Bone collagen levels exhibited a decrease across all samples (figure 58), with a minimum loss of 0.02 mg up to the greatest loss of 0.33 mg, and a calculated average of 0.09mg (11.2%, s.d.= 0.09). Conversely, rib 3 exhibited a slight increase of 0.02mg (3.4%), but this most likely a result of variation in instrument measurement rather than a true increase in collagen. All respective TGA thermograms for the hot water maceration method can be seen in appendix 3.

Table 6: Results of collagen quantification of ten porcine ribs (Sus scrofa domesticus) subjected to hot water maceration (approx. 80°C), including summary of changes in mass and collagen content.

Rib	Fresh			Macerated (Hot water approx. 80°C)			% change in collagen content	% change in bone mass
	Mass (g)	Total organic content (mg)	Calculated collagen content (90%)	Mass (g)	Total organic content (mg)	Calculated collagen content (90%)		
1	22.29	0.9010	0.785	18.51	0.8779	0.566	-2.6%	-17.0%
2	31.58	0.7063	0.824	27.03	0.6888	0.632	-2.5%	-14.4%
3	26.87	0.6192	0.853	24.35	0.6403	0.671	+3.4%	-9.4%
4	16.32	0.8599	0.823	14.68	0.8017	0.740	-6.8%	-10.0%
5	19.09	0.8927	0.837	15.92	0.7683	0.587	-13.9%	-16.6%
6	25.81	0.8919	0.893	22.31	0.7657	0.754	-14.1%	-13.6%
7	17.80	1.0841	0.975	15.00	0.7209	0.665	-33.5%	-15.7%
8	14.47	0.9146	0.835	12.24	0.7513	0.613	-17.9%	-15.4%
9	22.29	0.8622	0.862	18.38	0.7990	0.622	-7.3%	-17.5%
10	20.21	0.9056	0.805	16.62	0.7528	0.662	-16.9%	-17.8%
						Average	-11.2%	-14.7%

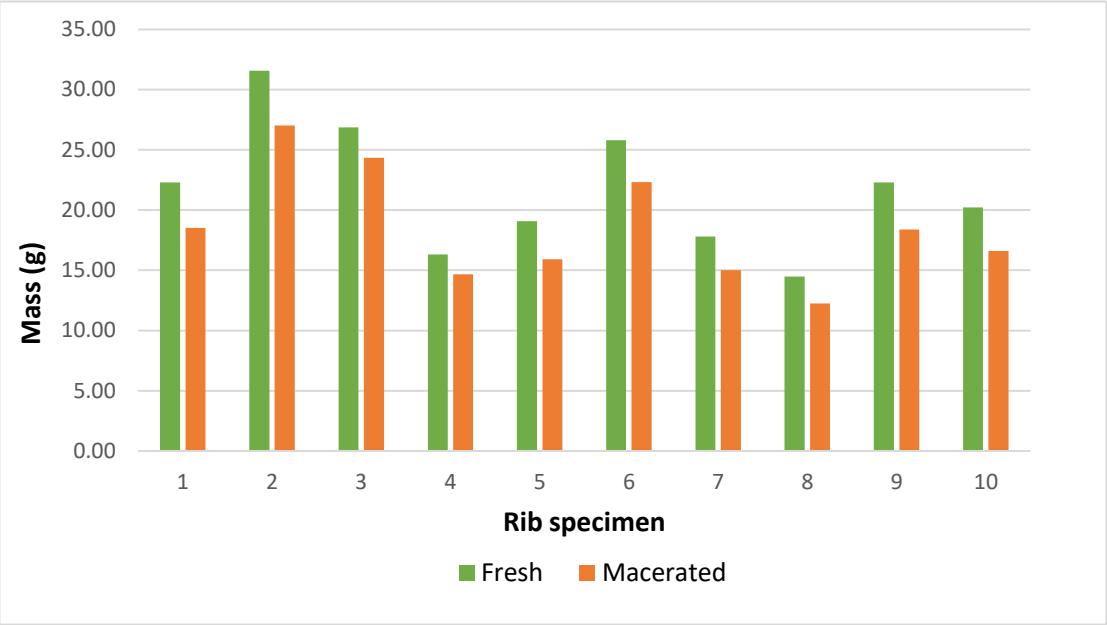

Figure 57: Changes in bone mass of ten porcine ribs (Sus scrofa domesticus) macerated in hot water (approx. 80°C)

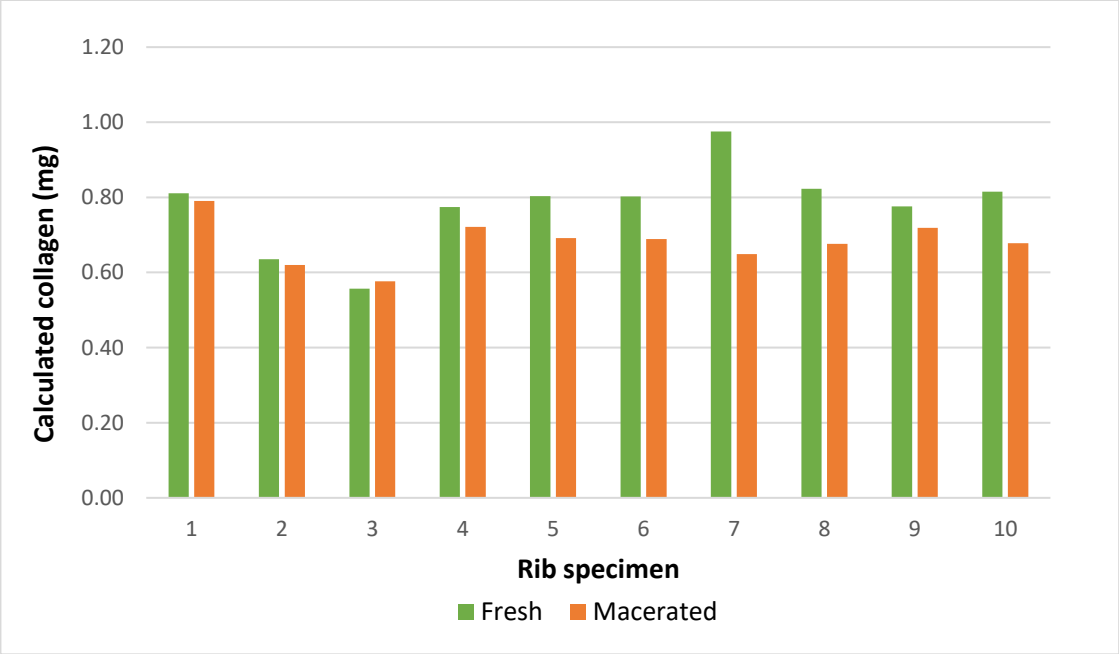

Figure 58: Changes in calculated bone collagen of ten porcine ribs (Sus scrofa domesticus) macerated in hot water (approx. 80°C)

14.1.2- FLUORESCENCE

Table 7 below summarises the photographic results for each porcine rib before and after hot water maceration. These photographs were selected as they were the most representative of the fluorescence results, however all fluorescence photographs can be seen in appendix 4.

Table 7: Summary of photographic results of 10 porcine ribs (Sus Scrofa Domesticus) before and after hot water maceration (approx. 80°C)

Rib	Fresh	Fluorescence	Macerated	Fluorescence
1		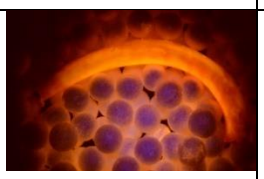		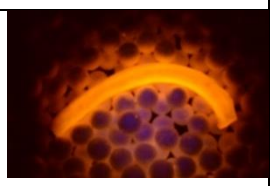
2		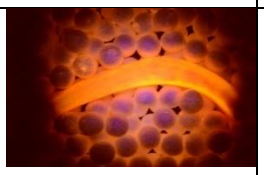		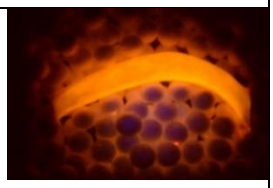
3		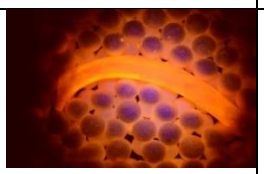		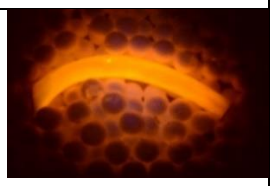
4		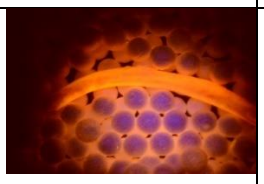		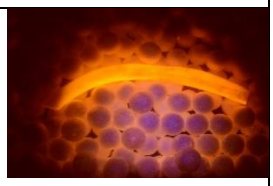
5		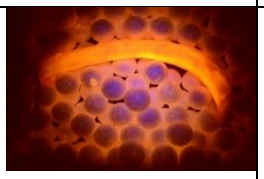		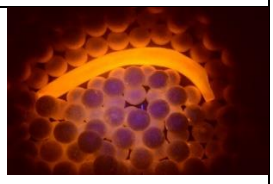
6		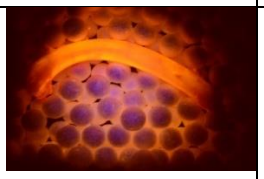		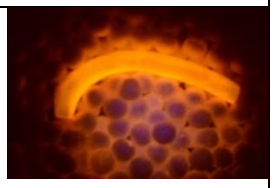
7		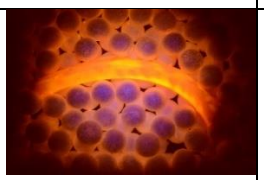		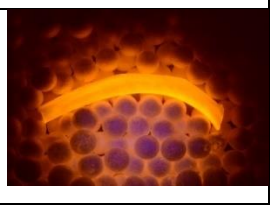

8		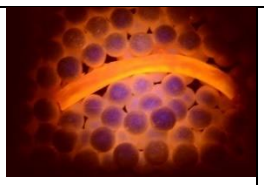		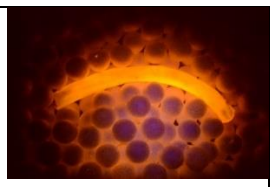
9				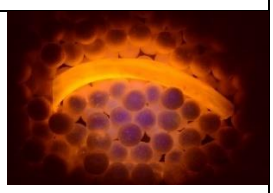
10		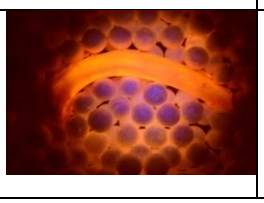		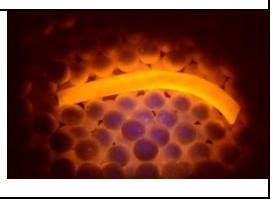

Table 8 and figure 59 display the changes in average bone fluorescence for each porcine rib after hot water maceration. The full list of fluorescence values for each ROI can be seen in appendix 5a.

As expected, there was generalised increase in observed fluorescence within the dataset, ranging from 1.56 up to 26.67, but with an average of 8.51 (5.5%, s.d.= 0.83). This increase in fluorescence can be attributed to the elimination of residual tissue and cartilage, exposing the bone underneath. However, rib 2 and rib 9 experienced a slight decrease in observed fluorescence by 6.78 and 1.44 respectively. This decrease was unexpected, and as it is limited to only two of the ten ribs it is more likely an anomalous result, possibly related to methodology, which will be examined in more detail in the discussion element of this pilot study.

Table 8: Average fluorescence values for porcine ribs (Sus scrofa domesticus) subject to hot water maceration (approx. 80°C), alongside calculated fluorescence and percentage change

Rib	Average fresh fluorescence	Average macerated fluorescence	Difference	% change
1	141.6	168.2	+26.67	+18.8%
2	173.6	166.8	-6.78	-3.9%
3	160.0	174.3	+14.33	+9.0%
4	152.4	168.7	+16.22	+10.6%
5	175.3	183.8	+8.44	+4.8%
6	160.3	161.9	+1.56	+1.0%
7	177.8	179.7	+1.89	+1.1%
8	171.2	182.1	+10.89	+6.4%
9	170.3	168.9	-1.44	-0.8%
10	163.7	177.0	+13.33	+8.1%
		Average	+8.51	+5.5%

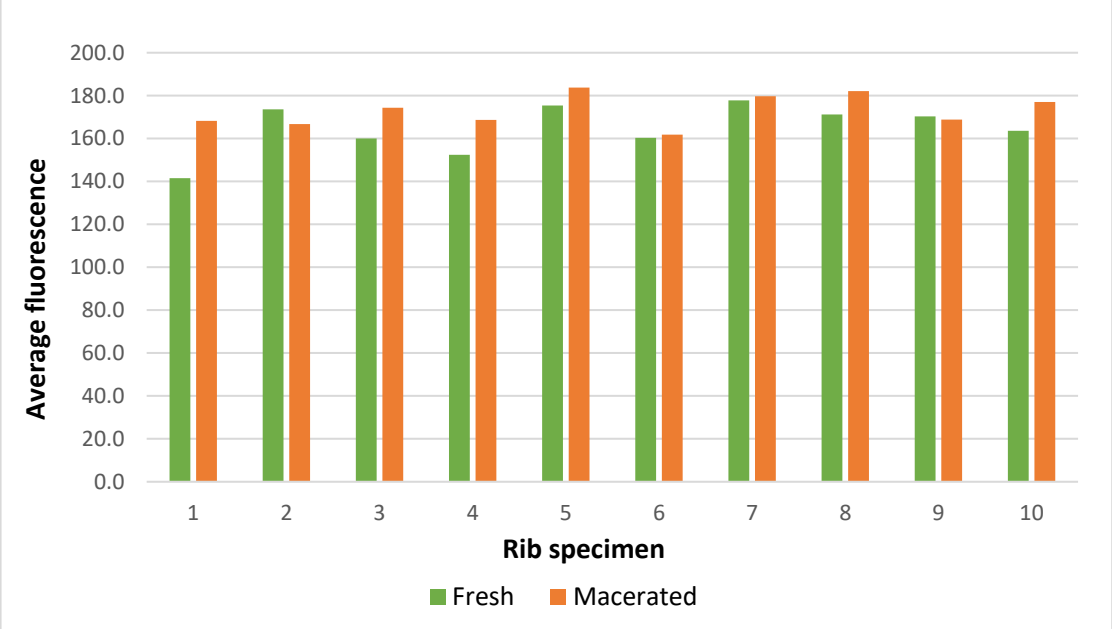

Figure 59: Changes in average fluorescence of 10 porcine ribs (Sus scrofa domesticus) macerated in hot water (approx. 80°C)

14.1.3 – STATISTICAL ANALYSIS

Histograms were produced in IBM™ SPSS Statistics v23 to test the normality of the data for the fresh and macerated average fluorescence values, and to inform consequent statistical analysis. As detailed in appendix 6a, the data was shown to be abnormally distributed, therefore a non-parametric Wilcoxon signed-rank test was conducted. The Wilcoxon signed-rank was chosen in favour of other nonparametric tests such as the Mann-Whitney U test, as the variables of pre and post maceration averaged fluorescence were considered dependent rather than independent. Results showed a strong statistically significant relationship (p= .022) between the fresh and macerated fluorescence values (fig. 60), and the subsequent recommendation to reject the null hypothesis.

Hypothesis Test Summary

	Null Hypothesis	Test	Sig.	Decision
1	The median of differences between Av.F.Fluor and Av.M.Fluor equals 0.	Related-Samples Wilcoxon Signed Rank Test	.022	Reject the null hypothesis.

Asymptotic significances are displayed. The significance level is .05.

Figure 60: Results of Wilcoxon signed-rank test, comparing fresh and macerated fluorescence values of ten porcine ribs (Sus scrofa domesticus) subjected to hot water maceration (approx. 80°C)

Histograms testing the distribution for bone mass and collagen data indicated a normal distribution, therefore parametric paired samples student t-tests were performed to test the hypothesis that hot water maceration led to the changes in mass and collagen. The results showed statistically significant differences between fresh and macerated bone mass (M= 3.169, SD= .27) p= .000, as well as between fresh and macerated collagen content (M= .092, SD= .029) p= .012, as shown in figure 61 below.

Paired Samples Statistics

		Mean	N	Std. Deviation	Std. Error Mean
Pair 1	F.Mass	21.6730	10	5.24281	1.65792
	M.Mass	18.5040	10	4.68727	1.48225
Pair 2	F.Coll1	.7350	10	.10554	.03337
	M.Coll1	.6430	10	.05658	.01789
Pair 3	Av.F.Fluor	164.6200	10	11.37285	3.59641
	Av.M.Fluor	173.1400	10	7.31683	2.31378

Paired Samples Correlations

		N	Correlation	Sig.
Pair 1	F.Mass & M.Mass	10	.991	.000
Pair 2	F.Coll1 & M.Coll1	10	.477	.163
Pair 3	Av.F.Fluor & Av.M.Fluor	10	.515	.127

Paired Samples Test

		Paired Differences					t	df	Sig. (2-tailed)
		Mean	Std. Deviation	Std. Error Mean	95% Confidence Interval of the Difference Lower	Upper			
Pair 1	F.Mass - M.Mass	3.16900	.87517	.27675	2.54294	3.79506	11.451	9	.000
Pair 2	F.Coll1 - M.Coll1	.09200	.09295	.02939	.02551	.15849	3.130	9	.012
Pair 3	Av.F.Fluor - Av.M.Fluor	-8.52000	9.85538	3.11654	-15.57011	-1.46989	-2.734	9	.023

Figure 61: Results of paired-samples t-test analysis, comparing the changes in bone mass, calculated collagen content, and average fluorescence, of the ten ribs subjected to hot water maceration (approx. 80°C)

These results suggest that the observed changes in bone mass, collagen content, and emitted fluorescence were the direct result of the hot water maceration preparation technique.

14.2 – BIOLOGICAL WASHING POWDER

The biological washing powder technique took a maximum of 3 hours and 30 minutes to reach completion. All ribs produced a mostly pale grey-white final colouration, with particularly white areas along prominent edges. Patches of darker brown pigmentation were evident where the cortical bone had been eroded and/or was flaking, producing an overall inconsistent appearance across each bone and the dataset (fig. 62 and 63). Although there were no obvious structural changes, such as fractures or splitting, and the bones still felt robust, there was a noticeable reduction in weight when handled.

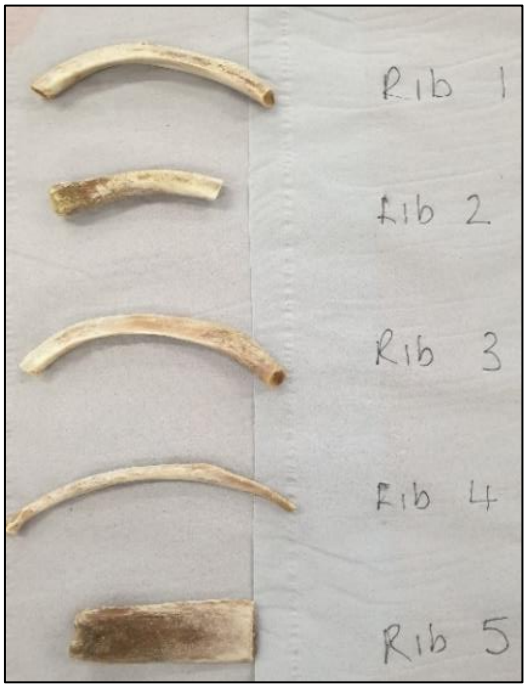

Figure 62: Final appearance of porcine ribs (Sus scrofa domesticus) post biological washing powder maceration (approx. 50°C), ribs 1 – 5

Figure 63: Final appearance of porcine ribs (Sus scrofa domesticus) post biological washing powder maceration (approx. 50°C), ribs 6 - 10

Nine out of the ten bones also displayed more advanced bone modifications including fraying at the epiphyses and along the inferior margins, with evidence of increased porosity noted in ribs 2, 6, 8, and 10. Figures 64-66 provide more detailed images of the surface changes found on ribs 2, 6 and 8 respectively. Correspondingly, bone quality scores were poorer compared to the hot water maceration results, with a median score of 4 and an overall average score of 4.3. However, based on the criteria outlined by Steadman et al (2005), a score of 4.3 is still indicative of good preservation.

Figure 64: Surface changes exhibited by rib 2 after being macerated in the washing powder solution (approx. 50°C)

Figure 65: Surface changes exhibited by rib 6 after being macerated in the washing powder solution (approx. 50°C)

Figure 66: Surface changes exhibited by rib 8 after being macerated in the washing powder solution (approx. 50°C)

14.2.1 – COLLAGEN QUANTIFICATION AND BONE MASS

The results of the collagen quantification conducted using TGA, as well as the changes in bone mass, can be seen in table 9 and figures 67 and 68. All bones subjected to

maceration with biological washing powder experienced a substantial loss of bone mass and collagen content, with an average collagen loss of 0.19 mg (22.9%, s.d. = 0.05) but a range between 0.08 mg and 0.27 mg. The reduction in bone mass ranged from 0.98 g to 4.55 g, with an average loss of 2.6 g (12.6%, s.d. = 1.02). All fresh and macerated TGA thermograms for the washing powder dataset are available in appendix 7.

Table 9: Results of collagen quantification of ten porcine ribs (Sus scrofa domesticus) subjected to maceration with biological washing powder (approx. 50°C), including summary of changes in mass and collagen content.

Rib	Fresh			Macerated (Biological washing powder approx. 50°C)			% change in collagen content	% change in bone mass
	Mass (g)	Total organic content (mg)	Calculated collagen content (90%)	Mass (g)	Total organic content (mg)	Calculated collagen content (90%)		
1	16.51	0.8722	0.785	14.30	0.6294	0.566	-27.8%	-13.4%
2	12.55	0.9154	0.824	10.78	0.7021	0.632	-23.3%	-14.1%
3	18.37	0.9478	0.853	16.78	0.7459	0.671	-21.3%	-8.7%
4	7.58	0.9148	0.823	6.60	0.8222	0.740	-10.1%	-12.9%
5	21.72	0.9296	0.837	17.17	0.6518	0.587	-29.9%	-20.9%
6	17.31	0.9922	0.893	15.77	0.8378	0.754	-15.6%	-8.9%
7	23.63	1.0346	0.931	20.16	0.7391	0.665	-28.6%	-14.7%
8	15.94	0.9278	0.835	14.40	0.6811	0.613	-26.6%	-9.7%
9	15.67	0.9580	0.862	14.05	0.6906	0.622	-27.9%	-10.3%
10	18.45	0.8948	0.805	16.13	0.7353	0.662	-17.8%	-12.6%
						Average	-22.9%	-12.6%

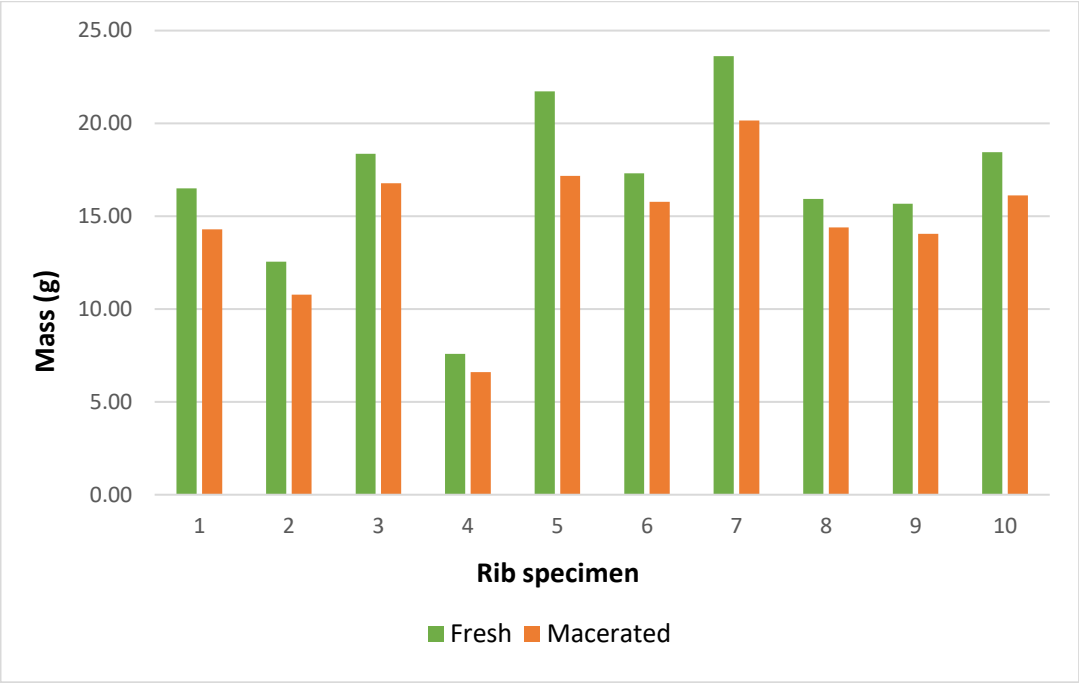

Figure 67: Changes in mass of ten porcine ribs (Sus scrofa domesticus) macerated in biological washing powder (approx. 50°C)

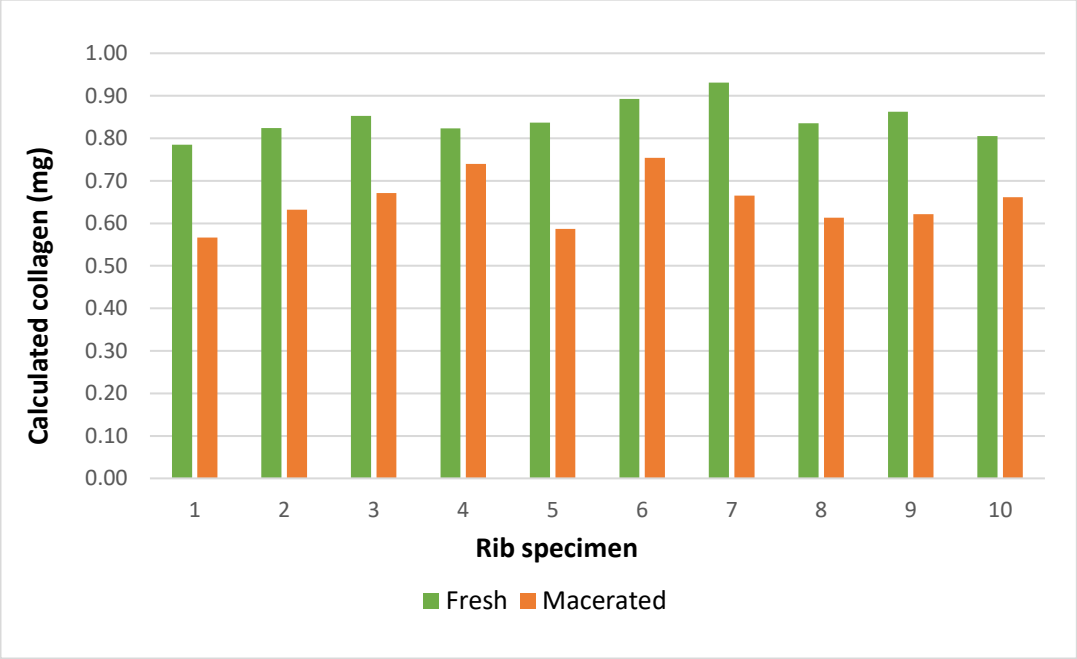

Figure 68: Changes in collagen content of the ten porcine ribs (Sus scrofa domesticus) macerated in biological washing powder (approx. 50°C)

14.2.2 – FLUORESCENCE ANALYSIS

Table 10 below summarises the photographic results for each rib before and after maceration with biological washing powder. These photographs were included as they are the most representative of the fluorescence results, however all fluorescence photographs for this technique are available in appendix 8.

Table 10: Summary of photographic results of ten porcine ribs (Sus scrofa domesticus) before and after maceration with biological washing powder (approx. 50°C)

Rib	Fresh	Fluorescence	Macerated	Fluorescence
1		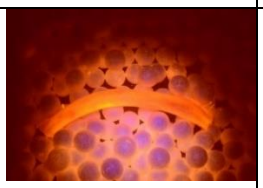		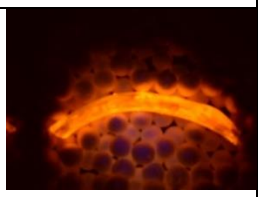
2		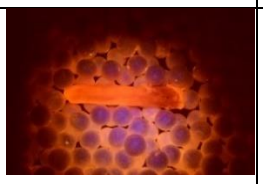		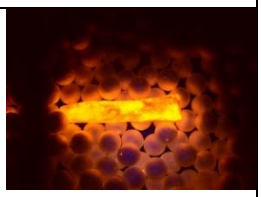
3		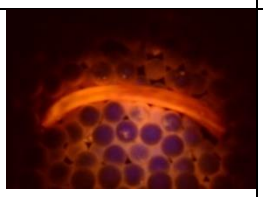		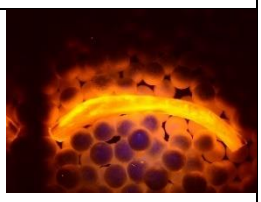
4		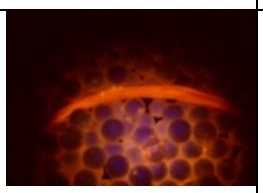		
5		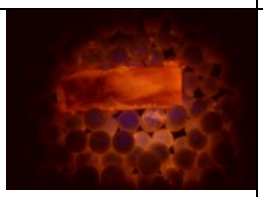	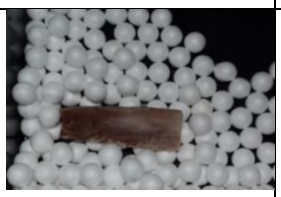	
6		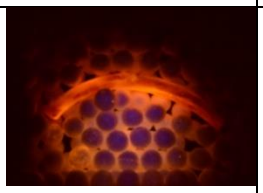		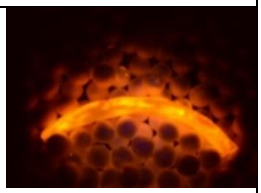

7		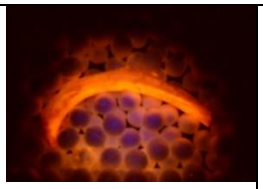		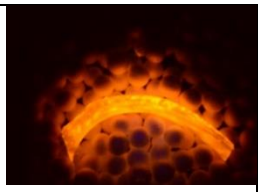
8		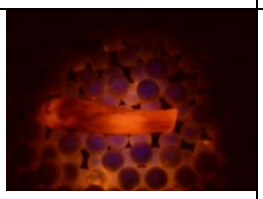		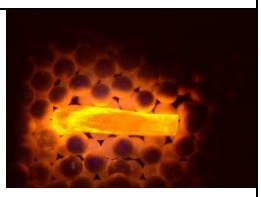
9		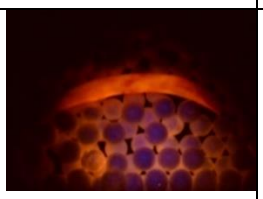		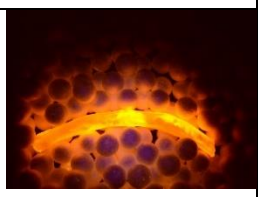
10		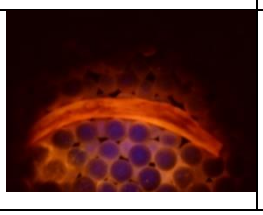		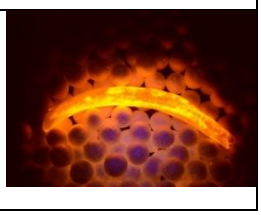

A comparison of average fluorescence values of the porcine ribs before and after maceration, alongside the calculated changes, can be seen in table 11 and figure 69 below. Overall, this maceration technique produced the greatest increase in observed bone fluorescence and was the only technique in the pilot study where all the ribs within the group experienced an increase in fluorescence. A wide spread of fluorescence increases was recorded, from 1 up to 103.33 with an overall average increase of 54.49 (49.3%, s.d.= 27.46). A full list of fluorescence results for each photograph and ROI can be seen in appendix 5b.

Table 11: Average fluorescence values for ten porcine ribs (Sus scrofa domesticus) subject to biological washing powder maceration (approx. 50°C), alongside calculated fluorescence and percentage change

Rib	Average fresh fluorescence	Average macerated fluorescence	Difference	% change
1	150.9	153.0	+2.11	+1.4%
2	128.4	197.8	+69.33	+54.0%
3	121.1	186.0	+64.89	+53.6%
4	92.3	143.3	+51.00	+55.2%
5	106.4	128.7	+22.22	+20.9%
6	107.4	169.3	+61.89	+57.6%
7	140.0	180.2	+40.22	+28.7%
8	114.3	162.7	+48.33	+42.3%
9	104.6	207.9	+103.33	+98.8%
10	101.3	182.9	+81.56	+80.5%
		Average	+54.49	+49.3%

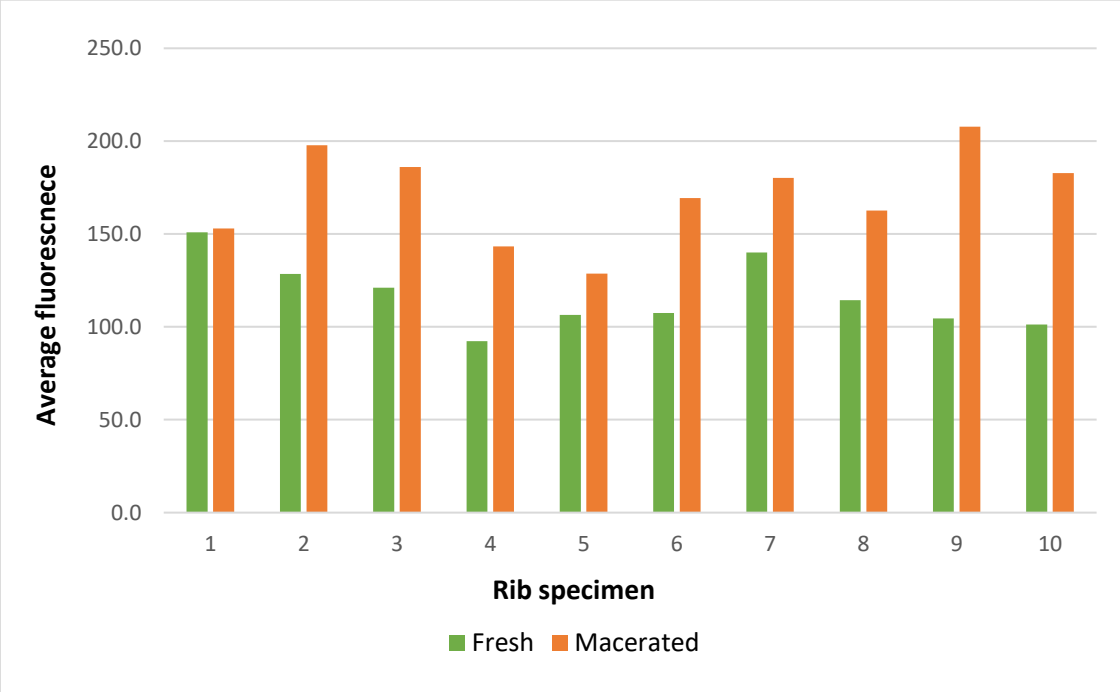

Figure 69: Changes in average fluorescence of the ten porcine ribs (Sus scrofa domesticus) macerated in biological washing powder (approx. 50°C)

14.2.3 – STATISTICAL ANALYSIS

Histograms (available in appendix 6b) identified normalised distributions for the bone mass and calculated collagen data, therefore paired samples student t-tests were produced. Results indicated strong statistically significant relationships between pre and post maceration bone mass (M= 2.15, SD= 1.07) p= .000 and collagen content (M= 0.18, SD= 0.05) p= .000 (Fig. 70), indicating that the biological washing powder maceration was responsible for the observed reduction in bone collagen and mass.

Paired Samples Statistics

		Mean	N	Std. Deviation	Std. Error Mean
Pair 1	F.Mass	16.7730	10	4.49032	1.41996
	M.Mass	14.6140	10	3.72683	1.17853
Pair 2	F.Coll2	.7980	10	.03994	.01263
	M.Coll2	.6150	10	.05817	.01839
Pair 3	Av.F.Fluor	142.840	10	21.7160	6.8672
	Av.M.Fluor	154.060	10	19.5471	6.1813

Paired Samples Correlations

		N	Correlation	Sig.
Pair 1	F.Mass & M.Mass	10	.983	.000
Pair 2	F.Coll2 & M.Coll2	10	.430	.214
Pair 3	Av.F.Fluor & Av.M.Fluor	10	.304	.394

Paired Samples Test

		Paired Differences					t	df	Sig. (2-tailed)
		Mean	Std. Deviation	Std. Error Mean	95% Confidence Interval of the Difference Lower	Upper			
Pair 1	F.Mass - M.Mass	2.15900	1.07425	.33971	1.39053	2.92747	6.355	9	.000
Pair 2	F.Coll2 - M.Coll2	.18300	.05458	.01726	.14396	.22204	10.603	9	.000
Pair 3	Av.F.Fluor - Av.M.Fluor	-11.2200	24.4119	7.7197	-28.6832	6.2432	-1.453	9	.180

Figure 70: Results of paired-samples t-test analysis, comparing the changes in bone mass, calculated collagen content, and average fluorescence, of the ten ribs subjected to biological washing powder maceration (approx. 50°C)

The averaged fluorescence data produced an abnormal distribution when inputted into a histogram (appendix 6b). Consequently, a nonparametric test of related samples, Wilcoxon signed-rank test, was performed (fig. 71).

Hypothesis Test Summary

	Null Hypothesis	Test	Sig.	Decision
1	The median of differences between Av.F.Fluor and Av.M.Fluor equals 0.	Related-Samples Wilcoxon Signed Rank Test	.241	Retain the null hypothesis.

Asymptotic significances are displayed. The significance level is .05.

Figure 71: Results of Wilcoxon signed-rank test, comparing fresh and macerated fluorescence values of ten porcine ribs (Sus scrofa domesticus) subjected to biological washing powder maceration (approx. 50°C)

The outcome of this test suggests acceptance of the null hypothesis as there was no statistically significant relationship in the observed average fluorescence before and after maceration (p= .241). However, this result was expected due to the inconsistent spread in fluorescence levels identified during image analysis.

14.3 – ENZYMATIC MACERATION

Enzymatic maceration of the porcine ribs took a maximum of 1 hours and 15 minutes and resulted in a generalised grey-beige colouration across all ribs (figures 72 and 73). However, some patches of diffuse pinkish-red discolouration could be seen in ribs 2-4, with bands of dark brown staining observed at the neck of most ribs, graduating to paler pigmentation towards the distal margin. Some cartilage remained at the proximal ends, but the previously adherent tissue was completely removed. There was also slight evidence of fraying noted on the proximal ends of ribs 1, 3, 8 and 10. There was no evidence of major structural changes, and the bones felt robust, although a greasy residue was noted on all bones post maceration. Bone quality scoring produced an average of 4.6, with a median of 5, indicating high levels of preservation, greater than the biological washing dataset, but not as high as hot water maceration.

Figure 72: Final appearance of porcine ribs (Sus scrofa domesticus) post enzymatic maceration (approx. 55°C), ribs 1 - 5

Figure 73: Final appearance of porcine ribs (Sus scrofa domesticus) post enzymatic maceration (approx. 55°C, ribs 6 -10

14.3.1- COLLAGEN

Table 12 and figures 74 and 75 display the results of the collagen quantification obtained through TGA, as well as the calculated changes in bone mass and collagen content. As

with both previous maceration techniques, this maceration technique produced an overall loss in bone mass across all ten ribs, with a minimum loss of 1.34 g and a maximum loss of 7.51 g, there was an average reduction of 3.23 g (19%, S.D 1.84). With regards to collagen, this technique produced intermediate results compared to the previous two maceration techniques, resulting in a 0.15 mg (19.5%, S.D 0.09) average loss in collagen content, ranging from 0.03mg to 0.31mg. All TGA thermograms for the enzymatic dataset can be seen in appendix 9.

Table 12: Results of collagen quantification for the ten porcine ribs (Sus scrofa domesticus) subjected to enzymatic maceration (approx. 55°C)

Rib	Fresh			Macerated (enzymatic approx. 55°C)			% change in collagen content	% change in bone mass
	Mass (g)	Total organic content (mg)	Calculated collagen content (90%)	Mass (g)	Total organic content (mg)	Calculated collagen content (90%)		
1	16.47	0.8586	0.73	14.09	0.7814	0.66	-9.0%	-14.5%
2	19.43	0.7959	0.68	14.49	0.7641	0.65	-4.0%	-25.4%
3	17.63	0.8219	0.70	13.33	0.7589	0.65	-7.7%	-24.4%
4	18.83	0.9139	0.78	17.2	0.7709	0.66	-15.6%	-8.7%
5	19.51	0.9156	0.78	12.00	0.6576	0.56	-28.2%	-38.5%
6	13.69	0.8799	0.75	10.33	0.6143	0.52	-30.2%	-24.5%
7	11.67	0.8419	0.72	10.33	0.6565	0.56	-22.0%	-11.5%
8	24.00	0.7648	0.65	20.67	0.6679	0.57	-12.7%	-13.9%
9	14.92	0.9368	0.80	13.08	0.5891	0.50	-37.1%	-12.3%
10	9.71	0.8633	0.73	8.08	0.6207	0.53	-28.1%	-16.8%
						Average	-19.5%	-19.0%

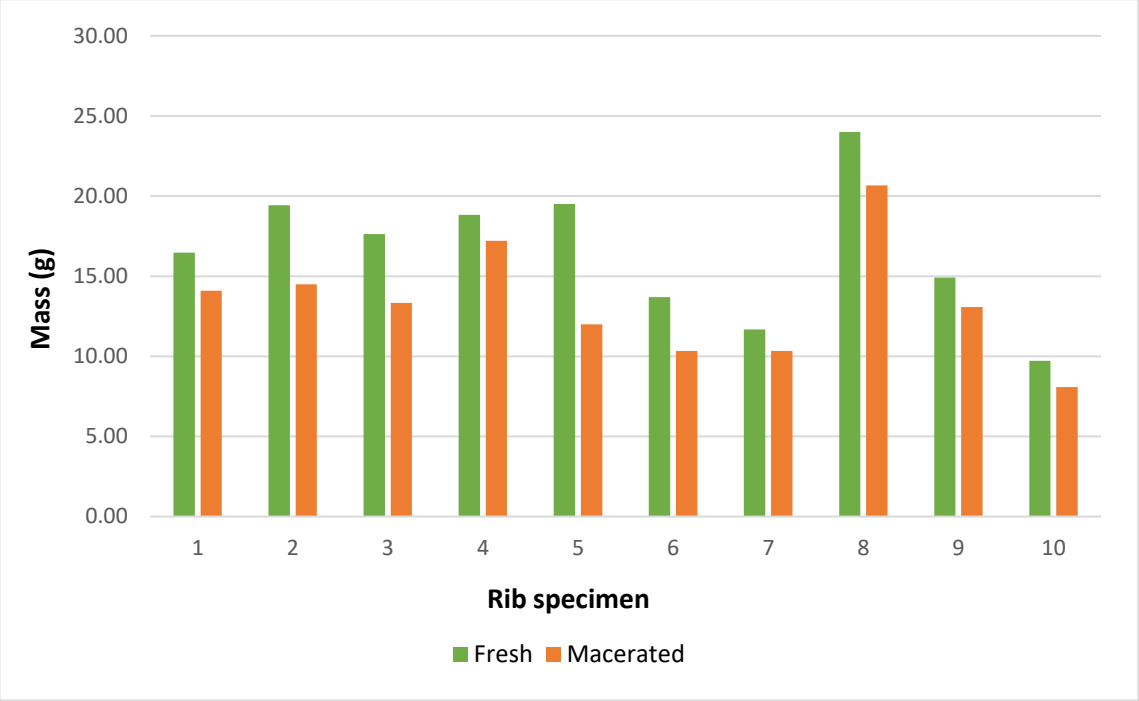

Figure 74: Changes in bone mass of ten porcine ribs (Sus scrofa domesticus) subjected to enzymatic maceration (approx. 55°C)

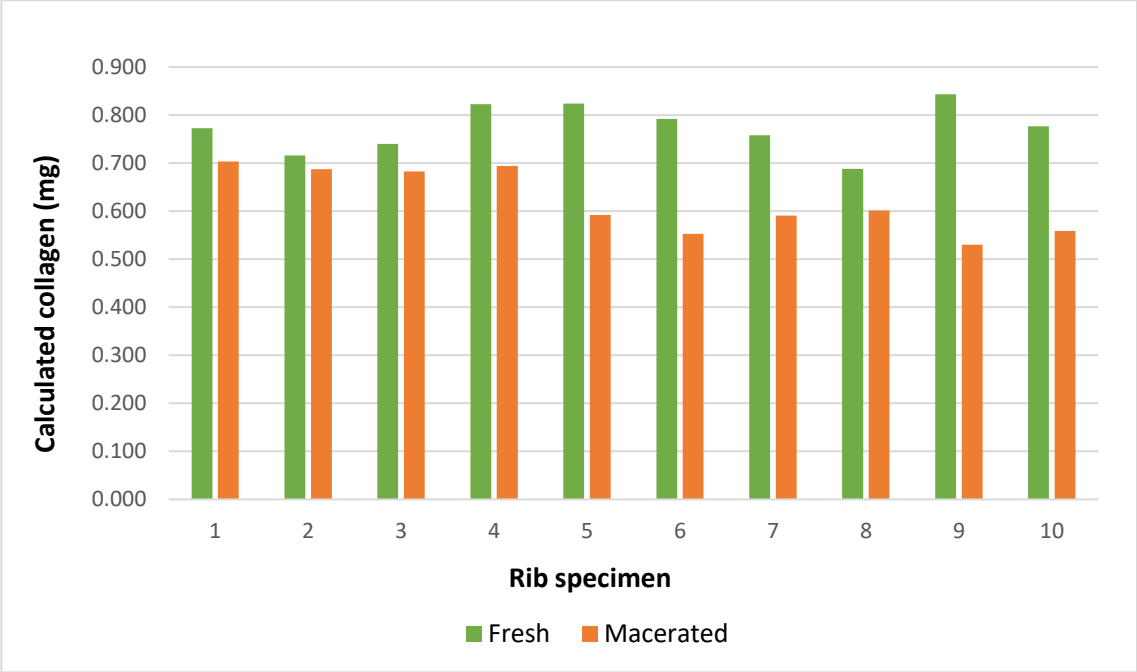

Figure 75: Changes in collagen content of ten porcine ribs (Sus scrofa domesticus) subjected to enzymatic maceration (approx. 55°C)

14.3.2- FLUORESCENCE

Table 13 summarises the photographic results for each porcine rib before and after

maceration with enzymatic maceration (55°C). The photographs in the table were chosen as the most representative of the fluorescence seen, but all fluorescence photographs for this technique can be seen in appendix 10.

Table 13: Summary of photographic results of ten porcine ribs (Sus scrofa domesticus) before and after enzymatic maceration (approx. 55°C)

Rib	Fresh	Fluorescence	Macerated	Fluorescence
1		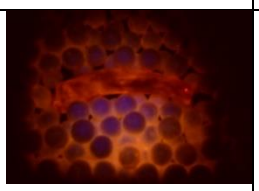		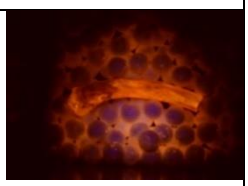
2		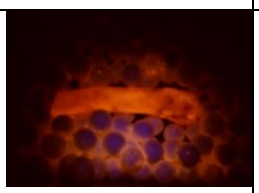		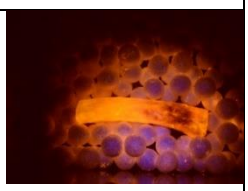
3		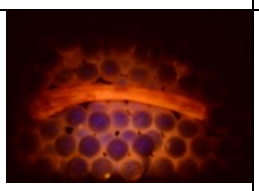		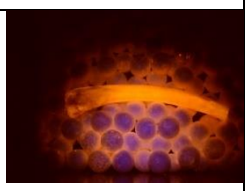
4		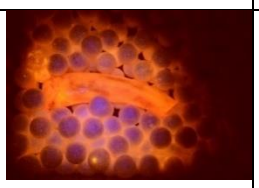		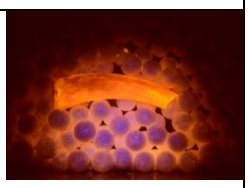
5		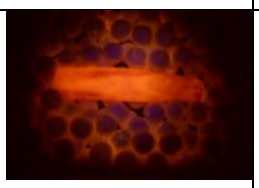		
6				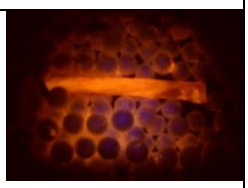
7		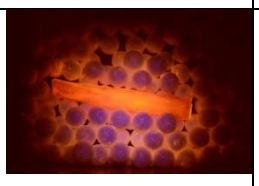		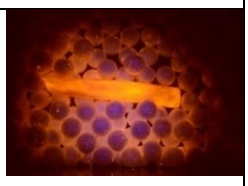
8		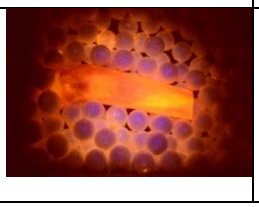		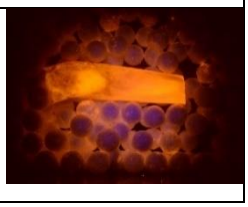

9		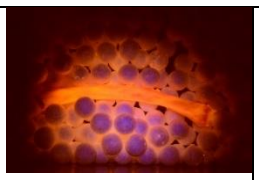		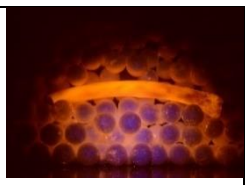
10		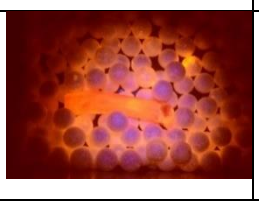	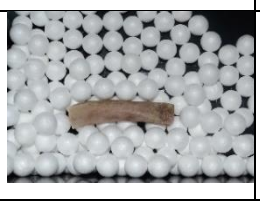	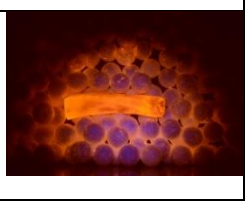

A comparison of the average fluorescence values before and after enzymatic maceration is detailed in table 14 and figure 76 below, alongside the calculated percentage changes.

Table 14: Average fluorescence values for porcine ribs (Sus scrofa domesticus) subject to enzymatic maceration (approx. 55°C), alongside calculated fluorescence and percentage change

Rib	Average fresh fluorescence	Average macerated fluorescence	Difference	% change
1	44.3	105.3	+61.00	+137.6%
2	107.4	155.3	+47.89	+44.6%
3	130.6	167.7	+37.11	+28.4%
4	146.4	162.3	+15.89	+10.8%
5	138.1	164.0	+25.89	+18.7%
6	155.8	138.9	-16.89	-10.8%
7	169.1	169.9	+0.78	+0.5%
8	155.0	150.9	-4.11	-2.7%
9	159.2	158.1	-1.11	-0.7%
10	159.4	168.2	+8.78	+5.5%
		Average	+17.52	+23.2%

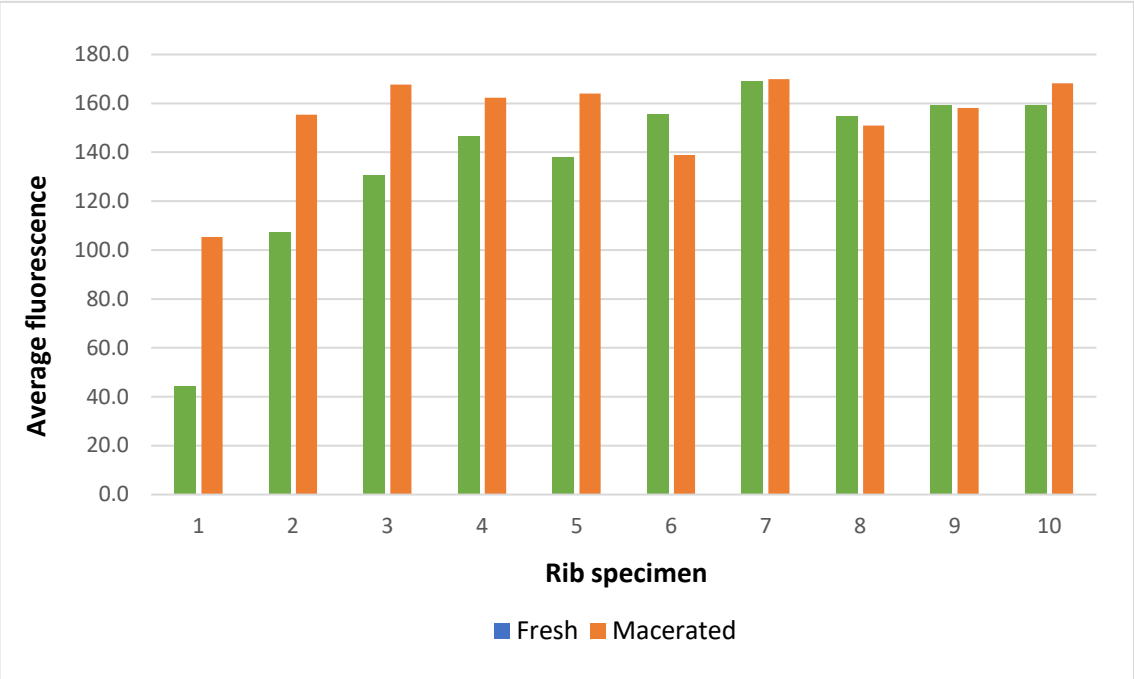

Figure 76: Changes in average fluorescence of the ten porcine ribs (Sus scrofa domesticus) subjected to enzymatic maceration (approx. 55°C)

Overall, the enzymatic maceration produced a moderate increase in fluorescence levels across most of the porcine ribs, with increases ranging from 0.78 to 61, with an average of 17.52 (23.2%, S.D.= 23.72). Visually the emitted fluorescence was generally more consistent across the length of the bone compared to the biological washing powder specimens. However, the dark patches located towards the neck of the ribs, as shown comparatively in figure 77 below, created some unexpected decreases in fluorescence levels.

Figure 77: Post maceration appearance of ribs 1-3 subjected to enzymatic maceration (approx. 55°C), dark staining present at the neck of the ribs (red circles).

14.3.3 – STATISTICAL ANALYSIS

Statistical analysis reflected similar fluorescence results to the washing powder maceration data set. As with the other techniques histogram analysis of the data distribution for the fresh and macerated bone mass datasets, and the fresh and macerated collagen content datasets identified normal distributions (appendix 6c), therefore parametric paired samples student t-tests were performed. Strong statistically significant relationships were noted in the comparisons of the fresh and macerated bone mass (M= 3.22, SD= 1.93) p= .001 and collagen content (M= .146, SD= 0.089) p= .001 (figure 78), indicating that the recorded changes in bone mass and bone collagen were the result of the enzymatic maceration.

Paired Samples Statistics

		Mean	N	Std. Deviation	Std. Error Mean
Pair 1	F.Mass	16.5860	10	4.22102	1.33480
	M.Mass	13.3600	10	3.62339	1.14582
Pair 2	F.Coll3	.7320	10	.04733	.01497
	M.Coll3	.5860	10	.06293	.01990
Pair 3	Av.F.Fluor	142.840	10	21.7160	6.8672
	Av.M.Fluor	154.060	10	19.5471	6.1813

Paired Samples Correlations

		N	Correlation	Sig.
Pair 1	F.Mass & M.Mass	10	.889	.001
Pair 2	F.Coll3 & M.Coll3	10	-.318	.371
Pair 3	Av.F.Fluor & Av.M.Fluor	10	.304	.394

Paired Samples Test

		Paired Differences					t	df	Sig. (2-tailed)
		Mean	Std. Deviation	Std. Error Mean	95% Confidence Interval of the Difference Lower	Upper			
Pair 1	F.Mass - M.Mass	3.22600	1.93680	.61247	1.84049	4.61151	5.267	9	.001
Pair 2	F.Coll3 - M.Coll3	.14600	.08996	.02845	.08164	.21036	5.132	9	.001
Pair 3	Av.F.Fluor - Av.M.Fluor	-11.2200	24.4119	7.7197	-28.6832	6.2432	-1.453	9	.180

Figure 78: Results of paired-samples t-test analysis, comparing the changes in bone mass, calculated collagen content, and average fluorescence, of the 10 ribs subjected to enzymatic maceration (approx. 55°C)

A histogram was also performed to test the distribution of the average fluorescence data for the fresh and macerated values to ascertain if it was normally distributed. As seen in appendix 6c, the data was abnormally distributed, therefore a Wilcoxon signed-rank test was conducted, figure 79 below.

Hypothesis Test Summary

	Null Hypothesis	Test	Sig.	Decision
1	The median of differences between Av.F.Fluor and Av.M.Fluor equals 0.	Related-Samples Wilcoxon Signed Rank Test	.241	Retain the null hypothesis.

Asymptotic significances are displayed. The significance level is .05.

Figure 79: Results of Wilcoxon signed-rank test, comparing fresh and macerated fluorescence values of 10 porcine ribs (Sus scrofa domesticus) subjected to enzymatic maceration (approx. 50°C)

The results of the Wilcoxon signed-rank test echoed those obtained during analysis of the biological washing powder maceration dataset, indicating no statistically significant

relationship between the pre and post maceration averaged fluorescence values. Therefore, acceptance of the null hypothesis was suggested. As with the washing powder maceration dataset, this was the expected outcome due to the discrepancies in the fluorescence data mentioned previously.

14.4 – MACERATION PILOT STUDY DISCUSSION

Overall, the most successful maceration technique was the hot water maceration, producing strong statistical relationships between fresh and macerated bone mass, fresh and macerated collagen content, and fresh and macerated fluorescence levels, as well as the most consistent visual fluorescence results. Hot water maceration was the least detrimental to bone collagen and overall bone mass, with bone quality scores of 5 for every bone, indicating maximum bone preservation. The small decrease in collagen content, and small increase in fluorescence can be attributed to the successful removal of residual tissue, with the final macerated results being the most representative of the original fresh results. A comparison of the average bone mass, fluorescence, collagen content, and bone scores for all three maceration techniques can been found in table 15.

Maceration with biological washing powder was the most destructive to bone structure and collagen content, producing the lowest average bone quality scores of the three maceration techniques: 4.3. This drop in bone quality was apparent from the surface texture of the bones, and subsequently the emitted fluorescence, as it had a far more irregular appearance compared to the homogeneous results of the ribs macerated with hot water. This irregularity was most likely a result of the concentrated enzymes and bleaching agents present in the washing powder, which abraded the cortical bone and artificially whitened the surface [149]. According to the ingredients list (appendix 11) the biological washing powder also contained optical brighteners, which are known to exhibit fluorescent properties, and are used to boost the appearance of white clothing.

In literature, optical brighteners and bleach have been shown to impede ALS examination of body fluids [120, 279], by creating confusing background fluorescence that makes differentiation between the stain and the fabric challenging [153]. In this pilot study, these destructive modifications have led to a substantial augmentation of

overall observed fluorescence, but with an inconsistent patchy appearance. Anatomical variation in bone structure and composition based on functional origins of the bones, i.e., closer to the spine (vertebral) or closer to the breastbone (sternal), could mean variable ratios of cortical and trabecular bone between the rib specimens. These compositional differences would also mean inequality in bone porosity across the sample population, and subsequently the absorption rate of the maceration solution. This variation in solution uptake likely created differential distribution of the washing powder throughout the structure of the ribs, further contributing to the irregular, patchy appearance.

Table 15: Comparison of the average bone mass, fluorescence, collagen content, and bone scores for all three maceration techniques

Maceration method	Average Mass (g)			Average Fluorescence			Average Collagen (mg) (90% of organic content)			Macerated bone quality score
	Fresh	Mac.	Change	Fresh	Mac.	Change	Fresh	Mac.	Change	
Hot water (80°C) N = 10	21.67	18.50	3.17 (-14.7%) s.d.=0.83	164.6	173.1	8.51 (+5.5%) s.d.=9.36	0.78	0.68	0.09 (-11.2%) s.d.=0.09	5
Bio. washing powder (50°C) N = 10	16.77	14.61	2.16 (-12.6%) s.d.=1.02	116.7	171.2	54.49 (+49.3%) s.d.=27.46	0.84	0.65	0.19 (-22.9%) s.d.=0.05	4.3
Enzymatic (55°C) N= 10	16.59	13.36	3.23 (-19%) s.d.=1.84	136.5	154.1	17.52 (+23.2%) s.d.=23.72	0.77	0.62	0.15 (-19.5%) s.d.=0.09	4.6

This asymmetrical distribution of the maceration solution would undoubtedly have been influential during the other maceration techniques, but it is more prominent in this dataset due to the caustic damage and discolouration created by the biological washing powder. These observations are supported by the statistical analysis of the pre and post maceration values for bone mass, calculated collagen, and average fluorescence. As the water temperature was kept low (50°C) the reduction in bone mass and collagen, as well as the drastically increased but patchy fluorescence, and the eroded and bleached surface texture, can be attributed to chemical alteration from the biological washing powder rather than water temperature. This is supported by the fact that no such surface or compositional changes were observed in the hot water maceration group, which was processed at the higher temperature of 80°C for a similar time frame.

Despite the substantial changes in bone quality identified through collagen, mass, and fluorescence quantification, the bone quality scores for the biological washing powder group did not drop below 4, which is still indicative of high bone quality according to Steadman et al (2005) [149]. Steadman et al (2005) created this scoring system to assess bone preservation and consequent suitability of bone samples destined for DNA analysis. Consequently, although the scale aided descriptive discussion of bone quality it is apparent that it lacks the required detail and descriptors relevant for bones undergoing ALS analysis. Furthermore, the criteria outlined for each bone quality score lacked definition and contained overlapping phrases [149]. Retrospectively, it may have been beneficial to have adapted the scoring system prior to analysis, but as this type of pilot study has not been conducted previously it was not clear what results to expect. A possible avenue for future work could be to create a scoring system applicable for this type of examination, however, investigations into maceration techniques were only conducted for this initial research question, and therefore the scoring system was not required for the remainder of the thesis.

Enzymatic maceration was the fastest maceration method and produced intermediate results with regards to reduction in bone mass and collagen, as well as the increase in fluorescence. Although it was more gentle on bone structure compared to the washing powder maceration, it was more destructive than the hot water technique. However, these results also demonstrated an inconsistent collagen loss with some bones experiencing a very small loss, such as rib 2 (0.18 mg), whereas over half of the ribs

exhibited 0.20 mg loss or greater. This disparity could be related to the variable size of the ribs and slightly different levels of tissue coverage left over from the manual defleshing. Bone composition was less likely to be influential in this data as all specimens were identified as sternal rib ends, but some natural interindividual variation could still be a factor. However, it is more likely these results are a consequence of the enzymatic formulation. The ratio of enzymes used for this technique was adapted from current literature [465, 490, 492], which includes maceration of whole mice and fleshed porcine rib, but not specifically defleshed porcine bone. Subsequently, the enzyme ratio used in this instance may have been suboptimal, and inadvertently detrimental to collagen content.

More specifically, ribs 6, 8, and 9 of the enzymatic dataset, experienced a decrease in average fluorescence with rib 6 notably displaying a 10.8% reduction. In this instance, all three ribs were from the second maceration session which overall took less time and was conducted at a slightly lower temperature compared to first session of ribs 1-5. These results highlight visual identification for maceration completion, as a possible limitation for this study, as these bones may have been removed from the solution too early. The mechanism of tissue removal during enzymatic maceration is very different compared to the other two maceration techniques, as the tissue is dissolved rather than softened and lifted away. Therefore, there were fewer physical indicators of completed maceration which made interpretation difficult. Furthermore, a greasy residue was noted on all bones post maceration, most likely where the tissue had dissolved rather than lifted away. Discussion in the literature suggests that during enzymatic maceration, lipids can disperse and settle into the external structure of the bone [463, 465], which may account for these observations. This in turn could have impeded the ALS, or altered the trajectory of ALS wavelengths, causing additional absorption or scattering and therefore lowering the observable fluorescence. Consequently, if enzymic maceration were to be pursued in the future, further testing would be needed to optimise formulation. The present method is currently not suitable for bone undergoing ALS analysis.

However, intraindividual variation was noted across all fluorescence values for all three maceration techniques in both pre and post maceration datasets. To assess this

variation further, an average range for pre and post fluorescence values was calculated based on the minimum and maximum fluorescence values obtained across the nine ROIs from the three photographs for each rib. In the pre-macerated fluorescence values for the hot water maceration group there was an average interindividual range in fluorescence values of 14, in the pre-macerated biological washing powder data group it was much higher at 24, whereas the enzymatic groups pre-macerated range was 15. In post maceration fluorescence values the range in average intraindividual fluorescence was reduced in both the hot water maceration and biological washing powder groups, with an average of 2.9 (-21%), and 1.2 (-5%) respectively. This result was expected, as the removal of residual tissue would facilitate the fluorescence photography by exposing the underlying bone and therefore a more consistent exposure to the ALS. However, the intraindividual variation in the enzymatic maceration group increased by 5.4 (+56%), as shown in table 16. This result was not entirely expected, but it is most likely the result of the discolouration created by the embedded lipid residue previously discussed.

Table 16: Comparison of intraindividual variation of pre and post maceration average fluorescence values, for each maceration dataset

Maceration technique	Avg. pre-maceration intraindividual range	Avg. post-maceration intraindividual range	Calculated changes
Hot water (80°C)	14	11	-2.9 (-21%) s.d.= 8.3
Bio. washing powder (50°C)	24	23	-1.2 (-5%) s.d.= 20
Enzymatic (55°C)	15	21	+5.4 (+56%) s.d.= 13.6

Although the intraindividual fluorescence range of the washing powder dataset was reduced by 5%, the overall intraindividual range of 23 was still high, with the greatest standard deviation of 20. As with the enzymatic macerated results, the high level of variation in the bones macerated with biological washing powder is most likely the result of the patchy surface texture created by the washing powder; however, the pre-macerated variance is unexpected, and is much higher than the other two techniques.

Despite the random allocation of the bone samples, retrospectively it was identified that the porcine ribs used in the hot water dataset where much more uniform in morphology and size compared to the other two maceration groups. More specifically, the ribs processed via washing powder maceration were the most varied in size and shape, and arguable possessed the greatest range in bone composition. The ribs used in the enzymatic maceration were generally smaller and less consistent in morphology compared to the hot water group, but more consistent than the washing powder dataset. This goes some way to explaining the greater range in intraindividual fluorescence noted in the latter two data groups. However, more prominent influencing factors most likely stem from the photography methodology.

Possible methodological contributing factors for the widespread fluorescence values include inconsistent bone positioning and the use of automatic camera settings. The lightweight polystyrene spheres used as a background and a control sometimes became displaced over time due to the weight of the bone pressing down and forcing the spheres to the side. Small vibrations from nearby movement could also displace the spheres, and differences in bone size and morphology could make initial positioning challenging, especially the smaller bone fragments. Similarly, once the bones were macerated, the smoother and drier bone texture meant that the bones would often fall through the spheres to the bottom of the box. Consequently, exact replication of bone positioning was not always possible, particularly between pre and post maceration photography sessions. Natural variation in bone morphology and size would also have contributed some variation when calculating the recorded fluorescence with the OFC, as smaller or more curved bones may have led to the inclusion of more background, and therefore lowered the fluorescence result within that ROI. This affect would have been exacerbated if the bone had changed position between photographs, due to the drifting polystyrene spheres.

Although some intraindividual variation will be the result of natural discolouration or uneven distribution of residual soft tissue left over from manual defleshing, as demonstrated by the changes in fluorescence average ranges, the use of automatic camera settings is most likely the primary contributing factor. When operating with automatic camera settings, the camera automatically selects the optimal exposure time,

F-stop, and ISO level for each photograph [124]. However, the purpose of the automatic camera settings is to optimise picture quality and clarity, ensuring accurate image capture [124, 202], but in the context of this research, accurate documentation of the observed fluorescence is paramount over image clarity. Even minor changes in bone positioning or ambient light may have led to deviations in how the ALS wavelengths interacted with the bones, which would then have been automatically compensated for by the camera. Exposure time, ISO, and F-stop, all control the amount of light hitting the camera lens [203], therefore any adjustments made to these settings will ultimately impact the amount of fluorescence captured. Consequently, in method development work was undertaken to firstly develop standardised photography parameters to ensure accurate fluorescence capture, and to potentially establish a protocol for bone fluorescence documentation.

14.5 – MACERATION PILOT STUDY CONCLUSIONS

Hot water maceration was identified as a suitable preparation technique for bone undergoing ALS analysis, as it produced fluorescence results similar to pre-macerated values, with limited collagen degradation. The hot water macerated bones also retained the highest level of bone preservation, with no evidence of major surface or structural modification. Consequently, hot water maceration was used as the designated preparation technique for the remainder of this PhD research, where applicable.

It was also established that maceration with biological washing powder was not suitable for bone undergoing ALS analysis, even at the low temperature of 50°C, as it was the most destructive to bone collagen and bone integrity whilst creating drastic alterations to surface texture and colour. These alterations to the bone subsequently manifested exaggerated and patchy fluorescence results. As a result, biological washing powder was not used any further in this research project, and it is recommended that it should be avoided for future research, particularly if molecular or histological analyses are required.

The formulation for the enzymatic maceration method was found to be partially successful. Although this technique successfully removed all adherent tissue, a greasy, undissolved lipid residue persisted on the bone's surface, leading to differential staining, and some inconsistency in fluorescence results. However, the enzymic maceration was completed in the fastest time, and overall was not as destructive to bone collagen and integrity as the biological washing powder solution. Further research dedicated to optimising the enzymatic formulation could be beneficial for future projects, but it will not be considered further in this PhD project.

Finally, due to the issues experienced with the photography protocol, additional photography refinement was carried out to determine a suitable replacement background for the polystyrene spheres and to standardise the camera settings. As bone composition possibly played a role in the fluorescence variation, additional photographs were taken to investigate the differences in fluorescence between the rib epiphyses and diaphysis.

15.0 - SECTION A, QUESTIONS 2-5:
PHOTOGRAPHY REFINEMENT METHODOLOGY

Due to the issues highlighted during the maceration study, and the introduction of an additional light source for underwater imagery, a series of photography refinement experiments were carried out with the aim of improving the data capture for section B research questions.

Although the bone samples used in the pilot study were all porcine ribs, differences in bone composition arising from anatomical variation, was still thought to be a possible source of inconsistency in the fluorescence results. Consequently, question 2 examines the distribution of bone fluorescence across the length of porcine ribs by quantifying the fluorescence emissions photographed at the vertebral, diaphysis, and sternal regions of three, manually defleshed porcine ribs.

Question 3 focused on identifying a suitable replacement background for the polystyrene spheres previously used during fluorescence photography. This was due to the mobile polystyrene spheres drifting during photography and therefore creating slight variations in bone positioning, which may have led to variation in observed bone autofluorescence. Consequently, a selection of different materials including a polystyrene sheet, 10 mm polystyrene spheres, play sand, black card (200 gsm), white card (220 gsm), clear plastic tub, and black plastic box were photographed with fresh and/or macerated porcine bone to see whether the different substrates were able to maintain bone positioning and performed under the ALS.

In addition to this, question 4 aimed to determine the optimal camera settings needed during submerged and terrestrial fluorescence photography, so that they could be standardised throughout the remaining research questions in section B. In the previous maceration pilot study, the use of automatic camera settings appeared to create a substantial range in values, even within the same fluorescence photograph, therefore standardised camera settings could help to achieve more consistent results. Similarly, as underwater bone fluorescence research forms a substantial aspect of section B, and included the use of a different, submersible ALS, additional photography questions were

explored to determine the optimal camera settings, particularly as there are currently no publications in literature specifically examining the photography of underwater bone fluorescence.

Finally, in question 5, the optimal distance between the camera, the specimen, and the light source was investigated. The addition of the aquatic photographic context required specialised underwater housing for the camera, which ultimately modified the camera positioning and zoom capabilities. Similarly, as the Hammerhead technical specifications were different to Crime-lite 2 the parameters for successful ALS stimulation and coverage were required.

In the following chapters, each research question is addressed individually, and the results were used to inform the remaining aspects of the overall research project, section B.

15.1 – MATERIALS

Sections 15.1.1 to 15.1.2 below describe the materials applicable to all remaining research questions in section A.

15.1.1 – PORCINE RIBS

For all four research questions discussed in this section, porcine ribs (*Sus scrofa domesticus*) were obtained fresh from a local butcher based in Huddersfield and handled in accordance with ethical considerations outlined in chapter 10.0. The ribs were manually defleshed using a PM40 scalpel to remove any large portions of soft tissue. Prior to examination all bones were kept frozen at -18˚C until use and defrosted overnight in the refrigerator (2˚C) the night before use. During transportation to the laboratory all ribs were kept within a cool bag alongside gel ice blocks to reduce any bacterial proliferation. The distribution of porcine ribs per research question is outlined in table 17:

Table 17: The distribution of porcine ribs (Sus scrofa domesticus) per research question, including the preparation method used.

Research question	No. of ribs	Preparation
2	3	Macerated
3	2	1 x Fresh, 1 x Macerated
4	3	1 x Fresh, 2 x Macerated
5	1	Macerated

15.1.2 – LIGHT SOURCES

Two models of ALS were used; the single LED blue (420-470 nm, peak 450nm) Crime-lite 2 from Foster and Freeman Ltd™ (fig. 80), as used in the maceration pilot study, and the 450 nm blue light Hammerhead by FoxFury Ltd. (fig. 81). The Crime-lite 2 was not designed to be used in aquatic environments therefore the Hammerhead was selected as a secondary light to compliment the terrestrial Crime-lite 2 and conduct the underwater experimentation. The Hammerhead has two LED bulbs, is fully submersible to a depth of 3 m, and has the capability of using one or both LEDs. To ensure maximum intensity and experimental consistency both LEDs were used throughout this project.

The technical specifications for each light source are shown in appendix 12a and b respectively.

Figure 80: Foster and Freeman Ltd™ Crime-lite 2 ALS

Figure 81: FoxFury Ltd. Hammerhead ALS

16.0: SECTION A, QUESTION 2:

COLLAGEN AND FLUORESCENCE DISTRIBUTION

Does the intensity of bone fluorescence in porcine ribs vary between the vertebral, diaphysis, and sternal regions of the bone, when photographed in a terrestrial context using blue light (450 nm) and an orange camera filter?

16.1 – METHOD

Three porcine ribs were macerated according to the hot water (approx. 80°C) protocol discussed in chapter 13.3. The macerated ribs were then photographed using the equipment configuration used during the maceration pilot study, also described in chapter 13.3, to investigate the distribution of fluorescence and collagen throughout the length of the bone. In addition to the standard central image, photographs of the vertebral and sternal ends of the ribs were taken (fig. 82) as well as corresponding collagen scrapings for TG analysis from each region of the bone, using the method outlined in chapter 13.3. Fluorescence analysis was conducted using the OFC as defined in chapter 13.3, but one ROI was selected for each anatomical region, and an average calculated using three photographs.

Figure 82: Vertebral, central, and sternal regions of a porcine rib (Sus scrofa domesticus)

16.2 – RESULTS AND DISCUSSION

Table 18 summarises the photographic results for each of the anatomical regions of the porcine ribs. The photographs in the table were chosen as the most representative of the fluorescence seen but all photographs can be seen in appendix 13. The quantified fluorescence values for each anatomical region of each rib can be seen in table 19, and the corresponding thermograms are included in appendix 14. Thermograms displaying the combined TGA curves of the anatomical regions for each rib are available in appendix 15. Table 19 also contains the calculated collagen content for each rib region. For orientation and sampling purposes, the central and original site of collagen sampling is referred to as 'A', the vertebral side of rib is labelled as 'B', and the sternal aspect is annotated as 'C'. The rib specimens are labelled with specimen numbers 1, 5, and 6, as they also formed part of another research question, therefore the numbering system was maintained to ensure consistency and cross-referencing if required.

Table 18: Summary of fluorescence results of anatomical regions of macerated porcine ribs (Sus scrofa domesticus); central (A), vertebral (B), sternal (C).

Rib	Central (A)	Vertebral (B)	Sternal (C)
1	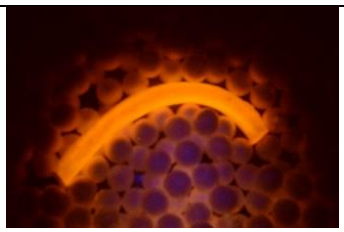	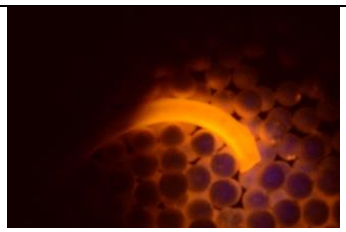	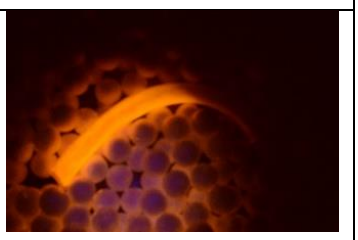
5	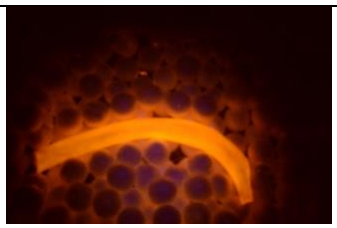	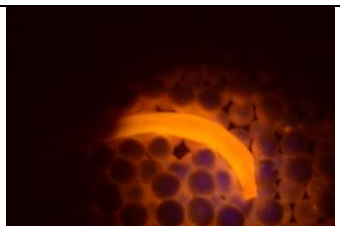	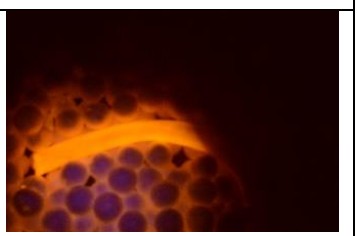
6	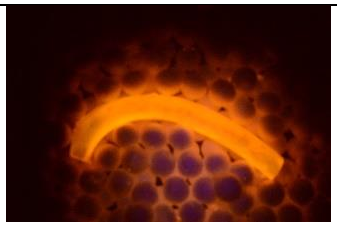	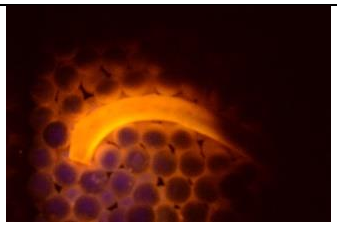	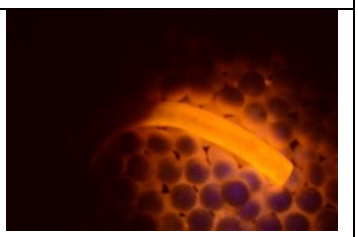

Table 19: Fluorescence and collagen results of central, vertebral, and sternal aspects of macerated porcine ribs (Sus scrofa domesticus), where (A) refers to the central/diaphysis, (B) refers to the vertebral end, and (C) refers to the sternal end.

Specimen (Rib region A-C)	Fluorescence				Collagen (mg)
	Photo 1	Photo 2	Photo 3	Average	
Rib 1A	154	147	146	149	0.79
Rib 1B	145	144	140	143	0.68
Rib 1C	162	159	158	160	0.72
Rib 5A	141	144	143	143	0.69
Rib 5B	151	153	152	152	0.64
Rib 5C	154	152	153	153	0.66
Rib 6A	148	150	150	149	0.69
Rib 6B	158	158	158	158	0.68
Rib 6C	161	162	161	161	0.71

Table 20 below, summarises the average fluorescence and calculated collagen content for each anatomical rib region using data from all three ribs.

Table 20: Average fluorescence and calculated collagen content calculated for each anatomical region based on the three examined porcine ribs (Sus scrofa domesticus)

Rib Region	Average fluorescence	Average collagen content (90%) (mg)
Vertebral	151 (s.d = 3.8)	0.67 (s.d. = 0.05)
Diaphysis (Central)	147 (s.d. = 6.3)	0.72 (s.d. = 0.02)
Sternal	158 (s.d. = 3.8)	0.70 (s.d. = 0.03)

The data showed that there was very little variation in collagen content between the three anatomical regions, suggesting an even distribution of collagen across the length of the bone. However, some minor differences were noted in the observed fluorescence levels. Across all three specimens the sternal end of the ribs appeared to fluoresce

slightly higher, with an average of 11 (6.7%) compared to the central aspect, whereas the vertebral ends were on average only 4 higher (2.7%) with rib 1 showing the largest difference of 17 compared to rib 5 which showed the smallest difference of 1. As this experiment was carried out at the same time as the maceration pilot study and consequently used the same methodology, some limitations experienced during that experiment may also be present here. For example, the use of automatic camera settings may have introduced some variation in fluorescence as the camera automatically adjusts the exposure time, ISO, and f-stop for each photograph, to ensure the best quality image is obtained. This issue may have been exacerbated by changing bone position precipitated by adjusting the light source between rib regions, and consequently causing the polystyrene spheres to move. However, as these differences are not substantial, it is possible that they are the result of natural variation in bone dimensions and morphology, as rib bones are not uniform throughout their entire length. The surface of rib bones exhibits natural fluctuations in width and shape based on their position in the thorax cavity, such as the presence of facets to articulate with vertebrae, and when providing protection to the heart, lungs, and related connective tissues, such as the coastal groove, and the groove for the subclavian vein [116]. It is also possible that these differences in fluorescence may have been slightly amplified due to the issues already discussed regarding the photography protocol. Overall, the differences found were not large enough to warrant changing the core methodology but do highlight the need for refinement of the photography methodology, more specifically the use of polystyrene spheres and automatic camera settings, to eliminate this potential route of variation.

17.0: SECTION A, QUESTION 3:
BACKGROUNDS AND POSITIONING

What material makes the most suitable photographic background between, play sand, polystyrene sheet, 10 mm polystyrene spheres, white card (220 gsm), black card (200 gsm), clear plastic box, and black plastic box, when photographing porcine bone in a terrestrial context, using blue light (450 nm) and orange camera filter?

17.1– ADDITIONAL MATERIALS AND METHOD

Two porcine ribs (*Sus scrofa domesticus*) were obtained fresh from a local butcher in Huddersfield. One rib was manually defleshed using a PM40, and the other was macerated in hot water (80°C) as per the method discussed in chapter 13.3. A selection of backgrounds and container configurations were used to test contrast and stability, this included black card (200 gsm), white card (220 gsm), the black box alone, 10 mm polystyrene spheres, polystyrene sheet, play sand in a round clear plastic container, 10 mm polystyrene spheres in a round clear plastic container, and 10mm polystyrene spheres with play sand in a round clear plastic container. The same photography methodology used for the maceration pilot study (chapter 13.3) was implemented during this investigation. Fluorescence calculations were not conducted during this experiment, as the presence or absence of fluorescence was considered a sufficient indicator of success, rather than quantification. The fresh porcine bone was first photographed in natural light with a scale and then photographed using the 10 mm polystyrene spheres in a round clear plastic container, play sand in a round clear plastic container, and then the 10 mm polystyrene spheres with play sand in a round clear plastic container, to see which configuration maintained the best specimen positioning and stability. The macerated rib was photographed on black card (200 gsm), white card (220 gsm), in the empty black box, on a polystyrene sheet, and in the play sand within the round plastic container. The round clear plastic container was included as it was thought the smaller diameter would restrict the movement of the polystyrene spheres and the sand.

17.2 – RESULTS AND DISCUSSION

Table 21 below summarises the results of the fluorescence photography positioning tests. These images were selected as the most representative but all photographs for this question can be found in appendix 16. Based on these results, none of these techniques were successful. Placing the polystyrene spheres in a smaller container only resulted in the spheres being displaced once the bone was added, most likely due to its much heavier weight. Although this test was conducted with a fresh bone, this issue was exacerbated once remaining tissue was removed as the macerated bone surface was much smoother and drier than fresh bone. The sand was successful at maintaining bone positioning but did not provide the contrast necessary for the fluorescence photography, like the polystyrene spheres. The sand with the spheres was more successful, but due to there being only one layer of polystyrene the contrast was also reduced compared to polystyrene spheres alone. Table 22 below summarises the results of further tests carried out with the other backgrounds and the macerated rib, all photographs for this test are available in appendix 17. Here, the results were more promising, with the polystyrene sheet, empty black box, and play sand performing well. However as hypothesised the empty black box did produce reflections, which the polystyrene spheres were previously used to overcome. The polystyrene sheet created the same contrasting effect as the spheres, whilst facilitating easier and more consistent bone positioning due to its flat, stable form. The sand was also more successful in this test, creating a good level of contrast and standardised positioning, however it did not perform well with the fresh bone and overall was not as successful as the polystyrene. Conversely, the white and black card both exhibited poor results, with the white card producing virtually no contrast with the bone. With this in mind, the polystyrene sheet was identified as the most suitable replacement for the polystyrene spheres.

Table 21: A summary of the photographic results for positioning methodology testing

Context	Image
Natural light with scale	
Natural light: In-situ with 10mm polystyrene spheres	
Fluorescence image: In-situ with 10 mm polystyrene spheres	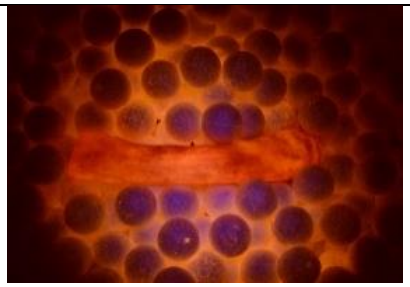
Fluorescence image: play sand	
Fluorescence image: Play sand embedded with 10 mm polystyrene spheres	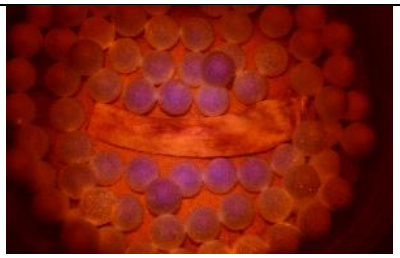

Table 22: A summary of the photographic results for background testing

Material	In-situ	Fluorescence
Polystyrene sheet		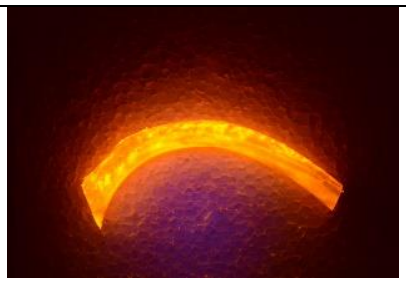
Black card (200 gsm)		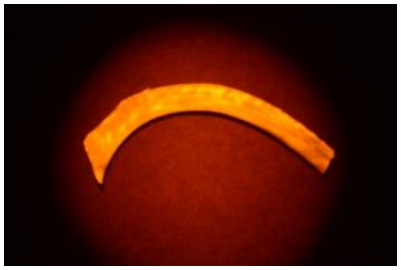
White card (220 gsm)		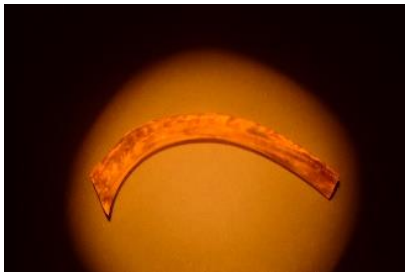
Empty black box		
Sand		

18.0: SECTION A, QUESTIONS 4 & 5: PHOTOGRAPHY REFINEMENT

Question 4: *What is the optimal exposure time, f-stop and ISO level required to visualise bone fluorescence when photographing porcine bone (Sus scrofa domesticus) in a terrestrial setting using blue light (approximately 450 nm) and orange and yellow filters?*

Question 5*: What is the optimal distance from the sample to the light source when photographing porcine bone (Sus scrofa domesticus) using the Crime-lite 2 and the FoxFury Hammerhead devices, in combination with orange and yellow filters in terrestrial and tap water contexts?*

Research questions 4 and 5 were explored during the same experiment as they both related to photography settings refinement. Efforts were made to keep the photography methodologies as similar as possible for both light sources, to maintain consistency and the production of comparable results. However, as the Crime-lite 2 and the Hammerhead light have different technical specifications, (appendix 12), refinement of the light positioning was required to optimise fluorescence output and data collection.

18.1 – TERRESTRIAL PHOTOGRAPHY REFINEMENT

The equipment configuration for terrestrial studies was updated from the maceration pilot study to include a flexible tripod, capable of being positioned perpendicular to the specimen, and the inclusion of a retort stand with a boss and clamp to secure the ALS. These changes enabled more controlled equipment placement, which could be easily measured, and reproduced for the submerged studies. Figure 83 displays a diagram of the improved equipment configuration, including the polystyrene sheet in place of the polystyrene spheres. Furthermore, a more modern camera; the Sony™ A6000 Mirrorless digital Camera was purchased to aid image capture, with an improved 24-megapixel resolution compared to the 14.2-megapixel Nikon D3100 DSLR. The Sony™ A6000 is also lighter and more compact which enabled the tripod to support the camera when perpendicular. It also contained a mirrorless sensor which is advantageous when

conducting fluorescence photography as the lens can be constantly exposed to the light, and by not containing a reflex mirror or optical viewfinder the image displayed on the screen is a true representation of the image being captured [204, 212]. During terrestrial photography the optical zoom was set at 40 mm to ensure full coverage, with the specimens placed on a 10 mm thick polystyrene insert, developed based on the success of the background study discussed in chapter 18.0, the full dimensions can be seen in figures 84 and 85.

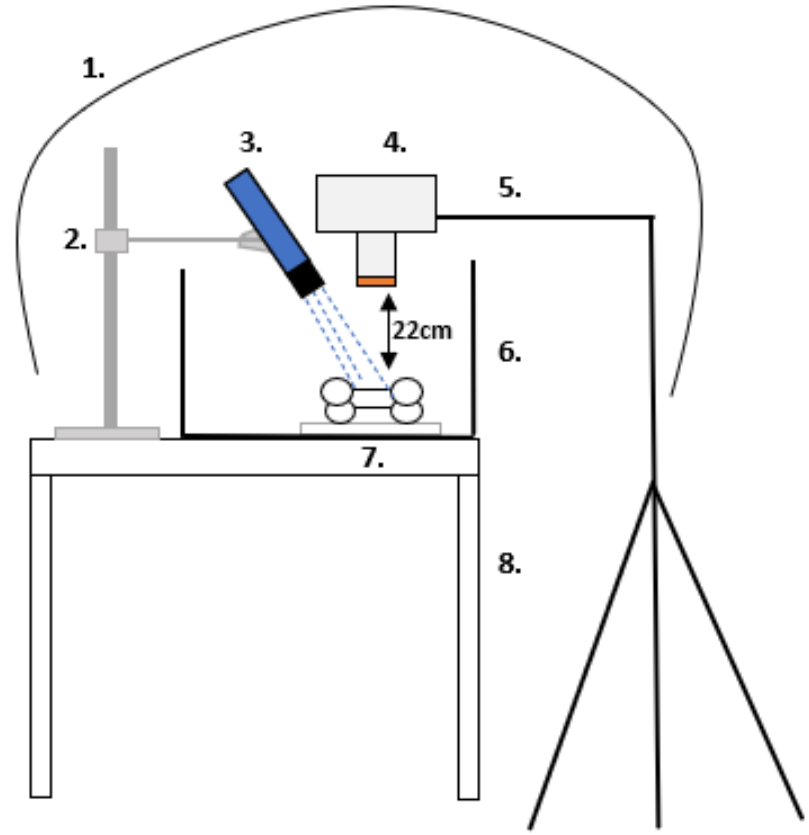

1. Photography cloth
2. Retort stand, boss, and clamp
3. ALS
4. Camera with coloured filter
5. Tripod
6. Black box
7. Polystyrene insert
8. Table

Figure 83: Improved equipment configuration for fluorescence photography

A non-reflective photography scale (Pasthorizontools.com) was secured to the polystyrene insert using Unibond™ No more nails double sided adhesive tape, which was also used to secure the insert to the base of the 39.5 x 29 x 31.5 cm 24 L black plastic box (plasticboxcompany.com), as used in the maceration pilot study.

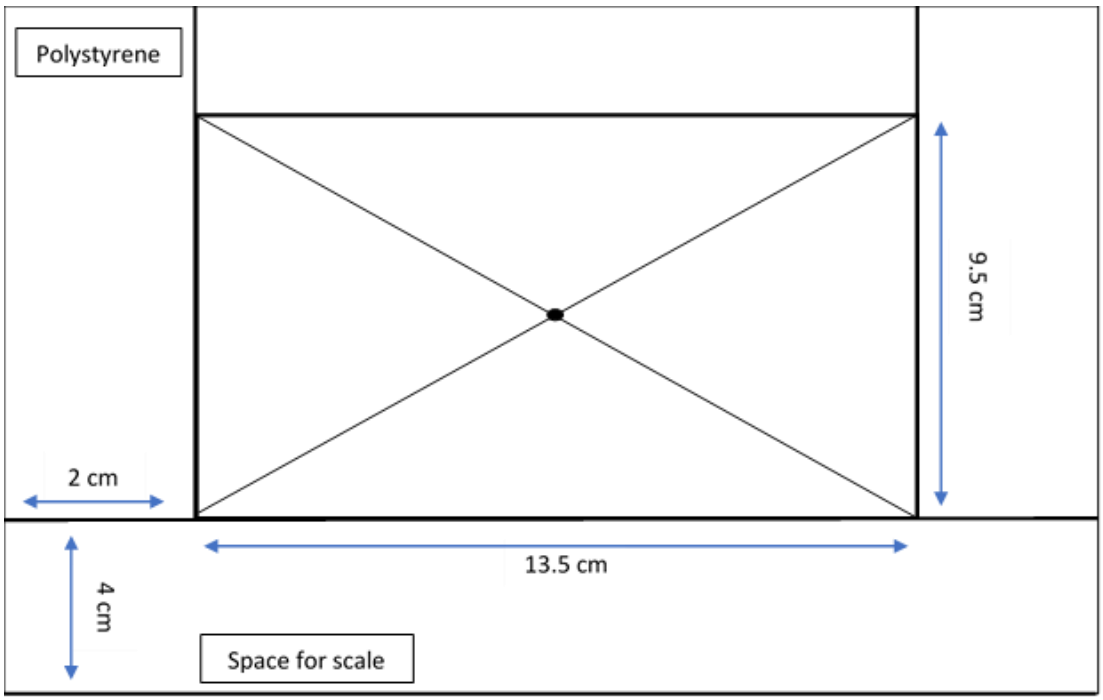

Figure 84: Diagram illustrating the dimensions of the polystyrene insert used during fluorescence photography.

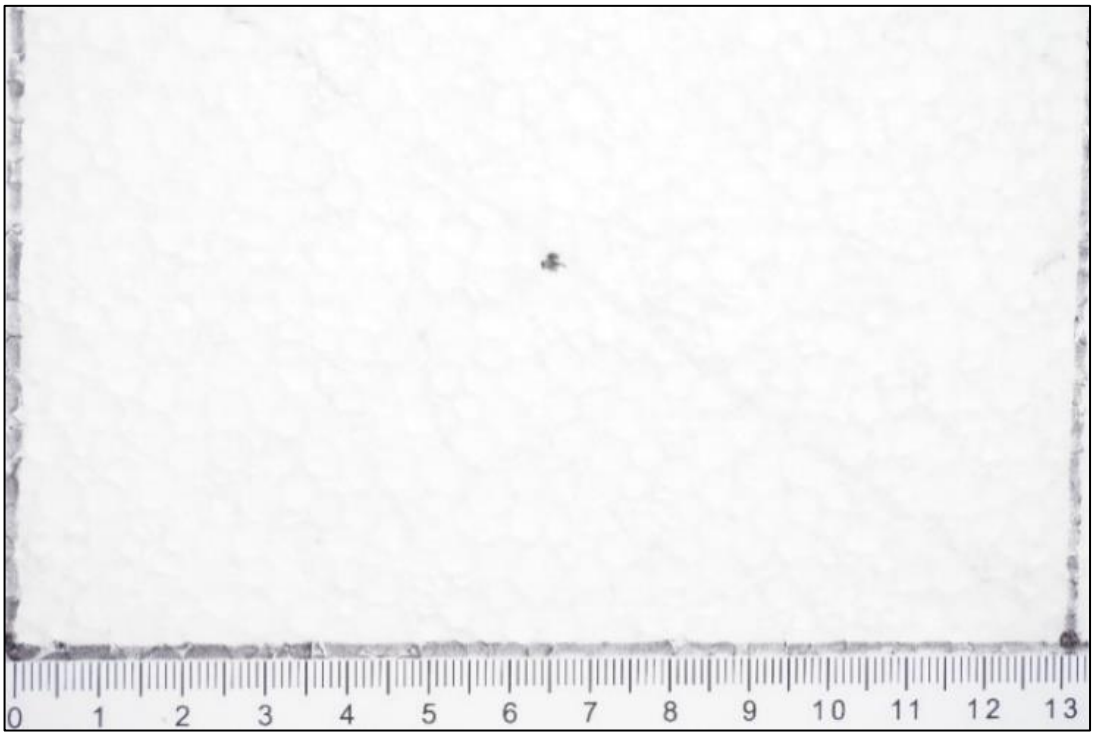

Figure 85: Photograph of the polystyrene insert used during fluorescence photography.

18.2 – OPTIMAL PHOTOGRAPHY DISTANCE

To investigate the light projection limits of the Hammerhead ALS and to establish an effective distance for photography, a fresh, manually defleshed, porcine rib (*Sus scrofa domesticus*) was photographed using the Hammerhead light source, positioned at 14, 18, and then 22 cm from the bone, using standardised camera settings ISO 1600, F5.6 and exposure time 0.4. These camera settings were selected, as during previous feasibility sessions testing to see if the light source was capable of activating bone fluorescence (not reported here), automatic camera settings were used to provide a initial indicator of the most frequently automatically selected settings and therefore provide a starting point for further testing. Upon evaluation ISO 1600, F5.6 and exposure time 0.4 were selected most frequently and produced the most successful photographs. Similarly, during the maceration pilot study and the background testing studies the distance from the camera to the Crime-lite 2 was 22 cm, therefore this was considered a suitable starting point for comparison. Results of the distance investigations are summarised in table 23:

Table 23: Summarised results of terrestrial photographs taken at 14, 18, 22cm with the Hammerhead ALS and orange filter

14 cm
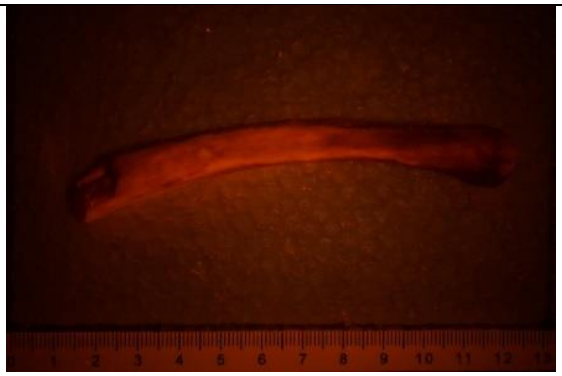
18 cm
22 cm

Based on these results it was clear that 18 cm was the most successful, due to the strong fluorescence, more consistent coverage, and good contrast with the background. Consequently, this distance was used for the Hammerhead light throughout the remaining terrestrial experiments. In the first instance orange and yellow filters were used in conjunction with both ALS light sources, however further testing showed that although the orange filter was successful, the yellow filter was not compatible with the

Hammerhead light. The images produced were overexposed with no obvious fluorescence in terrestrial or underwater contexts when photographing either fresh or macerated bone, as summarised in figures 86 and 87. This is most likely due to a slightly different peak wavelength compared to the Crime-lite 2. Subsequently, both orange and yellow filters were used with the Crime-lite 2 but only the orange filter was used for the Hammerhead. Terrestrial testing was not required for the Crime-lite 2 as it had been used in previously in the maceration pilot study.

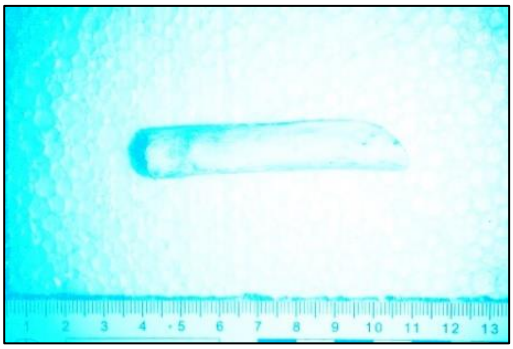

Figure 86: Terrestrial photograph of fresh porcine rib (Sus scrofa domesticus) using the Hammerhead ALS and yellow filter

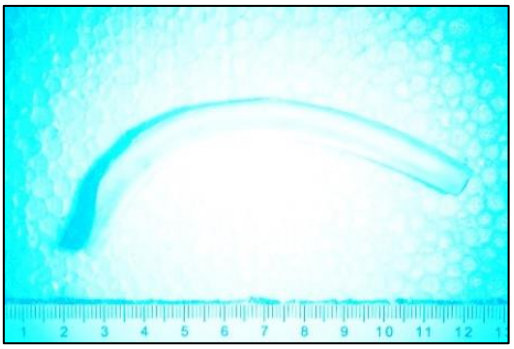

Figure 87: Submerged photograph of macerated porcine rib (Sus scrofa domesticus) using the Hammerhead ALS and yellow filter.

18.3 – SUBMERGED PHOTOGRAPHY REFINEMENT

Extensive testing was undertaken to ascertain the most effective experimental design for submerged fluorescence photography. A very similar equipment configuration described in the terrestrial testing was applied to submerged photography, with the addition of a Seafrogs™ underwater hard case housing unit to prevent water damage to the Sony™ A6000. An optical zoom of 34 mm rather than 40 mm was implemented, as once the coloured filter was fitted to the camera this was the maximum zoom achievable when housed in the underwater casing. A diagram illustrating the full underwater fluorescence photography equipment configuration is displayed in figure 88.

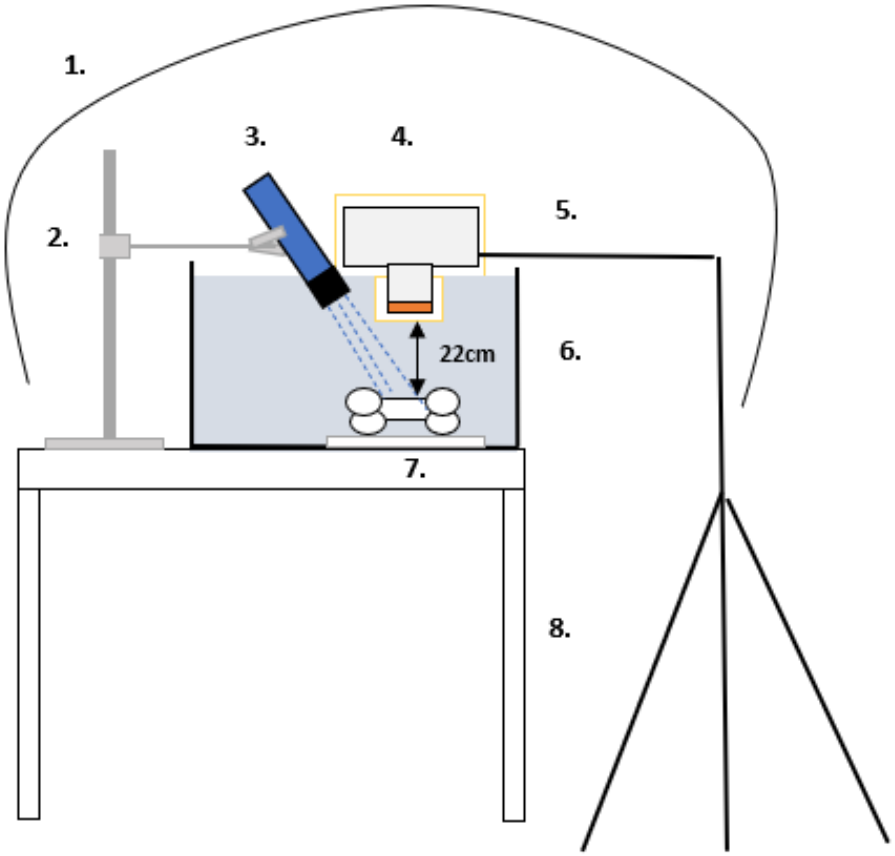

1. Photography cloth
2. Retort stand, boss, and clamp
3. ALS
4. Camera with coloured filter and underwater case
5. Tripod
6. Black box
7. Polystyrene insert
8. Table

Figure 88: Equipment configuration for underwater fluorescence photography

Initially thirty combinations of camera settings were used to photograph a macerated porcine rib (*Sus scrofa domesticus*) submerged in 21 L of tap water, coupled with the orange barrier filter, and illuminated by the Hammerhead light as shown in appendix 18. Visually, results suggested that a combination of F11 and ISO 1600 (appendix 18, no.15) produced the most successful fluorescence results. More focused photography testing was then conducted to validate these identified settings, and as outlined in the table 24 below, there was very little difference noted between f-stops 11 and 10, and ISO 1600 and 2000. Consequently, F11 with ISO 1600 was selected as it was the most similar to the terrestrial settings and therefore would be make a closer analytical comparison.

Table 24: Summarised fluorescence results of submerged macerated porcine rib (Sus scrofa domesticus) photographed using refined camera settings, Hammerhead light, and orange filter.

F11, ISO 1600, Exp. 0.6	F 11, ISO 2000, Exp. 0.6
F10, ISO 1600, Exp. 0.6	F10, ISO 2000, Exp. 0.6

To try and maximise aquatic fluorescence results, the Crime-lite 2 was also tested at several distances from a macerated porcine rib whilst submerged in 21 L of tap water, with the orange and yellow barrier filters. As this light is not engineered for aquatic environments, a clear polythene bag was placed over the submerged end of the light and secured with an elastic band to prevent water damage. This equipment configuration as used successfully in previous MSc work [134]. Short intervals of activity were completed to ensure the Crime-lite did not overheat. Photographs were taken of the macerated porcine rib (*Sus scrofa domesticus*) using the barrier filters, and the Crime-lite 2 positioned at incremental distances between 22 and 25 cm. Table 25 summarises the results seen.

Table 25: Summarised fluorescence results of submerged macerated porcine rib (Sus scrofa domesticus) photographed using Crime-lite 2 covered with plastic bag, in conjunction with orange and yellow barrier filters.

Distance (cm)	Orange filter	Yellow filter
22	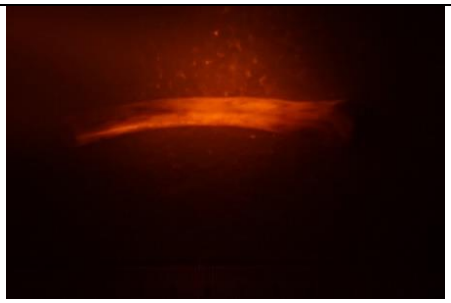	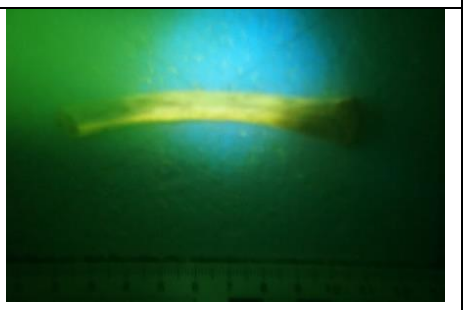
23	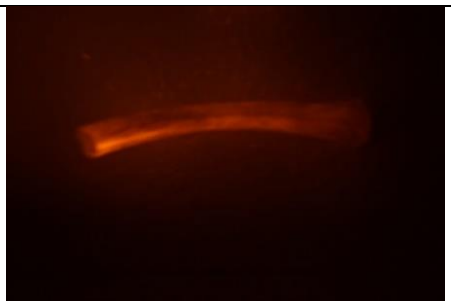	
24	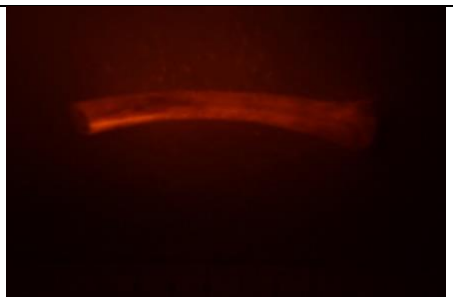	
25	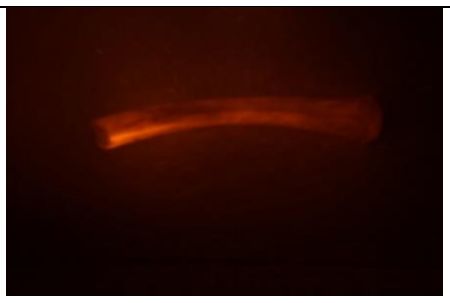	

Initial observations showed the overall light coverage of the bone increased as the ALS is positioned further away, with 24 and 25 cm providing the most comprehensive coverage. However, there are also significant inconsistencies in fluorescence across all distances and filters, producing a generally dark and hazy appearance, which was not expected. More specifically in the images produced using the yellow filter, areas of linear

demarcation can be seen, as highlighted in the photograph taken at 25 cm. Upon reflection it was hypothesised that this was due to the light struggling to penetrate the plastic covering, causing irregular diffraction and aberrations. Therefore, testing was carried out without the bag, but with the light suspended just above the water line rather than submerged. Overall, the results were much clearer, more defined fluorescence seen when using both filters (table 26). As a result, this approach was adopted for the submerged photography for the Crime-lite 2, keeping the camera at 22 cm and the light at 23 cm, ensuring fluorescence collection whilst complying with manufacturer's guidelines.

Table 26: Summarised fluorescence results of submerged macerated porcine rib (Sus scrofa domesticus) photographed using Crime-lite 2 without the plastic bag, in conjunction with orange and yellow barrier filters.

Distance (cm)	Orange filter	Yellow filter
23		

19.0 - SECTION A: SUMMARY

The results of the preparation and refinement research questions identified that hot water maceration (80°C) was the most suitable maceration preparation technique out of the three methods analysed. Furthermore, hot water maceration (80°C) provided similar fluorescence results to the fresh fluorescence intensities, with very little change in the collagen content. The small increase in fluorescence was in keeping with the removal of residual soft tissue. Consequently, hot water maceration was used to prepare all the macerated bones, when required, in section B.

With regards to the distribution of collagen and fluorescence throughout the length of the porcine ribs, fluorescence intensity was seen to be slightly more intense towards the emphasises of the examined ribs. However, the fluorescence differences where so small (sternal ends: average 11 (6.7%), vertebral ends: average 4 (2.7%) higher compared with the central, anterior diaphysis), that this increase was attributed to possible movement in ALS positioning, and the degree of retained tissue within the samples. Furthermore, there was very little variation in collagen content between the three anatomical regions, which suggested an even distribution of collagen across the length of the bone. Consequently, collagen sampling and fluorescence quantification was kept standardised to the central, anterior aspect of the porcine ribs.

The experimentation results into a suitable replacement for the polystyrene spheres for fluorescence photography identified the polystyrene sheet as the most successful for maintaining bone positioning whilst reducing reflections from the light source and black box, whilst creating a sufficient level of contrast and not intrinsic fluorescence emissions. Consequently, a standardised polystyrene insert was created for use in all future fluorescence photography (fig. 85)

The implementation of a new mirrorless camera and flexible tripod, in conjunction with the retort stand, boss, and clamp, enabled measurable, standardised equipment positioning for both terrestrial and submerged fluorescence photography.

For Hammerhead light source, camera settings of ISO 1600, F5.6 was determined to be the most successful for terrestrial photography, and F11 with ISO 1600 in aquatic

conditions, when positioned at 18 cm from the bone specimen. These configurations ensured even distribution of the ALS light and fluorescence production.

Although the Crime-lite 2 could not be submerged, refinement testing demonstrated that bone autofluorescence was still achievable when the Crime-lite 2 was positioned just above the water at 23 cm from the bone specimen and was capable of viewing fluorescence with both the yellow and orange filters.

These results led to the creation of a core methodology (chapter 20.0), which was utilised throughout the research questions in section B.

SECTION B:

THE APPLICATION OF ALS TO DETECT BONE

Section B focused on investigating the hypothesised collagen-fluorescence relationship and the taphonomic factors that may influence bone collagen content and subsequently autofluorescence.

Question 1: Is there a statistical difference in observed bone fluorescence of fresh porcine bone (*Sus scrofa domesticus*) between terrestrial and tap water contexts? A comparison of terrestrial and underwater fluorescence levels of 30 fresh porcine ribs (*Sus scrofa domesticus*). photographed using blue light (approximately 450 nm) and orange and yellow filters.

Question 2: Is there a correlation between the amount of collagen content in bone and the level of bone fluorescence seen when photographed using blue light (approximately 450 nm) and orange and yellow filters? A statistical comparison of fluorescence and collagen levels of 54 macerated porcine ribs (Sus scrofa domesticus).

Question 3a: Is it possible to distinguish between porcine bone (*Sus scrofa domesticus*) and other 27 non-bone control items when photographed using blue light (approximately 450 nm) and orange and yellow filters, in terrestrial and tap water contexts?

Question 3b: To what extent does pure porcine collagen powder fluoresce when exposed to ALS? Quantifying the fluorescence levels of pure porcine collagen powder photographed using blue light (approximately 450 nm) and orange and yellow filters, in terrestrial and tap water contexts

Question 3c: Will demineralised and deproteinised porcine bone (*Sus scrofa domesticus*) fluoresce when photographed using blue light (approximately 450 nm) and orange and yellow filters in terrestrial and tap water contexts?

Question 4: Is high water salinity destructive to bone collagen and subsequent fluorescence over time? Comparison of changes in bone fluorescence and collagen content of 54 macerated porcine ribs (*Sus scrofa domesticus*) submerged in tap water and simulated sea water, at 2-month intervals over a 6-month period, photographed using blue light (approximately 450 nm) and orange and yellow filters.

Hypotheses:

1. Hypothesis: Alternative light sources can be used to preliminarily identify bone in terrestrial and underwater environments using blue light (450-470 nm) when photographed with an orange camera filter

   Null hypothesis: Alternative light sources cannot be used to preliminarily identify bone in terrestrial and underwater environments using blue light (450-470 nm) when photographed with an orange camera filter

2. Hypothesis: Porcine bone (*Sus scrofa domesticus*) produces fluorescence in both terrestrial and underwater environments when exposed to blue light (450-470 nm) and viewed with a coloured filter.

   Null hypothesis: Porcine bone (*Sus scrofa domesticus*) does not produce fluorescence in terrestrial and underwater environments when exposed to blue light (450-470 nm) and viewed with a coloured filter.

3. Hypothesis: There is a correlation between the amount of bone collagen in porcine bone (*Sus scrofa domesticus*) and the levels of fluorescence seen when exposed to blue light (450-470 nm) and photographed with an orange camera filter.

   Null hypothesis: There is no correlation between the amount of bone collagen in porcine bone (*Sus scrofa domesticus*) and the levels of fluorescence seen when exposed to blue light (450-470 nm) and photographed with an orange camera filter.

4. Hypothesis: Exposure times need to be adjusted when photographing macerated porcine bone compared to fresh porcine bone when exposed to blue light (450-470 nm) and photographed with an orange camera filter.

   Null hypothesis: Exposure times do not need to be adjusted when photographing macerated porcine bone compared to fresh porcine bone when exposed to blue light (450-470 nm) and photographed with an orange camera filter.

5. Hypothesis: Macerated bone produces higher fluorescence levels compared to fresh bone due to removal of residual tissue when exposed to blue light (450-470 nm) and photographed with an orange camera filter.

   Null hypothesis: Macerated bone does not produce higher fluorescence levels compared to fresh bone when removed of residual tissue and exposed to blue light (450-470 nm) and photographed with an orange camera filter.

6. Hypothesis: When using blue light (450-470 nm) and a camera fitted with an orange or yellow camera filter it is possible to differentiate between bone and other environmental items within terrestrial and underwater contexts

   Null hypothesis: When using blue light (450-470 nm) and a camera fitted with an orange or yellow camera filter it is not possible to differentiate between bone and other environmental items within terrestrial and underwater contexts.

7. Hypothesis: Environmental items produce different levels of fluorescence compared to porcine bone (*Sus scrofa domesticus*) when exposed to blue light (450-470 nm) and photographed with an orange camera filter.

   Null hypothesis: Environmental items do not produce different levels of fluorescence compared to porcine bone (*Sus scrofa domesticus*) when exposed to blue light (450-470 nm) and photographed with an orange camera filter.

8. Hypothesis: High water salinity is destructive to porcine bone collagen when submerged for 6 months, which leads to a reduction in observed fluorescence levels when using blue light (450-470 nm) and photographed with an orange camera filter.

   Null hypothesis: High water salinity is not destructive to porcine bone collagen when submerged for 6 months, which leads to a reduction in observed fluorescence levels when using blue light (450-470 nm) and photographed with an orange camera filter.

The research questions in this section utilised the core methodology outlined in chapter 20.0, but with some adaptations where necessary to meet the needs of the parameters of the research question. These adaptations are outlined in the specific method section for each individual research question.

20.0 - CORE METHODOLOGY

Based on the results of section A, the following methodology was developed as a core foundation for the remaining research questions. Some adaptation of this core methodology was required for individual research questions to accommodate specific research aims, and to maximise results within project timescales. These adaptations are discussed during the respective research questions.

20.1- MATERIALS

20.1.1- SPECIMENS

All porcine ribs (*Sus scrofa domesticus*) utilised in section B were obtained fresh from a Sainsbury's supermarket and kept frozen at -18°C until required. All ribs were defrosted the night before use in a refrigerator (approx. 4°C) and manually defleshed using a PM40 knife as outlined in chapter 13.3. Prior to examination all bones were kept in a cooler bag with frozen gel blocks to limit bacterial growth and slow deterioration during transit. All ribs were handled in accordance with the ethical considerations discussed in chapter 10.0. Table 27 below provides an overview of how many ribs were used in each research question and the corresponding preparation method.

Table 27: Distribution of porcine ribs (Sus scrofa domesticus) per research question and corresponding preparation method

Research question	No. of porcine ribs (*Sus scrofa domesticus*)	Preparation
1	30	Fresh
2	54	Macerated
3	No ribs used	N/A
4	54	Macerated

20.1.2 – EQUIPMENT

Photographs were taken using the Sony™ A6000 Mirrorless digital camera fitted with a 16-50 mm lens and supported by a K&F Concept overhead tripod. When conducting underwater photography, the Sony™ A6000 was secured in the Seafrogs® underwater hard case housing unit to prevent water damage. The optical zoom was set at 40 mm for terrestrial photography, and 34 mm for submerged specimens as once the filter was fitted to the camera this was the maximum zoom achievable when housed in the underwater casing. During photography, the specimens were placed on a 10 mm polystyrene insert as described in chapter 20.0, with a non-reflective photography scale (Pasthorizontools.com) which were secured to the base of a 39.5 x 29 x 31.5 cm 24 L black plastic box (plasticboxcompany.com) using Unibond™ No more nails double sided adhesive tape.

20.1.3 – LIGHT SOURCES

Two models of ALS were used throughout the remainder of this project. The single LED blue (420-470 nm) Crime-lite 2 from Foster and Freeman Ltd™ (peak wavelength of 450 nm) and the 450 nm blue light Hammerhead by FoxFury Ltd. The general equipment configuration for both terrestrial and underwater experimentation is illustrated in figures 89 and 90 respectively. Throughout the photography process, ambient lights were turned off and a 1.6 x 2.1 m sheet of black photography cloth was placed over the camera and box to limit any interference from natural light. The distance of the camera from the bone specimens was fixed at 22 cm for both the terrestrial and tap water contexts. The distance between the specimen and the Hammerhead light source was set at 18 cm and the distance between the Crime-lite 2 and the specimen was fixed at 22 cm.

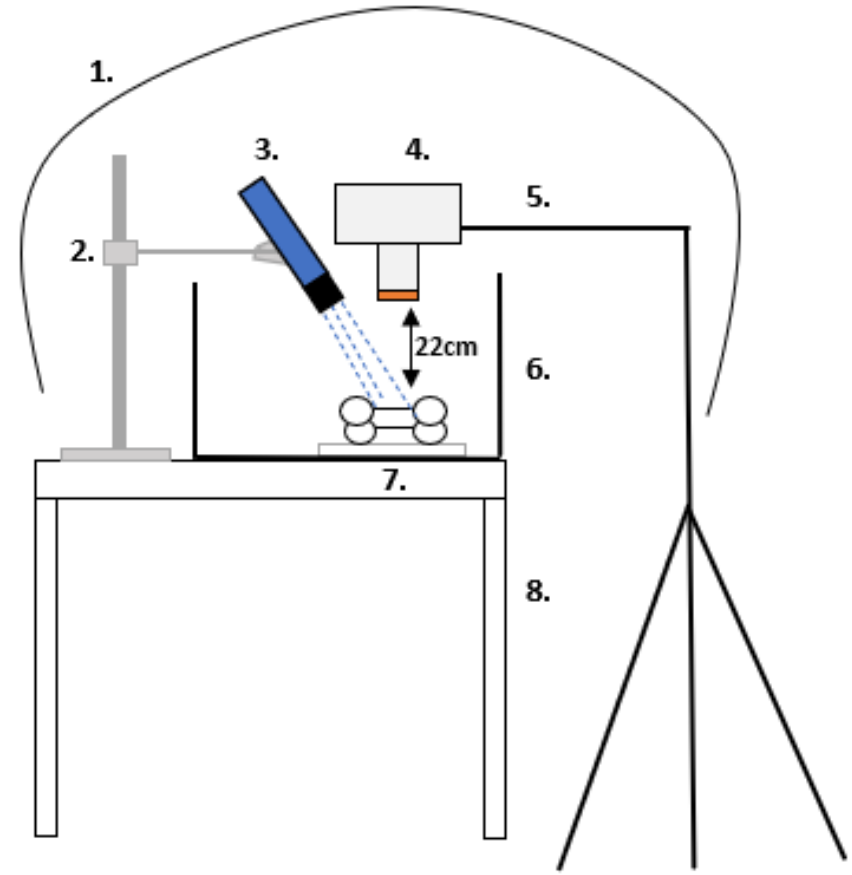

1. Photography cloth
2. Retort stand, boss, and clamp
3. ALS
4. Camera with coloured filter
5. Tripod
6. Black box
7. Polystyrene insert
8. Table

Figure 89: Diagram of equipment configuration for terrestrial fluorescence photography

Standardised camera settings for terrestrial photography for both light sources were set at ISO 1600 and F5.6, and F11 with ISO 1600 was used for aquatic conditions.

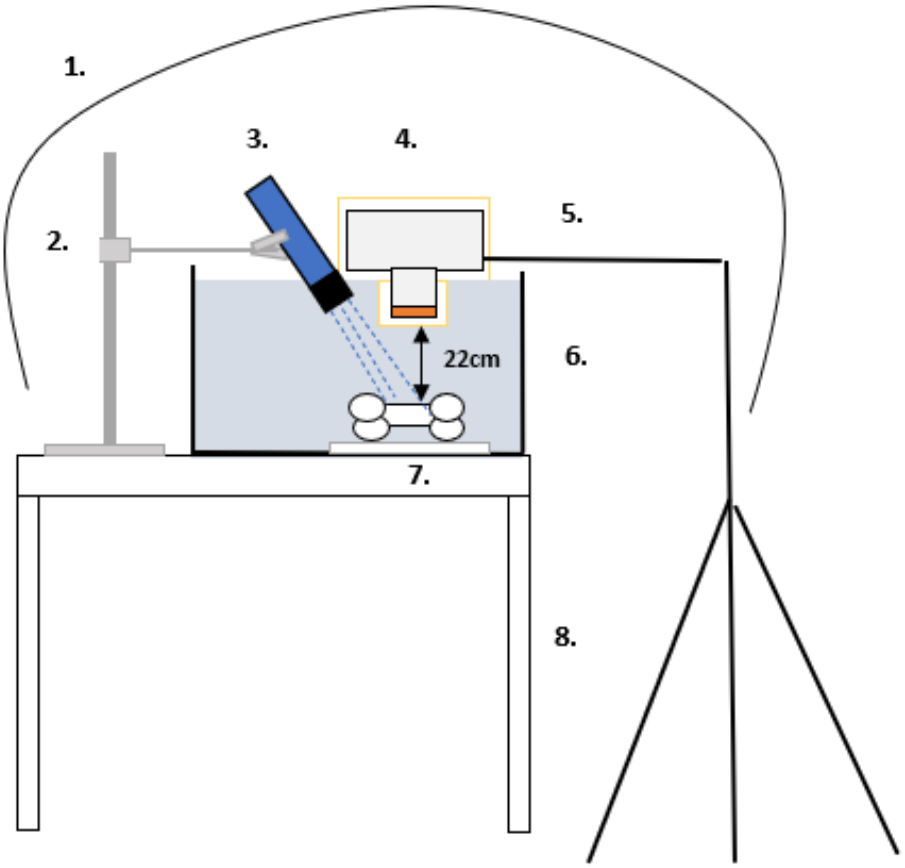

1. Photography cloth
2. Retort stand, boss, and clamp
3. ALS
4. Camera with coloured filter and underwater case
5. Tripod
6. Black box
7. Polystyrene insert
8. Table

Figure 90: Diagram of equipment configuration for submerged fluorescence photography

20.2 – METHOD

20.2.1 – MACERATION

Hot water maceration was used to prepare bones for any research questions examining the bone fluorescence of macerated bone. As described in the maceration pilot study (chapter 14.1), for each session, porcine ribs (*Sus scrofa domesticus*) were submerged in 1 L of tap water within a Morphy Richards™ 48709 stainless steel 3.5 L slow cooker set to high. Once the water had reached the desired temperature (80°C) (measured using a digital thermometer), the ribs were added. The ribs were initially observed every 30 mins until nearing completion when the intervals were reduced to 15 mins, 10 mins and then 5 mins to ensure maximum maceration but prevent overcooking. Maceration was

considered complete once all grease was removed, and any remaining tissue could be lifted away easily. Once the process was complete, the ribs were removed from the water and rinsed with cold deionised water to prevent any further changes. The ribs were then left overnight at room temperature (approximately 18°C) to dry. When analyses took several days to complete, the macerated bones were frozen at -18°C until required and defrosted the night before in a refrigerator (approx. 4°C).

20.2.2 – COLLAGEN

Collagen quantification was conducted using thermogravimetric analysis (TGA). Approximately 15 mg of bone shavings were scraped from the central anterior surface of each rib onto a clean piece of filter paper using a size 10 scalpel, before being transferred to 2ml plastic tubes. The scrapings were frozen (-18°C) to limit bacterial growth and defrosted overnight in the refrigerator (2°C) before processing. For each sample, 5 mg was loaded into alumina crucible (70 µl) and processed in a Nitrogen atmosphere using a Mettler Toledo TGA machine at a flow rate of 50 ml per minute. Each sample ran for 75 mins with an insertion temperature of 25°C increasing 10°C per minute to a final temperature of 800°C. Interpretation and analysis concentrated on phase 2 of the profile i.e., the organic content (as discussed chapter 12.4), so that collagen levels could be quantified.

20.2.3 – FLUORESCENCE

After each photography session, all images were transferred from the Sony™ A6000 camera to a desktop computer (Windows 10). Fluorescence intensity was quantified using the OFC as discussed in detail in chapters 11.0 and 13.3.3. In summary, the OFC uses the *luminosity* method to covert each image to grayscale before layering the image with a coloured 300 x 300-pixel grid, with each square labelled with coordinates, and calculated fluorescence of 90,000 pixels within that square. Three adjacent ROIs located at the central anterior surface of the ribs are selected. These fluorescence values and the corresponding grid coordinates of the selected ROIs were collated into an excel spreadsheet. Overall, three photographs were taken for each specimen under each experimental condition, and an average calculated.

20.2.4 – STATISTICAL ANALYSIS

All statistical analysis was conducted using IBM™ SPSS Statistics v23 and Microsoft Excel, exploring the relationships between collagen content and bone fluorescence in aquatic and terrestrial contexts, as well as between the two models of ALS. Specific statistical analyses for each research question will be addressed during the statistical analysis section for each individual question.

21.0 - SECTION B, QUESTION 1:

TERRESTRIAL AND UNDERWATER BONE FLUORESCENCE

Is there a statistical difference in observed bone fluorescence of fresh porcine bone (Sus scrofa domesticus) between terrestrial and tap water contexts? A comparison of terrestrial and underwater fluorescence levels of 30 fresh porcine ribs (Sus scrofa domesticus). photographed using blue light (approximately 450 nm) and orange and yellow filters.

21.1- MATERIALS

Thirty fresh, manually defleshed, porcine ribs (*Sus scrofa domesticus*), with an average mass of 18.23g, were photographed in terrestrial and tap water contexts using the Crime-lite 2 with the orange and then the yellow barrier filters, in accordance with the methodology outlined in chapter 20.0. Furthermore, the same ribs were also photographed under the same conditions using the Hammerhead light source as outlined in chapter 20.0, but with the orange filter only as the hammerhead was not capable with the yellow filter. The Hammerhead ALS was also used to photograph the porcine ribs in 21 L of tap water (also outlined in chapter 20.0), which had at the start of the experiment, had a temperature of 14.2°C (measured using a digital thermometer), pH 8, total dissolved solids (TDS) of 74 ppm and a turbidity of 0.04 NTU. pH was measured using a handheld digital pH meter (range 0.00 – 14.00) calibrated using factory supplied known pH 4.01 and pH 9.18 solutions (± 0.01 accuracy). TDS was measured using a factory calibrated E-1 portable TDS & EC meter, which could detect between 0-9999 µ/cm (± 2% accuracy). Turbidity (cloudiness) of the water was measured using Eutech™ TN-100 waterproof portable turbidity meter from Thermo Scientific™, calibrated using four factory supplied standards of 800 NTU, 100 NTU, 20.0 NTU, and 0.02 NTU. The turbidity meter has a detection range of 0 to 2000 NTU, and an accuracy range of < 0.1 NTU for 0.02 NTU standard; ±2 % of reading ±1 digit for 0 to 500 NTU; ±3 % of reading ±1 digit for 501 to 2000 NTU. In Huddersfield, where this experiment was carried out, the tap water is considered to have an average hardness rating of 'moderately soft', containing on average 20.4 mg/L of dissolved calcium (fig.91) [496].

Supply Zone:	Colne Valley 2019
Areas Covered:	Birkby, Cliff End, Egerton, Honley, Linthwaite, Marsden, Meltham, Rowley Hill, Slaithwaite, Hall Ings, Upperthong, Almondbury, Fenay Bridge, Cowmes
Report Period:	1st January 2021 - 31st December 2021
Water hardness type:	Moderately soft
Water hardness average:	20.4 mg/l calcium

Figure 91: Water hardness classification for Huddersfield, as reported by Yorkshire Water [496]

Full details of the average reported chemical composition of the tap water can be found in appendix 20. Prior to photography, the mass of each bone was measured using a Brifit kitchen scale (0.05–500 g), and the length, width, and anterior to posterior (front to back) measurement of each rib was recorded using a Yakamoz electronic digital callipers (±0.1 mm).

21.2 – RESEARCH QUESTION SPECIFIC METHOD

21.2.1- PHOTOGRAPHY

Firstly, each specimen was photographed terrestrially under natural light with scale. Terrestrial and submerged photographs were then taken using the Crime-lite 2, in conjunction with the orange and yellow filters, at three exposure times; 0.6, 0.4, 1/3s (slowest to fastest), using the camera settings outlined in chapter 20.0. Three photographs were taken at each exposure time. This sequence was repeated for the Hammerhead light using only the orange filter, as described in chapter 20.0. Submerged photographs were taken in 21 L of tap water, with the camera lens submerged 2 cm below the surface.

21.2.2 – COLLAGEN

Collagen scrapings were collected as per the core methodology (chapter 20.0).

21.2.3- FLUORESCENCE

Fluorescence quantification was conducted using the OFC software, as outlined in chapter 20.0.

21.2.4 – STATISTICAL ANALYSES

Statistical analysis was conducted using IBM™ SPSS Statistics v23 software and Microsoft Excel spreadsheets, using a combination of paired-samples t-tests, Wilcox signed rank tests, and graphical presentations to interpret potential relationships/correlations between collagen, fluorescence, and the different models of ALS. More specifically, analyses focused on comparing the terrestrial and submerged fluorescence values of the porcine ribs.

21.3 – RESULTS AND DISCUSSION

21.3.1 – FLUORESCENCE

Table 28 below summarises all photographic fluorescence results for rib 1 stimulated using the Crime-lite 2 with the orange and yellow filters in terrestrial and underwater setting respectively, as well as the Hammerhead light coupled with the orange filter. Due to the high volume of photographs taken, rib 1 is included here for representation, but all fluorescence photographic tables for all ribs can be seen in appendices 20-26. All fluorescence photographs and OFC outputs for the thirty ribs taken in all deposition contexts and ALS/filter combinations are also available in appendices 27-30.

Furthermore, table 29 below summarises the overall average fluorescence levels for each filter, ALS device, exposure time, and context, including the calculated differences between the fluorescence levels exhibited in terrestrial and underwater environments. The coloured squares represent the orange and yellow filters, the blue text highlights the underwater fluorescence values, and the red text indicates a reduction in values. Appendix 31 details the average terrestrial and underwater fluorescence values for all ribs using the Crime-lite 2 and the orange and yellow filters across all exposure times (0.6s, 0.4s, 1/3s), including the calculated difference in average fluorescence between the filters. Detailed individual fluorescence values for all selected regions of interest for the Crime-lite 2 are tabulated in appendices 33-36, alongside the calculated averages, arranged according to exposure time and deposition context. The equivalent data for the Hammerhead fluorescence images is contained in appendices 37-39. Due to an oversight, rib 17 was omitted at some points during the photography process, and as several months had passed since the photography had been completed, it was decided to remove rib 17 from the data set to maintain analytical consistency.

In all experimental configurations, the 0.6s exposure time captured the brightest fluorescence results, whereas the faster 1/3s exposure time recorded the lowest fluorescence results. For the Crime-lite 2, the data demonstrated that fluorescence values obtained using the yellow filter were overall much higher compared to the orange filter, across all photographic conditions, with an average overall difference (including all exposure times) of 88.6 in terrestrial contexts, and 77.5 in aquatic. Similarly, it is apparent from the photographs and the average fluorescence data, that higher levels of

fluorescence were detected when photographing the porcine bones in air compared to tap water, illustrated by a uniform decrease in fluorescence levels across both ALS devices, filters, and all exposure times. These findings were in keeping with expectations, as water is denser compared to air [168].

As discussed in chapter 7.1, when light passes through a medium it stimulates excitation of the surrounding molecules throughout its route, leading to loss of energy through refraction and scattering, and an overall reduction in speed of travel [497]. Consequently, the denser the material i.e., the more particles in a given volume, the greater the absorption, and the much the level of scattering and refraction. Water is optically denser than air [168], and consequently the fluorescence observed in an aquatic context would be overall lower compared to the same parameters conducted in a terrestrial context. Comparatively, the Crime-lite 2 produced higher fluorescence levels compared to the Hammerhead light in terrestrial and submerged contexts, when using the orange filter.

21.3.2- CRIME-LITE 2: FLUORESCENCE ANALYSIS

Across all three exposure times, the fluorescence produced using the Crime-lite 2, observed with the orange filter suffered an average reduction of 68.2 (48.1%) in fluorescence when photographing porcine rib bone in an aquatic context compared to in air. When using the yellow filter, the average reduction was technically higher at 79.3 (34.4%), but due to the overall much higher fluorescence intensities recorded, this figure equated to a smaller overall percentage change.

However, ribs 5, 7, and 8 in the Crime-lite 2 dataset experienced an increase in fluorescence, when photographed in tap water compared to the terrestrial context, when using the orange filter. When considering results for all exposure times, rib 5 experienced the largest average increase in fluorescence of 57.6 (60.3%), rib 7 exhibited the lowest average increase of 13.9 (9.2%), and rib 8 produced a slightly higher average increase compared to rib 7, of 17.4 (11%). These increases were not seen in the yellow filter dataset, nor in the Hammerhead with the orange filter results. Consequently, these increases may be the result of human error during photography, or the photography equipment not being set up correctly. Throughout a photography session the position of the camera could sometimes be disturbed by nearby movement or due to the weight of

the camera pulling the tripod closer to the specimen over time. The movement of the camera closer to the specimen may have led to overexposure, and therefore account for the increase, which was seen to be especially high in rib 5 at 60.3%. Although rib 5 exhibited some areas of surface discolouration along the diaphysis, if this were a contributing factor to the fluorescence increase it would be present in all the datasets. Therefore, these discrepancies are more likely a result of the photography methodology.

All photographs in this experiment were taken manually, a remote shutter release was considered during method development, but the underwater case prevented the attachment of a remote shutter release, therefore it was not used for all photography sessions, including terrestrial contexts, to prevent the introduction of additional variability. Due to the volume of bones, the photographs were also completed in batches. Therefore, this small number of anomalies may be a result of slight variation in camera movement when taking the photographs or slight differences when reassembling the equipment between batches. As the discrepancies were seen almost uniformly across all three exposure times, it could be suggested the issue was with the photography set up rather than the camera malfunctioning, particularly as the ribs are almost sequential in rib number, and most likely examined in the same batch. As a result, ribs 5, 7, 8 were removed from subsequent analyses.

Table 28: Summary of all photographic fluorescence results for rib 1 stimulated using the Crime-lite 2 with the orange and yellow filters in terrestrial and underwater setting respectively, as well as the Hammerhead light coupled with the orange filter in terrestrial and underwater contexts.

Natural		
Terrestrial fluorescence		
Crime-lite 2		Hammerhead
Orange	Yellow	Orange
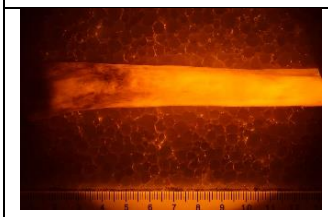		
0.6		
	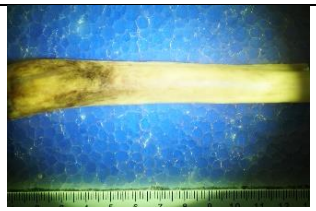	
0.4		
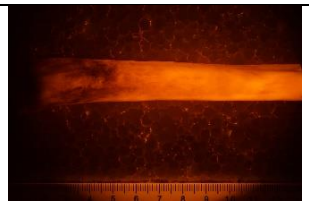	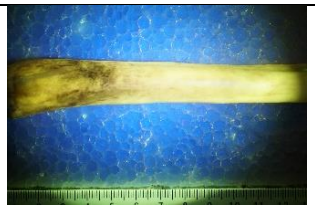	
1/3		
Underwater fluorescence		
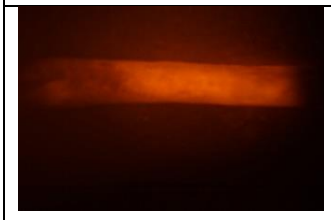	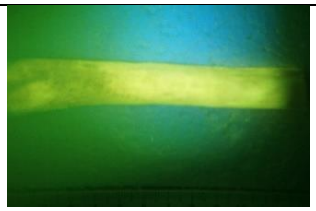	
0.6		

	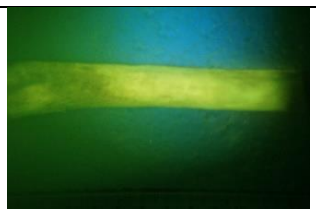	
0.4		
	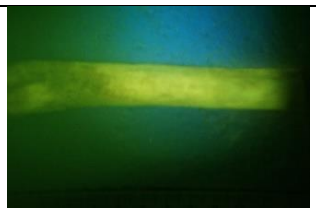	
1/3		

Table 29: Summary of average changes in averaged fluorescence levels of porcine bone when photographed with ALS and the appropriate orange and/or yellow filters in terrestrial and underwater contexts.

ALS	Crime-lite 2						Hammerhead			Context
Exp. time (s)	0.6		0.4		1/3		0.6	0.4	1/3	
Average Fluor.	160.2 (s.d.=23.8)	242.5 (s.d. =11.4)	141.3 (s.d=24.8)	232.7 (s.d.=14.5)	128.6 (s.d.=28.6)	220.7 (s.d.=22.1)	158.4 (s.d.=30.1)	127.5 (s.d.=33.5)	111.2 (s.d.=32.3)	Air
	94.6 (s.d.=37.2)	179 (s.d.=41)	71.3 (s.d.=33)	147.5 (s.d.=40.3)	59.4 (s.d.=27.8)	131.3 (s.d.=38.6)	63.3 (s.d.= 17.2)	42.5 (s.d.=12.8)	34.2 (s.d.=11.1)	Tap water
Diff. in fluor.	-65.6	-63.5	-70	-85.2	-69.2	-89.4	-95.1	-85	-77	Changes
% Diff. in fluor.	-40.9%	-26.2%	-49.6%	-36.6%	-53.8%	-40.5%	-60%	-66.6%	-69.2%	

In the terrestrial environment, fluorescence values stimulated using the Crime-lite 2 showed greater consistency at the longest exposure time of 0.6s, when photographed using an orange filter, compared to the shorter exposure times used in the same context. This result is illustrated by the tighter, clustered appearance on chart 92, and supported by the lower standard deviation of 23.8 reported in table 29, in comparison to the higher 28.6 calculated for 1/3s. Conversely, fluorescence results obtained using the yellow filter within the terrestrial environment with the Crime-lite 2, demonstrated an overall lower standard deviation in fluorescence values ranging from 11.4, when using exposure time 0.6s, up to 22.1 when using 1/3s (chart 94). However, although the standard deviation was overall lower, the deviation from the mean across exposure times was greater in the fluorescence values produced using the yellow filter, almost doubling (9.7), whereas the total increase was 4.8 when using the orange filter.

Irrespective of this difference, these results indicate that the 0.6s exposure time is the most suitable for imaging bone fluorescence in a terrestrial environment, when using the Crime-lite 2. The longer exposure time was the most optimal, as it allowed greater time for fluorescence capture, by allowing longer exposure to the camera sensor. The shorter exposure time possibly led to greater variation in fluorescence levels as it may not have been long enough for all bones within the sample. Natural variation in bone morphology, composition, and dimensions may have been influential in the degree and rate of fluorescence excitation and emission. For example, a larger bone may require more sustained stimulation compared to smaller bones as the overall volume of bone is greater. Similarly, differences in bone composition and density may also influence how readily accessible and consequently responsive the bone is to molecular excitation. Although all the bone samples are porcine ribs, anatomical variation based on the position of the ribs within the ribcage means differences in trabecular to cortical bone ratios, as well as overall size and shape.

When photographing porcine bone autofluorescence in the aquatic context, the results of the yellow filter echoed those obtained using the orange filter (charts 93 and 95). The results for both filters exhibited an inverse trend of the terrestrial values, with the degree of distribution within fluorescence values reducing as the exposure time became faster, with an optimal exposure time of 1/3s identified for both filters. The results obtained using the orange filter ranges from 37.2 when using 0.6s exposure time, down to 27.8 at

1/3s exposure time, a reduction of 9.4. Fluorescence values visualised with the yellow filter exhibited overall wider deviation from the mean compared to the orange filter results, ranging from 41 when using 0.6s exposure time to 38.6 when using the 1/3s exposure, but an overall much smaller reduction of 1.4 across exposure times, indicating greater consistency. Charts comparing the average terrestrial and underwater fluorescence values for all exposure times can be seen in figures 96-101.

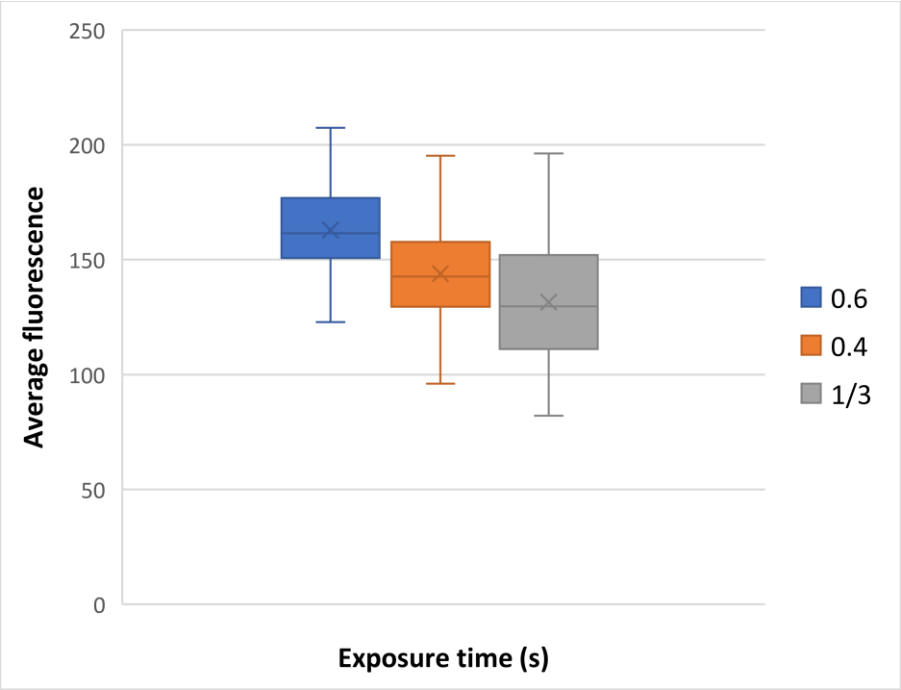

Figure 92: Comparison of average terrestrial fluorescence values of porcine ribs photographed with the Crime-lite 2 and the orange filter at 0.6, 0.4 and 1/3s exposure times.

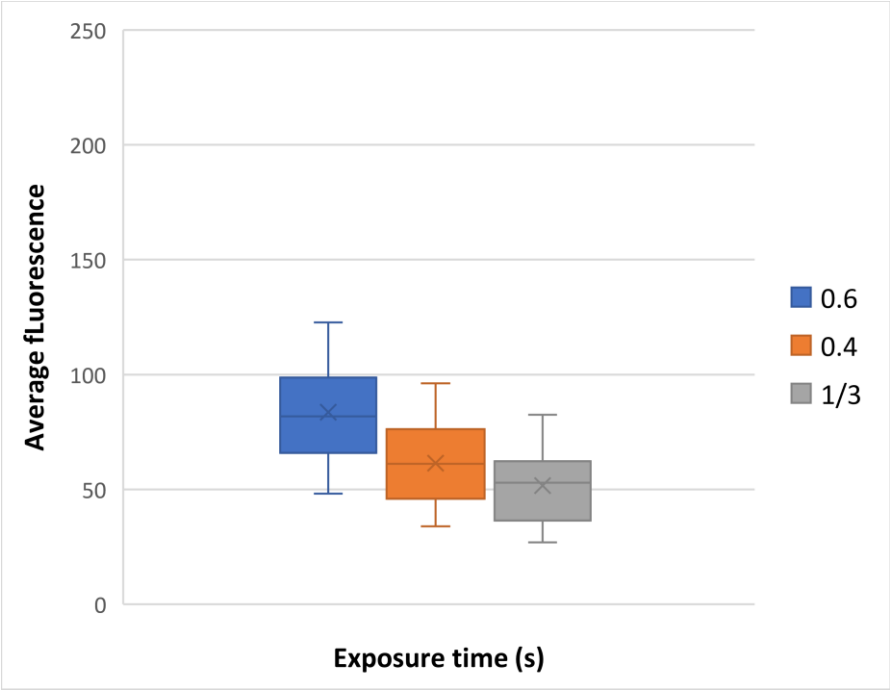

Figure 93: Comparison of average underwater fluorescence values of porcine ribs photographed with the Crime-lite 2 and the orange filter at 0.6, 0.4 and 1/3s exposure times.

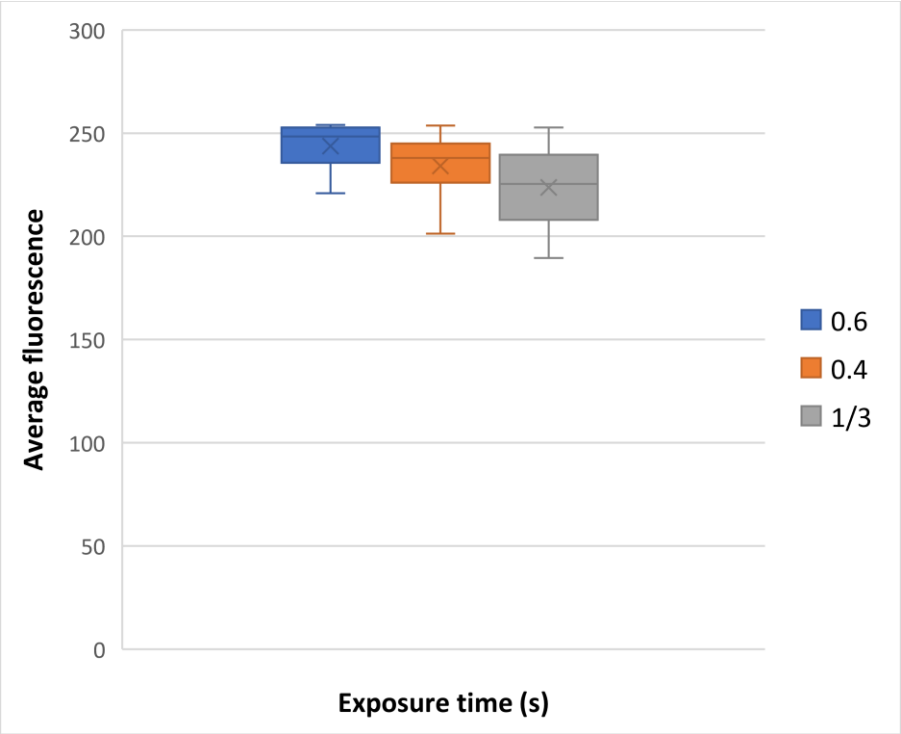

Figure 94: Comparison of average terrestrial fluorescence values of porcine ribs photographed with the Crime-lite 2 and the yellow filter at 0.6, 0.4 and 1/3s exposure times.

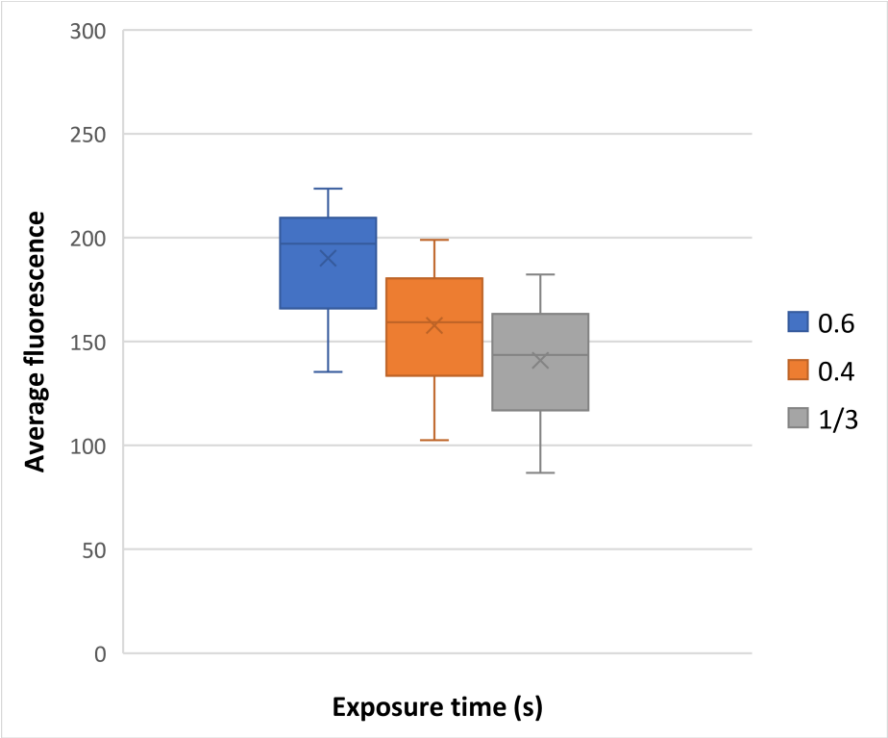

Figure 95: Comparison of average underwater fluorescence values of porcine ribs photographed with the Crime-lite 2 and the yellow filter at 0.6, 0.4 and 1/3s exposure times.

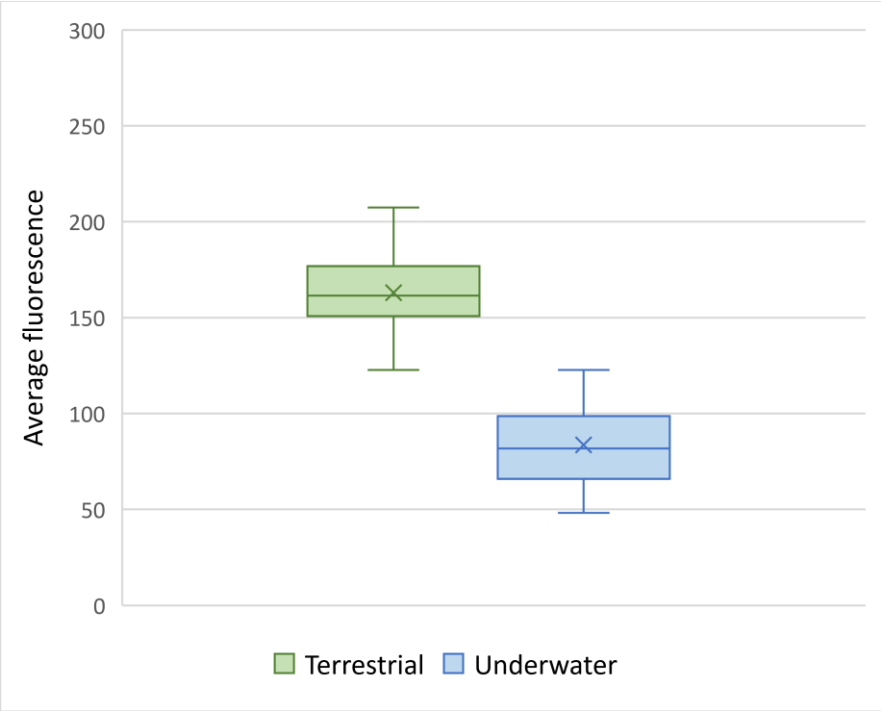

Figure 96: Comparison of average terrestrial and underwater fluorescence values of porcine ribs photographed with the Crime-lite 2 and the orange filter at 0.6s exposure time

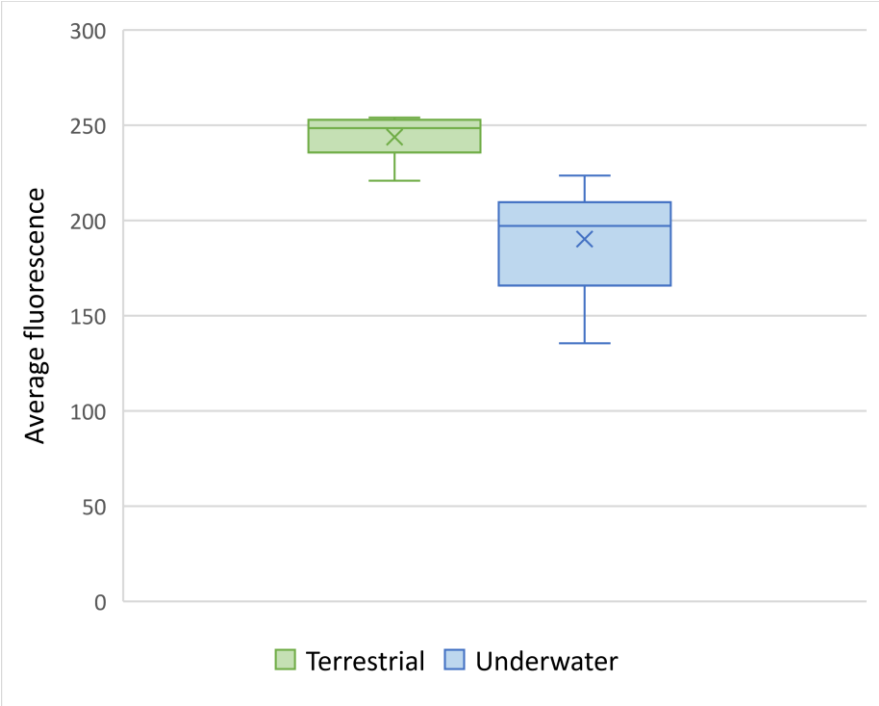

Figure 97: Comparison of average terrestrial and underwater fluorescence values of porcine ribs photographed with the Crime-lite 2 and the yellow filter at 0.6s exposure time

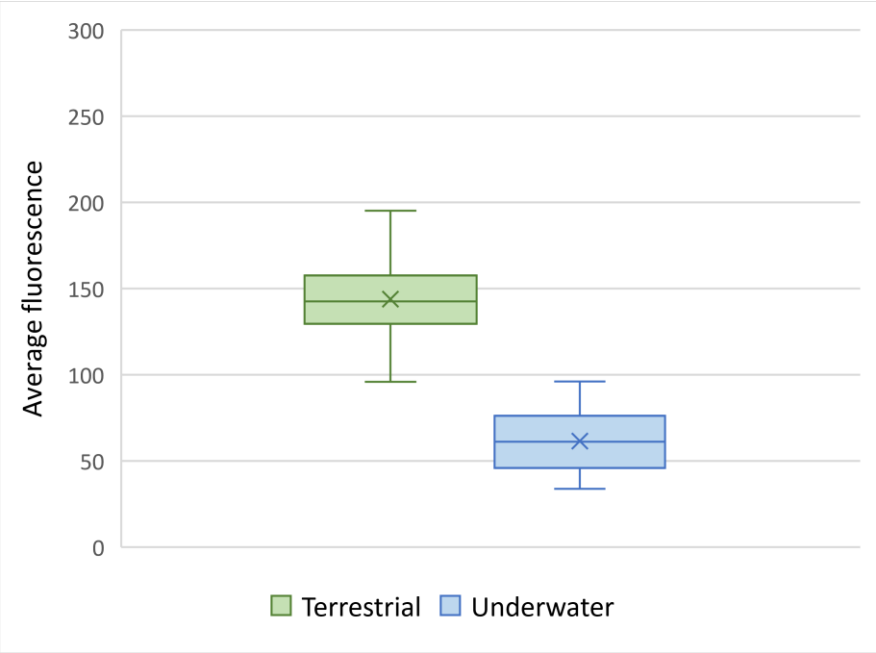

Figure 98: Comparison of average terrestrial and underwater fluorescence values of porcine ribs photographed with the Crime-lite 2 and the orange filter at 0.4s exposure time.

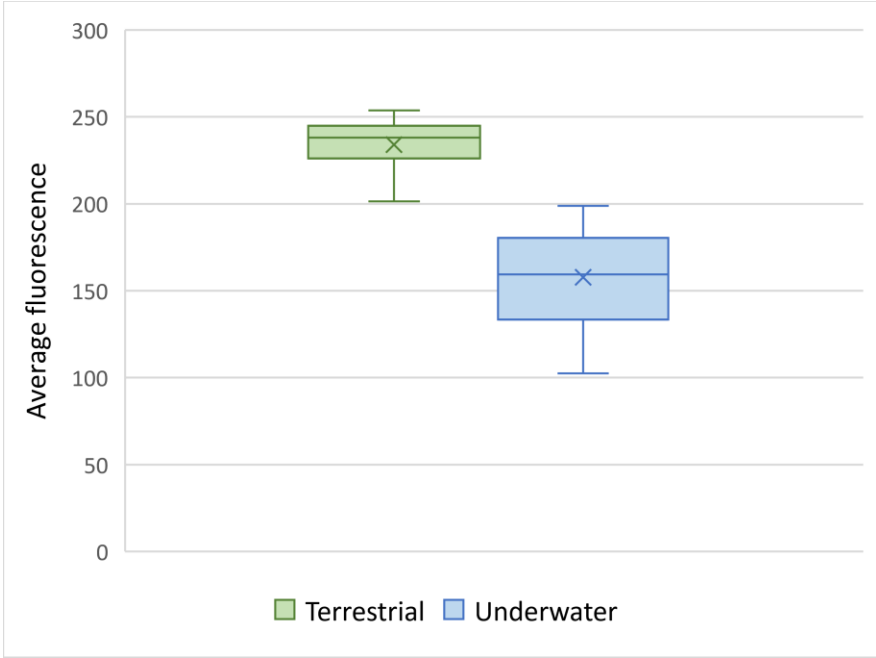

Figure 99: Comparison of average terrestrial and underwater fluorescence values of porcine ribs photographed with the Crime-lite 2 and the yellow filter at 0.4s exposure time.

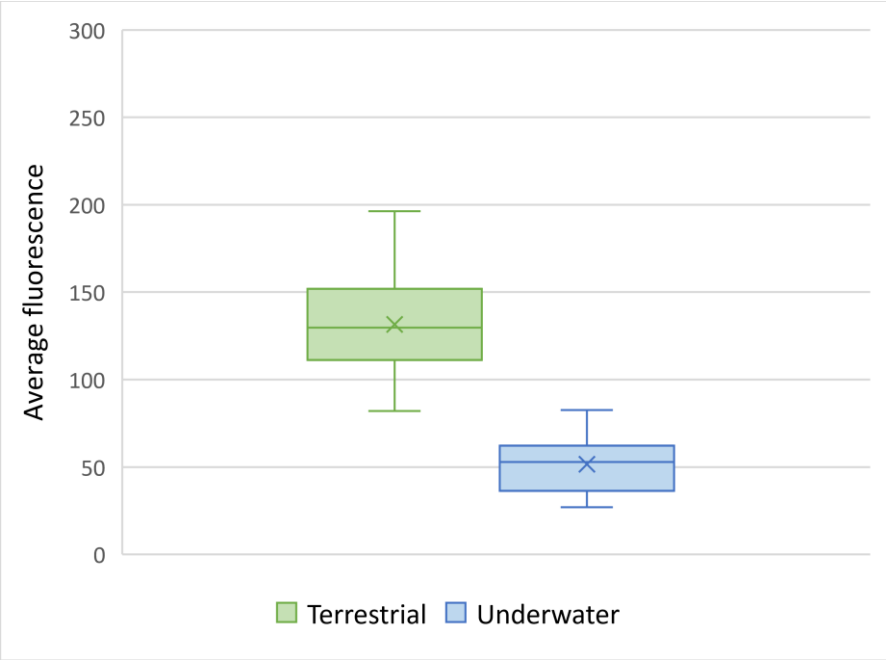

Figure 100: Comparison of average terrestrial and underwater fluorescence values of porcine ribs photographed with the Crime-lite 2 and the orange filter at 1/3s exposure time.

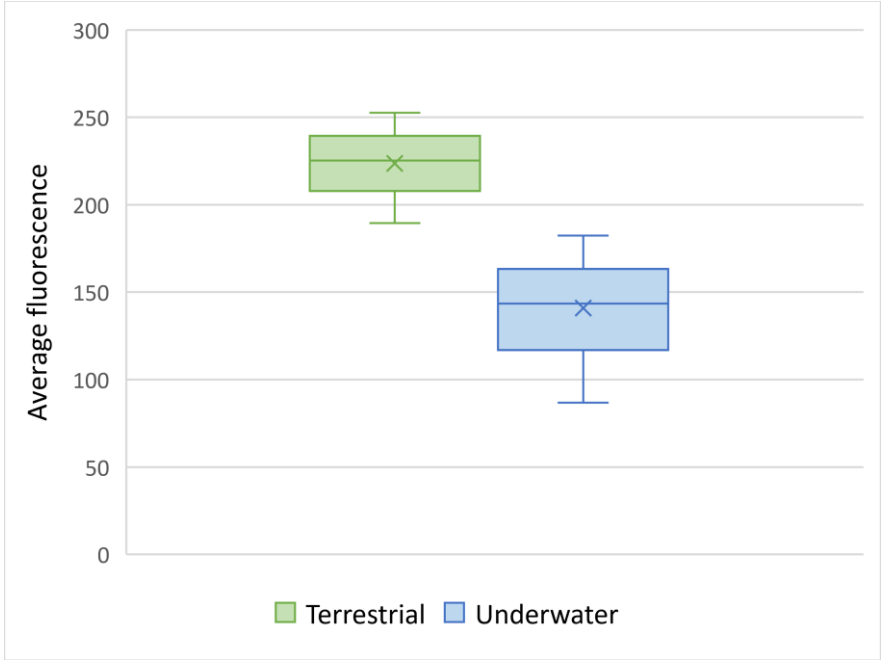

Figure 101: Comparison of average terrestrial and underwater fluorescence values of porcine ribs photographed with the Crime-lite 2 and the yellow filter at 1/3s exposure time.

The identification of a more rapid exposure time was somewhat expected, due to the denser aqueous medium, and probable movement caused by the water, there is a much higher possibility of scattering and reflection of the fluorescence wavelengths. Consequently, although a longer exposure time could allow for maximum fluorescence return due to longer exposure of the sensor, movement from the water could hinder assessment of the resulting photographs. If water was moving the angle of incidence will continue to change and increasing the subsequent refraction of light, leading to greater levels of scattering.

Similarly, although the same source of water was used throughout the experiment, the exact chemical composition may have slightly varied, potentially leading to differences in how the wavelengths behaved. More significantly, the degree and pattern of movement within the water would ultimately vary significantly between photography sessions, and therefore it would be impossible to truly replicate the aquatic environment each time, which subsequently could have led to fluctuations in how many wavelengths eventually interacted with the camera sensor. Submersion of the camera lens helped to reduce the impact, but only a depth of 2 cm was possible and therefore still close to the surface. Deeper submersion may have increased stability but could not be achieved due to restrictions within the equipment and workspace availability. Movement created outside the box whilst taking the photographs also disturbed the water and may have led to some changes in bone positioning, exacerbated by the small size of the bones, differences in bone composition, and the momentum of the water. Small specimens, particularly those comprised of sternal ends would occasionally float, most likely due to a higher ratio of trabecular bone (spongy bone) compared to cortical bone (compact bone). Its woven composition creates multiple cavities, trapping air and increasing buoyancy as illustrated in figure 102:

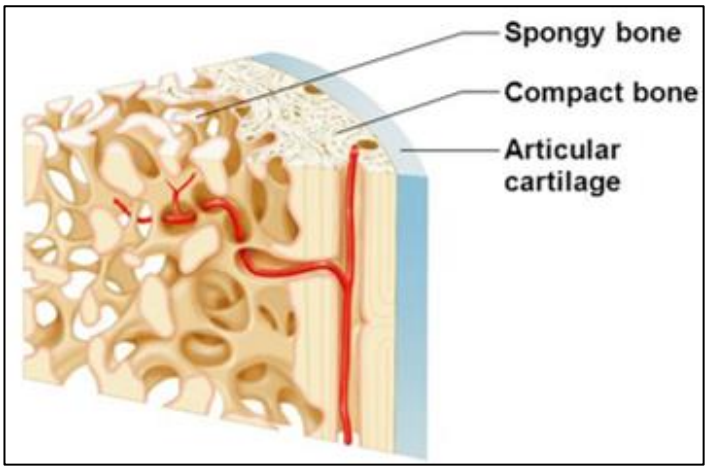

Figure 102: Graphical representation showing the general compositional differences between trabecular (spongy) bone and cortical (compact) bone.

Consequently, these specimens were secured in place with Blu Tac, meaning that bone positioning was not entirely consistent, and potentially contributed to some variation in fluorescence levels. However, a faster exposure time could in theory limit the impact of water on the overall fluoresce emissions. In the photography industry, faster exposure times are often implemented when photographing moving objects, to 'freeze' the subject in the frame, and consequently eliminating movement blur and over exposure [203], as previously discussed in chapter 6.0.

Comparatively, the yellow filter produced much greater variation in fluorescence values when used in the terrestrial environment, whereas the orange filter created greater levels of variation within the aquatic context. This result demonstrates how the filter, light source, camera, and deposition context are all influential in the production of bone fluorescence and will need to be tailored to each case.

When comparing individual images, such as with rib 23 in figures 103-104 below, it could be suggested that although 0.6s provided stronger fluorescence levels, the photograph taken at 1/3s provides an overall better representation of the bones image, enabling a higher degree of topological detail. This result varies between ribs due to natural diversity and the use of standardise camera settings, but therefore also infers that exposure times may need to be adapted depending on whether documentation or ALS analysis is the goal of examination. For example, if searching for bone at the crime scene, or triaging bone for further anthropological examination, rapid preliminary identification

would most likely be a higher priority compared to high quality detailed images. On the other hand, laboratory ALS analysis would possibly require a greater emphasis on accurate documentation, in order to inform further downstream analyses, and/or form part of expert witness reports and evidential reporting.

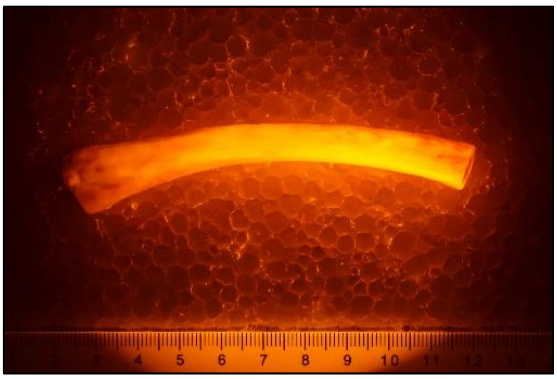

Figure 103: Porcine rib 23 photographed terrestrially using the Crime-lite 2 with the orange filter at 0.6s exposure time

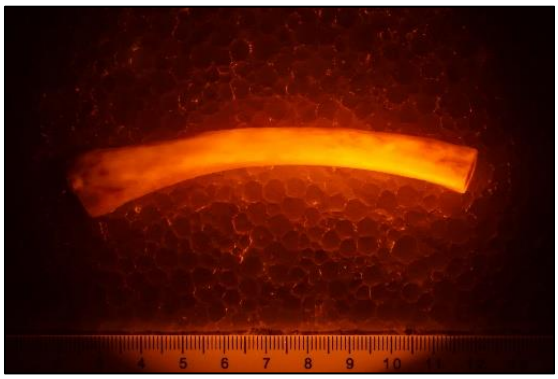

Figure 104: Porcine rib 23 photographed terrestrially using the Crime-lite 2 with the orange filter at 1/3s exposure time.

Furthermore, although the photographs taken with the yellow filter produced higher fluorescence values, it is not necessarily an indicator of the most successful filter choice. As the OFC uses a weighted RGB methodology, the higher the number out of 255 the closer the image is to pure white. Therefore, a high value of 254, as seen in several ribs in this dataset, equates to an almost true white. This could be more suggestive of overexposure rather than high autofluorescence levels, with the possibility that one of the RGB channels has been overexposed. Figures 105-106 below show comparable images of rib 20, photographed at 0.6s exposure time using the yellow and orange filters. The orange filtered image has an average fluorescence reading of 187 but 254 with the yellow.

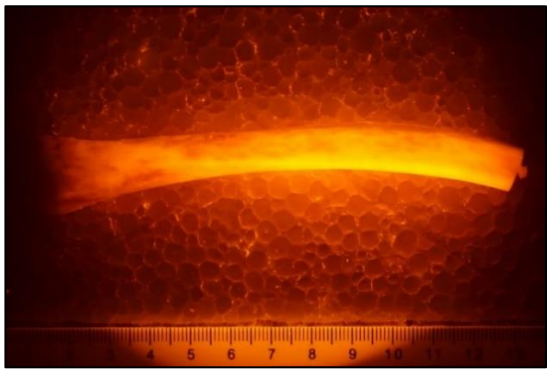

Figure 105: Porcine rib 20 photographed using the Crime-lite 2 with the orange filter at 0.6s exposure time.

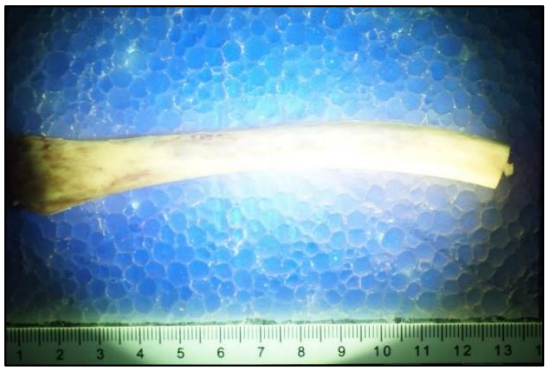

Figure 106: Porcine rib 20 photographed using the Crime-lite 2 with the yellow filter at 0.6s exposure time.

The centre of the bone, where the fluorescence was measured, is very white, creating a 'hot spot' of over exposure, with an observable reduction in contrast between the bone and the background. In comparison, the photograph created using the orange filter, which produced an overall lower fluorescence level, has better defined contrast between the polystyrene and the bone, and the fluorescence is more evenly distributed, arguable making it the more successful image. The yellow filter was investigated as it has been used in the current literature [135, 146], however authors for those papers used light sources other than the Crime-lite 2. Subsequently these ALS could have exhibited slightly different wavelengths of blue light, as well as differences in intensity and type of transmission, for example a laser rather than an LED bulb. Consequently, this supports the idea that successful visualisation of fluorescence is dependent on the pairing of a complimentary filter with a specific wavelength (as mentioned in chapter 7.0), in conjunction with optimal positioning of the camera and light. Based on these observations it is argued that in this project and specific equipment configuration, the visualisation of fluorescence was most successful when pairing the Crime-lite 2 with the orange filter rather than the yellow filter.

The issue of overexposure is less prevalent in the submerged photographs, potentially due to the absorption of some light by the water, and possibly the reduced zoom (34 mm instead of 40 mm) imposed by using the underwater housing. However, comparatively, the orange filtered results still appear visually superior compared to the yellow filter (figures 107-108). In the yellow filtered photograph, there is a halo of discolouration at the edges of the bone image, most likely a result of scattering by the water and incomplete barrier filtration. The orange filtered image lacks these extraneous

wavelengths, producing a clearer image.

Figure 107: Porcine rib 23 photographed underwater using the Crime-lite 2 with the orange filter at 0.6s exposure time.

Figure 108: Porcine rib 23 photographed underwater using the Crime-lite 2 with the yellow filter at 0.6s exposure time.

However, as mentioned previously, variation in specimen dimensions could also have had an impact on the success of fluorescence imaging. Differences in morphology, and general dimensions could influence the amount of fluorescence produced, as well as its intensity, due to the accessibility of light to the bone's surface. Rib bones have a natural curve due to their protective role in the thoracic cavity, with depressions and grooves at points of articulation and for anchorage of vessels. Consequently, the light from the ALS will undoubtedly encounter some variation in bone coverage.

As the bones were also manually defleshed, the ALS may have been impeded due to retention of some cartilage and tissue, as noted as a limiting factor in previous MSc work [134], with distribution of this tissue varying between individual bones. All bones were defleshed by this author to make the method as consistent as possible, but ultimately it would not have been identical. Similarly, no provenance information about the ribs was obtained. Intrinsic factors such as bone composition, the part of the rib the specimens were from, if the ribs were from the same animal, the age of the pig, or rearing environment such as diet, could also have created some diversity in the fluorescence data as there would have been variations in bone morphology and composition.

Appendix 40 shows all recorded measurements of the porcine ribs, with table 30 below summarising the average mass, length, width, and anterior-posterior (front to back) measurements including standard deviation and range.

Table 30: Summary of average bone mass, length, width and anterior to posterior measurements of the photographed porcine bones (excluding rib 17)

	Mass (g)	Length (mm)	Width (mm)	A/P (mm)
Average	18.23	102.6	14.84	9.65
Max	29.8	125.2	27	17.1
Min	8.56	73.4	6.8	6.9
SD	7.04	15.23	4.1	2.60
Range	21.33	51.8	20.2	10.2

To investigate this issue further, statistical comparisons were conducted between the different bone measurements, mass, length, width, and anterior-posterior, with the level of calculated fluorescence for each filter and across all exposure times. All charts can be seen in appendix 41.

21.3.3 – CRIME-LITE 2: BONE DIMENSIONS

With regards to mass, most comparisons produced a positive correlation, but in every case, it was not significant, as the highest R^2 value was 0.04, which was seen in the fluorescence data from the terrestrial context, visualised with an orange filter, at 0.6s exposure time. Additionally, the terrestrial fluorescence results captured using the yellow filter at 1/3s exposure time, only produced an R^2 value of 0.0008 indicating no relationship between bone mass and observed fluorescence. The anterior to posterior measurements and bone fluorescence comparisons produced similar results, as seven out of the twelve experimental combinations produced R^2 values very close to 0, indicating no correlation, and the highest R^2 value was only 0.0584, which was observed when using the orange filter, in a terrestrial context, captured using 1/3s exposure time. Investigations into bone length did not show any consistent correlations, as a mixture of positive, negative, and no correlations were observed. The only discernible trends that could be identified in this dataset, were that all underwater correlations appeared to be positive, and all terrestrial fluorescence data observed with an orange filter presented with a negative correlation. However, none of these results were significant, and overall,

the R^2 values were uniformly approximately 0.02 or less, and therefore were not considered any further.

The most indicative relationships were observed when comparing the measured width of the porcine ribs with the level of autofluorescence seen. All comparisons demonstrated a positive correlation, with the lowest R^2 value of 0.341 observed when comparing bone width with terrestrial fluorescence values produced using the orange filter and 1/3s exposure time. Conversely, the highest, and only significant R^2 value of 0.9 was seen when comparing bone width with the underwater fluorescence values obtained using the orange filter at 0.4s exposure time (figure 109). This R^2 value provides strong support for the proposition that the wider the bone, the higher the level of autofluorescence produced. However, none of the other comparisons produced a similar level of significance with the subsequent next highest R^2 value of 0.1204 identified when comparing bone width with autofluorescence visualised with the orange filter, recorded using 0.6s exposure time, in the tap water context.

A similar R^2 figure of 0.0959 was noted when comparing bone width with autofluorescence photographed with the orange filter and 1/3s exposure time, in the tap water context. These results consequently highlight an interesting trend that all comparisons between bone width and underwater fluorescence observed with an orange filter, produced the highest R^2 values in the dataset, and in all cases were substantially higher when compared to the same photographic conditions in the terrestrial environment. Therefore, it could be suggested that the width of porcine bone may be influential in the volume of porcine bone autofluorescence seen, particularly in the tap water environment, and therefore warrants further investigation. However, due to variation in bone morphology and size, the quantification of the fluorescence using the OFC was not always accurate, as some smaller or narrow bones did not completely fill the squares used for selecting the ROIs, and therefore some background may have been included in the result. Consequently, more investigation in the influence of bone dimensions on fluorescence levels is required.

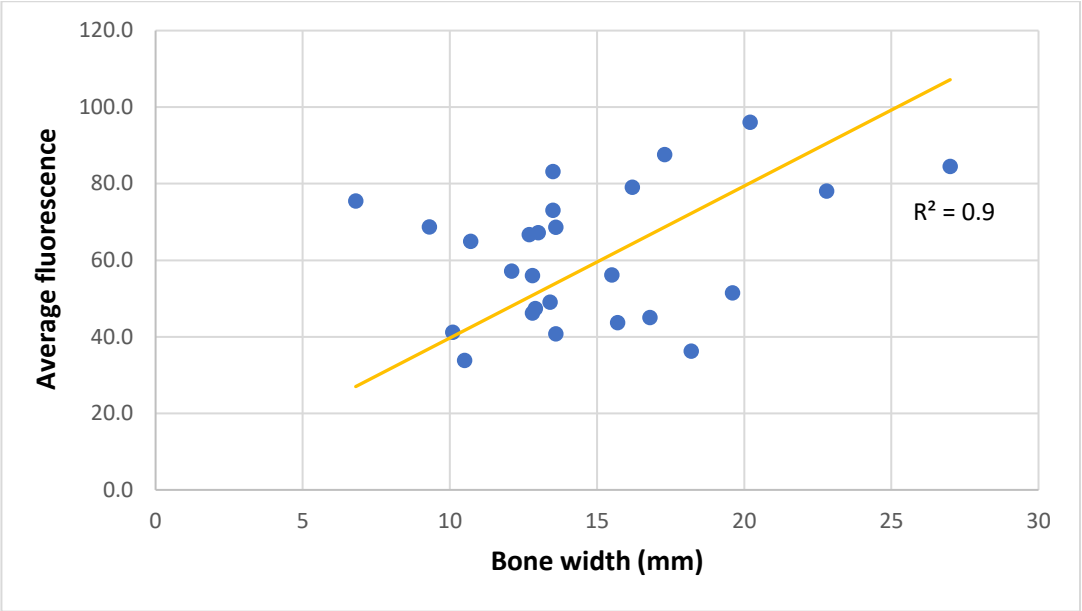

Figure 109: Comparison of average underwater fluorescence values compared with the measured width of the 29 porcine bones. Photographed using the Crime-lite 2, orange filter, and 0.4s exposure time.

This trend is subverted when considering the comparisons between bone width and the fluorescence levels produced using the yellow filter. In all cases, the correlations were overall stronger in the terrestrial contexts in comparison to the underwater comparisons when the same photographic parameters were used. The highest R^2 value of 0.0873, was observed when comparing bone width with the terrestrial fluorescence values photographed with a yellow filter and 0.6s exposure time. The R^2 values are then seen to decrease as the exposure time is reduced, dropping to R^2= 0.0514 at 0.4s, then to R^2=0.0409 at 1/3s exposure time. The aquatic comparisons of bone width and autofluorescence observed with the yellow filter do not follow the same declining trend, and instead produce very similar R^2 across the three exposure times, including R^2= 0.0416, R^2= 0.0448, and R^2= 0.0395, for 0.6s, 0.4s, and 1/3s exposure times respectively.

These results infer some corroboration that bone dimensions and composition may be influential in the level of fluorescence seen. The fact that bone width appears to be the most influential makes sense in the context of this PhD research due to the specific method employed. The Crime-lite 2 uses a single, LED (diameter 23 mm, fig. 110) to deliver the blue wavelengths of light, consequently producing a narrow beam. Therefore, it is logical that width would be the greatest morphological factor, as the whole length of the bone is not always included within the perimeter of the light beam, and the anterior-posterior margin always directly exposed to the light source during

photography. Additionally, the width measurements exhibited one of the greatest degrees of variation across the sample population, including a minimum width of 6.8 mm up to a maximum of 27 mm, and producing a range of 20.2 mm (s.d.= 4.1 mm).

Figure 110: Photograph of the Crime-lite 2 single LED (diameter 23 mm)

Figure 111: Photograph of the Hammerhead light source illustrating the two LEDs (diameter 18 mm each)

In comparison, the Hammerhead light source uses two LEDs (diameter 18 mm each, fig. 111) positioned side by side, creating a more diffuse beam of light, and therefore may produce different results compared to the Crime-lite 2.

21.3.4 – HAMMERHEAD: FLUORESCENCE ANALYSIS

The same analyses as discussed in the chapter 21.1.2 were also performed using the Hammerhead fluorescence dataset, to see if any trends noted in the Crime-lite 2 discussion were reproduced. The Hammerhead light source was only compatible with the orange filter, but comparisons between the two light sources could still be made, particularly with regards to understanding how the underwater context and porcine bone dimensions may possibly influence levels of emitted autofluorescence. Table 31 below summarises the results of the Hammerhead, initially reported in table 29. Box and whisker plots demonstrating the distribution of fluorescence values obtained with each exposure time are displayed in figures 112 and 113, and further charts comparing the distribution of bone fluorescence in the aquatic and terrestrial contexts for each exposure time can be seen in figures 114-116.

Table 31: Summary of average fluorescence of the photographed porcine bones (excluding rib 17) in terrestrial and underwater contexts, using the Hammerhead ALS, orange filter, and the three exposure times: 0.6s, 0.4s, and 1/3s.

	Context	Exposure time (s)		
		0.6	0.4	1/3
Average fluorescence	Air	158.4 (s.d.=30.1)	127.5 (s.d.=33.5)	111.2 (s.d.=32.3)
	Tap water	63.3 (s.d.= 17.2)	42.5 (s.d.=12.8)	34.2 (s.d.=11.1)
Difference in fluorescence		-95.1	-85	-77
% Difference in fluorescence		-60%	-66.6%	-69.2%

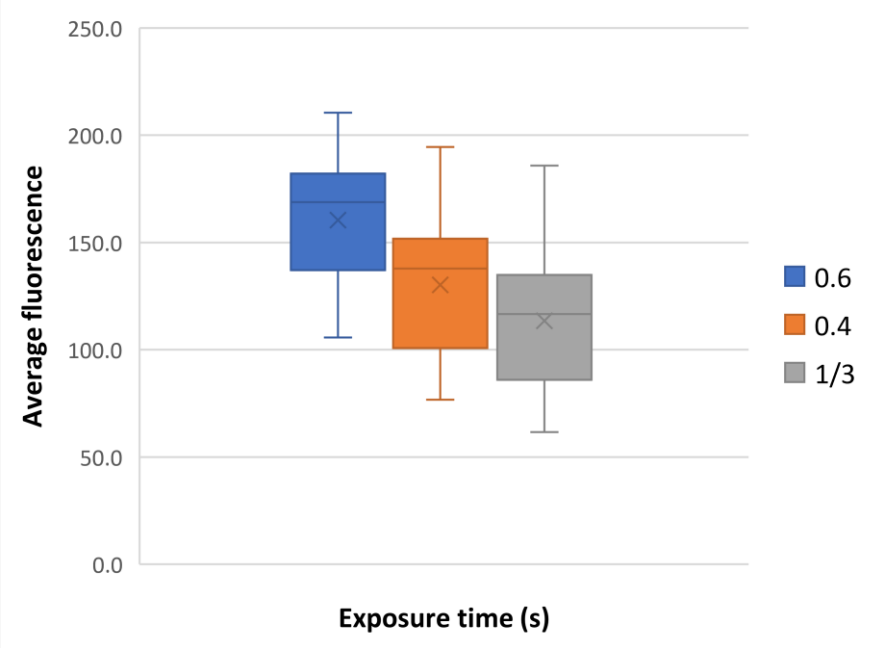

Figure 112: Comparison of average terrestrial fluorescence values of porcine ribs photographed with the Hammerhead and the orange filter at 0.6, 0.4 and 1/3s exposure times.

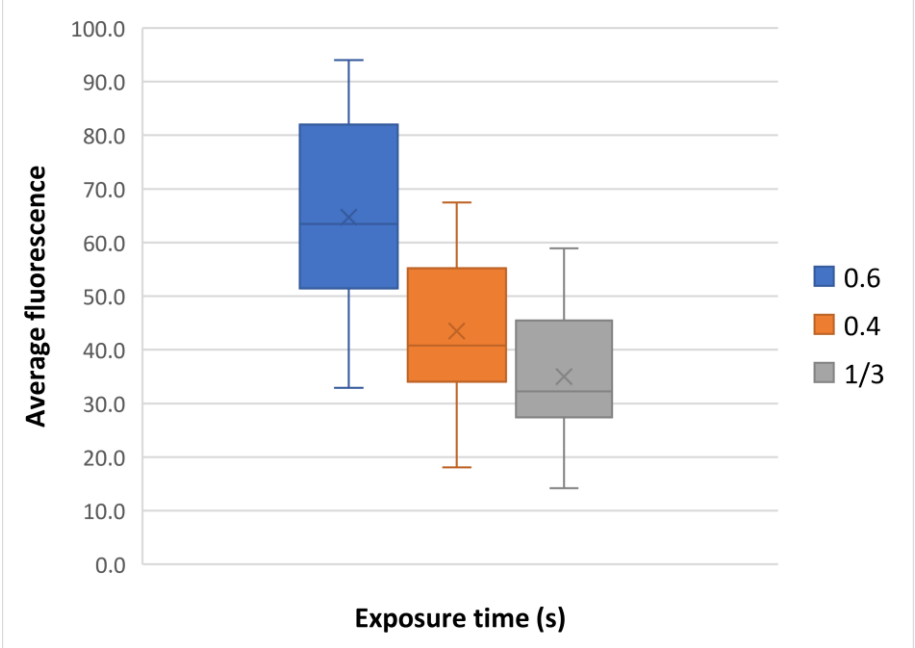

Figure 113: Comparison of average underwater fluorescence values of porcine ribs photographed with the Hammerhead and the orange filter at 0.6, 0.4 and 1/3s exposure times.

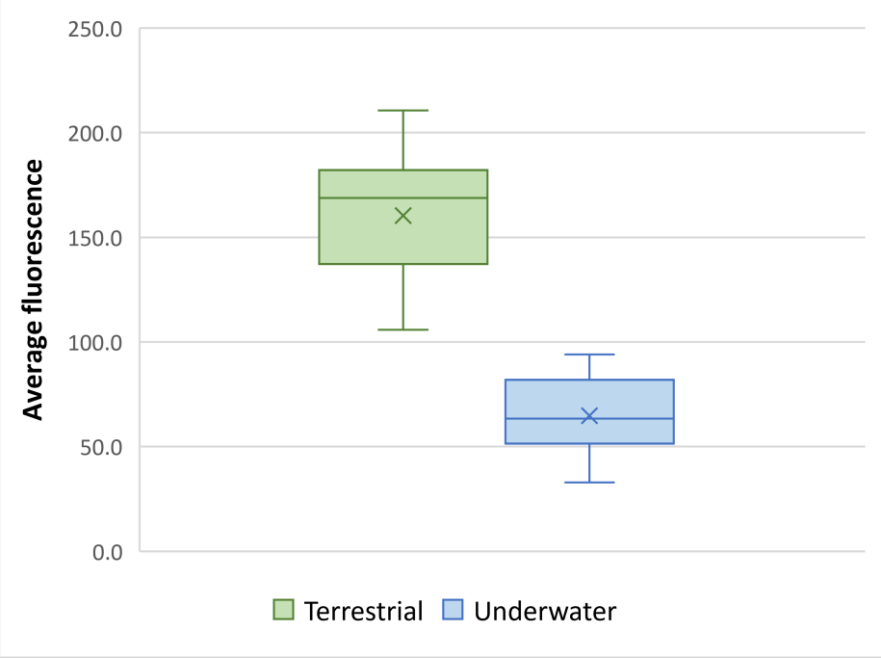

Figure 114: Comparison of average terrestrial and underwater fluorescence values of porcine ribs photographed with the Hammerhead and the orange filter at 0.6s exposure time.

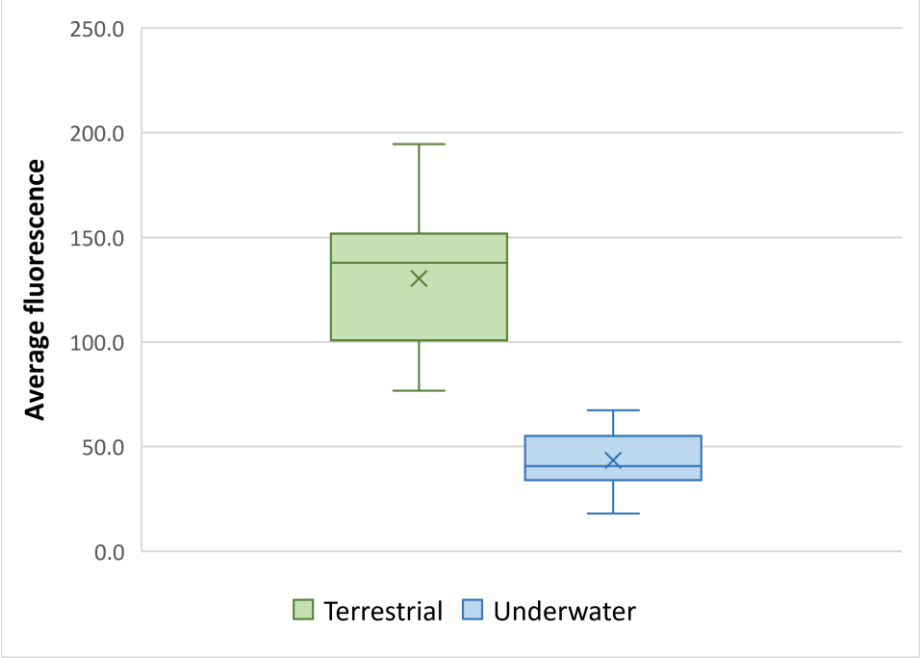

Figure 115: Comparison of average terrestrial and underwater fluorescence values of porcine ribs photographed with the Hammerhead and the orange filter at 0.4s exposure time.

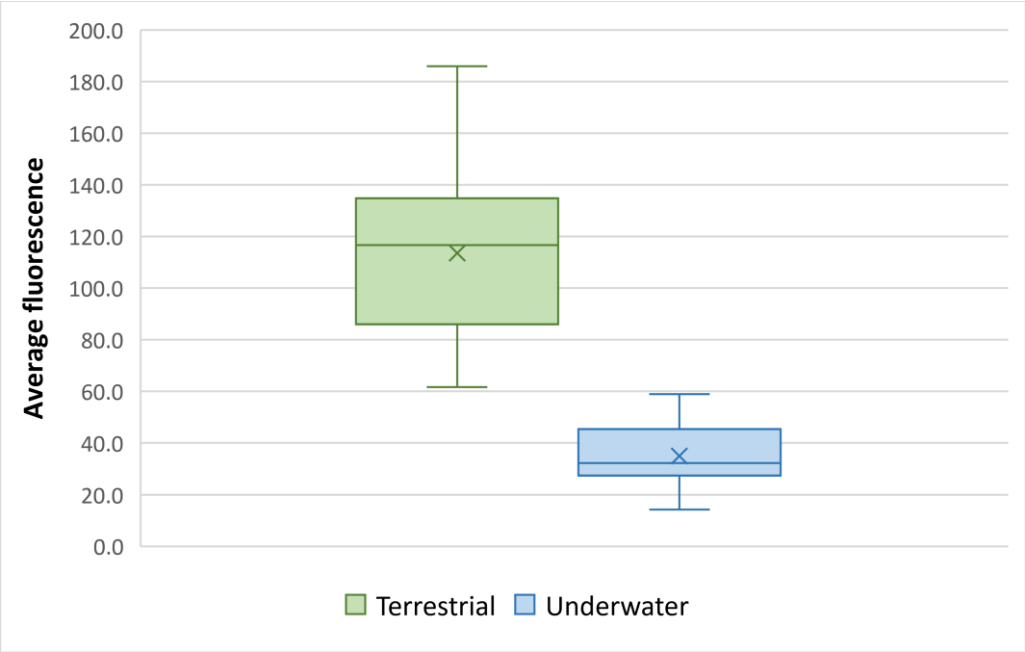

Figure 116: Comparison of average terrestrial and underwater fluorescence values of porcine ribs photographed with the Hammerhead and the orange filter at 1/3s exposure time.

In addition to the general results reported in section 24.1.1, the Hammerhead fluorescence data demonstrated a declining trend in fluorescence values across the exposure times, with the highest levels of fluorescence captured using the slowest exposure time of 0.6s, and the fastest 1/3s exposure time producing the lowest fluorescence results. This declining trend was mirrored in both aquatic and terrestrial contexts and as mentioned previously, this reduction in documented fluorescence is in keeping with expectations as the faster shutter speed would lead to shortened exposure of the sensor, and therefore shortened interval for the fluorescence to be detected. A 60–70% decrease in fluorescence level was noted when comparing the aquatic fluorescence values to the terrestrial results, a disparity that appeared to increase as the exposure time was shortened. However, the difference in the actual fluorescence values was seen to be smaller at the faster exposure times, with a difference of 95.1 seen between aquatic and terrestrial fluorescence exhibited when using the 0.6s exposure time, in comparison to 77 at 1/3s.

Standard deviation in the fluorescence values was overall much lower in the tap water context than in air, but proportionately it could be more impactful, as the fluorescence figures were so low, this equated to a deviation of almost 33% either side of the mean. For example, the aquatic average fluorescence value recorded using the 1/3s exposure time was 34.2, but with a standard deviation of 11.1, this creates an overall range of 23.1 to 45.3, indicating widespread fluorescence values and therefore greater inconsistency compared to the terrestrial fluorescence. However, comparatively, the Crime-lite 2 aquatic data produced an overall much higher rate of deviation, with an average value of 32.6 compared to the Hammerhead's 13.7 (including all exposure times) and where SD=27.8 for the 59.4 average fluorescence recorded for the 1/3s exposure. This figure equates to an almost 50% deviation around the mean, demonstrating extensive spread in fluorescence values and indicative of substantial variation. Despite this, both datasets experienced a decrease in standard deviation at faster exposure times, declining by approximately 25.7% and 35.5% respectively, when comparing the standard deviation of aquatic fluorescence values at 0.6s exposure times, to 1/3s exposure times, with the Hammerhead ALS results exhibiting the greatest reduction.

The extent of standard deviation was more constant in the terrestrial fluorescence values, ranging from 30.1 to 33.5 across the exposure times, with 0.4s producing the highest result of 33.5. These findings are similar to those reported in the Crime-lite 2 data, although the distribution of values in the terrestrial context for the Crime-lite 2 using the orange filter, was overall lower at 25.7 (when taking into account all exposure times), whereas the average standard deviation for the same context using the Hammerhead ALS was 31.9. However, when examining the deviation of the aquatic fluorescence levels, this relationship is reversed, with the Hammerhead ALS results producing an average standard deviation of 13.7 (when considering all exposure times) and the Crime-lite 2 presenting over double that figure at 32.6.

Overall, the Crime-lite 2 is more powerful compared to the Hammerhead, and as mentioned previously, emits a narrow beam of light due to a single LED, in comparison to the two LEDs used by the Hammerhead, which produces a wider, more diffuse incident beam. Consequently, some of the terrestrial inconsistencies and higher degree of deviation in fluorescence values observed in the terrestrial Hammerhead data, may be the result of slight variation in ALS coverage, and generally weaker emissions. As discussed in chapter 7.0, once a wavelength of light interacts with the examined material and is consequently converted to fluorescent emissions, the energy level of the reflected light is much lower than that of the original incident beam, and thus produces a shift in frequency and colour. It is therefore reasonable to suggest that light emitted from the Hammerhead would begin with comparatively lower energy levels and light from the Crime-lite 2, therefore perhaps some of the light was simply consumed during excitation of the bone rather, than being converted. If this scenario were true, similar results would be expected in the underwater context, or the effect potentially amplified, as light travelling through a denser medium will result in increased energy consumption [212]. This theory is supported by the fluorescence results, as a greater reduction in average fluorescence was noted in the Hammerhead results compared to the Crime-lite 2 dataset.

However, the standard deviation was also lower in the Hammerhead aquatic results, compared to the Crime-lite 2. This reduction in deviation could infer that the lower energy levels and more specific 450 nm were more conducive for imaging submerged

bone fluorescence. The high power and broader wavelength of the Crime-lite 2 potentially led to scattering and refraction of light, which could not be filtered out as successfully by the orange filter (as it was in the Hammerhead stimulated examples) as they may be, leading to a greater degree of variation in fluorescence results. Further evidence of this can be seen in the submerged images produced with the Crime-lite 2 and the yellow filter (fig. 108) where discolouration is noted at the perimeters of the bone, whereas these surplus wavelengths were either not present or filtered out in the orange filter images.

As the same porcine bones were examined with both ALS devices, the same limitations regarding bone density and water movement previously highlighted in the Crime-lite 2 dataset (chapter 21.1.1) should still apply. The fact that the faster exposure time of 1/3s led to the lowest level of variation in aquatic fluorescence results produced with the Hammerhead light, supports the interpretations reported for the Crime-lite 2; that faster exposure times potentially negate some the negative effects of the water movement. However, as there was a substantially lower level of fluorescence variation in the Hammerhead values compared to the Crime-lite 2, it could also be suggested that the model of ALS and consequently the wavelength was also influential.

Consequently, it could be argued that the specific 450 nm wavelength emitted by the Hammerhead light is better suited to the underwater context, although a more powerful light source using the same wavelength could help to boost overall fluorescence intensity. Although, the method development described in chapter 18.0, led to the Hammerhead light being positioned 4 cm closer to the porcine bones during photography, compared to the Crime-lite, it may be the case that this adaptation was not quite sufficient. Overall, this data iterates that considered selection of ALS wavelength and complementary coloured filter is integral for optimal bone fluorescence visualisation, and that there are undeniably differences between models of ALS, despite using similar wavelength

21.3.5 – HAMMERHEAD: BONE DIMENSIONS

The analysis into Hammerhead induced bone autofluorescence, photographed using the orange filter, in relation to bone dimensions, produced generally more consistent results compared to the Crime-lite 2 investigations, echoing some of the prominent statistical trends and provided additional insight into the role of bone metrics in autofluorescence. All graphical comparisons made between the bone dimensions: mass, length, width, and anterior-posterior, can be seen in appendix 42.

No relationship was found when comparing bone mass with autofluorescence, across any combination of context and exposure time. All R^2 values were approximately 0, with the highest being R^2= 0.0044, and the lowest being R^2= 0.0002. Although, overall positive correlations were recognised in the Crime-lite 2 discussions into mass and autofluorescence, the R^2 values were very low, and not significant, therefore these Hammerhead results are not too surprising. Similar R^2 values were discovered when analysing the anterior-posterior results compared with average bone fluorescence. All combinations of context and exposure time produced R^2 values close to 0, thus discounting any relationship, which supports with the findings from the Crime-lite 2 analysis (charts available in appendix 42).

Comparisons made between the autofluorescence results detected with an orange filter at each exposure time (0.6, 0.4, 1/3s), and each deposition context, compared to porcine bone width also produced similar results to the Crime-lite 2 dataset. Across all experimental configurations a positive correlation between bone width and autofluorescence was seen, as shown in figures 117-122 below. The highest R^2 value of 0.1142 was observed in the underwater fluorescence results photographed at 0.4s and the lowest R^2 figure of 0.0215 was identified in the terrestrial fluorescence results recorded at 0.6s exposure time. Although none of the figures were significant, the fact that all correlations were positive, and therefore echoed the Crime-lite 2 findings, provides credence to the theory that in the context of this PhD study, bone width was influential in determining the level of autofluorescence exhibited by porcine bone, stimulated by blue light. In addition to this, the higher levels of confidence for each exposure time were noted in the underwater fluorescence data. As previously discussed in section 24.1.3 above, the most consistent fluorescence values in the Hammerhead

dataset, identified by the lowest deviation from the mean, were the underwater fluorescence results.

In contrast, negative correlations between the length of porcine bone and the average fluorescence level, produced by the Hammerhead, were observed uniformly across all experimental configurations within this dataset (figures 123-128). This relationship was not observed in the Crime-lite 2 data, as the comparative investigations into bone length and autofluorescence produced a blend of negative, positive, and no correlations. There was a slight tendency towards positive correlations noted in the tap water context of the Crime-lite 2 comparisons with bone length, but all R^2 values were close to 0 (appendix 41). Similarly, in these comparisons using the Hammerhead fluorescence data none of the reported correlations are significant, as the highest R^2 value was 0.0605 observed in the underwater fluorescence values, at 1/3s exposure time and the least confident relationship was seen in the underwater data, but at 0.4s exposure time. The only other discernible pattern is that the terrestrial correlations were slightly more consistent, as all three exposure times demonstrated an R^2 value of approximately 0.04, although this does not add anything new to the current discourse regarding bone dimensions and autofluorescence.

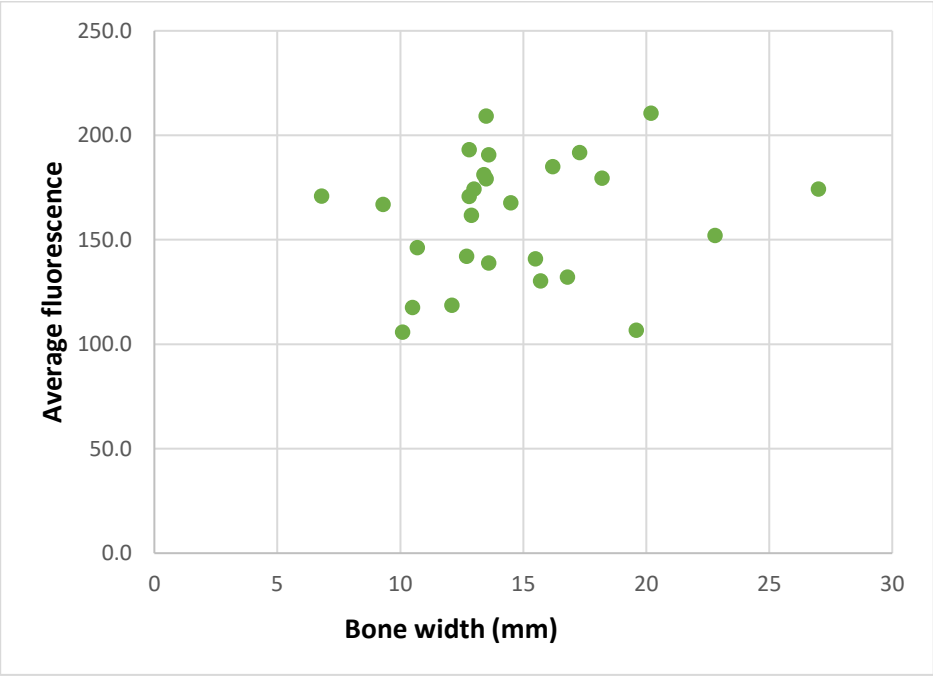

Figure 117: Comparison between bone width and terrestrial fluorescence taken with the orange filter, 0.6s

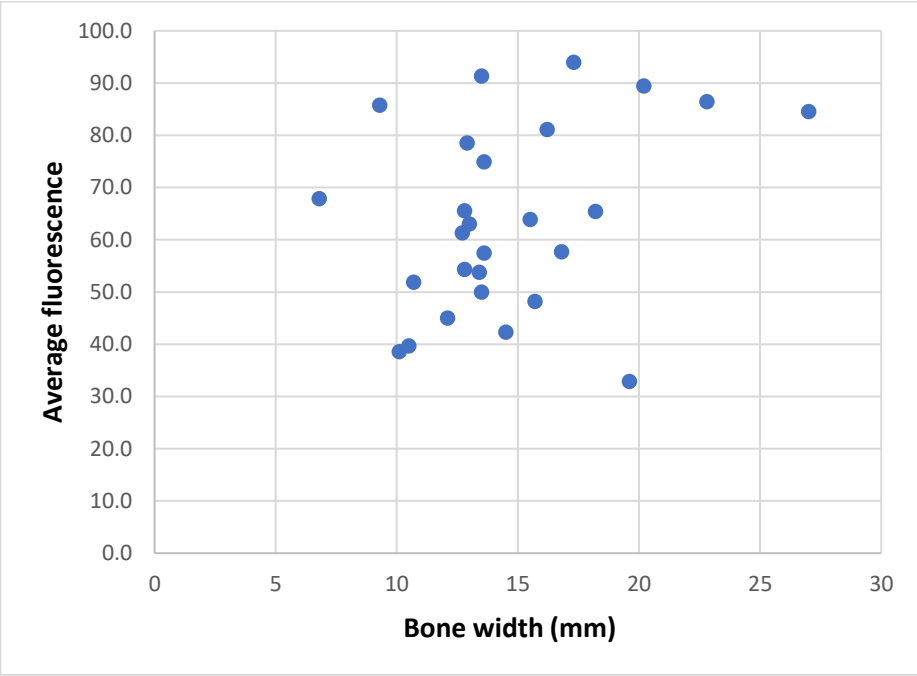

Figure 118: Comparison between bone width and underwater fluorescence taken with the orange filter, 0.6s

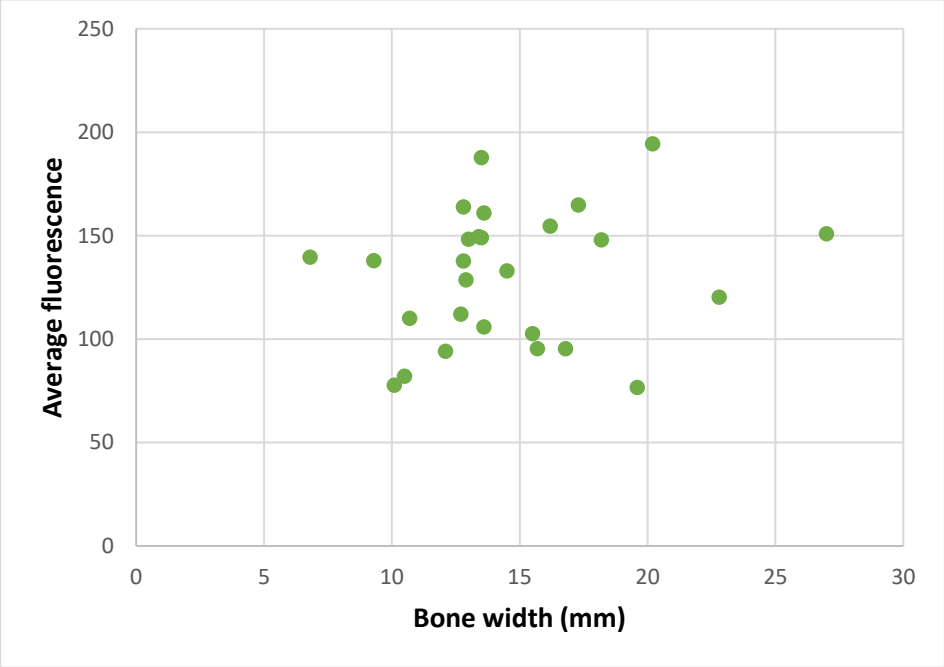

Figure 119: Comparison between bone width and terrestrial fluorescence taken with the orange filter, 0.4s

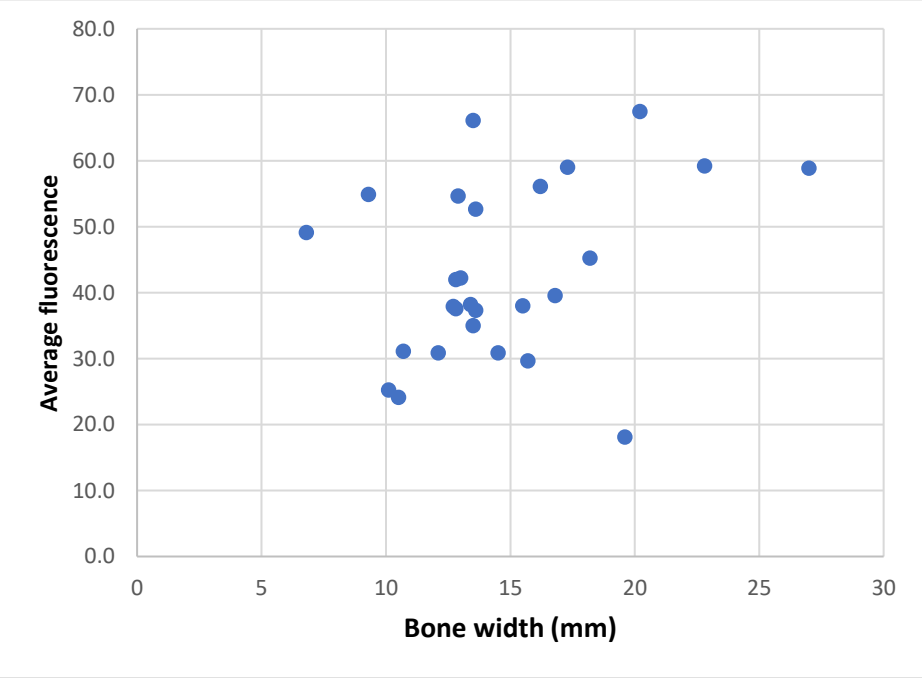

Figure 120: Comparison between bone width and underwater fluorescence taken with the orange filter, 0.4s

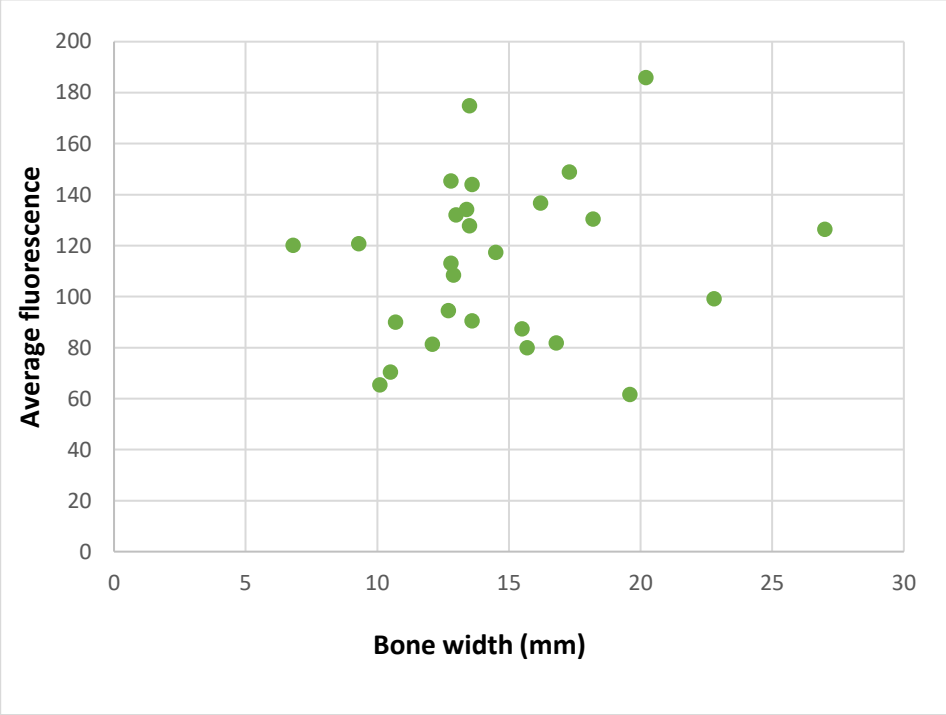

Figure 121: Comparison between bone width and terrestrial fluorescence taken with the orange filter, 1/3s

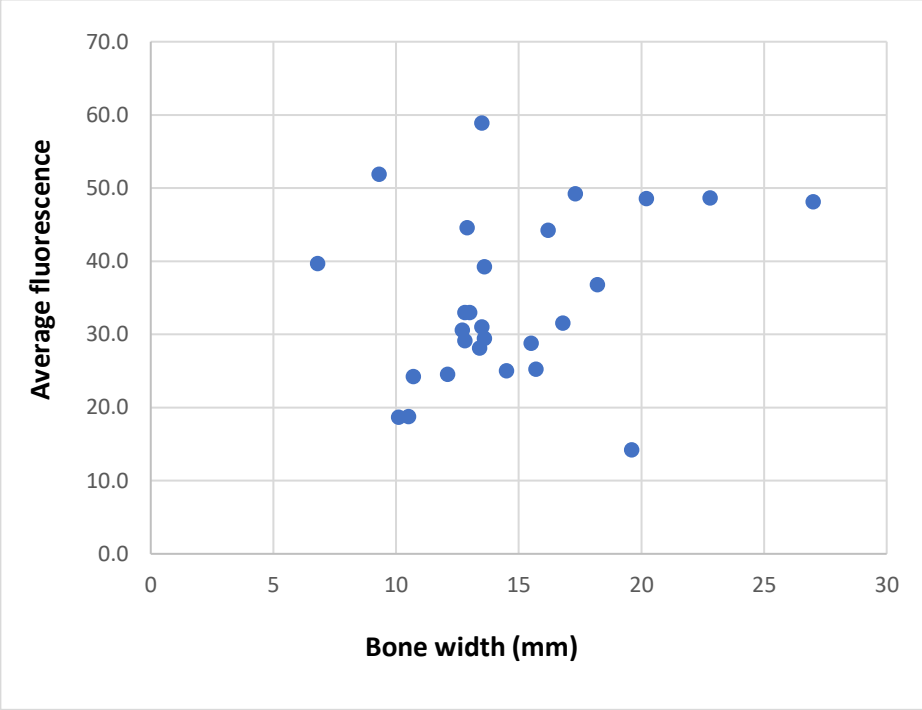

Figure 122: Comparison between bone width and underwater fluorescence taken with the orange filter, 1/3s

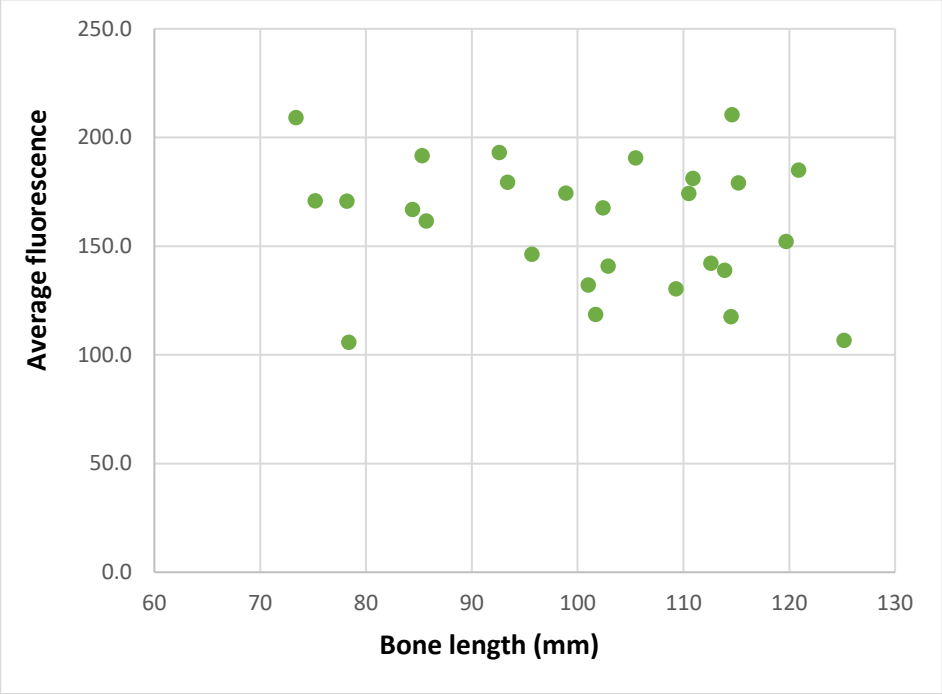

Figure 123: Comparison between bone length and terrestrial fluorescence taken with the orange filter, 0.6s

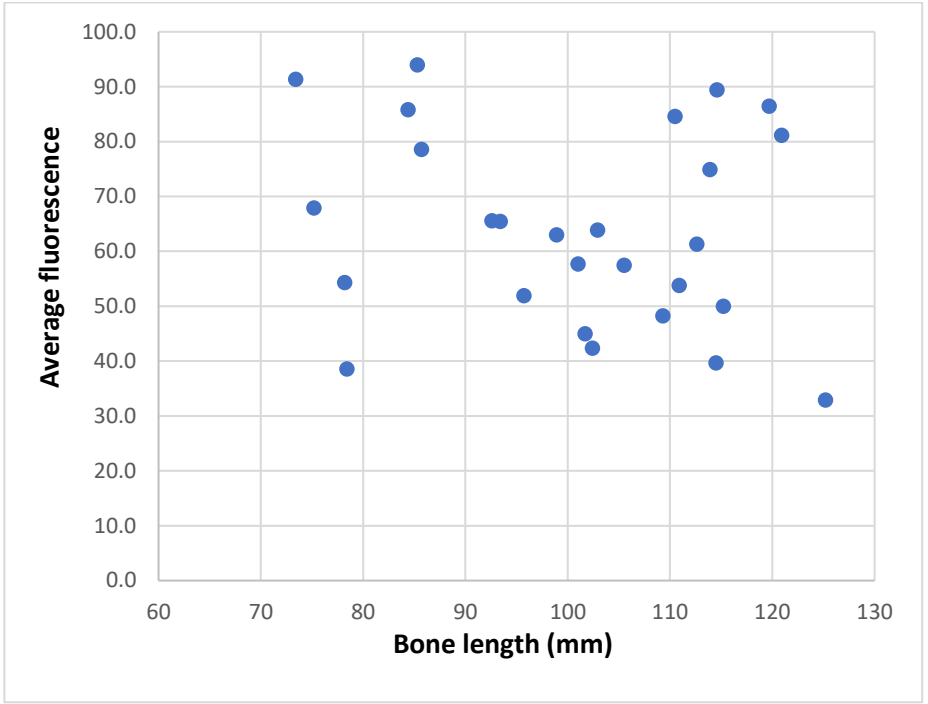

Figure 124: Comparison between bone length and underwater fluorescence taken with the orange filter, 0.6s

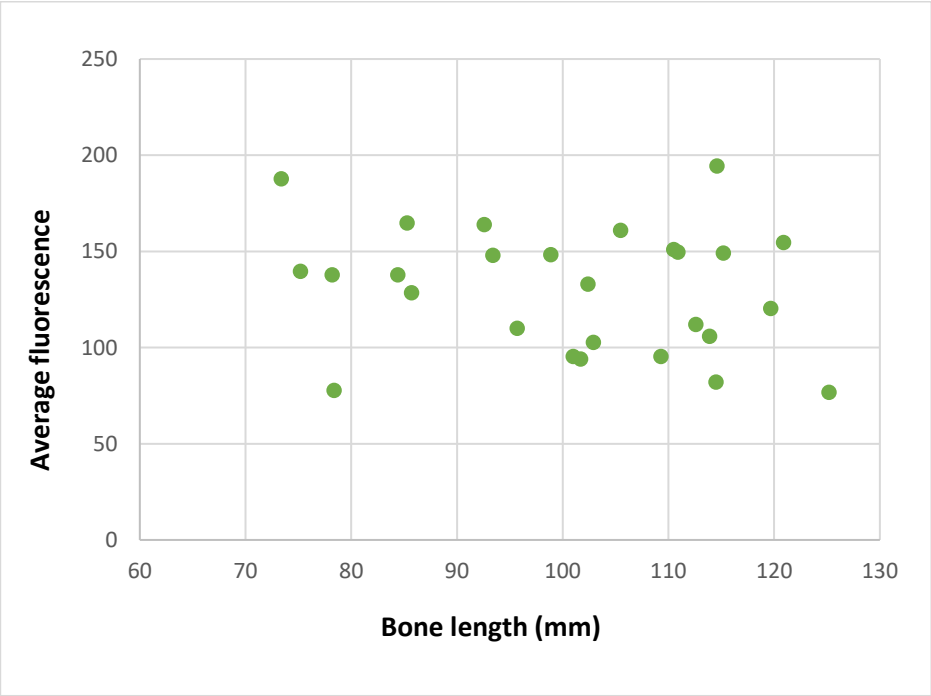

Figure 125: Comparison between bone length and terrestrial fluorescence taken with the orange filter, 0.4s

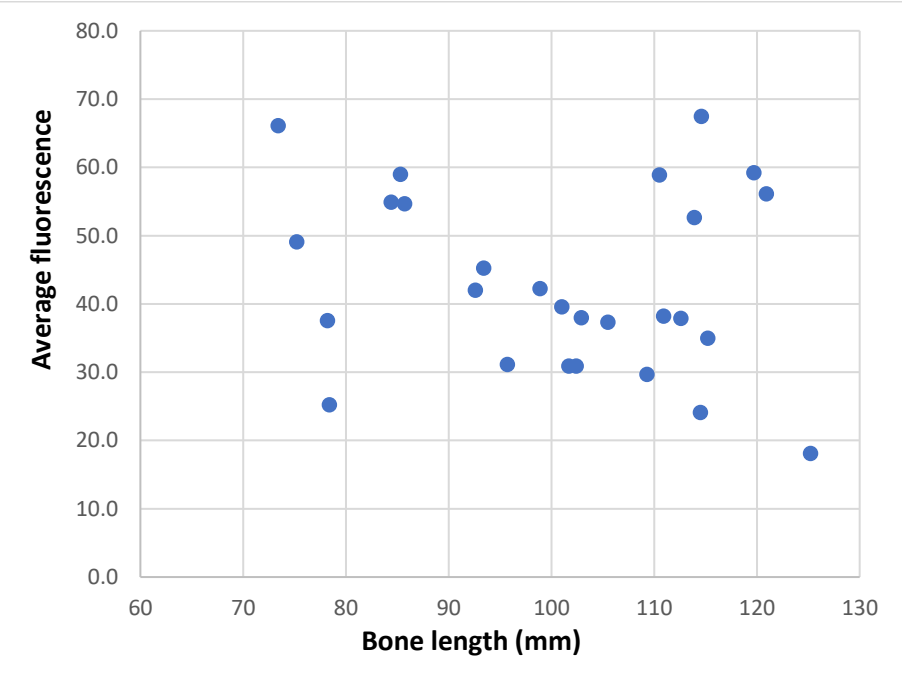

Figure 126: Comparison between bone length and underwater fluorescence taken with the orange filter, 0.4s

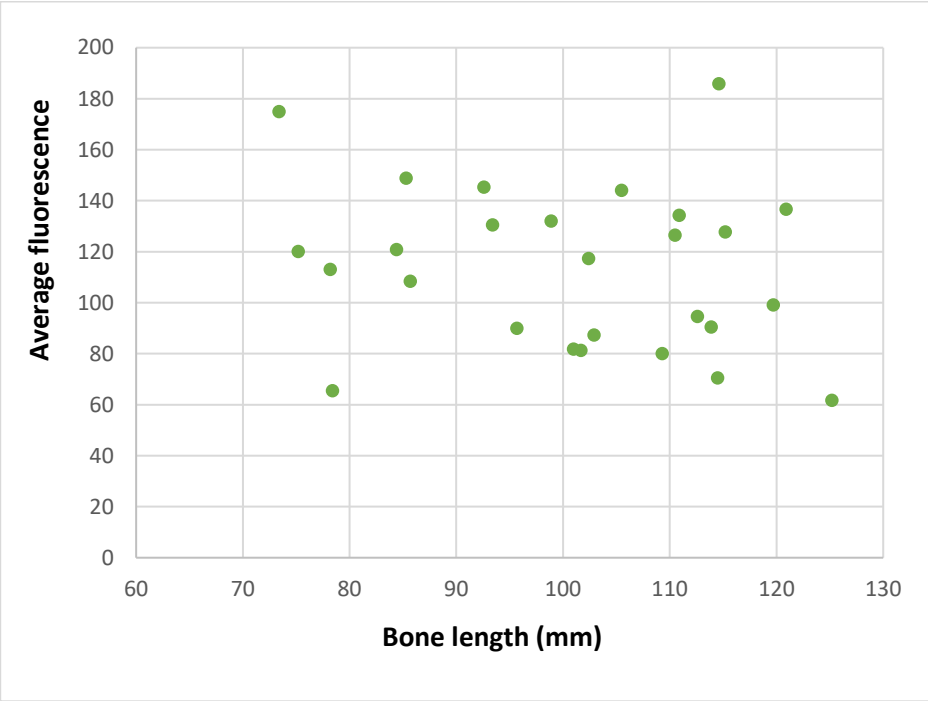

Figure 127: Comparison between bone length and terrestrial fluorescence taken with the orange filter, 1/3s

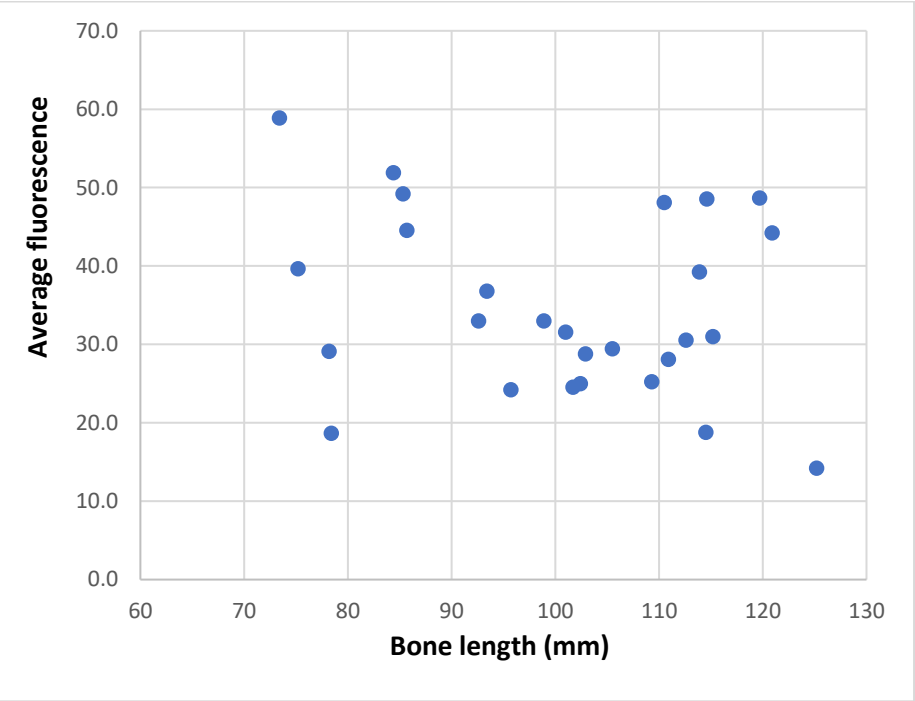

Figure 128: Comparison between bone length and underwater fluorescence taken with the orange filter, 1/3s

21.4 – COLLAGEN ANALYSIS

The other major analysis carried out during this research question was quantification of collagen content of the thirty porcine bones. As outlined in chapter 20.0, collagen quantification was conducted using TG analysis. All thermograms produced for the thirty porcine ribs can be found in appendix 43, but table 32 below summarises the collagen results.

Table 32: Calculated collagen content for the thirty porcine bones used in the terrestrial compared to underwater fluorescence dataset.

Rib	Total organic content (mg)	Calculated collagen (90%) (mg)
1	0.9030	0.81
2	0.6897	0.62
3	0.6920	0.62
4	0.6745	0.61
5	0.6896	0.62
6	0.6775	0.61
7	0.7133	0.64
8	0.6958	0.63
9	0.5915	0.53
10	0.6774	0.61
11	0.6667	0.60
12	0.7590	0.68
13	0.5946	0.54
14	0.6098	0.55
15	0.6272	0.56
16	0.5068	0.46
17	0.5564	0.50
18	0.5317	0.48
19	0.5967	0.54
20	0.4858	0.44
21	0.5761	0.52
22	0.6386	0.57

23	0.6227	0.56
24	0.5485	0.49
25	0.4375	0.39
26	0.5606	0.50
27	0.5500	0.50
28	0.5285	0.48
29	0.5445	0.49
30	0.5131	0.46
Average	0.62	0.55
Max	0.90	0.81
Min	0.44	0.39
Range	0.47	0.42
S.D.	0.09	0.08

Across the thirty ribs the lowest level of calculated collagen was 0.39 mg collected from rib 25, and the highest was rib 1 with 0.81 mg. This produced a range of 0.42 and a standard deviation of 0.08. Descriptive statistical analysis comparing the calculated collagen content of all thirty rib bones to their measured mass demonstrated a positive correlation of $R^2 = 0.398$. Although this result was not significant, it somewhat infers that the volume of bone collagen could be higher in heavier bones.

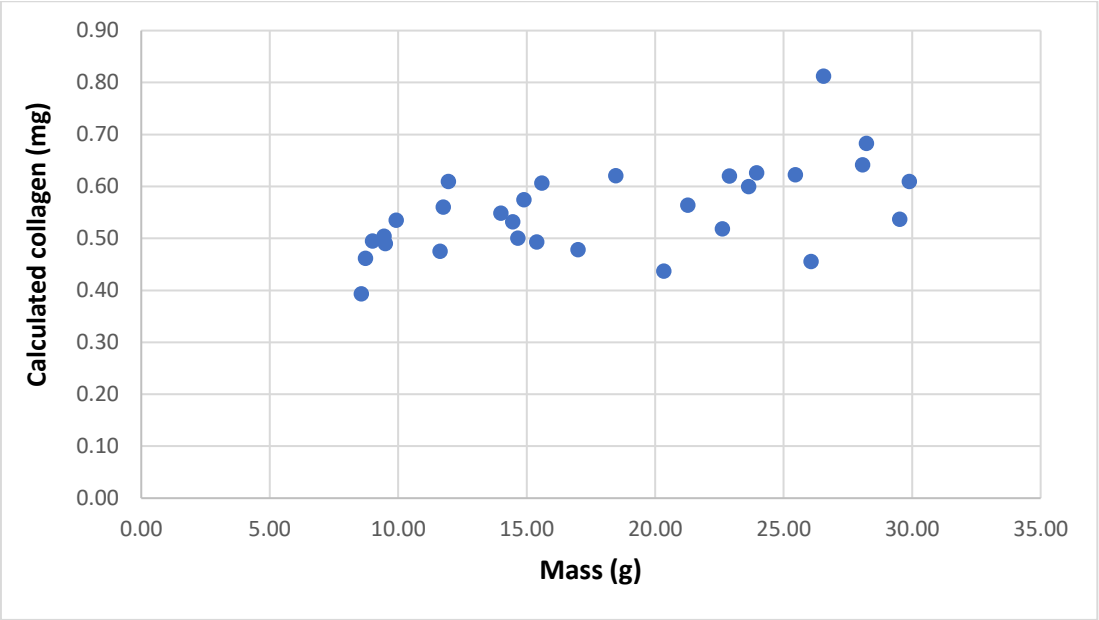

Figure 129: Comparison between the calculated collagen content and mass of the porcine bones (Sus scrofa domesticus)

When comparing the calculated collagen content with the average fluorescence values obtained with the Crime-lite 2 and the Hammerhead ALS, along with the respective filter and deposition combinations, no significant relationships were detected, as shown in appendices 44 and 45. Overall, the Crime-lite 2 terrestrial dataset demonstrated R^2 values of approximately 0 for both filters across all exposure times, therefore no discernible relationship was seen. The aquatic comparisons generated very slight positive correlations, potentially inferring that higher fluorescence intensity was produced in bones with higher collagen volume. However, the R^2 values were approximately 0.07 for the orange filter results and approximately 0.1 for the yellow filter results, consequently indicating no relationship.

Possible explanations could be that as the porcine bones were only manually defleshed, therefore some minor residual tissue may be influencing how the ALS wavelengths are interacting with the bone and subsequently negatively influencing the level of observable fluorescence by blocking ALS stimulation. In addition to this, as the potentially erroneous data was removed during statistical analysis, the overall sample size was reduced. Consequently, a larger sample size would have allowed for more robust calculations.

21.5 – STATISTICAL ANALYSIS

21.5.1 – FLUORESCENCE

Statistical analysis was conducted using IBM™ SPSS Statistics v23 to see if any of the potential relationships noted in sections 24.1.2-3, were statistically significant. Firstly, Histograms were performed for all data groups to ascertain if the data is normally distributed (appendix 46). All the data collected in the terrestrial environment using the orange filter was normally distributed therefore t-test analyses could be performed, figure 130 below:

Paired Samples Correlations

		N	Correlation	Sig.
Pair 1	T.Orange0.6 & T. Orange0.4	29	.976	.000
Pair 2	T.Orange0.6 & T. Orange1.3	29	.970	.000
Pair 3	T.Orange0.4 & T. Orange1.3	29	.967	.000

Paired Samples Test

		Paired Differences					t	df	Sig. (2-tailed)
		Mean	Std. Deviation	Std. Error Mean	95% Confidence Interval of the Difference Lower	Upper			
Pair 1	T.Orange0.6 - T.Orange0.4	19.53103	5.84540	1.08546	17.30757	21.75450	17.993	28	.000
Pair 2	T.Orange0.6 - T.Orange1.3	32.12414	8.69083	1.61385	28.81832	35.42995	19.905	28	.000
Pair 3	T.Orange0.4 - T.Orange1.3	12.59310	8.07779	1.50001	9.52048	15.66573	8.395	28	.000

Figure 130: T-test comparisons of the average terrestrial fluorescence results of the porcine bones (Sus scrofa domesticus) photographed using the Crime-lite 2 with the orange filter at 0.6s, 0.4s and 1/3s

As expected, strong statistically significant relationships were produced when comparing each exposure time (p= .000), indicating that it is highly unlikely that the relationships noted in the discussion above occurred by chance. Further concluding that the level of fluorescence exhibited in a terrestrial environment is dependant of effective use of exposure time. Histograms examining the data distribution for the yellow filter in the terrestrial context and data for both filters in the tap water environment display abnormal distributions (appendix 46a), therefore non-parametric tests of related samples; Wilcoxon signed rank tests, were performed. Results of the comparisons between exposure times for terrestrial photographs taken with the yellow filter presented strong statistically significant relationships, p = .000, with recommended rejection of the null hypothesis as displayed in figures 131 to 132.

Hypothesis Test Summary

	Null Hypothesis	Test	Sig.	Decision
1	The median of differences between T.Yellow0.6 and T.Yellow0.4 equals 0.	Related-Samples Wilcoxon Signed Rank Test	.000	Reject the null hypothesis.

Asymptotic significances are displayed. The significance level is .05.

Figure 131: Result of Wilcoxon signed rank test comparing the average fluorescence values of the terrestrial photographs taken at 0.6s and 0.4s exposure times using the yellow filter

Hypothesis Test Summary

	Null Hypothesis	Test	Sig.	Decision
1	The median of differences between T.Yellow0.6 and T.Yellow1.3 equals 0.	Related-Samples Wilcoxon Signed Rank Test	.000	Reject the null hypothesis.

Asymptotic significances are displayed. The significance level is .05.

Figure 132: Result of Wilcoxon signed rank test comparing the average fluorescence values of the terrestrial photographs taken at 0.6s and 1/3s exposure times using the yellow filter.

Hypothesis Test Summary

	Null Hypothesis	Test	Sig.	Decision
1	The median of differences between T.Yellow0.4 and T.Yellow1.3 equals 0.	Related-Samples Wilcoxon Signed Rank Test	.000	Reject the null hypothesis.

Asymptotic significances are displayed. The significance level is .05.

Figure 133: Result of Wilcoxon signed rank test comparing the average fluorescence values of the terrestrial photographs taken at 0.4s and 1/3s exposure times using the yellow filter

These findings are in keeping with the discussion outlined in section 6.0 and further demonstrates that exposure time directly contributes to the levels of fluorescence seen. Comparisons between the coloured filters also complimented these results, (figures 134-136), producing further strong statistically significant relationships; p= .000, and indicating that the coloured filter directly contributes to the level of fluorescence seen, across all examined exposure times. Consequently, this emphasises the requirement to select a suitable filter to optimise fluorescence production and documentation and

supports the selection of the orange filter as the recommended pairing with blue light (approx. 450 nm), rather than the yellow filter as commonly discussed in literature.

Hypothesis Test Summary

	Null Hypothesis	Test	Sig.	Decision
1	The median of differences between T.Orange0.6 and T.Yellow0.6 equals 0.	Related-Samples Wilcoxon Signed Rank Test	.000	Reject the null hypothesis.

Asymptotic significances are displayed. The significance level is .05.

Figure 134: Result of Wilcoxon signed rank test comparing the average fluorescence values of the terrestrial photographs taken using the orange and yellow filters at 0.6s exposure time.

Hypothesis Test Summary

	Null Hypothesis	Test	Sig.	Decision
1	The median of differences between T.Orange0.4 and T.Yellow0.4 equals 0.	Related-Samples Wilcoxon Signed Rank Test	.000	Reject the null hypothesis.

Asymptotic significances are displayed. The significance level is .05.

Figure 135: Result of Wilcoxon signed rank test comparing the average fluorescence values of the terrestrial photographs taken using the orange and yellow filters at 0.4s exposure time.

Hypothesis Test Summary

	Null Hypothesis	Test	Sig.	Decision
1	The median of differences between T.Orange1.3 and T.Yellow1.3 equals 0.	Related-Samples Wilcoxon Signed Rank Test	.000	Reject the null hypothesis.

Asymptotic significances are displayed. The significance level is .05.

Figure 136: Result of Wilcoxon signed rank test comparing the average fluorescence values of the terrestrial photographs taken using the orange and yellow filters at 1/3s exposure time.

Results of the Wilcoxon tests for the underwater exposure comparisons mirrored the terrestrial findings, all producing statistically significant relationships of p= .000, further supporting the determination that stimulation of bone autofluorescence levels relates to the selection of optimal exposure time, in keeping with the current hypothesis, figures 137-141 below.

Hypothesis Test Summary

	Null Hypothesis	Test	Sig.	Decision
1	The median of differences between U.Orange0.6 and U.Orange0.4 equals 0.	Related-Samples Wilcoxon Signed Rank Test	.000	Reject the null hypothesis.

Asymptotic significances are displayed. The significance level is .05.

Figure 137: Result of Wilcoxon signed rank test comparing the average fluorescence values of the underwater photographs taken using the orange filter at 0.6s and 0.4s exposure times

Hypothesis Test Summary

	Null Hypothesis	Test	Sig.	Decision
1	The median of differences between U.Orange0.6 and U.Orange1.3 equals 0.	Related-Samples Wilcoxon Signed Rank Test	.000	Reject the null hypothesis.

Asymptotic significances are displayed. The significance level is .05.

Figure 138: Result of Wilcoxon signed rank test comparing the average fluorescence values of the underwater photographs taken using the orange filter at 0.6s and 1/3s exposure times.

Hypothesis Test Summary

	Null Hypothesis	Test	Sig.	Decision
1	The median of differences between U.Orange0.4 and U.Orange1.3 equals 0.	Related-Samples Wilcoxon Signed Rank Test	.000	Reject the null hypothesis.

Asymptotic significances are displayed. The significance level is .05.

Figure 139: Result of Wilcoxon signed rank test comparing the average fluorescence values of the underwater photographs taken using the orange filter at 0.4s and 1/3s exposure times.

Hypothesis Test Summary

	Null Hypothesis	Test	Sig.	Decision
1	The median of differences between U.Yellow.0.6 and U.Yellow0.4 equals 0.	Related-Samples Wilcoxon Signed Rank Test	.000	Reject the null hypothesis.

Asymptotic significances are displayed. The significance level is .05.

Figure 140: Result of Wilcoxon signed rank test comparing the average fluorescence values of the underwater photographs taken using the yellow filter at 0.4s and 0.6s exposure times.

Hypothesis Test Summary

	Null Hypothesis	Test	Sig.	Decision
1	The median of differences between U.Yellow.0.6 and U.Yellow1.3 equals 0.	Related-Samples Wilcoxon Signed Rank Test	.000	Reject the null hypothesis.

Asymptotic significances are displayed. The significance level is .05.

Figure 141: Result of Wilcoxon signed rank test comparing the average fluorescence values of the underwater photographs taken using the yellow filter at 0.6s and 1/3s exposure times.

Hypothesis Test Summary

	Null Hypothesis	Test	Sig.	Decision
1	The median of differences between U.Yellow0.4 and U.Yellow1.3 equals 0.	Related-Samples Wilcoxon Signed Rank Test	.000	Reject the null hypothesis.

Asymptotic significances are displayed. The significance level is .05.

Figure 142: Result of Wilcoxon signed rank test comparing the average fluorescence values of the underwater photographs taken using the yellow filter at 0.4s and 1/3s exposure times

Finally, Wilcoxon signed rank tests comparing the underwater fluorescence values of the orange and yellow filters across the 3 exposure times produced similar results. As detailed in figures 143-145, statistically significant relationships were noted between the fluorescence levels of photographs taken with the orange and yellow filter at 0.6s and 0.4s exposure times, returning a significance value of p= .001, and 1/3s producing a significance of p= .000. Overall, this data shows that the correlations noted in previous section are highly unlikely to be the result of chance, inferring that exposure time and coloured filter selection have a direct impact on the level of fluorescence seen in both terrestrial and underwater contexts.

Hypothesis Test Summary

	Null Hypothesis	Test	Sig.	Decision
1	The median of differences between U.Orange0.6 and U.Yellow.0.6 equals 0.	Related-Samples Wilcoxon Signed Rank Test	.001	Reject the null hypothesis.

Asymptotic significances are displayed. The significance level is .05.

Figure 143: Result of Wilcoxon signed rank test comparing the average fluorescence values of the underwater photographs taken using the yellow and orange filters at 0.6s exposure time.

Hypothesis Test Summary

	Null Hypothesis	Test	Sig.	Decision
1	The median of differences between U.Orange0.4 and U.Yellow0.4 equals 0.	Related-Samples Wilcoxon Signed Rank Test	.001	Reject the null hypothesis.

Asymptotic significances are displayed. The significance level is .05.

Figure 144: Result of Wilcoxon signed rank test comparing the average fluorescence values of the underwater photographs taken using the yellow and orange filters at 0.4s exposure time

Hypothesis Test Summary

	Null Hypothesis	Test	Sig.	Decision
1	The median of differences between U.Orange1.3 and U.Yellow1.3 equals 0.	Related-Samples Wilcoxon Signed Rank Test	.000	Reject the null hypothesis.

Asymptotic significances are displayed. The significance level is .05.

Figure 145: Result of Wilcoxon signed rank test comparing the average fluorescence values of the underwater photographs taken using the yellow and orange filters at 1/3s exposure time

21.5.2 – BONE DIMENSIONS

21.5.2a- HAMMERHEAD ALS

Histograms were produced to assess the normality of the distribution of data for each bone measurement. In the Hammerhead terrestrial fluorescence dataset, all data was observed to be abnormally distributed for all categories of bone measurement, therefore non-parametric Wilcoxon signed rank tests were performed to test the relationship between each bone dimension and the quantified terrestrial fluorescence

(all exposure times) produced using the Hammerhead ALS in conjunction with the orange filter. All histograms for these analyses can be seen in appendix 46b.

Strong statistically significant relationships of p= .000, were observed between all bone dimensions (figures 146-149) and the terrestrial fluorescence comparisons, indicating that the observed fluorescence results produced during the terrestrial Hammerhead analysis were directly related to the dimensions of the rib bone being examined, and that the null hypothesis should be rejected, in keeping with expectations.

Hypothesis Test Summary

	Null Hypothesis	Test	Sig.	Decision
1	The median of differences between T.Fluor and Mass equals 0.	Related-Samples Wilcoxon Signed Rank Test	.000	Reject the null hypothesis.

Asymptotic significances are displayed. The significance level is .05.

Figure 146: Result of Wilcoxon ranked sign test comparing the average terrestrial fluorescence values produced using the Hammerhead light source, and bone mass.

Hypothesis Test Summary

	Null Hypothesis	Test	Sig.	Decision
1	The median of differences between T.Fluor and Width equals 0.	Related-Samples Wilcoxon Signed Rank Test	.000	Reject the null hypothesis.

Asymptotic significances are displayed. The significance level is .05.

Figure 147: Result of Wilcoxon signed rank test comparing the average terrestrial fluorescence values produced using the Hammerhead light source, and bone width.

Hypothesis Test Summary

	Null Hypothesis	Test	Sig.	Decision
1	The median of differences between T.Fluor and AP equals 0.	Related-Samples Wilcoxon Signed Rank Test	.000	Reject the null hypothesis.

Asymptotic significances are displayed. The significance level is .05.

Figure 148: Result of Wilcoxon signed rank test comparing the average terrestrial fluorescence values produced using the Hammerhead light source, and bone anterior-posterior.

Hypothesis Test Summary

	Null Hypothesis	Test	Sig.	Decision
1	The median of differences between T.Fluor and Length equals 0.	Related-Samples Wilcoxon Signed Rank Test	.000	Reject the null hypothesis.

Asymptotic significances are displayed. The significance level is .05.

Figure 149: Result of Wilcoxon signed rank test comparing the average terrestrial fluorescence values produced using the Hammerhead light source, and bone length.

Histograms were also produced to assess the normality of the data for each bone measurement in relation to the tap water fluorescence values produced using the Hammerhead ALS and orange filter, and the measured bone dimensions. All data except for the underwater fluorescence values was seen to abnormally distributed (appendix 46b). Consequently, non-parametric Wilcoxon signed rank tests were also performed for this data, as the majority of the data present an abnormal distribution.

In keeping with the results observed in the terrestrial Hammerhead dataset, strong statistically significant relationships of p= .000, were observed for all bone dimensions and the aquatic fluorescence comparisons (figures 150-157), indicating that the observed fluorescence results produced were directly related to the dimensions of the individual rib bones, and consequently supports the results of the terrestrial analysis.

21.5.2b- CRIME-LITE 2 COMPARISONS

As the same group of ribs was analysed using both light sources, the histograms were not repeated for the bone dimensions data, but histograms for the aquatic and terrestrial fluorescence levels (both filters, and all ROIs) for the Crime-lite 2 were completed, and can be seen in appendix 46. As with the Hammerhead datasets, the fluorescence and data generated abnormal distributions, therefore additional non-parametric Wilcoxon signed rank tests for related samples were carried out, to analyse the potential relationship between the Crime-lite 2 fluorescence values and bone dimensions.

Complimentarily to the results produced by the Hammerhead data, strong statistically significant relationships of p= .000, were observed across all bone dimensions and the ALS fluorescence results, observed in both terrestrial and aquatic contexts, produced using the terrestrial Crime-lite 2 (figures 150-157). These results provide further support for the hypothesis that the observed bone fluorescence intensity was a direct result of the dimensions of the individual rib samples, rather than due to chance. With all that in mind, the null hypothesis; that there is no statistically significant relationship between bone fluorescence and bone dimensions was rejected.

Hypothesis Test Summary

	Null Hypothesis	Test	Sig.	Decision
1	The median of differences between T.Flour and Mass equals 0.	Related-Samples Wilcoxon Signed Rank Test	.000	Reject the null hypothesis.

Asymptotic significances are displayed. The significance level is .05.

Figure 150: Result of Wilcoxon signed rank test comparing the average terrestrial fluorescence values produced using the Crime-lite 2, and bone mass.

Hypothesis Test Summary

	Null Hypothesis	Test	Sig.	Decision
1	The median of differences between T.Flour and Width equals 0.	Related-Samples Wilcoxon Signed Rank Test	.000	Reject the null hypothesis.

Asymptotic significances are displayed. The significance level is .05.

Figure 151: Result of Wilcoxon signed rank test comparing the average terrestrial fluorescence values produced using the Crime-lite 2, and bone width.

Hypothesis Test Summary

	Null Hypothesis	Test	Sig.	Decision
1	The median of differences between T.Flour and AP equals 0.	Related-Samples Wilcoxon Signed Rank Test	.000	Reject the null hypothesis.

Asymptotic significances are displayed. The significance level is .05.

Figure 152: Result of Wilcoxon signed rank test comparing the average terrestrial fluorescence values produced using the Crime-lite 2, and bone anterior-posterior

Hypothesis Test Summary

	Null Hypothesis	Test	Sig.	Decision
1	The median of differences between T.Flour and Length equals 0.	Related-Samples Wilcoxon Signed Rank Test	.000	Reject the null hypothesis.

Asymptotic significances are displayed. The significance level is .05.

Figure 153: Result of Wilcoxon signed rank test comparing the average terrestrial fluorescence values produced using the Crime-lite 2, and bone length.

Hypothesis Test Summary

	Null Hypothesis	Test	Sig.	Decision
1	The median of differences between U.Flour and Mass equals 0.	Related-Samples Wilcoxon Signed Rank Test	.000	Reject the null hypothesis.

Asymptotic significances are displayed. The significance level is .05.

Figure 154: Result of Wilcoxon signed rank test comparing the average underwater fluorescence values produced using the Crime-lite 2, and bone mass.

Hypothesis Test Summary

	Null Hypothesis	Test	Sig.	Decision
1	The median of differences between U.Flour and Width equals 0.	Related-Samples Wilcoxon Signed Rank Test	.000	Reject the null hypothesis.

Asymptotic significances are displayed. The significance level is .05.

Figure 155: Result of Wilcoxon signed rank test comparing the average underwater fluorescence values produced using the Crime-lite 2, and bone width.

Hypothesis Test Summary

	Null Hypothesis	Test	Sig.	Decision
1	The median of differences between AP and U.Flour equals 0.	Related-Samples Wilcoxon Signed Rank Test	.000	Reject the null hypothesis.

Asymptotic significances are displayed. The significance level is .05.

Figure 156: Result of Wilcoxon signed rank test comparing the average underwater fluorescence values produced using the Crime-lite 2, and bone anterior-posterior.

Hypothesis Test Summary

	Null Hypothesis	Test	Sig.	Decision
1	The median of differences between U.Flour and Length equals 0.	Related-Samples Wilcoxon Signed Rank Test	.000	Reject the null hypothesis.

Asymptotic significances are displayed. The significance level is .05.

Figure 157: Result of Wilcoxon signed rank test comparing the average underwater fluorescence values produced using the Crime-lite 2, and bone length.

21.5.3 – COLLAGEN

21.5.3a- CRIME-LITE 2 COMPARISONS

The quantified collagen data for the porcine ribs was also compared to the bone dimensions. Histogram analysis (appendix 46c) also identified an abnormal distribution in the collagen values, in keeping with the other bone dimension data, leading to further non-parametric Wilcoxon signed rank tests being completed. Strong statistically significant relationships of p= .000, were observed across all bone dimensions and the calculated collagen results (figures 158-161 below).

Hypothesis Test Summary

	Null Hypothesis	Test	Sig.	Decision
1	The median of differences between Collagen and Mass equals 0.	Related-Samples Wilcoxon Signed Rank Test	.000	Reject the null hypothesis.

Asymptotic significances are displayed. The significance level is .05.

Figure 158: Result of Wilcoxon signed rank test comparing the calculated bone collagen content and bone mass.

Hypothesis Test Summary

	Null Hypothesis	Test	Sig.	Decision
1	The median of differences between Width and Collagen equals 0.	Related-Samples Wilcoxon Signed Rank Test	.000	Reject the null hypothesis.

Asymptotic significances are displayed. The significance level is .05.

Figure 159: Result of Wilcoxon signed rank test comparing the calculated bone collagen content and bone width.

Hypothesis Test Summary

	Null Hypothesis	Test	Sig.	Decision
1	The median of differences between Collagen and AP equals 0.	Related-Samples Wilcoxon Signed Rank Test	.000	Reject the null hypothesis.

Asymptotic significances are displayed. The significance level is .05.

Figure 160: Result of Wilcoxon signed rank test comparing the calculated bone collagen content and bone anterior-posterior.

Hypothesis Test Summary

	Null Hypothesis	Test	Sig.	Decision
1	The median of differences between Collagen and Length equals 0.	Related-Samples Wilcoxon Signed Rank Test	.000	Reject the null hypothesis.

Asymptotic significances are displayed. The significance level is .05.

Figure 161: Result of Wilcoxon signed rank test comparing the calculated bone collagen content and bone length.

Due to the poor results noted in the collagen-fluorescence comparisons, statistical analysis was not completed for the collagen and average fluorescence values and instead deferred to section B, research question 2, which focused specifically on investigating the osteo-fluorescence relationship, by removing some of the possible limitations highlighted during this experiment. This included using a much bigger sample size of 54 porcine ribs, which were prepared using the hot water maceration (80°C), developed during the pilot study, protocol to eliminate all residual tissue.

21.6- CONCLUSIONS

In conclusion, the analyses conducted in this research question provided valuable insight into the impact of exposure time and coloured filter combination, as well as deposition environment, on observed bone fluorescence. Strong statistically significant relationships support the fact that both the filter and exposure time are influential on the level of fluorescence seen, with the strongest fluorescence results observed in a terrestrial environment rather than the tap water scenario, which was characterised by a substantial decrease in all fluorescence values. The bullet points below summarise the key significant relationships:

- Comparison between fluorescence levels produced using 3 exposure times; 0.6s, 0.4s and 1/3s, with the orange and yellow filters in a terrestrial context: p= .000
- Comparison between fluorescence levels produced using 3 exposure times; 0.6s, 0.4s and 1/3s, with the orange and yellow filters in an underwater context: p= .000
- Comparison between terrestrial and underwater fluorescence levels produced using 3 exposure times; 0.6s, 0.4s and 1/3s and the orange filter context: p= .000
- Comparison between terrestrial and underwater fluorescence levels produced using 3 exposure times; 0.6s, 0.4s and 1/3s and the yellow filter context: p= .000
- Comparison between the underwater fluorescence levels produced using the orange and yellow filters at 3 exposure times; 0.6s, 0.4s and 1/3s: p= .001

More specifically, the most effective combination of coloured filter and exposure time for the examination of fresh porcine bone in terrestrial and underwater environments, when using the Crime-lite 2, was 0.6s coupled with the orange filter. Although the faster exposure time 1/3 produced more representative photographs of bone detail, it proved to be too fast to capture consistent fluorescence levels, leading to a larger spread in values as the exposure time was reduced. In a practical setting, the exposure time may need to be adjusted depending on whether the aim is documentation or photographs for fluorescence analysis. This effect was amplified in the aquatic context where the higher density medium, increased the spread in fluorescence values. However, deeper submersion of the photography equipment may help to stabilise photograph in future and potentially reduce this variable. Although this was not possible during this study, when used at an aquatic crime scene, as intended, full submersion of the light source and camera would be attainable.

Furthermore, the Crime-lite 2 is not a submersible device and was positioned just above the waterline during examination. If the light was under the water the fluorescence levels may have been higher and/or more consistent. The Crime-lite 2 is a considerably more powerful light source, and subsequently produced intense fluorescence results, particularly in the terrestrial context, although this could lead to overexposure at slower exposure times, particularly when using the yellow filter, which also led to a loss of detail

in the resulting photographs. Overall, the orange filter produced the most successful fluorescence results with both light sources in both deposition contexts.

These results also emphasised how bone dimensions, composition, and specimen provenance, may also impact observed fluorescence levels. This theory was demonstrated by strong statistically significant relationships (p= .000) when comparing bone length, width, mass, anterior-posterior, to calculated collagen content, and quantified fluorescence, for both ALS devices in aquatic and terrestrial contexts. These results are supported by the statistically significant correlation of R^2= 0.9, identified in the scatter plot comparing bone width and underwater fluorescence, obtained using the Hammerhead light, orange filter, and 0.4s exposure time. Consequently, these results enabled acceptance of hypotheses 1 and 2, and rejection of the respective null hypotheses as bone auto-fluorescence was able to be successfully produced in both terrestrial and aquatic environments, indicating that this technique could be used to search for bone at crime scenes.

1. Hypothesis: Alternative light sources can be used to identify bone in terrestrial and underwater environments using blue light (450-470 nm) when photographed with an orange camera filter

   Null hypothesis: Alternative light sources cannot be used to identify bone in terrestrial and underwater environments using blue light (450-470 nm) when photographed with an orange camera filter.

2. Hypothesis: Porcine bone (*Sus scrofa domesticus*) produces fluorescence in both terrestrial and underwater environments when exposed to blue light (450-470 nm) and viewed with a coloured filter.

   Null hypothesis: Porcine bone (*Sus scrofa domesticus*) does not produce fluorescence in terrestrial and underwater environments when exposed to blue light (450-470 nm) and viewed with a coloured filter.

22.0 - SECTION B, QUESTION 2:

THE COLLAGEN-FLUORESCENCE RELATIONSHIP

Is there a correlation between the amount of collagen content in bone and the level of bone fluorescence seen when photographed using blue light (approximately 450 nm) and orange and yellow filters? A statistical comparison of fluorescence and collagen levels of 54 macerated porcine ribs (Sus scrofa domesticus).

22.1- MATERIALS

Fifty-four porcine ribs (*Sus scrofa domesticus*) were prepared using hot water (80°C) maceration as outlined in chapter 20.0. Due to the large volume of bones, maceration was completed in twelve batches of 4-5 each batch. The ribs were then photographed in terrestrial and tap water contexts using Hammerhead ALS with the orange filter, in accordance with the core methodology outlined in chapter 20.0. The Hammerhead light source was selected as the primary device for the remaining questions, due to the successful, consistent fluorescence results noted in question 1, as well as the inconsistencies discovered in previous Crime-lite 2 results. Tap water used for the aquatic context was from the same source as question 1 and therefore possessed the same chemical characteristics. However, the water temperature during this experiment was recorded as 14.7°C, as measured with a digital thermometer. The average dimensions for the 54 porcine ribs analysed in this question are displayed in table 33 below, whereas the full table of all bone measurements for each rib is available in appendix 47.

Table 33: Average dimensions for the 54 porcine ribs (sus scrofa domesticus) used during section B, research question 2; examining the collagen-fluorescence relationship.

Mass (g)	Length (mm)	Width (mm)	A/P (mm)
11.8	82.0	15.1	9.4

22.2 – RESEARCH QUESTION SPECIFIC METHOD

22.2.1- PHOTOGRAPHY

Firstly, each specimen was photographed terrestrially under natural light with scale. Terrestrial and submerged photographs were then taken using the Hammerhead ALS, in conjunction with the orange filter, at three exposure times; 0.6, 0.4, 1/3s (slowest to fastest), using the camera settings outlined in section 20.0. Three photographs were taken at each exposure time. Submerged photographs were taken in 21 L of tap water, with the camera lens submerged 2 cm below the surface, as discussed in chapter 20.0

22.2.2 – COLLAGEN

Collagen scrapings were collected as per the core methodology (chapter 20.0).

22.2.3- FLUORESCENCE

Fluorescence quantification was conducted using the OFC software, as outlined in chapter 20.0.

22.2.4 – STATISTICAL ANALYSES

Statistical analysis was conducted using IBM™ SPSS Statistics v23 software and Microsoft Excel spreadsheets using a combination of paired-sample student t-tests, Wilcox signed rank tests, and scatter plot correlations to interpret potential relationships/correlations between the quantified collagen content and observed fluorescence values, in terrestrial and tap water contexts.

22.3 – RESULTS AND DISCUSSION

Table 34 below provides an overview of the average collagen, mass, and fluorescence data collected from the 54 porcine ribs, at each exposure time, and during both deposition contexts.

Table 34: average collagen, mass, and fluorescence data collected from the 54 porcine ribs (Sus scrofa domesticus), at each exposure time, and during both deposition contexts.

Stat.	Collagen (90%) (mg)	Mass (g)	Fluorescence					
			Terrestrial: Exposure time (s)			Underwater: Exposure time (s)		
			0.6	0.4	1/3	0.6	0.4	1/3
Min.	0.34	5.2	78.3	54.89	45	47.1	31	24.2
Max.	0.80	24	187.3	158.44	142.67	154	133.3	109.1
Range	0.46	18.8	109	103.56	97.67	106.9	102.3	84.9
Average	0.53	1.82	136.95	109.37	95.87	100.81	74.72	62.02
S.D.	0.08	4.7	25.72	24.35	23.18	27.28	25.64	22.44

Table 35 provides a summary of example fluorescence photographic results for ribs 1 and 16 taken across each exposure time and context. These images were selected as an example due to their different composition and structure, to therefore demonstrate the anatomical range in the porcine rib specimens and subsequent fluorescence. Example photographic results for all 54 ribs can be seen in appendices 48 and 49, but all fluorescence and OFC processed photographs are available in appendices 50 and 51. The quantified collagen data for each ROI for all fluorescence photographs is available in appendices 52 (terrestrial) and 53 (underwater), tabulated accordingly to exposure time. The thermograms for all 54 ribs are included in appendix 54 and the corresponding calculated collagen data has been compiled into appendix 55.

Table 35: Summarised terrestrial and submerged photographic fluorescence results for porcine ribs 1 and 16 (Sus scrofa domesticus), generated using the Hammerhead ALS coupled with the orange filter, across each exposure time (0.6s, 0.4s, 1/3s)

Rib no. and context	Natural	Exposure time (s)		
		0.6	0.4	1/3
Rib 1 Terrestrial				
Rib 1 Tap water				
Rib 16 Terrestrial		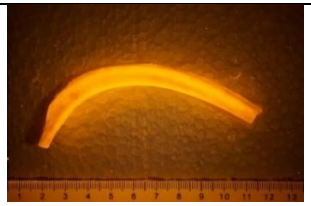	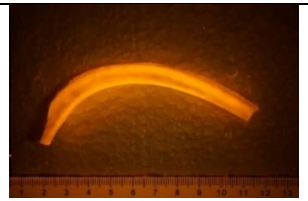	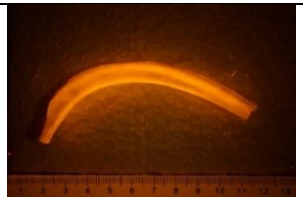
Rib 16 Tap water				

22.3.1- BONE DIMENSIONS

Similar to the results found in section B, research question 1, bone fluorescence values were seen to be lower at the faster exposure times, in air and underwater, and overall, the terrestrial fluorescence results were higher compared to underwater. Standard deviation was almost uniform across the whole fluorescence dataset with an average of 24.42 between the terrestrial fluorescence results, and 25.1 across the underwater values. The calculated collagen content of the porcine ribs ranged from 0.34 mg at the lowest, up to 0.80 mg at the highest, with an average of 0.53 mg, and a range of 0.46 mg.

Statistical comparisons were conducted based on the calculated bone collagen level, mass, and fluorescence intensity. When comparing the bone mass with the calculated collagen levels, a slight positive correlation was identified, but with a very low R^2 value of 0.0145 (fig. 162). This result indicated that there is no significant relationship between bone mass and collagen content. However, this result contradicted the results of similar analysis conducted in section B, question 1, where a more suggestive relationship between the mass of 30 fresh porcine bones and respective collagen content demonstrated an R^2 value of 0.3098. Although, the R^2 value for the fresh dataset was also not considered significant, it was more robust compared to the value found in this larger macerated dataset, therefore warranted further scrutiny.

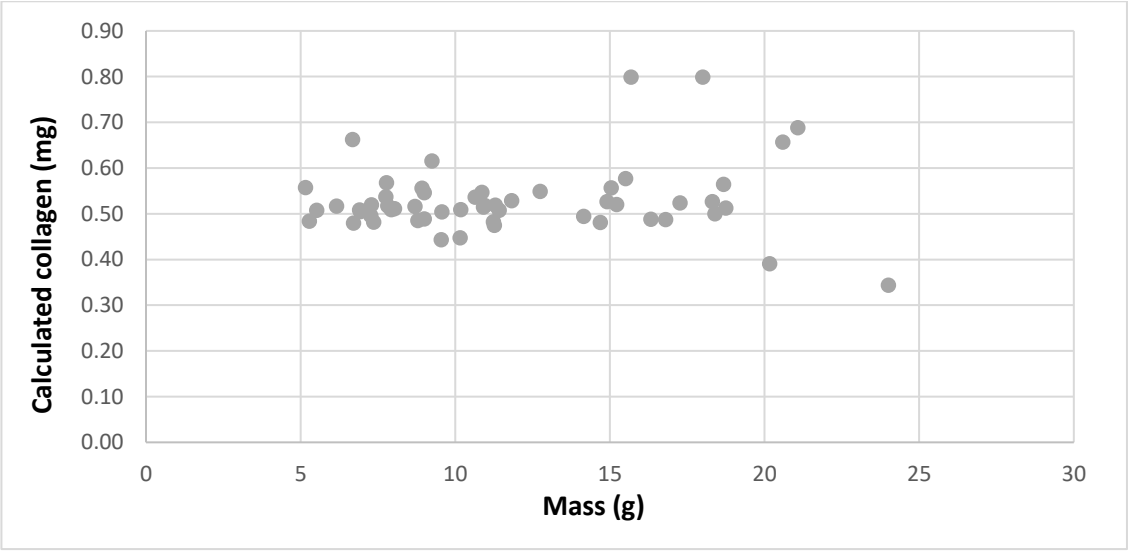

Figure 162: Comparison between calculated bone collagen level and bone mass

When comparing the averaged characteristics of the bone specimens in each dataset, most dimensions concur (tables 36 and 37 below). However, the average mass of the samples examined in question 2 was 6.43g (42.8%) lower compared to the fresh samples examined in question 1. This disparity can most likely be attributed to the removal of residual tissue and bone marrow during the hot water maceration. A reduction in bone mass was noted in the results of the maceration pilot study (chapter 13.0), as well as very little reduction in collagen levels. The same results are reflected here. Consequently, it is difficult to know whether mass is aligned with collagen content, as first thought, or if the initial comparison was not accurate, as the retained tissue and bone marrow added to the overall bone mass. Successful maceration leads to the elimination of the residual tissue, or at least a substantial reduction, therefore the comparison above could arguably be more representative of actual bone mass compared to collagen values, as the bones were devoid of soft tissue.

Table 36: Average bone dimensions of the fresh porcine ribs (Sus scrofa domesticus) (n=30), examined in section B, question 1

Analysis	Mass (g)	Length (mm)	Width (mm)	A/P (mm)	Coll. (mg)	Fluor. (0.6s)	Fluor. (0.4s)	Fluor. (1/3s)
Average	18.23	102.6	14.84	9.65	0.55	158.4	127.5	111.2
Max.	29.8	125.2	27	17.1	0.81	210.6	194.4	185.9
Min.	8.56	73.4	6.8	6.9	0.39	105.8	59.4	58.6
S.D.	7.04	15.23	4.1	2.60	0.08	30.1	33.5	127.3
Range	21.33	51.8	20.2	10.2	0.42	104.8	135.0	32.3

Table 37: Average bone dimensions of the macerated porcine ribs (Sus scrofa domesticus) (n=54), examined in section B, question 2

Analysis	Mass (g)	Length (mm)	Width (mm)	A/P (mm)	Coll. (mg)	Fluor. (0.6s)	Fluor. (0.4s)	Fluor. (1/3s)
Average	11.8	82	15.08	9.42	0.53	136.95	109.37	95.87
Max.	24	133.8	26.5	16.2	0.80	187.3	154.88	142.67
Min.	5.2	55.8	10.1	5.5	0.34	78.3	54.89	45
S.D.	4.7	17.0	4	2.4	0.08	25.72	24.35	23.18
Range	18.8	78	16.4	10.7	0.46	109	103.56	97.67

Consequently, these results imply that there is no correlation between bone mass and the amount of collagen found in porcine bone.

As with question 2, analyses between bone dimensions and exhibited fluorescence were also conducted to evaluate any potential relationships or trends. The underwater comparisons led to an almost unanimous result of $R^2 < 0.01$, across all configurations of bone measurement and observed fluorescence. The highest confidence level was noted in the comparison between anterior-posterior measurements and 0.6s exposure time, resulting in $R^2 = 0.0092$, whereas the lowest R^2 value of 0.0002 was seen when comparing bone width to bone fluorescence at 0.4s exposure time. All comparison charts for the underwater data can be seen in appendix 56.

In keeping with the results of the fresh dataset, the anterior-posterior measurements compared to terrestrial bone fluorescence also produced no evidence of a relationship, with all results producing an $R^2 < 0.02$ (appendix 57). On the contrary, the comparisons made between bone width and terrestrial fluorescence, and bone length and terrestrial fluorescence, contradicted the fresh results of question 1. Although no statistically significant relationships were found, a slight negative correlation was noted in all comparisons made between the fluorescence levels of each exposure time and bone width, whereas a slight positive correlation was observed in the analysis between bone length and terrestrial fluorescence. Similar results were seen across the exposure times, and a representative chart for each bone characteristic can be seen in figures 163 and 164 below, and all terrestrial charts are available in appendix 57.

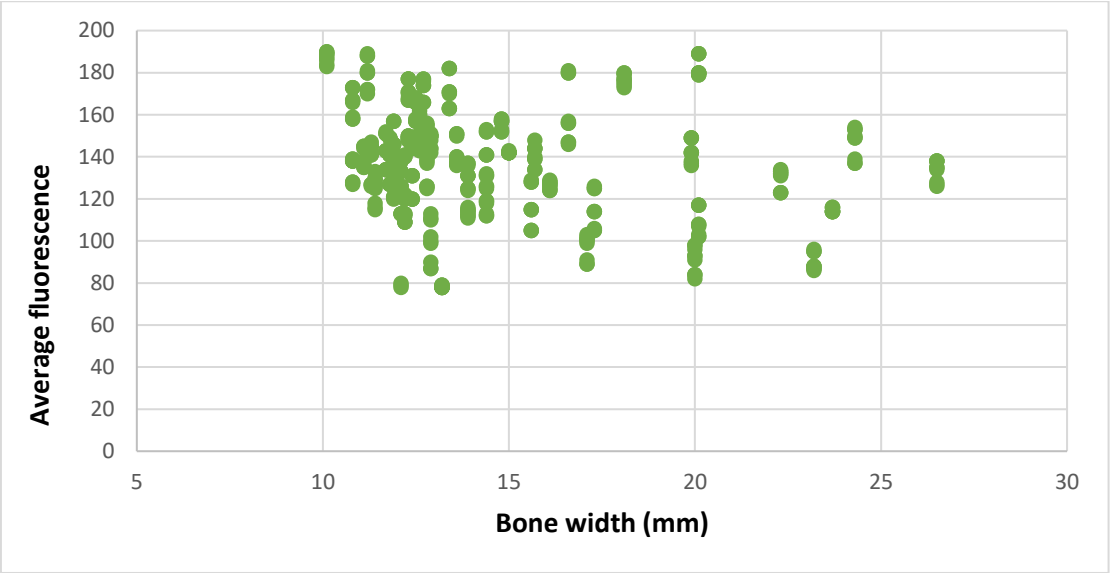

Figure 163: Comparison between bone width and terrestrial autofluorescence, photographed with the orange filter at 0.6s

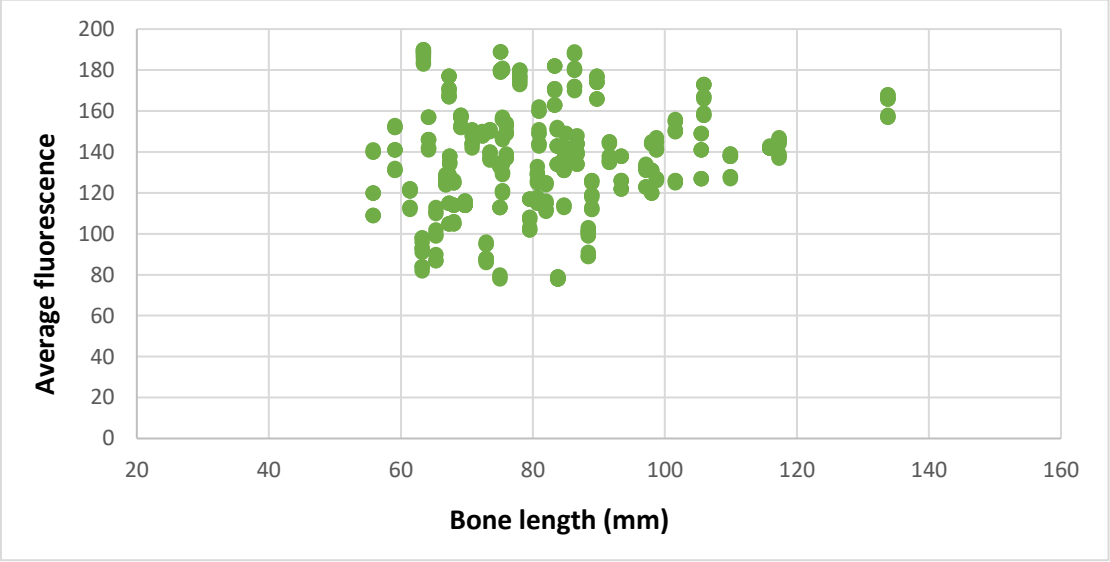

Figure 164: Comparison of between bone length and terrestrial autofluorescence, photographed with the orange filter at 0.6s

These trends are the reverse of the findings from the fresh dataset, which therefore now infers that the original interpretations in chapter 22.0 may not be entirely accurate. Changes in bone dimensions was not monitored during the maceration pilot study, as the focus was on the collagen content. Therefore, it's a possibility that this reversal in trends may be the result of shrinkage, or dissolution of bone, from the hot water maceration. However, each batch of ribs was only macerated for 1 hour and 30 mins, and no visible deterioration was observed upon completion. An alternative explanation may be that the small amount of residual tissue from manual defleshing in the fresh

dataset skewed the fresh measurements, but as the average values of both datasets were so similar it seems unlikely. In fact, this consistency in bone measurements across the two datasets further supports the idea that the bones did not suffer shrinkage. Similarly, the macerated dataset was double the number of bones examined in the fresh study, but the commonalities across the data groups imply that the sample size was not an influencing factor. More specifically, a greater sample size would normally amplify results if the hypothesis was accurate.

The most likely explanation for inverted trends, is that the ALS wavelengths responded differently to the macerated bone surface compared to the fresh bone. When comparing the average terrestrial fluorescence values (table 34), the fluorescence was higher in the macerated group, as expected, by an overall average (inclusive of all exposure times) of 18.3 (17.8%). Although this figure is not excessive, it is still substantial, and therefore could have influenced the statistical results. The reasoning for this change is unclear, but the results do demonstrate that further investigation into the influence of bone dimensions would be beneficial, and most significantly, that there may be differences in how fresh and macerated bone respond to ALS stimulation. Although the use of macerated porcine bone in research has provided some essential insight into bone fluorescence, particularly where fluorescence is the only criteria being measured, additional investigations using fresh bone are still required to help understand the aetiology of bone fluorescence and how it would be normally encountered at crime scenes.

22.3.2- COLLAGEN-FLUORESCENCE RELATIONSHIP

Upon initial examination of the collagen and bone fluorescence comparisons, no discernible trend could be detected. All comparisons demonstrated R^2 values of almost zero, as demonstrated by the example in figure 165. These results suggested that there is no relationship between collagen content and bone fluorescence. However, upon further examination of the data, four results were identified as possible outliers: ribs 4, 15, 24, and 51.

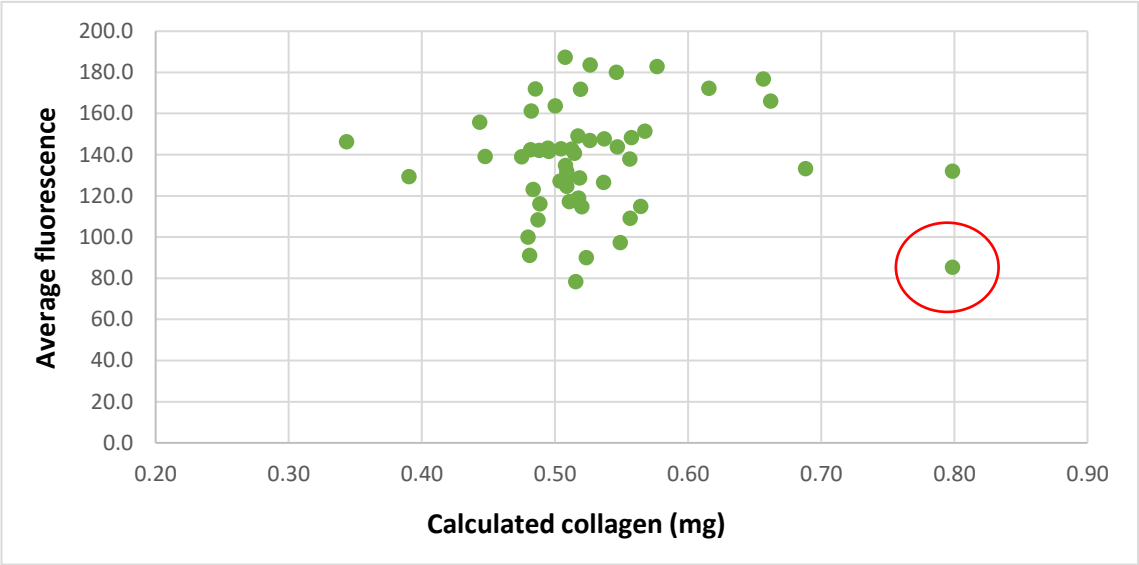

Figure 165: Comparison of calculated bone collagen and average terrestrial autofluorescence, photographed with the orange filter. A potentially erroneous result (rib 15) is circled in red.

Rib 4 was missing fluorescence data from the 0.4s exposure range, which was an oversight made during the photography process. The collagen level for rib 15 and 51 was 0.80 mg, which was 40.6% higher than the average for this dataset (0.53mg), and consistently appeared widely separate from the other values in each comparison chart (highlighted in red on figure 165). On the other hand, rib 24 presented with the lowest collagen value of 0.34, 43.6% lower than the calculated average. A low collagen content is not necessarily erroneous, but proportionally it seemed unlikely to be accurate, as rib 15 was comparatively one of the largest bones in the dataset, but much higher collagen values were noted in similar sized bones. Consequently, ribs 4, 15, 24, and 51 were removed from the sample population, and the data reanalysed.

Reanalysis of the calculated collagen volume and observed terrestrial and underwater fluorescence comparisons presented positive correlations across all comparisons. However, as with previous data, the correlations were not significant, but the uniformity of this trend was much more suggestive of the possible hypothesised relationship between bone collagen and fluorescence. Overall, the terrestrial results produced weaker relationships compared to the aquatic data, when considering individual exposure times, and when all data was compiled, figures 166-168 below.

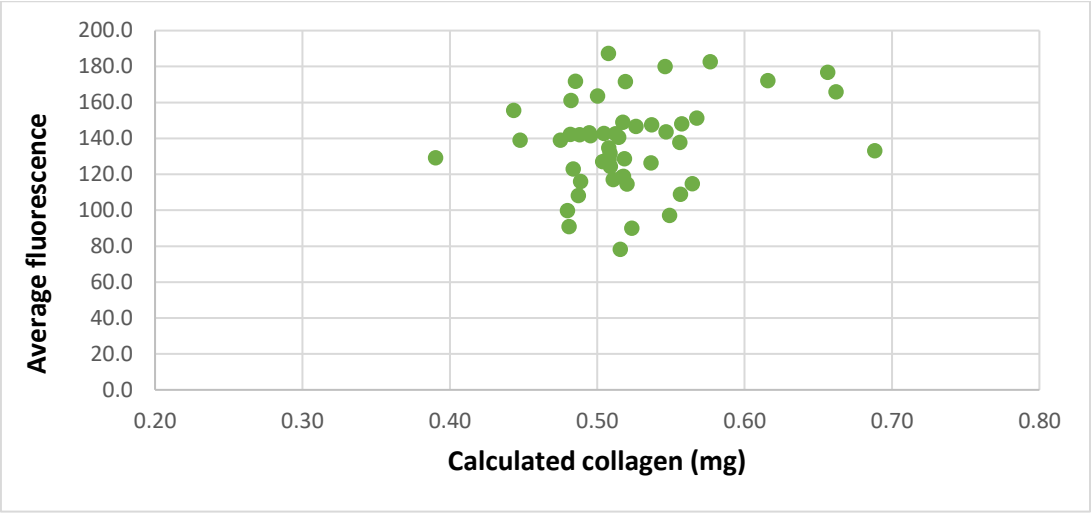

Figure 166: Comparison of calculated bone collagen and average terrestrial autofluorescence, photographed with the orange filter, and 0.6s exposure time.

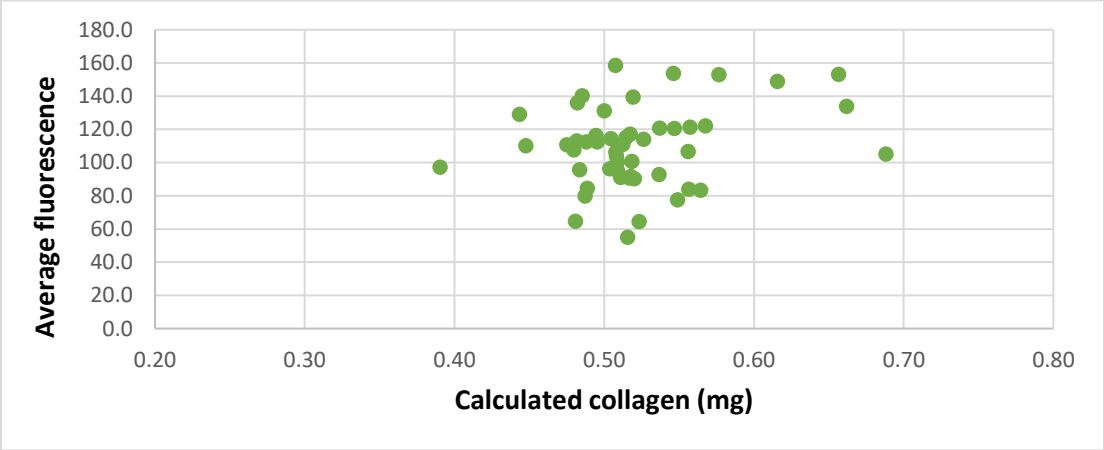

Figure 167: Comparison of calculated bone collagen and average terrestrial autofluorescence, photographed with the orange filter, and 0.4s exposure time.

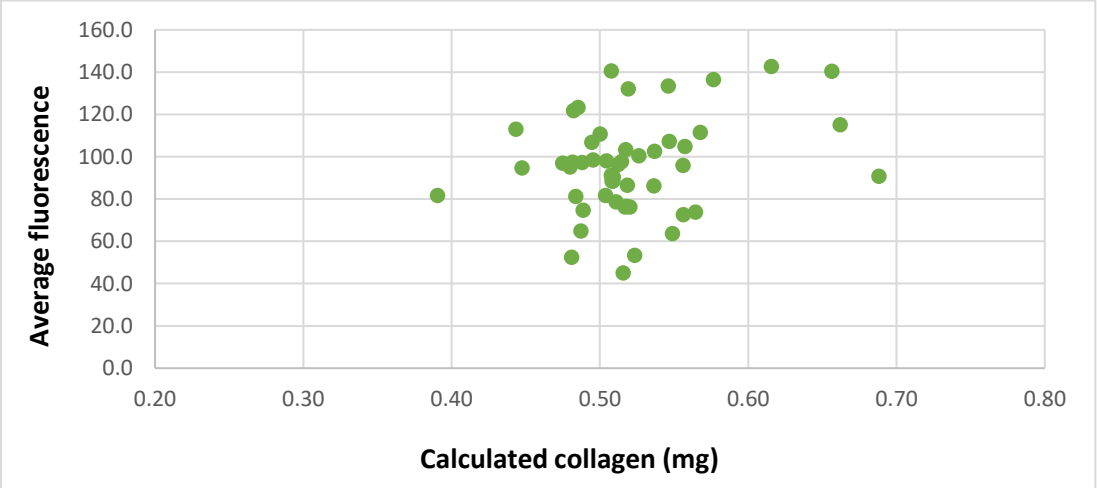

Figure 168: Comparison of calculated bone collagen and average terrestrial autofluorescence, photographed with the orange filter, and 1/3s exposure time.

The analysis of all terrestrial fluorescence data (all exposure times and all ROIs) compared to collagen content of led to a R^2 value of 0.599. When separated according

to exposure time, the correlation between calculated collagen content and average bone fluorescence increased as the exposure time became shorter. The 0.6s fluorescence data produced a correlation of R^2= 0.592, 0.4s data produced R^2= 0.636, and 1/3s led to an R^2 value of R^2= 0.0769.

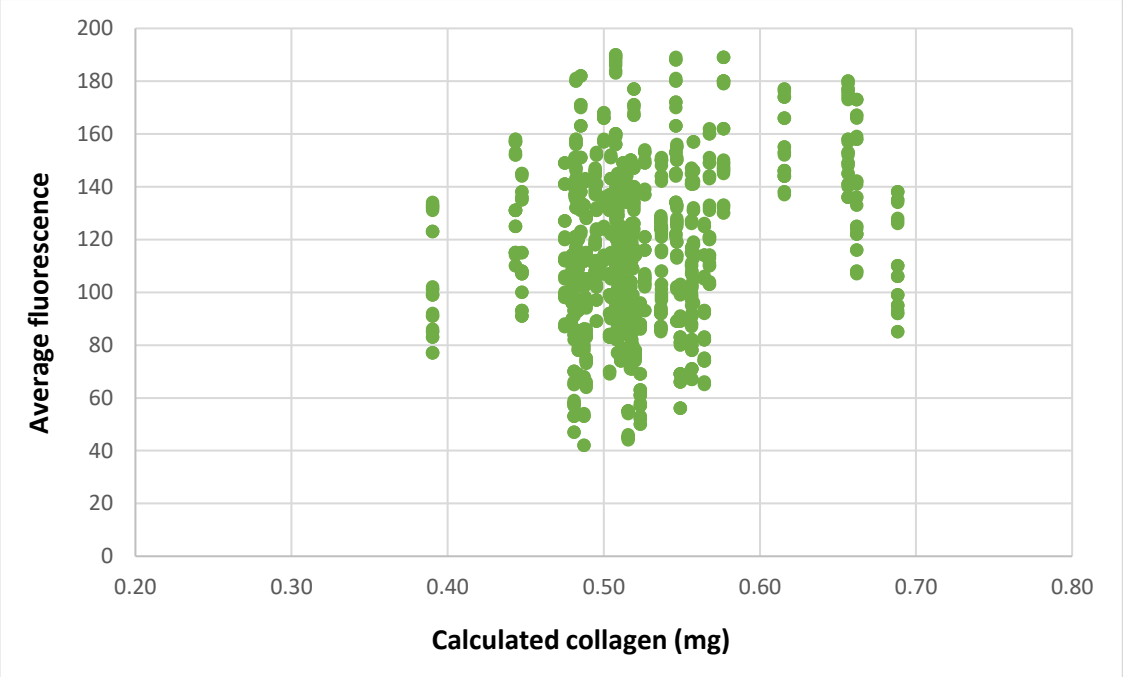

Figure 169: Comparison of all terrestrial fluorescence data points (all exposure times and all ROIs) compared with the calculated collagen content for each porcine bone (sus scrofa domesticus).

After the removal of the erroneous data, the underwater fluorescence data generated similar trends, although slightly stronger, and rather than increasing with shorter exposure times, the correlations were generally consistent across each exposure time (figs. 170-173). The fluorescence obtained at 0.4s exposure time produced the lowest R^2 value of R^2=0.749, and the fastest exposure time of 1/3s generated the highest R^2 value of 0.792. When compiled into one comparison examining all the underwater fluorescence data (all exposures, and ROIs), the correlation was almost the same as the 1/3s exposure time, producing an R^2 value of R^2= 0.794.

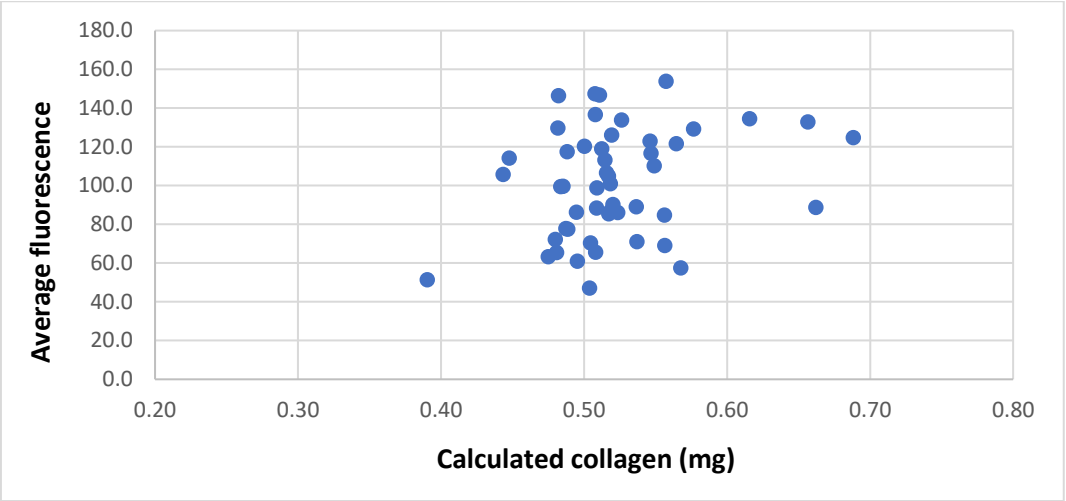

Figure 170: Comparison of calculated bone collagen and average underwater autofluorescence, photographed with the orange filter, and 0.6s exposure time.

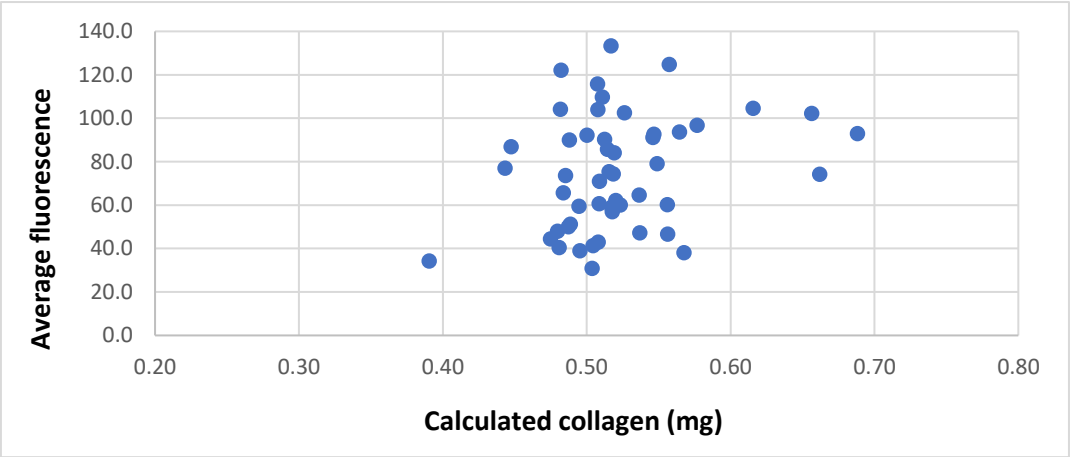

Figure 171: Comparison of calculated bone collagen and average underwater autofluorescence, photographed with the orange filter, and 0.4s exposure time.

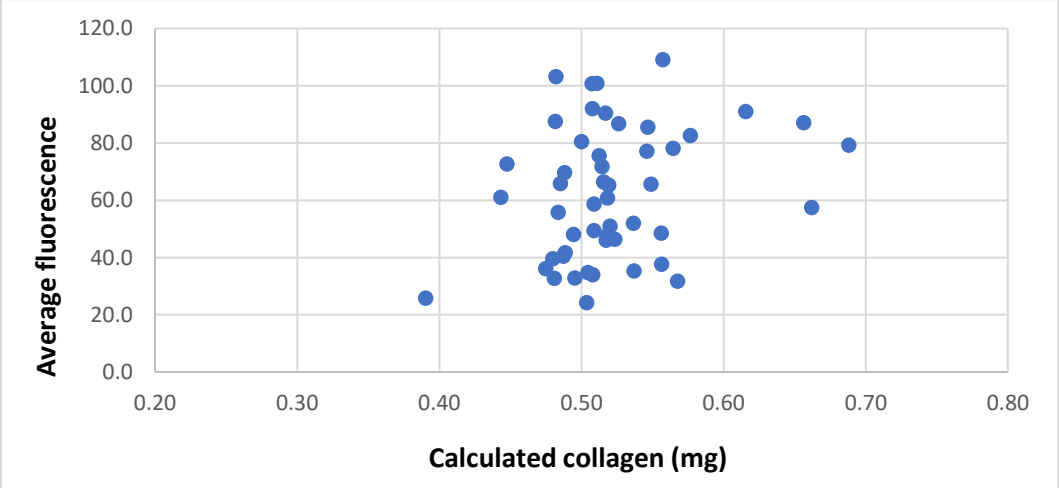

Figure 172: Comparison of calculated bone collagen and average underwater autofluorescence, photographed with the orange filter, and 1/3s exposure time.

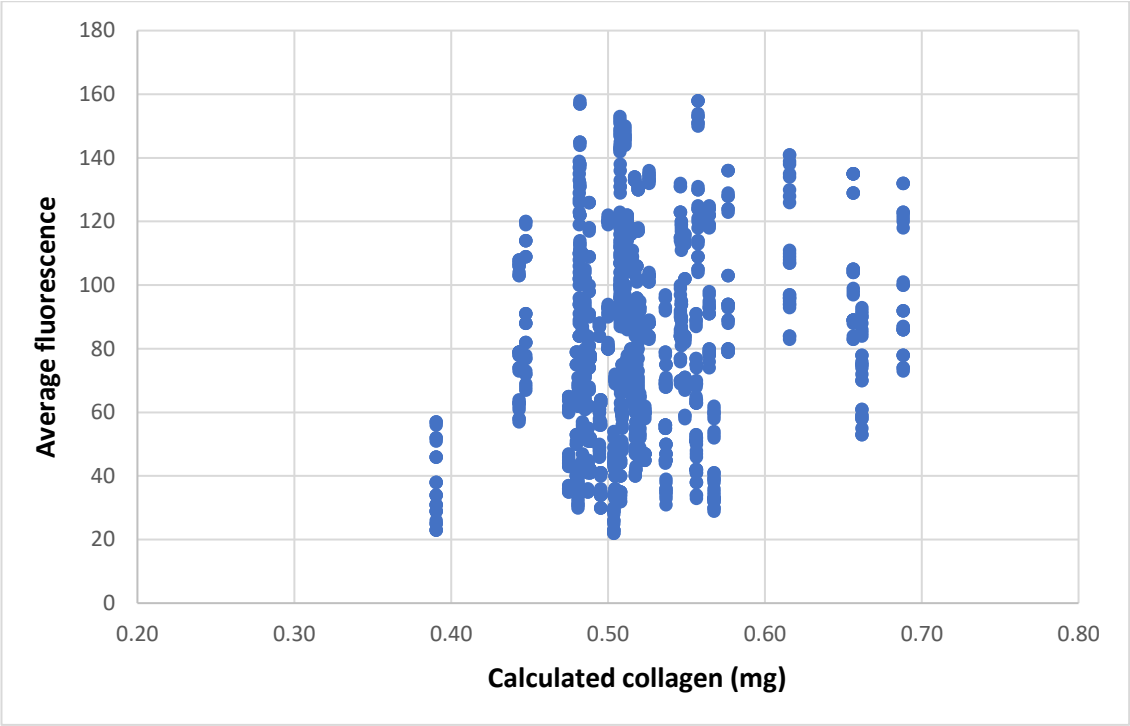

Figure 173: Comparison of all submerged fluorescence data points (all exposure times and all ROIs) compared with the calculated collagen content for each porcine bone (sus scrofa domesticus).

These results suggest a potential relationship between bone fluorescence and bone collagen levels, in keeping with the hypothesis discussed in literature (chapter 9.2). However, as none of these correlations were significant, further research will be required to investigate this theory further. The standard deviation in fluorescence values across all exposures within both terrestrial and aquatic datasets were very consistent, with the fastest exposure time in both contexts providing the smallest standard deviation of 23.18 and 22.44 for air and underwater respectively. The longest exposure time of 0.6s generated the widest spread in values for each condition, of 25.72 and 27.28 for air and underwater accordingly.

The presence of anomalous collagen data highlights the possibility that the chosen collagen quantification technique of TGA may not have been optimal. The inclusion of replicates may have helped to boost the reliability of the data, by allowing the creation of averages, as with the fluorescence values, rather than relying on one measurement. However, TG analysis can be very time consuming and expensive, particularly in the absence of an autosampler, and due to a range of additional challenges encountered

throughout this PhD including closure of the laboratories due to the coronavirus pandemic and a cyber-attack on the university, it was not possible to conduct replicates.

Other possibilities for the erroneous data could be the result of mismeasurement or malfunction by the TG machine. Throughout the duration of this PhD, the TG machine autosampler sometimes would fail to pick up a sample or drop it before processing. This would lead to delayed loading, and/or contamination of samples, particularly when left on the machine for a long time, which may have influenced the rate of burning. Although the TG machine was used communally, the crucibles used for this analysis were not, to limit cross contamination. However, this may still have been a possibility if other materials were spilt in the autosampler turntable, or on the laboratory bench prior to examination.

Although the bone samples were hot water macerated, it was only for a short duration, therefore the samples were still vulnerable to the natural decomposition process, and consequently may have degraded if not processed straight away. As many of the TG analysis was conducted over the night, with the assistance of university personnel, it is not known which samples may have been left out. In addition to this, a portion of the TG analysis was conducted at a different institution due to a university transfer, and although the TG machine was the same model, it may have been calibrated slightly differently. However, as there were only a small number of samples affected in a relatively large sample population, it is possible that these inconsistencies are the result of the small individual sample size. For all TGA samples, 5 mg of bone scrapings were used. After retrospective research, a greater volume of sample may have been required to ensure consistent and even burning. Figure 174 below, is an example of a TG thermogram produced for rib 2 during this research question.

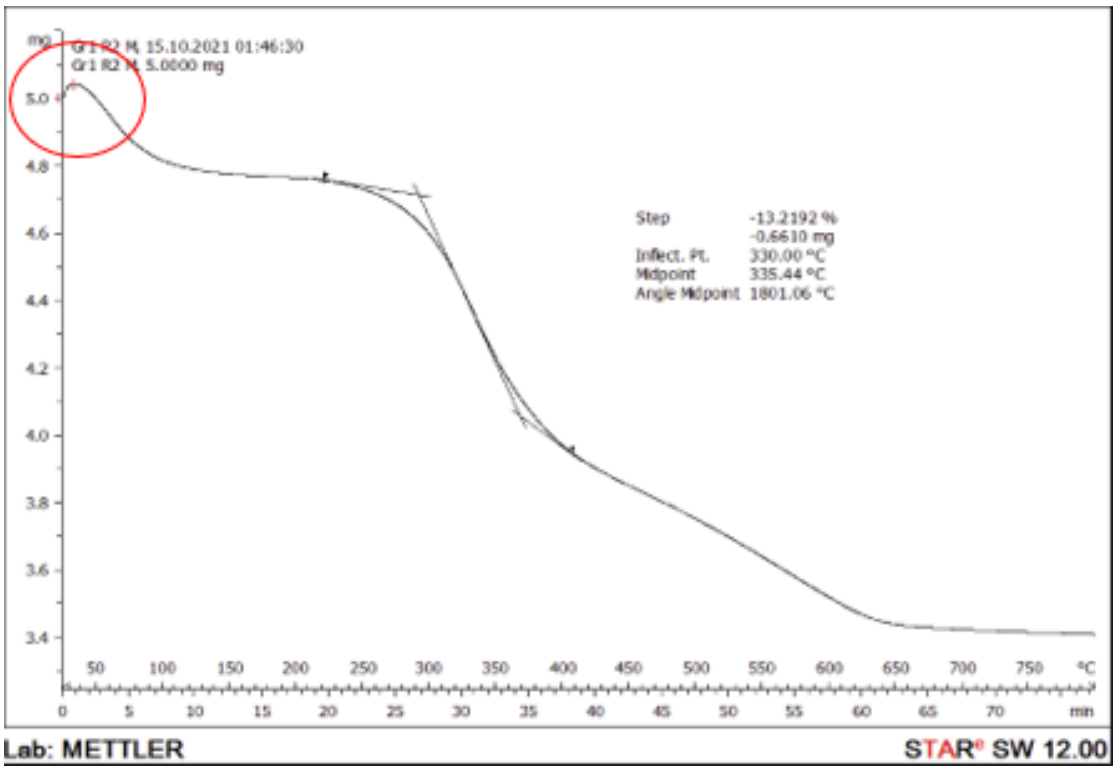

Figure 174: Example thermogram from porcine rib 2 demonstrating buoyancy artefact (circled in red)

At the beginning of the curve, a small increase in mass is reported (circled in red). This is an artefact commonly found in TG analysis and is referred to as the buoyancy effect [498]. This apparent rise in mass is not caused by the sample, but is a result of a sharp change in gas density as it is injected into the furnace [498]. This effect can be exacerbated if the type of gas is changed regularly, or if there are fluctuations in the gas flow rate [499]. However, it can also occur when a low sample volume is used, with the injection of gas leading to uneven thermal alterations [499, 500]. The buoyancy artefact is not responsible for the inconsistencies in collagen data, but its presence can be an indicator of low sample volume [499], and therefore provide some explanation for the erroneous measurements.

In future experimentation an increase in sample volume could help to reduce the buoyancy effect, or the use of an automatic blank curve subtraction during quantification of the curve [456]. Further issues also arose due to TGA being a destructive analysis, therefore when an error was encountered, the sample would still be consumed, and a new sample was required. As the samples were from bone, natural variation in bone composition could mean some variation in collagen content, meaning

it was impossible to run the exact sample again, even though it is from the same bone. However, based on the results from section A, question 3, the distribution in collagen content throughout bone is negligible, therefore it is unlikely this was the source of the inconsistency.

Despite these limitations, the TG analysis was arguably successful, as 48 of the 54 samples were not considered erroneous and provided some indicative results. Therefore, in future work, the inclusion of a supplementary and cheaper technique, such as FTIR, may provide additional data to support TGA, and enable deeper analysis of bone composition, and thus a fuller quantification of the collagen.

22.3.3- SPSS STATISTICS

Histograms were produced to assess the normality of the differences in distribution of data for the quantified collagen content for the 54 porcine bones, and average florescence data for each context and exposure time. The collagen data exhibited a normal distribution, as did the terrestrial fluorescence data across all exposure times. As a result, paired sample student T-tests were performed to compare the observed fluorescence values with the calculated collagen content. All histograms for these analyses can be seen in appendix 58.

All three comparisons produced statistically significant results, with the 0.6s exposure time reporting a value of t= -143.5, d.f= 49, p= .000, 0.4s produced a significance of t= -29.408, d.f= 49, p= .000, and the shortest exposure time of 1/3s produced a result of T=-29.4, d.f =49, p =.000. The SPSS output for the respective analyses can be seen in figures 175-178 below.

T-Test

Paired Samples Statistics

		Mean	N	Std. Deviation	Std. Error Mean
Pair 1	Collagen	.522400	50	.0533590	.0075461
	TFluor0.6	136.9740	50	25.05730	3.54364

Paired Samples Correlations

		N	Correlation	Sig.
Pair 1	Collagen & TFluor0.6	50	.248	.082

Paired Samples Test

		Paired Differences					t	df	Sig. (2-tailed)
		Mean	Std. Deviation	Std. Error Mean	95% Confidence Interval of the Difference Lower	Upper			
Pair 1	Collagen - TFluor0.6	-136.4516000	25.0441135	3.5417725	-143.5690583	-129.3341417	-38.526	49	.000

Figure 175: T-test comparisons of the average terrestrial fluorescence results of the porcine bones (Sus scrofa domesticus), photographed at 0.6s exposure time, compared to the calculated collagen content.

T-Test

Paired Samples Statistics

		Mean	N	Std. Deviation	Std. Error Mean
Pair 1	Collagen	.522400	50	.0533590	.0075461
	TFluor0.4	109.3760	50	23.87673	3.37668

Paired Samples Correlations

		N	Correlation	Sig.
Pair 1	Collagen & TFluor0.4	50	.258	.071

Paired Samples Test

		Paired Differences					t	df	Sig. (2-tailed)
		Mean	Std. Deviation	Std. Error Mean	95% Confidence Interval of the Difference Lower	Upper			
Pair 1	Collagen - TFluor0.4	-108.8536000	23.8630407	3.3747436	-115.6354011	-102.0717989	-32.255	49	.000

Figure 176: T-test comparisons of the average terrestrial fluorescence results of the porcine bones (Sus scrofa domesticus), photographed at 0.4s exposure time, compared to the calculated collagen content.

T-Test

Paired Samples Statistics

		Mean	N	Std. Deviation	Std. Error Mean
Pair 1	Collagen	.522400	50	.0533590	.0075461
	TFluor13	95.8140	50	22.92752	3.24244

Paired Samples Correlations

		N	Correlation	Sig.
Pair 1	Collagen & TFluor13	50	.283	.046

Paired Samples Test

		Paired Differences					t	df	Sig. (2-tailed)
		Mean	Std. Deviation	Std. Error Mean	95% Confidence Interval of the Difference Lower	Upper			
Pair 1	Collagen - TFluor13	-95.2916000	22.9124728	3.2403130	-101.8032527	-88.7799473	-29.408	49	.000

Figure 177: T-test comparisons of the average terrestrial fluorescence results of the porcine bones (Sus scrofa domesticus), photographed at 1/3s exposure time, compared to the calculated collagen content.

In contrast, all data groups within the underwater fluorescence dataset exhibited abnormal data distributions. Consequently, non-parametric Wilcoxon signed rank tests were performed to test the relationship between bone collagen and underwater fluorescence, as detailed in figures 178-180 below:

Hypothesis Test Summary

	Null Hypothesis	Test	Sig.	Decision
1	The median of differences between Collagen and UFluor0.6 equals 0.	Related-Samples Wilcoxon Signed Rank Test	.000	Reject the null hypothesis.

Asymptotic significances are displayed. The significance level is .05.

Figure 178: Result of the Wilcoxon signed rank test comparing the average underwater fluorescence results of the porcine bones (Sus scrofa domesticus), photographed at 0.6s exposure time, compared to the calculated collagen content.

Hypothesis Test Summary

	Null Hypothesis	Test	Sig.	Decision
1	The median of differences between Collagen and UFluor0.4 equals 0.	Related-Samples Wilcoxon Signed Rank Test	.000	Reject the null hypothesis.

Asymptotic significances are displayed. The significance level is .05.

Figure 179: Result of the Wilcoxon signed rank test comparing the average underwater fluorescence results of the porcine bones (Sus scrofa domesticus), photographed at 0.4s exposure time, compared to the calculated collagen content.

Hypothesis Test Summary

	Null Hypothesis	Test	Sig.	Decision
1	The median of differences between Collagen and UFluor13 equals 0.	Related-Samples Wilcoxon Signed Rank Test	.000	Reject the null hypothesis.

Asymptotic significances are displayed. The significance level is .05.

Figure 180: Result of the Wilcoxon signed rank test comparing the average underwater fluorescence results of the porcine bones (Sus scrofa domesticus), photographed at 1/3s exposure time, compared to the calculated collagen content.

In agreement with the results produced by the terrestrial dataset, strong statistically significant relationships of p= .000, were observed across all exposure times when comparing the collagen content and underwater ALS fluorescence results. In combination, these comparisons provide compelling support for the hypothesis that there is a relationship between bone collagen and observed bone fluorescence, which can be observed in both tap water and terrestrial contexts.

22.4 – CONCLUSIONS

In summary, the comparisons made between calculated bone collagen content and emitted fluorescence levels of the 54 macerated porcine ribs, provided strong support for a possible collagen-fluorescence relationship, with statistical analysis returning a unanimous result of p= .000 for all tested comparisons. However, a few anomalies noted in the collagen data suggest that the collagen quantification technique may not be entirely optimal, hence why there is some disparity in the statistical correlations. It is proposed that deeper sampling of the cortical bone, along with a larger sample volume, could boost the reliability of the TGA measurements, and overall make the statistical analysis more robust. Moreover, the addition of other quantification techniques such as FTIR, could help to provide a more comprehensive quantification of bone composition, without damaging the sample.

Comparisons between the question 1 fresh data, and the macerated dataset produced contrasting results regarding the influence of bone dimensions on the bone autofluorescence, suggesting that although maceration is not destructive to bone collagen, ALS wavelengths may interact differentially with fresh and macerated bone. This would be a particularly important area of ALS research to develop, as much of the ALS bone fluorescence published research in literature was generated using macerated bone, and historical skeletal collections.

With that being said, the strong statistical results produced during this result question offer a strong indication that there is most likely a positive correlation between the amount of bone collagen in porcine ribs, ergo the higher the bone collagen volume the greater intensity of emitted bone autofluorescence, when stimulated with blue light (450 nm), and photographed with an orange filter. This theory is supported by the fact that significant relationships were noted in both aquatic and terrestrial deposition contexts. Based on these results it is possible to accept hypothesis 3, detailed below, and reject the null hypothesis.

3. Hypothesis: There is a correlation between the amount of bone collagen in porcine bone (*Sus scrofa domesticus*) and the levels of fluorescence seen when exposed to blue light (450-470 nm) and photographed with an orange camera filter.

Null hypothesis: There is no correlation between the amount of bone collagen in porcine bone (*Sus scrofa domesticus*) and the levels of fluorescence seen when exposed to blue light (450-470 nm) and photographed with an orange camera filter.

However, the full extent of this collagen-fluorescence relationship, and how it potentially differs between macerated and fresh bone will need to be explored in future research.

23.0 - SECTION B, QUESTION 3:
DIFFERENTIATION AND CONTROLS

***Question 3a**: Is it possible to distinguish between porcine bone (Sus scrofa domesticus) and other 27 non-bone control items when photographed using blue light (approximately 450 nm) and orange and yellow filters, in terrestrial and tap water contexts?*

***Question 3b**: To what extent does pure porcine collagen powder fluoresce when exposed to ALS? Quantifying the fluorescence levels of pure porcine collagen powder photographed using blue light (approximately 450 nm) and orange and yellow filters, in terrestrial and tap water contexts.*

***Question 3c**: Will demineralised and deproteinised porcine bone (Sus scrofa domesticus) fluoresce when photographed using blue light (approximately 450 nm) and orange and yellow filters in terrestrial and tap water contexts?*

Research questions 3a to 3c focus on the production and analysis of a range of positive and negative controls including controls derived from bone, and non-bone items obtained from the environment. Each question is addressed individually and discussed comparatively at the end of the chapter.

23.1- QUESTION 3A: NON-BONE CONTROLS

23.1.1 MATERIALS

A selection of twenty-seven naturally occurring non-bone items were collected from terrestrial and aquatic contexts across the UK, as shown in table 38. Items represent both organic and inorganic materials that can commonly be confused with bone when conducting searches for skeletal remains. For items such as sea glass, ceramics and wood, measurements were completed using Yakamoz electronic digital callipers (±0.1 mm). All items were stored at room temperature, in a clean, dry plastic box throughout experimentation.

23.1.2- METHOD

Each item was photographed under natural light and then using the Hammerhead forensic light source in terrestrial and underwater contexts according to the core methodology described in chapter 20.0. The non-bone items were also photographed using the Crime-lite 2 with the orange and yellow filters. Exposure time was standardised to 1/3s for both light sources, to ensure a normalised comparison across the dataset, and as this exposure time had proven successful for porcine bone in previous experimentation. Fluorescence quantification was conducted using the OFC as also outlined in chapter 20.0.

Collagen quantification was not conducted in this research question, as the TGA protocol was designed to quantify bone collagen, based on similar methodologies in literature. Due to many different compositions of the non-bone items, the heating parameters for TGA would need to be altered for each individual item and therefore would not be truly comparable. Moreover, this research question was designed to focus on a fluorescence comparison, to investigate the possibility of differentiation whilst searching for skeletal remains at a crime scene, therefore fluorescence quantification was the premier focus of this research question, rather than a comparison between collagen and fluorescence.

23.1.3- STATISTICAL ANALYSIS

Statistical analysis focused on comparing the calculated fluorescence levels of the non-bone items within the dataset, with the aim of generating terrestrial and underwater fluorescence scales, and investigating the potential for differentiation.

Table 38: Twenty-seven naturally occurring non-bone items recovered from terrestrial and aquatic environments, alongside provenance data, descriptions, and dimensions.

No.	Item	Photo	Location	No.	Item	Photo	Location
1	Stick 1 117 x 18mm		West Yorkshire woodland	2	Stick 2 130 x 15mm		West Yorkshire woodland
3	Tree bark		West Yorkshire woodland	4	Driftwood 100 x 18mm		North Yorkshire coast
5	Blue mussel (*Mytilus edulis*)		North Yorkshire coast	6	Great scallop shell (*Pecten maximus*)		North Yorkshire coast
7	Queen scallop shell (*Aequipecten opercularis*)		North Yorkshire coast	8	Shield limpet (*Lottia pelta*)		North Yorkshire coast

9	Cockle shell (*Cerastoderma edule*)		North Yorkshire coast	10	Oyster shell (*Ostrea edulis*)		North Yorkshire coast
11	Freshwater mussel shell (*Margaritifera margaritifera*)		West Yorkshire canal	12	Stone 1 Yellow/orange 46.7 x 32.9mm		North Yorkshire coast
13	Stone 2 White 40.8 x 35.9mm		North Yorkshire coast	14	Stone 3 Pale grey/yellow Coarse texture 50 x 30.5mm		North Yorkshire coast
15	Stone 4 Dark grey 80 x 50mm		North Yorkshire coast	16	Stone 5 Light grey, speckled. 60 x 29.1mm		West Yorkshire garden

17	Ceramic fragment 1 White, crackle glaze 63 x 47mm		North Yorkshire coast	18	Ceramic fragment 2 Yellow/brown 61 x 55mm	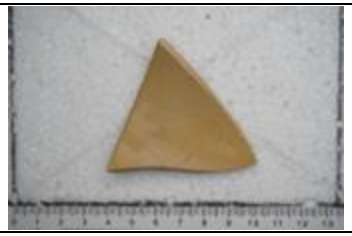	North Yorkshire coast
19	Ceramic fragment 3 Red/orange 54.9 x 22mm		North Yorkshire coast	20	Sea glass 1 Translucent, colourless 39.1 x 27.1mm	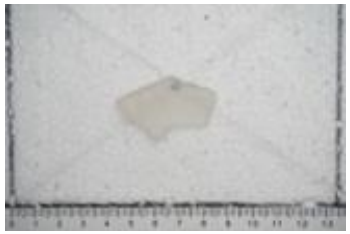	North Yorkshire coast
21	Sea glass 2 Frosted Colourless 33 x 26mm	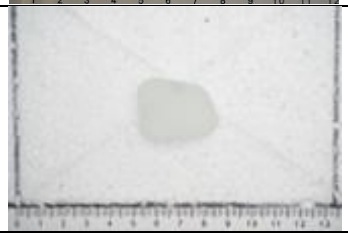	North Yorkshire coast	22	Fresh Leaf		West Yorkshire garden
23	Old leaf		West Yorkshire garden	24	Sea glass 3 Pale green, translucent 36.2 x 36.4mm	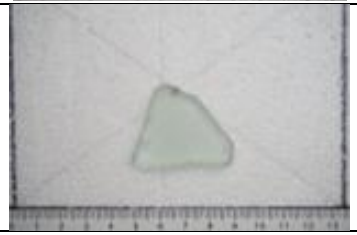	Cornish coast

25	Sea glass 4 Frosted Dark brown 31.1 x 18.9mm		Cornish coast	26	Sea glass 5 Frosted, dark green. 28.7 x 24.8mm		Cornish coast
27	Sea glass 6 Translucent Light brown 20.4 x 17.3mm		Cornish coast				

23.2- QUESTION 3A: NON-BONE CONTROLS RESULTS

The quantified average fluorescence for each non-bone item using the two light sources, in the terrestrial and aquatic contexts, are displayed in table 39. A full table of all fluorescence values for each ROI is available in appendix 59. Table 40 summarises the photographic fluorescence results for all the non-bone control items, and all the fluorescence photographs, alongside respective OFC processed images, are available in appendices 60 (Hammerhead) and 61 (Crime-lite 2).

The fresh leaf was not photographed using the Crime-lite 2 and the yellow filter, as it had begun to wilt before photographs could be taken, and therefore an accurate comparison could not be achieved. Similarly, stick 2, tree bark, fresh leaf, and old leaf were unable to be photographed in the underwater environment as they floated during submersion. As with the porcine bones that floated during previous research questions, attempts were made to try and secure the items to the polystyrene sheet using blu tac™ and then Unibond™ double sided mounting tape. However, the surface texture of these items was not conducive to either adhesive, and they could not be secured, and were not able to be photographed.

Table 39: Average fluorescence results for the 27 non-bone items recovered from terrestrial and aquatic environments, tabulated according to context and filter used.

No.	Specimen	Hammerhead		Crime-lite 2	
		Terrestrial	Underwater	Orange	Yellow
1	Stick 1	152.7	98.7	163.2	246.1
2	Stick 2	69	Not possible	87.3	183.3
3	Tree bark	148.9	Not possible	162.8	245.3
4	Driftwood	94.2	31.2	168.9	242.3
5	Blue mussel	22.0	5.7	30.4	91.1
6	Great scallop shell	74.9	22.2	99.9	213.1
7	Queen scallop shell	126.7	35.1	146.3	254.2
8	Shield limpet	111.6	49.0	126.6	224.1
9	Cockle shell	164.7	74.9	207.4	253.7
10	Oyster shell	54.3	35.0	111.2	216.2
11	Freshwater mussel shell	164.9	83.0	194.1	253.4
12	Stone 1	104.1	34.6	131.7	226.7
13	Stone 2	108.6	37.6	161.3	249.0
14	Stone 3	26.1	5.8	20.4	85.1
15	Stone 4	14.7	5.0	36.2	82.8
16	Stone 5	33.0	11.7	56.6	156.8
17	Ceramic fragment 1	54.9	24.6	54.8	252.0
18	Ceramic fragment 2	25.7	10.0	15.3	252.1
19	Ceramic fragment 3	26.4	7.7	26.4	218.2
20	Sea glass 1	76.0	25.9	137.3	242.3
21	Sea glass 2	75.7	24.4	132.2	240.3
22	Fresh Leaf	36.6	Not possible	77.8	Not possible
23	Old leaf	141.6	Not possible	156.7	243.7
24	Sea glass 3	142.7	26.3	116.4	232.3
25	Sea glass 4	29.1	6.2	29.6	97.2
26	Sea glass 5	27.1	6.8	24.7	71.0
27	Sea glass 6	26.2	8.0	22.3	75.1

Table 40: Summarised photographic fluorescence results for all 27 non-bone control items, including all filters, contexts, and ALS devices

No.	Natural	Hammerhead		Crime-lite 2	
		Orange terrestrial (1/3s)	Orange underwater (1/3s)	Orange terrestrial (1/3s)	Yellow terrestrial (1/3s)
1			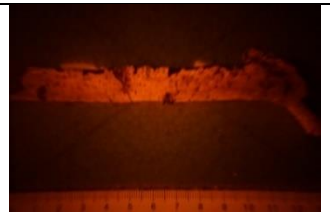	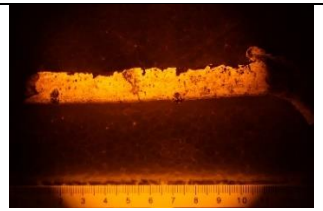	
2			Not possible	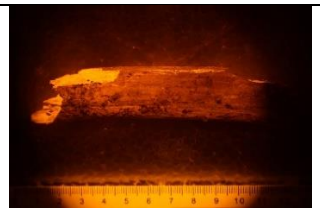	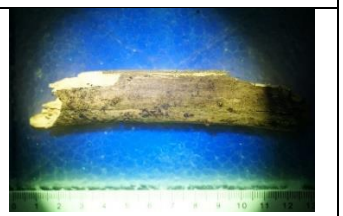
3			Not possible	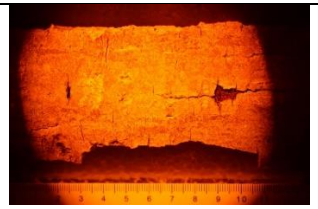	
4				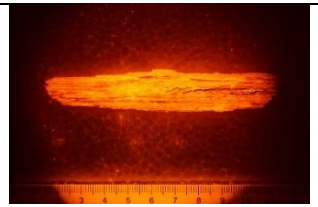	

No.	Natural	Hammerhead		Crime-lite 2	
		Orange terrestrial (1/3s)	Orange underwater (1/3s)	Orange terrestrial (1/3s)	Yellow terrestrial (1/3s)
5				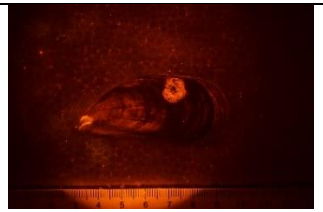	
6		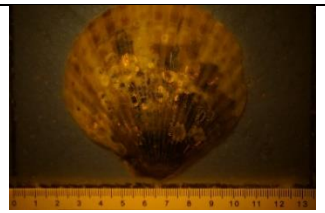	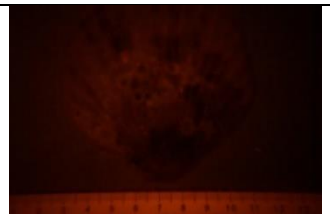	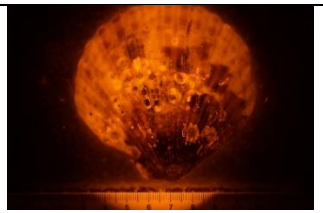	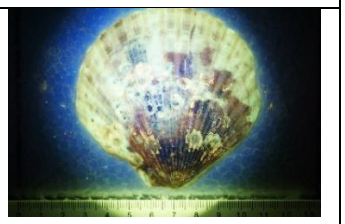
7				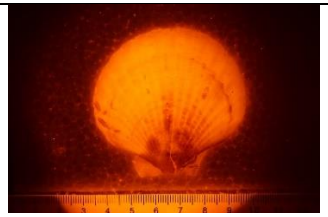	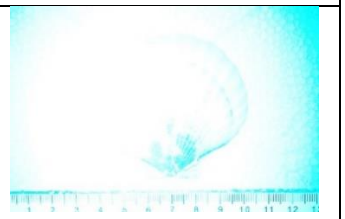
8		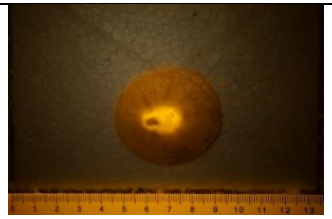	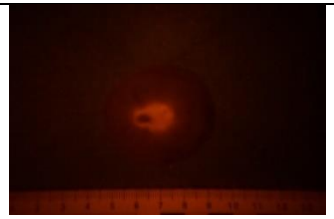	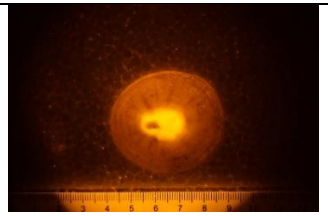	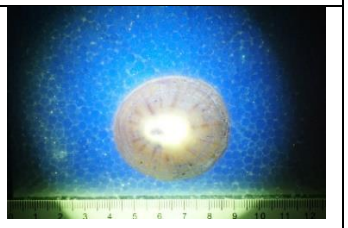

No.	Natural	Hammerhead		Crime-lite 2	
		Orange terrestrial (1/3s)	Orange underwater (1/3s)	Orange terrestrial (1/3s)	Yellow terrestrial (1/3s)
9				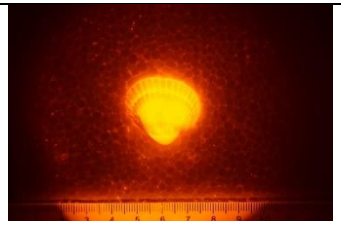	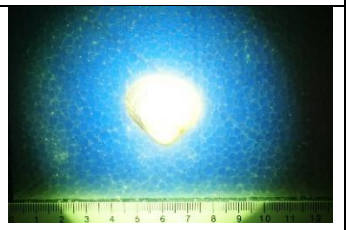
10				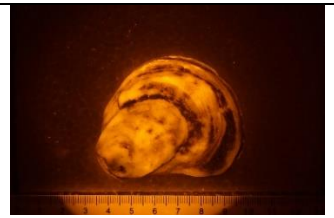	
11	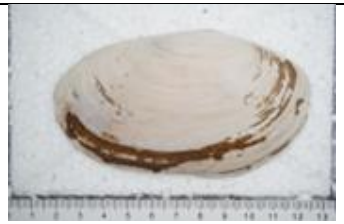		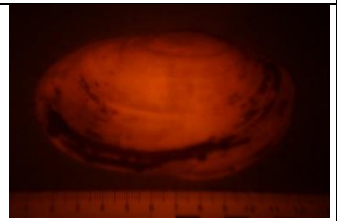	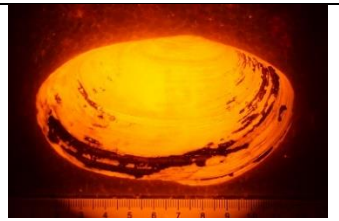	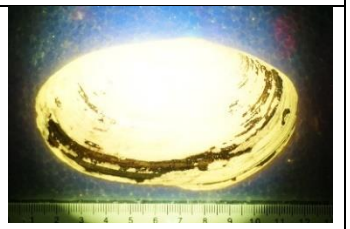
12			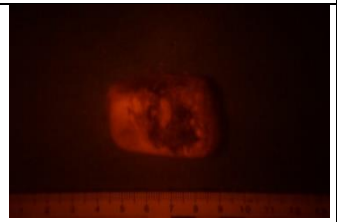	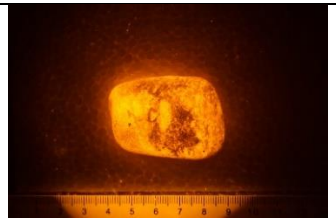	

No.	Natural	Hammerhead		Crime-lite 2	
		Orange terrestrial (1/3s)	Orange underwater (1/3s)	Orange terrestrial (1/3s)	Orange underwater (1/3s)
13			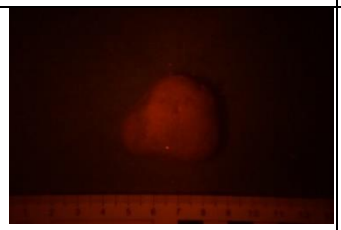	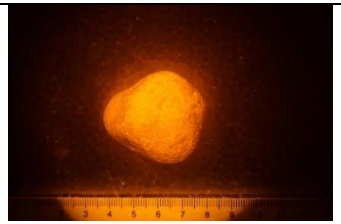	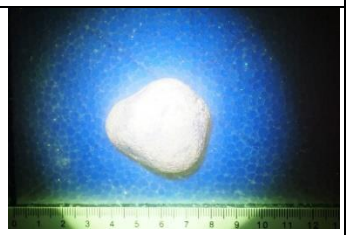
14				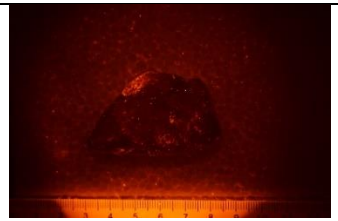	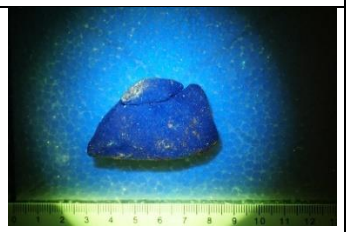
15				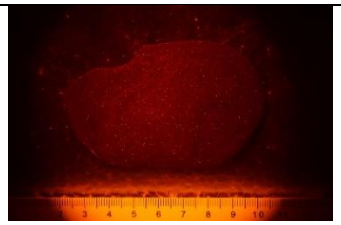	
16				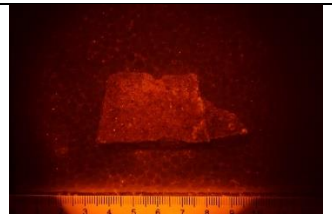	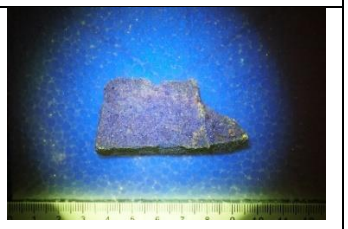

No.	Natural	Hammerhead		Crime-lite 2	
		Orange terrestrial (1/3s)	Orange underwater (1/3s)	Orange terrestrial (1/3s)	Yellow terrestrial (1/3s)
17	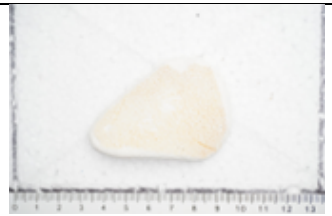	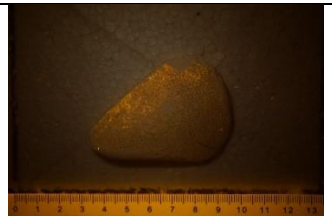	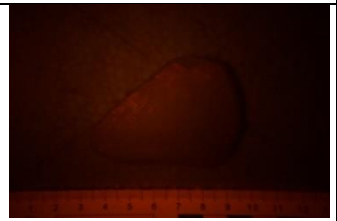	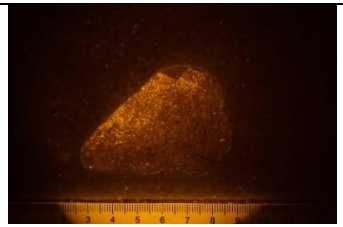	
18				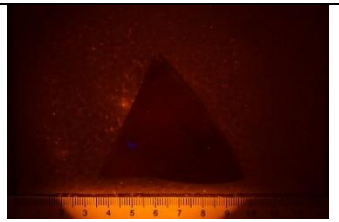	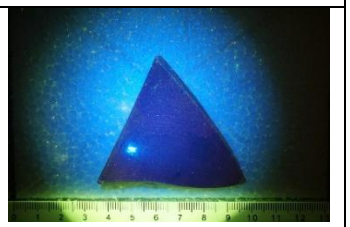
19				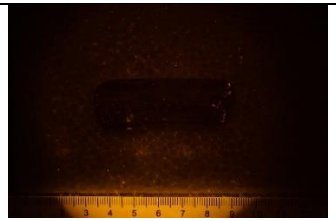	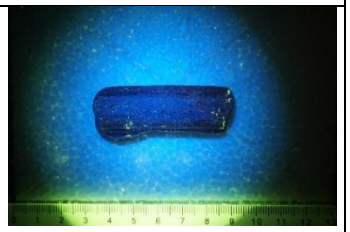
20	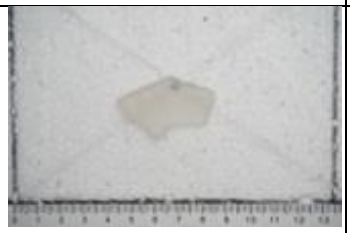	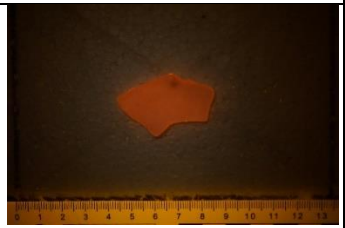	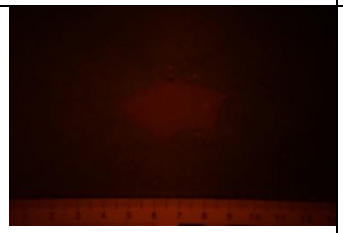	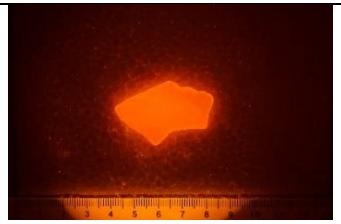	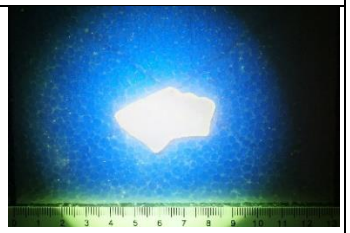

No.	Natural	Hammerhead		Crime-lite 2	
		Orange terrestrial (1/3s)	Orange underwater (1/3s)	Orange terrestrial (1/3s)	Yellow terrestrial (1/3s)
21	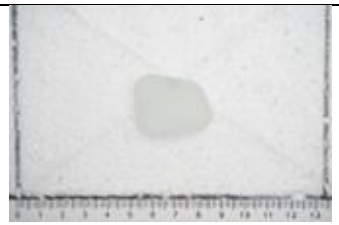			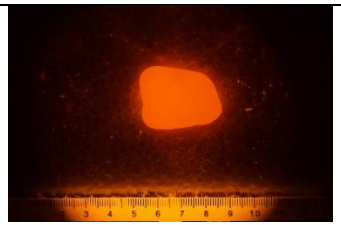	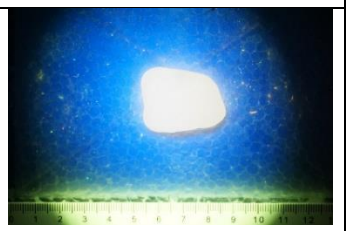
22			Not possible		Not possible
23			Not possible	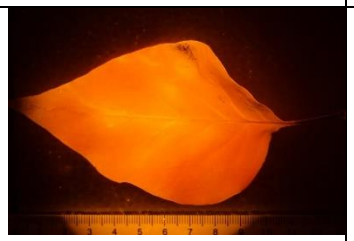	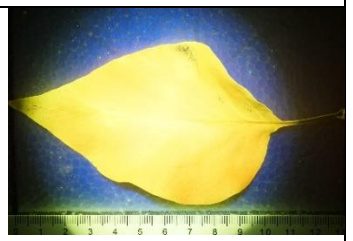
24	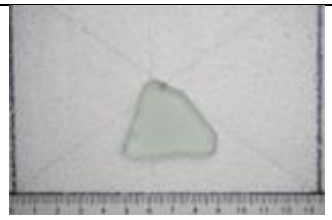	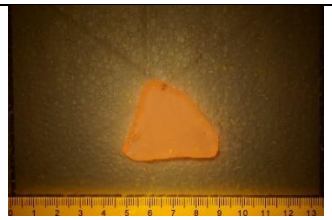		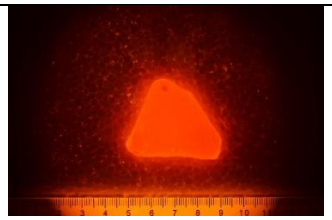	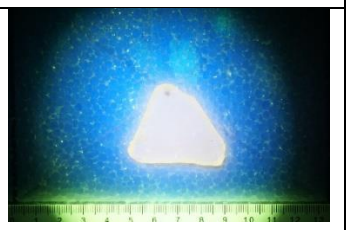

No.	Natural	Hammerhead		Crime-lite 2	
		Orange terrestrial (1/3s)	Orange underwater (1/3s)	Orange terrestrial (1/3s)	Yellow terrestrial (1/3s)
25				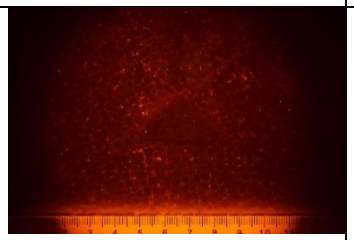	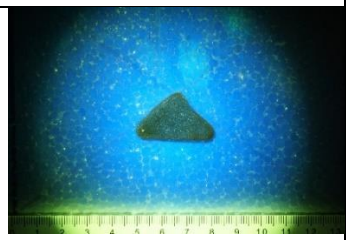
26			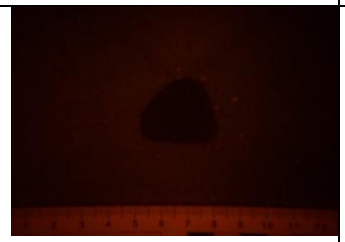	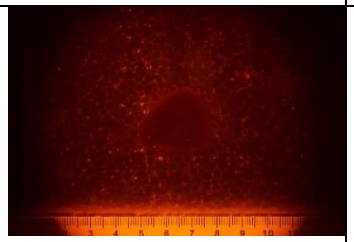	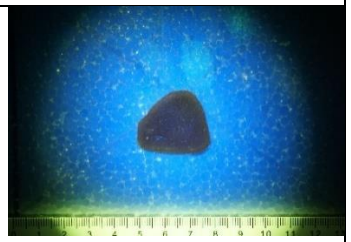
27			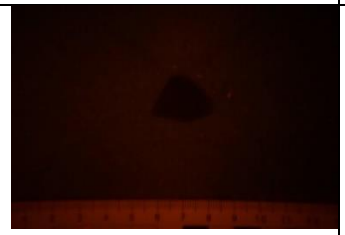	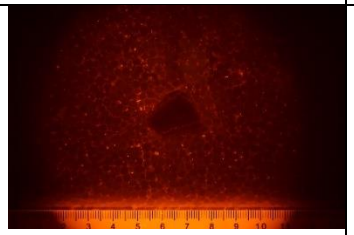	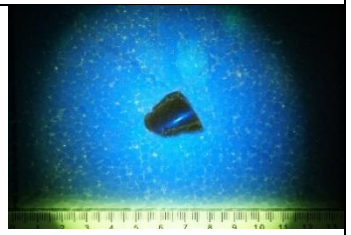

23.2.1- QUANTITATIVE ANALYSIS

Bar charts 181-183 below, describe the average fluorescence level of each examined non-bone control (arranged from highest fluorescence level to the lowest) when photographed in the terrestrial and underwater contexts using the Hammerhead light with the orange filter (1/3s exposure time). As with most comparisons within this thesis, the terrestrial fluorescence levels were higher compared to the tap water, as the terrestrial results produced an average of 79 and the underwater an average of 47 when incorporating the entire dataset. However as mentioned previously, four items could not be photographed underwater due to being buoyant, therefore this comparison is not entirely reflective. Once the terrestrial data for stick 2, tree bark, fresh leaf, and old leaf are removed, the terrestrial fluorescence average is reduced to 75 highlighting a decrease of 47 (37.8%) between the two contexts.

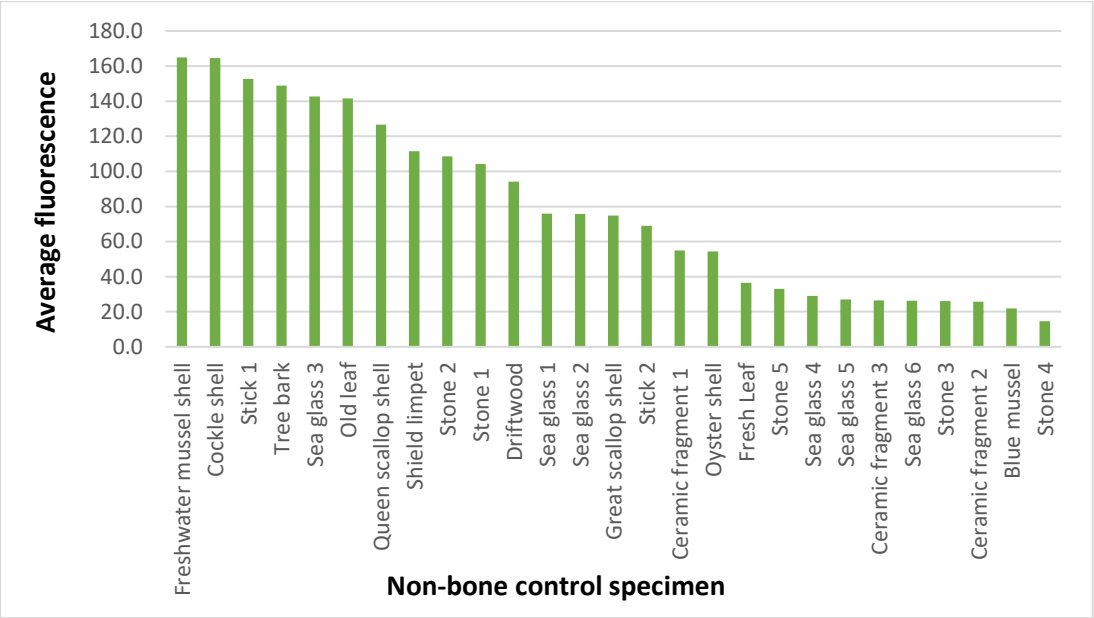

Figure 181: Average terrestrial fluorescence level of each non-bone control (arranged from highest fluorescence level to the lowest), photographed using the Hammerhead ALS and orange filter at 1/3s

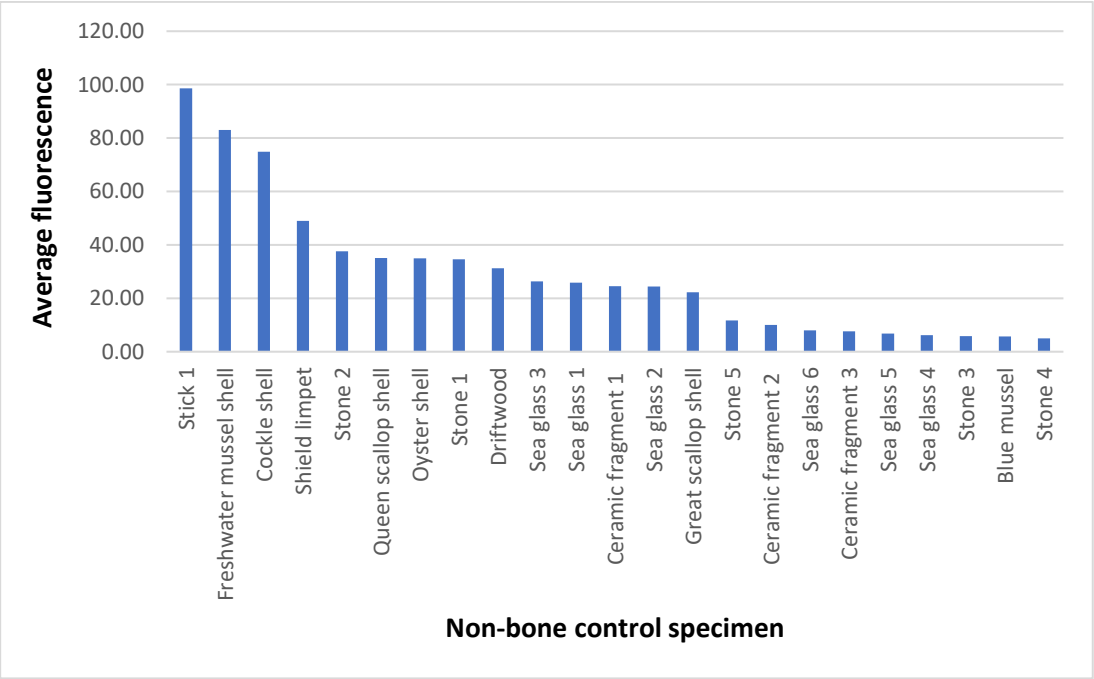

Figure 182: Average underwater fluorescence level of each non-bone control (arranged from highest fluorescence level to the lowest), photographed using the Hammerhead ALS and orange filter at 1/3s.

When comparing the fluorescence levels of individual items, the freshwater mussel shell produced the highest fluorescence intensity within the terrestrial Hammerhead dataset of 164.7, and lowest fluorescence was emitted by stone 4 at 14.7, a difference of 150.2. In contrast, in the aquatic fluorescence data, the highest fluorescence level of 120.9 was exhibited by stick 1, and the lowest of 8.8 also emitted by stone 4. The largest individual

difference in fluorescence intensity was experienced by stone 3, which lost 12.6 (48.3%) of its overall fluorescence intensity once submerged in tap water. The lowest reduction was observed in the fluorescence levels emitted by stick 1, which reduced from 152.7 to 120.9, a loss of 31.8 (20.8%).

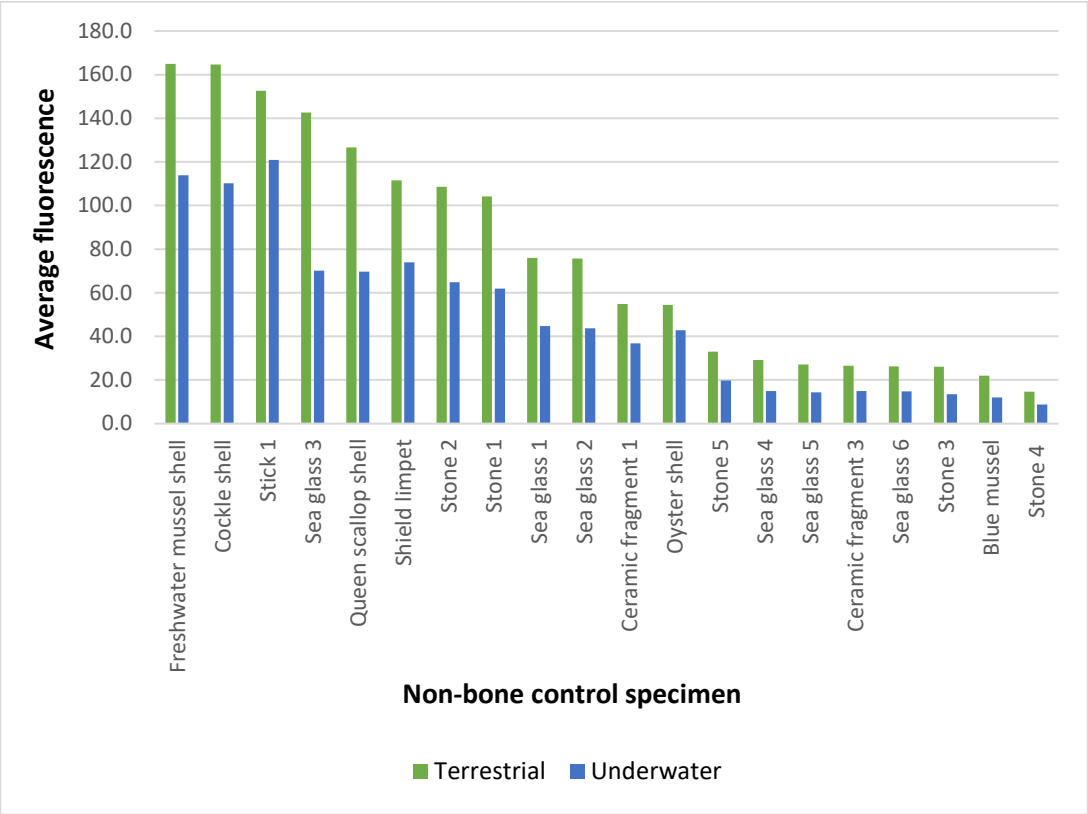

Figure 183: Comparison of average underwater and terrestrial fluorescence level of each non-bone control, photographed using the Hammerhead ALS and orange filter at 1/3s.

In keeping with fluorescence trends noted in the previous chapters, the Crime-lite 2, coupled with the orange filter in the terrestrial environment, produced higher fluorescence results compared to the Hammerhead. Ceramic fragment 2 generated the lowest value of 15.3, and the cockle shell produced the brightest fluorescence level of 207.4. Interestingly the non-bone objects exhibiting the highest and lowest fluorescence levels, varies between the Hammerhead and Crime-lite 2 ALS groups. This observation reinforces the theory that ALS wavelength and filter combination is crucial for optimised fluorescence visualisation, as well as the composition of the material under observation. Both light sources used in this PhD study, utilise the same region of the electromagnetic

spectrum, but due to differences in wavelength specificity, as well as technical specifications, the fluorescence results vary, despite examining the same subjects. Bar plot 184 below illustrates a comparison between the terrestrial fluorescence of the Crime-lite 2 and the Hammerhead, when observed with the orange filter, sorted into descending order according to the Crime-lite 2 results. Although the higher levels of fluorescence produced by the Crime-lite 2 were expected, the fluorescence levels generated by the Hammerhead do not follow the same trend as the Crime-lite 2, which was unexpected. For example, the driftwood control produced a fluorescence result of 94.2 when using the Hammerhead ALS but recorded a fluorescence value of 168.9 when exposed to the Crime-lite 2, making it the third highest result in the Crime-lite 2 dataset. Conversely, sea glass 3 produced an average fluorescence of 142.7 during Hammerhead excitation but only 116.4 when exposed to the Crime-lite 2. These quite major differences are most likely due to the different chemical composition in the control specimens responding differentially to slightly different ALS wavelengths.

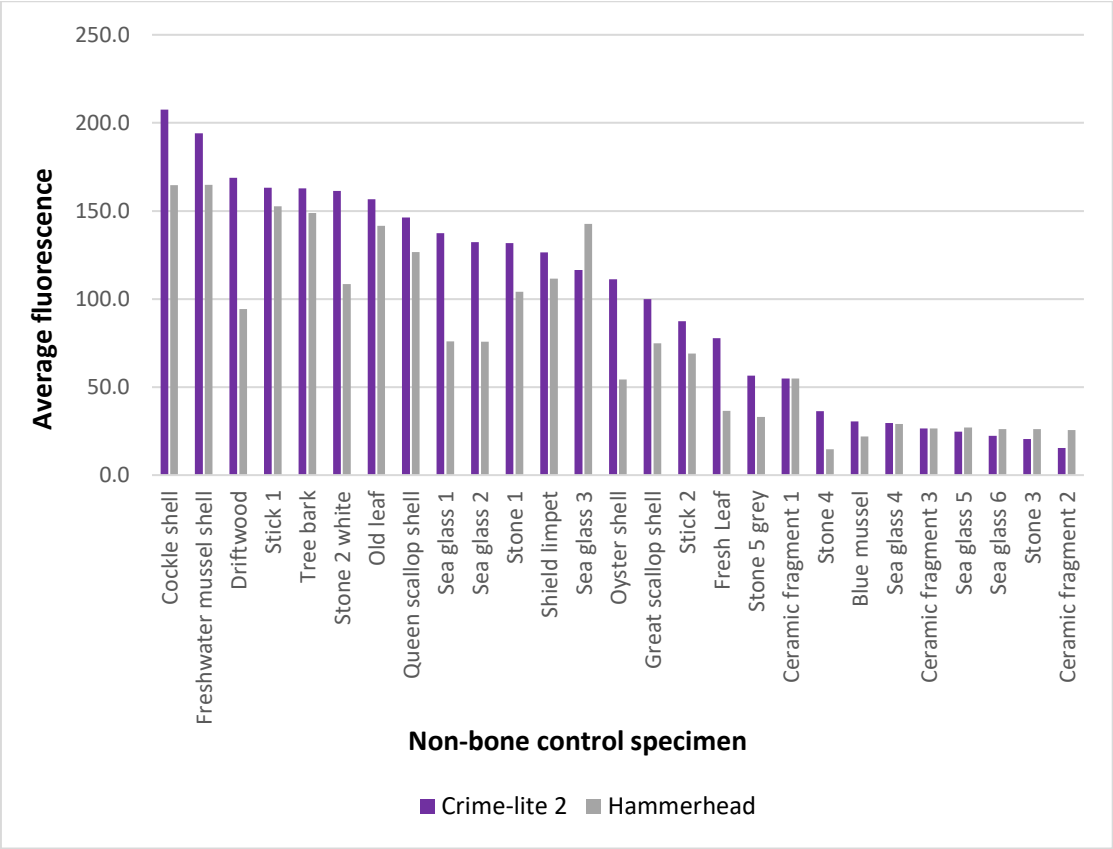

Figure 184: Comparison of average terrestrial fluorescence level of each non-bone control, photographed using the Hammerhead ALS and Crime-lite 2, coupled with the orange filter at 1/3s.

This interpretation is supported when comparing the terrestrial fluorescence results of the Crime-lite 2, when photographed with the orange and yellow filters, as displayed in chart 185 below. The data was sorted from highest to lowest according to the results obtained using the orange filter. Based on the analysis conducted in previous questions the higher levels of fluorescence observed in the yellow data were expected, but as seen in the Crime-lite 2 to Hammerhead ALS comparison, there are obvious disparities in the distribution of fluorescence intensity between the control specimens. More specifically all three ceramic fragments exhibited drastically higher fluorescence values when viewed with the yellow filter compared to the orange. For example, visualisation with Crime-lite 2 and the orange filter produce a fluorescence result of 54.8 for ceramic fragment 1 but rose to 252, a difference of 197.2, when examined with the yellow filter. For ceramic fragment 2 and the orange filter only produced a fluorescence value of 26.4 whereas the yellow filter a fluorescence intensity of 218.2, an increase of 191.8.

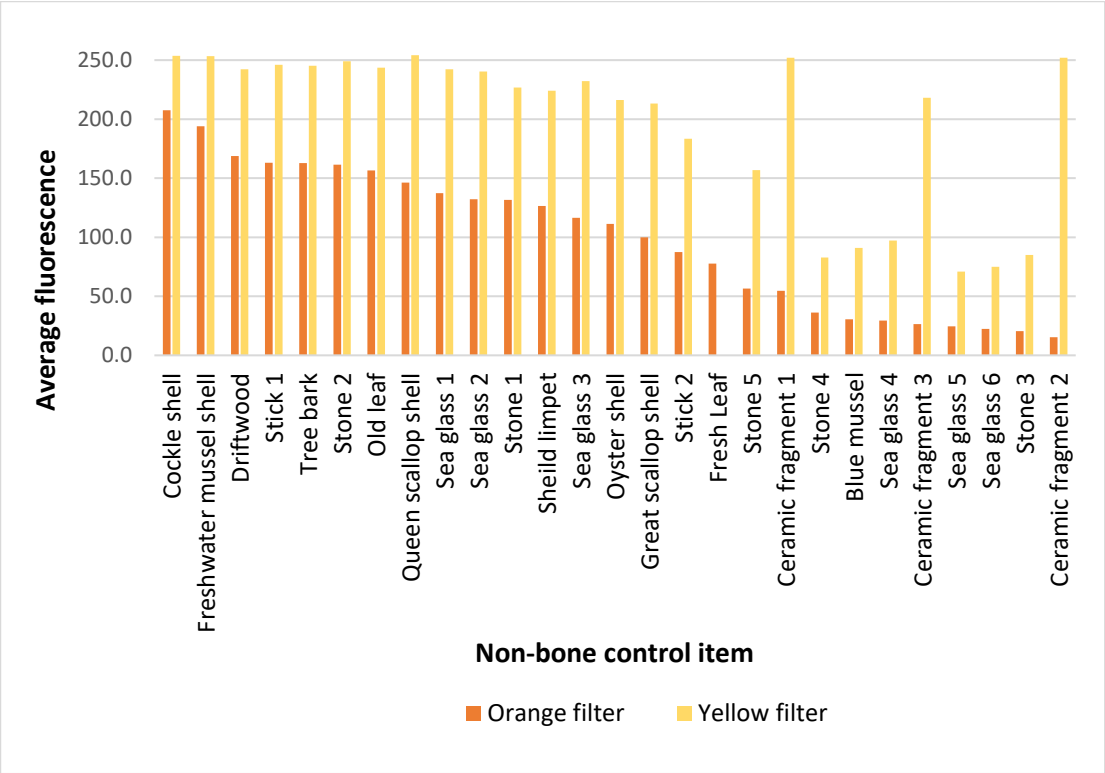

Figure 185: Comparison of average terrestrial fluorescence level of each non-bone control, photographed using Crime-lite 2, and the orange and yellow filters at 1/3s.

23.2.2- VISUAL EVALUATION

The ceramic fragments were retrieved from a North Yorkshire beach; therefore, no provenance information was available. However, from visual examination there are obvious differences in colour and texture. Ceramic fragment 1 is predominantly white in colour with a smooth texture and a crackle like glaze, whereas ceramic fragment 3 is an orangey/red with a more porous, coarse texture. The visual table below (table 41) displays the natural appearance of the ceramic fragments alongside the relevant fluorescence images obtained with the orange and yellow filters in conjunction with the Crime-lite 2. The fluorescence photographs further highlight how the different materials respond to ALS stimulation, and the importance of selecting the correct wavelength.

Table 41: Visual comparison of fluorescence levels of ceramic fragments 1 and 3, produced using the Crime-lite 2 at 1/3s exposure time with the orange and yellow filters.

Photograph	Ceramic fragment 1	Ceramic fragment 3
Natural	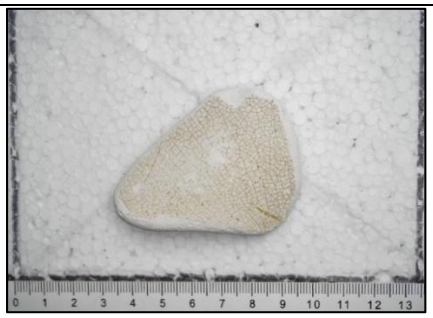	
Orange	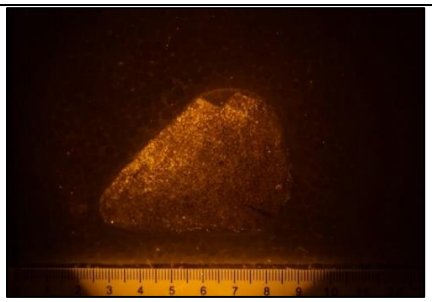	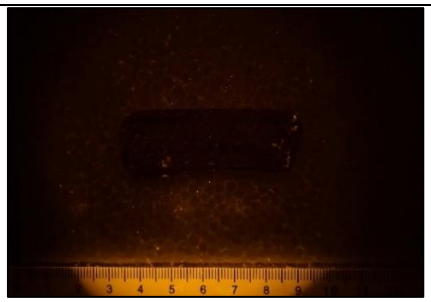
Yellow	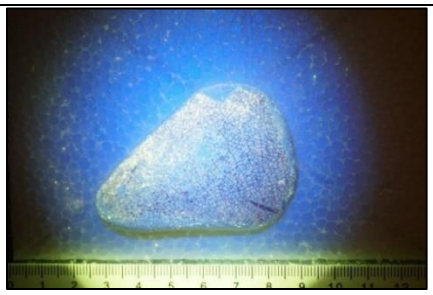	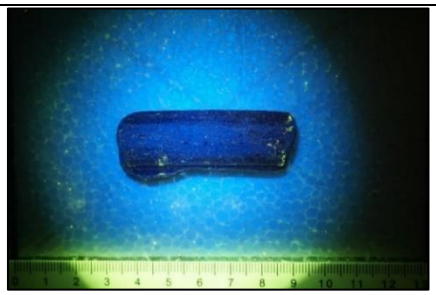

When exposed to the Crime-lite 2 and the orange filter the ceramic fragments appear dark, especially ceramic fragment 3 which is almost indistinguishable from background polystyrene. Fragment 1 emits slightly stronger levels of fluorescence, that appear confined to the glazed areas of the specimen, particularly at the apex of the shard where the glaze is absent, and consequently so is the fluorescence. These observations infer that the glaze most likely has a different chemical composition compared to the ceramic underneath. In pottery, glazes are used for decoration and to provide some protection against breakage [501], therefore it is reasonable to suggest there may be additional components in the glaze that is not present in the underlying ceramic. Common ingredients used to colour glazes include metal oxides such as iron, cobalt, copper, and chrome [502], which can generate autofluorescence depending on composition and concentration [503]. Without knowing the age and composition of the ceramic

fragments it is not possible to make further interpretations. In addition to this, as the glaze has a cracked appearance, although it is unclear whether this was the result of manufacture or acquired during submersion, these cracks could offer recesses for the accumulation and proliferation of bacteria, which can also produce autofluorescence [504], thus potentially contributing to the fluorescence seen.

Alternatively, the yellow filtered images appeared much brighter compared to the orange filter, which explains the substantial fluorescence levels calculated by the OFC. However, visual examination of the fluorescence images revealed that both ceramic fragments were not fluorescing as much as the OFC figures suggest. Ceramic fragment 3 appears dark against the background, and almost absent of fluorescence, and ceramic fragment 1 exhibits a similar level of fluorescence noted in the orange filtered photograph, but overall, also appeared much brighter.

Based on these images, it is suggested that the yellow filter delivered incomplete filtration of the incident wavelengths, an issue that was highlighted previously in chapter 21.3, and is the result of the broad 420-470 nm excitation range. This assessment is expounded by the high saturation of blue colour in the images, with a periphery of yellow, and the intense brightness, which can be attributed to general illumination rather than fluorescence. The OFC measures the brightness of images and as such cannot discriminate between fluorescence and other forms of light, including over exposure and illumination. This can therefore augment some results, as seen in the yellow filter dataset, and theoretically introduce misleading results and/or false positives. In retrospect, measurement of the filters prior to examination may have been able to provide a baseline result from which to help account for this overexposure and normalise the results.

This is a potential limitation of the OFC quantification methodology, but as the software does not alter the original fluorescence photograph, it would still be available for manual observation and assessment. This was a deliberate feature included in the application in order to comply with forensic science protocol, of a transparent record of demonstrable actions undertaken during the analysis of a piece of evidence, thus enabling critical review and retrospective analysis if required. It would be recommended that final identification would always be based on expert opinion, with the OFC providing a

quantitative tool to support these decision-making processes. Future OFC developments to help overcome the issue of potential false positives could be the implementation of features such as error messages to alert users to incompatible wavelength and filter combinations, to highlight fluorescence results that fall outside expected thresholds, and/or the inclusion of a reference library or trouble shooting gallery for assistance with identification. As the OFC is a novel application at the beginning of its development, there is still substantial room for improvement, but overall has proven successful during this PhD project, by providing an objective, quantitative approach for fluorescence analysis, which has not previously been conducted in this context.

Other potential contributors to the overexposure exhibited in the yellow filtered photographs could originate from the photography configuration. As the Crime-lite 2 is a powerful ALS, the positioning of the light in relation to the specimen may not have been optimal. Although the standardised distance was determined based on previous methodologies and method development discussed in section A, it distance was calibrated based on the characteristics of porcine bone, as this was the primary subject of analysis. Conversely, the non-bone dataset comprised of specimens that exhibited a range of sizes, colours, textures, and morphologies, which ultimately led to some variation in positioning, and differential interactions with the ALS wavelengths. For example, larger sized objects and those with projected surface morphology would have shortened the distance between the light source and the specimen, potentially leading to more intense ALS coverage and over exposure. Similarly, objects with a more reflective surface may have reflected some light wavelengths. These inferences are further demonstrated when examining the fluorescence results of the cockle shell (one of the control items that produced one of the highest fluorescence values) and the queen scallop shell.

The fluorescence results for the cockle shell and the queen scallop shell are summarised in table 42, including terrestrial images obtained using the Crime-lite 2 with the orange and yellow filters, and when using the Hammerhead ALS coupled with the orange filter in submerged and terrestrial contexts.

Table 42: Visual comparison of fluorescence levels of the cockle and queen scallop shells, produced using both light sources and all photography configurations.

ALS, filter, and deposition context	Cockle shell	Queen scallop shell
Natural		
Hammerhead Terrestrial Orange filter		
Hammerhead Submerged Orange filter	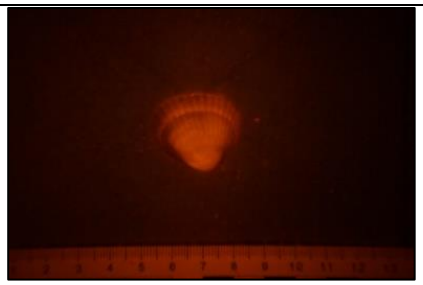	
Crime-lite 2 Terrestrial Orange filter	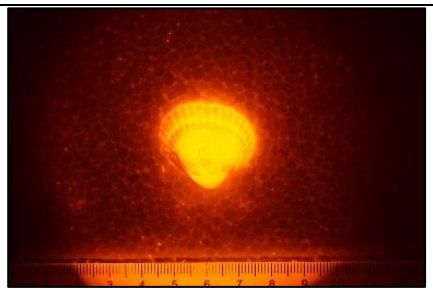	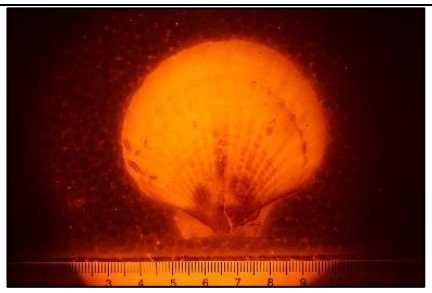
Crime-lite 2 Terrestrial Yellow filter	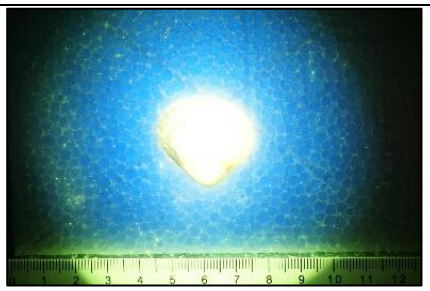	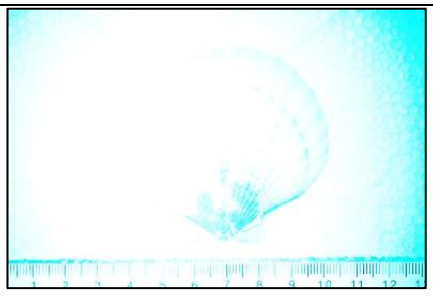

These images present a clear distinction between the fluorescence levels produced by the Hammerhead light source and the Crime-lite 2. In keeping with the general observations noted in previous paragraphs the cockle shell and the queen scallop both fluoresce under ALS stimulation, including underwater, with substantially higher levels of fluorescence observed in the Crime-lite 2 photographs. Furthermore, the yellow filtered images appear overexposed, characterised by the bright white colour in the centre of the frame, and loss of surface detail on the shells. Although the cockle shell was one of the smallest control items, it had a projecting profile in contrast to the flat but larger scallop shell. Subsequently, the cockle shell exhibited the brightest fluorescence intensity at the centre of its domed form, whereas the scallop shell experienced a much more complete coverage of light, which led to most of the scallop shell being obscured. These results reiterate that the yellow filter may not have been completely compatible with the Crime-lite 2, as the excessive amount of light indicates partial filtration of the excitation waves.

All photographs in this control group were taken using the same exposure time of 1/3s, to facilitate direct comparisons. The range of in quality of results demonstrates how intrinsic factors such as size, shape and colour can influence the fluorescence result, but also the model of the ALS and selected exposure time. Although the 1/3s image taken using the Crime-lite 2 and the orange filter was arguably over exposed, typified by the loss of shell detail and light penetration of the polystyrene background, when the same item was photographed at a much faster exposure time of 1/13s, these artefacts were reduced, and the fluorescence much clearer (figure 186). Similarly, the 1/3s terrestrial photograph of the cockle shell taken with the orange filter and the Hammerhead ALS (figure 187), produced homogeneous fluorescence, and distinct contrast with the polystyrene sheet. However, compared to the similar Crime-lite 2 photograph the fluorescence levels are lower, therefore a longer exposure time of 1.3s allows light to enter the camera for longer and boost the overall fluorescence appearance, albeit with some sacrifice of surface definition.

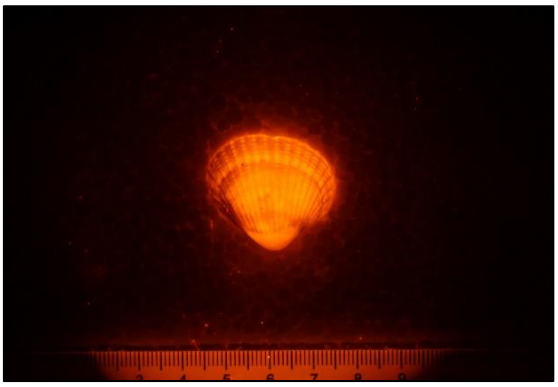

Figure 186: Terrestrial fluorescence of the cockle shell produced using the Crime-lite 2 and orange filter at 1/13s exposure time.

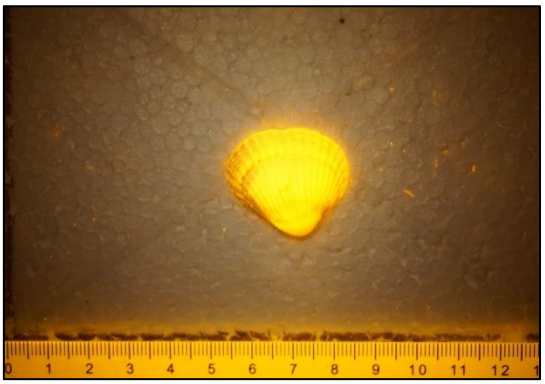

Figure 187: Terrestrial fluorescence of the cockle shell produced using the Hammerhead ALS and orange filter at 1.3s exposure time.

Consequently, it is suggested that the production and documentation of ALS is more nuanced than simply an absence or presence of fluorescence dictated by the volume of a specific compound but is instead a combination of factors including selecting a specific wavelength, model of ALS, and the correct complimentary barrier filter to optimise how the light will interact with the material under examination. It is therefore unlikely that there is a single methodology of coloured filter, ALS wavelength, and exposure time, suitable for all osseous searches, but recommendations based on the topography of the search area and target of examination could be possible. Furthermore, recommendations could be adapted based on the desired outcome, i.e., locating and identifying human remains in the field, or documentation of bone fluorescence at the scene or in the laboratory. In the future, these recommendations could form the basis of professional documentation, and/or be available through the OFC app.

The seashell fluorescence was an unexpected result. Christensen et al (2014) reported that bones and teeth could easily be differentiated from other debris such as shells, rocks and beach glass, using a 450 nm Rofin PoliLight-Flare™ Plus and a yellow filter, as these inorganic materials produced a dark, or bluish-purple appearance in contrast to the bright orange/yellow emissions from bone [135]. However, the findings in this PhD contradict this assessment, as fluorescence was detected in shells, ceramics, rocks, and sea glass, when using both the orange and yellow filters, and when using ALS light sources.

Calcium carbonate is the major constituent of bivalve mollusc shells such as mussels, clams, cockles, and scallops, referred to as nacre [505]. Shells form over time, as layers of nacre, in the form of crystalised aragonite or calcite (stable polymorphs of calcium carbonate) [103], are deposited through continuous exposure to the aquatic environment [506]. As calcium carbonate is a carbonate (a salt comprised of carbon and oxygen) [507] and consequently inorganic in composition [508], therefore the shell specimens in this study were not expected to fluorescence, in line with the theory that protein is most likely responsible for autofluorescence. However, the calcium carbonate nacre found in shells is an example of a biomineral [506], an inorganic-organic composite, where layers of mineral are interspersed with layers of organic matrix [508]. One of the most common proteins found in this organic matrix is hemocyanin, which contains tyrosinase, an enzyme that catalyses pigment production through oxidation of tyrosine [505].

The fluorescent properties of tyrosine were discussed in length during chapter 9.3, therefore its presence in shell colouration may provide some explanation as to why fluorescence was detected in some of the shells in this dataset. In total, seven different shells from different species were examined, and exhibited a variation in pigmentation. In addition to the primarily white colour of the cockle, scallop, and freshwater mussel shells, a blue mussel shell (fig. 188) and a shield limpet (Fig. 189) were also included, exhibiting deeper pigmentation in blue and orange.

Figure 188: Blue mussel shell (natural light)

Figure 189: Shield limpet (natural light)

When the fluorescence levels of the shells were compared (Hammerhead light, 1/3s, orange filter), a clear trend of higher fluorescence levels in the lighter pigments can be

seen (fig. 190). The shield limpet produced higher than expected results, but this was most likely the result of the white colouration in the centre of the shell.

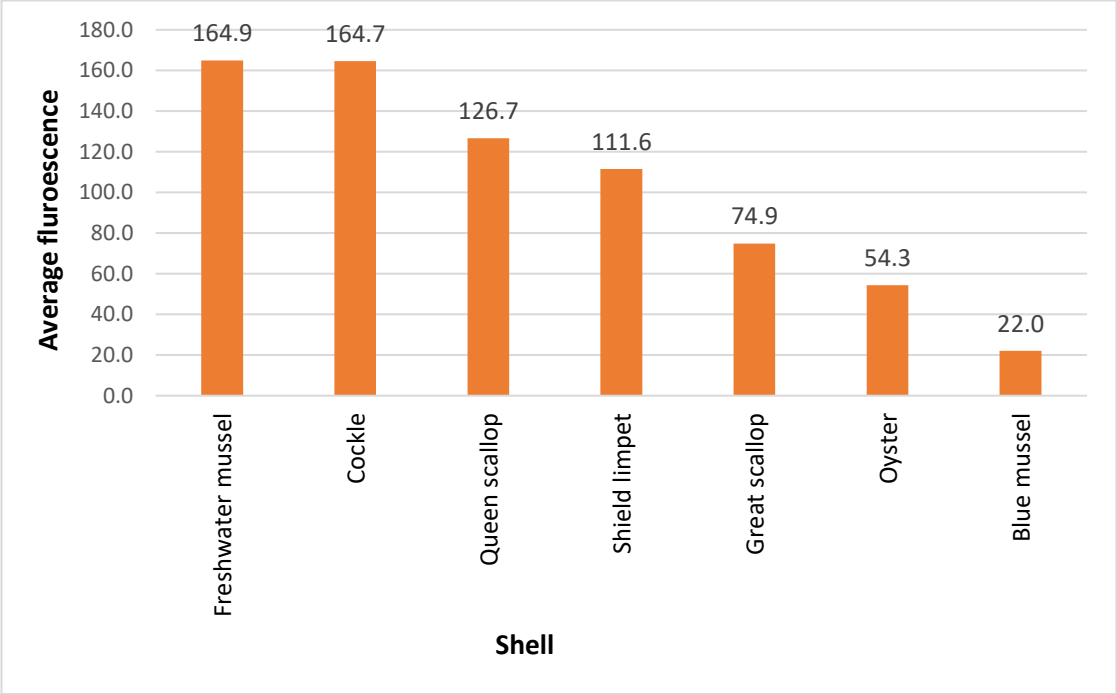

Figure 190: Comparison of terrestrial fluorescence levels of the seven shell specimens, produced using the Hammerhead light, orange filter, and 1/3s exposure time.

It is unclear whether the whiter pigmentation in the more fluorescent shells was the result of natural colouration or taphonomic alteration, such as bleaching or erosion, and although this sample size of seven shells is very small, these findings do pose potential ramifications for ALS identification of bone. Taphonomic degradation such as bleaching and erosion are prevalent in skeletal remains , due to extended PMI and sustained exposure to taphonomic agents (as explained in chapters 8.3 and 9.0), consequently, future work assessing differentiation between bone of varying preservations, and other environmental items of varying colour, size, and morphology, would provide deeper understanding of how taphonomic degradation and colour could influence the application of ALS to search for bone in real-world crime scenes. Christensen et (2014) reportedly investigated thirteen different shells during their laboratory comparison, including gastropod shells, bivalve shells, and echinoderm shells, reporting that virtually no fluorescence was detectable, but did not elaborate any further regarding fluorescence differences between the species [135]. No further information regarding

the composition of these shells was reported and therefore it's not possible to directly compare the results to the findings discussed here. However, what can be suggested is that interpretation of their results was hindered by the lack of fluorescence quantification, with all interpretations based on observations, and the absence of provenance data.

Christensen et al (2014) also examined eight examples of beach glass during their experimentation and concluded that it did not fluoresce when exposed to 450 nm blue light coupled with a yellow filter [135]. The terms beach glass and sea glass are used interchangeably and refer to fragments of glass recovered from beaches [509]. Typically, sea glass originates from common household items such as bottles, jars, and ceramics, and has a smooth, frosted appearance from being tumbled in the sea [509, 510].

Glass is a composite material made primarily from sand and calcium carbonate, which has been heated to a high temperature to form a liquid [511]. This liquid is then cooled, often rapidly, to consequently form glass. Additives such as lime-soda, boron oxide, lead oxide, and pigments, are added during this manufacturing process to either accelerate the production or imbue the glass with different characteristics and finishes [510, 511]. Soda-lime is one of the most common additives used to lower the cooling point of the glass and therefore speed up production [512]. Boron oxide is used to increase durability so is more often associated with cook ware or laboratory glass ware [511], and lead oxide is used to increase the reflective effect of glass and/or enable greater absorption of radiation, making it suitable for eyeglasses and thermometers [510]. Most sea glass is soda-lime and contains silicon dioxide, sodium carbonate, and calcium carbonate [510, 513]. This type of glass is commonly used to manufacture bottles, household glassware, and windowpanes [514]

The addition of Iron sulphide gives glass a brown colour, commonly seen in beer bottles [511]. This colour absorbs nearly all radiation and wavelengths of 450 nm and shorter [513], which helps protect products such as beer and drugs from UV degradation during transportation and storage [510]. Iron oxide can add a bluish-green colour to glass and absorbs wavelengths strongly in the UV spectrum and weakly between 420 - 440 nm in the visible electromagnetic spectrum [515]. The addition of chromium to glass can also produce a strong green colour but will manifest a range of optical properties depending

on the glass matrix it is combined with [516]. In general, the higher the concentration of these compounds the darker the colour [510].

Consequently, although the basic composition of glass may not be inherently fluorescent, aside from possible contamination from sand (silicon dioxide), the colour of glass may have implications for possible fluorescence emissions [503]. In this control dataset six examples of sea glass were examined, ranging from colourless, to pale green, dark green, brown, and dark brown, as shown in figure 191. Further photographs demonstrating a side-by-side comparison of all six shards of glass photographed terrestrially with the orange and yellow filters and the Crime-lite 2 are displayed in figures 192-193, and aquatic and terrestrial images visualised with the orange filter and Hammerhead light can be seen in figures 194-195. The average terrestrial fluorescence results for the sea glass control samples, generated using the Hammerhead light source are compared in the bar plot in figure 196. The fluorescence levels were calculated based on the photographs of the individual glass shards, rather than in the side-side configuration, to ensure standardised quantification.

Figure 191: Visual comparison of the six sea glass specimens, photographed under natural light

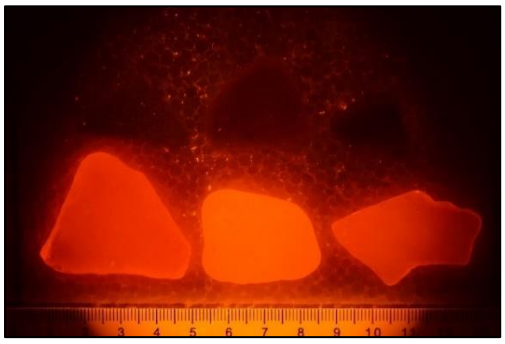

Figure 192: Visual comparison of terrestrial fluorescence of the six sea glass specimens, photographed using the Crime-lite 2, orange filter, and 1/3s exposure time.

Figure 193: Visual comparison of terrestrial fluorescence of the six sea glass specimens, photographed using the Crime-lite 2, yellow filter, and 1/3s exposure time.

Figure 194: Visual comparison of terrestrial fluorescence of the six sea glass specimens, photographed using the Hammerhead ALS, orange filter, and 1/3s exposure time.

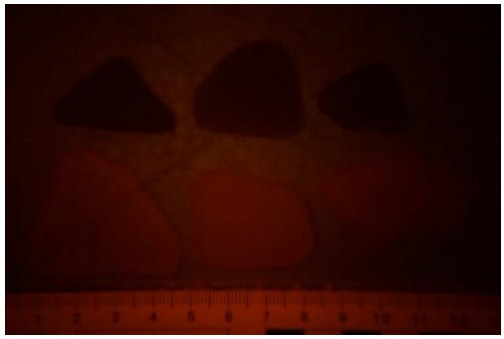

Figure 195: Visual comparison of submerged fluorescence of the six sea glass specimens, photographed using the Hammerhead ALS, orange filter, and 1/3s exposure time.

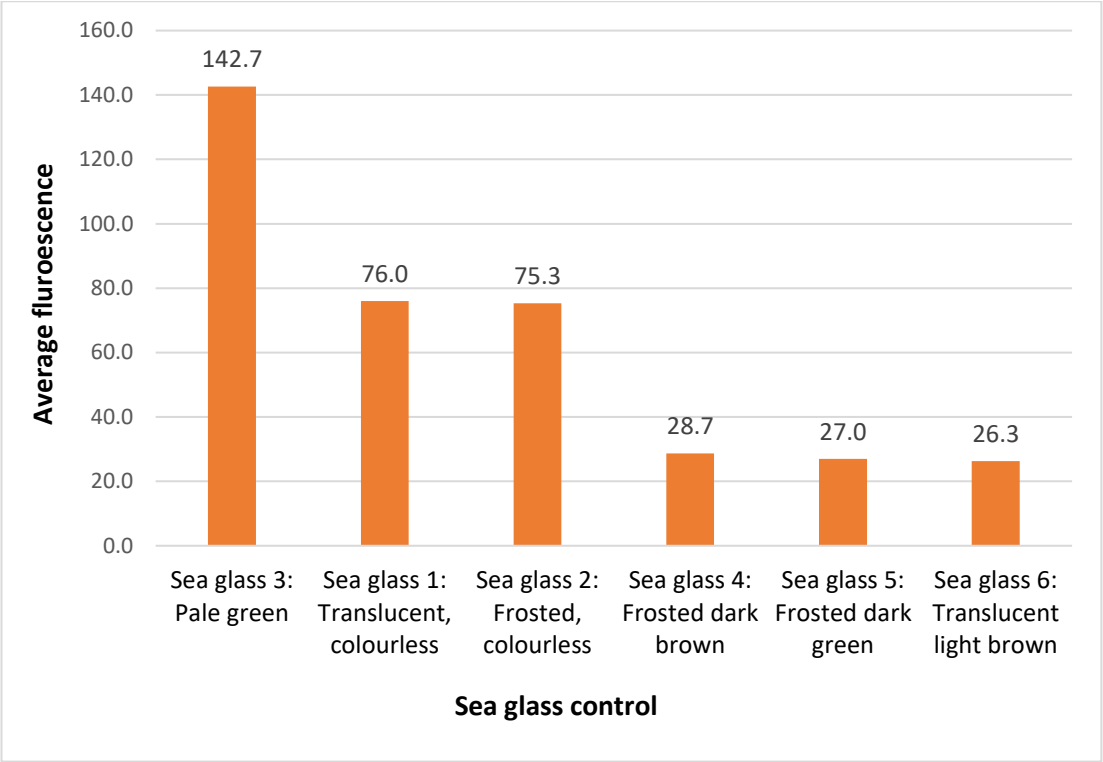

Figure 196: Comparison of terrestrial fluorescence levels of the six sea glass specimens, produced using the Hammerhead light, orange filter, and 1/3s exposure time.

The darker coloured glass samples exhibited very low levels of fluorescence, with the dark brown, dark green, and brown shards all exhibiting less than 30 (28.7, 27, 26.3 respectively). In contrast, the pale green sea glass control produced a very high fluorescence value of 142.7 when photographed in air with the orange filter and hammerhead light, which was surprisingly higher than the Crime-lite 2 average fluorescence result obtained under the same conditions, which produced a value of 116.4. The colourless glass samples exhibited fluorescence values almost half the intensity exhibited by the pale green glass, as sea glass 1 produced a fluorescence value of 76, and 75.3 for sea glass 2. These results were also echoed when using the yellow filter and the Crime-lite 2, although an element of overexposure is still present. Although the fluorescence was substantially lower in the submerged specimens, the pale glass examples are still visible, and differentiation may be boosted if using a more powerful light source.

The low fluorescence results of the dark glass samples support the findings by Christensen et al (2014) [135], but the intense fluorescence detected in the pale and colourless glass do not. It could be that all the glass samples examined by Christensen

et al (2014) were darker glass. The range of glass deposited on beaches will vary around the world and will be determined by the composition and manufacture of local products, as well as the chemical and mechanical characteristics of the marine environment [513]. Although the location of Christensen et al's (2014) study, and the provenance of the environmental objects, were not disclosed, the inclusion of USA based institutional correspondent addresses suggests it was not based in the UK. Consequently, it is likely there would be variation in glass manufacture as well as the prevalence in different glass compositions. However, as no photographs or other details about the glass samples were provided in the publication it is not possible to make any deeper interpretations.

In this study, it can be suggested that the dark glass samples absorbed most of the ALS wavelengths, due to the likely addition of iron sulphide, as described previously. The high fluorescence level emitted by the pale green sample, suggests the possible presence of iron oxide or chromium, which both possess fluorescence capabilities [104, 516]. However confirmatory elemental analysis would need to be conducted. On the contrary, the colourless glass samples most likely did not contain any additional metals or oxides, due to the lack of perceivable pigment However, the most common method of making flat glass in the UK, such as for windows, is the floated glass method, which may have contributed to the fluorescence levels seen.

Floated glass is made by pouring molten glass into a bath of liquid tin [511]. The glass consequently floats on top of the metal, resulting in an almost perfectly flat pane of glass once cooled [514]. Historically, flat glass in the UK used to be produced by rolling, but this method often led to imperfections and distortions in the final product due to inconsistent rolling pressure and uneven cooling [512]. Consequently, almost all flat glass in the UK is now made almost exclusively using the float method [514], and most significantly, the exposure to the tin during manufacture infuses the glass with fluorescent properties, which can then be excited under ALS [514]. This is a method already deployed at crime scenes, and in the laboratory, to search for trace glass evidence [514], and thus could be a possible source of fluorescence in the colourless glass samples examined here.

23.2.3- ORGANIC AND INORGANIC COMPARISONS

Part of this research question was to investigate the fluorescence levels of environmental items that are commonly confused with bone. Organic items such as wood can mimic the colour and texture of bone, including the characteristic spicules associated with trabecular bone. This effect is exaggerated when bone is altered by the taphonomic environment as discussed in chapter 8.3. The surface texture and colour of stone also can intimate taphonomically altered bone, particularly bone that has been submerged in an aquatic environment, where the mechanical action of currents, waves, and scavengers, can erode morphology, increase porosity, and bleach the surface. Consequently, a selection of organic and inorganic specimens from the 27 non-bone control samples were examined, and the photographic fluorescence results for eight examples are displayed in table 43 below.

Table 43: Visual comparison of terrestrial fluorescence levels of four organic and four inorganic non-bone control samples, photographed using the Hammerhead light source, orange filter, 1/3s exposure time.

Fresh leaf	Bark
Stick 1	Driftwood
Stone 1	Stone 2
Stone 3	Stone 4

Fluorescence levels of common organic non-bone items were of particular interest as it is the organic component of bone that is thought to respond to ALS stimulation. Bar chart 197 below compares the average terrestrial fluorescence results of the eight control items in table 43, as produced by the Hammerhead ALS and orange filter, the Crime-lite 2 and orange filter, and the Crime-lite 2 with yellow filter, all captured at 1/3s exposure time (sorted according to the Hammerhead values). An aquatic comparison could not be carried out as most of the organic non-bone control items floated when immersed in the tap water, as explained previously.

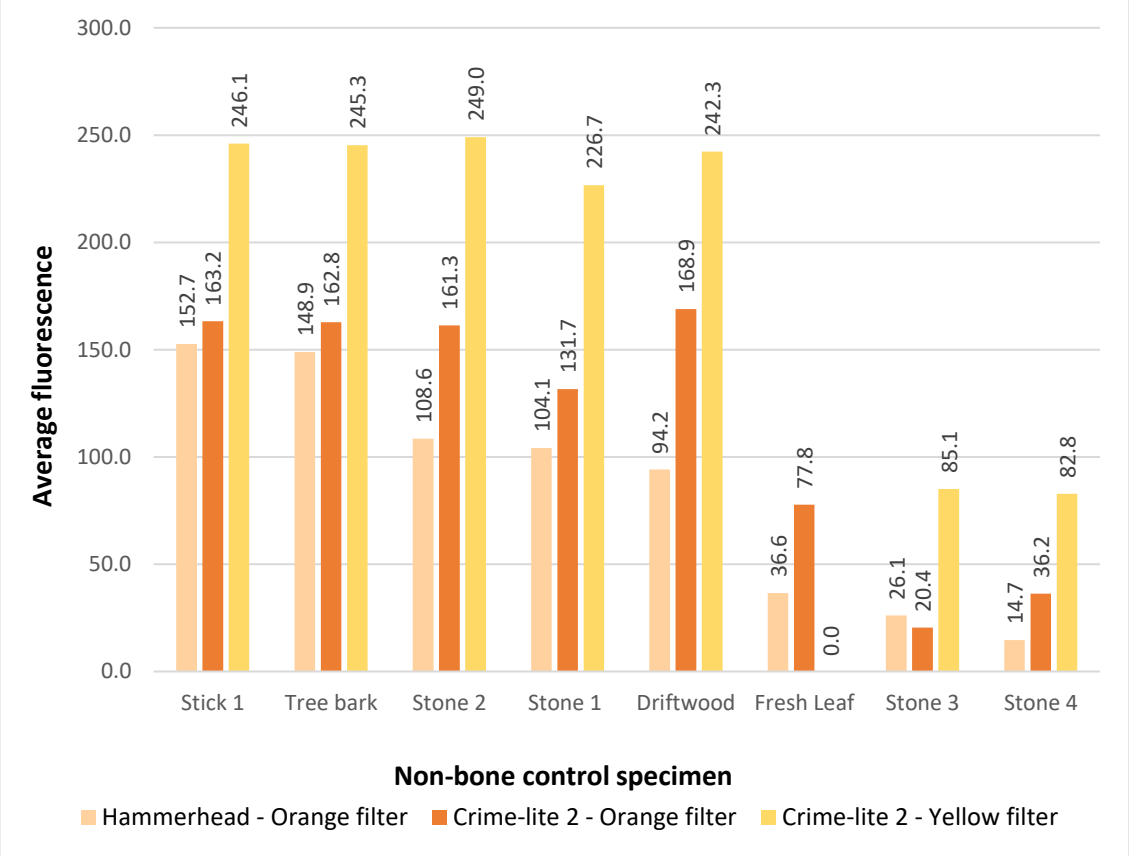

Figure 197: Average terrestrial fluorescence results of the eight control items in table 43, as produced by the Hammerhead ALS and orange filter, the Crime-lite 2 and orange filter, and the Crime-lite 2 with yellow filter, all captured at 1/3s exposure time (sorted according to the Hammerhead values).

The results from this comparison demonstrated, that the organic items overall produced the highest levels of fluorescence across all ALS model and filter combinations, in keeping with the current hypothesis. However, stone 1 and 2 produced fluorescence levels higher than the driftwood and the fresh leaf, and comparatively higher than other

items in the wider non-bone dataset, such as the sea glass and shells. This result was not expected, as stone has a mineral composition, therefore very low fluorescence was expected. However, when comparing the four stone specimens under natural light (table 44), there are distinct differences in colour, with the two highest fluorescence intensities of 108.6 and 104.1 belonging to stone 2 and 1 respectively, which are white and orange/yellow in colouration. These result support the findings discussed in the sea glass and shell fluorescence results, indicating that the colour of an object, as well as its composition, most likely contributes to the production and visualisation of fluorescence, and therefore requires further research. Without analytical examination of the chemical composition of each of the non-bone items it is not possible to conduct further interpretations, particularly as the sample is deficient in organic control items compared to inorganic.

Table 44: Colour comparison of the four stone specimens from the non-bone control dataset, photographed under natural light.

Stone 1	Stone 2
Stone 3	Stone 4

A primary focus of this PhD was the use of ALS in underwater contexts, consequently most of the environmental controls analysed during this research question were marine

in origin, to enable a closer comparison with current literature. However, in retrospect, additional organic controls such as grass, mud, and other foliage, would have been beneficial to help explore terrestrial deposition, as well as better understand the implementation of ALS in more actualistic contexts. Consequently, this would be a key focus for future work. The fluorescence results from all control specimens, examined across all control research questions, are compared in chapter 34.5, alongside examples of fresh and macerated porcine bone to aid interpretation.

24.0 - SECTION B, QUESTION 3B: PORCINE COLLAGEN POWDER

24.1- RESEARCH QUESTION SPECIFIC METHOD

24.1.1- MATERIALS

A collagen control was created using Health Leads UK Ltd (Healthleads.co.uk) pure porcine collagen hydrolysate powder, embedded into clear epoxy resin, to act as a positive control. The porcine powder was embedded in resin to prevent the collagen powder from dissolving during underwater photography, and to ensure an even, standardised surface to fluorescence quantification.

1600 mg of porcine collagen powder was combined with 3ml of Easteverlast Crystal Clear Epoxy Resin and 1 ml of complimentary Easteverlast Crystal Clear Curing Agent and stirred slowly for 3 mins until fully combined. The solution was transferred to an oval silicon mould measuring 40 x 30 x 10 mm and left at room temperature for 24 hrs to harden. The final product can be seen in figure 198 below. A further control block made only of the epoxy resin (figure 199) of the same dimensions was produced to ensure any possible fluorescence from the epoxy resin could be taken into consideration when interpreting fluorescence results.

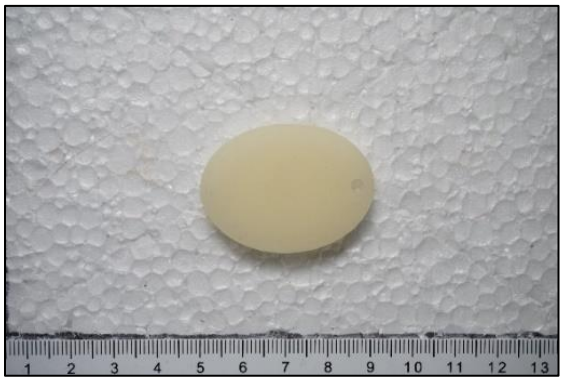

Figure 198: Porcine collagen powder embedded in epoxy resin to form a collagen control block.

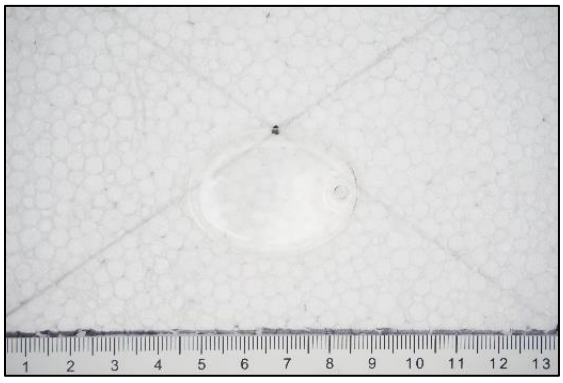

Figure 199: Epoxy resin only control block.

24.1.2 – METHOD

24.1.2a- PHOTOGRAPHY

The porcine collagen control block and epoxy resin only block was photographed in terrestrial and tap water contexts using the core methodology outlined in chapter 20.0, firstly under natural light with scale and then using the Hammerhead light. Photographs were taken in conjunction with the orange filter at 1/3s exposure time, using the camera settings and equipment configuration established in chapter 20.0.

24.1.2b- FLUORESCENCE

All images were processed using the OFC as outlined in section chapter 20.0.

24.1.2c- STATISTICAL ANALYSIS

Analyses focused on the quantification of fluorescence levels seen between deposition contexts, and between the resin and collagen powder, and to consequently contribute to the fluorescence scale in chapter 25.4.4.

24.2- RESULTS AND DISCUSSION

Table 45 below summarises the fluorescence results for the porcine powder embedded in epoxy resin, and the epoxy resin only controls. All fluorescence and OFC processed photographs can be seen in appendix 62, and all the calculated fluorescence values for each photograph and ROI are displayed in appendix 63.

Table 45: Visual table summarising the photographic fluorescence results of the porcine collagen powder and epoxy resin control blocks, photographed using the Hammerhead light in terrestrial and aquatic settings, with the orange filter at 1/3s exposure time.

Context	Embedded porcine collagen powder block	Epoxy resin only block
Natural	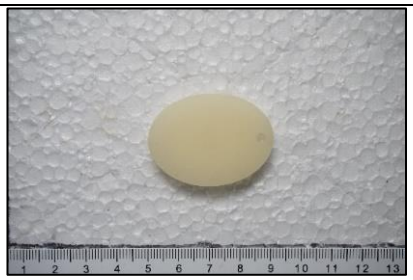	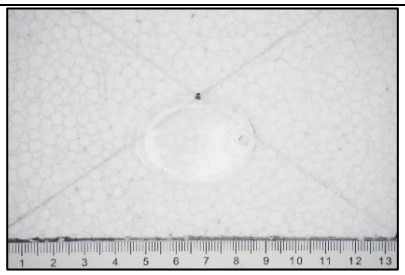
Terrestrial	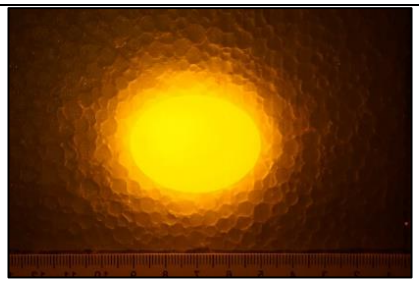	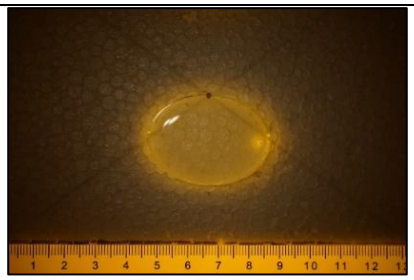
Underwater	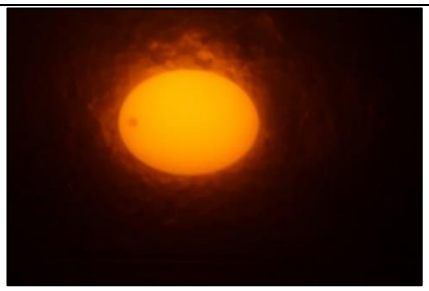	
Side by side embedded porcine collagen powder block and the epoxy resin only block		
Terrestrial	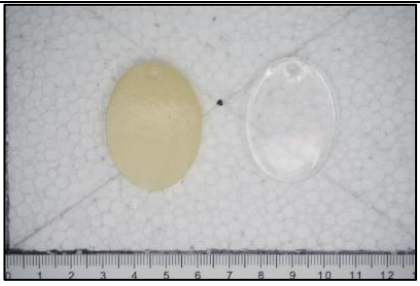	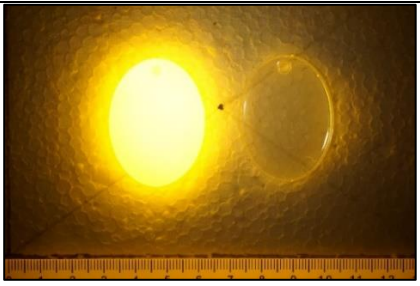

In keeping with expectations, the collagen powder produced very high fluorescence results in both the terrestrial (218) and tap water contexts (184.7), only exhibiting a difference of 33.3 (16.5%). The resin only block produced a higher than anticipated terrestrial fluorescence value of 141.7, as shown comparatively in figure 200 below.

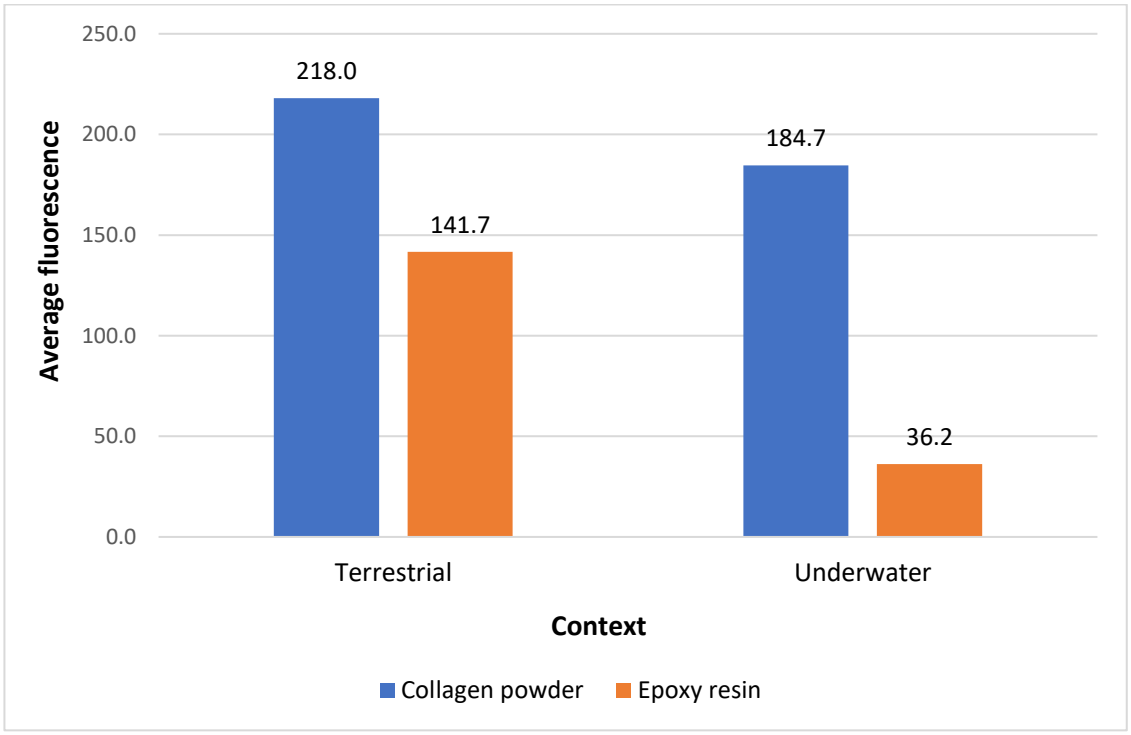

Figure 200: Comparison of terrestrial and underwater average fluorescence levels of the porcine collagen powder and epoxy resin only control blocks.

Initially it was thought that this may be due to residual collagen powder left inside the mould after making the collagen powder control. Therefore, another resin only control block was made in a different mould, of similar dimensions, and using the same protocol listed in the method. This square resin only block produced very similar levels of fluorescence as the original oval block, 142.1 in the terrestrial context, and 38.7 in the underwater environment (figures 201-203). It was therefore surmised that the high fluorescence response could be due to the chemical composition of the epoxy resin, although it was advertised as UV resistant when purchased. The more likely explanation could be that the fluorescence was the result of the transparent, shiny surface, and overall morphology causing reflections and scattering of light. This explanation is more compelling when scrutinising the fluorescence distribution within the terrestrial

fluorescence photographs of the resin only controls. The fluorescence was brightest at edges, where the resin is most dense and exhibits more complex topography, whereas the centre of the shape is almost transparent due to the flatter, smoother surface. This effect is mirrored in both the oval and square epoxy resin controls. This theory is further supported by the substantial reduction in calculated fluorescence once the blocks were submerged. The oval resin only block experienced a reduction of 105.5, and the square resin only block decreased by 103.4, as the greater density of water impeded the trajectory of the fluorescence wavelengths, but also absorbed or redirected scattered reflections.

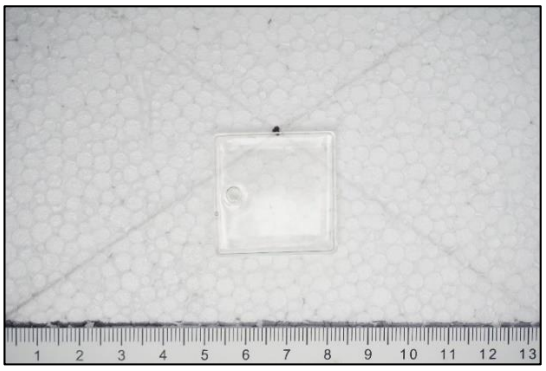

Figure 201: Square epoxy resin only control block, photographed under natural light.

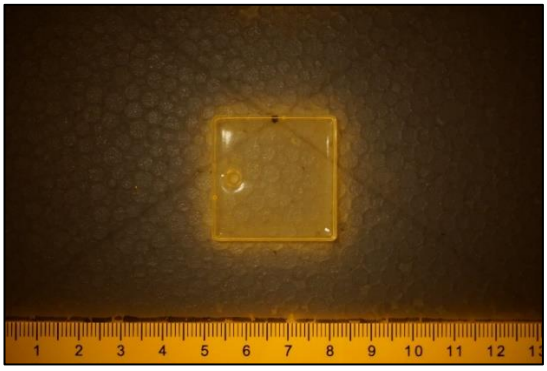

Figure 202: Terrestrial fluorescence of the square epoxy resin only control block, photographed with the Hammerhead ALS, orange filter, and 1/3s exposure time.

Figure 203: Submerged fluorescence of the square epoxy resin only control block, photographed with the Hammerhead ALS, orange filter, and 1/3s exposure time.

Subsequently, these findings support the hypothesis that porcine collagen does exhibit strong fluorescent properties when stimulated by blue light (450 nm) and photographed with an orange filter, in both terrestrial and submerged deposition contexts. Although a small proportion of the fluorescence recorded in this research question could be

attributed to the embedding medium, it is proposed that the high fluorescence results recorded in terrestrial context for the resin only blocks were primarily the product of light scattering precipitated by the transparency and block morphology. It is likely that this effect would have been negated in the porcine collagen powder block, due to overall increased opacity. Comparisons between all control specimens can be found in chapter 25.4.4.

25.0 - SECTION B, QUESTION 3C

DEMINERALISED AND DEPROTEINISED PORCINE BONE

25.1- DEMINERALISED BONE

25.1.1- MATERIALS

Six portions of fresh porcine bone (*Sus scrofa domesticus*) measuring 3 cm in length were cut from the diaphysis of three manually defleshed porcine ribs using a Dremel™ 3000 130 W Rotary Multi Tool, fitted with a diamond edge circular blade (figures 204 and 205). The ribs were obtained fresh from a local butcher and defleshed in accordance with the methodology outlined in chapter 20.0. Prior to demineralisation all bone chunks were weighed using a Brifit digital kitchen scale (0.05-500 g) and their length, width, depth, and anterior-posterior dimensions measured using Yakamoz electronic digital callipers (±0.1 mm). Table 46 displays the exact measurements of the six portions of porcine bone used in this research question.

Figure 204: Dremel™ 3000 130 W Rotary Multi Tool, fitted with a diamond edge circular blade

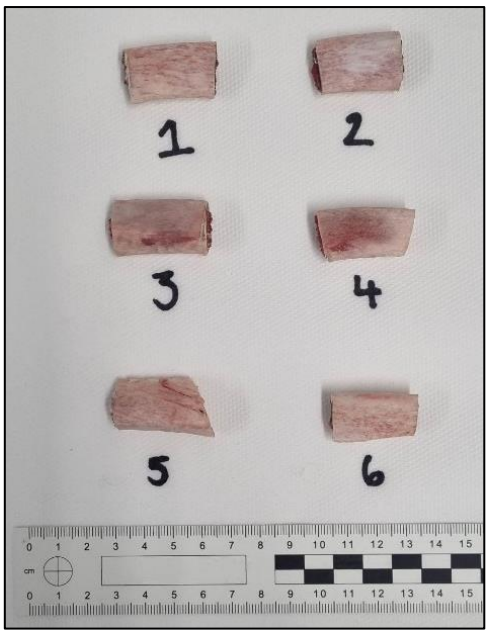

Figure 205: The six sections of porcine rib (Sus scrofa domesticus) prior to demineralisation.

Table 46: Dimensions of the six portions of porcine rib (Sus scrofa domesticus).

Rib sample	Mass (g)	Length (mm)	Width (mm)	A/P (mm)
1	5.4	31	16.9	10.2
2	4.67	30.1	18.4	9.3
3	5.84	32.6	18.3	10.3
4	5.54	30.3	16.1	10.6
5	5.67	29.6	17.7	1.1
6	3.95	29	15.5	9.4
Average	5.18	30.43	17.15	8.48

25.1.2- METHOD

To remove the lipids from the bone, each portion of porcine rib was placed in an individual boiling tube filled with 30 ml of a 2:1 chloroform methanol solution. Each boiling tube was sealed with a rubber bung, wrapped in aluminium foil, and secured with a rubber band. All six boiling tubes were labelled, placed in a test tube rack, and secured in place with a cable tie to keep them secure during agitation. The test tube rack was placed on a Cole-Parmer™ Stuart™ See-Saw Rocker, housed within a fume cupboard, and continuously rocked at a speed of 70 rpm for 6 weeks at room temperature (approx. 18°C). The solution was replenished on a weekly basis. Figures 206 and 207 illustrate the equipment configuration.

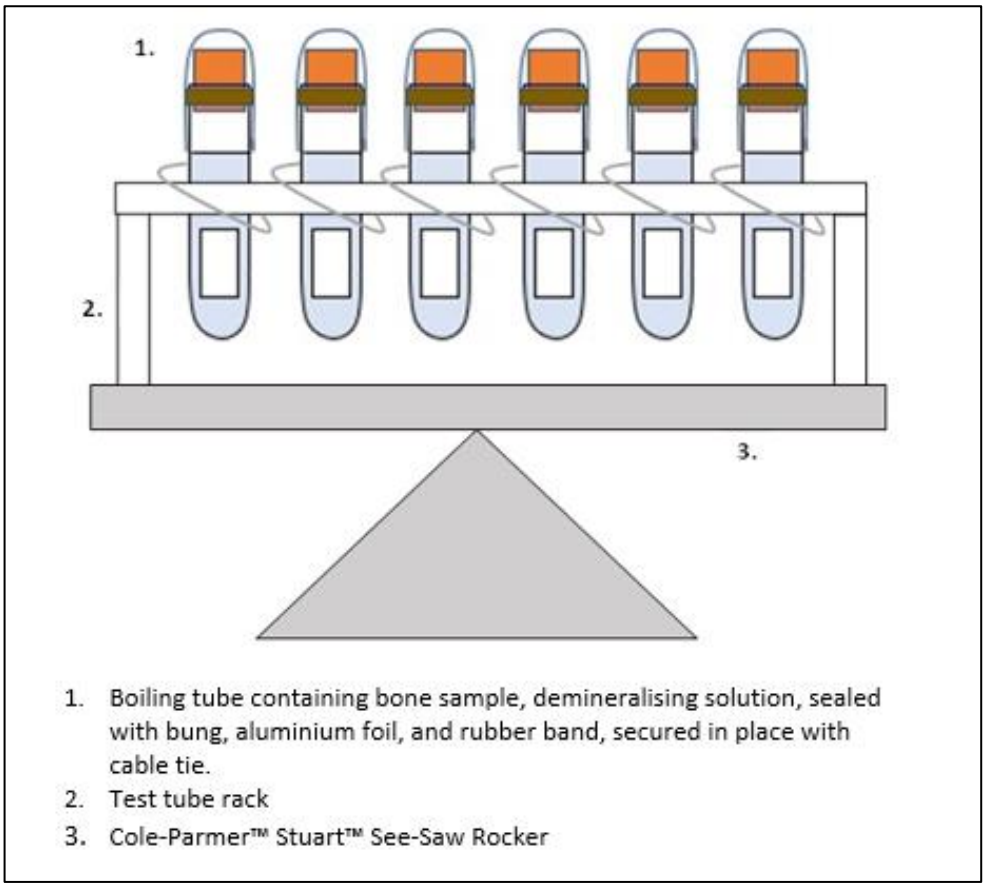

Figure 206: Diagram of the demineralising bone equipment configuration

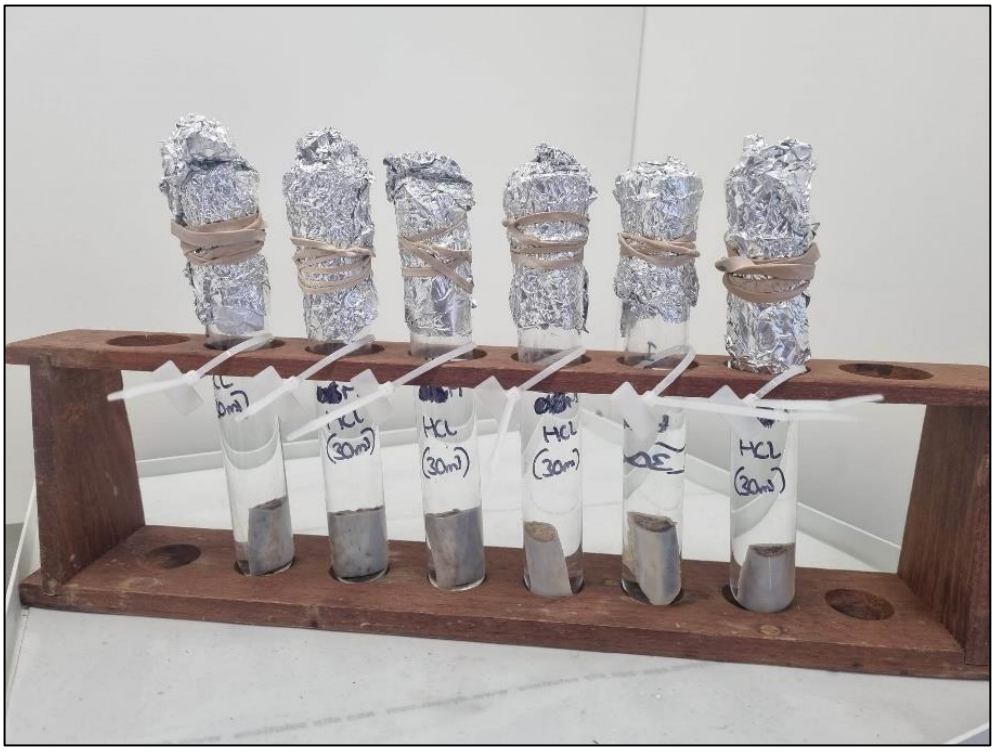

Figure 207: Photograph of the demineralising bone equipment configuration

After 6 weeks, the chloroform methanol solution was replaced with 30 ml 1M hydrochloric acid to eliminate the mineral content from the bone. The samples continued to be rocked at a speed of 70 rpm for 5 weeks at room temperature (approx. 18°C), with the solution being replaced weekly until the bones became pale and pliable, signifying the loss of mineral content. Once demineralisation was complete the samples were rinsed with deionised water three times to neutralise the acid and left overnight in Ph 4 buffer to halt any further acidic action. For transportation the bone samples were housed in universal containers with deionised water, to later be photographed underwater and terrestrially according to the methodology outlined in chapter 20.0. The resulting images were analysed using the OFC as also outlined in the core methodology chapter 20.0.

25.2- DEPROTEINISED BONE

25.2.1- MATERIALS AND METHOD

A negative photographic fluorescence control was created by deproteinising porcine bone through burning. Firstly, six porcine ribs were manually defleshed using the methodology discussed in chapter 20.0. Whole ribs rather than bone fragments were selected, due to the anticipated loss in bone integrity associated with high heat, which would lead to the collapse of small bone samples and therefore render photography impossible. The ribs were kept frozen until the day of burning where they were defrosted in a refrigerator overnight (4°C) and then left at room temperature (16.8°C) for two hours, to reach ambient temperature before burning. Each rib was weighed using a Brifit digital kitchen scale (0.05-500 g) and their length, width, depth, and anterior-posterior dimensions measured using Yakamoz electronic digital callipers (±0.1 mm). Figure 208 and table 47 below summarise the dimensions and appearance of the porcine ribs prior to burning.

Figure 208: Appearance of the manually defleshed porcine ribs (Sus scrofa domesticus) prior to burning, photographed under natural light.

Table 47: Dimensions of the fresh porcine ribs (Sus scrofa domesticus) prior to burning.

Rib	Mass (g)	Length (mm)	Width (mm)	A/P (mm)
1	18.55	87.4	19.8	11
2	20.73	88.8	18.9	12.3
3	19.4	82.5	21.3	10
4	19.95	107.3	17.2	8.9
5	15.76	109.4	11.6	11.4
6	17.22	120.1	14.6	11.3
Av.	18.60	99.25	17.23	10.82

The rib samples were burned in a methane gas powered roll top BillyOh.com 3 burner hooded domestic BBQ (grill dimensions: 48.4cm x 37.6cm) (figures 209 and 210), for a total of 2 hrs and 30 mins with the temperature set at maximum. The ribs were monitored every 15 mins and the temperature measured at each interval using a digital

thermometer. The lid of the BBQ was kept closed, other than to measure temperature, during the entire burning session.

Figure 209: Methane gas powered roll top BillyOh.com 3 burner hooded domestic BBQ

Figure 210: Photograph showing the porcine ribs (Sus scrofa domesticus) in-situ in the BBQ.

After the burning was complete, the ribs were left to cool for 30 mins before being stored in small dry plastic container, lined with absorbent tissue paper, at room temperature until photography.

25.2.2- FLUORESCENCE

Firstly photographs were taken of the burnt bones under natural light with scale. The extent of burning was determined using the Munsell colour chart (1994) [517] to record any discolouration to the bone's surface, at the sternal epiphysis, diaphysis, and vertebral epiphysis, alongside percentage coverage, and documentation of any deterioration in surface texture and bone integrity such as patina, fractures, or delamination. Fluorescence photography was then conducted using the terrestrial methodology outlined in chapter 20.0, using the Hammerhead light source and orange filter, at an exposure time of 1/3s, to align with the method used for the other control specimens. Underwater photography could not be completed for the burnt bone samples, as the thermal degradation of the mineral content leads to the loss of structural integrity, which would have destroyed the sample if submerged. Once complete all photographs were uploaded to a desk top computer and analysed using the OFC as outlined in the core methodology.

25.3- CALCINED BONE ASH

25.3.1- MATERIALS AND METHOD

To act as a further negative control, 1600 mg of bone ash powder, purchased from PotClays Ltd (www.potclays.co.uk,) comprising of calcined animal bone (technical data sheet: appendix 64) was combined with 3 ml of Easteverlast Crystal Clear Epoxy Resin and 1ml of complimentary Easteverlast Crystal Clear Curing Agent in the same manner as the powdered collagen control, and stirred slowly for 3 mins until fully combined. Calcinated bone was selected as a negative control as it has been heated to the point where the organic aspect has been destroyed (in excess of approx. 600°C), as discussed in section 9.6, and therefore would not be expected to produce fluorescence.

The solution was transferred to the same oval silicon mould used for the collagen powder measuring 40 x 30 x 10 mm and left at room temperature for 24 hrs to harden. The bone ash block was then photographed using the Hammerhead light source in accordance with the terrestrial methodology outlined in chapter 20.0, using the orange camera filter and 1/3s exposure time. Underwater fluorescence photography was not conducted for the bone ash, as bone ash would not be a common underwater finding.

As with the collagen powder, the calcined bone ash was embedded in resin to enable a standardised surface area and dimensions for fluorescence photography. However, it was noticed that when the bone ash was combined with the epoxy resin the bone ash developed a much darker appearance, changing from a pale grey to a dark grey as shown in figures 211-212. This could have been purely a result of combining the powder with moisture, but possibly due to the slight exothermic reaction that occurs during the resin curing. To ensure that the fluorescence results were an accurate reflection of calcined bone, 1.6 g of only powdered bone ash was photographed separately using the same photography protocol. Once complete all photographs were uploaded to a desk top computer and analysed using the OFC as discussed in chapter 20.0.

Figure 211: Calcined bone ash photographed under natural light.

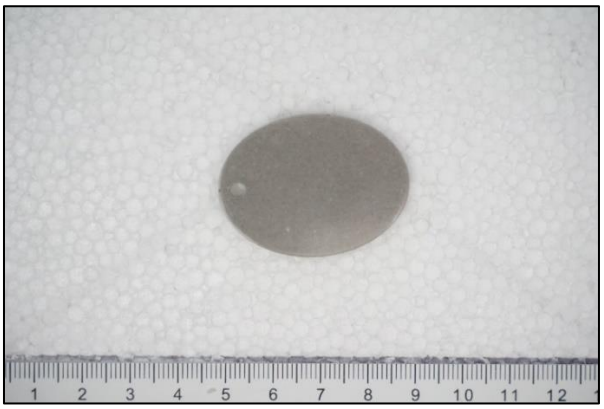

Figure 212: Calcined bone ash embedded in epoxy resin, photographed under natural light.

25.3.2- STATISTICAL ANALYSIS

Fluorescence data was analysed using Microsoft Excel and compared with the results from each part of research Section B, questions 3a-c, with the aim of constructing a fluorescence scale to aid interpretation, and as a model for future guidance for investigators using the OFC. Comparisons were made between organic and inorganic materials as well as terrestrial and submerged values.

25.4- RESULTS AND DISCUSSION

25.4.1- DEMINERALISED BONE

Table 48 below summarises the photographic fluorescence results of the six demineralised bone samples, and table 49 displays the average calculated fluorescence results, alongside the overall average fluorescence for each context and the calculated standard deviation. All the fluorescence images, OFC processed images, and subsequent calculated fluorescence values for each ROI of each bone segment, across both deposition contexts, can be seen in appendices 66-67.

Table 48: Photographic fluorescence results of the six demineralised bone samples photographed using the Hammerhead ALS, orange filter, at 1/3s exposure time, in terrestrial and submerged contexts.

Rib	Natural	Terrestrial	Submerged
1	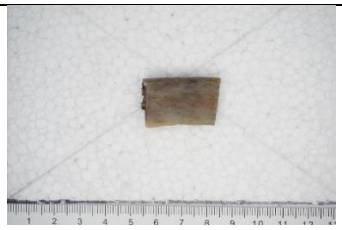	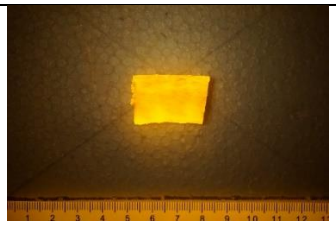	
2	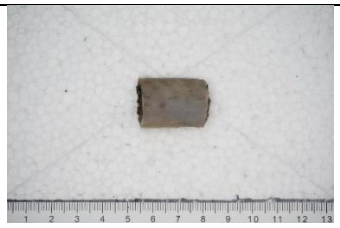	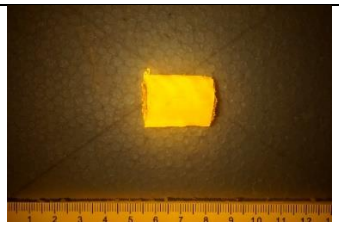	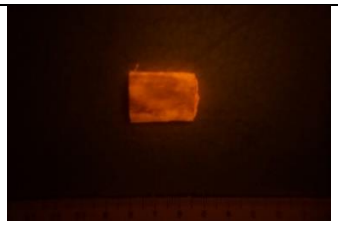
3	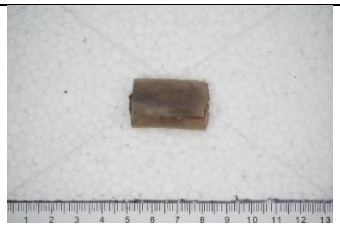	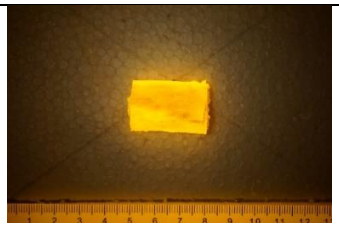	
4		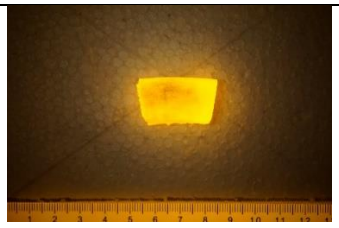	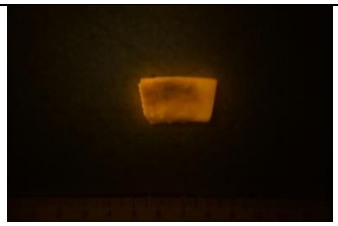

5	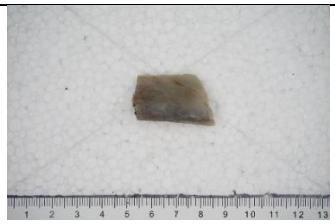	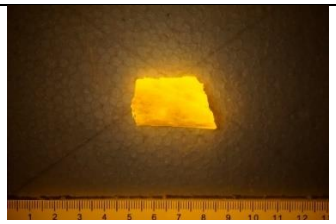	
6	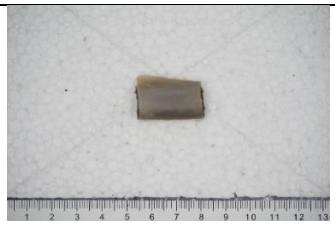	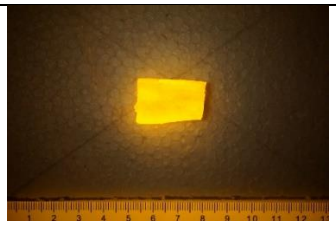	

Table 49: Average calculated terrestrial and aquatic fluorescence results, standard deviation, and range, for the six demineralised porcine bone (Sus scrofa domesticus) sections. Photographed with the Hammerhead light, orange filter, and 1/3s exposure time.

Rib sample	Fluorescence	
	Terrestrial	Underwater
1	192.3	90.9
2	153.3	79.7
3	186.7	74.1
4	185.0	69.0
5	202.3	96.1
6	201.7	82.2
Average	186.9	83
Min	153.3	69
Max	202.3	96.1
Range	49	27.1
S.D.	15.2	8.8

Overall, the results of the demineralised bone samples photographed with the Hammerhead ALS, orange filter and exposure time of 1/3s, produced an average terrestrial fluorescence of 186.9 (s.d= 15.2), and an underwater fluorescence level of 83 (s.d= 8.8), a difference of 103.9 (76.9%), as shown in table 49. In agreement with all the

terrestrial and underwater comparisons conducted in this thesis, the submerged fluorescence was much lower compared to the terrestrial values (figure 213) but had a smaller standard deviation of 8.8 compared to 15.2, indicating slightly more variation in the terrestrial values compared to the underwater fluorescence. Individually, rib segment 5 produced the highest fluorescence results in both the terrestrial context (202.3) and the tap water (96.1), whereas rib 2 produced the lowest terrestrial level of 153.3, and rib 4 generated the lowest aquatic result of 69 (appendix 67).

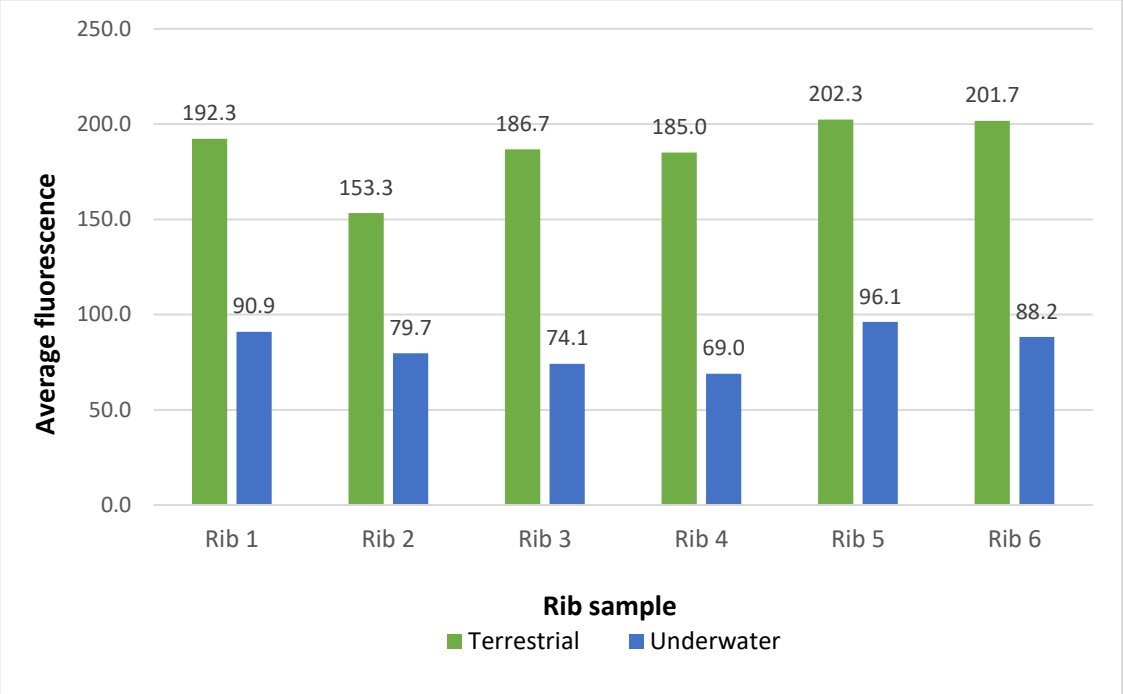

Figure 213: Comparison of average calculated terrestrial and aquatic fluorescence results for the six demineralised porcine bone (Sus scrofa domesticus) sections. Photographed with the Hammerhead light, orange filter, and 1/3s exposure time.

When compared to the average fluorescence of the fresh rib dataset discussed in Section B, research question 1 (terrestrial 111.2, aquatic 34.2), the average fluorescence demineralised results were on average 75.7 (50%) and 48.8 (83%) higher in the terrestrial and aquatic contexts respectively (table 49). Similarly, when compared to the macerated rib dataset from Section B, research question 2, (terrestrial 95.87, aquatic 62.02) the demineralised bone fluorescence was on average 91.03 (64.3%), and 20.9 (28.9%) (table 49). Consequently, this provides support for the theory that bone protein is the primary source of bone autofluorescence, as the calculated fluorescence levels increased

dramatically after the removal of the mineral component. However, it is recognised that the sample population in this research question of N=6, was very low compared to the datasets from questions 1 and 2 (N=30 and N=54 respectively), therefore these findings are not as statistically robust. However, as all the demineralised samples exhibited comparatively very high fluorescence levels to fresh and macerated bone, particularly in the terrestrial context, it is still considered an informative finding, and highly suggestive of effective demineralisation.

Ideally fluorescence measurements would also have been conducted prior to demineralisation to quantify the changes in fluorescence levels, but as this research question was focused on differentiation and controls, this was not carried out during this study. However, it would be beneficial to explore this technique in future to help advance the understanding of the collagen-fluorescence relationship. Similarly, no quantification of collagen or mineral content was conducted during this research question, therefore it can't be confirmed if all mineral content was removed. This decision was due to uncertainty regarding how the demineralisation would affect the final curve, and thus subsequently effect interpretation and quantification. Furthermore, the possibility of retained chloroform and methanol solution, and/or hydrochloric acid, would have required extensive research, as it is unclear if the samples would have been suitable for thermal analysis. Chloroform fumes are toxic, methanol is highly flammable, and hydrochloric acid is toxic and corrosive, which may have raised safety concerns when using TGA. However, as this thesis was focused on foundational understanding of bone fluorescence, the demineralised bone was intended to be used as a visual positive fluorescence control to compare to other controls derived from bone, as well as non-bone samples, to create a fluorescence scale. Consequently, confirmation of total mineral removal was not necessarily crucial to interpret the overall fluorescence results.

Table 50: Comparison of terrestrial and aquatic average fluorescence values of the demineralised porcine bone segments (sus scrofa domesticus), and the fresh and macerated porcine bone datasets from section B, research questions 1 & 2. Photographed using the Hammerhead ALS, orange filter, and 1/3s exposure time.

Statistic	Average fluorescence					
	Fresh (Qu. 1) (N=30)		Macerated (Qu. 2) (N=54)		Demineralised (Qu. 3b) (N=6)	
	Terrestrial	Aquatic	Terrestrial	Aquatic	Terrestrial	Aquatic
Average	111.2	34.2	95.8	62	186.9	83
S.D.	33.8	11.6	23.2	22.4	15.2	8.8
Median	114	33	94	61	192	83

25.4.2- DEPROTEINISED BONE

Table 51 below summarises the photographic results of the deproteinised bone samples, including visual surface changes. Appendix 68, details the observed bone modifications, assigned Munsell colour readings, and the estimated percentage coverage. Table 52 details the intervals and associated temperatures recorded during the burning session, and chart 214 and table 53, display the calculated average fluorescence values for each burned porcine rib. A full table of results, detailing the fluorescence value for each ROI within each fluorescence photograph can be seen in appendix 69, and the OFC processed photographs are available in appendix 70.

Table 51: Summarised fluorescence results of the deproteinised porcine ribs (Sus scrofa domesticus), photographed using the Hammerhead ALS, orange filter, and 1/3s exposure time in a terrestrial context.

Rib	Natural	Fluorescence		Natural	Fluorescence
1			4		
2			5		
3		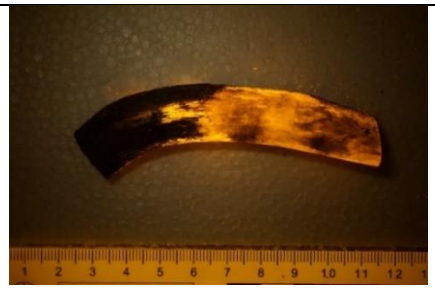	6		

Table 52: Recorded intervals and burning temperatures.

Time (Mins)	Temp (°C)
15	176.8
30	250.3
45	253.6
60	285.1
75	283.3
90	283.8
105	269.3
120	269.8
135	270.2
150	271.3

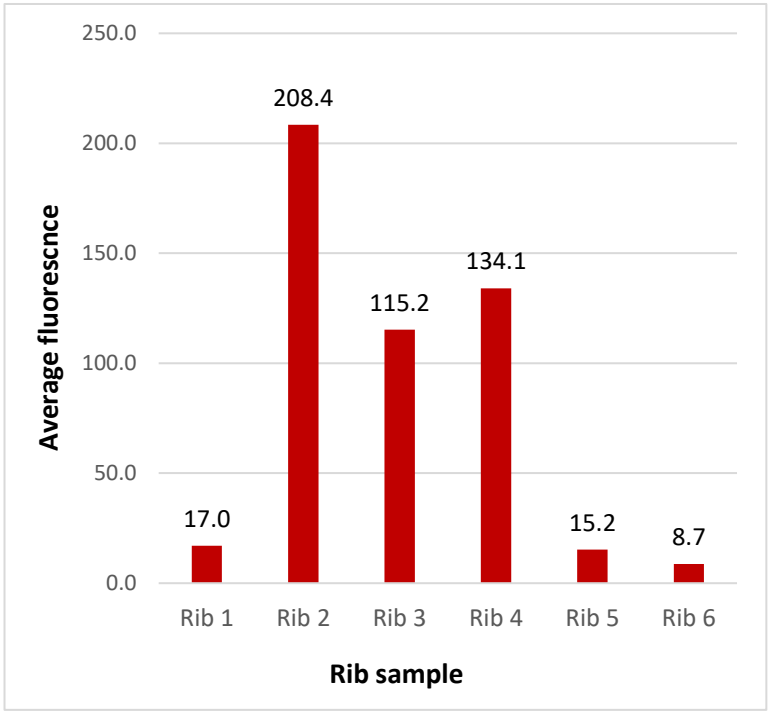

Figure 214: calculated average fluorescence values for each burned porcine rib.

Table 53: Calculated average fluorescence values for each burned porcine rib, photographed using the Hammerhead ALS, orange filter, and 1/3s exposure time in a terrestrial context.

Rib sample	Fluorescence
1	17
2	208
3	115.2
4	134.1
5	15.2
6	8.7
Average	83.1
Min	8.7
Max	208
Range	199.8
S.D.	77.3

Overall, the calculated fluorescence values of the photographs produced using the Hammerhead light, orange filter, and 1/3s exposure time in the terrestrial context, exhibited an expansive range in fluorescence values. The highest fluorescence value was recorded in rib 2 at 208, and the lowest fluorescence level was seen in rib 6 at 8.7, presenting a range of 199.8 and standard deviation of 77.3. This substantial range in values is due to the differential burning observed between ribs and across the surface of each individual rib, despite all ribs being burned at the same time and under the same conditions. However, as a domestic BBQ was used rather than a furnace, the burning environment was not completely stable, which is demonstrated by the fluctuating temperatures shown in table 52. Furthermore, although the attempts were made to ensure that all ribs were placed at an equal distance from the BBQ burner, to standardise the level of burning within the dataset, due to the different dimensions and morphology of the ribs, as well as the central placement of the burner, this was not achievable.

The photographs of the ribs taken under natural light (table 51), illustrate the range in burning modifications sustained within this small dataset. For example, ribs 1, 5, and 6 have experienced almost complete charring with small areas of probably calcination. On the contrary, ribs 2 and 4 showed signs of drying out, but very little colour change of the anterior surface. The posterior surface, which was closest to the BBQ burners, exhibited greater levels of modification including charring and loss of cortical bone (appendix 68), but it was the anterior surface that was exposed to the ALS and subsequently photographed, thus still producing high fluorescence results. Rib 3 exhibited the most complex burning patterns out of the six ribs, including areas of charring and other zones absent of significant change.

Table 54: Comparison of terrestrial average fluorescence values of the deproteinised porcine bones (sus scrofa domesticus), six demineralised porcine bone segments, and the fresh and macerated porcine bone terrestrial datasets from section B, research questions 1 & 2. Photographed using the Hammerhead ALS, orange filter, and 1/3s exposure time in a terrestrial context.

Stat.	Average fluorescence			
	Fresh (Qu. 1) (N=30)	Macerated (Qu. 2) (N=54)	Demineralised (Qu. 3b) (N=6)	Deproteinised (Qu. 3b) (N=6)
Avg.	111.2	95.87	186.9	83.1
S.D.	33.8	23.18	15.2	77.3
Median	114	94	192	55.5

When comparing the deproteinised results to the rib bone datasets from previous research questions (table 54), it is still evident that the deproteinised bone samples did produce the lowest fluorescence intensities, as intended, including a 28.1 (28.9%) difference in average fluorescence compared to fresh bone and a 103.8 (76.8%) difference compared to the demineralised bone. These findings infer that the burning process did substantially reduce the overall organic content of the bone as anticipated. This interpretation is supported by the fact that the median value for average fluorescence of the deproteinised bone (when comparing all ROIs of all the ribs), was as low as 55.5, identifying the rib 2 result of over 200 average fluorescence as an outlier and not representative of the overall dataset. However, the method used to burn the bone in this experiment was arguably flawed and could have been improved with the use of a furnace. The differential burning patterns were mostly a result of bone placement, variation in bone morphology, and the fluctuating burning temperature. Moreover, the peak temperature achieved during the burning process was 283.8 °C, which based on studies in literature, would not have been sufficient to induce calcination, particularly in the relatively short timescale of 2 hours and 30 mins. Sustained temperatures in excess of 600 °C are usually required for homogenous calcination [485]. Consequently, this disparity in fluorescence figures prompted the inclusion of the calcined porcine bone ash. Although some examples of the burned bone were still included in the final fluorescence scale in chapter 25.4.4, as the examination

of burned bone is a relatively common use for ALS, and to ensure a wide diversity of samples.

25.4.3- CALCINED BONE ASH

Examples of the photographic fluorescence results of the bone ash controls can be seen in table 55 below, and the calculated average fluorescence results (using all ROIs) can be seen in table 56. All fluorescence photographs, processed OFC, and full table of fluorescence results for each ROI can be found in appendices 71 and 72 accordingly. The bone ash results generated with Hammerhead light source and orange filter, at 1/3s exposure time, were in accordance with expectations, as they overall exhibited lower fluorescence levels compared to other bone preparations such as fresh, macerated, and demineralised bone. The powdered bone ash generated an average fluorescence value of 87.3 (s.d.= 3.1), and the bone ash embedded in epoxy resin produced an average fluorescence level of 60.8 (s.d.= 3.1).

Table 55: Example of the photographic fluorescence results of the bone ash control, photographed using the Hammerhead ALS, orange filter, and 1/3s exposure time in a terrestrial context.

Control	Natural	Fluorescence
Bone ash powder	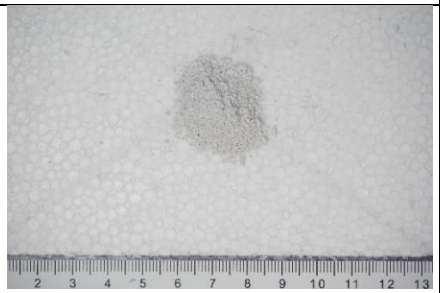	
Embedded bone ash	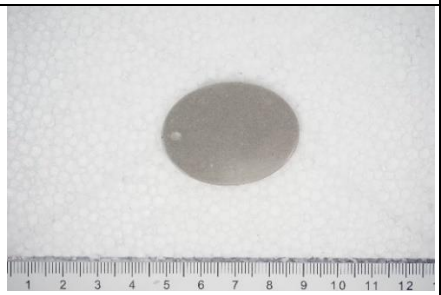	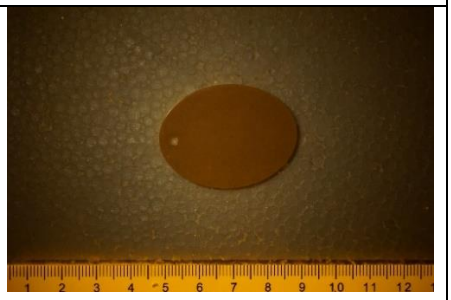

Table 56: Calculated average fluorescence values for each burned porcine rib, photographed using the Hammerhead ALS, orange filter, and 1/3s exposure time in a terrestrial context.

Specimen	Average	SD	Median
Embedded bone ash	60.8	3.1	62
Bone ash powder	87.3	3.1	89

This was a surprising result, as during the collagen powder analysis the epoxy resin was found to possess a low level of inherent fluorescence, and therefore it was presumed it may boost the fluorescence levels of the embedded bone ash, whereas comparatively it was 26.5 (35.7%) lower than the powdered bone ash. This difference in average fluorescence intensity could be the result of the darkened colour generated during the embedding process, either the result of moisture being added to the compound or due to the slight exothermic reaction. Furthermore, the bone ash powder was very white in colour, due to the organic component being destroyed during production. Consequently, this white colouration may also be causing a level of reflection, as noted in the non-bone control group, where paler pigmentation was seen to produce higher levels of fluorescence.

These possible reflections would be the result of how different colours absorb and respond to different wavelengths of the visible spectrum [518]. As in colour theory, white items appear white as all colours are reflected [518], as explained in chapter 7.1. However, this reflective property, was less expected in the bone ash powder as it also has a matte consistency, which was thought to facilitate some level of absorption rather than promoting reflection. Conversely, based on these results, it could be argued that the colour of the examined material plays a more significant role in fluorescence emission compared to the texture, and that it should be a major consideration when proposing ALS examination. The impact of substrate colour on autofluorescence is discussed in the literature in relation to ALS examination of clothing, fibres, and other trace evidence [120, 519], but currently not in relation to bone ALS, other than when categorising the burning conditions of thermally altered bone [158].

Moreover, the process of calcination in bone is characterised by the elimination of the organic component, and consequently collagen [138], which leads to fragile, brittle bone texture, loss of bone integrity, and an overall white/grey/blue colour [485]. Based on the fluorescence results observed here, there is justification for the hypothesis that bone mineral may also contribute to bone fluorescence, rather than protein alone, although based on the relatively low levels of fluorescence reported, it is in lesser capacity compared to protein. However, further research into how substrate colour influences autofluorescence production would assist with future interpretations of bone autofluorescence, especially bone samples that exhibit extensive taphonomic alteration to bone colour such as bleaching or soil staining.

A possible limitation for the inclusion of these bone ash control samples, is that although the standard molecular composition of the bone ash was obtained (appendix 64), the source of the bone ash is not fully understood. Although the safety data sheet describes the bone ash as 'animal bone ash', the Potclays Ltd's website is more specific, describing it as a mixture of porcine and bovine bone [520]. Pure porcine bone would have been preferable for this study, to complement the porcine bone examined throughout the rest of the research. However, bovine bone has been used extensively in forensic science and forensic anthropology and taphonomy research [130, 154, 316]. It was highlighted during the evaluation of the literature in this thesis, that different animal species exhibit different volumes of collagen, and that different anatomical specimens such as ligaments will exhibit different types of collagens [328]. However, as the focus of this control sample is to function as a negative control, devoid of protein and therefore collagen, the use of bovine bone is less detrimental.

Table 57 below, provides a summative overview of the bone derived control samples discussed in this research question (Section B, question 3a-c), alongside an example of a manually defleshed fresh porcine bone, to demonstrate the range of autofluorescence levels that were obtained using the 450 nm Hammerhead light source, orange filter, and 1/3s exposure time in terrestrial and underwater contexts.

Table 57: Overview of the bone derived control samples discussed in research question section B, question 3a-c, alongside an example of a manually defleshed fresh porcine bone (sus scrofa domesticus), obtained using the 450 nm Hammerhead light source, orange filter, and 1/3s exposure time in terrestrial and tap water contexts.

Context	Porcine collagen powder embedded in epoxy resin	Calcined bone ash	Fresh, manually defleshed	Deproteinised bone	Demineralised
Natural		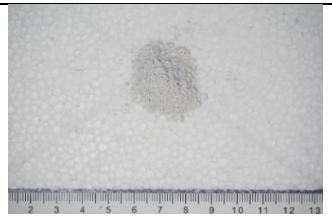			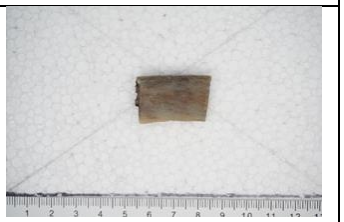
Terrestrial	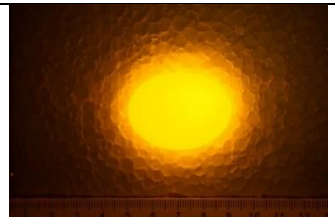	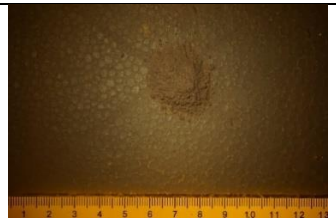			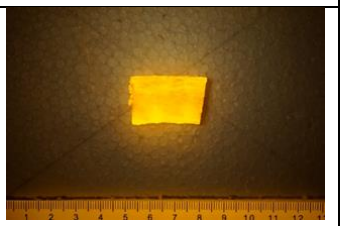
Tap water	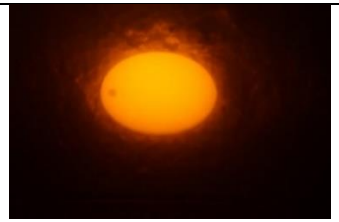	Not possible		Not possible	

25.4.4- FLUORESCENCE SCALE

Graphs 215 and 216 below depict the average fluorescence results for all examined control specimens, produced using the Hammerhead light source, orange camera filter, and photographed at 1/3s exposure time in the terrestrial and aquatic contexts. The results are arranged from highest to lowest, with the addition of the average fluorescence value of the macerated porcine bone dataset discussed in question 1, and the average fluorescence value of the macerated porcine bone dataset examined in research question 2, to enable comparison. As deproteinised bone 2 was identified as an outlier in Section B, question 3c, it was not included in the chart. The submerged fluorescence chart only displays the average fluorescence values of the applicable control items, therefore does not include, deproteinised bone, bone ash, or the non-bone items that floated during photography.

The terrestrial graph clearly identifies the porcine collagen powder control as the most fluorescent material examined during this research question, presenting an average fluorescence of 218. This result is closely followed by all the demineralised porcine bone control samples, and some of the organic controls such as stick 1 (152.7) and the tree bark (148.9). The lowest end of the chart is predominantly occupied by the negative controls, such as deproteinised bone 6, which exhibited the lowest overall fluorescence intensity of 8.7, and therefore led to an overall difference of 209.3 across the control samples dataset. Most stone specimens, sea glass, and ceramic shards were also positioned at the latter side of the chart, including stone 4 (14.7), ceramic fragment 2 (25.7), and sea glass 6 (26.2). It is proposed that the lower fluorescence values were most likely due to a higher mineral content, and darker pigmentation, such as the deproteinised bone, which exhibited lower collagen levels due to the burning, as well as black charring. Interestingly the blue mussel shell also produced very low fluorescence intensity (22), and in theory would also possess a high mineral content, and due to its blue pigmentation would potentially more readily absorb the 450 nm excitation waves.

Consequently, the distribution of organic and inorganic control specimens does provide support for the hypothesis that the protein element of the bone is the primary contributor to the production of autofluorescence. However, additional factors such as colour, texture, and morphology may also influence the level of fluorescence seen and therefore may pose challenges when attempting to differentiate between bone and

other debris at the scene. This is demonstrated by items such as stone 2 (108.6) and the cockle shell (164.7), which generated comparable or higher fluorescence intensities than many of the organic controls, including the fresh (111.2) and macerated bone (95.87), despite presumed high mineral concentration. Some of this fluorescence could be attributed to the pale colour of the item, the more reflective surface of the shell, but also implies that the mineral content of bone may also contribute to autofluorescence, particularly biominerals, as it is a composite material of organic and inorganic compounds. In addition to this, the bone ash control specimen produced higher than expected levels of fluorescence (87.3), which positioned it within the central portion of the dataset and provides further endorsement to the idea of mixed organic and inorganic fluorescence contributors.

The collated average submerged fluorescence results for the control specimens (fig. 2016) illustrate the overall lower fluorescence levels in the tap water context. The distribution of specimens mirrors the terrestrial results, with the highest still being the porcine collagen powder (186), and stone 4 producing the lowest level of fluorescence 8.8.

Overall, this research question has highlighted the requirement for fluorescence quantification to enable direct comparisons and drive deeper interpretation, which was lacking in literature. However, the use of the OFC program also promoted critical evaluation of the fluorescence quantification methodology, due to the possibility of misinterpretations from overexposed photographs as a result of unsuitable wavelength and filter pairings. In the context of this PhD, and the two light sources analysed, the 450 nm Hammerhead light source paired with the orange camera filter was the most successful and most consistent device for documenting autofluorescence in underwater and terrestrial contexts. In comparison, the broader and more intense 420-470 nm spectra of the Crime-lite 2, led to high autofluorescence in bone, but also in many of the control items, and particularly when coupled with the yellow filter, which produced incomplete filtering of fluorescence and excess excitation wavelengths.

These intense levels of fluorescence, and unfiltered wavelengths, could make differentiation even more challenging. If many different types of objects are exhibiting similar levels of fluorescence at the same time, or overall producing extremely intense

fluorescence emissions, it could obscure important forensic details on individual exhibits, hinder documentation, or completely obscure smaller items or fragments. Conversely, in an aquatic context, a more powerful light sources could be beneficial, as the results of this PhD have shown that the greater density of water substantially reduces fluorescence levels, compared to terrestrial visualisation, in a tap water context. In forensic casework, the waterways being investigated for skeletal remains will exhibit a far greater diversity in colour, turbidity, chemical composition, and suspended particulates, all factors that may respond differentially to the ALS, and the camera filter, and exposure time would need to be adjusted accordingly.

As a result, these findings also exposed the need for the construction of possible recommendations to assist investigators when interpreting fluorescence results in the field. For example, recommendations for optimal filter combinations based on the wavelength and model of the ALS in use, the deposition context under investigation, and the proposed goal of examination i.e., to locate and identify potential bone, or analytical documentation and quantification. It was clear from the results obtained during this research question that a standardised ALS methodology for all environments is not feasible, but a more agile working approach will be required to accurately perform bone fluorescence photography at the scene. Furthermore, although digital tools such as the OFC could support investigators in the field, professional judgement to make accurate bone identification will still be required.

Subsequently, development of the OFC program could provide further support for investigators, in addition to fluorescence quantification, by indicating potential false positives associated with over exposure or incompatible filter and wavelength combinations, and a reference library to facilitate decision making, and cataloguing helpful examples of fluorescence encountered during searches. With that in mind, figures 217 and 218 below illustrate examples of a fluorescence scale for terrestrial and underwater contexts, based on the results of the control dataset. As well as visually demonstrating the possible differentiation between bone and other materials, these photographic scales also offer a basic paradigm for the type of visual tools that could be created to assist with bone identification at the crime scene, including tangible examples

so that even personnel not trained in anthropology would still feel confident performing interpretations, thus helping to maximise the recovery of potential osseous material.

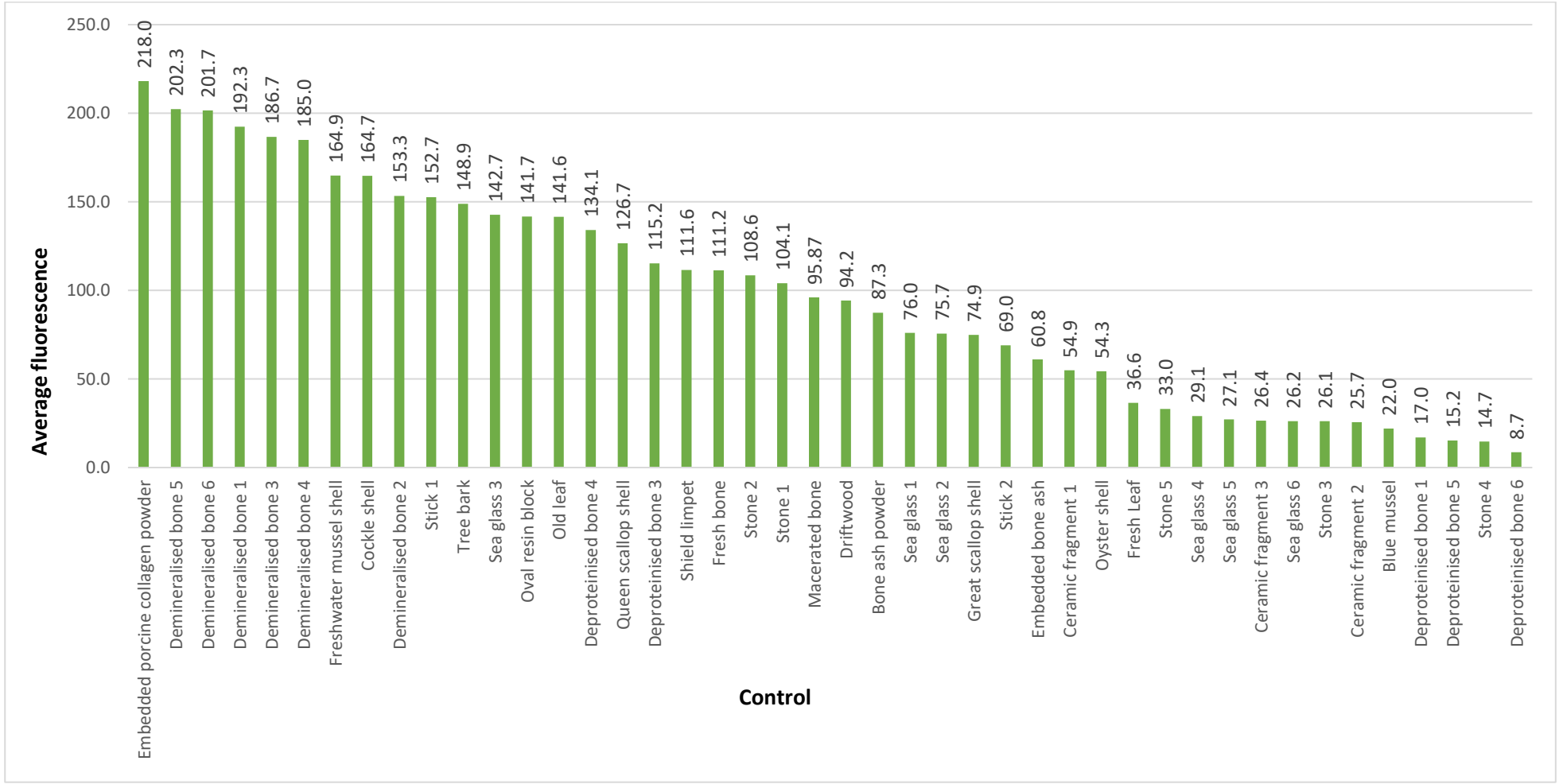

Figure 215: Average terrestrial fluorescence values of all examined control specimens (except deproteinised bone 2), produced using the Hammerhead light source, orange filter, and photographed at 1/3s exposure time.

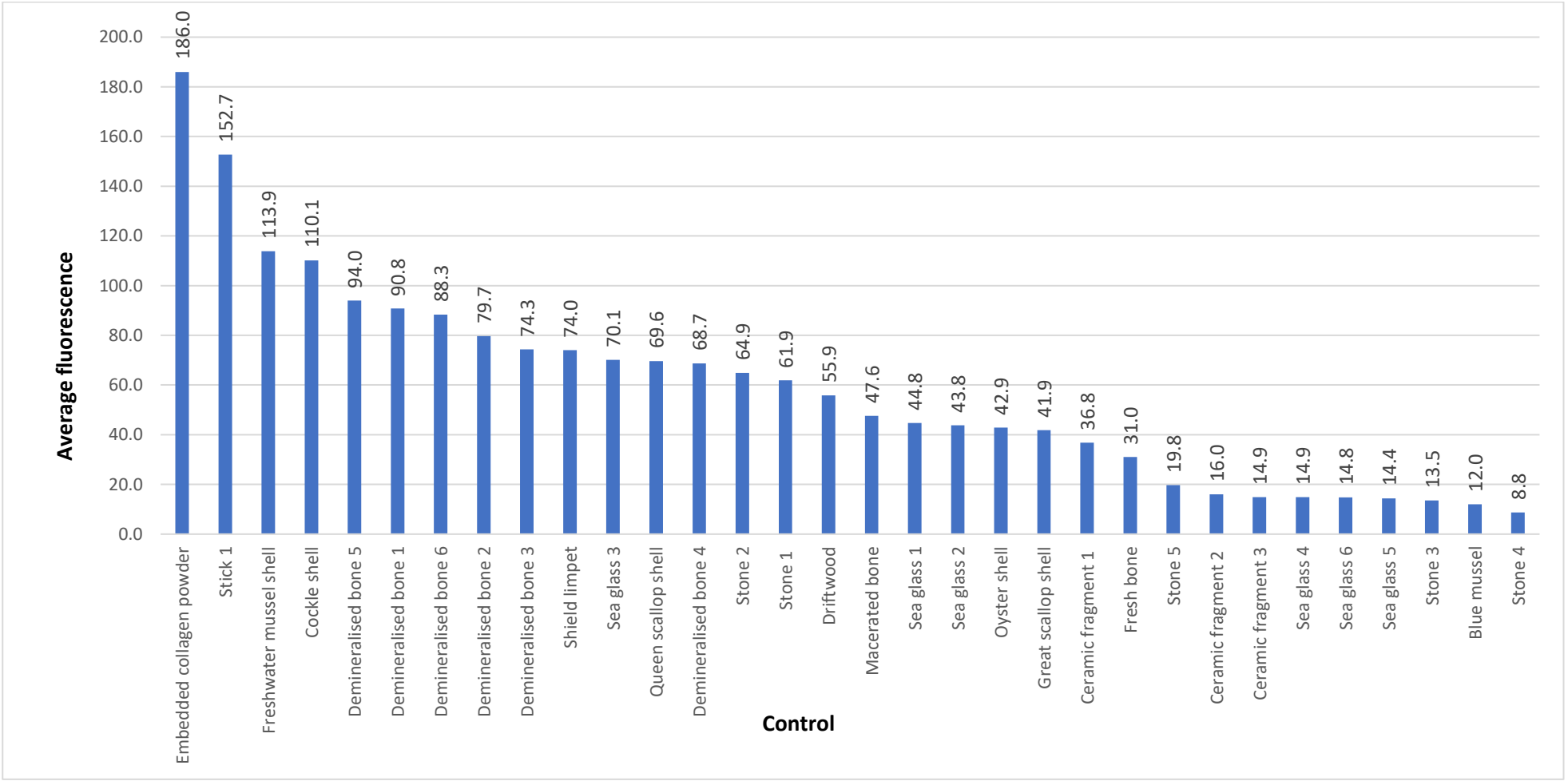

Figure 216: Average submerged fluorescence values of all applicable control specimens, produced using the Hammerhead light source, orange filter, and photographed at 1/3s exposure time.

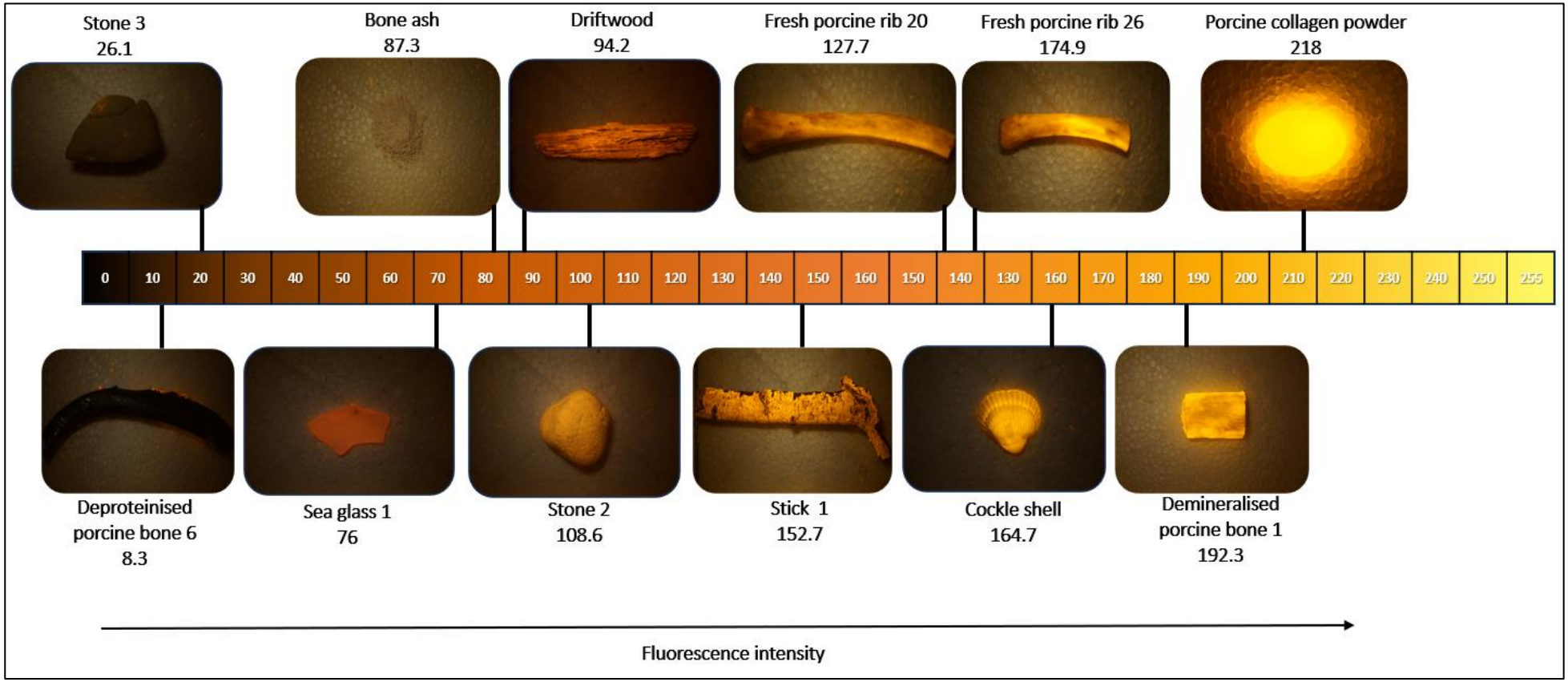

Figure 217: Terrestrial fluorescence scale

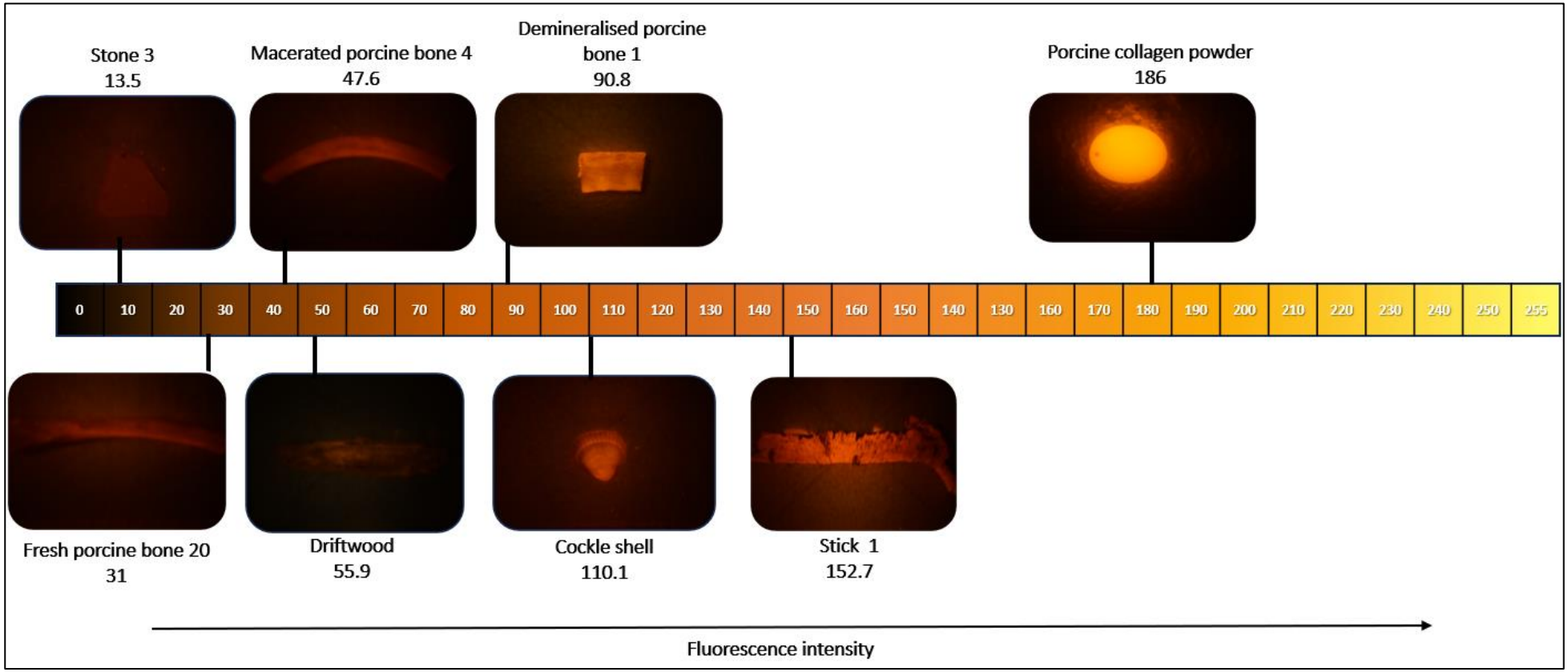

Figure 218: Underwater fluorescence scale

25.5- CONCLUSIONS

It was established that different environmental items emit varying levels of fluorescence, most likely due to variation in molecular composition, colour, texture, and morphology, as illustrated by the fluorescence scales (fig. 217 & 218) and comparative bar charts (fig. 215 & 216). Furthermore, the environmental specimens responded differentially to the blue ALS 450 nm wavelength compared to the different porcine bone specimens. These results consequently provide validity to the possibility of differentiation between bone and other items when searching for skeletal remains in submerged and terrestrial contexts, when using blue light and a camera fitted with an orange camera. Thus, leading to acceptance of hypotheses 6 and 7 below, and the subsequent rejection of the associated null hypotheses.

6. Hypothesis: When using blue light (450-470 nm) and a camera fitted with an orange or yellow camera filter it is possible to differentiate between bone and other environmental items within terrestrial and underwater contexts

   Null hypothesis: When using blue light (450-470 nm) and a camera fitted with an orange or yellow camera filter it is not possible to differentiate between bone and other environmental items within terrestrial and underwater contexts.

7. Hypothesis: Environmental items produce different levels of fluorescence compared to porcine bone (*Sus scrofa domesticus*) when exposed to blue light (450-470 nm) and photographed with an orange camera filter.

   Null hypothesis: Environmental items do not produce different levels of fluorescence compared to porcine bone (*Sus scrofa domesticus*) when exposed to blue light (450-470 nm) and photographed with an orange camera filter.

Although organic material, is likely the primary source of bone autofluorescence, in keeping with the primary hypothesis, and as established through the positive porcine collagen powder and demineralised bone controls, the positive fluorescence results observed in the calcined bone ash, and some of the inorganic non-bone specimens such

as sea glass and shells, poses the scenario, that contrary to the collective hypothesis in literature, the mineral content may also play a role in autofluorescence production.

Recommendations regarding ALS wavelength, coloured filter, and exposure time could provide support for investigators when working at the scene, as it is unlikely that a standardised fluorescence photography protocol would be appropriate for all forensic scenarios. Suboptimal filter and wavelength pairings can lead to overexposure and observation impairment, which presents the possibility of misidentifications and false positives. However, the implementation of fluorescence quantification via the OFC enabled objective comparison of fluorescence values for a variety of environmental items, which had not been conducted previously in literature. The results also emphasised how professional judgement would still be required to execute accurate searches for skeletal remains, to avoid false positives, but crucially, a one size fits all fluorescence photography methodology is not realistic and would not be appropriate. However, recommendations for filter, wavelength, and exposure time, could help to reduce preparation time and triage results at the scene.

The use of the OFC assisted with the discrimination between control items, including highlighting possible misconceptions regarding the origins of autofluorescence, with results reiterating that collagen and protein are not the only compounds capable of autofluorescence production. However, as the overall sample size of the non-bone controls was small, particularly with regards to specimens of organic origin, further research is required to investigate environmental sources of autofluorescence more comprehensively, and how they may impact the use of ALS search for bone. Quantification of specimen composition was not undertaken in this research question, as the focus was on visual fluorescence discrimination. However, in future work the addition of analytical techniques such as FTIR or Raman spectroscopy, could help to elucidate some of the findings that have been established here.

26.0 - SECTION B, QUESTION 4

Is high water salinity destructive to bone collagen and subsequent fluorescence over time? Comparison of changes in bone fluorescence and collagen content of 54 macerated porcine ribs (Sus scrofa domesticus) submerged in tap water and simulated sea water, at 2-month intervals over a 6-month period, photographed using blue light (approximately 450 nm) and orange filter.

26.1- MATERIALS

Fifty-four porcine ribs were manually defleshed and subjected to hot water maceration using the methodology described in chapter 20.0. Tables showing the temperature monitoring of the maceration process can be seen in appendix 73, and the average mass, length, width, and anterior-posterior measurements are displayed in table 58. The ribs were randomly separated into three groups of eighteen ribs, based on the three intervals to be conducted: 2-month, 4-month, and 6-months. All ribs were labelled with a numbered plastic tie for future reference, as shown in table 59 below. Each group of eighteen ribs was randomly distributed between two water conditions (nine bones in each) per timescale. One 24 L black plastic box contained 21 L of tap water, and the other 21 L of high salinity saltwater, to simulate seawater. Kosher salt was used to produce the saltwater conditions, obtained online from the Herb and Spice emporium. Kosher salt was selected as it contains fewer additives and preservatives compared to many other types of salt, such as iodine and caking agents, the formulation used is described in the method section below.

Table 58: Average dimensions for the 54 porcine ribs (sus scrofa domesticus) used during section B, research question 4: the impact of salinity.

Mass (g)	Length (mm)	Width (mm)	A/P (mm)
11.8	82.0	15.1	9.4

26.2- METHOD

In total six 24 L black plastic boxes were used to house the specimens during submersion, two for each interval, with one box containing 21 L of tap water and the other containing 21 L of saltwater. The purpose of the saltwater was to simulate seawater to provide insight into potential degradation of bones at sea. On average seawater contains approximately 35 g of salt per litre [188], consequently 735 g of salt was dissolved in 21 L of tap water for each box of saltwater. A polystyrene insert with scale was attached to the base of each box using Unibond™ double sided mounting tape to prevent it floating during submersion and to ensure photography could be carried out. Nine ribs with plastic labels were added to each box as well as a datalogger enclosed in a labelled plastic bag, to allow for temperature monitoring, as shown in table 59 and figures 219-223 below. Figure 224 illustrates the overall equipment configuration.

The water chemistry for each box was recorded. pH was measured using a handheld digital pH meter (range 0.00 – 14.00) calibrated using factory supplied known pH 4.01 and pH 9.18 solutions (± 0.01 accuracy). TDS was measured using a factory calibrated E-1 portable TDS & EC meter, which could detect between 0-9999 µ/cm (± 2% accuracy). Turbidity was measured using Eutech™ TN-100 waterproof portable turbidity meter from Thermo Scientific™, calibrated using four factory supplied standards of 800 NTU, 100 NTU, 20.0 NTU, and 0.02 NTU. The turbidity meter has a detection range of 0 to 2000 NTU, and an accuracy range of < 0.1 NTU for 0.02 NTU standard; ±2 % of reading ±1 digit for 0 to 500 NTU; ±3 % of reading ±1 digit for 501 to 2000 NTU. In Huddersfield, where this experiment was carried out, the tap water is considered to have an average hardness rating of 'moderately soft', containing 20.4 mg/L of calcium (YorkshireWater.com). Full details of the average reported chemical composition of the tap water can be found in appendix 20.

On day 0, the ambient temperature, and temperature of the water for all six boxes, was recorded using a digital thermometer. This process was repeated at each interval for the two boxes being sampled that day. Prior to submersion, all ribs were weighed and measured as outlined in the core methodology in chapter 20.0, and the eighteen ribs being analysed at each interval were subsequently weighed, and measured upon

retrieval, to record any changes in bone dimensions.

Table 59: Photographs of all 54 porcine ribs (Sus scrofa domesticus) before and after maceration, with labels attached.

Interval (Months)	Fresh	Macerated
2		
4		
6		

Figure 219: External view of the black plastic boxes used to house the submerged porcine bone specimens (Sus scrofa domesticus).

Figure 220: Internal view of the black plastic boxes used to house the submerged porcine bone specimens (Sus scrofa domesticus).

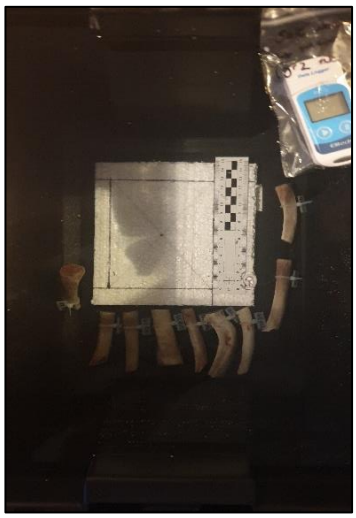

Figure 221: Internal view of plastic boxes with porcine ribs in-situ (Sus scrofa domesticus) and filled with water.

Figure 222: Position of boxes in the outside environment

Figure 223: Position of boxes covered with tarpaulin sheet.

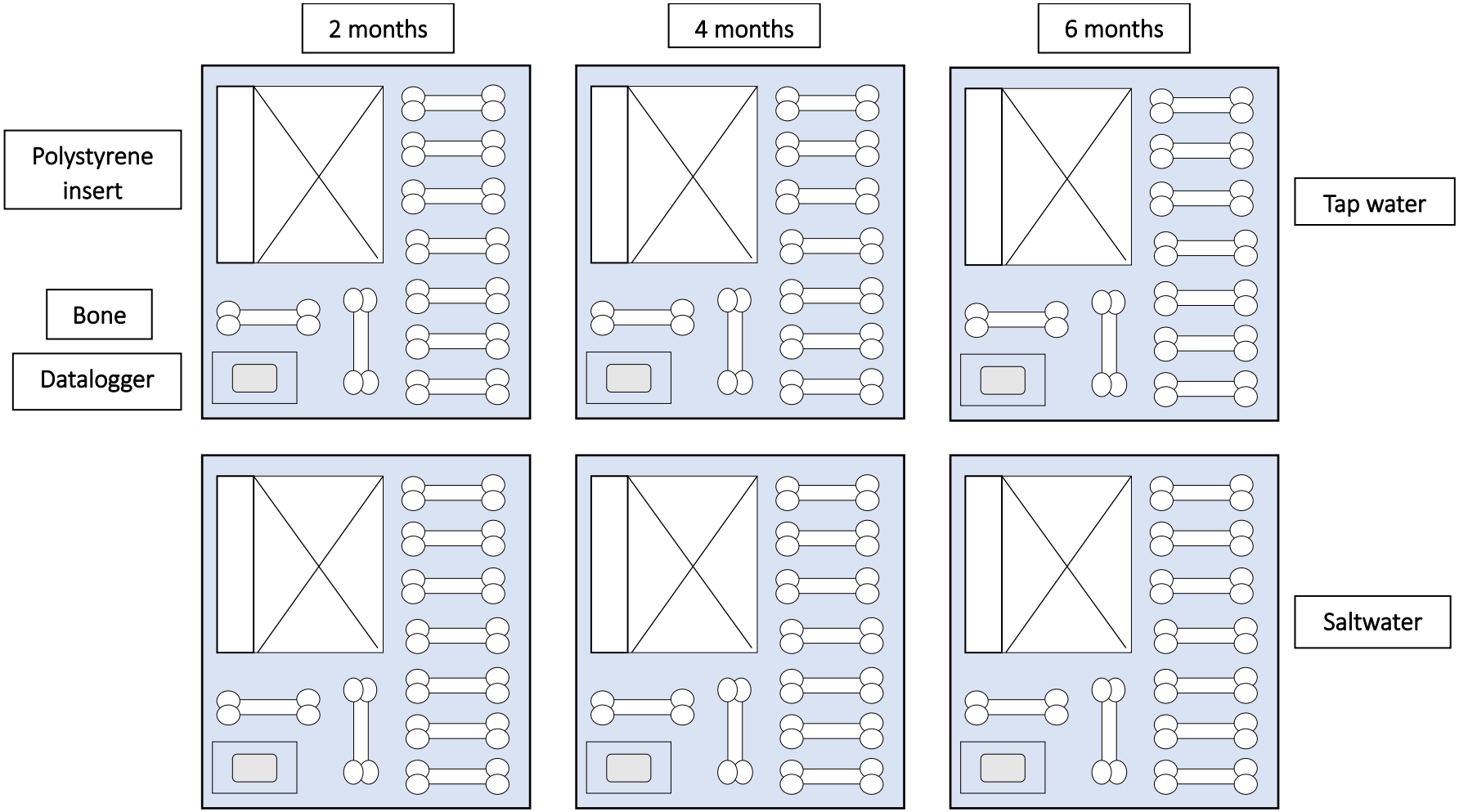

Figure 224: Diagram of the equipment configuration for the aquatic taphonomy salinity experiment

Once assembled, the boxes were placed outside in an enclosed garden comprised of slate shards. The lids were placed on and then the whole configuration covered with a 1.8 x 2.4 m waterproof tarpaulin sheet weighed down by bricks (figures 223) to prevent scavenger access and infiltration by rain. At each subsequent sampling date, the same water chemistry characteristics, as detailed above, were recorded for two boxes being withdrawn. Photographs of the physical/visual changes to the water environments were collected prior to removing the ribs. Approximately 50 ml (two universal containers) of water was collected from each of the two containers being withdrawn, to enable turbidity testing. The water samples were refrigerated (2°C) until analysis to limit bacterial growth and any subsequent chemical changes. The experiment ran from July 2020 to November 2020.

26.2.1- FLUORESCENCE

Fluorescence photography was conducted using the same methodology outlined in section 20.0. Terrestrial and submerged photographs (tap water) were taken at day 0 (after maceration) using the Hammerhead light in conjunction with the orange filter and using the camera settings determined in 20.0. Submerged and terrestrial photography were also completed for each 2-month interval using the same settings. Initially, the plan was to photograph the porcine bones at the end of each submersion interval, whilst still in-situ within the aquatic context. However, as expected the water became very turbid over time (actual turbidity values are displayed in table 62), however, the Hammerhead light source was unable to penetrate the turbid water. This effect may have been exacerbated by the use of highly saline water, as the higher the salinity the greater the density of the water [188]. Consequently, the contaminated water was replaced with tap water to enable submerged photography to still take place.

26.2.2- COLLAGEN

Day 0 bone scrapings for all ribs were collected using the same process described in chapter 20.0. Six ribs were selected for additional collagen sampling, including pre maceration, post maceration (day 0) and after submersion, so that any influence of maceration could also be documented. TGA scrapings were then collected from the 18 ribs being withdrawn at each submersion interval to see if prolonged submersion altered the volume of collagen, and consequently the fluorescence.

26.2.3- STATISTICAL ANALYSIS

Statistical analysis utilised IBM™ SPSS Statistics v23 software and Microsoft Excel to explore how prolonged submersion in tap or salt water may alter the structural integrity of the bones, the collagen levels, and the subsequent fluorescence emissions. Non-parametric Kruskal-Wallis tests and Wilcoxon signed rank tests were used to compare the changes in bone fluorescence and collagen content over time, across the three temporal groups and well as between the two aquatic environments. Discussion also focused on comparisons regarding collagen and fluorescence differences between terrestrial and submerged contexts.

26.3- RESULTS AND DISCUSSION

Table 60 below summarises quantified collagen changes of the six randomly selected ribs, two from each group of eighteen ribs designated for each submersion interval (2, 4, 6 months). When comparing the average pre-maceration and post-maceration collagen values this sample exhibited a relatively minor average reduction 0.07 mg (12.8%). The lowest recorded loss in collagen was 0 mg (0%), however the highest loss was 0.22 mg, equating to 34.9%. This result was slightly higher than expected, and not quite in keeping with other findings in this PhD. Possible explanations are that a potential mismeasurement of the collagen content by the TG machine, as discussed in chapter 22.3.1, or during interpretation of the thermogram. This is somewhat supported by the fact that the pre-maceration collagen content for this rib was unusually high compared to the other specimens, as well as compared to the overall average of 0.55 mg for the dataset. However, it is also plausible that this disparity is due to natural variation in rib composition. Excluding this potentially erroneous result from the dataset, reduces the average collagen loss to 0.04 mg (7.5%), which seems potentially more realistic. However, overall, the hot water maceration preparation exerted minimal changes on bone collagen content of the ribs and therefore limited impact on the subsequent analysis conducted in this research question. The thermograms for the pre-maceration and post-maceration data for these samples can be seen in appendix 74.

Table 60: Quantified collagen levels of the six porcine ribs (Sus scrofa domesticus), pre and post hot water maceration (80°C), including the calculated reductions.

Group	Rib	Before (mg)	After (mg)	Diff (mg)	% change
1	2	0.57	0.48	0.09	-15.8%
	13	0.55	0.54	0.01	-1.8%
2	4	0.63	0.41	0.22	-34.9%
	18	0.44	0.44	0	0.0%
3	1	0.53	0.49	0.04	-7.5%
	4	0.57	0.51	0.06	-10.5%
Average		0.55	0.48	0.07	-12.8%

26.3.1- WATER ANALYSIS

Images of the visual changes observed in each aquatic context can be seen in table 61, beginning with day 0, followed by images of the boxes immediately before sample collection. Turbidity was seen to have increased substantially for both aquatic contexts by the 2-month interval, and drastically more so by the 4-month sampling session. However, after 6 months, visual turbidity was seen to be much lower compared to the 2-month and 4-month intervals. In addition to this, the saltwater context at all intervals exhibited higher levels of turbidity compared to the tap water contexts. These observations were reflected in the chemical analysis of the water conducted at each sampling date, as detailed in tables 62.

Table 61: Visual changes observed in each aquatic context and the applicable interval.

Interval	Tap water (ribs 1-9)	Saltwater (ribs 10-18)
Day 0	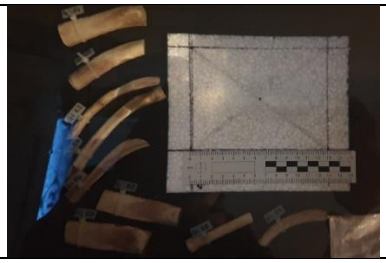	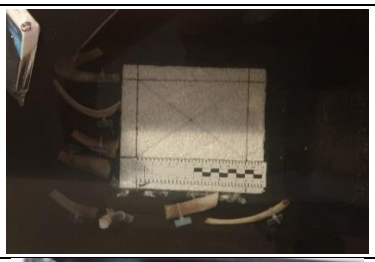
2 Months		
4 Months		
6 Months		

Table 62: Water chemistry measurements recorded at each interval, and the calculated changes observed overtime.

	Day 0				2 months				Changes			
Water	**pH**	**TDS (ppm)**	**EC (µs/cm)**	**Turb. (NTU)**	**pH**	**TDS (ppm)**	**EC (µs/cm)**	**Turb. (NTU)**	**pH**	**TDS (ppm)**	**EC (µs/cm)**	**Turb. (NTU)**
Tap	8.36	74	146	0.04	11.93	287	588	3.93	3.57 (+42.7%)	213 (+287.8%)	442 (+302.7%)	3.89 (+9,725%)
Salt	6.84	3515	4764	0.04	12.08	20,150	30,300	4.84	5.24 (+76.6 %)	26,785 (+473.3%)	25,536 (+536%)	4.80 (+12,000%)
	Day 0				**4 months**				**Changes**			
Water	**pH**	**TDS (ppm)**	**EC (µs/cm)**	**Turb. (NTU)**	**pH**	**TDS (ppm)**	**EC (µs/cm)**	**Turb. (NTU)**	**pH**	**TDS (ppm)**	**EC (µs/cm)**	**Turb. (NTU)**
Tap	7.62	73	146	0.02	7.8	199	400	1.84	0.18 (+2.4%)	126 (+63.3%)	254 (+174%)	1.82 (+9,100%)
Salt	6.93	3515	4764	0.05	8.7	20150	30,300	42.1	1.77 (+25.5 %)	26,785 (+473.3%	25,536 (+536%)	42.05 (+84,100%)
	Day 0				**6 months**				**Changes**			
Water	**pH**	**TDS (ppm)**	**EC (µs/cm)**	**Turb. (NTU)**	**pH**	**TDS (ppm)**	**EC (µs/cm)**	**Turb. (NTU)**	**pH**	**TDS (ppm)**	**EC (µs/cm)**	**Turb. (NTU)**
Tap	7.29	74	144	0.03	7	131	262	5.96	0.29 (-4%)	57 (+77%)	118 (+81.9%)	5.93 (+19,766%)
Salt	6.67	3515	4764	0.06	8.22	20,150	40,300	1.48	1.55 (+23.2%)	35,536 (+473.3%	35,536 (+745.9%)	1.42 (+2,366%)

At day 0 the pH of the aquatic environments was close to neutral for both saltwater and tap water contexts, although saltwater was slightly more acidic overall, with an average pH of 6.8 compared to the tap water pH of 7.8. However, at the 2-month interval, the pH was seen to rise substantially in both the saltwater and tap water, producing similar readings of 11.93 (+42.7%) and 12.08 (76.6%) respectively, and indicating a change to a more alkaline composition. However, these increases were not replicated at the 4-month and 6-month intervals, as the tap water contexts instead developed closer to neutral pH levels, as seen at day 0, including 7.8 at the 4-month interval, and 7 at the 6-month interval. In contrast, the saltwater contexts remained more alkaline, exhibiting a pH of 8.7 at the 4-month interval, and 8.22 at the 6-month interval.

In a similar trend to the pH levels, the TDS findings for the tap water context were seen to have dramatically increased at the 2-month interval, over doubling, from 74 ppm to 213 (287.8%). However, in the latter intervals, recorded tap water TDS levels were still higher than day 0, but not by such a large margin, with the 4-month exhibiting 126 (63.3%) increase, and 131 at the 6-month sampling session, an increase of 131 (77%) from day 0. The TDS measurements for the saltwater contexts at day 0 were obviously much higher due to the saline formulation, with a baseline value of 3515 ppm recorded in each day 0 box. At the 2-month interval the TDS of the saltwater context had increased substantially, up to 20,150 ppm (473.3%), which was replicated in the subsequent 4-month and 6-month intervals.

Conductivity measurements for the saltwater environment followed a similar trend, with a higher baseline value of 4764 µs/cm compared to the 146 µs/cm noted in the tap water. At the 2-month interval this figure rose to 30,300 µs/cm (536%), which was maintained at the 4-month interval, but was elevated to 40,300 µs/cm at the 6-month interval, a 35,536 µs/cm (745.9%) increase from day 0. The conductivity of the tap water environments experienced a different trend. From a day 0 baseline of 146 µs/cm the 2-month interval sample exhibited an increase of 442 µs/cm (302.7%) up to 588 µs/cm. The 4-month samples however exhibited lower conductivity compared to the 2-month samples but still higher than day 0, with a reading of 400 µs/cm, an increase of 254 µs/cm from the baseline. The 6-month conductivity increase from day 0 was also lower compared to the increase recorded at the 2-month sampling, reporting a reading of 262 µs/cm, an increase of 118 µs/cm from day 0.

The measured turbidity values saw the greatest increase in values throughout the experiment, as illustrated by the photographs in table 61 and the results in table 62. The highest turbidity levels were recorded in the saltwater contexts at the 2-month and 4-month intervals of 4.84 NTU, and 42.1 NTU respectively. This was an increase of 4.8 NTU (12,000% at the 2-month interval, and 42.05 (84,1000%) at 4-months, from the day 0 value of 0.04 NTU. In each of these intervals the tap water contexts also registered a substantial increase in turbidity from day 0, with a final reading of 3.93 NTU and 1.84 NTU for the 2-month and 4-month sampling dates. However, at the 6-month interval the tap water context exhibited the higher turbidity level of 5.96, compared to the 1.48 seen in the saltwater. Although both readings were elevated compared to day 0, by 5.93 NTU (19,766%) for the tap water, and 1.42 NTU (2,366%) in the salt water. Charts 225-228 below illustrate all the trends in the water chemistry data detailed above, using a logarithmic scale.

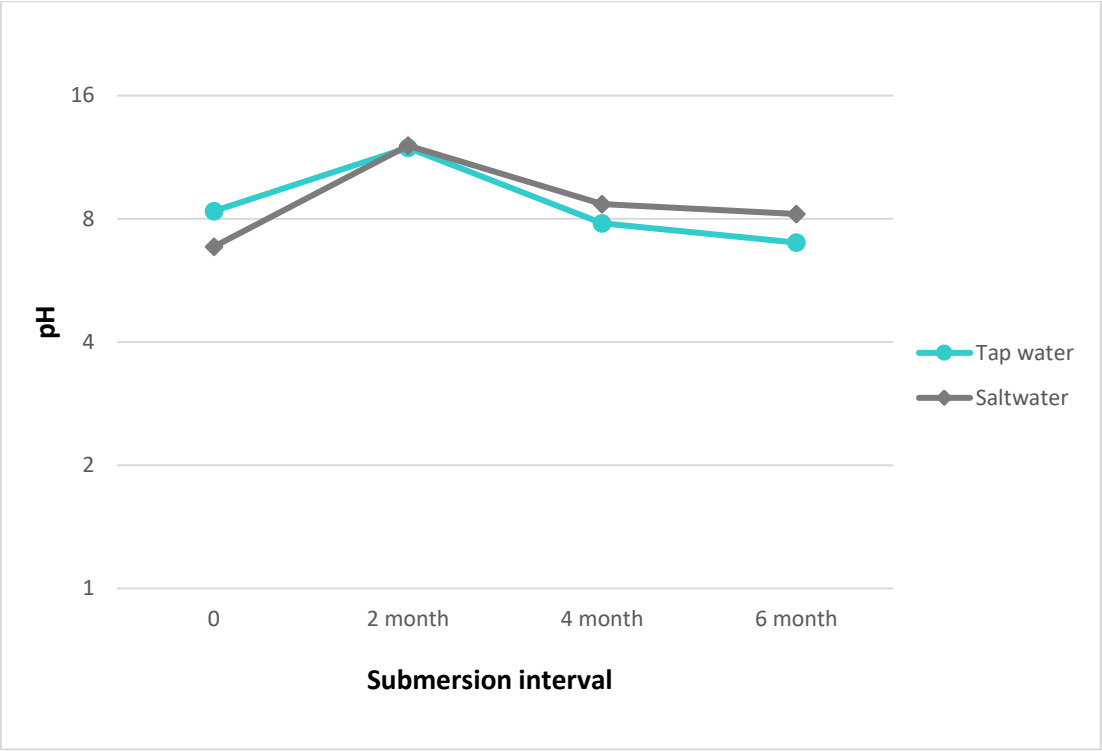

Figure 225: Measured changes in pH in the tap water and saltwater contexts over the 6-month period (reading taken at each 2-month interval)

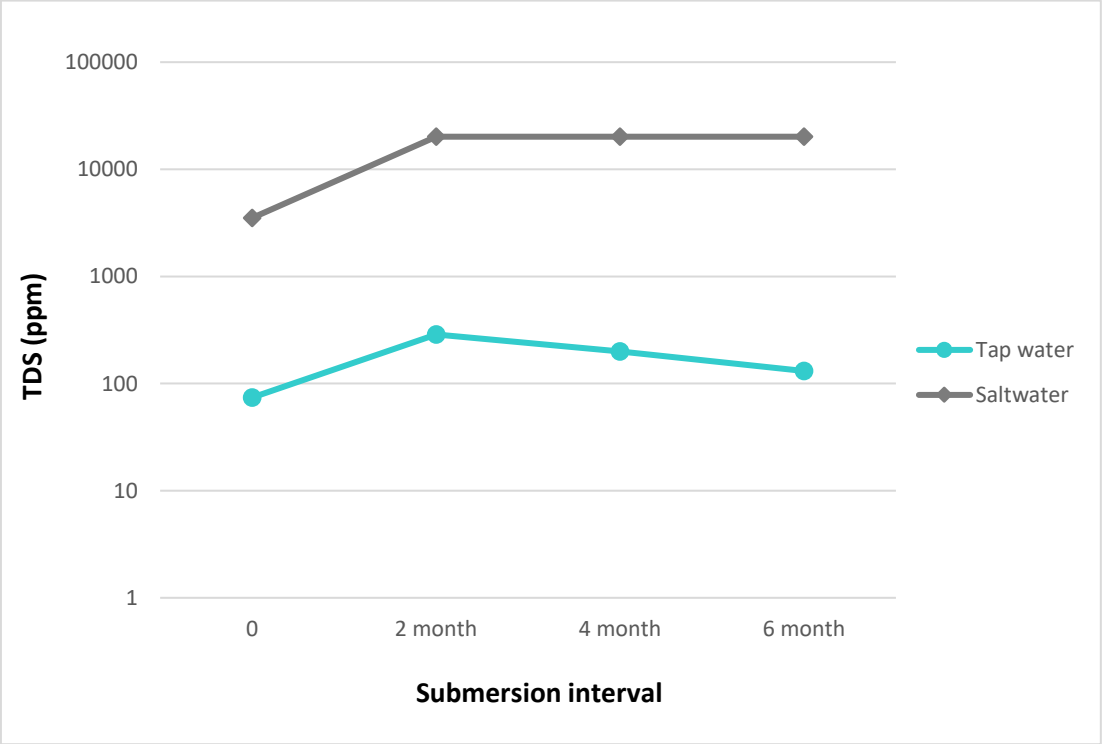

Figure 226: Measured changes in total dissolved solids (TDS) in the tap water and saltwater contexts over the 6-month period (reading taken at each 2-month interval)

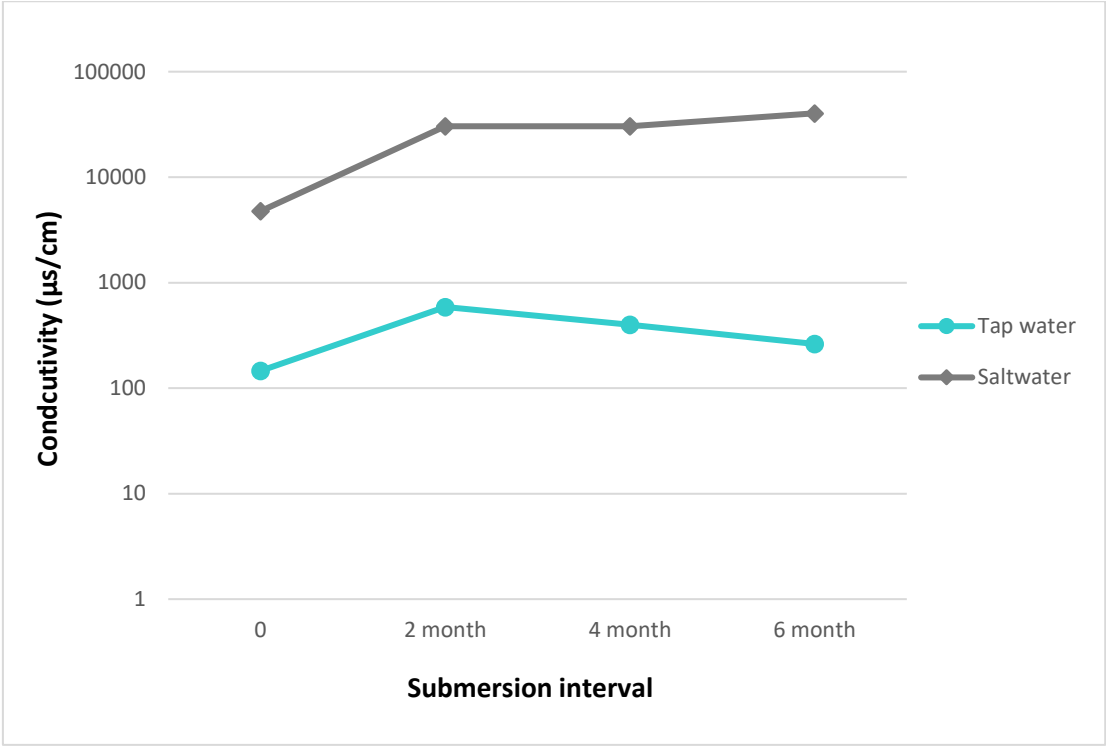

Figure 227: Measured changes in conductivity in the tap water and saltwater contexts over the 6-month period (reading taken at each 2-month interval)

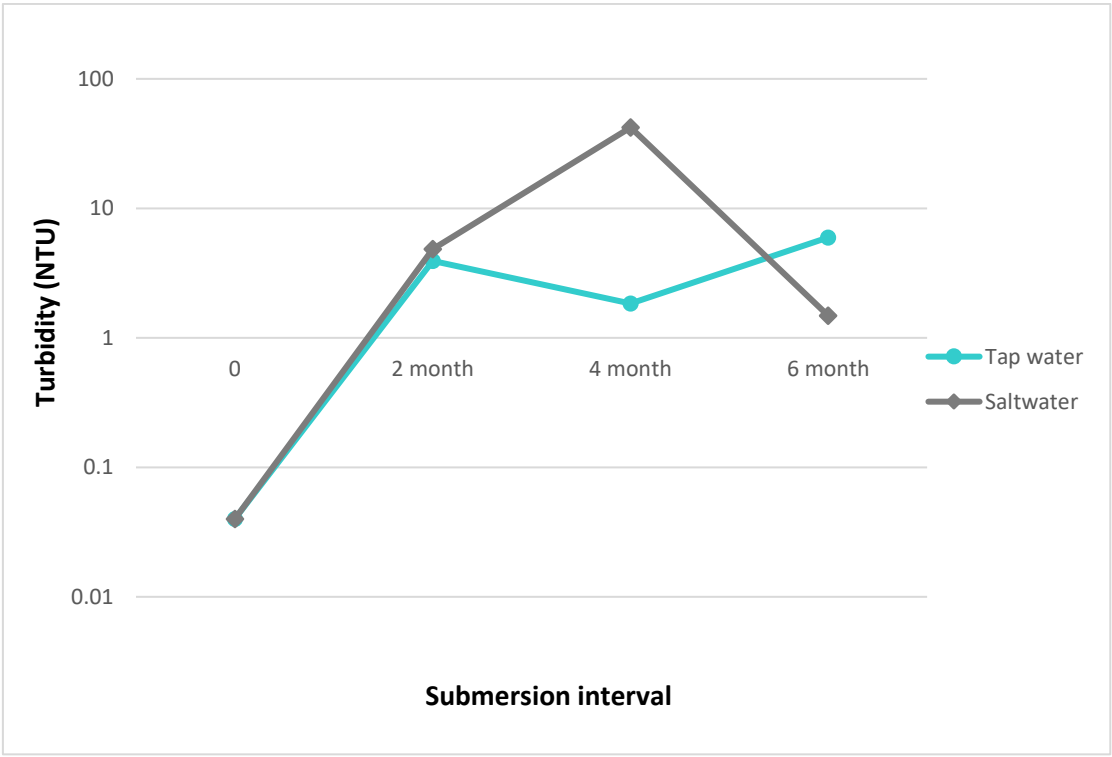

Figure 228: Measured changes in turbidity in the tap water and saltwater contexts over the 6-month period (reading taken at each 2-month interval)

26.3.2- BONE CHANGES

Photographic table 63 summarises the post-submersion appearance for each set of ribs retrieved from each submersion interval and deposition context.

Table 63: Photographic summary of the post-submersion appearance for each set of porcine ribs (Sus scrofa domesticus) retrieved at each submersion interval and deposition context, photographed under natural light.

Interval	Tap water (ribs 1-9)	Saltwater (ribs 10-18)
2 Months		
4 Months		
6 Months		

All rib samples experienced taphonomic alteration due to prolonged submersion. The most prevalent modification was discolouration, documented at all submersion intervals and in all aquatic contexts. The ribs submerged in tap water for 2 months exhibited a pinkish grey/brown pigmentation (figure 229), with some darker areas of discolouration noted at the sternal ends of some of the shorter ribs. This red hue of discolouration is typically caused by the haemolysis of red blood cells during decomposition [102]. Rib samples submerged for 2 months in saltwater exhibited yellow/orange discolouration and yellow greasy deposits on the bone surface (figure 230), which was most likely the leaching of fat precipitated by the high salinity environment.

Figure 229: Photographs of the porcine ribs (Sus scrofa domesticus), taken in natural light, after submersion in tap water for 2 months, exhibiting a pinkish grey/brown pigmentation.

Figure 230: Photographs of the porcine ribs (Sus scrofa domesticus), taken in natural light, after submersion in saltwater for 2 months, exhibiting yellow/orange discolouration and yellow greasy deposits on the bone surface.

The porcine ribs submerged in saltwater for 4 months developed a dark pink pigmentation, which was more concentrated towards the epiphyses. In most of the ribs a white, crystalline deposit was also noted at the butchered epiphyses (figure 231). In the surface of the shorter, wider ribs, a similar white deposit was also noted, with a visual increase in porosity (figure 232). It is hypothesised that the white material leaching from the bones is most likely the organic content, and the pink/red discolouration is the decomposition of any blood and marrow, as also seen in the tap water specimens from the 2-month interval. This sequential colour change could be indicative of a slower decomposition rate in the saltwater environment, inhibiting bacterial proliferation and therefore taking longer to reach a similar stage of discolouration and decay. However, due to the vast variability associated with aquatic depositions, and decomposition processes in general, it cannot be assumed that decomposition would naturally follow the same sequence of changes. It is well known in forensic taphonomy that despite the identification of five key stages of decomposition (chapter 1.0), with verified commonality in characteristics and timescales, in reality, the sequence, duration, and presentation of decomposition modifications can vary drastically, even within similar deposition contexts [28, 45].

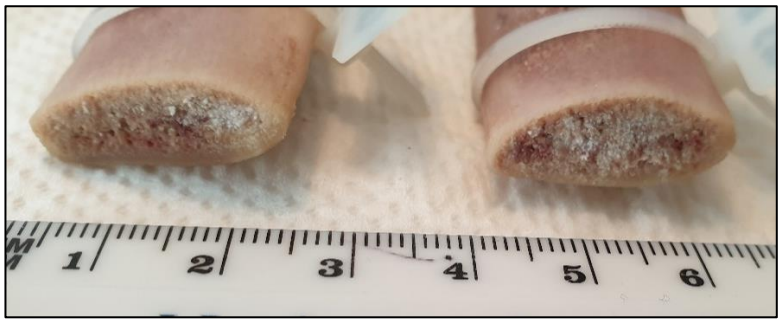

Figure 231: White, crystalline deposit at the butchered epiphyses and dark pink pigmentation, seen in the porcine ribs (Sus scrofa domesticus) that had been submerged in saltwater for 4 months.

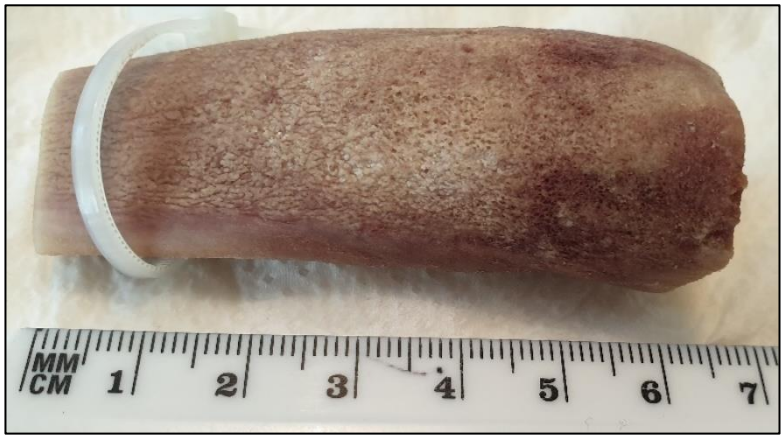

Figure 232: White deposit and visual increase in porosity noted in the shorter, wider porcine ribs (Sus scrofa domesticus) that had been submerged in saltwater for 4 months.

The tap water specimens exhibited a predominantly pale pink discolouration, which was darker towards the epiphyses, but with some yellowing across the diaphysis, where some of the lipid content appears to have leached from the bone. Evidence of minor surface deterioration was noted in several ribs, including fraying and delamination, and possible microbial tunnelling (red circles, figures 233 & 234). However, there was no evidence of the white deposits observed in the saltwater specimens.

Figure 233: Photographs of the tap water porcine bones (Sus scrofa domesticus) after submersion for 4 months, exhibiting a pale pink discolouration with yellowing across the diaphysis. Some surface damage and increased porosity (red circle).

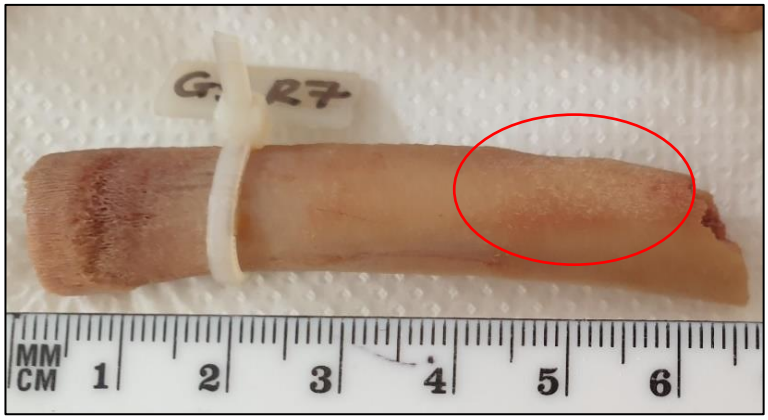

Figure 234: Photographs of the tap water porcine bones (Sus scrofa domesticus) after submersion for 4 months, exhibiting a pale pink discolouration with yellowing across the diaphysis. Possible evidence of microbial tunnelling (red circle).

The porcine bones that were submerged for 6 months in the tap water context produced a similar appearance to some of the 4-month specimens, but to a greater intensity. The prominent surface colour was pink/red, which graduated to a considerably darker reddish/brown towards the epiphyses, especially in the shorter, wider rib fragments (figure 235). This colour change is indicative of advancing decomposition of red blood cells [102], and interestingly is as prominent in the simulated seawater specimens, potentially indicating a slower rate of decomposition. There was some of evidence

organic content leaching noted on the diaphysis of most ribs, characterised by the yellow colour, and the presence of a subtle greasy film. Surface texture was smooth, and there was no evidence of textural modification.

Figure 235: Diffuse pink/red discolouration graduating to a darker reddish/brown towards the epiphyses in the porcine ribs (Sus scrofa domesticus), submerged in tap water for 6 months.

The saltwater specimens presented with an intense yellow pigmentation, in the form of a thick layer of greasy/fatty deposit on the surface of all bones (figure 236). Although this greasy deposit encompassed the entire bone, in most ribs there was a greater concentration accumulated at each epiphysis, where obvious globules were manifesting on the bone surface (figure 236), which were not seen across the diaphysis. This leaching distribution could be the result of the anatomical distribution of cortical and trabecular bone within the rib, as a greater concentration of trabecular bone is usually contained towards the ends of bone and therefore a higher volume of bone marrow and bone vessels [101]. The diaphysis of ribs is predominantly cortical bone, with a narrow intramedullary cavity, due to the protective role within the thoracic cavity. Consequently, it is reasonable to suggest that the greater concentration of fat leaching would occur in the areas of bone with the richer fat reserves. Furthermore, it would also be logical for the leaching of organic material to be evident at the sites of trauma and butchery, as the penetration of the cortical bone creates an access point for the infiltration of water and bacteria, as well as an exit route for leaching material. This theory is supported by the

accumulation of white material at the butchered ends of the bone, which was present in greater volume compared to previous submersion intervals (figure 237).

Figure 236: Appearance of two example porcine ribs (Sus scrofa domesticus) displaying yellow pigmentation and a thick layer of greasy/fatty surface deposits, after submersion in saltwater for 6 months.

Figure 237: White surface deposits seen at the butchered epiphyses of two porcine ribs (Sus scrofa domesticus), after submersion in saltwater for 6 months.

Table 64 below details the recorded changes in bone dimensions; mass, length, width and anterior-posterior, for each submersion interval, including the calculated percentage change for each measurement. The top half of the table contains the data for the tap water specimens and the lower half of table details the measurements for the bones

submerged in the simulated sea water. The day 0 figures for all ribs are the post-maceration measurements.

At all submersion intervals the porcine ribs deposited in the saline environment experienced an increase in mass. The greatest mass gain was seen in the 2-month interval, where the ribs on average experienced 0.80 g (8.1%) increase. Although mass increases were also present for the 4-month and 6-month saltwater specimens, the volume of gain was lower, as the duration increased. The 4-month specimens exhibited an average mass increase of 0.57 g (5.1%), and the 6-month saline data set experience a 0.49 g (3.6%) increase. The tap water specimens exhibited a mixture of mass losses and gains, with an overall 0.34 g (2.4%) loss in mass seen in the 2-month specimens, whereas a 0.68 g (5.7%) average gain was found when examining the 4-month tap water bones. The 6-month tap water specimens also exhibited an overall average loss of 0.68 g (7.2%). The ribs submerged in saltwater generally exhibited a uniform change across the dataset, whereas the tap water groups experienced a mixture of reductions and increases of mass within the same dataset, especially in the 2-month submersion samples.

Increases in mass were anticipated, due to the infiltration of the water through the porous bone structure. However, there was some expectation that the porcine ribs submerged in the saltwater conditions would eventually experience a decrease in mass, due to the high salinity creating an osmotic gradient and subsequent leaching of water and organic material. As mentioned in the previous paragraphs, there was clear evidence of fat and organic leaching seen in the saltwater datasets, due to the presence of the yellow, greasy material found on the surface of the bones. This greasy substrate was in the highest quantities in the final 6-month dataset, where a mass increase was still recorded for the porcine bones, but it was the smallest increase. Consequently, it is feasible that the submersion duration was not long enough to see a loss in mass.

The loss in bone mass experienced by the tap water bones was not anticipated, especially in the relatively short 2-month duration of the first sampling interval. However, the initial loss experienced in the 2-month submersion samples was low (0.33 g, 1.8%), and therefore may have been the result of mismeasurement. The increase in bone mass noted at the 4-month submersion interval was in keeping with expectations, as bone will absorb water due to its porous texture. It is unclear why mass gain was

observed in the saltwater datasets earlier than the tap water, as it was hypothesised that the high salinity would cause a decrease in mass due to the osmotic gradient drawing moisture/organic content from the bone. The leaching of the organic content was most prevalent at the 6-month interval, but this is not reflected by any changes in bone mass. These results further highlight that the overall timescale of the experiment would have benefited from being longer to allow further taphonomic alterations to develop.

Table 64: Changes in mass, length, width and anterior-posterior for all porcine bones (Sus scrofa domesticus) across each submersion interval, including the calculated percentage change for each measurement. Data for the tap water specimens is contained in the top half and the saltwater data in the lower half.

		Day 0				2 Months				Changes							
	Rib	Mass (g)	Length (mm)	Width (mm)	A/P (mm)	Mass (g)	Length (mm)	Width (mm)	A/P (mm)	Mass (g)		Length (mm)		Width (mm)		A/P (mm)	
Tap water	1	20.59	78	18.1	13.9	19.63	77.2	19	13	-0.96	4.9%	-0.80	1%	+0.90	4.7%	-0.90	6.9%
	2	11.23	75.4	16.6	9.3	11.8	74.5	16	9.2	+0.57	4.8%	-0.90	1.2%	-0.60	3.8%	-0.10	1.1%
	3	8.92	98.7	11.3	7.9	8.68	99.2	10.7	8.1	-0.24	2.8%	+0.50	0.5%	-0.60	5.6%	+0.20	2.5%
	4	14.91	118.8	14.6	9.3	14.64	118	14.9	8.6	-0.27	2.8%	-0.80	0.7%	+0.30	2%	-0.70	8.1%
	5	15.51	75.1	20.1	10.9	14.76	73.5	20	10.2	-0.75	5.1%	-1.60	2.2%	-0.10	0.5%	-0.70	6.9%
	6	9	86.3	11.2	9.6	8.4	84.7	11	10.8	-0.60	7.1%	-1.60	1.9%	-0.20	1.8%	+1.20	11.1%
	7	18.31	76	24.3	8.9	17.04	74.8	23.6	9.2	-1.27	7.5%	-1.20	1.6%	-0.70	3%	+0.30	3.3%
	8	5.52	63.4	10.1	7	5.63	62.2	9.8	7	+0.11	2%	-1.20	1.9%	-0.30	3.1%	0.00	
	9	18.39	133.8	12.5	10.6	18.72	133.7	14.7	10.3	+0.33	1.8%	-0.10	0.1%	+2.20	15%	-0.30	2.9%
Av.		13.60	89.50	15.42	9.71	13.26	88.64	15.52	9.60	-0.34	2.3%	-0.86	1.1%	+0.10	0.4%	-0.11	1%
Saltwater	10	6.68	105.9	10.8	6.9	7.29	105.5	10.7	6.8	+0.61	8.4%	-0.40	0.4%	-0.10	0.9%	-0.10	1.5%
	11	9	67.3	15.6	8.2	9.55	67.7	15.3	8.1	+0.55	5.8%	+0.40	0.6%	-0.30	2%	-0.10	1.2%
	12	7.77	80.9	12.6	7.1	9.13	79.3	12.4	6.9	+1.36	14.9%	-1.60	2%	-0.20	1.6%	-0.20	2.9%
	13	10.64	66.8	16.1	9.9	11.38	65.8	16	9.6	+0.74	6.5%	-1.00	1.5%	-0.10	0.6%	-0.30	3.1%
	14	18.67	68	17.3	15.3	19	68.5	17	14.9	+0.33	1.7%	+0.50	0.7%	-0.30	1.8%	-0.40	2.7%
	15	15.68	63.7	17.1	14.1	16.16	61.9	17.1	13.5	+0.48	3%	-1.80	2.9%	0.00		-0.60	4.4%
	16	9.24	89.7	12.7	7.8	9.9	86.9	12.6	8.4	+0.66	6.7%	-2.80	3.2%	-0.10	0.8%	+0.60	7.1%
	17	8.79	83.3	13.4	7.5	10.07	82.7	13	7.2	+1.28	12.7%	-0.60	0.7%	-0.40	3.1%	-0.30	4.2%
	18	7.29	67.3	12.3	8.4	8.45	65.6	12.2	8.4	+1.16	13.7%	-1.70	2.6%	-0.10	0.8%	0.00	
Av.		10.42	76.99	14.21	9.47	11.21	75.99	14.03	9.31	+0.80	8.1%	-1.00	1.3%	-0.18	1.3%	-0.16	1.4%

		Day 0				4 Months				Changes							
	Rib	Mass (g)	Length (mm)	Width (mm)	A/P (mm)	Mass (g)	Length (mm)	Width (mm)	A/P (mm)	Mass (g)		Length (mm)		Width (mm)		A/P (mm)	
Tap water	1	16.32	115.9	15	9.4	17.59	115.5	15	9.1	+1.27	7.2%	-0.40	0.3%	0.00	0.0%	-0.30	3.3%
	2	18.75	85	19.9	12.2	19.97	84.4	20.1	11.8	+1.22	6.1%	-0.60	0.7%	+0.20	1.0%	-0.40	3.4%
	3	10.15	91.6	11.1	10.5	10.66	91.4	10.3	9.9	+0.51	4.8%	-0.20	0.2%	-0.80	7.8%	-0.60	6.1%
	4	8.03	82	13.9	6.6	8.63	81.1	13.6	6.4	+0.60	7.0%	-0.90	1.1%	-0.30	2.2%	-0.20	3.1%
	5	11.29	93.4	12.1	9.8	12.08	92.2	12.3	9.5	+0.79	6.5%	-1.20	1.3%	+0.20	1.6%	-0.30	3.2%
	6	24	71.5	22.1	16.2	24	72.1	22	14.7	0.00		+0.60	0.8%	-0.10	0.5%	-1.50	10.2%
	7	7.36	73.5	13.6	7.1	7.84	72.9	13	6.7	+0.48	6.1%	-0.60	0.8%	-0.60	4.6%	-0.40	6%
	8	11.42	109.9	10.8	9.7	11.93	108.1	10.6	8.9	+0.51	4.3%	-1.80	1.7%	-0.20	1.9%	-0.80	9%
	9	7.27	59.1	14.4	9.2	8	58.4	14.3	9.1	+0.73	9.1%	-0.70	1.2%	-0.10	0.7%	-0.10	1.1%
Av.		12.73	86.88	14.77	10.08	13.41	86.23	14.58	9.57	+0.68	5.7%	-0.64	0.7%	-0.19	1.7%	-0.51	5%
Salt water	10	21.07	67.4	26.5	13.8	21.37	68.6	25.6	11.6	+0.30	1.4%	+1.20	1.7%	-0.90	3.5%	-2.20	19%
	11	6.16	61.4	12.2	8.2	6.61	60.5	11.6	7.2	+0.45	6.8%	-0.90	1.5%	-0.60	5.2%	-1.00	13.9%
	12	15.22	69.7	23.7	10.8	16.22	70.9	24.3	8.6	+1.00	6.2%	+1.20	1.7%	+0.60	2.5 %	-2.20	25.6%
	13	12.74	88.4	17.1	8.8	13.45	86.4	17.1	8.4	+0.71	5.3%	-2.00	2.3%	0.00		-0.40	4.8%
	14	8.7	83.8	13.2	7.9	9.88	83.3	13.3	7.6	+1.18	11.9%	-0.50	0.6%	+0.10	0.8%	-0.30	3.9%
	15	10.91	86.7	15.7	8.6	11.71	11.71	15.6	8.6	+0.80	6.8%	-1.10	1.3%	-0.10	0.6%	0.00	
	16	10.86	101.6	12.8	7.8	11.53	11.53	12.5	7.7	+0.67	5.8%	-0.50	0.5%	-0.30	2.4%	-0.10	1.3%
	17	5.16	64.2	11.9	5.5	5.27	5.27	12.5	5.1	+0.11	2.1%	-0.40	0.63%	+0.60	4.8%	-0.40	7.8%
	18	17.27	72.9	23.2	12.3	17.15	17.15	22.8	10.8	-0.12	0.7%	-2.10	3.0%	-0.40	1.8%	-1.50	13.9%
Av.		12.01	77.34	17.37	9.30	12.58	46.15	17.26	8.40	+0.57	5.1%	-0.57	0.7%	-0.11	0.6%	-0.90	10%

		Day 0				6 Months				Changes							
	Rib	Mass (g)	Length (mm)	Width (mm)	A/P (mm)	Mass (g)	Length (mm)	Width (mm)	A/P (mm)	Mass (g)		Length (mm)		Width (mm)		A/P (mm)	
Tap water	1	7.75	70.8	12.9	6.8	7.29	72.7	12.7	6.4	-0.46	6.3%	+1.90	2.6%	-0.20	1.6%	-0.40	6.2%
	2	9.57	84.7	13.9	8.9	8.73	83.7	13.1	7.7	-0.84	9.6%	-1.00	1.2%	-0.80	6.1%	-1.20	15.6%
	3	14.15	117.3	12.8	9	14.35	117	13.1	8.9	+0.20	1.4%	-0.30	0.3%	+0.30	2.3%	-0.10	1.1%
	4	10.18	98	12.4	9.3	9.58	96.8	12.3	8.3	-0.60	6.3%	-1.20	1.2%	-0.10	0.8%	-1.00	12%
	5	6.94	83.7	11.7	7.6	6.87	84.4	11	7.4	-0.07	1%	+0.70	0.8%	-0.70	6.4%	-0.20	2.7%
	6	11.26	105.5	11.8	8.2	10.3	103.1	11.5	7.2	-0.96	9.3%	-2.40	2.3%	-0.30	2.6%	-1.00	13.9%
	7	16.8	75	12.1	13.2	14.89	73.1	16.3	11.8	-1.91	12.8%	-1.90	2.6%	+4.20	25.8%	-1.40	11.9%
	8	20.16	97.1	22.3	10.9	19.51	95.4	22.1	10.2	-0.65	3.3%	-1.70	1.8%	-0.20	0.9%	-0.70	6.9%
	9	5.28	55.8	12.2	6.5	4.48	55.3	11.4	6.4	-0.80	17.9%	-0.50	0.9%	-0.80	7%	-0.10	1.6%
Av.		11.34	87.54	13.57	8.93	10.67	86.83	13.72	8.26	-0.68	7.2%	-0.71	0.8%	+0.16	0.3%	-0.68	8%
Saltwater	10	9.54	69.1	14.8	8.2	9.69	68.3	14.8	7.4	+0.15	1.5%	-0.80	1.2%	0.00		-0.80	10.8%
	11	10.95	88.9	14.4	7.6	11.08	87.8	14.4	6.9	+0.13	1.2%	-1.10	1.3%	0.00		-0.70	10.1%
	12	7.93	80.7	11.4	8.2	8.5	78.4	11.3	7	+0.57	6.7%	-2.30	2.9%	-0.10	0.9%	-1.20	17.1%
	13	15.04	79.5	20.1	10.3	15.04	77.4	19.4	9.4	0.00		-2.10	2.7%	-0.70	3.6%	-0.90	9.6%
	14	6.9	75.4	11.9	6.9	7	75.7	12.4	6.4	+0.10	1.4%	+0.30	0.4%	+0.50	4.0%	-0.50	7.8%
	15	18	67.2	18.3	13.5	19.3	65.5	18.2	13	+1.30	6.7%	-1.70	2.6%	-0.10	0.5%	-0.50	3.8%
	16	7.82	72.4	12.3	7	8.05	71.1	12.5	6.8	+0.23	2.9%	-1.30	1.8%	+0.20	1.6%	-0.20	2.9%
	17	6.71	65.3	12.9	7.2	6.74	65.1	13	6.8	+0.03	0.4%	-0.20	0.3%	+0.10	0.8%	-0.40	5.9%
	18	14.69	63.2	20	12.6	16.55	60.9	20	10.7	+1.86	11.2%	-2.30	3.8%	0.00		-1.90	17.8%
Av.		11.11	80.90	14.30	8.99	11.33	72.24	15.11	8.27	+0.49	3.6%	-1.28	1.8%	-0.01	0.2%	-0.79	9.5%

With regards to bone dimensions, no discernible relationship between the observed changes in bone dimension and the deposition context was detected. All ribs across all contexts and timescales experienced a minor change in bone dimensions, usually a small loss of between 0.1-2%, but with some ribs experiencing an increase of a similar magnitude at different submersion intervals. The most consistent and largest decreases were recorded in the anterior-posterior measurement in both the tap water and saline contexts. At the 2-month interval the reduction was relatively minor for both aquatic contexts, as the tap water bones lost on average 0.11 mm (1%), and the saltwater specimens lost 0.16 mm (1.4%). At the 4-month interval, the tap water dataset experienced larger average loss of 0.51 mm (5%) in anterior-posterior volume, whilst the saltwater porcine ribs exhibited a 0.90 mm (10%) average loss, almost double the tap water measurement. This result was then echoed in the 6-month results data, as the saltwater porcine ribs were subjected to a 0.79 mm (9.5%) average reduction in A/P measurements, and the tap water bones experienced a similar loss of 0.68 mm (8%). These results correspond with the macroscopic changes noted during initial observations, such as the surface changes to the cortical bone, leaching of the organic component, and early diagenetic alterations including increased porosity, and microbial tunnelling, which all could contribute to loss of bone volume, and therefore shrinkage of A/P dimensions [101].

However, these findings were not in keeping with expectations, as it was anticipated that more drastic structural changes would be exhibited with more disparity between the tap and saltwater results. A possible explanation is the use of still aquatic environment. Literature states that a fluctuating environment is the most conducive to bone degradation [101, 368], such as extreme changes in temperature, water composition, moisture levels, or movement [101]. However, as this experiment simulated a still aquatic context, there was no means of mechanical decomposition such as waves or currents, and no abrasive terrain for the bones to interact with. Based on the temperature data from the data loggers (table 65) there were sizable diurnal fluctuations in temperature throughout the experiment. Over the course of the 6-months ambient temperature ranged from 5.3 to 25.6 °C, with an average temperature of 31.1 °C. The recorded temperature within the aquatic contexts were overall slightly higher compared to the ambient, and based on the 4-month readings, there was a negligible difference

between the tap water and saltwater readings. Consequently, it is less likely that temperature impeded decomposition, but as many of the data loggers failed to record, it is not possible to make any further interpretations.

The lids to the containers were kept closed throughout the experiment, and then all containers were covered with a tarpaulin to prevent scavenging activity and dilution of the solutions from rain. Although the lids were not airtight, the presence of multiple physical barriers would also have limited oxygen levels within the boxes, and thus slowing bacterial proliferation. It was the intention to drill holes in the side of the boxes to allow a flow of air but due to the shutdown of the laboratories and limited access to equipment due to the coronavirus lockdown, it was not possible. In addition to this, the inclusion of the holes at the side of the boxes would have meant lower water levels, which would have impeded the fluorescence photography.

The pH of each context remained relatively stable throughout the experimentation, and close to neutral. It was expected that the decomposition of the porcine rib bones would have had a greater influence on the aqueous environments, as is commonly reported in taphonomic studies [95]. The lack of tissue may have been an influencing factor, as there would have been diminished resources for putrefactive bacteria to consume. A more acidic environment would have been more conducive to diagenetic change [370].

Table 65: Average recorded temperature data for each interval and ambient temperature for the duration of the submerged salinity experiment.

Context	Ambient (°C)			2-month (°C)			4-month (°C)			6-month (°C)		
	Min	Av.	Max	Min	Av.	Max	Min	Av.	Max	Min	Av.	Max
Tap	5.3	13.1	25.6	Data logger failed			10.2	17.9	34.5	Data logger failed		
Salt				Data logger failed			9.8	17.9	36	4.8	14.1	33.2

26.3.3- FLUORESENCE

Tables 66-71 summarise the photographic fluorescence results for three example porcine ribs for each context and each submersion interval, photographed using the Hammerhead ALS (450 nm), orange filter and 1/3s exposure time. The final fluorescence and OFC processed images are available in appendix 76. The full fluorescence photographic tables can be seen in appendix 77.

Table 66: Summarised photographic fluorescence results for the 2-month tap water specimens.

Day 0			2 months (tap water)		
Natural	Terrestrial	Submerged	Natural	Terrestrial	Submerged
					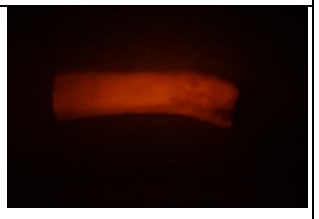
	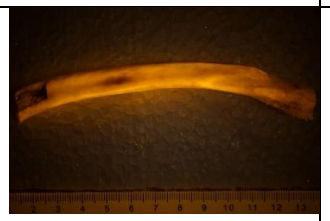			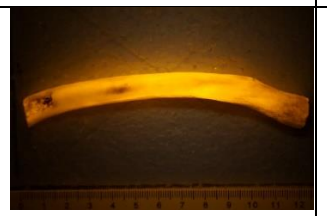	
		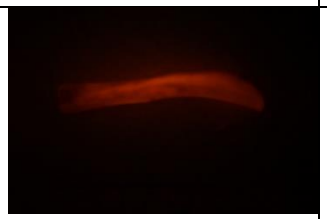			

Table 67: Summarised photographic fluorescence results for the 2-month saltwater specimens.

Day 0			2 months (Saltwater)		
Natural	Terrestrial	Submerged	Natural	Terrestrial	Submerged
			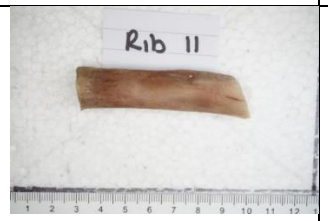		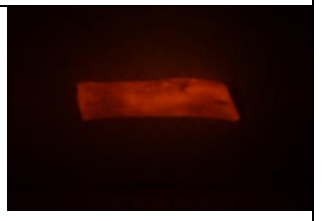
	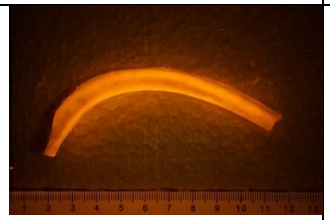				

Table 68: Summarised photographic fluorescence results for the 4-month tap water specimens.

Day 0			4 months (tap water)		
Natural	Terrestrial	Submerged	Natural	Terrestrial	Submerged
		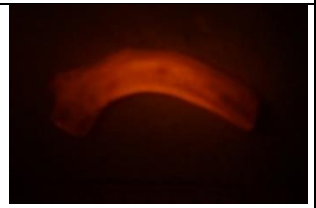			
	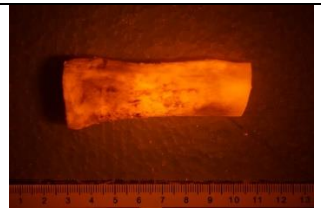				
	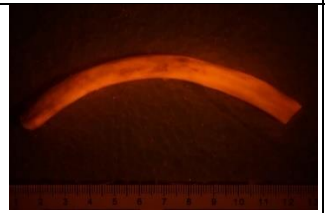			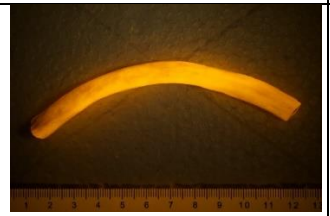	

Table 69: Summarised photographic fluorescence results for the 4-month saltwater specimens.

Day 0			4 months (Saltwater)		
Natural	Terrestrial	Submerged	Natural	Terrestrial	Submerged
	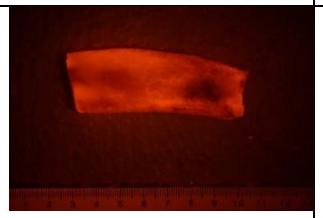			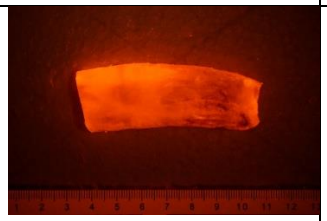	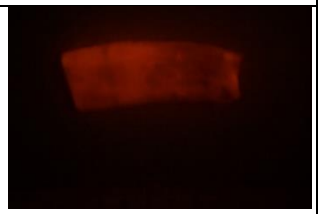
	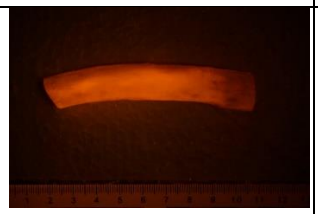				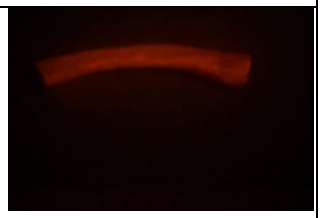
	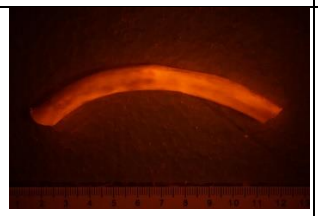			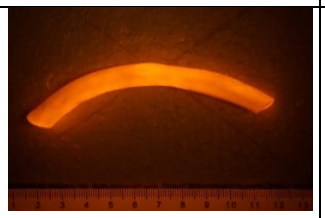	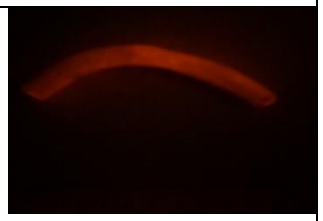

Table 70: Summarised photographic fluorescence results for the 6-month tap water specimens.

Day 0			6 months (tap water)		
Natural	Terrestrial	Submerged	Natural	Terrestrial	Submerged
	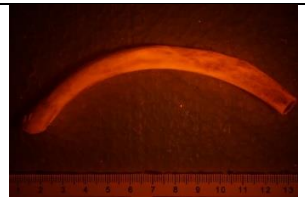			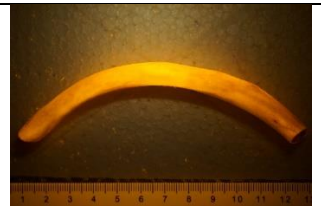	
				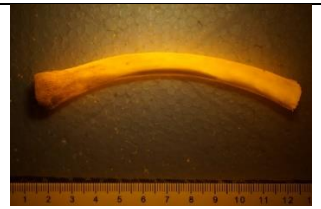	
	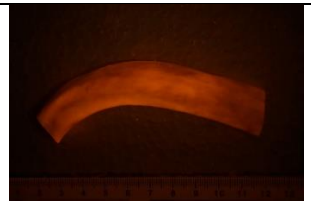	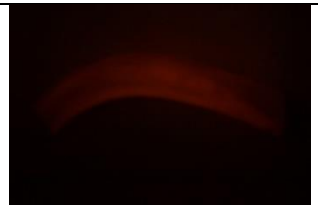			

Table 71: Summarised photographic fluorescence results for the 6-month saltwater specimens.

Day 0			6 months (saltwater)		
Natural	Terrestrial	Submerged	Natural	Terrestrial	Submerged
		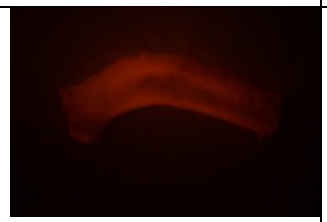			

Table 72 and bar charts 238 and 239, comparatively illustrate the average differences in emitted florescence in the porcine ribs prior to submersion compared to post submersion, for each interval. Overall, the highest fluorescence results were seen in the terrestrial contexts and increased exponentially at each submersion interval. The largest increase in fluorescence was observed in the 6-month dataset set, where prior to submersion the ribs exhibited an average fluorescence result of 88.0, but after 6-months submersion in an aquatic environment experienced an average fluorescence value of 184.4 when photographed terrestrially with the Hammerhead light source. When the same ribs were consequently photographed in tap water environment, the average fluorescence values were substantially lower, decreasing from 184.4 to 84.8, a reduction of 99.6 (73.9%).

In contrast, the recorded fluorescence values captured in the tap water environment experienced a minor decrease in fluorescence values in the 2-month and 4-month datasets, a 9.4% and 1% respectively, however, the porcine bones that were submerged for 6 months, almost doubled in fluorescence intensity, with a pre-submersion fluorescence value of 43.3 rising to 85.8, post-submersion, difference of 42.5 (98.1%) when photographed in tap water.

When the saltwater and tap water fluorescence changes are compared (table 73), the bones submerged in saltwater can be seen to increase in fluorescence intensity at each temporal interval and in both photography contexts, other than at the 4-month interval, where a small average loss of 20 (37.1%) was seen. The bones submerged in tap water initially experience a loss in fluorescence at the 2-month interval in the underwater photography context, then went on to generate an increase at the 4-month and 6-month intervals, in both terrestrial and aquatic photography conditions. Overall, the highest fluorescence values were observed in the terrestrial contexts, in keeping with the results of the previous research questions.

Table 72: Calculated average differences in emitted florescence in porcine ribs (Sus scrofa domesticus) after each submersion interval, when photographed using the Hammerhead ALS, orange filter, at 1/3s exposure time, in terrestrial and aquatic contexts.

Interval (months)	Terrestrial				Underwater			
	Before submersion	Post submersion	Diff	% change	Before submersion	Post submersion	Diff	% change
2	112.9	170.8	+58.0	+51.4%	67.3	61.0	-6.3	-9.4%
4	86.8	147.5	+60.7	+70.0%	74.3	73.6	-0.8	-1.0%
6	88.0	184.8	+96.9	+110.1%	43.3	85.8	+42.5	+98.1%

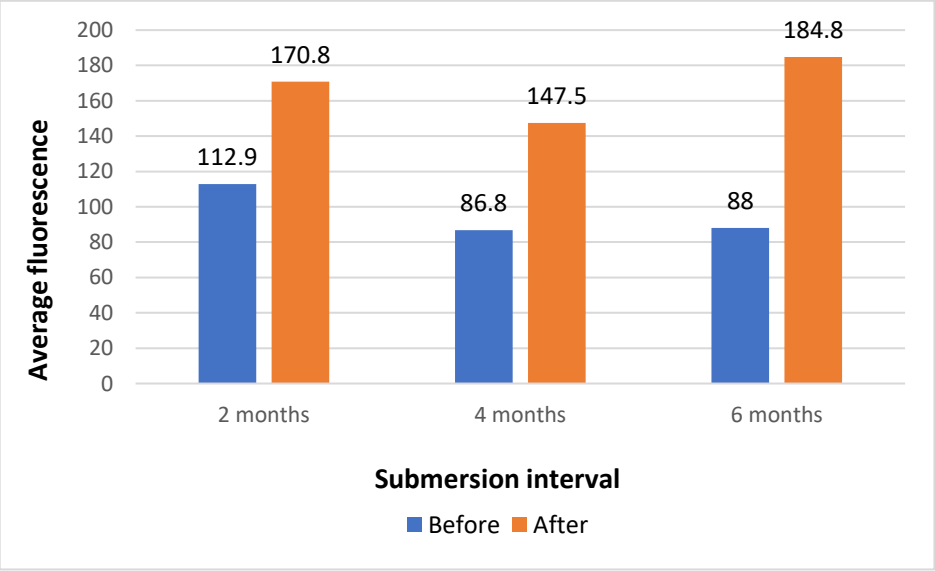

Figure 238: Average changes in terrestrial fluorescence of the 18 porcine ribs (Sus scrofa domesticus), seen at each submersion interval.

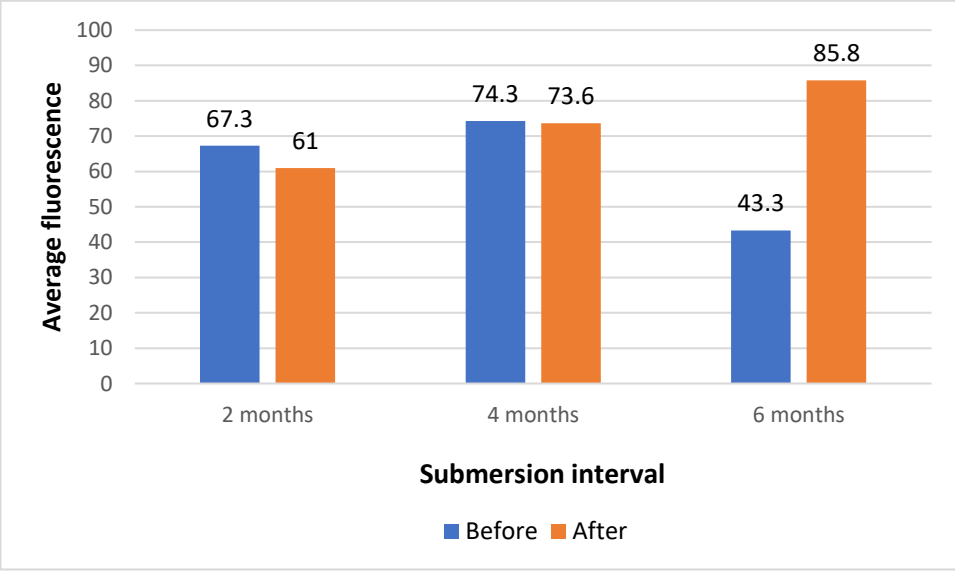

Figure 239: Average changes in underwater fluorescence of the 18 porcine ribs (Sus scrofa domesticus), seen at each submersion interval.

Table 73: Comparison of calculated average differences in emitted florescence in porcine ribs (Sus scrofa domesticus) after each submersion interval, and across each aquatic context. Photographed using the Hammerhead ALS, orange filter, at 1/3s exposure time.

Terrestrial fluorescence												
Deposition context	2 months				4 months				6 months			
	Before submersion	After submersion	Diff.	% diff.	Before submersion	After submersion	Diff.	% diff.	Before submersion	After submersion	Diff.	% diff.
Tap	123.9	172.3	+48.4	28.1%	94	170.4	+76.4	44.8%	89.2	86.8	-0.6	2.8%
Salt	101.8	169.4	+67.6	39.9%	79.5	124.5	+45	36.2%	179.4	190.3	+10.9	5.8%
Diff.	22.1	2.9			14.6	45.9			2.4	10.9		
Underwater fluorescence												
Tap	79.3	56.5	-22.8	40.4%	74.8	93.2	+18.4	19.9%	38.8	69.4	+30.6	44.1%
Salt	57.6	65.6	+8	12.2%	73.9	53.9	-20	37.1%	47.8	102.2	+54.4	53.2%
Diff.	22.8	8.1			0.9	39.3			9	32.8		

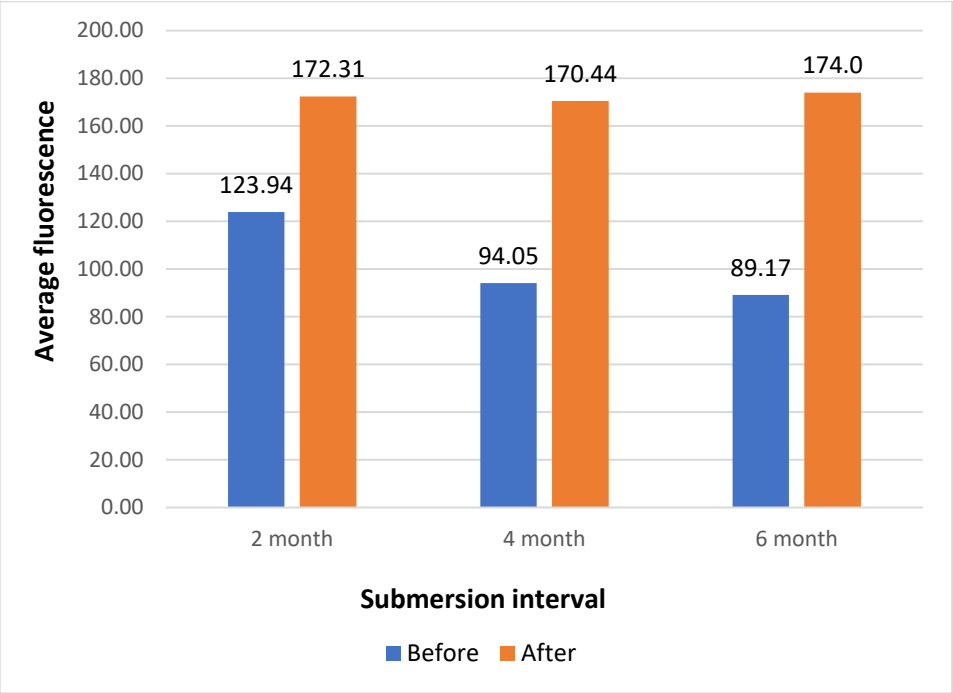

Figure 240: Differences in average terrestrial bone fluorescence observed in porcine bone (Sus scrofa domesticus) that had been submerged in tap water for 2-, 4-, and 6-month durations.

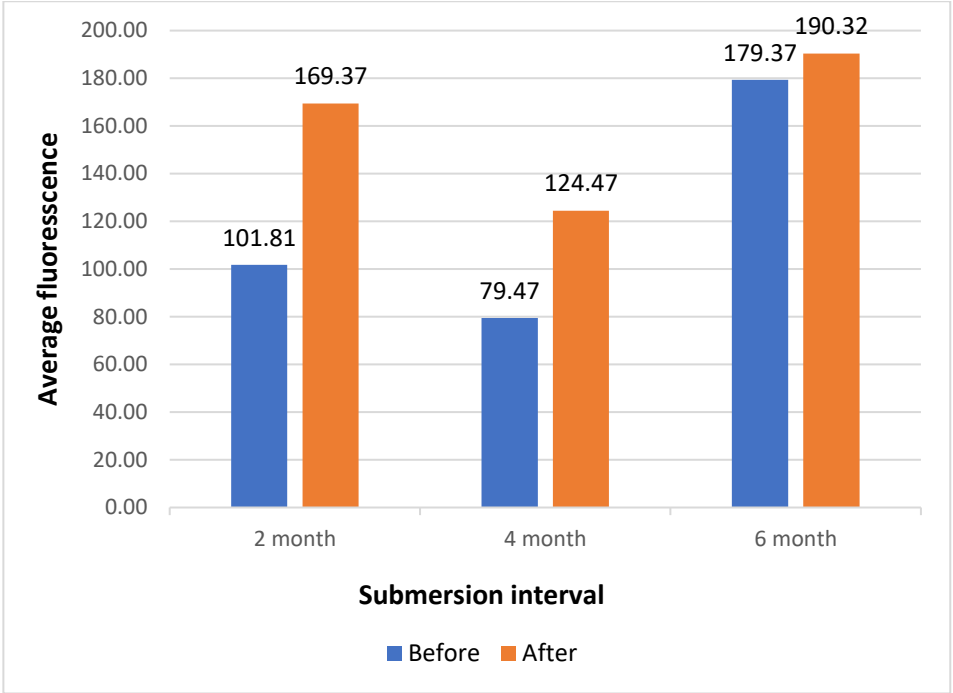

Figure 241: Differences in average terrestrial bone fluorescence observed in porcine bone (Sus scrofa domesticus) that had been submerged in saltwater for 2-, 4-, and 6-month durations.

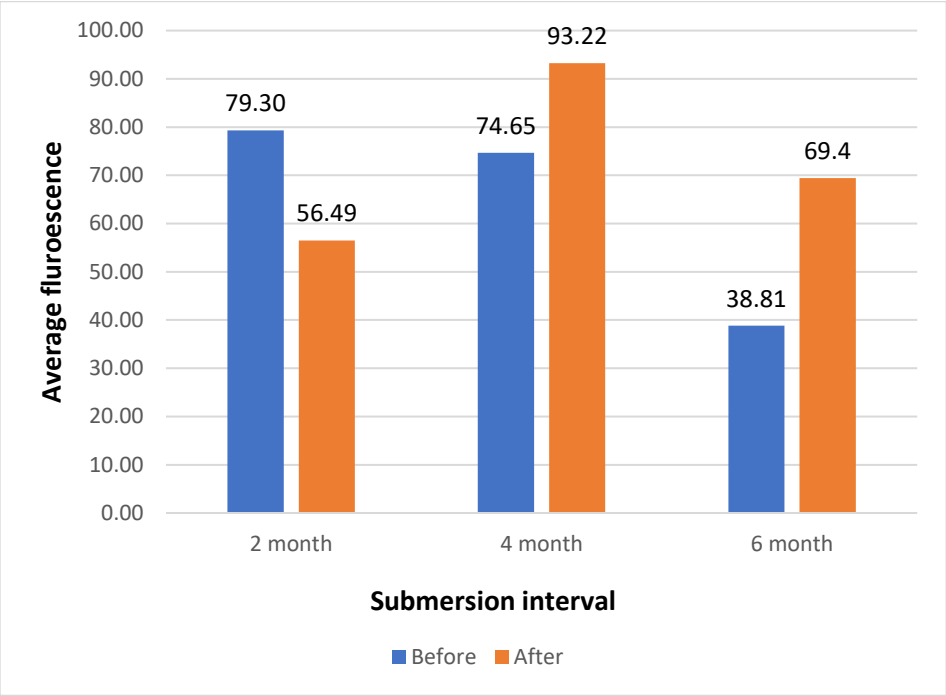

Figure 242: Differences in average underwater bone fluorescence observed in porcine bone (Sus scrofa domesticus) that had been submerged in tap water for 2-, 4-, and 6-month durations.

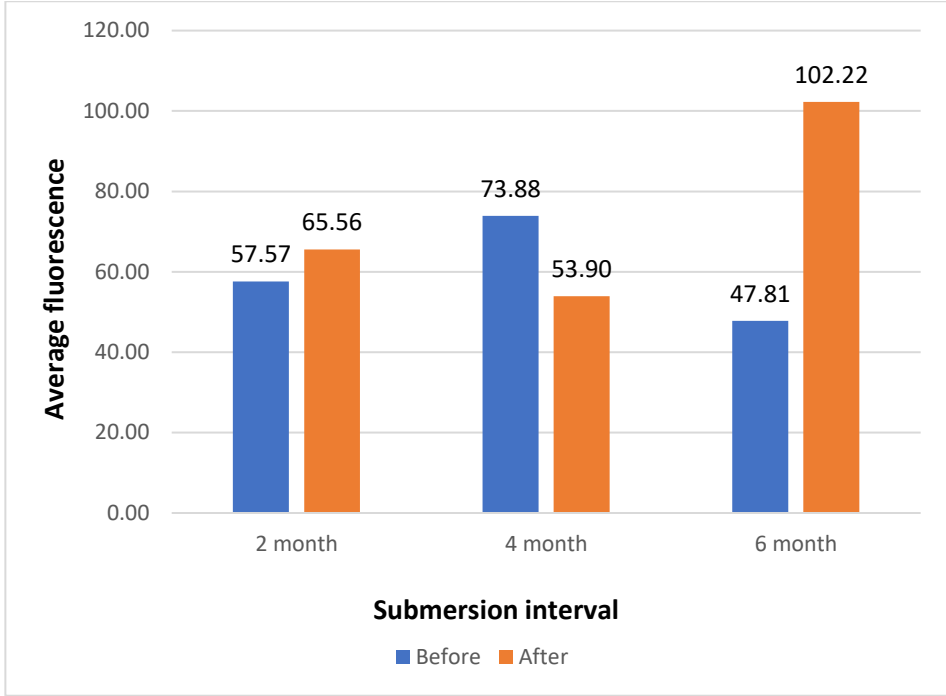

Figure 243: Differences in average underwater bone fluorescence observed in porcine bone (Sus scrofa domesticus) that had been submerged in saltwater for 2-, 4-, and 6-month durations.

26.3.4- COLLAGEN

Tables 74-76 and figures 244 and 245 summarise the collagen results for the salinity experiment for each submersion interval, including the calculated decreases and percent change. All thermograms for this research question can be found in appendix 78. All the porcine ribs experienced a loss of collagen. In all cases, the ribs submerged in saltwater experienced on average the greatest and most consistent decreases in collagen content, with the most substantial reduction recorded at the 2-month interval of 0.07 mg (s.d = 0.09, 10.48%), and the lowest in the 4-month interval of 0.048 mg (s.d = 0.04, 8.21%). The tap water specimens overall experienced smaller losses in calculated content, but also experienced the greatest loss at the first interval, (2 months submersion) of 0.07 (s.d = 0.05, 12.2%), echoing the trend seen in the saltwater specimens. A reduction in collagen content in the 2-month and 6-month intervals was greater than the equivalent saltwater samples.

Table 74: Changes in calculated collagen levels for the porcine ribs (Sus scrofa domesticus) submerged in the tap water and saltwater contexts for 2-months.

Context	Rib	Day 0 Collagen (mg)	2 months Collagen (mg)	Difference (mg)	% Difference
Tap water	1	0.66	0.54	-0.12	-17.7%
	2	0.48	0.33	-0.15	-31.2%
	3	0.56	0.47	-0.08	-14.9%
	4	0.53	0.50	-0.03	-5.2%
	5	0.58	0.47	-0.11	-18.7%
	6	0.55	0.51	-0.03	-6.2%
	7	0.53	0.49	-0.04	-7.7%
	8	0.51	0.48	-0.03	-5.9%
	9	0.50	0.49	-0.01	-1.6%
	Av.	0.54	0.48	-0.07	-12.12%
	S.D.	0.05	0.06	0.05	8.4%
Saltwater	10	0.66	0.56	-0.10	-15.5%
	11	0.49	0.48	0.01	-1.6%
	12	0.57	0.55	-0.02	-3.5%
	13	0.54	0.52	-0.02	-3.3%
	14	0.56	0.53	-0.03	-5.5%
	15	0.80	0.50	-0.30	-37.9%
	16	0.62	0.51	-0.10	-17.0%
	17	0.49	0.49	-0.00	-0.7%
	18	0.52	0.46	-0.06	-10.8%
	Av.	0.58	0.51	-0.07	-10.48%
	S.D.	0.09	0.03	0.09	10.7%

Table 75: Changes in calculated collagen levels for the porcine ribs (Sus scrofa domesticus) submerged in the tap water and saltwater contexts for 4-months.

Context	Rib	Day 0 Collagen (mg)	4 months Collagen (mg)	Difference (mg)	% Difference
Tap water	1	0.49	0.47	-0.02	-3.2%
	2	0.51	0.44	-0.07	-14.1%
	3	0.45	0.44	-0.01	-1.4%
	4	0.51	0.47	-0.04	-8.4%
	5	0.52	0.49	-0.03	-6.2%
	6	0.34	0.30	-0.04	-12.8%
	7	0.48	0.47	-0.01	-1.8%
	8	0.51	0.47	-0.04	-7.5%
	9	0.50	0.43	-0.07	-13.2%
	Av.	0.48	0.44	-0.036	-6.90%
	S.D.	0.05	0.05	0.02	4.7%
Saltwater	10	0.69	0.54	-0.15	-21.3%
	11	0.52	0.48	-0.03	-6.5%
	12	0.52	0.53	-0.01	-2.7%
	13	0.55	0.53	-0.02	-3.3%
	14	0.52	0.48	-0.04	-6.9%
	15	0.51	0.48	-0.04	-7.3%
	16	0.55	0.48	-0.07	-12.6%
	17	0.56	0.47	-0.08	-15.0%
	18	0.52	0.50	-0.02	-3.7%
	Av.	0.55	0.50	-0.048	-8.21%
	S.D.	0.05	0.03	0.04	6.7%

Table 76: Changes in calculated collagen levels for the porcine ribs (Sus scrofa domesticus) submerged in the tap water and saltwater contexts for 6-months.

Context	Rib	Day 0 Collagen (mg)	6 months Collagen (mg)	Difference (mg)	% Difference
Tap water	1	0.54	0.45	-0.08	-15.3%
	2	0.50	0.44	-0.07	-13.3%
	3	0.49	0.43	-0.06	-12.9%
	4	0.51	0.44	-0.07	-14.3%
	5	0.50	0.46	-0.04	-8.7%
	6	0.47	0.46	-0.01	-3.1%
	7	0.49	0.44	-0.04	-8.7%
	8	0.39	0.39	0.00	0
	9	0.48	0.41	-0.07	-14.7%
	Av.	0.49	0.44	-0.05	-10.07%
	S.D.	0.04	0.02	0.03	5.3%
Saltwater	10	0.44	0.39	-0.05	-12.2%
	11	0.52	0.51	-0.01	-1.8%
	12	0.51	0.47	-0.04	-8.5%
	13	0.56	0.48	-0.08	-14.5%
	14	0.51	0.46	-0.05	-9.7%
	15	0.80	0.60	-0.20	-24.8%
	16	0.52	0.47	-0.05	-9.1%
	17	0.48	0.47	-0.01	-2.3%
	18	0.48	0.47	-0.01	-3.1%
	Av.	0.53	0.48	-0.06	-9.56%
	S.D.	0.10	0.05	0.05	6.8%

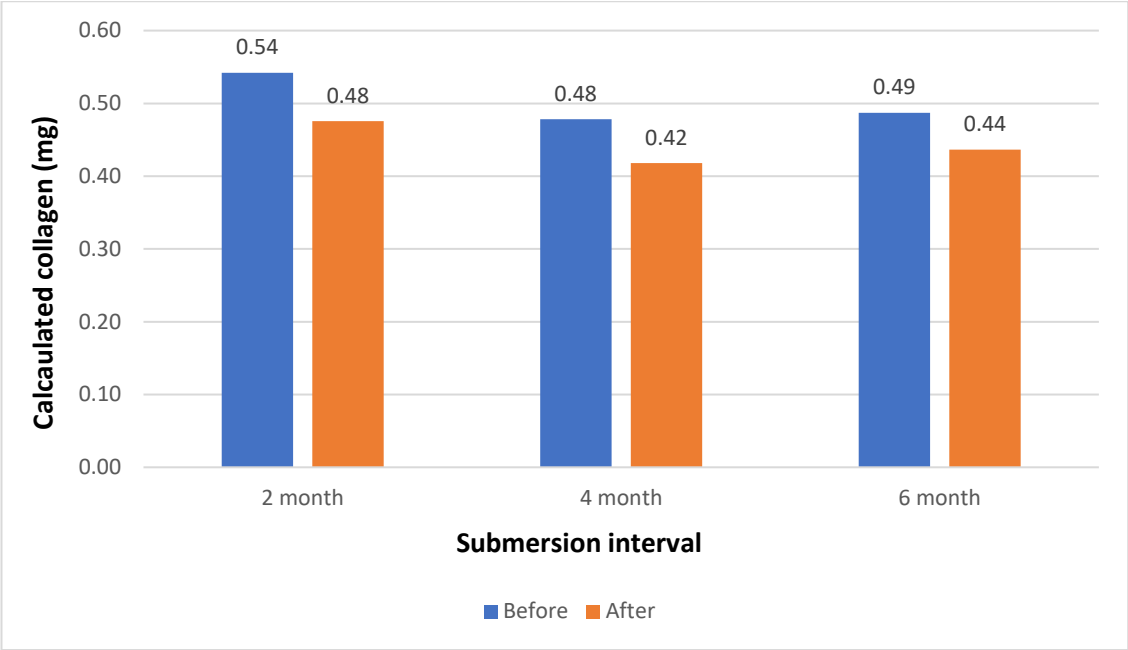

Figure 244: Differences in calculated collagen content in porcine bones (Sus scrofa domesticus) that had been submerged in tap water for 2-, 4-, and 6-month durations.

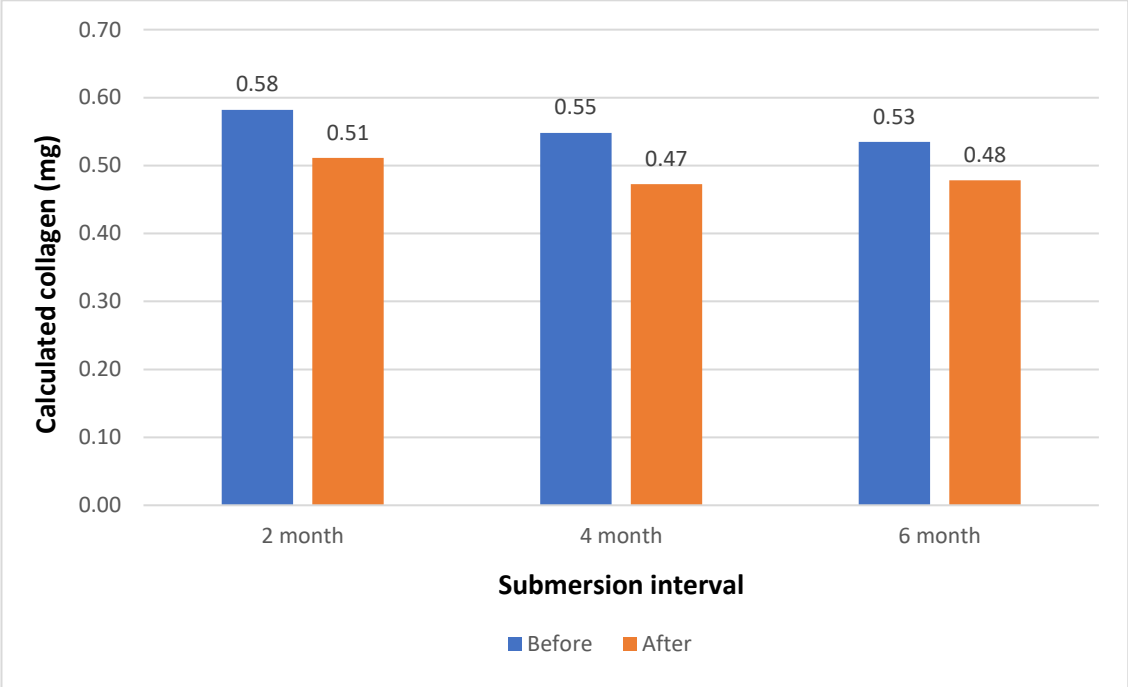

Figure 245: Differences in calculated collagen content in porcine bones (Sus scrofa domesticus) that had been submerged in saltwater for 2-, 4-, and 6-month durations.

26.3.5- STATISTICAL ANALYSIS

The aim of this research question was to investigate the impact of the aquatic taphonomic environment on the calculated collagen content and observed fluorescence. Consequently, statistical analysis focused on the 2 month and 6-month datasets. The dataset of 54 macerated porcine ribs discussed in question 2, was the secondary analysis of the original data for this salinity-based question. Consequently, histogram analysis of the data distribution for the pre-submersion bone dimensions, collagen content, and fluorescence levels has already been completed (appendix 58). Therefore, histograms were only performed on the post-submersions data for each interval, and context, (appendix 79).

All histograms produced for the 2-month and 6-month datasets demonstrated abnormal data distributions, indicating non-parametric data, and therefore, unsuitable for ANOVA statistical analysis. The Friedman test was discounted as the measurements were not repeated samples. Consequently, non-parametric independent samples median tests were conducted, followed by the non-parametric Kruskal-Wallis tests, to see whether there were any significant differences between any of the bone dimensions, calculated collagen content, and average fluorescence data. The output for each temporal group can be seen in images 246-249 below.

Hypothesis Test Summary

	Null Hypothesis	Test	Sig.	Decision
1	The medians of DayOTerrF are the same across categories of DayOColl.	Independent-Samples Median Test	.528	Retain the null hypothesis.
2	The medians of DayOUnWF are the same across categories of DayOColl.	Independent-Samples Median Test	.528	Retain the null hypothesis.
3	The medians of DayOmass are the same across categories of DayOColl.	Independent-Samples Median Test	.374	Retain the null hypothesis.
4	The medians of DayOWidth are the same across categories of DayOColl.	Independent-Samples Median Test	.528	Retain the null hypothesis.
5	The medians of DayOLength are the same across categories of DayOColl.	Independent-Samples Median Test	.528	Retain the null hypothesis.
6	The medians of DayOAP are the same across categories of DayOColl.	Independent-Samples Median Test	.528	Retain the null hypothesis.

Asymptotic significances are displayed. The significance level is .05.

Figure 246: Results of the independent samples median test comparing the day 0 data from the 2-month data group.

Hypothesis Test Summary

	Null Hypothesis	Test	Sig.	Decision
1	The medians of Mass2mon are the same across categories of Coll2mon.	Independent-Samples Median Test	.272	Retain the null hypothesis.
2	The medians of Width2mon are the same across categories of Coll2mon.	Independent-Samples Median Test	.416	Retain the null hypothesis.
3	The medians of Length2mon are the same across categories of Coll2mon.	Independent-Samples Median Test	.416	Retain the null hypothesis.
4	The medians of AP2mon are the same across categories of Coll2mon.	Independent-Samples Median Test	.591	Retain the null hypothesis.
5	The medians of Terr2monF are the same across categories of Coll2mon.	Independent-Samples Median Test	.591	Retain the null hypothesis.
6	The medians of UnW2monF are the same across categories of Coll2mon.	Independent-Samples Median Test	.591	Retain the null hypothesis.

Asymptotic significances are displayed. The significance level is .05.

Figure 247: Results of the independent samples median test comparing the 2-month post-submersion data from the 2-month data group.

Test Statistics[a,b]

	Day0UnWF	Day0Coll	Day0mass	Day0Width	Day0Length	Day0AP
Chi-Square	16.930	14.670	11.925	13.053	15.577	13.558
df	16	16	16	16	16	16
Asymp. Sig.	.390	.549	.749	.669	.483	.632

a. Kruskal Wallis Test

b. Grouping Variable: Day0TerrF

Figure 248: Result of the Kruskal Wallis test for day 0 data for the 2-month dataset, grouped according to terrestrial fluorescence

Test Statistics[a,b]

	Coll2mon	Width2mon	Length2mon	AP2mon	Mass2mon	UnW2monF
Chi-Square	16.284	16.240	16.772	15.513	14.860	16.702
df	15	15	15	15	15	15
Asymp. Sig.	.363	.366	.333	.415	.462	.337

a. Kruskal Wallis Test

b. Grouping Variable: Terr2monF

Figure 249: Result of the Kruskal Wallis test for the 2-month data for the 2-month dataset, grouped according to terrestrial fluorescence.

The statistical analysis of the 2-month data group did not demonstrate any statistically significant results, when comparing bone dimensions, calculated collagen content and average fluorescence levels, as shown in figures 246-249, as all comparisons returned a value greater than .05. These results infer that there is no relationship between bone collagen and observed fluorescence in either a submerged or terrestrial context, and thus the null hypothesis should be accepted. This lack of significance was also echoed in the results of the same statistical comparisons completed using the 6-month dataset (figures 251-255). This result was not entirely unexpected as no discernible trends could be deciphered based on the descriptive statistics examining the changes in bone dimensions, fluorescence levels, and calculated collagen. However, these results consequently reiterate that the aetiology of bone autofluorescence, and its contributing factors, is more complex than first hypothesised in literature, and deeper research into bone composition, colour, texture, and morphology is required.

Non-parametric Wilcoxon paired sign rank tests were carried out to evaluate the relationships between day 0 values and the 2-month measurements for bone dimensions, collagen content, and fluorescence, (figure 250). This analysis produced statistically significant relationships of Z= -3.724, p= .000 for the terrestrial fluorescence values and the calculated collagen content Z= -3.625, p= .000. All other comparisons returned values greater than .05 and therefore were not considered significant, other than bone length which was also statistically significant (Z= -3.226, p= .001). These results indicate that the observed differences in terrestrial bone fluorescence, pre- and post-submersion collagen content, and bone length, were the direct result of exposure to the aquatic environment. This result endorses the theory that an aquatic deposition context influences the collagen content and the autofluorescence of porcine bone, even in a still aqueous medium, which complements the terrestrial findings reported by Swaraldahab and Christensen's paper (2016) [146].

Interestingly, the comparisons examining the relationship between pre- and post-submersion measurements of bone dimensions, only produced a significant result for bone length, which infers that it unlikely that the aquatic environment was influential in these changes. This outcome was less expected but does reflect the variable changes

noted throughout all intervals. As all these measurements were conducted by hand using digital callipers, it is possible that the measurements were not always taken from the exact same location on the rib. This is especially true for width and A/P measurements which were much more difficult to judge compared to the length, and therefore more prone to inconsistency. Moreover, this result further emphasises that natural variation in bone morphology and composition were a major influencing factor in this experimentation, and wider PhD project. Specifically, differences in levels of bone marrow and fat content seem to have led to variable decomposition rates, characterised by the colour changes noted in the post-submersion observations. This effect was apparent in bones even within the same context, which may be due to greater marrow contents offering greater resources for microbes. Similarly, variation in bone porosity and the ratio of trabecular to cortical bone, may have created inequalities in moisture absorption rates and retention, and thus contributed to the variable changes in bone dimensions.

However, the non-parametric Wilcoxon paired sign rank test results comparing day 0 values to 6-month findings (fig. 250) produced statistically significant relationships for the terrestrial (Z= -3.724, p= .000) and underwater fluorescence values (Z= -3.724, p= .000), as well as calculated collagen content (Z= -3.633, p= .000)., and A/P bone dimensions (Z= -3.727, p= .000).

Additionally, the length of bone produced a statistically significant value of Z= -3.727, p= .005. These results validate the discussions in the preceding paragraphs, further supporting the conclusion that the aquatic deposition context does influence bone collagen content and autofluorescence emissions. The fact that the underwater fluorescence levels, and bone A/P comparisons have also produced significant relationships in this dataset introduces the theory that the bones may have reached more of an equilibrium with the aquatic environment by the 6-month interval, whereas at the 2-month interval the bones were all at different stages of absorption and decomposition. This is demonstrated by the greater level of inconsistency noted in the bone changes data in table 64. This observation is further support for the fact that the duration of this experiment would have benefitted from being longer, to see if this trend continued.

The results of the independent samples median tests and Kruskal Wallis tests examining the relationships between collagen content, bone dimensions, and fluorescence levels within each temporal dataset, echoed the results of the 2-month findings. No statistically significant results were found, as shown in figures (252-255), as all comparisons returned a value greater than .05, which further reflects the inconsistencies noted during this experiment.

Test Statistics[a]

	Terr2monF - Day0TerrF	UnW2monF - Day0UnWF	Coll2mon - Day0Coll	Mass2mon - Day0mass	Width2mon - Day0Width	Length2mon - Day0Length	AP2mon - Day0AP
Z	-3.724[b]	-1.263[c]	-3.625[c]	-1.241[b]	-1.617[c]	-3.226[c]	-1.478[c]
Asymp. Sig. (2-tailed)	.000	.206	.000	.214	.106	.001	.139

a. Wilcoxon Signed Ranks Test

b. Based on negative ranks.

c. Based on positive ranks.

Figure 250: Result of the Wilcoxon Signed Ranks tests comparing day 0 measurements to the 2-month fluorescence, collagen, and bone dimension values.

Test Statistics[a]

	Terr6monF - Day0TerrF	UnW6monF - Day0UnWF	Coll6mon - Day0Coll	Mass6mon - Day0mass	Width6mon - Day0Width	Length6mon - Day0Length	AP6mon - Day0AP
Z	-3.724[b]	-3.724[b]	-3.633[c]	-.497[c]	-1.026[c]	-2.810[c]	-3.727[c]
Asymp. Sig. (2-tailed)	.000	.000	.000	.619	.305	.005	.000

a. Wilcoxon Signed Ranks Test

b. Based on negative ranks.

c. Based on positive ranks.

Figure 251: Result of the Wilcoxon Signed Ranks tests comparing day 0 measurements to the 6-month values.

Hypothesis Test Summary

	Null Hypothesis	Test	Sig.	Decision
1	The medians of Day0TerrF are the same across categories of Day0Coll.	Independent-Samples Median Test	.769	Retain the null hypothesis.
2	The medians of Day0UnWF are the same across categories of Day0Coll.	Independent-Samples Median Test	.243	Retain the null hypothesis.
3	The medians of Day0mass are the same across categories of Day0Coll.	Independent-Samples Median Test	.384	Retain the null hypothesis.
4	The medians of Day0Width are the same across categories of Day0Coll.	Independent-Samples Median Test	.332	Retain the null hypothesis.
5	The medians of Day0Length are the same across categories of Day0Coll.	Independent-Samples Median Test	.332	Retain the null hypothesis.
6	The medians of Day0AP are the same across categories of Day0Coll.	Independent-Samples Median Test	.392	Retain the null hypothesis.

Asymptotic significances are displayed. The significance level is .05.

Figure 252: Results of the independent samples median test comparing the day 0 data from the 6-month data group.

Hypothesis Test Summary

	Null Hypothesis	Test	Sig.	Decision
1	The medians of Terr6monF are the same across categories of Coll6mon.	Independent-Samples Median Test	.148	Retain the null hypothesis.
2	The medians of UnW6monF are the same across categories of Coll6mon.	Independent-Samples Median Test	.324	Retain the null hypothesis.
3	The medians of Mass6mon are the same across categories of Coll6mon.	Independent-Samples Median Test	.378	Retain the null hypothesis.
4	The medians of Width6mon are the same across categories of Coll6mon.	Independent-Samples Median Test	.195	Retain the null hypothesis.
5	The medians of Length6mon are the same across categories of Coll6mon.	Independent-Samples Median Test	.568	Retain the null hypothesis.
6	The medians of AP6mon are the same across categories of Coll6mon.	Independent-Samples Median Test	.165	Retain the null hypothesis.

Asymptotic significances are displayed. The significance level is .05.

Figure 253: Results of the independent samples median test comparing the 6-month post-submersion data from the 6-month data group.

Test Statistics[a,b]

	Day0UnWF	Day0Coll	Day0mass	Day0Width	Day0Length	Day0AP
Chi-Square	9.070	14.865	8.485	12.293	10.427	9.217
df	13	13	13	13	13	13
Asymp. Sig.	.768	.316	.811	.504	.659	.756

a. Kruskal Wallis Test

b. Grouping Variable: Day0TerrF

Figure 254: Result of the Kruskal Wallis test for day 0 data, for the 6-month dataset, grouped according to terrestrial fluorescence

Test Statistics[a,b]

	UnW6monF	Coll6mon	Mass6mon	Width6mon	Length6mon	AP6mon
Chi-Square	14.316	9.636	15.064	15.872	14.029	13.889
df	13	13	13	13	13	13
Asymp. Sig.	.352	.723	.303	.256	.372	.382

a. Kruskal Wallis Test

b. Grouping Variable: Terr6monF

Figure 255: Result of the Kruskal Wallis test for 6-month data for the 6-month dataset, grouped according to terrestrial fluorescence

To further investigate the possible impact of salinity on bone autofluorescence, comparisons between recorded fluorescence values of the individual saltwater and tap water submerged groups of ribs for the 2-month and 6-month submersion intervals were compared to the calculated collagen content. Histograms were also produced for each of these datasets, which produced homogeneous abnormal distributions across all groups (appendix 80). Consequently, non-parametric Wilcoxon Signed Ranks tests were completed. When comparing the quantified fluorescence levels of each dataset statistically significant results were reported in both the terrestrial saltwater to tap water comparisons in the 6-month ribs (terrestrial and submerged recorded fluorescence) Z= -1.955, p= .051 and Z= -2.666, p= .008 respectively (figure 256).

On the other hand, the equivalent analyses completed with the 2-month data produced no statistically significant results. Interestingly this supports the theory that the porcine bones and the subsequent aquatic environments were in a state of flux at the 2-month interval, and that decomposition had progressed differentially throughout the dataset.

Furthermore, it implies that there is no significant difference between the fluorescence values from bones exposed to a tap water environment and those generated from bones previously submerged in a saltwater context. In contrast, the significant relationships noted in the 6-month data suggests that there is a significance difference in the fluorescence emissions generated from bones exposed to a tap water context compared to those exposed to a saltwater environment. This result infers that high salinity is an influencing factor in bone autofluorescence, but not in the detrimental capacity as hypothesised.

Both sets of ribs experienced a similar level of collagen loss at the 6-month interval, as the tap water specimens exhibited on average a 10.07% reduction and the saltwater specimens on average a 9.56% loss. However, both groups exhibited a substantial increase in fluorescence intensity, an average increase of 44.1% was recorded in the tap water specimens and a 53.2% increase in the saltwater group. This was not expected, as based on previous MSc work and discussion in literature [134, 146], it was thought that the destruction of the collagen would lead to a reduction in observable bone fluorescence. However, this outcome supports the ongoing finding of this PhD, that the relationship between bone and autofluorescence is more complex that just molecular composition, and that additional factors such as colour, texture, dimensions, and morphology, as well as the ALS model, filter, and camera settings, will impact the level of fluorescence seen. In this scenario, a possible explanation could be the discolouration noted in the porcine bones.

The tap water bones exhibited a pink/red pigmentation, whereas the saltwater exhibited yellow/orange due to the leaching of lipids. Consequently, this may have influenced how the ALS light waves interacted with the bone due to differing levels of absorption, reflectance, and scattering. However, the red discolouration noted in the tap water specimens was thought to be the result of decomposing blood [102], and as discussed in chapter 7.4, blood is known to absorb ALS wavelengths (including in aged stains) [249, 521], and does not possess intrinsic fluorescence capabilities [178], a reduction in fluorescence would have been expected. However, this may explain why the increase in fluorescence in the tap water bones was lower and more inconsistent compared to the saltwater.

An alternative theory is that there was some element of mineral decomposition. Depletion of the cortical bone may have led to greater exposure of the organic component, much like the results of the demineralised bone controls, which produced a much greater level of fluorescence compared to macerated and fresh equivalents. This theory is supported by the fact that in literature some authors suggest that due to protective composition of bone, taphonomic dissolution of the mineral aspect is required before degradation of the organic content can take place [145]. Diagenetic microbial tunnelling and increased porosity were evident on the surface of some of the ribs, which is indicative of mineral modification, and therefore adds credence to this hypothesis, particularly as the reduction in collagen content was so small. In future, quantification of both the mineral aspect and collagen levels would enable a fuller interpretation of the taphonomic interactions and the subsequent impact on bone autofluorescence. These findings are further supported by the uniform statistically significant relationships ($Z= -2.666$, $p= .008$) reported for all contexts and datasets when comparing the calculated collagen levels with the quantified fluorescence (figure, 257).

Test Statistics[a]

	Tsalt2mon - Ttap2mon	Ssalt2mon - Stap2mon	Tsalt6mon - Ttap6mon	Ssalt6mon - Stap6mon
Z	-.533[b]	-1.362[b]	-1.955[b]	-2.666[b]
Asymp. Sig. (2-tailed)	.594	.173	.051	.008

a. Wilcoxon Signed Ranks Test

b. Based on negative ranks.

Figure 256: Result of the Wilcoxon Signed Ranks tests comparing salt and tap water fluorescence values in the 2-month and 6-month temporal groups.

Test Statistics[a]

	Ttap2monCol I - Ttap2mon	Tsalt2monCo II - Tsalt2mon	Stap2monCol I - Stap2mon	Ssalt2monCo II - Ssalt2mon	Ttap6monCol I - Ttap6mon	Tsalt2monCo II - Tsalt6mon	Stap2monCol I - Stap6mon	Ssalt6monCo II - Ssalt6mon
Z	-2.666[b]	-2.666[b]	-2.666[b]	-2.666[b]	-2.666[b]	-2.666[b]	-2.666[b]	-2.666[b]
Asymp. Sig. (2-tailed)	.008	.008	.008	.008	.008	.008	.008	.008

a. Wilcoxon Signed Ranks Test

b. Based on positive ranks.

Figure 257: Result of the Wilcoxon Signed Ranks tests comparing salt and tap water fluorescence values of the 2-month and 6-month temporal groups, to the respective calculated collagen values.

26.4: CONCLUSIONS

Overall, the salinity experiment provided mixed results. Macroscopic observations of colour and bone surface modifications suggested that the saltwater environment slowed the progress of decomposition in comparison to the tap water context. However statistical analysis indicated that the aquatic contexts were equally detrimental to bone collagen by the 6-month interval, as both the tap water and saltwater specimens exhibited very similar levels of collagen loss, approximately 10%.

However, this relatively low reduction in bone collagen content means that ALS could be used to locate skeletal remains for at least 6-months after tissue removal in aquatic contexts. These results also highlight the need for further research at greater timescales, and comparative terrestrial studies to further explore the scope of this methodology.

Furthermore, despite the slight reduction in bone collagen content, fluorescence quantification demonstrated a substantial increase in fluorescence levels after prolonged aquatic exposure, in both the tap water and saltwater bone groups, contrary to the initial hypothesis. It is unclear why fluorescence levels increased, but it could be due to the dissolution of surface mineral content of the porcine ribs, evidenced by the presence of microbial tunnelling, increased porosity, and leaching. Similarly, variation in bone porosity, bone marrow volume, and the ratio of trabecular to cortical bone, may have created inequalities in moisture absorption rates, bacterial infiltration, and consequently the rate of decomposition. This variability was particularly noticeable in the 2-month tap water specimens, due to the greatly variable changes in bone dimensions.

The results endorse the theory that an aquatic deposition context influences the collagen content and the autofluorescence of porcine bone, even in a still aqueous medium, supported by the following statistically significant relationships:

2-month:

- Terrestrial day 0 fluorescence compared to terrestrial fluorescence after 2-month submersion ($Z= -3.724$, $p= .000$).
- Day 0 calculated collagen content compared to collagen levels after 2-months submersion ($Z= -3.625$, $p= .000$).

- Day 0 bone length measurements compared to bone length after 2-month submersion (Z= -3.226, p= .001).

6-month:

- Day 0 terrestrial fluorescence compared to 6-month terrestrial fluorescence (Z= -3.724, p= .000)
- Day 0 underwater fluorescence compared to 6-month underwater fluorescence (Z= -3.724, p= .000).
- Day 0 calculated collagen content compared to 6-month collagen content (Z= -3.633, p= .000)
- Day 0 A/P bone measurements compared to A/P bone measurements after 6-month submersion (Z= -3.727, p= .000).
- Day 0 bone length measurements compared to bone length after 6-month submersion (Z= -3.727, p= .005).

Salinity:

- Post-submersion terrestrial fluorescence after 6-month submersion in saltwater compared to the post-submersion terrestrial fluorescence of bones submerged in tap water (Z= -1.955, p= .051)
- Post-submersion submerged fluorescence after 6-month submersion in saltwater compared to the post-submersion submerged fluorescence of bones submerged in tap water (Z= -2.666, p= .008)
- Statistically significant relationships (Z= -2.666, p= .008) reported for all contexts and datasets when comparing the calculated collagen levels with the quantified fluorescence.

However, no statistically significant relationships were found when comparing calculated collagen levels to quantified fluorescence in either a terrestrial or aquatic context, which supports the theory that osseous autofluorescence production relies on more than just the presence of collagen, and that further research into the role of mineral content, colour, and bone composition are needed. Furthermore, the duration of this experiment was long enough to see substantial changes, therefore comparative terrestrial and underwater degradation studies, for longer durations, would be

beneficial to test the full scope of this technique, as well as sequential sampling of the same bones to reduce some of the inter-bone variation.

In summary, although the high salinity aquatic content had a slight detrimental effect on the collagen content, it was in no greater capacity compared to the tap water investigations, and in fact submersion led to higher bone autofluorescence intensities rather than a reduction. This result consequently leads to partial acceptance of null hypothesis 8 (shown below), as although submersion in high salinity water was shown to be somewhat destructive to porcine bone collagen content, it did not lead to a reduction in bone autofluorescence.

8. Hypothesis: High water salinity is destructive to porcine bone collagen when submerged for 6 months, which leads to a reduction in observed fluorescence levels when using blue light (450-470 nm) and photographed with an orange camera filter.

   Null hypothesis: High water salinity is destructive to porcine bone collagen when submerged for 6 months, which leads to a reduction in observed fluorescence levels when using blue light (450-470 nm) and photographed with an orange camera filter.

27.0 - SECTION B: SUMMARY

Section B produced some conflicting results regarding the collagen-fluorescence relationship. In the fresh dataset examined in question 1 results suggested that bone dimensions, composition, and specimen provenance, may impact observed fluorescence levels due to strong statistically significant relationships (p= .000) when comparing bone length, width, mass, anterior-posterior bone measurements, to calculated collagen content, and quantified fluorescence. Strong, indicative results were seen for both ALS devices in aquatic and terrestrial contexts. Similarly, the 54 macerated porcine ribs, provided support for a possible collagen-fluorescence relationship, with statistical analysis returning a unanimous result of p= .000 for all tested comparisons terrestrial and underwater fluorescence at 0.6s, 0.4s, and 1/3s exposure times, when compared to calculated collagen content. However, a few anomalies noted in the collagen data led to a reduction in sample size, and collagen quantification technique may not be entirely optimal, hence why there is some disparity in the correlation data.

However, comparisons between the question 1 fresh data, and the macerated dataset produced contrasting results regarding the influence of bone dimensions on the bone autofluorescence, suggesting that although maceration is not destructive to bone collagen, ALS wavelengths may interact differentially with fresh and macerated bone. This would be a particularly important area of ALS research to develop, as much of the ALS bone fluorescence published research in literature was generated using macerated bone.

Results of the non-bone and bone derived positive and negative controls provided support for the potential for differentiation between bone and other environmental debris due to the varying levels of fluorescence observed. As the demineralised bone and many of the organic items generated higher levels of observed fluorescence these results also reinforce the ongoing discourse that the organic component of bone is most likely the primary contributor to bone autofluorescence. However, fluorescence emissions observed in shells and sea glass also highlight the fact that the mineral content, as well as the colour and morphology of the examined material are also instrumental in fluorescence production. As such, it is not possible to recommend a

singular combination of camera settings that would be suitable for all skeletal searches, particularly as the aquatic taphonomic environment was seen to alter bone fluorescence levels, and collagen content. In addition to this, there are many more influencing factors such as water composition, camera specifications, and different light sources need to be explored in the future, in order to gain a more comprehensive understanding into the feasibility of this technique.

Question 4 results did not provide any support for a potential collagen relationship but did endorse the theory that prolonged exposure to a still aquatic deposition environment (tap or saltwater) will lead to small reductions in bone collagen content, albeit at a slow pace. Conversely, the results of the fluorescence analysis subverted expectations by producing amplified post-submersion fluorescence values in porcine bone that had been submerged in tap water and saltwater contexts. This increase in fluorescence may be due to bone surface modifications but more complete analysis of the bone mineral and collagen content would be required.

28.0 – THESIS DISCUSSION AND FUTURE WORK

Overall, the results of this PhD research have provided valuable insight into how ALS technology could be used to search for skeletal remains in terrestrial and aquatic contexts. By combining feasibility, maceration, and refinement research questions with simulated deposition scenarios and collagen and fluorescence quantification, it has enabled novel, deeper interpretation of the collagen-fluorescence relationship, the taphonomic impact on bone autofluorescence, and the scope of the methodology.

It was shown that blue 450 nm ALS wavelengths stimulated bone autofluorescence in both terrestrial and submerged context and produced the most successful results when coupled with an orange filter, rather than a yellow filter, as commonly reported in literature [135]. Comparisons between the calculated collagen content and recorded fluorescence levels of fresh and macerated bone dataset overall demonstrated that there is likely a positive correlation between collagen content and fluorescence emissions. However contradictory data was seen in the submerged salinity studies and bone dimension analyses. Therefore, it is apparent that the source of bone autofluorescence is more complex than literature suggests, and most likely a result of multiple contributors, rather than just the organic component.

As this research project focused on the surface fluorescence of bone, in future, deeper and measured bone sampling, to include cortical and trabecular aspects, could provide more detail into how different bone compositions may influence fluorescence, and inclusion of different bone types and preservations, as well as refinement of the size of the squares used in the OFC would enable more comprehensive investigation into the collagen fluorescence relationship.

Although TG analysis was able to provide a suitable level of quantification for this project, retrospective evaluation suggests that additional techniques such as FTIR or Raman spectroscopy, would be able to offer additional detail regarding bone composition, and consequently help create a more comprehensive overview of the collagen-fluorescence relationship. Moreover, additional research into the influence of

bone mineral content, as well as the colour, texture, and morphology of bone, would also facilitate deeper understanding of autofluorescence production.

Findings from the differentiation and controls study confirm that differentiation between bone and other non-bone items is possible in aquatic and terrestrial environments, which mostly supports the findings of the terrestrial differentiation studies in literature, such as Swaraldahab and Christensen (2014) [146], Green et al (2019) [133], and Craig and Vezaro (1998) [256] successfully demonstrated how ALS can be used to assist investigators with presumptive identification of potential osseous material at the scene, as all the examined items produced varying levels of fluorescence. Although professional judgement and confirmatory analysis would be required, presumptive, non-destructive, identification using ALS could help to speed up searches and increase the number of bones being recovered. This would not only benefit downstream analyses by preserving molecular and evidential material, but also contribute to the production of a fuller osteological profile, to assist identification and continued forensic enquiries. More specifically, this ALS methodology would be especially beneficial to underwater searches, where there are currently no search strategies focused on locating human remains in the later stages of decomposition, including bone.

However, several of the inorganic non-bone items, including sea glass and shells, also produced intense fluorescence emissions when stimulated with ALS, which contradicts published data in literature [135]. Consequently, this study has highlighted the requirement for further research into the degree of differentiation, by examining other common deposition materials, and perhaps constructing a similar study to Brown et al [266], and assess how easily volunteers and/or serving forensic personnel can identify potential bone from amongst other items. Not only would this help to discern the validity of this search technique but also garner insight into how it would be applied in the field, alongside feedback from the proposed end users. Overall, more actualistic experimentation involving human remains, and fieldwork would be a major requirement for future research to see how well the technique performs in less controlled and more representative conditions. This type of experimentation could include comparative studies of different durations, various bone types, as well as macerated, fresh, and

burned bone, to comprehensively explore the influence of both intrinsic and extrinsic variables.

Throughout this thesis, all hypotheses were fully met, other than hypothesis 8 (as discussed in chapter 26.4), as although the high salinity aquatic context had a slight detrimental effect on the collagen volume, it was in no greater capacity compared to the tap water investigations, but submersion led to an increase in bone autofluorescence intensities rather than the hypothesised reduction. However, the increased levels of autofluorescence demonstrated by the porcine ribs after prolonged submersion was a surprising but beneficial finding, as increased fluorescence intensity would help increase bone visibility in search environment which are known to be usually dark, with very limited visibility [80]. It would be particularly beneficial when conducting fingertip searches in more confined waterways, where other search strategies would not be possible. Furthermore, as this technology is already readily used by operating personnel, this new methodology has the potential to be easily adopted by current constabulary, and should not pose any additional encumberment when in the water as hand held sonar is already used [96]. Additional research into different water types and variables such as colour, depth, turbidity, and currents, would help to understand the scope of this technique as well as inform the development of further recommendations.

Similarly, the implementation of the OFC software enabled objective and quantitative comparisons to help direct discussion and evaluate fluorescence output, rather than relying on descriptive and subjective examination but has been frequently used in literature [142, 304]. Experimentation also highlighted potential features for further development such as the inclusion of a reference library and fluorescence scales. The use of a simple, automated, fluorescence quantification process means that quantification could be carried out at the scene as well as in the laboratory, enabling contemporaneous documentation and interpretation of potential osseous material, which is currently not possible when using ImageJ or Photoshop programs.

In summary, this PhD research has demonstrated that ALS technology offers a potential new approach for locating skeletal remains, as well as a preliminary indicator to whether a material is bone. In addition to this, as this research is still in early, foundational stages, there are many avenues for future research, which offers the opportunity of crafting a

multidimensional methodology that can support forensic investigators at terrestrial and aquatic crime scenes, as well as in the laboratory.

29.0 – FINAL CONCLUSIONS AND RECOMMENDATIONS

Based on all the data produced during this research project, the following conclusions and recommendations were established:

- Hot water maceration was identified as a suitable preparation technique for bone undergoing ALS analysis, as it produced fluorescence results similar to pre-macerated values, with limited collagen degradation. The hot water macerated bones also retained the highest level of bone preservation, with no evidence of major surface or structural modification.

- Biological washing powder is not a suitable preparation method for bone undergoing ALS analysis, even at the low temperature of 50°C, as it was destructive to bone collagen and bone integrity, creating drastic alterations to surface texture and colour as well as exaggerated and patchy fluorescence.

- Bone fluorescence can be produced in a terrestrial and submerged tap water context, when excited by blue light (450 nm), coupled with an orange filter.

- Fluorescence levels are shown to reduce in an aquatic context compared to in air when examining the same porcine bone and the same light source. This is due to the optically denser aquatic environment creating greater levels of scattering and greater refraction indices.

- ALS can be used as a presumptive tool to search for bone in terrestrial and submerged environments.

- Different models of ALS and coloured filter may produce varying results; therefore, it is recommended that a narrow ALS wavelength of 450 nm is selected, to ensure better compatibility with the orange filter and reduce the possibility of overexposure or incomplete filtration of light. However more

research is required.

- Variable levels of fluorescence between bone and other non-bone items can assist with differentiation when searching for bone in terrestrial and aquatic scenes, but a reference standard would be required to provide deeper comparisons.

- Overall, slower exposure times were seen to produce higher levels of fluorescence compared to faster exposure times, therefore adjustment of exposure time will be required based on whether the primary aim is to document or quantify bone fluorescence.

- A faster exposure time is recommended for aquatic contexts to reduce blurring from moving water.

- The demineralised bone samples and porcine collagen powder controls demonstrate that the organic component of bone is most likely the primary contributor to osseous autofluorescence. However, the mechanism behind bone autofluorescence production is more complex then described in literature, and that other characteristics such as colour, preservation, and morphology are also influential.

- Submersion in an aquatic deposition up to 6 months only led to a small decrease in calculated bone collagen content.

- Porcine bones submerged in an aquatic environment for up to 6-months led to a substantial increase in recordable bone fluorescence when photographed in a terrestrial and tap water context.

- The high salinity aquatic deposition context was just as detrimental to calculated bone collagen content as submersion in tap water.

- Submersion in an aquatic context directly contributed to the rise in bone fluorescence intensity and the small reduction in calculated collagen content.

- Bone colour, texture, and morphology most likely contribute to bone autofluorescence in addition to bone composition.

- Future forensic research should endeavour to include quantification of both bone fluorescence and bone composition, to better understand the source of bone fluorescence and enable more objective analysis of bone fluorescence.

- Similarly, although a positive fluorescence result is indicative of bone, further confirmatory analysis will be required, as simply measuring the intensity of observed fluorescence does not offer a higher enough level of discrimination.

- The OFC provided a simple and efficient method of bone fluorescence quantification, and presents many opportunities for further development, whilst ultimately providing a supportive tool to be used in the field and in the laboratory when analysing skeletal remains.

- Additional osteology training for attending crime scene investigators would also help to maximise bone identification and collection, alongside using the OFC.

30.0 – APPENDICES

Please see volume 2

31.0 - REFERENCES

1. Haglund WD, Sorg MH. *Advances in forensic taphonomy: method, theory, and archaeological perspectives*

Boca Raton: CRC Press; 2002.
2. Mateus M, de Pablo H, Vaz N. An investigation on body displacement after two drowning accidents. *Forensic Sci Int*. 2013;229(1-3):e6-12.
3. UK Centre for Ecology and Hydrology. The UK Lakes Portal - 40,000 lakes at your fingertips 2016 [updated 2019; cited 29/06/2020. Available from: https://www.ceh.ac.uk/
4. The Department for Environment Food & Rural Affairs. Factsheet Marine Conservation Zones 2009 [updated 2019; cited 29/06/2020.
5. National River Flow Archive. UK River and Flow Regimes [Internet]. 2020 [updated 2019; cited 29th July 2020. Available from: https://nrfa.ceh.ac.uk/.
6. National Water Safety Forum. 2018 UK Water Related Fatalities [Internet]. 2018 [updated 2019; cited 29/06/2020. Available from: ww.nationalwatersafety.org.uk.
7. Mahmoudain N. Titan submersible disaster underscores dangers of deep-sea exploration – an engineer explains why most ocean science is conducted with crewless submarines: The Conversation; 2023 [
8. Howie M, Chantler-Hicks L. Nicola Bulley drowned after accidentally falling into water, inquest coroner rules. Evening Standard. 2023 27/06/2023.
9. Organisation WH. Global report of drowning; Preventing a leading killer. World Health Organisation; 2014.
10. Suppasri A, Shuto N, Imamura F, Koshimura S, Mas E, Yalciner AC. Lessons learned from the 2011 Great East Japan tsunami: Performance of tsunami countermeasures, coastal buildings, and tsunami evacuation in Japan. *Pure and Applied Geophysics*. 2013;170(6-8):993-1018.
11. Smith WH, Marks KM. Seafloor in the Malaysia Airlines flight MH370 search area. *Eos, Transactions American Geophysical Union*. 2014;95(21):173-4.
12. Schotsmans EM, Márquez-Grant N, S F. *Taphonomy of human remains: Forensic analysis of the dead and the depositional environment*. Chichester: West Sussex: Wiley; 2017.
13. Abate D, Sturdy Colls C, Moyssi N, Karsili D, Faka M, Anilir A, et al. Optimizing search strategies in mass grave location through the combination of digital technologies. *Forensic Sci Int Synerg*. 2019;1:95-107.
14. Tilstone J, Hastrup ML, Hald C. *Fisher's Techniques of Crime Scene Investigation First International Edition*: CRC Press; 2013.
15. Fish JT, Miller LS, Braswell MC, EW W. *Crime Scene Investigation*: Routledge; 2013.
16. Tuller H, Durić' M. Keeping the pieces together: comparison of mass grave excavation methodology. *Forensic Sci Int*. 2004;27(156):192-200.
17. Schotsmans EM, Van de Voorde W, De Winne J, Wilson AS. The impact of shallow burial on differential decomposition to the body: a temperate case study. *Forensic Sci Int*. 2011;206(1-3):e43-8.
18. Zangarini S, Trombino L, Cattaneo C. Micromorphological and ultramicroscopic aspects of buried remains: Time-dependent markers of decomposition and permanence in soil in experimental burial. *Forensic Sci Int*. 2016;263:74-82.
19. Doro KO, Kolapkar AM, Bank CG, Wescott DJ, Mickleburgh HL. Geophysical imaging of buried human remains in simulated mass and single graves: Experiment design and results from pre-burial to six months after burial. *Forensic Sci Int*. 2022;335:111289.

20. Dupras TL, Schultz JJ, Wheeler SM, Williams LJ. *Forensic recovery of human remains: archaeological approaches*. 2 ed: CRC Press; 2011.
21. Becker RF. *Crime scene: Underwater Crime Investigative Techniques*: Boca Raton, FL; 1995.
22. Pokines JT, Symes SA. *Manual of forensic taphonomy*. Boca Raton: CRC Press; 2014.
23. Maloney M S. Aquatic recovery of human remains. *Death scene investigation procedural guide*. Hoboken: Taylor and Francis; 2017. p. 137-45.
24. Ebbesmeyer CC, Haglund WD. Trajectories of a Floating Human Body Simulated in a Hydraulic Model of Puget Sound. *Journal of Forensic Sciences*. 1994;39(1):231-40.
25. Winskog C. Underwater disaster victim identification: the process and the problems. *Forensic Sci Med Pathol*. 2012;8(2):174-8.
26. Stuart BH, Maiken U. Decomposition in Aquatic Environments. In: Schotsmans EMJ, Márquez-Grant N, Forbes SL, editors. *Taphonomy of Human Remains: Forensic Analysis of the Dead and the Depositional Environment*: John Wiley & Sons Ltd; 2017. p. 235-50.
27. Petrik MS, Hobischak NR, Anderson GS. Examination of Factors Surrounding Human Decomposition in Freshwater: A Review of Body Recoveries and Coroner Cases In British Columbia. *Canadian Society of Forensic Science Journal*. 2004;37(1):9-17.
28. Haglund WD, Sorg MH. *Forensic taphonomy: the postmortem fate of human remains*. Boca Raton: CRC Press; 1997.
29. Delabarde T, Keyser C, Tracqui A, Charabidze D, Ludes B. The potential of forensic analysis on human bones found in riverine environment. *Forensic Sci Int*. 2013;228(1-3):e1-5.
30. Pokines JT. Differential Diagnosis of the Taphonomic Histories of Common Types of Forensic Osseous Remains. *Journal of Forensic Identification*. 2018;68(1):87-145.
31. Guidance on the management recording and investigation of missing persons. National Centre for Policing Excellence; 2005.
32. Practice Advice on Search Management and Procedures. National Centre for Policing Excellence; 2006.
33. Gibb GJ, Woolnough C. Missing Persons Understanding Planning Responding. Grampian Police; 2007.
34. Mateus M, Vieira V. Study on the postmortem submersion interval and accumulated degree days for a multiple drowning accident. *Forensic Sci Int*. 2014;238:e15-9.
35. Carniel S, Umgiesser G, Sclavo M, Kantha LH, Monti S. Tracking the drift of a human body in the coastal ocean using numerical prediction models of the oceanic, atmospheric and wave conditions. *Sci Justice*. 2002;42(3):143-51.
36. Heaton V, Lagden A, Moffatt C, Simmons T. Predicting the postmortem submersion interval for human remains recovered from U.K. waterways. *J Forensic Sci*. 2010;55(2):302-7.
37. Mateus M, Pinto L, Chambel-Leitão P. Evaluating the predictive skills of ocean circulation models in tracking the drift of a human body: a case study. *Australian Journal of Forensic Sciences*. 2014;47(3):322-31.
38. Molenaar J. Behaviour of Dead Bodies in Water. In: Bierens JJLM, Branche CM, Brewster BC, editors. *Handbook on Drowning: Prevention, Rescue, Treatment*. 1 ed. Berlin / Heidelberg: Springer 2005.
39. Williams A, Rogers CJ, Cassella JP. Why does the UK need a Human Taphonomy Facility? *Forensic Sci Int*. 2019;296:74-9.
40. Palmer C. Estimating the Impact of Laminar Flow on the Pattern and Rate of Decomposition in Aquatic Environments-Is There a Better Way of Modeling Decomposition? *J Forensic Sci*. 2020;65(5):1601-9.
41. Palazzo C, Pelletti G, Fais P, Boscolo-Berto R, Fersini F, Gaudio RM, et al. Postmortem submersion interval in human bodies recovered from fresh water in an area of Mediterranean climate. Application and comparison of preexisting models. *Forensic Sci Int*. 2020;306:110051.

42. Palazzo C, Pelletti G, Fais P, Giorgetti A, Boscolo-Berto R, Gaudio RM, et al. Application of aquatic decomposition scores for the determination of the Post Mortem Submersion Interval on human bodies recovered from the Northern Adriatic Sea. *Forensic Sci Int*. 2021;318:110599.
43. Megyesi MS, Nawrocki SP, Haskell NH. Using Accumulated Degree Days to Estimate the Postmortem Interval From Decomposed Human Remains. *Journal of Forensic Sciences*. 2005;50(3):618-26.
44. Stejskal SM. *Death, Decomposition, and Detector Dogs*. Boca Raton: CRC Press; 2022.
45. Lee Goff M. Early post-mortem changes and stages of decomposition in exposed cadavers. *Exp Appl Acarol*. 2009;49(1-2):21-36.
46. Cockle DL, Bell LS. Human decomposition and the reliability of a 'Universal' model for post mortem interval estimations. *Forensic Sci Int*. 2015;253:136 e1-9.
47. Card A, Cross P, Moffatt C, Simmons T. The Effect of Clothing on the Rate of Decomposition and Diptera Colonization on Sus scrofa Carcasses. *J Forensic Sci*. 2015;60(4):979-82.
48. Bates LN, Wescott DJ. Comparison of decomposition rates between autopsied and non-autopsied human remains. *Forensic Sci Int*. 2016;261:93-100.
49. Mann RW, Bass WM, Meadows L. Time Since Death And Decomposition Of The Human Body: Variables And Observations In Case And Experimental Field Studies. *Journal of Forensic Sciences*. 1990;35(1):103-11.
50. Caruso JL. Decomposition Changes in Bodies Recovered from Water. *Acad Forensic Pathol*. 2016;6(1):19-27.
51. van Daalen MA, de Kat DS, Oude Grotebevelsborg BF, de Leeuwe R, Warnaar J, Oostra RJ, et al. An Aquatic Decomposition Scoring Method to Potentially Predict the Postmortem Submersion Interval of Bodies Recovered from the North Sea. *J Forensic Sci*. 2017;62(2):369-73.
52. Magni PA, Tingey E, Armstrong NJ, Verduin J. Evaluation of barnacle (Crustacea: Cirripedia) colonisation on different fabrics to support the estimation of the time spent in water by human remains. *Forensic Sci Int*. 2021;318:110526.
53. Haglund WD, Sorg MH. Human Remains in Water Environments. In: Haglund WD, Sorg MH, editors. *Advances in Forensic Taphonomy: Method, Theory, and Archaeological Perspectives*. 1st ed. Boca Raton: CRC Press; 2002. p. 201-18.
54. Higgs ND, Pokines JT. Marine Environmental Alterations to Bone. In: Pokines JT, Symes SA, editors. *Manual of Forensic Taphonomy*: CRC Press; 2014. p. 143-79.
55. Lunetta P. Autopsy Findings: Drowning and Submersion Deaths. *Encyclopedia of Forensic and Legal Medicine*2016. p. 315-22.
56. Armstrong EJ, Erskine KL. *Water-related death investigation: practical methods and forensic applications.* 2nd ed. Boca Raton, FL: CRC Press,; 2021.
57. Gleason M. *The Search for Human Remains in the Search and Rescue Environment*: SARTI; 2008.
58. Breglia GA, Uzal MH, Herbstein JA. Time of immersion of bodies found in water in Northern Patagonia Argentina. *Spanish Journal of Legal Medicine*. 2023;49(1):20-7.
59. Byard RW. Putrefaction: An Additional Complicating Factor in the Assessment of Freshwater Drownings in Rivers. *J Forensic Sci*. 2018;63(3):899-901.
60. Olowe I. The Effect of Water Conditions on Decomposition Rate: A Comparative Study on the Estimation of PMSI. [Unpublished doctoral thesis]. In press 2023.
61. Reijnen G, Gelderman HT, Oude Grotebevelsborg BFL, Reijnders UJL, Duijst W. The correlation between the Aquatic Decomposition Score (ADS) and the post-mortem submersion interval measured in Accumulated Degree Days (ADD) in bodies recovered from fresh water. *Forensic Sci Med Pathol*. 2018;14(3):301-6.
62. De Donno A, Campobasso CP, Santoro V, Leonardi S, Tafuri S, Introna F. Bodies in sequestered and non-sequestered aquatic environments: a comparative taphonomic study using decompositional scoring system. *Sci Justice*. 2014;54(6):439-46.
63. Golden F, Tipton M. *Essentials of Sea Survival*: Human Kinetics Publishers; 2002.

64. Barwood MJ, Bates V, Long G, Tipton MJ. "Float First": Trapped air between clothing layers signficantly improves buoyancy after immersion. *International Journal of Aquatic Research and Education*. 2011;5:147-63.
65. Dennison-Wilkins L, Hackman L, Hayatdavoodi M. The Body Recovery From Water Study: The application of science to missing person search. *Policing: A Journal of Policy and Practice*. 2023;17.
66. Notter SJ, Stuart BH. The effect of body coverings on the formation of adipocere in an aqueous environment. *J Forensic Sci*. 2012;57(1):120-5.
67. Ruffell A, Pringle JK, Cassella JP, Morgan RM, Ferguson M, Heaton VG, et al. The use of geoscience methods for aquatic forensic searches. *Earth-Science Reviews*. 2017;171:323-37.
68. Dennison-Wilkins L. Body Recovery from Water Study2021 10/11/2022. Available from: www.college.police.uk/article/body-recovery-water-study.
69. Williams P, Whitfield M, Biggs J, Bray S, Fox G, Nicolet P, et al. Comparative biodiversity of rivers, streams, ditches and ponds in an agricultural landscape in Southern England. *Biological Conservation*. 2004;115(2):329-41.
70. Inland waterways and categorisation of waters: GOV.UK; 2023 [Available from: www.gov.uk/guidance/inland-waterways-and-categorisation-of-waters.
71. Hannah DM, Garner G. River water temperature in the United Kingdom. *Progress in Physical Geography: Earth and Environment*. 2015;39(1):68-92.
72. Pakosh CM, Rogers TL. Soft tissue decomposition of submerged, dismembered pig limbs enclosed in plastic bags. *J Forensic Sci*. 2009;54(6):1223-8.
73. Houck MM, Crispino F, McAdam T. *The Science of Crime Scenes*. 2nd ed: Academic Press; 2018.
74. Howe J. Search and Recovery in Near-Shore Waters. In: Bierens JJLM, Branche CM, Brewster BC, editors. *Handbook on Drowning: Prevention, Rescue, Treatment*. 1 ed. Berlin / Heidelberg: Springer 2005. p. 622-4.
75. Ruffell A. Lacustrine flow (divers, side scan sonar, hydrogeology, water penetrating radar) used to understand the location of a drowned person. *Journal of Hydrology*. 2014;513:164-8.
76. Williamson R. Search Techniques for Drowning Victims: Recovery Using Side Scan Sonars. In: Bierens JJLM, Branche CM, Brewster BC, editors. *Handbook on Drowning: Prevention, Rescue, Treatment*. 1 ed. Berlin / Heidelberg: Springer 2005. p. 627-30.
77. Ruffell A. Under-water scene investigation using ground penetrating radar (GPR) in the search for a sunken jet ski, Northern Ireland. *Sci Justice*. 2006;46(4):221-30.
78. Ruffell A, King L. Water penetrating radar (WPR) in archaeology: A crannog case study. *Journal of Archaeological Science: Reports*. 2022;41.
79. Erskine KL. Investigative Duties on Scene. In: Armstrong EJ, Erskine KL, editors. *Water-related death investigation: practical methods and forensic applications*. 2nd ed. Boca Raton, FL: CRC Press,; 2021. p. 29-131.
80. Paba R, Moniz R, Magni PA. Optimizing underwater visual records for crime scene investigations in water with clear to reduced visibility. *Forensic Sci Int Synerg*. 2023;6:100329.
81. Healy CA, Schultz JJ, Parker K, B L. Controlled research using Side-Scan sonar to detect submerged proxy cadavers. *Journal of Forensic Sciences*. 2015;60(3):743-52.
82. Schultz JJ, Healy CA, Parker K, Lowers B. Detecting submerged objects: The application of side scan sonar to forensic contexts. *Journal of Forensic Sciences*. 2013;231(1-3):306.
83. Parker R, Ruffell A, Hughes D, Pringle J. Geophysics and the search of freshwater bodies: a review. *Sci Justice*. 2010;50(3):141-9.
84. Fancher JP, Aitkenhead-Peterson JA, Farris T, Mix K, Schwab AP, Wescott DJ, et al. An evaluation of soil chemistry in human cadaver decomposition islands: Potential for estimating postmortem interval (PMI). *Forensic Sci Int*. 2017;279:130-9.
85. Schoon A. Search Techniques for Dead Bodies: Searching with Dogs. In: Bierens JJLM, Branche CM, Brewster BC, editors. *Handbook on Drowning: Prevention, Rescue, Treatment*. 1 ed. Berlin / Heidelberg: Springer 2005. p. 625-7.

86. Rebmann A, David D, Sorg M, H,. *Cadaver Dog Handbook: Forensic Training and Tactics for the Recovery of Human Remains*: CRC Press; 2000.
87. Forbes SL, Perrault KA, Stefanuto PH, Nizio KD, Focant JF. Comparison of the decomposition VOC profile during winter and summer in a moist, mid-latitude (Cfb) climate. *PLoS One*. 2014;9(11):e113681.
88. Healy CA, Schultz JJ, Parker K, Lowers B. Detecting submerged bodies: controlled research using side-scan sonar to detect submerged proxy cadavers. *J Forensic Sci*. 2015;60(3):743-52.
89. Haglund WD, Reay DT. Problems of Recovering Partial Human Remains at Different Times and Locations: Concerns for Death Investigators. *Journal of Forensic Sciences*. 1993;38(1):69-80.
90. Haglund WD. Disappearance of soft tissue and the disarticualtion of human remains from aqueous environments. *Journal of Forensic Sciences*. 1993;38:806-15.
91. Houck MM, Crispino F, McAdam T. Underwater and Underground Crime Scenes. *The Science of Crime Scenes*2012. p. 373-86.
92. Guareschi EE, Tobe SS, Nicholls PK, Magni PA. Taphonomy and Diagenesis of Human Bone in Underwater Archaeology: A Review of the Current Status and the Proposal of Post-Mortem Submersion Interval (PMSI) as a Potential Forensic Application. *Journal of Maritime Archaeology*. 2021;16(1):57-75.
93. Ellingham STD, Perich P, Tidball-Binz M. The fate of human remains in a maritime context and feasibility for forensic humanitarian action to assist in their recovery and identification. *Forensic Sci Int*. 2017;279:229-34.
94. Pinheiro J. Decay Process of a Cadaver. In: Schimtt A, Cunha E, Pinheiro J, editors. *Forensic Anthropology and Medicine: Complementary Sciences From Recovery to Cause of Death*. Totowa, NJ: Humana Press Inc; 2006. p. 85-116.
95. Christensen AM, Myers SW. Macroscopic observations of the effects of varying fresh water pH on bone. *J Forensic Sci*. 2011;56(2):475-9.
96. McGrane O, Cronin A, Hile D. Use of handheld sonar to locate a missing diver. *Wilderness & Environmental Medicine*. 2013;24(1):28-31.
97. (NAS) NA Lastnautical Archaeology Society (NAS). *Underwater Archaeology : The NAS Guide to Principles and Practice*. Hoboken: John Wiley & Sons; 2008.
98. Byers SN. *Introduction to forensic anthropology: A textbook*. Boston: Allyn and Bacon; 2002.
99. Huculak MA, Rogers TL. Reconstructing the sequence of events surrounding body disposition based on color staining of bone*. *J Forensic Sci*. 2009;54(5):979-84.
100. Tibbett M, Carter DO, editors. Soil Analysis in Forensic Taphonomy. 1 ed. Boca Raton: CRC Press; 2008.
101. Kendall C, Eriksen AMH, Kontopoulos I, Collins MJ, Turner-Walker G. Diagenesis of archaeological bone and tooth. *Palaeogeography, Palaeoclimatology, Palaeoecology*. 2018;491:21-37.
102. Dupras TL, Schultz JJ. Taphonomic Bone Staining and Color Changes in Forensic Contexts. In: Pokines JT, Symes SA, editors. *Manual of Forensic Taphonomy*. Boca Raton: CRC Press; 2014.
103. Toffolo MB, Ricci G, Caneve L, Kaplan-Ashiri I. Luminescence reveals variations in local structural order of calcium carbonate polymorphs formed by different mechanisms. *Sci Rep*. 2019;9(1):16170.
104. Shi D, Sadat ME, Dunn AW, Mast DB. Photo-fluorescent and magnetic properties of iron oxide nanoparticles for biomedical applications. *Nanoscale*. 2015;7(18):8209-32.
105. Evans T. Fluvial Taphonomy. In: Pokines JT, Symes SA, editors. *Manual of Forensic Taphonomy*: CRC Press; 2014. p. 115-41.
106. Pokines J T, Higgs N. Macroscopic Taphonomic Alterations to Human Bone Recovered from Marine Environments. *Journal of Forensic Identification*. 2015;65(6):953.

107. Ubelaker DH. Taphonomy applications in forensic anthropology. In: Haglund WD, Sorg MH, editors. *Forensic taphonomy: the postmortem fate of human remains*. Boca Raton: CRC Press; 1997.
108. Stokes S, Marquez-Grant N, Greenwood C. Establishing a minimum PMI for bone sun bleaching in a UK environment with a controlled desert-simulated comparison. *Int J Legal Med*. 2020;134(6):2297-306.
109. Thompson CEL, Ball S, Thompson TJU, Gowland R. The abrasion of modern and archaeological bones by mobile sediments: the importance of transport modes. *Journal of Archaeological Science*. 2011;38(4):784-93.
110. Buikstra JE, Ubelaker DH. *Standards for data collection from human skeletal remains: proceedings of a seminar at the Field Museum of Natural History*1994.
111. Pokines JT. Faunal Dispersal, Reconstruction, and Gnawing Damage. In: Pokines JT, Symes SA, editors. *Manual of Forensic Taphonomy*: CRC Press; 2014. p. 201-48.
112. Spradley MK, Hamilton MD, Giordano A. Spatial patterning of vulture scavenged human remains. *Forensic Sci Int*. 2012;219(1-3):57-63.
113. Kjorlien YP, Beattie OB, Peterson AE. Scavenging activity can produce predictable patterns in surface skeletal remains scattering: observations and comments from two experiments. *Forensic Sci Int*. 2009;188(1-3):103-6.
114. Haglund WD, Connor M, Scott DD. The Effect of Cultivation on Buried Human Remains. In: Haglund WD, Sorg MH, editors. *Advances in Forensic Taphonomy: Method, Theory, and Archaeological Perspectives*. 1st ed. Boca Raton: CRC Press; 2002. p. 133-50.
115. Coard R. One Bone, Two Bones, Wet Bones, Dry Bones: Transport Potentials Under Experimental Conditions. *Journal of Archaeological Science*. 1999;26(11):1369-75.
116. White T D, Folkens P A. *The Human Bone Manual*. Amsterdam;Boston: Elsevier Academic; 2005.
117. Kersh KL, Childers JM, Justice D, Karim G. Detection of gunshot residue on Dark-Colored clothing prior to chemical analysis. *Journal of Forensic Sciences*. 2014;59(3):754-62.
118. Robertson J, Roux C, Wiggins K G. From Crime Scene to Laboratory. *Forensic Examination of Fibres*. 3rd ed. Boca Raton: CRC Press; 2017. p. 99-143.
119. Lincoln CA, McBride PM, Turbett GR, Garbin CD, MacDonald EJ. The use of an alternative light source to detect semen in clinical forensic medical practice. *Journal of Clinical Forensic Medicine*. 2006;13(4):215-8.
120. Miranda GE, Prado FB, Delwing F, Daruge E, Jr. Analysis of the fluorescence of body fluids on different surfaces and times. *Sci Justice*. 2014;54(6):427-31.
121. Li B, Beveridge P, O'Hare WT, Islam M. The application of visible wavelength reflectance hyperspectral imaging for the detection and identification of blood stains. *Science & Justice: Journal of the Forensic Science Society*. 2014;54(6):432-8.
122. Capasso L, D'Anastasio R, Guarnieri S, Viciano J, Mariggiò M. Bone natural autofluorescence and confocal laser scanning microscopy: Preliminary results of a novel useful tool to distinguish between forensic and ancient human skeletal remains. *Forensic Science International*. 2017;272:87-96.
123. Hoke N, Grigat A, Grupe G, Harbeck M. Reconsideration of bone postmortem interval estimation by UV-induced autofluorescence. *Forensic Sci Int*. 2013;228(1-3):176 e1-6.
124. Marin N, Buszka J. *Alternate Light Source Imaging: Forensic Photography Techniques*. New York: Routledge; 2013.
125. Vecellio ME, Bryant EP. *Pocket Guide to Crime Scene Photography*. 1st ed: Taylor & Francis; 2017.
126. Wawryk J, Odell M. Fluorescent identification of biological and other stains on skin by the use of alternative light sources. *J Clin Forensic Med*. 2005;12(6):296-301.
127. Sheppard K, Cassella JP, Fieldhouse S, King R. The adaptation of a 360 degrees camera utilising an alternate light source (ALS) for the detection of biological fluids at crime scenes. *Sci Justice*. 2017;57(4):239-49.

128. Hayman J, Oxenham M. *Human Body Decompostion*. 1st ed: Academic Press; 2016.
129. Prentice AID. Autofluorescence of bone tissues. *Journal of clinical pathology*. 1967;20(5):717-9.
130. Lambrecht G, Mallol C. Autofluorescence of experimentally heated bone: Potential archaeological applications and relevance for estimating degree of burning. *Journal of Archaeological Science: Reports*. 2020;31.
131. Krap T, Nota K, Wilk LS, van de Goot FRW, Ruijter JM, Duijst W, et al. Luminescence of thermally altered human skeletal remains. *Int J Legal Med*. 2017;131(4):1165-77.
132. Miranda GE, Melani RFH, Francisquini Júnior L., Daruge Júnior E. Use of an Alternate Light Source to Detect Tooth and Bone. *Brazilian Dental Journal*. 2017;28(1):78-81.
133. Green H, Jabez J, Nelson J. Optimizing parameters for the use of alternate light sources in detecting fragmentary bones: a pilot study. *Australian Journal of Forensic Sciences*. 2019;51(sup1):S201-S4.
134. Maidment C. The Use of Alternative Light Sources to Detect Skeletal Remains Underwater: A Study of Collagen, Fluorescence, and Taphonomic Environment. [Unpublished master's thesis]. In press 2017.
135. Christensen AM, Horn KJ, Smith VA. The use of an alternate light source for detecting bones underwater. *J Forensic Sci*. 2014;59(4):1046-8.
136. Johnsen S. *The optics of life: a biologist's guide to light in nature*: Princeton University Press; 2012.
137. Harte A, Cassella JP, McCullagh NA. Recovery of trace evidence in forensic archaeology and the use of alternate light sources (ALS). *Forensic Sci Int*. 2020;316:110475.
138. Thompson T. Heat-induced dimensional changes in bone and their consequences for forensic anthropology. *Journal of Forensic Science*. 2005;50(5):1008.
139. Gallo G, Fyhrie M, Paine C, Ushakov SV, Izuho M, Gunchinsuren B, et al. Characterization of structural changes in modern and archaeological burnt bone: Implications for differential preservation bias. *PLoS One*. 2021;16(7):e0254529.
140. Thompson TJU. Recent advances in the study of burned bone and their implications for forensic anthropology. *Forensic Science International*.146:S203-S5.
141. Ellingham STD, Thompson TJU, Islam M. Thermogravimetric analysis of property changes and weight loss in incinerated bone. *Palaeogeography, Palaeoclimatology, Palaeoecology*. 2015;438:239-44.
142. Krap T, Busscher L, Oostra RJ, Aalders MCG, Duijst W. Phosphorescence of thermally altered human bone. *Int J Legal Med*. 2021;135(3):1025-34.
143. Gallant AS. Alternate light sources in the detection of bone after an accelerated fire: a pilot study. *J Forensic Sci*. 2013;58 Suppl 1:S221-6.
144. Louys J. Practice and prospects in underwater palaeontology. *Palaeontologia Electronica*. 2018.
145. Bertoglio B, Messina C, Cappella A, Maderna E, Mazzarelli D, Lucheschi S, et al. Bone tissue preservation in seawater environment: a preliminary comparative analysis of bones with different post-mortem histories through anthropological and radiological perspectives. *Int J Legal Med*. 2021;135(6):2581-94.
146. Swaraldahab MAH, Christensen AM. The Effect of Time on Bone Fluorescence: Implications for Using Alternate Light Sources to Search for Skeletal Remains. *J Forensic Sci*. 2016;61(2):442-4.
147. Sterzik V, Holz F, Ohlwarther TEN, Thali M, Birngruber CG. Estimating the postmortem interval of human skeletal remains by analyzing their fluorescence at 365 and 490 nm. *Int J Legal Med*. 2018;132(3):933-8.
148. Sterzik V, Jung T, Jellinghaus K, Bohnert M. Estimating the postmortem interval of human skeletal remains by analyzing their optical behavior. *Int J Legal Med*. 2016;130(6):1557-66.

149. Steadman DW, DiAntonio LL, Wilson JJ, Sheridan KE, Tammariello SP. The Effects of Chemical and Heat Maceration Techniques on the Recovery of Nuclear and Mitochondrial DNA from Bone. *Journal of Forensic Sciences*. 2006;51(1):11-7.
150. Couse T, Connor M. A comparison of maceration techniques for use in forensic skeletal preparations. *Journal of Forensic Sciences*. 2015;3(1):1-6.
151. Husch C, Berner M, Goldammer H, Lichtscheidl-Schultz I. Technical note: A novel method for gentle and non-destructive removal of flesh from bones. *Forensic Sci Int*. 2021;323:110778.
152. Gent L, Schwalbe EC, Procopio N. The impact of maceration on the 'Osteo-ome'; a pilot investigation. *J Proteomics*. 2023;271:104754.
153. Mahon TJ, Maboke N, Myburgh J. The use of different detergents in skeletal preparations. *Forensic Sci Int*. 2021;327:110967.
154. Bonicelli A, Cheung W, Hughes S, Wescott DJ, Procopio N. Preliminary Investigation of the Effect of Maceration Procedures on Bone Metabolome and Lipidome. *Metabolites*. 2022;12(11).
155. Lee EJ, Luedtke JG, Allison JL, Arber CE, Merriwether DA, Steadman DW. The effects of different maceration techniques on nuclear DNA amplification using human bone. *Journal of Forensic Sciences*. 2010;55(4):1032-8.
156. King C, Birch W. Assessment of maceration techniques used to remove soft tissue from bone in cut mark analysis. *J Forensic Sci*. 2015;60(1):124-35.
157. Marin N, Buszka J. Light and the Electromagnetic Spectrum. *Alternate Light Source Imaging: Forensic Photography Techniques*. New York: Routledge; 2013. p. 1-7.
158. Schariatmadary P, Aalders MCG, Oostra RJ, Krap T. Temperature-specific spectral shift of luminescing thermally altered human remains. *Int J Legal Med*. 2023;137(4):1277-86.
159. Killam EW. *The Detection of Human Remains*. 2nd ed. Springfield, Illonois: Charles C Thomas; 2004.
160. Martini G. Infrared Detection Systems for Maritime Search And Rescue Units. In: Bierens JJLM, Branche CM, Brewster BC, editors. *Handbook on Drowning: Prevention, Rescue, Treatment*. 1 ed. Berlin / Heidelberg: Springer 2005. p. 630-3.
161. Thomas TB, Finley SJ, Wilkinson JE, Wescott DJ, Gorski A, Javan GT. Postmortem microbial communities in burial soil layers of skeletonized humans. *J Forensic Leg Med*. 2017;49:43-9.
162. Forbes SL, Samson C, Watson CJ. Seasonal impact of scavenger guilds as taphonomic agents in central and northern Ontario, Canada. *J Forensic Sci*. 2022;67(6):2203-17.
163. Pringle JK, Stimpson IG, Wisniewski KD, Heaton V, Davenward B, Mirosch N, et al. Geophysical monitoring of simulated homicide burials for forensic investigations. *Sci Rep*. 2020;10(1):7544.
164. Pringle JK, Ruffell A, Jervis JR, Donnelly L, McKinley J, Hansen J, et al. The use of geoscience methods for terrestrial forensic searches. *Earth-Science Reviews*. 2012;114(1-2):108-23.
165. Armstrong EJ, Erskine KL. *Water-related death investigation: practical methods and forensic applications*. 1st ed. Baco Raton, FL: CRC Press; 2016.
166. Ruffell A, Powell N. Search Strategy for Buried Objects in Water: Geophysics, Probes and Dogs. *Forensic Sciences*. 2021;1(3):130-7.
167. Becker R. Crime Scene Investigation and Examination: Underwater Crime Scenes. In: Payne-James J, Byard RW, editors. *Encyclopedia of Forensic and Legal Medicine*. 1. 2nd ed2016. p. 709-21.
168. Becker RF. *Underwater forensic investigation*. Boca Raton: CRC Press; 2013.
169. Alexander MB, Hodges TK, Bytheway J, Aitkenhead-Peterson JA. Application of soil in forensic science: residual odor and HRD dogs. *Forensic Sci Int*. 2015;249:304-13.
170. Forbes SL, Troobnikoff AN, Ueland M, Nizio KD, Perrault KA. Profiling the decomposition odour at the grave surface before and after probing. *Forensic Sci Int*. 2016;259:193-9.
171. Dorriety JK. Cadaver Dogs as a Forensic Tool: An Analysis of Prior Studies. *Journal of Forensic Identification*. 2007;57(5):717-25.

172. Oesterhelweg L, Krober S, Rottmann K, Willhoft J, Braun C, Thies N, et al. Cadaver dogs--a study on detection of contaminated carpet squares. *Forensic Sci Int*. 2008;174(1):35-9.
173. Watney MM, editor Ethical and Legal Aspects Pertaining to Law Enforcement use of Drones. International Conference on Cyber Warfare and Security; 2022: Academic Conferences International Limited.
174. Cicek M, Pasli S, Imamoglu M, Yadigaroglu M, Beser MF, Gunduz A. Simulation-Based Drone Assisted Search Operations in a River. *Wilderness Environ Med*. 2022;33(3):311-7.
175. Ruffell A, Lally A, Rocke B. Dronar—Geoforensic Search Sonar from a Drone. *Forensic Sciences*. 2021;1(3):202-12.
176. Georgiou A, Masters P, Johnson S, Feetham L. UAV-assisted real-time evidence detection in outdoor crime scene investigations. *J Forensic Sci*. 2022;67(3):1221-32.
177. Lyle AL, Johnson M. Drone Photography. *Handbook of Forensic Photography*. Boca Raton: CRC Press; 2022. p. 459-73.
178. Maloney MS, Housman DG. *Crime Scene Investigation Procedural Guide*. 1st ed: CRC Press; 2014.
179. Konieczny M. Air Accidents over Water — Selected Forensic Aspects. *Internal Security*. 2016;8(2):51-65.
180. Siddiqi MA, Iwendi C, Jaroslava K, Anumbe N. Analysis on security-related concerns of unmanned aerial vehicle: attacks, limitations, and recommendations. *Math Biosci Eng*. 2022;19(3):2641-70.
181. Yaacoub J-P, Noura H, Salman O, Chehab A. Security analysis of drones systems: Attacks, limitations, and recommendations. *Internet of Things*. 2020;11.
182. Scholl V, Gerace A. Removing Glint With Video Processing to Enhance Underwater Target Detection. IEEE Western New York Image Processing Workshop2013.
183. Simmons T, Cross PA, Adlam RE, Moffatt C. The influence of insects on decomposition rate in buried and surface remains. *J Forensic Sci*. 2010;55(4):889-92.
184. Butters O, Krosch MN, Roberts M, MacGregor D. Application of forward-looking infrared (FLIR) imaging from an unmanned aerial platform in the search for decomposing remains. *J Forensic Sci*. 2021;66(1):347-55.
185. Lee MJ, Voss SC, Franklin D, Dadour IR. Preliminary investigation of aircraft mounted thermal imaging to locate decomposing remains via the heat produced by larval aggregations. *Forensic Sci Int*. 2018;289:175-85.
186. Rocke B, Ruffell A. Detection of Single Burials Using Multispectral Drone Data: Three Case Studies. *Forensic Sciences*. 2022;2(1):72-87.
187. Franceschetti L, Palamenghi A, Mazzarelli D, Cappella A, Gibelli DM, De Angelis D, et al. Taphonomic study on drowned victims in a non-sequestered aquatic environment in the Mediterranean Sea. *Int J Legal Med*. 2022;136(3):887-95.
188. Martlin BA, Anderson GS, Bell LS. A review of human decomposition in marine environments. *Canadian Society of Forensic Science Journal*. 2022;56(2):92-121.
189. Urbanova P, Jurda M, Vojtisek T, Krajsa J. Using drone-mounted cameras for on-site body documentation: 3D mapping and active survey. *Forensic Sci Int*. 2017;281:52-62.
190. McLean DL, Parsons MJG, Gates AR, Benfield MC, Bond T, Booth DJ, et al. Enhancing the Scientific Value of Industry Remotely Operated Vehicles (ROVs) in Our Oceans. *Frontiers in Marine Science*. 2020;7.
191. Singh H, Roman C, Pizarro O, Eustice R, Can A. Towards High-resolution Imaging from Underwater Vehicles. *The International Journal of Robotics Research*. 2016;26(1):55-74.
192. Bucci G. Hydrographic Drone Non-Invasive Underwater Investigations: New Archaeological Discoveries in Valle Fossa di Porto (Comacchio—FE, Italy). *Heritage*. 2023;6(2):1804-23.
193. Diela T, Jensen F, Schuettler D. Underwater drone finds bodies, motorcycles from sunken Indonesia ferry 2018 [updated 06/06/2018. Available from: https://www.reuters.com/article/us-indonesia-ferry-idUSKBN1JP0JF.

194. Gately I. Exploring the potential for the archaeological application of remotely operated underwater vehicles (ROVs) in the Australian context. *Bulletin of the Australasian Institue for Maritime Archaeology*. 2013;37:26-32.
195. Atherton MW. *Echoes and Images: The Encyclopedia of Side-Scan and Scanning Sonar Operations*: OysterInk Publications; 2011.
196. Tan Q, Zhao Y, Shufan H, Cong A, Chunfeng R, Dexiang G. Profiling experiment of a lake using ground penetrating radar. 2017 9th International Workshop on Advanced Ground Penetrating Radar (IWAGPR)2017. p. 1-5.
197. Ruffell A, Parker R. Water penetrating radar. *Journal of Hydrology*. 2021;597.
198. Voillot JF. Examination of Vehicles Recovered Underwater. In: Stauffer E, Bonfanti MS, editors. *Forensic Investigation of Stolen-Recovered and other Crime-related Vehicles*. 1st ed: Academic Press; 2006. p. 337-65.
199. City of Orlando Jurisdiction Map: City of Orlando; 2021.
200. Shaler RC. *Crime scene forensics: A scientific method approach*. Boca Raton: CRC Press; 2012.
201. Gilmour PM. The application of photography in investigating fraud. *The Imaging Science Journal*. 2019;67(4):215-23.
202. Miller M, Marin N. *Police Photography*. 7th ed: Routledge; 2015.
203. Dutelle AW. *Basic Crime Scene Photography*. 2nd ed: CreateSpace; 2016.
204. Duncan CD. *Advanced crime scene photography*: CRC Press; 2015.
205. Suboch G. Forensic Photography. *Real-World Crime Scene Investigation: A Step-by-Step Pocedure Manual*. Boca Raton: CRC Press; 2016. p. 29-66.
206. Pepper IK. *Crime Scene Investigation: Methods and Procedures*. 2nd ed. Maidenhead: Open University Press; 2010.
207. Robinson EM, Richards GB. *Crime Scene Photography*. 2nd ed: Elsevier Science & Technology; 2010.
208. Crowe C, Moran C. Police photography, video recording, 3D laser scanning. In: Sutton R, Trueman K, Moran C, editors. *Crime Scene Management: Scene Specific Methods*: John Wiley & Sons, Ltd; 2017.
209. Marsh N. *Forensic Photography: A Practitioner's Guide*. 1st ed: John Wiley & Sons, Inc; 2014.
210. Redsicker DR. *The Practical Metholodolgy of Forensic Photography*. 2nd ed. Boca Raton, Fla.; London: CRC; 2001.
211. Understanding Your Camera Settings: There's More To Taking Pictures Than The 'Auto' Function: Digital Relativity; 2013 [updated 10/01/2013. Available from: https://digitalrelativity.com/camera-settings-basics/.
212. Mancini K, Sidoriak J. *Fundamentals of Forensic Photography: Practical Techniques for Evidence Documentation on Location and in the Laboratory*. 1st ed. New York: Routledge; 2017.
213. Mansurov N. What is a Mirrorless Camera? : Photography life; 2018 [updated 11/02/2018. Available from: https://photographylife.com/what-is-a-mirrorless-camera.
214. Weiss SL, Wyman R. Getting Ready to Go. In: Weiner SL, editor. *Handbook of Forensic Photography*: CRC Press; 2022. p. 23-36.
215. Watkins D, Brown K. Impression and Pattern Evidence. In: Weiss S, editor. *Handbook of Forensic Photography*. Boca Raton: CRC Press; 2022. p. 122-37.
216. Gouse S, Karnam S, Girish HC, Murgod S. Forensic photography: Prospect through the lens. *J Forensic Dent Sci*. 2018;10(1):2-4.
217. Elizarov V. The Exposure Triangle: A Beginner's Guide: PetaPixel; 2022 [updated 09/11/2022. Available from: https://petapixel.com/exposure-triangle/.
218. Jones P, Gerbeth VJ. *Practical Forensic Digital Imaging: Applications and Techniques*. 1st ed: CRC Press; 2011.
219. Porter G. Specialised photography and imaging. In: Horswell J, editor. *The Practice of Crime Scene Investigation*. 1st ed. Boca Raton: CRC Press; 2004. p. 139-59.

220. Carapezza EM, Barazzetti L, Sala R, Scaioni M, Cattaneo C, Gibelli D, et al. 3D scanning and imaging for quick documentation of crime and accident scenes. Sensors, and Command, Control, Communications, and Intelligence (C3I) Technologies for Homeland Security and Homeland Defense XI2012. p. 835910--14.
221. Buck U. 3D crime scene reconstruction. *Forensic Sci Int*. 2019;304:109901.
222. Wink AE. Pubic symphyseal age estimation from three-dimensional reconstructions of pelvic CT scans of live individuals. *J Forensic Sci*. 2014;59(3):696-702.
223. Sheppard K, Cassella JP, Fieldhouse S. A comparative study of photogrammetric methods using panoramic photography in a forensic context. *Forensic Sci Int*. 2017;273:29-38.
224. Siebke I, Campana L, Ramstein M, Furtwängler A, Hafner A, Lösch S. The application of different 3D-scan-systems and photogrammetry at an excavation — A Neolithic dolmen from Switzerland. *Digital Applications in Archaeology and Cultural Heritage*. 2018;10.
225. Errickson D, Thompson TJU, Rankin BWJ. The application of 3D visualization of osteological trauma for the courtroom: A critical review. *Journal of Forensic Radiology and Imaging*. 2014;2(3):132-7.
226. Urbanova P, Hejna P, Jurda M. Testing photogrammetry-based techniques for three-dimensional surface documentation in forensic pathology. *Forensic Sci Int*. 2015;250:77-86.
227. Hacker R. Laser Scanning. In: Weiner S, editor. *Handbook of Forensic Photography*. Boca Raton: CRC Press; 2022. p. 388-97.
228. Liscio E. Crime Scene Photogrammetry. In: Weiner S, editor. *Handbook of Forensic Photography*. Boca Raton: CRC Press; 2022. p. 435-43.
229. Weiss SL. Three-dimensional photography and its applications. In: Weiner S, editor. *Handbook of Forensic Photography*. Boca Raton: CRC Press; 2022. p. 179-205.
230. Edelman. G.J, Aalders MC. Photogrammetry using visible, infrared, hyperspectral and thermal imaging of crime scenes. *Forensic Science International*. 2018;292(11):181-9.
231. Larsen JL. Large scene investigation. In: Weiner S, editor. *Handbook of Forensic Photography*. Boca Raton: CRC Press; 2022. p. 399-404.
232. Moran C, Forest D. Managing complex scenes and multiple or mass fatality scenes. In: Sutton R, Trueman K, Moran C, editors. *Crime Scene Management: Scene Specific Methods*. 2nd ed: John Wiley & Sons Inc.; 2017. p. 252-66.
233. Daluz HM. *Fundamentals of fingerprint analysis*. Boca Raton: CRC Press; 2015.
234. Bandey HL, Bleay SM, Gibson AP. Powders for Fingerprint Development. In: Ramotowski R, editor. *Lee and Gaensslen's Advances in Fingerprint Technology*. 3rd ed: CRC Press; 2021. p. 191-216.
235. Hawthorne MR. *Fingerprints: processing, analysis and understanding*. Boca Raton: CRC Press; 2020.
236. Wargacki SP, Lewis LA, Dadmun MD. Enhancing the quality of aged latent fingerprints developed by superglue fuming: loss and replenishment of initiator. *J Forensic Sci*. 2008;53(5):1138-44.
237. Lewis LA. Cyanoacrylate fuming method. In: Ramotowski R, editor. *Lee and Gaensslen's Advances in Fingerprint Technology*. 3rd ed: CRC Press; 2012. p. 263-91.
238. Chen CC, Yu YC, Lee HC, Giang YS, Wang SM. Latent Fingerprint Development on Thermal Paper Using Traditional Ninhydrin and 1,2-indanedione. *J Forensic Sci*. 2016;61(1):219-25.
239. Almog J. Ninhydrin and ninhydrin analogues. In: Ramotowski R, editor. *Lee and Gaensslen's Advances in Fingerprint Technology*. 3rd ed: CRC Press; 2012. p. 293-305.
240. Lee WC, Khoo BE, Abdullah AF, Aziz A, Binti Z. Statistical evaluation of alternative light sources for bloodstain photography. *Journal of Forensic Sciences*. 2013;58(3):658-63.
241. Marin N, Buszka J. Polarized Light Photography. *Alternate Light Source Imaging: Forensic Photography Techniques*. New York: Routledge; 2013. p. 89-96.
242. Lawson C, Lancaster M, Jasra S, Jasra P. Estimation of Firing Distance by Analysis of Gunshot Residue Patterns Using An Alternative Light Source with Validation using SEM. *Identification Canada*. 2016:76-99.

243. Baxter Jr E. *Complete Crime Scene Investigation Workbook*. 1st ed. Boca Raton: CRC Press; 2015.
244. Kottner S, Schulz MM, Berger F, Thali M, Gascho D. Beyond the visible spectrum - applying 3D multispectral full-body imaging to the VirtoScan system. *Forensic Sci Med Pathol*. 2021;17(4):565-76.
245. Gartshore A, Kidd M, Joshi LT. Applications of Microwave Energy in Medicine. *Biosensors (Basel)*. 2021;11(4).
246. James ME. Degrees of contrast: Detection of latent bloodstains on fabric using an alternate light source (ALS) and the effects of washing. *J Forensic Sci*. 2021;66(3):1024-32.
247. Radi HA, Rasmussen JO. *Principles of Physics*. Berlin, Heidelberg: Springer; 2013.
248. Aparna R, Iyer RS. Detection and visualization of human tears using alternate light sources for forensic purposes. *Sci Justice*. 2021;61(6):771-8.
249. Oner Kaya D, Karadayi S, Karadayi B, Cetin G. Evaluation of the detectability of different ages of bloodstains on fabrics in different washing conditions and at various wavelengths. *J Forensic Leg Med*. 2023;94:102486.
250. Tay JW, Joudo J, Tran T, Ta H, Botting JL, Liew YC, et al. Comparison of Crime-lite® 82S, Polilight® PL400 and Polilight® PL500 for the detection of semen and saliva stains. *Australian Journal of Forensic Sciences*. 2020;53(4):483-93.
251. Miller MT. Visualization and Enhancement. *Crime Scene Investigation Laboratory Manual*2014. p. 129-46.
252. Baxter Jr E. *Complete Crime Scene Investigation Handbook*. 1st ed. Boca Raton: CRC Press; 2015.
253. Jolley EM, Smith FT. Interactions between a heavy particle, air, and a layer of liquid. *Physics of Fluids*. 2023;35(4).
254. Qiao X, Yamashita A, Asama H. Underwater Structure from Motion for Cameras Under Refractive Surfaces. *Journal of Robotics and Mechatronics*. 2019;31(4):603-11.
255. Hoth J, Kowalczyk W. Colour reconstruction of underwater images. *Underwater Technology*. 2017;34(2):51-61.
256. Craig EA, Vezaro N. Use of an Alternate Light Source to Locate Bone and Tooth Fragments. *Journal of Forensic Identification*. 1998;48(4):451-8.
257. Lakowicz RJ. *Solvent Effects on Emission Spectra*. 2nd ed: Springer Science; 1999.
258. Marian CM. Understanding and Controlling Intersystem Crossing in Molecules. *Annu Rev Phys Chem*. 2021;72:617-40.
259. Marin N, Buszka J. UV and Narrowband Visible Light Imaging. *Alternate Light Source Imaging: Forensic Photography Techniques*. New York: Routledge; 2013. p. 25-45.
260. Dutelle AW. *An Introduction to Crime Scence Investigation*. 3rd ed: Jones and Bartlett; 2016.
261. Marin N, Buszka J. Photographic Equipment for Alternate Light Photography Source Imaging. *Alternate Light Source Imaging: Forensic Photography Techniques*. New York: Routledge; 2013. p. 10-9.
262. Landscape study of alternate light sources. Forensic Technology Center of Excellence: National Institute of Justice, Office of Investigative and Forensic Science; 2018.
263. Barrera V, Haas C, Meixner EA, Fliss B. Detection of painted-over traces of blood and seminal fluid. *Int J Legal Med*. 2018;132(4):1067-74.
264. Lennard C, Stoilovic M. Application of forensic light sources at the crime scene. *The Practice of Crime Scene Investigation* CRC Press; 2004. p. 97-123.
265. Stoilovic M. Detection of semen and blood stains using polilight as a light source. *Forensic Science International*. 1991;51:289-96.
266. Brown T, Christensen A. Using an Alternate Light Source (ALS) to Search for Surface Deposited Skeletal Remains. *Forensic Anthropology*. 2018;1(1):68-73.
267. Finnis J, Davidson G, Fraser I, Murphy C, Hargreaves C, Stevenson N, et al. Illuminating the benefits and limitations of forensic light sources. *Sci Justice*. 2023;63(1):127-34.

268. Schulz MM, Wehner F, Wehner HD. The use of a tunable light source (Mini-Crimescope MCS-400, SPEX Forensics) in dissecting microscopic detection of cryptic epithelial particles. *J Forensic Sci*. 2007;52(4):879-83.
269. Howard MC, Nessan M. Detecting bloodstains under multiple layers of paint. *Journal of Forensic Identification*. 2010;60(6):682-717.
270. Rust L, Nizio KD, Wand MP, Forbes SL. Investigating the detection limits of scent-detection dogs to residual blood odour on clothing. *Forensic Chemistry*. 2018;9:62-75.
271. Vandenberg N, van Oorschot RA. The use of Polilight in the detection of seminal fluid, saliva, and bloodstains and comparison with conventional chemical-based screening tests. *J Forensic Sci*. 2006;51(2):361-70.
272. Bulut O, Wedge A. Forensic anthropology and photography. In: Weiner S, editor. *Handbook of Forensic Photography*. Boca Raton: CRC Press; 2022. p. 611-38.
273. Barbaro A, Mishra A. *Manual of Crime Scene Investigation*. 1st ed. Boca Raton: CRC Press; 2022.
274. Guidelines to the Standards for Recording Human Remains. BABAO and the Institute of Field Archaeologists; 2004.
275. Nelson DG. An Alternate Light Source to Detect Semen. *Academic Emergency Medicine*. 2002;9(10):1045-8.
276. Sterzik V, Hinderberger P, Panzer S, Bohnert M. Visualizing old biological traces on different materials without using chemicals. *Int J Legal Med*. 2018;132(1):35-41.
277. McAllister P, Graham E, Deacon P, Farrugia KJ. The effect of mark enhancement techniques on the subsequent detection of saliva. *Sci Justice*. 2016;56(5):305-20.
278. Camilleri E, Silenieks E, Henry J. Locating Saliva Stains using the Polilight and SALIgAE Spray. Evidence Recovery and Biology Anlaytical Groups, Government of South Australia: Florida International University; 2006.
279. Lloyd JB. Forensic significance of fluorescent brighteners: their qualitative TLC characterisation in small quantities of fibre and detergents. *J Forensic Sci Soc*. 1978;17(2-3):145-52.
280. Viner TC, Kagan RA, Johnson JL. Using an alternate light source to detect electrically singed feathers and hair in a forensic setting. *Forensic Sci Int*. 2014;234:e25-9.
281. Wallace JS. *Chemical Analysis of Firearms, Ammunition, and Gunshot Residue*. 2nd ed. Boca Raton: CRC Press; 2018.
282. Barrera V, Fliss B, Panzer S, Bolliger SA. Gunshot residue on dark materials: a comparison between infrared photography and the use of an alternative light source. *Int J Legal Med*. 2019;133(4):1115-20.
283. Husak J. Noninvasive, visual examination for the presence of gunshot residue on human skin. *J Forensic Sci*. 2022;67(3):1191-7.
284. Golden GS. Use of Alternative Light Source Illumination in Bite Mark Photography. *Journal of Forensic Sciences*. 1994;39(3):815-23.
285. Glauche J, Ondruschka B, Wenzel V, Dreßler J, Hädrich C. Examination of invisible injuries. *Rechtsmedizin*. 2015;25(6):543-7.
286. Sully CJ, Olds KL, Langlois NE. Evaluation of a model of bruising in pigmented skin for investigating the potential for alternate light source illumination to enhance the appearance of bruises by photography of visible and infrared light. *Forensic Science, Medicine and Pathology*. 2019;15:555-63.
287. Limmen RM, Ceelen M, Reijnders UJ, Joris Stomp S, de Keijzer KC, Das K. Enhancing the visibility of injuries with narrow-banded beams of light within the visible light spectrum. *J Forensic Sci*. 2013;58(2):518-22.
288. Lombardi M, Canter J, Patrick PA, Altman R. Is fluorescence under an alternate light source sufficient to accurately diagnose subclinical bruising? *J Forensic Sci*. 2015;60(2):444-9.
289. Lynnerup N, Hjalgrim H. The routine use of ultraviolet light in medicolegal examinations to evaluate stains and skin trauma. *Medicine, Science and the Law*. 1995;35(2):165-8.

290. Scafide KN, Downing NR, Kutahyalioglu NS, Sheridan DJ, Langlois NE, Hayat MJ. Predicting alternate light absorption in areas of trauma based on degree of skin pigmentation: Not all wavelengths are equal. *Forensic Sci Int*. 2022;339:111410.
291. Olds K, Byard RW, Winskog C, Langlois NE. Validation of ultraviolet, infrared, and narrow band light alternate light sources for detection of bruises in a pigskin model. *Forensic Sci Med Pathol*. 2016;12(4):435-43.
292. Holbrook DS, Jackson MC. Use of an alternative light source to assess strangulation victims. *J Forensic Nurs*. 2013;9(3):140-5.
293. Ellen D, Day S, Davies C. *Scientific Examination of Documents*. 4th ed. Boca Raton: CRC Press; 2018.
294. King RSP, Davis LWL, Skros DA. The use of longwave reflected UV imaging for the enhancement of cyanoacrylate developed fingermarks: A simple, safe and effective imaging tool. *Forensic Sci Int*. 2018;289:329-36.
295. Bandey H, Bleay S, Bowman V, Fitzgerald L, Gibson A, Hart A, et al. Fingerprint imaging across EM spectrum. *The Imaging Science Journal*. 2013;54(4):211-8.
296. Becue A, Moret S, Champod C, Margot P. Use of stains to detect fingermarks. *Biotech Histochem*. 2011;86(3):140-60.
297. Gaw A. *Lee and Gaensslen's Advances in Fingerprint Technology*. 3rd ed. Boca Raton: CRC Press; 2012.
298. Bond JW. A Noninvasive and Speculative Method of Visualizing Latent Fingerprint Deposits on Thermal Paper. *J Forensic Sci*. 2015;60(4):1034-9.
299. Richards A, Leintz R. Forensic Reflected Ultraviolet Imaging. *Journal of Forensic Identification*. 2013;63(1):46-69.
300. Lennard C. Fingerprint detection: current capabilities. *Australian Journal of Forensic Sciences*. 2007;39(2):55-71.
301. Cantú AA. The Physical Principles of the Reflected Ultraviolet Imaging Systems. *Journal of Forensic Identification*. 2014;64(2):123-1441.
302. Senior S, Hamed E, Masoud M, Shehata E. Characterization and dating of blue ballpoint pen inks using principal component analysis of UV-Vis absorption spectra, IR spectroscopy, and HPTLC. *J Forensic Sci*. 2012;57(4):1087-93.
303. Houlgrave S, LaPorte GM, Stephens JC. The use of filtered light for the evaluation of writing inks analyzed using thin layer chromatography. *J Forensic Sci*. 2011;56(3):778-82.
304. Hoke N, Burger J, Weber C, Benecke N, Grupe G, Harbeck M. Estimating the chance of success of archaeometric analyses of bone: UV-induced bone fluorescence compared to histological screening. *Palaeogeography, Palaeoclimatology, Palaeoecology*. 2011;310(1-2):23-31.
305. Stoops G. Fluorescence Microscopy. In: Nicosia C, Stoops G, editors. *Archaeological Soil and Sediment Micromorphology*: John Wiley & Sons Ltd.; 2017. p. 383-91.
306. Knight B, Lauder I. Methods of dating skeletal remains. *Human Biology*. 1969;41(3):322-41.
307. Scheirs S, Malgosa A, Galtes I. The use of ultraviolet light to reveal and enhance burned areas on human bone. *Forensic Sci Med Pathol*. 2015;11(4):618-21.
308. Virkler K, Lednev IK. Analysis of body fluids for forensic purposes: from laboratory testing to non-destructive rapid confirmatory identification at a crime scene. *Forensic Science International*. 2009;188(1):1-17.
309. Mazel CH. Underwater fluorescence photography in the presence of ambient light. *Limnology and Oceanography: Methods*. 2005;3(11):499-510.
310. Pollitt EN, Anderson JC, Scafide KN, Holbrook D, D'Silva G, Sheridan DJ. Alternate Light Source Findings of Common Topical Products. *J Forensic Nurs*. 2016;12(3):97-103.
311. Blau S, Briggs CA. The role of forensic anthropology in Disaster Victim Identification (DVI). *Forensic Sci Int*. 2011;205(1-3):29-35.

312. Martinez GIA, Azorin NJ, Sosam FR. Radiation damage UV and γ-rays on pig and bovine bones by fluorescence techniques. 19th International Symposium on Solid State Dosimetry; Mexico: ISSSD; 2019.
313. Schmidt CW, Symes SA. *The analysis of burned human remains* 2nd ed. Amsterdam: Academic Press; 2015.
314. Ramsthaler F, Amendt J, Grassberger M, Verhoff MA. Recovery of human remains with severe burn damage. *Legal Medicine*. 2013;23:267-80.
315. Hillier ML, Bell LS. Differentiating human bone from animal bone: a review of histological methods. *J Forensic Sci*. 2007;52(2):249-63.
316. Cattaneo C, Porta D, Gibelli D, Gamba C. Histological determination of the human origin of bone fragments. *J Forensic Sci*. 2009;54(3):531-3.
317. Zimmerman HA, Meizel-Lambert CJ, Schultz JJ, Sigman ME. Chemical Differentiation of Osseous, Dental, and Non-skeletal Materials in Forensic Anthropology using Elemental Analysis. *Sci Justice*. 2015;55(2):131-8.
318. Buddhachat K, Klinhom S, Siengdee P, Brown JL, Nomsiri R, Kaewmong P, et al. Elemental Analysis of Bone, Teeth, Horn and Antler in Different Animal Species Using Non-Invasive Handheld X-Ray Fluorescence. *PLoS One*. 2016;11(5):e0155458.
319. Wang Q, Li W, Liu R, Zhang K, Zhang H, Fan S, et al. Human and non-human bone identification using FTIR spectroscopy. *Int J Legal Med*. 2019;133(1):269-76.
320. Imbert L, Gourion-Arsiquaud S, Villarreal-Ramirez E, Spevak L, Taleb H, van der Meulen MC, et al. Dynamic structure and composition of bone investigated by nanoscale infrared spectroscopy. *PLoS One*. 2018;13(9).
321. Paschalis EP, Recker R, Dicarlo E, Doty SB, Boskey AL. Distribution of collagen cross links in normal trabecular bone. *Journal of Bone and Mineral Research*. 2003;18(11):1942-6.
322. Shah FA, Stoica A, Cardemil C, Palmquist A. Multiscale characterization of cortical bone composition, microstructure, and nanomechanical properties in experimentally induced osteoporosis. *Journal of Biomedical Materials Research Part A*. 2018;106(4):997-1007.
323. Tomassetti M, Marini F, Campanella L, Coppa A. Study of modern or ancient collagen and human fossil bones from an archaeological site of middle Nile by thermal analysis and chemometrics. *Microchemical Journal*. 2013;108:7-13.
324. Currey JD. *Bones: Structure and mechanics* Princeton: Princeton University Press; 2013.
325. Myllyharju J, Kivirikko KI. Collagens and collagen-related diseases. *Annals of medicine*. 2001;33(1):7-21.
326. Henriques ME, Pinto, M. *Type I collagen: biological functions, synthesis and medicinal applications*. New York: Nova Science Publishers, Inc; 2012.
327. Lodish HF, Darnell JE. *Molecular Cell Biology*. 4th ed. New York: W.H. Freeman; 2000.
328. Marcu L, Cohen D, Maarek JM, Grundfest WS. Characterization of type I, II, III, IV, and V collagens by time-resolved laser-induced fluorescence spectroscopy. *InOptical Biopsy III* 2000;3917:93-102.
329. Shekhonin BV, Domogatsky SP, Muzykantov VR, Idelson GL, Rukosuev VS. Distribution of type I, III, IV and V collagen in normal and atherosclerotic human arterial wall: immunomorphological characteristics. *Collagen and related research*. 1985;5(4):355-68.
330. Hudson BG, Tryggvason K, Sundaramoorthy M, Neilson EG. Alport's syndrome, Goodpasture's syndrome, and type IV collagen. *New England Journal of Medicine*. 2003;348(25):2543-56.
331. Minor RR. Collagen metabolism: a comparison of diseases of collagen and diseases affecting collagen. *The American journal of pathology*. 1980;98(1):225.
332. Wang X, Shen X, Li X, Agrawal CM. Age-related changes in the collagen network and toughness of bone. *Bone*. 2002;31(1):1-7.
333. Buckley M, Collins M, Thomas-Oates J, Wilson JC. Species identification by analysis of bone collagen using matrix-assisted laser desorption/ionisation time-of-flight mass spectrometry. *Rapid Communications in Mass Spectrometry: An International Journal Devoted*

to the Rapid Dissemination of Up-to-the-Minute Research in Mass Spectrometry. 2009;23(23):3843-54.
334. Depalle B, Duarte AG, Fiedler IAK, Pujo-Menjouet L, Buehler MJ, Berteau JP. The different distribution of enzymatic collagen cross-links found in adult and children bone result in different mechanical behavior of collagen. *Bone*. 2018;110:107-14.
335. Monici M. Cell and tissue autofluorescence research and diagnostic applications. *Biotechnology annual review*. 2005;1(11):227-56.
336. Prentice AID. Bone Autofluorescence and Mineral Content. *Nature*. 1965;4959:1167.
337. Drzazga ZK, Kluczewska-Galka A, Michnik A, Kaszuba M, Trzeciak H. Fluorescence spectroscopy as tool for bone development monitoring in newborn rats. *J Fluoresc*. 2011;21(3):851-7.
338. Madden O, Chan DMW, Dundon M, France CAM. Quantifying collagen quality in archaeological bone: Improving data accuracy with benchtop and handheld Raman spectrometers. *Journal of Archaeological Science: Reports*. 2018;18:596-605.
339. Boskey AL, Coleman R. Aging and bone. *J Dent Res*. 2010;89(12):1333-48.
340. Hall BK. *Bones and Cartilage: Developmental and Evolutionary Skeletal Biology.* Australia;San Diego, Calif: Elsevier Academic Press; 2005.
341. Bielajew BJ, Hu JC, Athanasiou KA. Collagen: quantification, biomechanics, and role of minor subtypes in cartilage. *Nat Rev Mater*. 2020;5(10):730-47.
342. Pilolli GP, Lucchese A, Maiorano E, Favia G. New approach for static bone histomorphometry: confocal laser scanning microscopy of maxillo-facial normal bone. *Ultrastruct Pathol*. 2008;32(5):189-92.
343. Maggiano C, Dupras T, Schultz M, Biggerstaff J. Spectral and photobleaching analysis using confocal laser scanning microscopy: a comparison of modern and archaeological bone fluorescence. *Mol Cell Probes*. 2006;20(3-4):154-62.
344. Ren P-G, Ma T, Huang Z, Smith RL, Goodman SB. Quantitation of Bone Area in Undecalcified Frozen Sections With Fluorescent Microscopy. *Journal of Histotechnology*. 2013;31(1):15-7.
345. Via GG, Jerele JL. Bone fluorescence and fluorescence-guided debridement in orthopaedic surgery: Current evidence and practice. *Journal of Orthopaedic Reports*. 2023;2(1).
346. Akram M, Daniyal M, Ali A, Zainab R, Shah SMA, Munir N, et al. Role of Phenylalanine and Its Metabolites in Health and Neurological Disorders In: Surguchov A, editor. *Synucleins: Biochemistry and Role in Diseases*2020.
347. Ding KH, Cain M, Davis M, Bergson C, McGee-Lawrence M, Perkins C, et al. Amino acids as signaling molecules modulating bone turnover. *Bone*. 2018;115:15-24.
348. Ghisaidoobe AB, Chung SJ. Intrinsic tryptophan fluorescence in the detection and analysis of proteins: a focus on Forster resonance energy transfer techniques. *Int J Mol Sci*. 2014;15(12):22518-38.
349. MacDonell R, Hamrick MW, Isales CM. Protein/amino-acid modulation of bone cell function. *Bonekey Rep*. 2016;5:827.
350. Shalev M, Elson A. The roles of protein tyrosine phosphatases in bone-resorbing osteoclasts. *Biochim Biophys Acta Mol Cell Res*. 2019;1866(1):114-23.
351. Nayak BN, Singh RB, Buttar HS. Role of Tryptophan in Health and Disease: Systematic Review of the Anti-Oxidant, Anti-Inflammation, and Nutritional Aspects of Tryptophan and Its Metabolites. *World heart journal*. 2019;11(2):161-78.
352. Al Saedi A, Sharma S, Summers MA, Nurgali K, Duque G. The multiple faces of tryptophan in bone biology. *Exp Gerontol*. 2020;129:110778.
353. Jamme F, Kascakova S, Villette S, Allouche F, Pallu S, Rouam V, et al. Deep UV autofluorescence microscopy for cell biology and tissue histology. *Biol Cell*. 2013;105(7):277-88.
354. Pham HT, Ono M, Hara ES, Nguyen HTT, Dang AT, Do HT, et al. Tryptophan and Kynurenine Enhances the Stemness and Osteogenic Differentiation of Bone Marrow-Derived Mesenchymal Stromal Cells In Vitro and In Vivo. *Materials (Basel)*. 2021;14(1).

355. Hoerman KC, Manecewicz SA. Fluorometric Demonstration of Tryptophan in Dentin and Bone Protein. *Journal of Dental Research*. 1963;43(2):276-80.
356. Nuytinck L, Tükel T, Kayserili H, Apak MY, Paepe AD. Glycine to tryprophan substitution in type I collagen in a patient with OI type III a unique collagen mutation. *American Journal of Medical Genetics*. 2000;37:371-5.
357. Shen Y, Zhu D, Lu W, Liu B, Li Y, Cao S. The Characteristics of Intrinsic Fluorescence of Type I Collagen Influenced by Collagenase I. *Applied Sciences*. 2018;8(10).
358. Alfano RR, Marcu L, Cohen D, Maarek J-MI, Grundfest WS. Characterization of type I, II, III, IV, and V collagens by time-resolved laser-induced fluorescence spectroscopy. Optical Biopsy III2000. p. 93-101.
359. Hanson DA, Eyre DR. Molecular site specificity of pyridinoline and pyrrole cross-links in type I collagen of human bone. *J Biol Chem*. 1996;271(43):26508-16.
360. Eyre DR. Cross-linking in collagen and elastin. *Annual Review of Biochemistry*. 1984;33:717-48.
361. Takeuchi S, Arai K, Saitoh H, Yoshida K, Miura M. Urinary pyridinoline and deoxypyridinoline as potential markers of bone metastasis in patients with prostate cancer. *The Journal of Urology*. 1996;156(5):1691-5.
362. Knott L, Bailey A. Collagen Cross-Links in Mineralizing Tissues A Review of Their Chemistry, Function, and Clinical Relevance. *Bone*. 1998;22(3):181-7.
363. Eyre DR. The specificity of collagen cross-links as markers of bone and connective tissue degradation. *Acta Orthopaedica Scandinavica*. 2009;66(sup266):166-70.
364. Boaks A, Siwek D, Mortazavi F. The temporal degradation of bone collagen: A histochemical approach. *Forensic Sci Int*. 2014;240:104-10.
365. Loy C, Brock F, Dyer C. Investigating diagenesis of archaeological bones from Etton Causewayed enclosure, UK. *Quaternary International*. 2023;660:21-30.
366. Wu S, Zhou X, Jin Z, Cheng H. Collagenases and their inhibitors: a review. *Collagen and Leather*. 2023;5(1).
367. Durga R, Jimenez N, Ramanathan S, Suraneni P, Pestle WJ. Use of thermogravimetric analysis to estimate collagen and hydroxyapatite contents in archaeological bone. *Journal of Archaeological Science*. 2022;145.
368. Nielsen-Marsh CM, Hedges REM. Patterns of Diagenesis in Bone I: The Effects of Site Environments. *Journal of Archaeological Science*. 2000;27(12):1139-50.
369. Trueman CN, Martill DM. The long–term survival of bone: The role of bioerosion. *Archaeometry*. 2002;44(3).
370. Eriksen AMH, Nielsen TK, Matthiesen H, Caroe C, Hansen LH, Gregory DJ, et al. Bone biodeterioration-The effect of marine and terrestrial depositional environments on early diagenesis and bone bacterial community. *PLoS One*. 2020;15(10):e0240512.
371. Mein C, Williams A. Assessing the extent of bone bioerosion in short timescales – A novel approach for quantifying microstructural loss. *Quaternary International*. 2023;660:65-74.
372. Collins M J, Nielsen–Marsh C M, Hiller J, Smith C I, Roberts J P, Prigodich R V, et al. The survival of organic matter in bone: a review. *Archaeometry*. 2002;44(3).
373. DeBattista R, Thompson TJ, Thompson CE, Gowland RL. A comparison of surface features on submerged and non-submerged bone using scanning electron microscopy. *J Forensic Leg Med*. 2013;20(6):770-6.
374. Stone TT, Dickel DN, Doran GH. The Preservation and Conservation of Waterlogged Bone from the Windover Site, Florida: A Comparison of Methods. *Journal of Field Archaeology*. 1990;17(2):177-86.
375. Pfretzschner H-U. Fossilization of Haversian bone in aquatic environments. *Comptes Rendus Palevol*. 2004;3(6-7):605-16.
376. Child AM. Microbial taphonomy of archaeological bone. *Studies in Conservation*. 1995;40(1).

377. Jellinghaus K, Urban PK, Hachmann C, Bohnert M, Hotz G, Rosendahl W, et al. Collagen degradation as a possibility to determine the post-mortem interval (PMI) of human bones in a forensic context - A survey. *Leg Med (Tokyo)*. 2019;36:96-102.
378. Luo Q, Leng H, Wang X, Zhou Y, Rong Q. The role of water and mineral-collagen interfacial bonding on microdamage progression in bone. *J Orthop Res*. 2014;32(2):217-23.
379. Hunt DR, Albanese J. History and demographic composition of the Robert J. Terry anatomical collection. *Am J Phys Anthropol*. 2005;127(4):406-17.
380. Bassett EJ, Keith AS, Armelagos GJ, Martin D L, Villanueva AR. Tetracycline-Labeled Human Bone from Ancient Sudanese Nubia. *Science*. 1980;209(4464):1532-4.
381. Hummert JR, Van Gaerven DP. Tetracycline Labeled Human Bone From A Medieval Population in Nubias Batn El Hajar. *Human Biology*. 1982;54(2):355-63.
382. Cook M, Molto E, Anderson C. Fluorochrome labelling in Roman period skeletons from Dakhleh Oasis, Egypt. *Am J Phys Anthropol*. 1989;80(2):137-43.
383. Piepenbrink H, Herrmann B, Hoffmann P. Tetracycline-like fluorescence in buried human skeleton parts. *Rechtsmedizin*. 1983;91(1):71-4.
384. Ristow O, Nehrbass D, Zeiter S, Arens D, Moratin J, Pautke C, et al. Differences between auto-fluorescence and tetracycline-fluorescence in medication-related osteonecrosis of the jaw—a preclinical proof of concept study in the mini-pig. *Clinical Oral Investigations*. 2020;24(12):4625-37.
385. Fondi C, Franchi A. Definition of Bone Necrosis by the Pathologists. *Clinical Cases in Mineral and Bone Metabolism*. 2007;4(1):21-6.
386. Al-Ghaithi A, Husband J, Al-Maskari S. Analysis of Bone Microarchitectural Changes and Structural Damage in Sickle Cell Disease-Induced Avascular Necrosis Using Raman Spectroscopy: Is there potential for medical management? *Sultan Qaboos Univ Med J*. 2021;21(2):e297-e301.
387. Gonzalez G, Costa-Vera C, Borrero LJ, Soto D, Lozada L, Chango JI, et al. Effect of carbonates on hydroxyapatite self-activated photoluminescence response. *Journal of Luminescence*. 2018;195:385-95.
388. Barreiro MB, Ferreira MT, Makhoul C, Morgado M. Distinguishing thermally altered bones from debris using imaging and fluorescence spectrometry. *J Forensic Leg Med*. 2022;91:102416.
389. Keough N, Myburgh J, Steyn M. Scoring of Decomposition: A Proposed Amendment to the Method When Using a Pig Model for Human Studies. *J Forensic Sci*. 2017;62(4):986-93.
390. Connor M, Baigent C, Hansen ES. Testing the Use of Pigs as Human Proxies in Decomposition Studies. *J Forensic Sci*. 2018;63(5):1350-5.
391. Dautartas A, Kenyhercz MW, Vidoli GM, Meadows Jantz L, Mundorff A, Steadman DW. Differential Decomposition Among Pig, Rabbit, and Human Remains. *J Forensic Sci*. 2018;63(6):1673-83.
392. Matuszewski S, Konwerski S, Fratczak K, Szafalowicz M. Effect of body mass and clothing on decomposition of pig carcasses. *Int J Legal Med*. 2014;128(6):1039-48.
393. Forbes S. Body farms. *Forensic Sci Med Pathol*. 2017;13(4):477-9.
394. Varlet V, Joye C, Forbes SL, Grabherr S. Revolution in death sciences: body farms and taphonomics blooming. A review investigating the advantages, ethical and legal aspects in a Swiss context. *Int J Legal Med*. 2020;134(5):1875-95.
395. Wallman JF. Body farms. *Forensic Sci Med Pathol*. 2017;13(4):487-9.
396. Oostra RJ, Gelderman T, Groen WJM, Uiterdijk HG, Cammeraat ELH, Krap T, et al. Amsterdam Research Initiative for Sub-surface Taphonomy and Anthropology (ARISTA) - A taphonomic research facility in the Netherlands for the study of human remains. *Forensic Sci Int*. 2020;317:110483.
397. Byard RW. Body farms - characteristics and contributions. *Forensic Sci Med Pathol*. 2017;13(4):473-4.
398. Human Tissue Act, (2004).

399. Matuszewski S, Hall MJR, Moreau G, Schoenly KG, Tarone AM, Villet MH. Pigs vs people: the use of pigs as analogues for humans in forensic entomology and taphonomy research. *Int J Legal Med*. 2020;134(2):793-810.
400. Carter DO, Tibbett M. Does repeated burial of skeletal muscle tissue (Ovis aries) in soil affect subsequent decomposition? *Applied Soil Ecology*. 2008;40(3):529-35.
401. Crescimanno A, Stout SD. Differentiating fragmented human and nonhuman long bone using osteon circularity. *J Forensic Sci*. 2012;57(2):287-94.
402. Mickleburgh HL, Wescott DJ. Controlled experimental observations on joint disarticulation and bone displacement of a human body in an open pit: Implications for funerary archaeology. *Journal of Archaeological Science: Reports*. 2018;20:158-67.
403. Soni V. *Fundamentals of Computers*: Himalaya Publishing House; 2008.
404. Pratt WK. *Introduction to Digital Image Processing*: Taylor & Francis Group; 2013.
405. Dalrymple B, Smith J. *Forensic Digital Image Processing: Optimization of Impression Evidence*: CRC Press; 2018.
406. Mather PM, Koch M. *Computer Processing of Remotely-Sensed Images: An Introduction*. 4th ed: John Wiley & Sons, Inc; 2011.
407. Kanan C, Cottrell GW. Color-to-grayscale: does the method matter in image recognition? *PLoS One*. 2012;7(1):e29740.
408. Burger W, Burge MJ. *Principles of Digital Image Processing: Fundamental Techniques*. London: Springer; 2009.
409. Solomon C, Breckon T. *Fundamentals of digital image processing: a practical approach with examples in Matlab*. 2 ed: John Wiley & Sons; 2011.
410. Harbeck M, Schleuder R, Schneider J, Wiechmann I, Schmahl WW, Grupe G. Research potential and limitations of trace analyses of cremated remains. *Forensic Sci Int*. 2011;204(1-3):191-200.
411. Connah D, Finlayson GD, Blof M, editors. Seeing beyond luminance: A psychophysical comparison of techniques for converting colour images to greyscale. 15th Color Imaging Conference; 2007: Society for Imaging Science and Technology.
412. Whitt P. *Beginning photo retouching and restoration usin GIMP*. CA: Berkeley; 2014.
413. Hahn BD. *Essential MATLAB for engineers and scientists*. 8th ed. London: Academic Press; 2023.
414. Taylor AB, Ioannou MS, Watanabe T, Hahn K, Chew TL. Perceptually accurate display of two greyscale images as a single colour image. *J Microsc*. 2017;268(1):73-83.
415. Hoerricks J. *Forensic PhotoShop: a comprehensive imaging workflow for forenisc professionals*: Blurb; 2008.
416. Schindelin J, Rueden CT, Hiner MC, Eliceiri KW. The ImageJ ecosystem: An open platform for biomedical image analysis. *Mol Reprod Dev*. 2015;82(7-8):518-29.
417. Rueden CT, Schindelin J, Hiner MC, DeZonia BE, Walter AE, Arena ET, et al. ImageJ2: ImageJ for the next generation of scientific image data. *BMC Bioinformatics*. 2017;18(1):529.
418. Schroeder AB, Dobson ETA, Rueden CT, Tomancak P, Jug F, Eliceiri KW. The ImageJ ecosystem: Open-source software for image visualization, processing, and analysis. *Protein Sci*. 2021;30(1):234-49.
419. Miura M, Sladoje N. *Bioimage Data Analysis Workflows - Advanced Components and Methods*. 1 ed: Springer Cham; 2022.
420. Rasband W. Plugins NIH.gov: National Institutes of Health; 2023 [Available from: https://imagej.nih.gov/ij/plugins/index.html.
421. Rasband W. ImageJ (version 1.54f). 2023.
422. Adobe Photoshop www.adobe.com: Adobe; 2023 [Available from: https://www.adobe.com/uk/products/photoshop.html.
423. Evans S, Noorbhai S, Lawson Z, Stacey-Jones S, Carabott R. Contrast enhancement of bite mark images using the grayscale mixer in ACR in Photoshop(R). *J Forensic Sci*. 2013;58(3):804-10.

424. Chuk H. The Effects of High Dynamic Range on Fingerprint Images Processed by Photoshop. *J Forensic Sci*. 2019;64(4):1173-80.
425. France CAM, Thomas DB, Doney CR, Madden O. FT-Raman spectroscopy as a method for screening collagen diagenesis in bone. *Journal of Archaeological Science*. 2014;42:346-55.
426. Zioupos P, Williams A, Christodoulou G, Giles R. Determinig 'age at death' for forensic purposes using human bone by a laboratory-based analytical method. *Journal of the Mechanical Behavior of Biomedical Materials*. 2014;33(1):109-23.
427. Lozano LF, Peña-Rico MA, Heredia A, Ocotlán-Flores J, Gómez-Cortés A, Velázquez R, et al. Thermal Analysis of Human Bone. *Journal of Materials Science*. 2003;38(23):4777-82.
428. Kontopoulos I, Van de Vijver K, Robberechts B, von Tersch M, Turner-Walker G, Penkman K, et al. Histological and stable isotope analysis of archeological bones from St. Rombout's cemetery (Mechelen, Belgium): Intrasite, intraindividual, and intrabone variability. *International Journal of Osteoarchaeology*. 2022;32(5):1142-56.
429. Tsutaya T. Post-weaning diet in archaeological human populations: A meta-analysis of carbon and nitrogen stable isotope ratios of child skeletons. *Am J Phys Anthropol*. 2017;164(3):546-57.
430. Privat KL, O'Connell TC, Hedges REM. The distinction between freshwater- and terrestrial-based diets: methodological concerns and archaeological applications of sulphur stable isotope analysis. *Journal of Archaeological Science*. 2007;34(8):1197-204.
431. Meier-Augenstein W. *Stable Isotope Forensics: An Introduction to the Forensic Application of Stable Isotope Analysis*. Chichester: John Wiley & Sons Ltd; 2010.
432. Richards MP, Britton K. *Archaeological science: an introduction*. Cambridge: Cambridge University Press; 2020.
433. Pestle WJ. Chemical, elemental, and isotopic effects of acid concentration and treatment duration on ancient bone collagen: an exploratory study. *Journal of Archaeological Science*. 2010;37(12):3124-8.
434. Sealy J, Johnson M, Richards M, Nehlich O. Comparison of two methods of extracting bone collagen for stable carbon and nitrogen isotope analysis: comparing whole bone demineralization with gelatinization and ultrafiltration. *Journal of Archaeological Science*. 2014;47:64-9.
435. Semal P, Orban R. Collagen Extraction from Recent and Fossil Bones Quantitative and Qualitative Aspects. *Journal of Archaeological Science*. 1994;22:463-7.
436. Harbeck M, Grupe G. Experimental chemical degradation compared to natural diagenetic alteration of collagen: implications for collagen quality indicators for stable isotope analysis. *Archaeological and Anthropological Sciences*. 2009;1(1):43-57.
437. Jørkov MLS, Heinemeier J, Lynnerup N. Evaluating bone collagen extraction methods for stable isotope analysis in dietary studies. *Journal of Archaeological Science*. 2007;34(11):1824-9.
438. Brock F, Higham T, Ramsey CB. Pre-screening techniques for identification of samples suitable for radiocarbon dating of poorly preserved bones. *Journal of Archaeological Science*. 2010;37(4):855-65.
439. Yinon J. *Advances in Forensic Applications of Mass Spectrometry*. 1st ed. Boca Raton: CRC Press; 2003.
440. Aparicio S, Doty SB, Camacho NP, Paschalis EP, Spevak L, Mendelsohn R, et al. Optimal methods for processing mineralized tissues for Fourier transform infrared microspectroscopy. *Calcif Tissue Int*. 2002;70(5):422-9.
441. Stuart BH. *Infrared Spectroscopy: Fundamentals and Applications*. 1st ed. Chichester: John Wiley & Sons Ltd; 2004.
442. Surovell TA, Stiner MC. Standardizing Infra-red Measures of Bone Mineral Crystallinity: an Experimental Approach. *Journal of Archaeological Science*. 2001;28(6):633-42.

443. Pal Chowdhury M, Choudhury KD, Bouchard GP, Riel-Salvatore J, Negrino F, Benazzi S, et al. Machine learning ATR-FTIR spectroscopy data for the screening of collagen for ZooMS analysis and mtDNA in archaeological bone. *Journal of Archaeological Science*. 2021;126.
444. Sponheimer M, Ryder CM, Fewlass H, Smith EK, Pestle WJ, Talamo S. Saving Old Bones: a non-destructive method for bone collagen prescreening. *Sci Rep*. 2019;9(1):13928.
445. Schmidt VM, Zelger P, Woss C, Huck CW, Arora R, Bechtel E, et al. Post-Mortem Interval of Human Skeletal Remains Estimated with Handheld NIR Spectrometry. *Biology (Basel)*. 2022;11(7).
446. Adamiano A, Fabbri D, Falini G, Giovanna Belcastro M. A complementary approach using analytical pyrolysis to evaluate collagen degradation and mineral fossilisation in archaeological bones: The case study of Vicenne-Campochiaro necropolis (Italy). *Journal of Analytical and Applied Pyrolysis*. 2013;100:173-80.
447. Hedges REM, Van Klinken GJ. A Review of Current Approaches in the Pretreatment of Bone for Radiocarbon Dating by AMS. *Radiocarbon*. 2016;34(3):279-91.
448. Schwarcz HP, Nahal H. Theoretical and observed C/N ratios in human bone collagen. *Journal of Archaeological Science*. 2021;131.
449. Lebon M, Reiche I, Gallet X, Bellot-Gurlet L, Zazzo A. Rapid Quantification of Bone Collagen Content by ATR-FTIR Spectroscopy. *Radiocarbon*. 2016;58(1):131-45.
450. Onishi A, Thomas PS, Stuart BH, J.P G, Forbes S. TG-MS characterisation of pig bone in an inert atmosphere. *Journal of Thermal Analysis and Calorimetry*. 2007;88(2):405-9.
451. Devièse T, Colombini MP, Regert M, Stuart BH, Guerbois JP. TGMS analysis of archaeological bone from burials of the late Roman period. *Journal of Thermal Analysis and Calorimetry*. 2009;99(3):811-3.
452. Crompton TR. *Thermal methods of polymer analysis*: Smithers Rapra Technology; 2013.
453. Haines P. *Thermal methods of analysis: principles, applications, and problems*: Springer Science & Business Media; 2012.
454. Mkukuma LD, Skakle JM, Gibson IR, Imrie CT, Aspden RM, Hukins DW. Effect of the proportion of organic material in bone on thermal decomposition of bone mineral: an investigation of a variety of bones from different species using thermogravimetric analysis coupled to mass spectrometry, high-temperature X-ray diffraction, and Fourier transform infrared spectroscopy. *Calcif Tissue Int*. 2004;75(4):321-8.
455. Lim JJ. Thermogravimetric analysis of human femur bone. *Physical Biological Sciences*. 1975;3:111-29.
456. Gabbott P. *Principles and applications of thermal analysis*: John Wiley & Sons; 2008.
457. Kubisz L, Mielcarek S. Differential scanning calorimetry and temperature dependence of electric conductivity in studies on denaturation process of bone collagen. *Journal of Non-Crystalline Solids*. 2005;351(33-36):2935-9.
458. Figueiredo M, Fernando A, Martins G, Freitas J, Judas F, Figueiredo H. Effect of the calcination temperature on the composition and microstructure of hydroxyapatite derived from human and animal bone. *Ceramics International*. 2010;36(8):2383-93.
459. Etok SE, Valsami-Jones E, Wess TJ, Hiller JC, Maxwell CA, Rogers KD, et al. Structural and chemical changes of thermally treated bone apatite. *Journal of Materials Science*. 2007;42(23):9807-16.
460. Iafisco M, Foltran I, Sabbatini S, Tosi G, Roveri N. Electrospun nanostructured fibers of collagen-biomimetic apatite on titanium alloy. *Bioinorg Chem Appl*. 2012;2012:123953.
461. Gabbott P. A Practical Introduction to Differential Scanning Calorimetry. In: Gabbott P, editor. *Princples and Applications of Thermal Analysis*: Blackwell Publishing Ltd.; 2008. p. 1-50.
462. Lambri ML, Giordano ED, Bozzano PB, Bonifacich FG, Pérez-Landazábal JI, Zelada GI, et al. Thermal Degradation of Type I Collagen from Bones. *Journal of Renewable Materials*. 2016;4(4):251-7.

463. Lai PS, Khoo LS, Mohd Hilmi S, Ahmad Hafizam H, Mohd Shah M, Nurliza A, et al. Effectiveness of bone cleaning process using chemical and entomology approaches: Time and cost. *Malaysian Journal of Pathology*. 2015;37(2):123.
464. Lander SL, Brits D, Hosie M. The effects of freezing, boiling and degreasing on the microstructure of bone. *Homo*. 2014;65(2):131-42.
465. Simonsen KP, Rasmussen AR, Mathisen P, Petersen H, Borup F. A Fast Preparation of Skeletal Materials Using Enzyme Maceration. *Journal of Forensic Sciences*. 2011;56(2):480-4.
466. Offele D, Harbeck M, Dobberstein RC, von Wurmb-Schwark N, Ritz-Timme S. Soft tissue removal by maceration and feeding of Dermestes sp.: impact on morphological and biomolecular analyses of dental tissues in forensic medicine. *International Journal of Legal Medicine*. 2007;121(5):341348.
467. Fernández-Jalvo Y, Monfort MDM. Experimental taphonomy in museums: Preparation protocols for skeletons and fossil vertebrates under the scanning electron microscopy. *Geobios*. 2008;41(1):157-81.
468. Ajayi A, O.T I, Edjomariegwe O. A Review of Bone Preparation Techniques for Anatomical Studies. *Malaya Journal of Biosciences*. 2016;3(2):76-80.
469. Galloway A, Snodgrass J. Biological and Chemical Hazards of Forensic Skeletal Analysis. *Journal of Forensic Sciences*. 1998;43(5):940-8.
470. Mann RW, Berryman HE. A Method for Defleshing Human Remains Using Household Bleach. *Journal of Forensic Sciences*. 2012;57(2):440-2.
471. Fernández-Jalvo Y, Andrews P, Pesquero D, Smith C, Marín-Monfort D, Sánchez B, et al. Early bone diagenesis in temperate environments. *Palaeogeography, Palaeoclimatology, Palaeoecology*. 2010;288(1-4):62-81.
472. Dix J. *Color atlas of forensic pathology*: CRC Press; 2000.
473. Geissenberger J, Ehrenfellner B, Monticelli FC, Pittner S, Steinbacher P. Dismembered porcine limbs as a proxy for postmortem muscle protein degradation. *Int J Legal Med*. 2021;135(4):1627-36.
474. Mairs S, Swift B, Rutty GN. Detergent: an alternative approach to traditional bone cleaning methods for forensic practice. *Am J Forensic Med Pathol*. 2004;25(4):276-84.
475. Hefti E, Trechsel U, Rüfenacht H, Fleisch H. Use of dermestid beetles for cleaning bones. *Calcified Tissue International*. 1980;31(1):45-7.
476. Charabidze D, Colard T, Becart A, Hedouin V. Use of larder beetles (Coleoptera: Dermestidae) to deflesh human jaws. *Forensic Science International*. 2013;234:162-4.
477. Fenton T, Birkby W, Cornelison J. A Fast and Non-Bleaching Method for Forensic Skeletal Preparation. *Journal of Forensic Science*. 2003;48(2):1-3.
478. Pahl A. Skeleton Preparation Best Practices in the Modern Museum: The Dermestid Approach. *Curator: The Museum Journal*. 2019;63(1):99-113.
479. Charabidze D, Lavieille V, Colard T. Experimental Evidence of Bone Lesions Due to Larder Beetle Dermestes maculatus (Coleoptera: Dermestidae). *Biology (Basel)*. 2022;11(9).
480. Drusini AG. Age-related changes in root transparency of teeth in males and females. *American Journal of Human Biology*. 1991;3(6):629-37.
481. Hobischak NR, Anderson GS. Time of Submergence Using Aquatic Invertebrate Succession and Decompositional Changes. *Journal of Forensic Sciences*. 2002;47(1):142-51.
482. Wescott DJ. Recent advances in forensic anthropology: decomposition research. *Forensic Sci Res*. 2018;3(4):327-42.
483. Mooney MP, Kraus EM, Bardach J, Snodgass JI. Skull preparation using the exzyme-active detergent technique. *Anat Rec*. 1982;202(1):125-9.
484. Frank EM, Mundorff AZ, Davoren JM. The effect of common imaging and hot water maceration on DNA recovery from skeletal remains. *Forensic Sci Int*. 2015;257:189-95.
485. Symes SA, L'Abbe EN, Pokines JT, Yuzwa T, Messer D, Stromquist A, et al. Thermal Alteration to Bone. In: Pokines JT, Symes SA, editors. *Manual of Forensic Taphonomy*: CRC Press; 2013. p. 367-402.

486. Arismendi JL, Baker LE, Matteson KJ. Effects of Processing Techniques on the Forensic DNA Analysis of Human Skeletal Remains. *Journal of Forensic Science*. 2004;49(5).
487. Rennick SL, Fenton TW, Foran DR. The effects of skeletal preparation techniques on DNA from human and non-human bone. *Journal of Forensic Science*. 2005;50(5).
488. Horak O, Pyszko M, Paral V, Sandor O. Degreasing and bleaching bones using light sources as a tool to increase the safety of teaching osteology at the University of Veterinary Sciences Brno. *PeerJ*. 2022;10:e14036.
489. O'Neil Wyatt S. A Study of the Effectiveness of a Common Household Chemical for Maceration: Louisiana State University and Agricultural and Mechanical College; 2012.
490. Hill FC. Techniques for Skeletonizing Vertebrates. *American Antiquity*. 1975;40(2):215-9.
491. Meyer M. Macroscopic and microscopic effects of various chemicals on the degreasing of bone. [Dissertation]. In press 2021.
492. Uhre M, Eriksen AM, Simonsen KP, Rasmussen AR, Hjort BB, N. L. Enzymatic maceration of bone: a gentler technique than boiling. *Medicine, Science and the Law*. 2015;50(2):90-6.
493. Yin L, Venkatesan S, Kalyanasundaram S, Qin QH. Influence of enzymatic maceration on the microstructure and microhardness of compact bone. *Biomed Mater*. 2010;5(1):15006.
494. Hoshi K. Fine structure of bone matrix calcification. *Journal of Oral Biosciences*. 2012;54(1).
495. Manning HB, Nickdel MB, Yamamoto K, Lagarto JL, Kelly DJ, Talbot CB, et al. Detection of cartilage matrix degradation by autofluorescence lifetime. *Matrix Biology*. 2013;32(1).
496. Check your water hardness Yorkshirewater.com: Yorkshire Water; 2023 [Available from: https://www.yorkshirewater.com/your-water/water-hardness/.
497. Webb RH. *Elementary Wave Optics*: Dover Publications; 2012.
498. Tsioptsias C. On the latent limit of detection of thermogravimetric analysis. *Measurement*. 2022;204.
499. Lukaszewski GM. Accuracy in Thermogravimetric Analysis. *Nature*. 1962;194:959-61.
500. Prime RB, Bair HE, Vyazokin S, Gallagher PK, Riga A. Thermogravimetric Analysis (TGA). In: Menczel JD, Prime RB, editors. *Thermal Analysis of Polmers: Fundamentals and Applications*: John Wiley & Sons; 2008. p. 241-317.
501. Rhodes D. *Clay and Glazes for the Potter*. London: A&C Black; 1988.
502. Kline G. *Amazing glaze recipes and combinations : 200+ surefire finishes for low-fire, mid-range, and high-fire pottery*. Irvine: Quarry Brooks; 2021.
503. Ehrt D. Photoluminescence in glasses and glass ceramics. *IOP Conference Series: Materials Science and Engineering*. 2009;2.
504. Surre J, Saint-Ruf C, Collin V, Orenga S, Ramjeet M, Matic I. Strong increase in the autofluorescence of cells signals struggle for survival. *Sci Rep*. 2018;8(1):12088.
505. Ji X, Huang J, Wang Z, Xu Z, Liu C. Proteins Are Well-Preserved in Shells Toasted at 300°C Revealed by Proteomics. *Frontiers in Marine Science*. 2022;9.
506. Marin F, Luquet G, Marie B, Medakovic D. Molluscan Shell Proteins: Primary Structure, Origin, and Evolution. *Current Topics in Developmental Biology*. 2007;80:209-76.
507. Mohamed M, Suzup S, Maitra S. Decomposition study of calcium carbonate in cockle shell. *Journal of Engineering Science and Technology*. 2012;7(1):1-10.
508. Addadi L, Joester D, Nudelman F, Weiner S. Mollusk Shell Formation A Source of New Concepts for Understanding. *Chemistry - A European Journal*. 2006;12(4):963-1295.
509. Tiwari A. What Is Sea Glass And Where Does It Come From? Science ABC2022 [Available from: https://www.scienceabc.com/nature/what-is-sea-glass-and-where-does-it-come-from.html.
510. Stewart J, S. Spectroscopic investigations of luminescent sea glass. [[Unpublished dissertation thesis]. In press 2022.
511. Copley GJ. The composition and manufacture ofglass and its domestic and industrialapplications. *Forensic Examination of Glass and Paint*. 1 ed: CRC Press; 2001.

512. Tooley F, V,. *The Handbook of Glass Manufacture: A Book of Reference for the Plant Executive, Technologist, and Engineer*: Ashlee Publishing Company; 1984.
513. La Motte R. *Pure Sea Glass*: Sea Glass Publishing; 2009.
514. Almirall J, Buckleton J, Curran J, Hicks T, N. Examination of glass. *Forensic Interpretation of Glass Evidence*. 1 ed. Boca Raton: CRC Press; 2000. p. 1-26.
515. Ceglia A, Nuyts G, Meulebroeck W, Cagno S, Silvestri A, Zoleo A, et al. Iron speciation in soda-lime-silica glass: a comparison of XANES and UV-vis-NIR spectroscopy. *Journal of Analytical Atomic Spectrometry*. 2015;30(7):1552-61.
516. Lachheb R, Herrmann A, Damak K, Rüssel C, Maâlej R. Optical absorption and photoluminescence properties of chromium in different host glass. *Journal of Luminescence*. 2017;186:152-7.
517. *Munsell Soil Color Charts*. New York: Macbeth Division of Kallmorgen Instruments Corporation; 1994.
518. Bisi O. *Visible and invisible: the wonders of light phenomena*. Cham: Springer; 2014.
519. Lee WC, Khooa BE. Forensic Light Sources for Detection of Biological Evidences in Crime Scene Investigation: A Review. *Malaysian Journal of Forensic Science*. 2010;1(1):18-28.
520. Bone Ash www.potclays.co.uk2023 [Available from: https://www.potclays.co.uk/bone-ash.
521. Indalecio-Céspedes CR, Hernández-Romero D, Legaz I, Sánchez Rodríguez MF, Osuna E. Occult bloodstains detection in crime scene analysis. *Forensic Chemistry*. 2021;26.

Shining a Light on Forensic Anthropology:

The Use of Alternative Light Sources to Detect Skeletal Remains Underwater.

By

Catherine Anne Maidment

A thesis submitted in partial fulfilment for the requirements for the degree of Doctor of Philosophy at the University of Central Lancashire.

Volume 2 of 2

August 2023

STUDENT DECLARATION

Concurrent registration

I declare that while registered as a candidate for the research degree, I have not been a registered candidate or enrolled student for another award of the University or other academic or professional institution.

Material submitted for another award

I declare that no material contained in the thesis has been used in any other submission for an academic award and is solely my own work.

Collaboration

I declare that this research project was not part of a collaboration.

Signature of Candidate:

C. A. Maidment

Type of Award: Doctor of Philosophy

School: Natural Science

30.0 – APPENDICES

Appendix 1: Transcript of the Osteo-Fluorescence calculator C++ source code is available on OneDrive: 1 - Transcript of the Osteo-Fluorescence calculator (OFC) C++ source code

Appendix 2: Bone quality scores completed for all macerated ribs for Section A: Research 1, produced using Steadman et al (2005).

A) Hot water maceration.

Rib	Observations	Bone quality score
1	All ribs exhibited a uniform pale grey/beige colouration and were clean of all residual tissue. No evidence of porosity, erosion, flaking or fractures, although some slightly drier surface patches on the anterior surface of ribs 1-3.	5
2		5
3		5
4		5
5		5
6		5
7		5
8		5
9		5
10		5
Average		5

B) Biological washing powder maceration

Rib	Observations	Bone quality score
1	All ribs generally exhibit a very pale grey/white colouration, with patches of darker brown where cortical bone has been eroded/is flaking, producing a more inconsistent appearance. Most bones exhibit significant fraying at the epiphyses and edges with increased porosity noted in ribs 2,6,8, and 10	4
2		4
3		4
4		5
5		5
6		4
7		5
8		4
9		4
10		4
Average		4.3

C) Enzymatic maceration

Rib	Observations	Bone quality score
1	All ribs exhibit general grey/beige colouration but with some pinkish patches seen in ribs 2-4, and large patches of dark brown discolouration predominantly around the neck of the ribs with paler colouring towards the cut epiphyses. Some cartilage remains at the proximal ends but no tissue present. Slight fraying noted on the proximal ends of ribs 1,3,8 and 10	4
2		5
3		4
4		5
5		5
6		5
7		5
8		4
9		5
10		4
Average		4.6

Appendix 3: All thermograms for the hot water maceration dataset are available on OneDrive: 3 - Thermograms for hot water maceration dataset

Appendix 4: All fluorescence photographs for the hot water maceration dataset are available on OneDrive: 4 - Fluorescence photographs for hot water maceration dataset

Appendix 5: A) The fresh and macerated fluorescence values for the porcine ribs subjected to hot water maceration.

Rib	Fresh fluorescence values									Avg.
	Photograph 1			Photograph 2			Photograph 3			
	ROI 1	ROI 2	ROI 3	ROI 1	ROI 2	ROI 3	ROI 1	ROI 2	ROI 3	
1	144	147	141	149	150	143	136	135	129	141.6
2	180	171	168	179	170	167	184	174	169	173.6
3	158	164	166	156	161	161	156	159	159	160.0
4	154	153	154	150	149	152	154	153	153	152.4
5	171	169	183	174	168	185	175	167	186	175.3
6	167	159	159	164	159	161	161	155	158	160.3
7	173	180	174	178	182	178	177	180	178	177.8
8	185	184	169	179	174	161	164	165	160	171.2
9	173	171	171	170	170	171	168	169	170	170.3
10	166	166	158	164	164	157	169	168	161	163.7
Macerated fluorescence values										
1	165	169	168	166	170	169	167	171	169	168.2
2	167	168	167	166	167	166	166	167	167	166.8
3	176	176	172	175	176	172	175	176	171	174.3
4	167	165	165	171	169	166	174	171	170	168.7
5	194	195	187	189	188	182	173	175	171	183.8
6	163	164	161	162	163	159	162	164	159	161.9
7	181	183	182	175	177	175	180	183	181	179.7
8	183	187	176	169	181	180	182	192	189	182.1
9	176	167	163	177	167	161	179	168	162	168.9
10	179	176	173	177	178	176	179	179	176	177.0

Appendix 5: B) The fresh and macerated fluorescence values for the porcine ribs subjected to biological washing powder maceration.

Rib	Fresh fluorescence values									Avg.
	Photograph 1			Photograph 2			Photograph 3			
	ROI 1	ROI 2	ROI 3	ROI 1	ROI 2	ROI 3	ROI 1	ROI 2	ROI 3	
1	153	150	152	154	149	148	154	152	146	150.9
2	145	141	127	134	127	111	132	127	112	128.4
3	124	120	113	128	125	119	124	122	115	121.1
4	89	109	99	84	104	93	74	96	83	92.3
5	105	116	114	98	111	112	90	105	107	106.4
6	107	114	102	106	113	102	107	114	102	107.4
7	137	140	145	136	139	144	136	139	144	140.0
8	91	127	133	84	120	128	88	125	133	114.3
9	94	116	108	94	114	106	91	113	105	104.6
10	91	110	112	88	108	110	84	103	106	101.3
Macerated fluorescence values										
1	132	167	167	137	170	161	124	167	152	153.0
2	189	212	194	187	210	193	189	212	194	197.8
3	177	186	177	184	195	188	184	195	188	186.0
4	140	147	144	141	148	145	138	145	142	143.3
5	114	130	146	112	128	145	111	127	145	128.7
6	177	173	158	177	173	158	177	173	158	169.3
7	175	177	189	175	177	188	175	177	189	180.2
8	161	165	166	158	162	163	160	164	165	162.7
9	200	218	213	196	213	212	195	213	211	207.9
10	196	183	168	199	188	173	190	181	168	182.9

Appendix 5: C) The fresh and macerated fluorescence values for the porcine ribs subjected to enzymatic maceration.

Rib	Fresh fluorescence values (RGB)									Avg.
	Photograph 1			Photograph 2			Photograph 3			
	ROI 1	ROI 2	ROI 3	ROI 1	ROI 2	ROI 3	ROI 1	ROI 2	ROI 3	
1	102	110	108	103	112	108	104	112	108	107.4
2	139	135	122	137	133	121	136	132	120	130.6
3	141	148	147	142	149	148	142	151	150	146.4
4	140	140	141	138	139	140	133	135	137	138.1
5	156	160	161	154	157	159	153	152	150	155.8
6	165	172	175	162	166	167	166	173	176	169.1
7	160	151	156	158	149	156	157	150	158	155.0
8	158	154	151	157	154	152	173	170	164	159.2
9	149	154	163	153	160	174	150	159	173	159.4
10	102	110	108	103	112	108	104	112	108	107.4
Macerated fluorescence values (RGB)										
1	106	115	106	99	110	111	90	102	109	105.3
2	175	163	144	172	161	139	163	153	128	155.3
3	172	170	167	168	166	165	168	167	166	167.7
4	155	160	171	156	159	167	159	162	172	162.3
5	164	166	160	164	166	162	164	167	163	164.0
6	145	141	136	141	137	132	143	140	135	138.9
7	163	169	175	169	176	184	158	164	171	169.9
8	146	155	160	132	145	154	148	156	162	150.9
9	165	164	155	161	161	152	158	158	149	158.1
10	159	161	157	169	172	174	170	175	177	168.2

Appendix 6: A) Histograms for the hot water maceration dataset

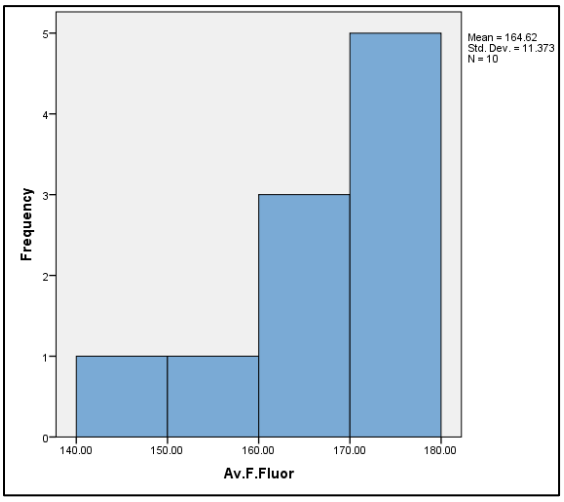

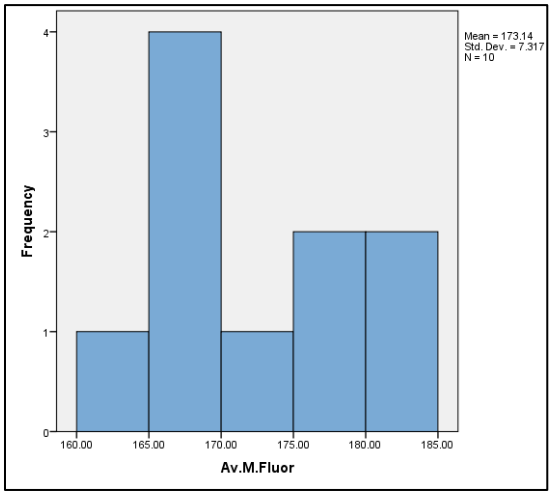

Average fluorescence

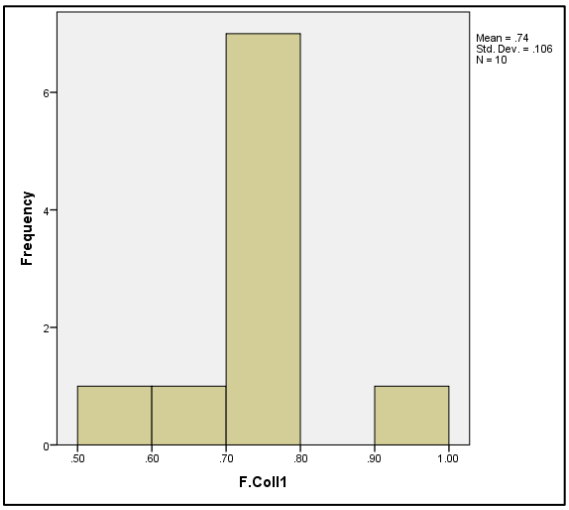

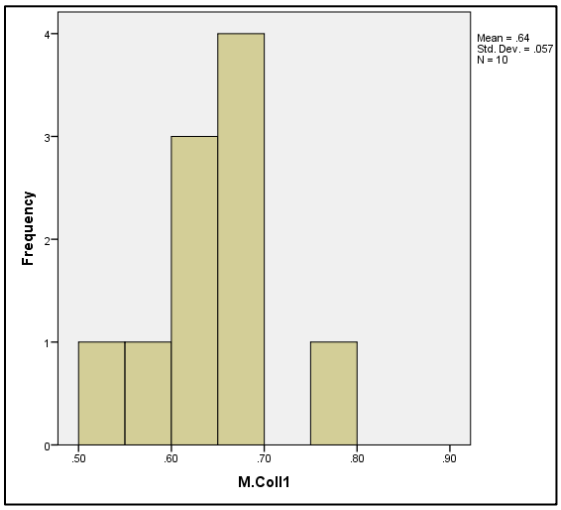

Calculated collagen content

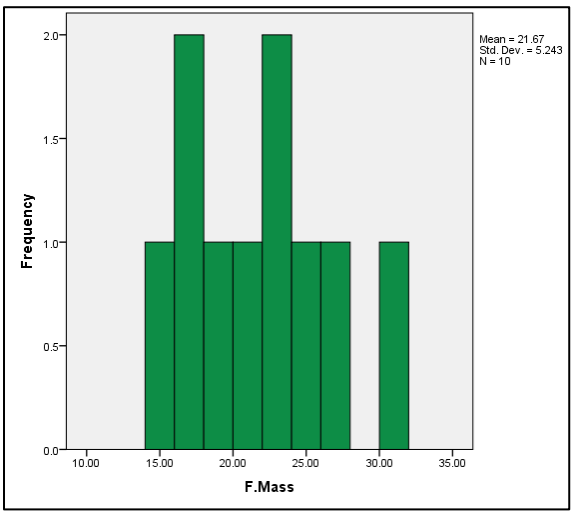

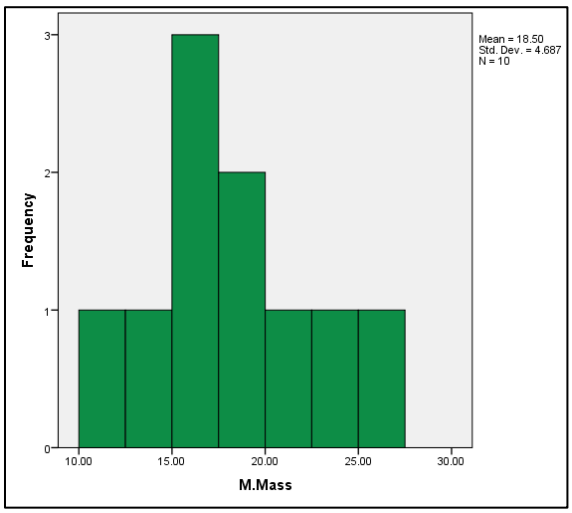

Mass

Appendix 6: B) Histograms for the biological washing powder maceration dataset

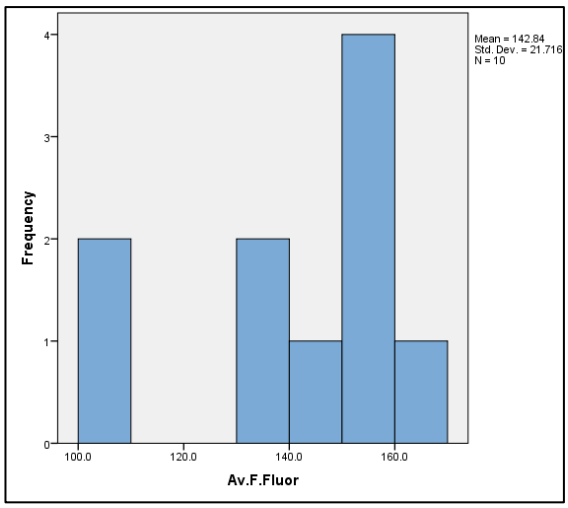

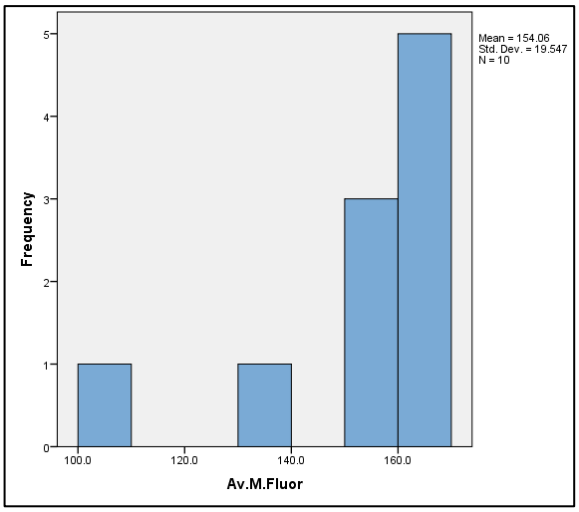

Average fluorescence

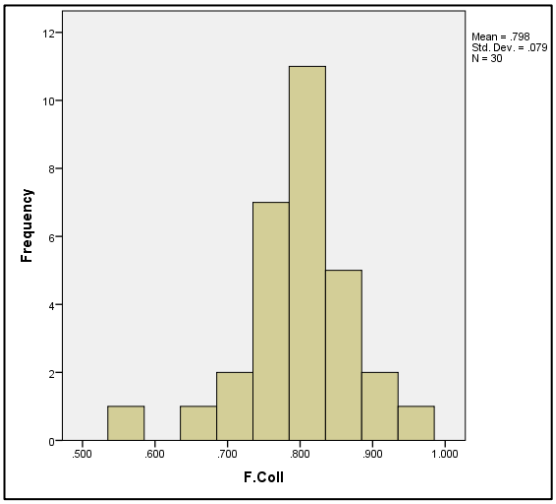

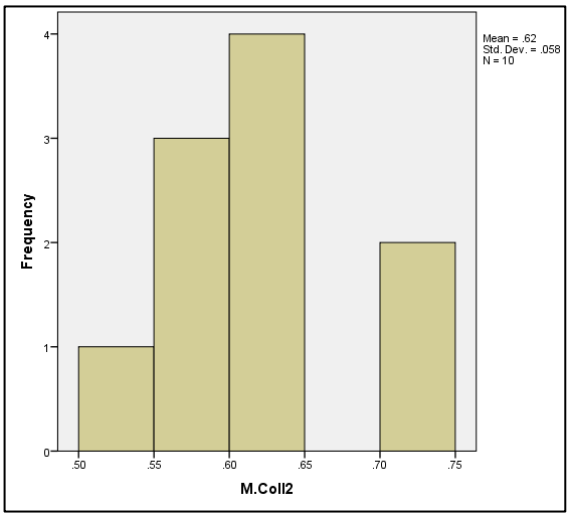

Calculated collagen content

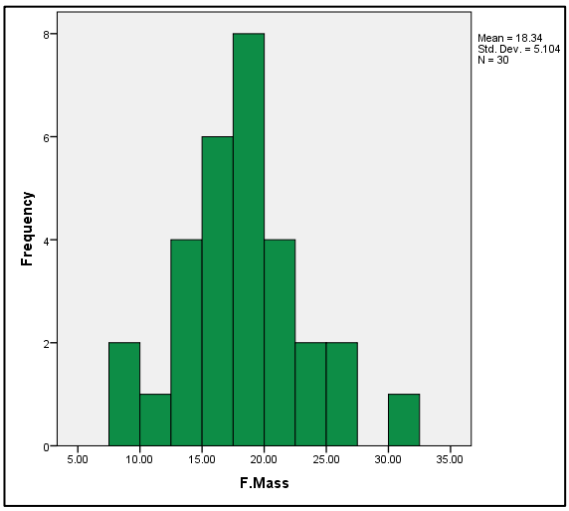

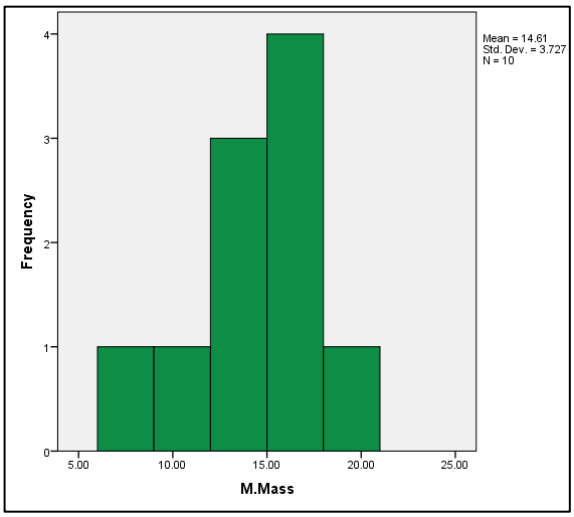

Mass

Appendix 6: C) Histograms for the enzymatic maceration dataset

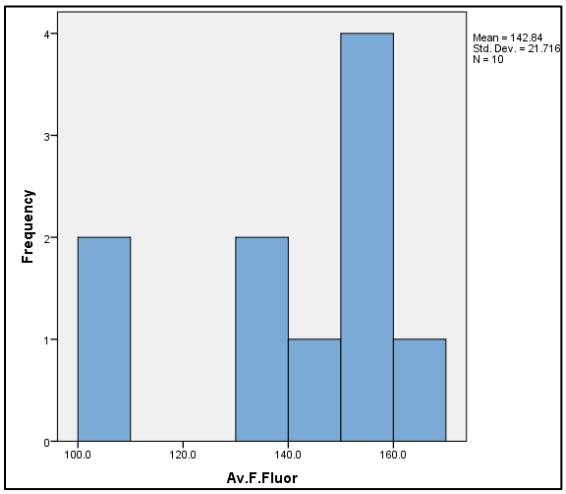

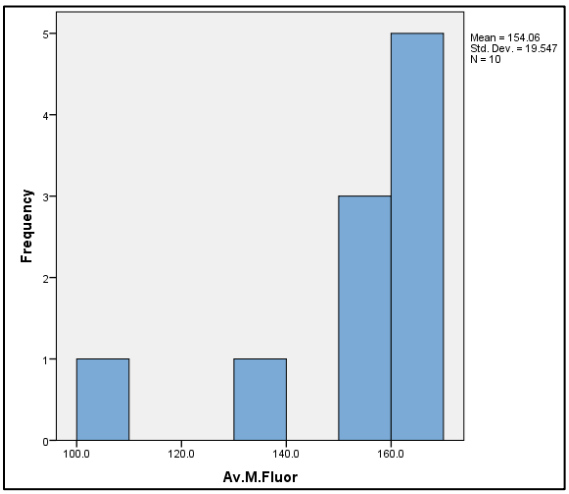

Average fluorescence

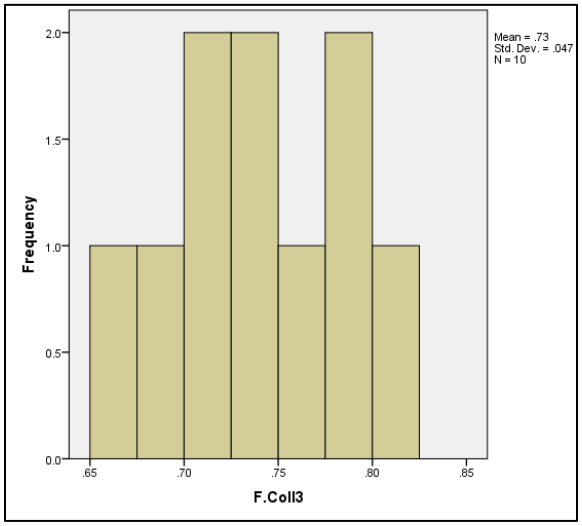

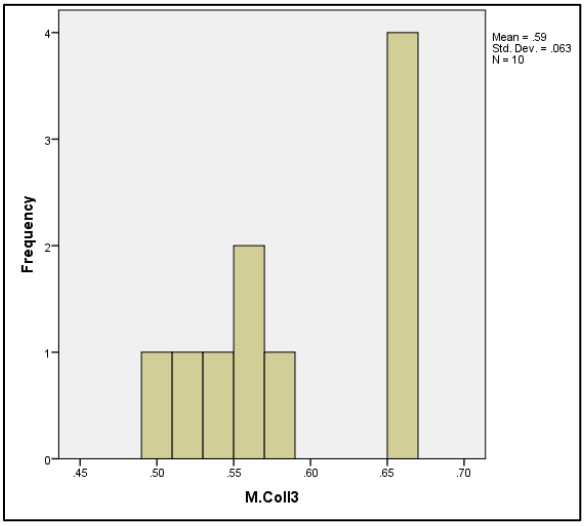

Calculated collagen content

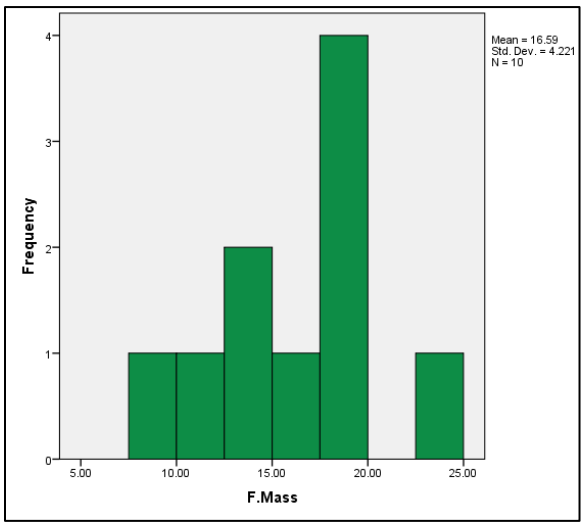

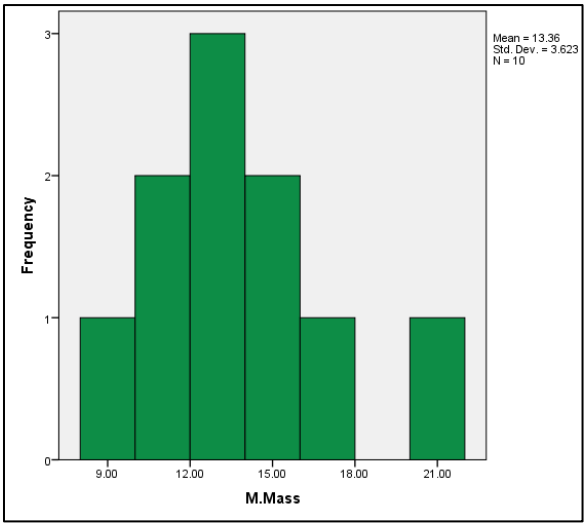

Mass

Appendix 7: All thermograms for the biological washing powder maceration dataset are available on OneDrive: 7 - Thermograms for biological washing powder dataset

Appendix 8: All fluorescence photographs for the biological washing powder maceration dataset are available on OneDrive: 8 - Fluorescence photographs for biological washing powder dataset

Appendix 9: All thermograms for the enzymatic maceration dataset are available on OneDrive: 9 - Thermograms for the enzymatic maceration dataset

Appendix 10: All fluorescence photographs for the enzymatic maceration dataset are available on OneDrive: 10 - Fluorescence photographs for the enzymatic maceration dataset

Appendix 11: Surf ingredients list and safety data sheet

A) Ingredients list

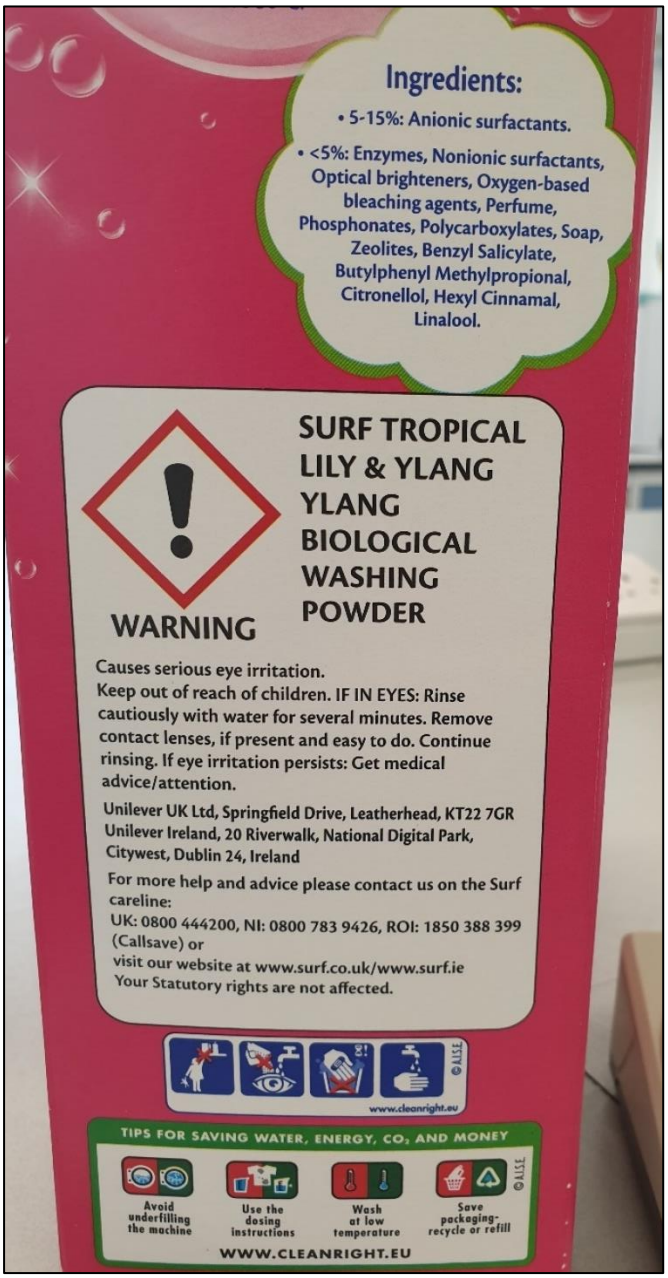

B) Surf safety data sheet available on OneDrive: [11b - Surf safety data sheet]

Appendix 12: Advertised specifications of the Foster and Freeman Ltd™ blue 420-470nm Crime-lite 2 and FoxFury Ltd blue 450 nm Hammerhead light

A) Crime-lite 2:

Crime-lite® 2

FOR CRIME SCENE INVESTIGATION AND LABORATORY EXAMINATION

Suitable for use in the forensic laboratory and for crime scene investigation, Crime-lite 2 light sources are compact and versatile tools for the detection and examination of evidence.

The range includes a white light model for general search and eight narrow band wavelengths in UV, violet, blue, blue-green, green, orange, red and IR.

With thousands of units in active use by forensic investigators worldwide the Crime-lite 2 demonstrates effectiveness, exceptional build quality and reliability.

Product Features

- Fitted with a high power LED
- Constructed from anodised aluminium
- Lightweight, high capacity batteries
- 2 to 4 hours of operating time on fully charged battery
- Wavelength tuned to match viewing goggles

Output	10% band width	Peak
White	400-700nm	N/A
UV	350-380nm	365nm
Violet	400-430nm	410nm
Blue	420-470nm	445nm
Blue/Green	445-510nm	475nm
Green	480-560nm	520nm
Orange	570-610nm	590nm
Red	600-660nm	640nm
Infrared	800-900nm	860nm

LEDs	1 x high efficiency LED
LED Power Output	up to 1.2W dependent on wavelength
Runtime	Continuous with adaptor
Battery life	Up to 290 minutes
Charge time	10 - 100 minutes
Weight	460g

B) Hammerhead light:

Description	Specifications	Downloads

Wavelength	450nm
Battery Life	1.5 - 4 hours
Power Source	(2) CR123 batteries or (1) 18650 batteries - not included
Modes	2 (Low, High)
Weight	8.4 oz (239 g)
Length	6.6 in (168 mm)
Diameter Body or Handle	1.1 in (28 mm)
Head Size	2.2 x 1.5 in (56 x 38 mm)
Certifications	CE-EMC
Fire Resistant	Meets Requirements of NFPA 1971-8.6 (2013)
Waterproof	9.8 ft (3 m)
Impact Resistant	6.6 ft (2 m)
LED Color	Blue
Beam Angle	8 degree
Operating Temperature	-4°F (-20°C) to 300°F (149°C)
Materials	6061-T6 Aluminum hard anodized housing
Features	Anti-roll design, Diffuser lens for smooth hotspot, Thumb rest
Evidence Seen	Trace evidence (hairs, fibers, etc.), gunshot residue, biological fluids including blood treated with fluorescein and footwear (and other) impressions
Max.Operational	10 ft (3 m)

Appendix 13: All fluorescence photographs for collagen/fluorescence distribution dataset are available on OneDrive: 13 - Fluorescence photographs for the distribution of collagen and fluorescence dataset

Appendix 14: All thermograms for the enzymatic maceration dataset are available on OneDrive: 14 - Thermograms for the collagen distribution dataset

Appendix 15: Thermograms displaying the combined TGA curves of the anatomical regions for each of the three ribs discussed in section B, question 2.

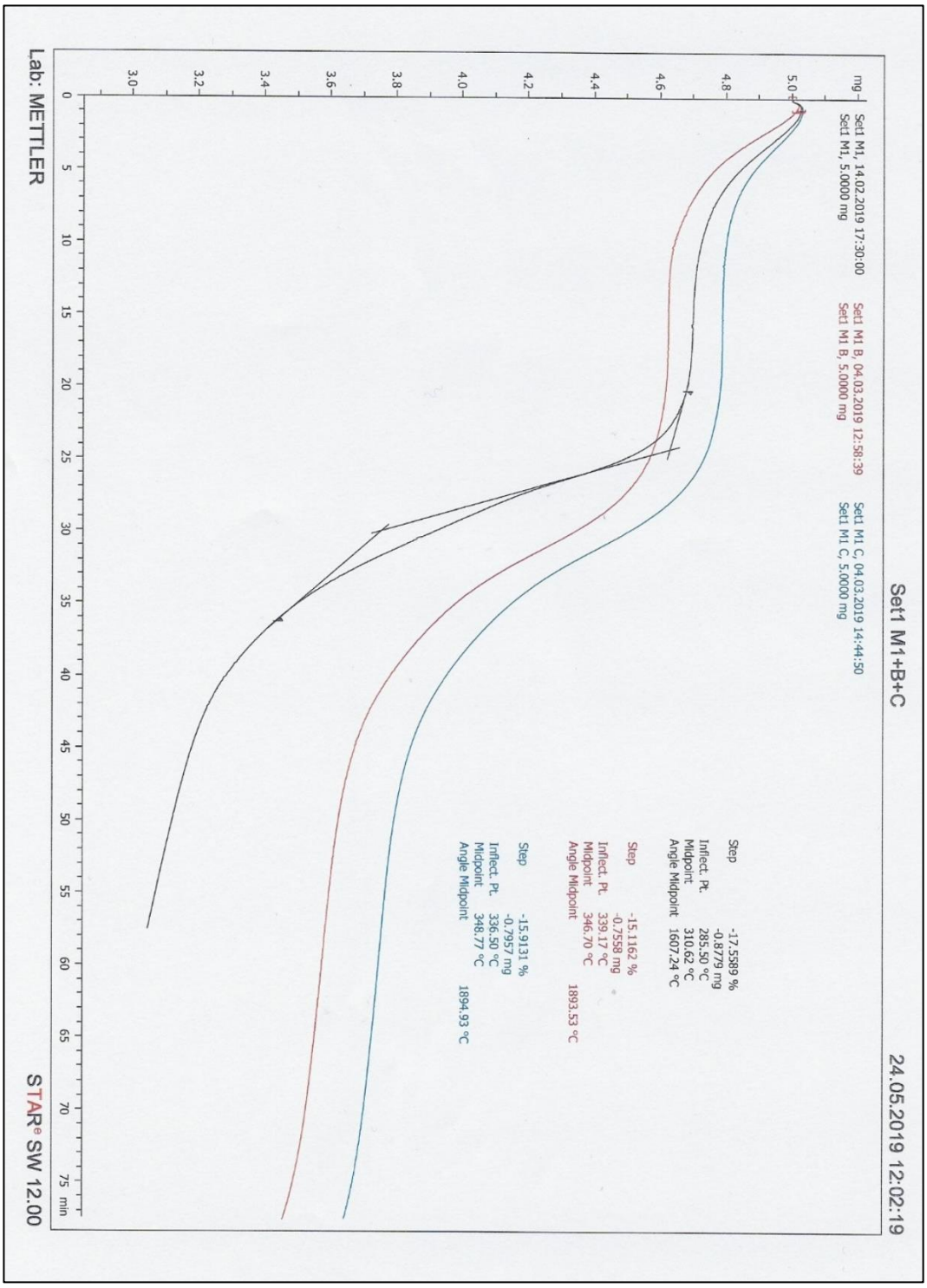

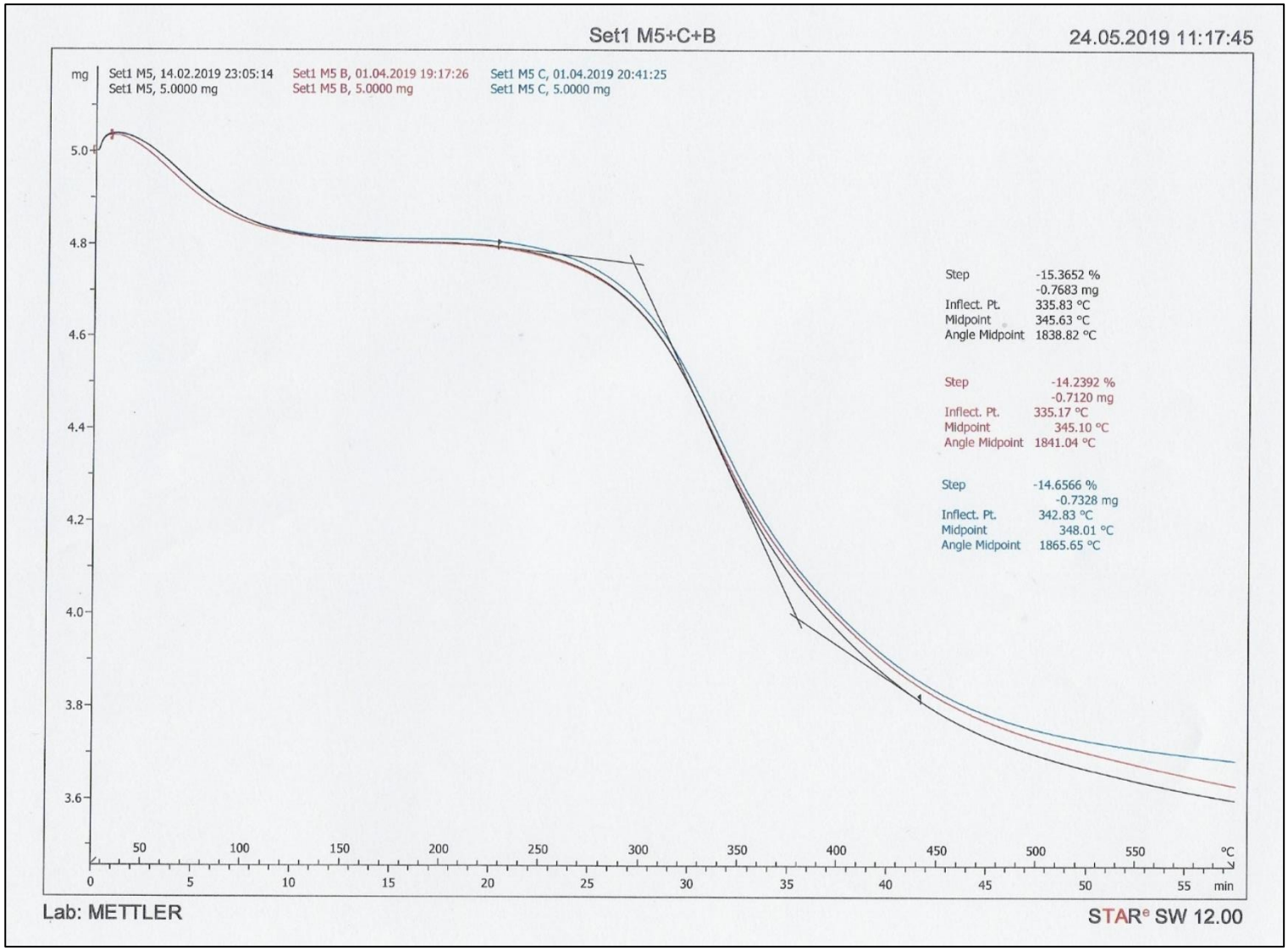
Set1 M5+C+B
24.05.2019 11:17:45
mg
Set1 M5, 14.02.2019 23:05:14
Set1 M5, 5.0000 mg
Set1 M5 B, 01.04.2019 19:17:26
Set1 M5 B, 5.0000 mg
Set1 M5 C, 01.04.2019 20:41:25
Set1 M5 C, 5.0000 mg
5.0
4.8
4.6
4.4
4.2
4.0
3.8
3.6
Step -15.3652 %
-0.7683 mg
Inflect. Pt. 335.83 °C
Midpoint 345.63 °C
Angle Midpoint 1838.82 °C
Step -14.2392 %
-0.7120 mg
Inflect. Pt. 335.17 °C
Midpoint 345.10 °C
Angle Midpoint 1841.04 °C
Step -14.6566 %
-0.7328 mg
Inflect. Pt. 342.83 °C
Midpoint 348.01 °C
Angle Midpoint 1865.65 °C
50 100 150 200 250 300 350 400 450 500 550 °C
0 5 10 15 20 25 30 35 40 45 50 55 min
Lab: METTLER
STARe SW 12.00

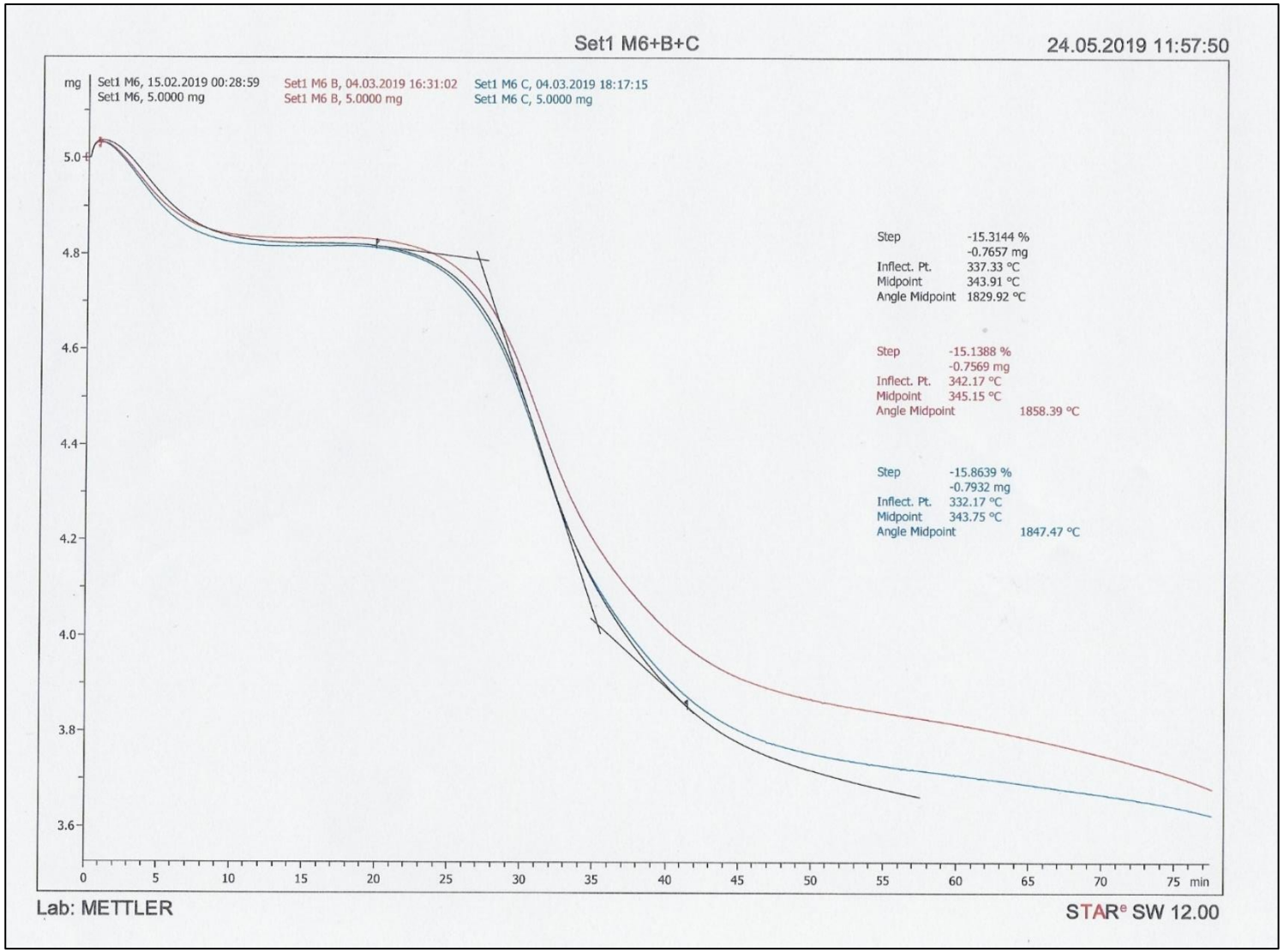
Set1 M6+B+C
24.05.2019 11:57:50
mg
Set1 M6, 15.02.2019 00:28:59
Set1 M6, 5.0000 mg
Set1 M6 B, 04.03.2019 16:31:02
Set1 M6 B, 5.0000 mg
Set1 M6 C, 04.03.2019 18:17:15
Set1 M6 C, 5.0000 mg
Step -15.3144 %
-0.7657 mg
Inflect. Pt. 337.33 °C
Midpoint 343.91 °C
Angle Midpoint 1829.92 °C
Step -15.1388 %
-0.7569 mg
Inflect. Pt. 342.17 °C
Midpoint 345.15 °C
Angle Midpoint 1858.39 °C
Step -15.8639 %
-0.7932 mg
Inflect. Pt. 332.17 °C
Midpoint 343.75 °C
Angle Midpoint 1847.47 °C
5.0
4.8
4.6
4.4
4.2
4.0
3.8
3.6
0
5
10
15
20
25
30
35
40
45
50
55
60
65
70
75 min
Lab: METTLER
STARe SW 12.00

Appendix 16: All fluorescence photographs for bone positioning dataset are available on OneDrive: 16 - Fluorescence photographs for bone positioning dataset

Appendix 17: All fluorescence photographs for background testing dataset are available on OneDrive: 17 - Fluorescence photographs for background testing

Appendix 18: Comparison of camera settings for submerged macerated porcine bone (*Sus scrofa domesticus*) using the Hammerhead light with orange filter

30mm zoom			34mm zoom		
No.	**Config.**	**Example photograph**	**No.**	**Config.**	Example photograph
1	F20 ISO 2000 Exp. 0.8		**16**	F20 ISO 4000 1/20	
2	F 5.6 (lowest possible) ISO 2000 Exp. 0.8		**17**	F20 ISO 4000 1/50	
3	F25 ISO 1600 Exp. 1/3		**18**	F20 ISO 4000 1/200	
4	F25 ISO 2500 Exp. 0.8		**19**	F20 ISO 3200 1/200	
5	F18 ISO 2000 Exp. 0.8		**20**	F10 ISO 3200 1/100	
6	F10 ISO 2000 Exp. 0.8		**21**	F10 ISO 3200 1/200	

7	F10 ISO 2500 Exp. 0.8		**22**	F5.6 ISO 3200 1/200	
8	F8 ISO 2000 Exp. 0.8		**23**	F5.6 ISO 3200 1/20	
9	F8 ISO 2500 Exp. 0.8		**24**	F5.6 ISO 3200 1/6	
10	F8 ISO 1000 Exp. 0.8		**25**	F5.6 ISO 4000 1/6	
11	F14 ISO 1000 Exp. 0.8		**26**	F20 ISO 4000 1/6	
12	F14 ISO 1000 Exp. 0.6	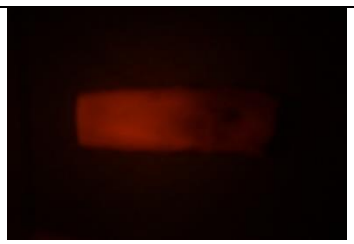	**27**	F10 ISO 4000 1/6	
13	F13 ISO 1000 Exp. 0.6		28	F8 ISO 4000 1/6	

14	F11 ISO 1000 Exp. 0.6		**29**	F8 ISO 4000 1/10	
15	F 11 ISO 1600 Exp. 0.6		**30**	F5 ISO 6400 1/200	

Appendix 20: Reported chemical composition of the tap water in Huddersfield.

Substance	Typical Value	UK/European limit	Unit
Calcium	16.9		mg Ca/l
Magnesium	2.1		mg Mg/l
Residual chlorine - free	0.31		mg/l Cl2
Residual chlorine - total	0.41		mg/l Cl2
TotalColiforms	0	0	no/100ml
EColi	0	0	no/100ml
Aluminium	13.2	200	µg Al/l
Colour	2.9	20	mg/l Pt/Co Scale
Conductivity	144	2500	µS/cm
Fluoride	0.06	1.5	mg F/l
Turbidity	0.18	4	NTU
pHHydrogenIon	7.6	6.5 - 9.5	pH Units
Iron	14.8	200	µg Fe/l
Manganese	1.1	50	µg Mn/l
Nitrate	2.76	50	mg NO3/l
Nitrite	0.002	0.5	mg NO2/l
Sodium	8.1	200	mg Na/l
Copper	0.0175	2	mg Cu/l
Lead	0.32	10	µg Pb/l

Appendix 21: Summarised terrestrial photographic results of all 30 porcine ribs photographed with the orange filter and Crime-lite 2, in section B, research question 1.

Rib	Exposure time (s)			
	Natural	0.6	0.4	1/3
1		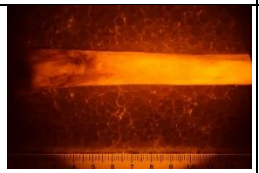		
2		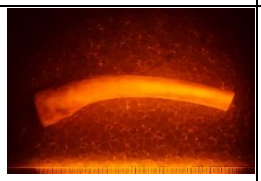	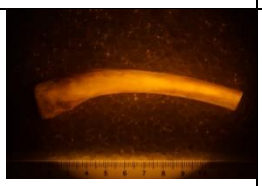	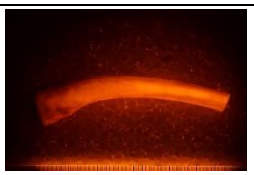
3		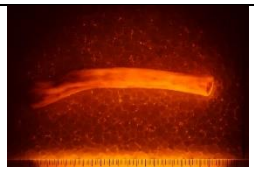	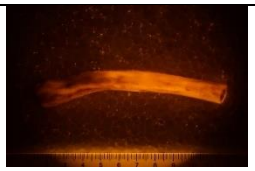	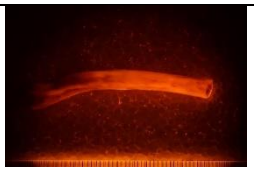
4		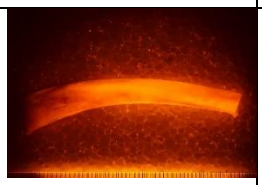	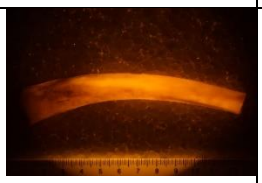	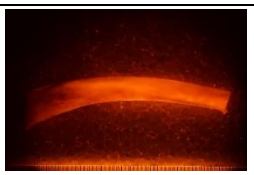
5		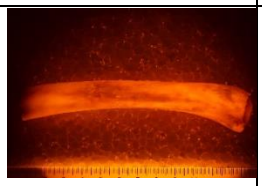	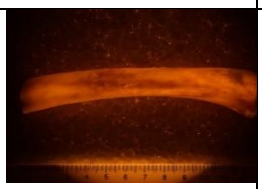	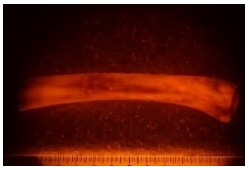
6		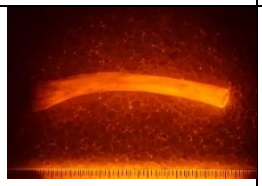	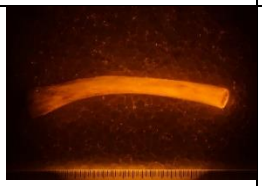	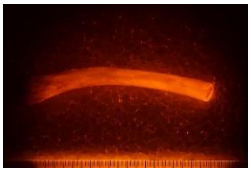
7		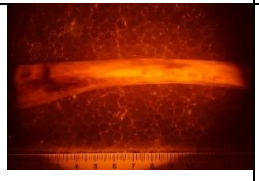	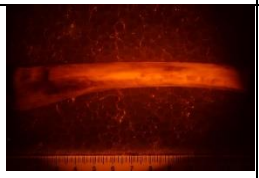	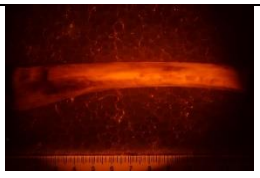

8		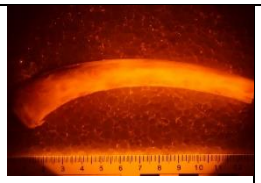		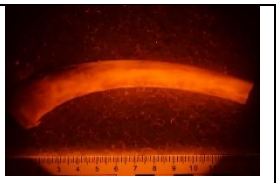
9		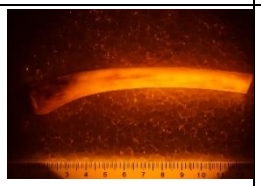		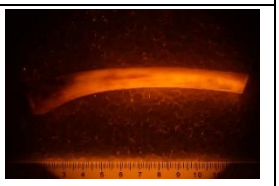
10		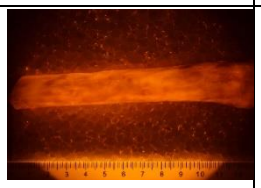	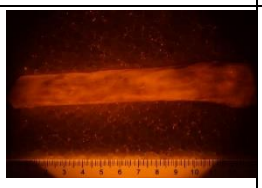	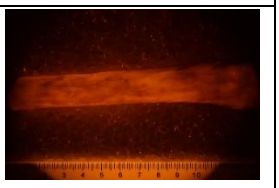
11		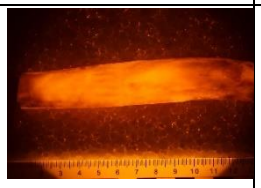	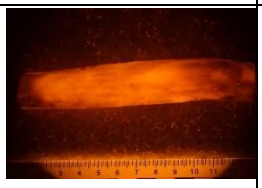	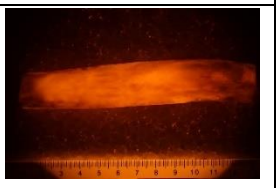
12		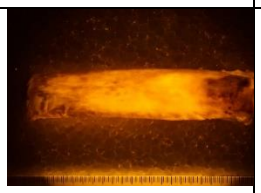	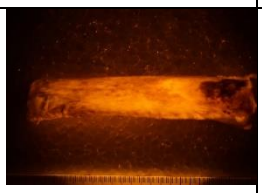	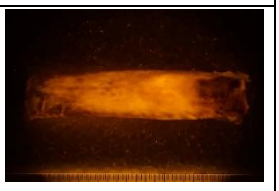
13		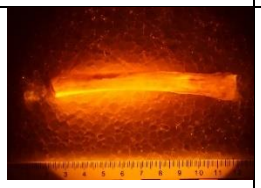	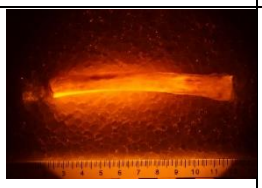	
14		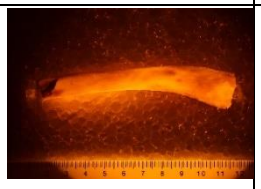	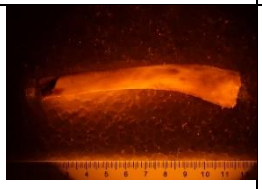	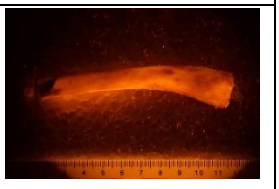
15		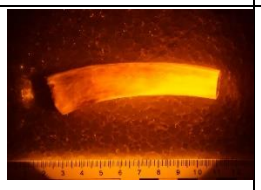	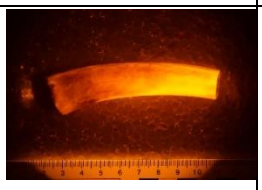	

16		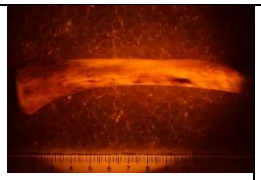		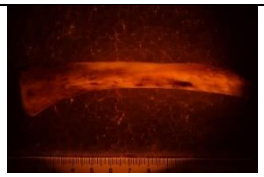
17		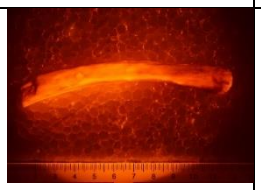		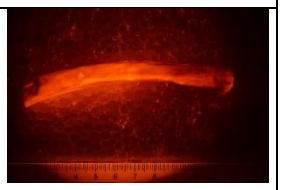
18		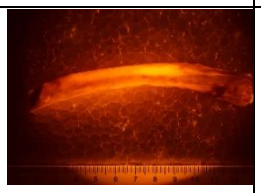	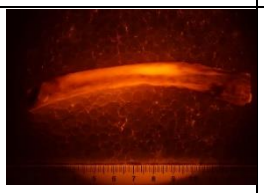	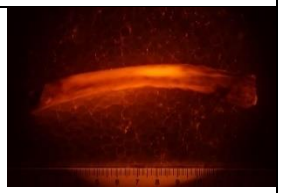
19			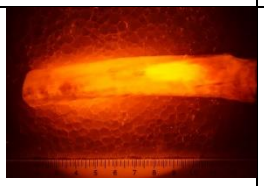	
20	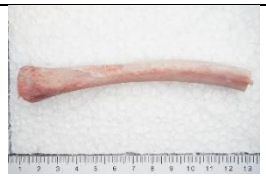	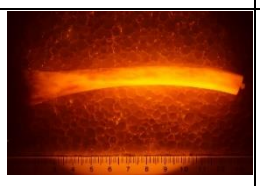		
21		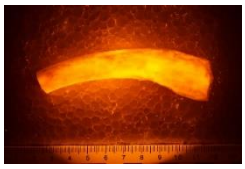	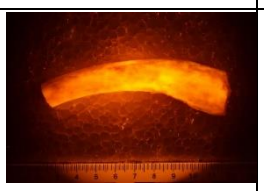	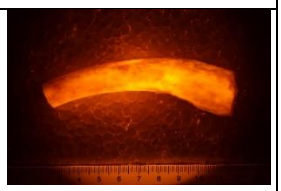
22		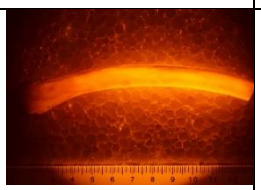	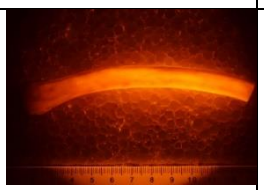	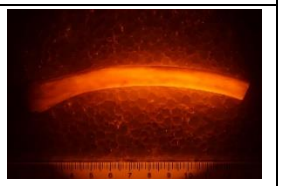
23		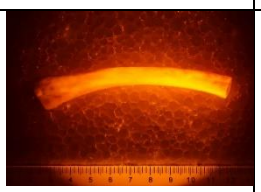	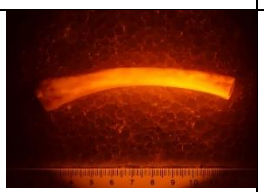	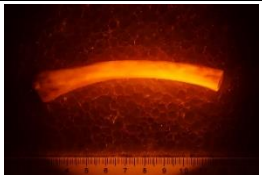
24		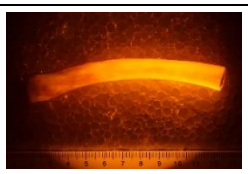	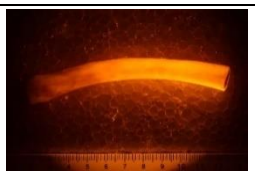	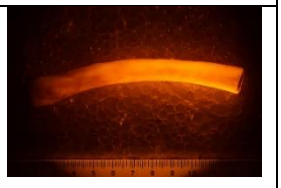

25		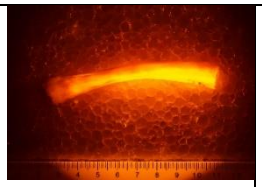	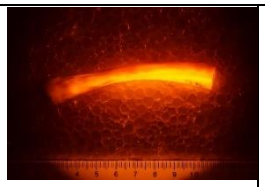	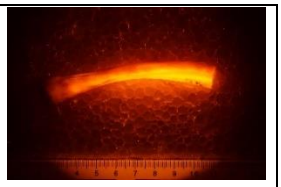
26			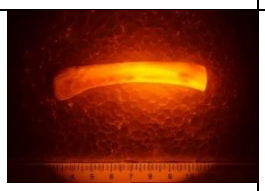	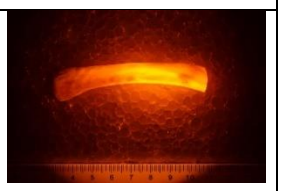
27		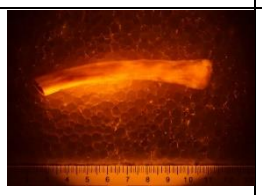	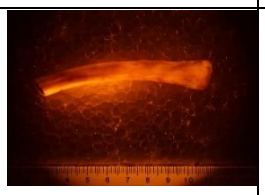	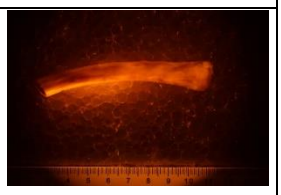
28	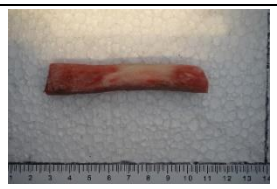	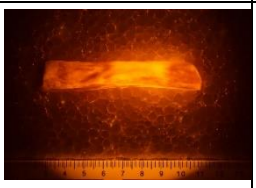	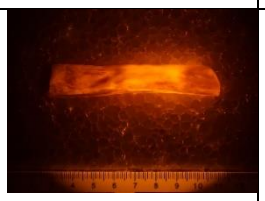	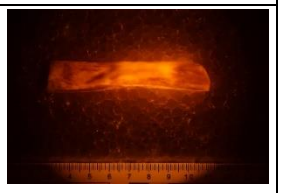
29		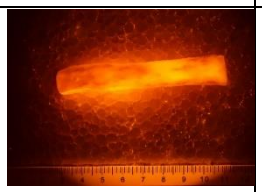	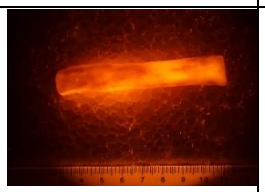	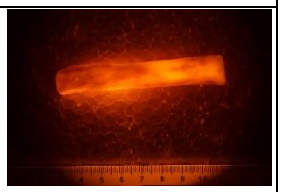
30		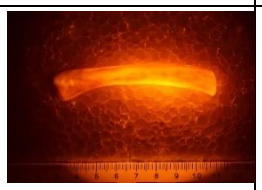		

Appendix 22: Summarised terrestrial photographic results of all 30 porcine ribs photographed with the yellow filter and Crime-lite 2, in section B, research question 1.

Rib	Exposure time (s)			
	Natural	0.6	0.4	1/3
1				
2				
3				
4			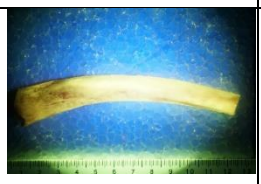	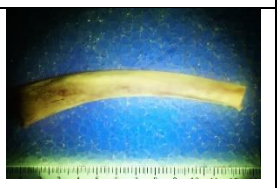
5		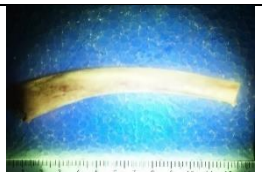	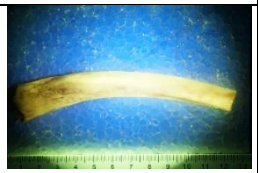	
6		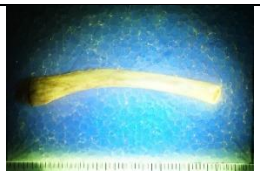		
7				

8		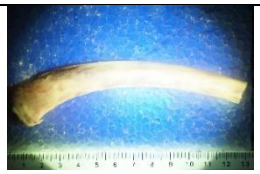		
9				
10		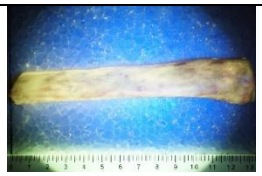	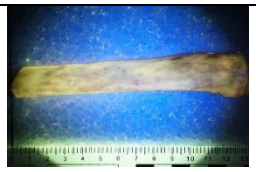	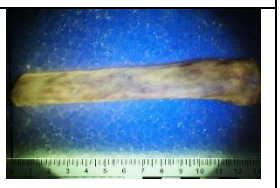
11				
12				
13				
Rib 14				
15				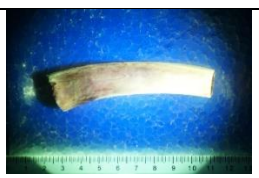
16		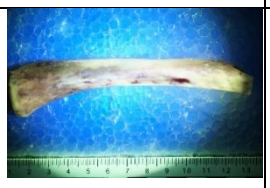	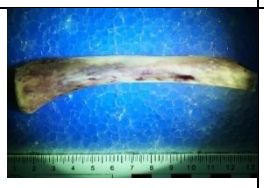	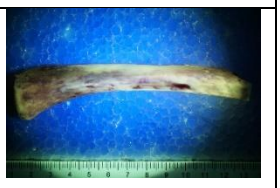

17				
18		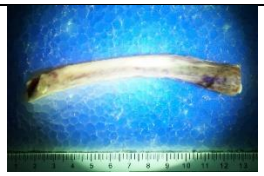	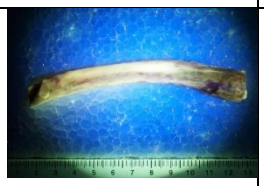	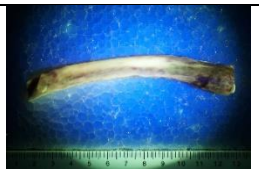
19		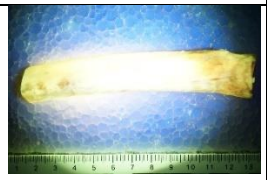	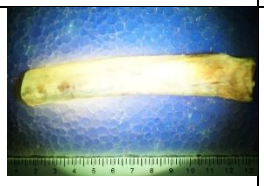	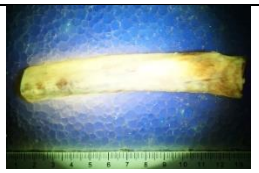
20	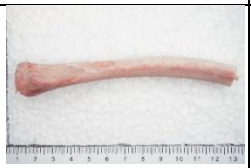	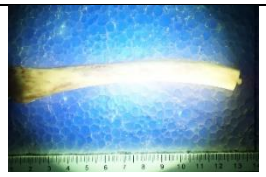	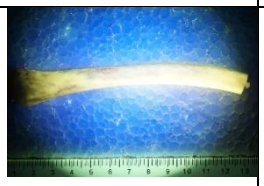	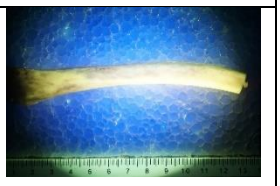
21				
22	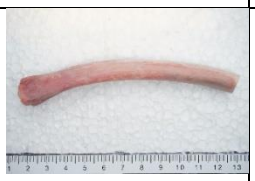	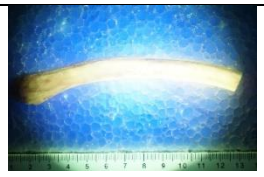		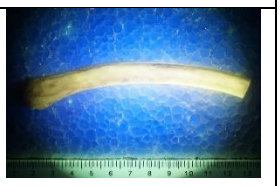
23				
24		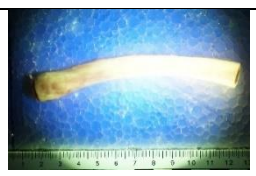		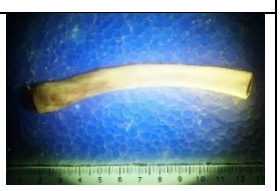
25			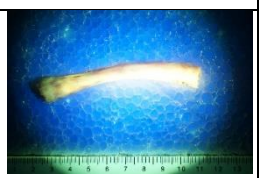	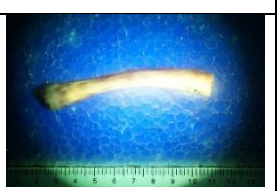

26			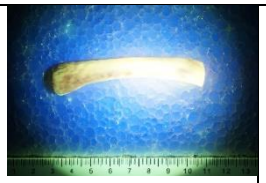	
27		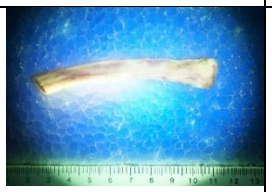		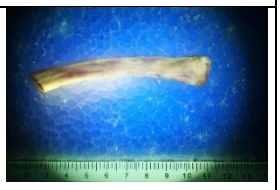
28		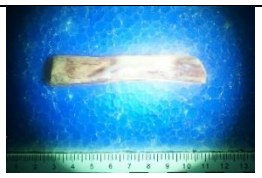	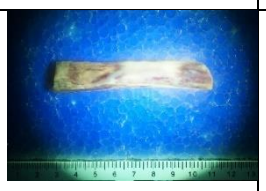	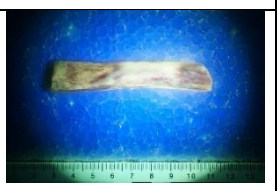
29				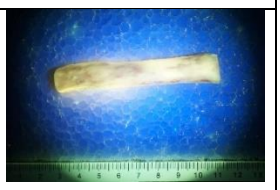
30			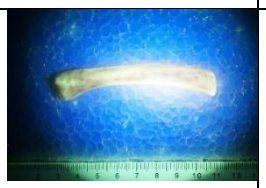	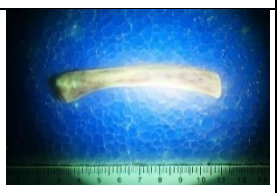

Appendix 23: Summarised underwater photographic results of all 30 porcine ribs photographed with the orange filter and Crime-lite 2, in section B, research question 1.

Rib	Exposure time (s)			
	Natural	0.6	0.4	1/3
1		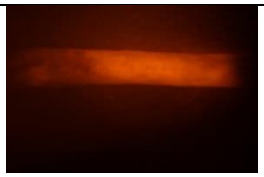		
2				
3			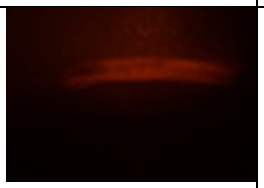	
4				
5				
6		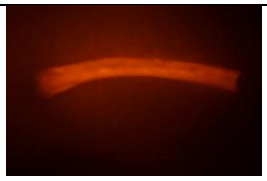		
7				

8				
9				
10				
11				
12				
13				
14				
15		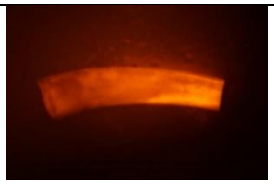	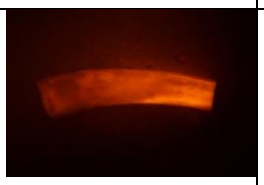	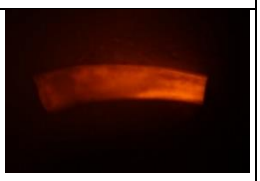

16				
17		Not taken	Not taken	
18			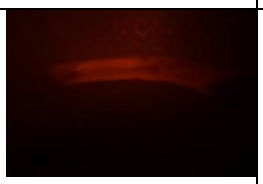	
19				
20	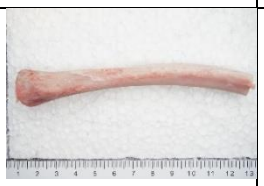			
21				
22				
23		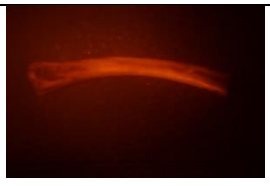		
24				

25		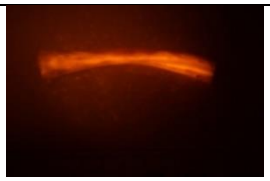	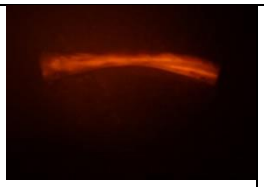	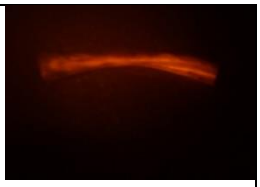
26			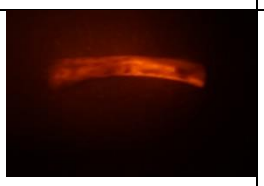	
27				
28				
29				
30				

Appendix 24: Summarised underwater photographic results of all 30 porcine ribs photographed with the yellow filter and Crime-lite 2, in section B, research question 1.

Rib	Exposure time (s)			
	Natural	0.6	0.4	1/3
1		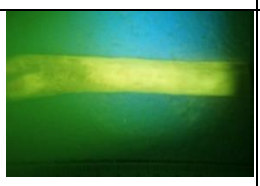	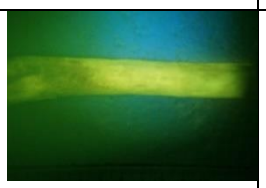	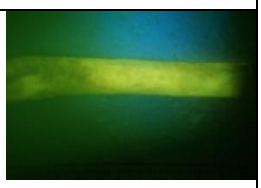
2		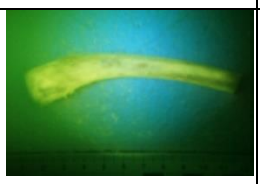		
3				
4				
5				
6			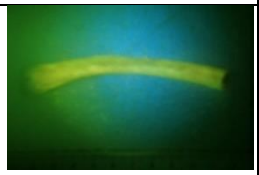	
7				

8				
9				
10		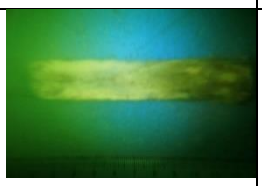	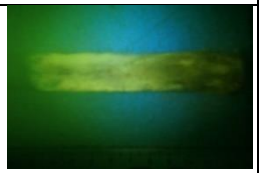	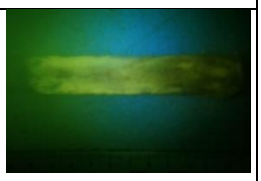
11				
12				
13		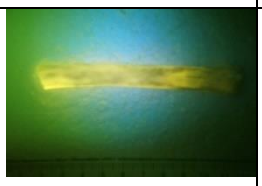	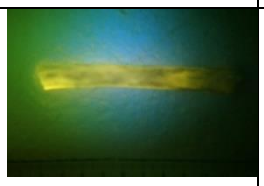	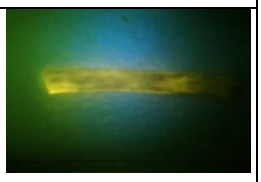
14				
15		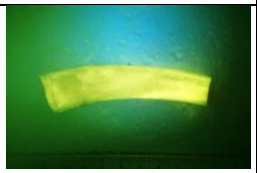	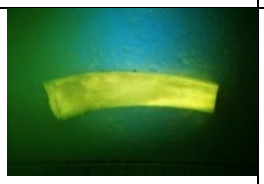	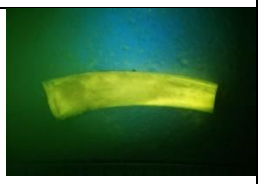
16		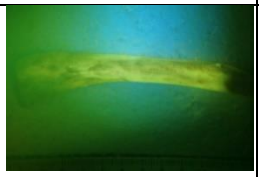	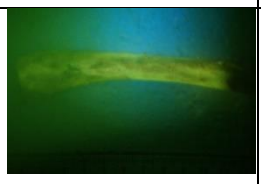	

17		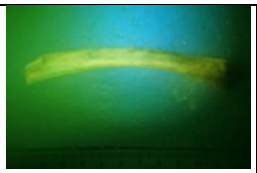		
18		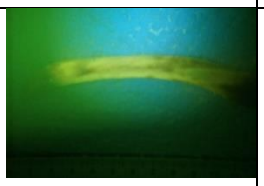		
19		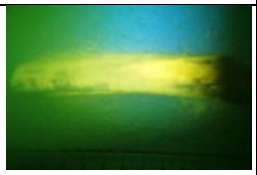		
20	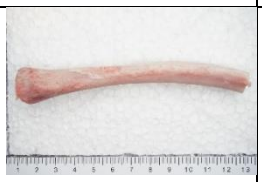	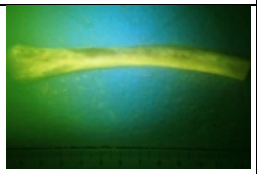		
21				
22				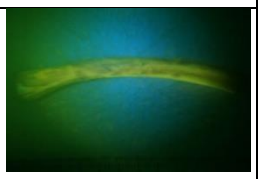
23				
24				
25		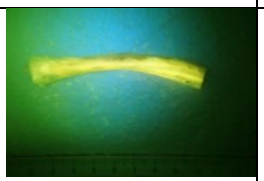	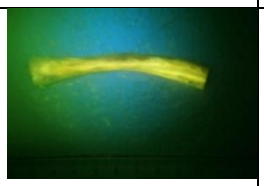	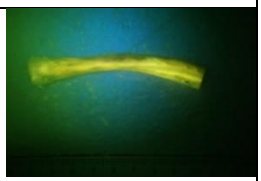

26				
27				
28	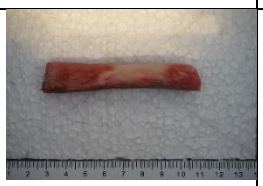			
29			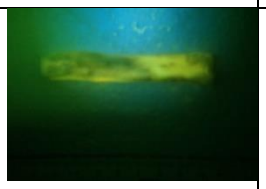	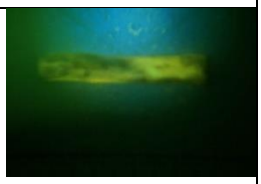
30				

Appendix 25: Summarised photographic results of all 30 porcine ribs photographed with the orange filter and Hammerhead light source, in section B, research question 1.

Rib	Exposure time (s)			
	Natural	0.6	0.4	1/3
1				
2				
3				
4				
5				
6				
7				

8				
9				
10				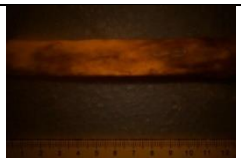
11				
12				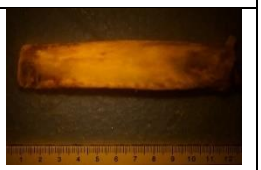
13				
14				
16				
17				

18				
19		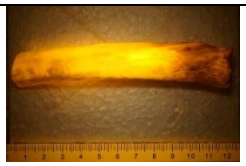	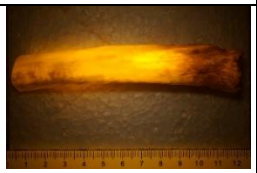	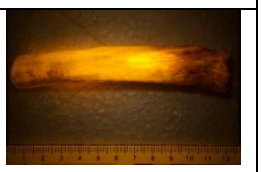
20				
21				
22				
23				
24				
25				
26				

27				
28				
29	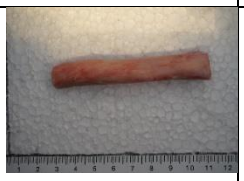			
30				

Appendix 26: Summarised photographic results of all 30 porcine ribs photographed with the orange filter and Hammerhead light source, in section B, research question 1.

Rib	Exposure time (s)			
	Natural	0.6	0.4	1/3
1				
2		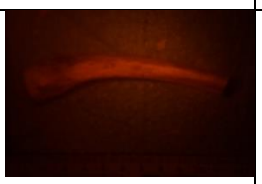		
3				
4				
5				
6				
7				

8				
9				
10				
11				
12				
13			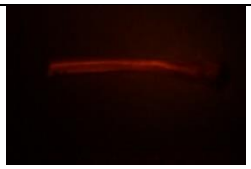	
14				
15				
16				

17				
18				
19				
20	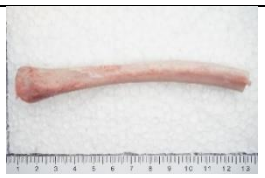			
21				
22				
23				
24				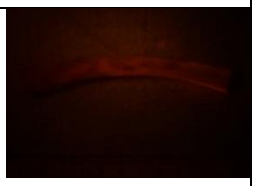

25			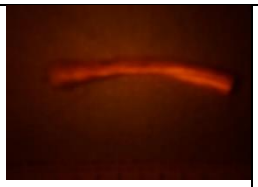	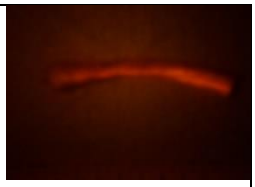
26				
27				
28				
29				
30				

Appendix 27: All terrestrial fluorescence and OFC processed photographs for the Crime-lite 2 are available on OneDrive: 27 - Terrestrial fluorescence and OFC processed images for Crime-Lite 2

Appendix 28: All terrestrial fluorescence and OFC processed photographs for the Hammerhead ALS are available on OneDrive: 28 - Terrestrial fluorescence and OFC processed images for the Hammerhead ALS

Appendix 29: All underwater fluorescence and OFC processed photographs for the Crime-lite 2 are available on OneDrive: 29 - Underwater fluorescence and OFC processed images for the Crime-Lite 2

Appendix 30: All underwater fluorescence and OFC processed photographs for the Hammerhead ALS are available on OneDrive: 30 - Underwater fluorescence and OFC processed images for the Hammerhead ALS

Appendix 31: Summary of averaged fluorescence values for 29 porcine ribs photographed using the Crime-Lite 2 at 0.6, 0.4 and 1/3s exposure times, with the orange and yellow filters, in terrestrial and tap water contexts, including calculated changes in fluorescence seen between filters within the same context.

Rib	Exposure time (s)																	
	0.6						0.4						1/3					
	Terrestrial			Underwater			Terrestrial			Underwater			Terrestrial			Underwater		
	O	Y	Diff.	O	Y	Diff.	O	Y	Diff	O	Y	Diff.	O	Y	Diff.	O	Y	Diff.
1	172.5	249.0	+76.5	103.3	218.9	+115.6	151.6	239.1	+87.5	79.0	192.5	+113.5	137.1	232.6	+95.5	66	176	+110.4
2	166.6	250.1	+83.5	85.6	197.5	+111.9	147.3	236.9	+89.6	55.9	160.1	+104.3	131.8	232.8	+101.0	49	141	+91.4
3	137.9	231.3	+93.4	65.0	181.8	+116.8	123.3	231.6	+108.4	45.1	145.5	+100.4	106.0	194.1	+88.1	37	127	+90.3
4	157.0	243.4	+86.4	91.8	219.1	+127.4	144.5	244.6	+100.1	67.8	191.0	+123.3	123.0	216.0	+93.0	55	174	+118.6
5	112.0	216.9	+104.9	184.8	69.8	-115.0	84.1	214.0	+129.9	152.5	48.8	-103.8	64.8	163.1	+98.4	128	40	-88.3
6	125.0	220.9	+95.9	79.6	186.6	+107.0	119.8	226.8	+107.0	57.1	153.1	+96.0	81.5	197.0	+115.5	50	133	+82.4
7	156.6	246.6	+90.0	184.1	82.6	-101.5	134.4	233.6	+99.3	149.5	57.9	-91.6	121.4	225.3	+103.9	117	47	-69.6
8	168.0	250.0	+82.0	199.8	78.0	-121.8	149.3	238.9	+89.6	164.8	52.4	-112.4	140.9	231.8	+90.9	146	43	-102.9
9	163.6	249.9	+86.3	82.8	200.6	+117.9	144.4	242.1	+97.8	66.6	169.3	+102.6	132.3	231.1	+98.9	55	152	+96.3
10	121.6	230.8	+109.1	76.1	178.4	+102.3	94.9	204.1	+109.3	51.1	143.9	+92.8	82.3	188.1	+105.9	42	126	+83.5
11	161.3	247.5	+86.3	105.3	199.1	+93.9	141.0	233.6	+92.6	78.6	165.6	+87.0	129.8	221.5	+91.8	65	148	+83.5
12	174.5	253.0	+78.5	111.3	220.4	+109.1	141.9	242.1	+100.3	84.9	191.4	+106.5	134.3	238.6	+104.4	72	173	+101.3
13	160.9	252.4	+91.5	92.9	188.6	+95.8	139.4	244.5	+105.1	66.6	152.8	+86.1	127.9	238.6	+110.8	55	144	+89.4

14	154.0	241.5	+87.5	81.5	203.8	+122.3	131.8	225.6	+93.9	68.3	173.1	+104.9	121.5	215.6	+94.1	57	158	+100.9
15	174.1	248.6	+74.5	115.4	223.3	+107.9	156.0	238.1	+82.1	87.1	198.4	+111.3	150.5	227.4	+76.9	78	182	+103.6
16	128.8	220.9	+92.1	51.6	163.6	+112.0	104.5	211.1	+106.6	33.8	125.0	+91.3	93.1	191.9	+98.8	27	109	+81.5
18	158.5	244.9	+86.4	64.5	168.0	+103.5	143.6	226.5	+82.9	44.1	131.8	+87.6	115.0	216.9	+101.9	36	115	+78.6
19	207.1	254.0	+46.9	121.5	222.0	+100.5	194.1	253.6	+59.5	95.1	194.6	+99.5	195.4	252.6	+57.3	81	179	+97.9
20	187.0	253.9	+66.9	100.0	206.1	+106.1	167.5	248.8	+81.3	73.3	173.9	+100.6	158.8	245.6	+86.9	60	156	+96.1
21	202.3	254.0	+51.8	49.6	137.3	+87.6	190.8	253.0	+62.3	37.6	104.3	+66.6	184.0	252.0	+68.0	31	89	+57.4
22	177.0	252.6	+75.6	74.6	178.3	+103.6	161.4	243.9	+82.5	49.1	140.8	+91.6	153.9	239.0	+85.1	42	122	+80.4
23	155.9	238.6	+82.8	81.4	197.1	+115.8	131.1	229.3	+98.1	56.5	159.4	+102.9	111.4	218.5	+107.1	51	144	+93.3
24	181.9	254.0	+72.1	62.3	162.1	+99.9	160.5	249.3	+88.8	40.8	126.6	+85.9	143.0	243.4	+100.4	31	110	+78.8
25	125.3	225.9	+100.6	90.1	209.4	+119.3	111.1	200.5	+89.4	69.0	180.4	+111.4	108.4	189.8	+81.4	61	163	+101.6
26	203.5	253.3	+49.8	96.6	207.1	+110.5	190.4	246.8	+56.4	79.8	178.1	+98.4	177.0	248.1	+71.1	68	162	+94.8
27	142.6	234.5	+91.9	66.6	159.3	+92.6	114.4	216.1	+101.8	47.8	135.9	+88.1	100.5	205.0	+104.5	38	119	+80.9
28	155.6	234.4	+78.8	59.6	153.3	+93.6	135.6	214.0	+78.4	41.4	117.9	+76.5	126.4	206.1	+79.8	34	102	+67.6
29	153.5	240.8	+87.3	68.6	153.1	+84.5	133.3	227.9	+94.6	46.5	118.9	+72.4	123.8	219.5	+95.8	36	101	+64.9
30	175.3	251.8	+76.5	98.3	207.5	+109.3	151.5	244.5	+93.0	75.9	177.5	+101.6	152.5	239.1	+86.6	62	160	+97.8
Avg.	160.7	242.9	+82.3	94.6	178.4	+83.7	140.2	232.4	+92.2	71.2	147.5	+78.6	127.7	220.3	+92.6	59.3	131.2	+71.9

Appendix 32: Changes in average fluorescence levels exhibited by porcine bone when photographed with the Crime-lite 2 and the orange and filter in terrestrial and tap water contexts.

A) 0.6s exposure time

Rib	0.6s exposure time							
	Terrest.	Underw.	Changes		Terrest.	Underw.	Changes	
	O	O	Diff	% Change	Y	Y	Diff	% Change
1	172.5	103.3	-69.3	-40.1%	249.0	218.9	-30.1	-12.1%
2	166.6	85.6	-81.0	-48.6%	250.1	197.5	-52.6	-21.0%
3	137.9	65.0	-72.9	-52.9%	231.3	181.8	-49.5	-21.4%
4	157.0	91.8	-65.3	-41.6%	243.4	219.1	-24.3	-10.0%
5	112.0	184.8	+72.8	65.0%	216.9	69.8	-147.1	-67.8%
6	125.0	79.6	-45.4	-36.3%	220.9	186.6	-34.3	-15.5%
7	156.6	184.1	+27.5	17.6%	246.6	82.6	-164.0	-66.5%
8	168.0	199.8	+31.8	18.9%	250.0	78.0	-172.0	-68.8%
9	163.6	82.8	-80.9	-49.4%	249.9	200.6	-49.3	-19.7%
10	121.6	76.1	-45.5	-37.4%	230.8	178.4	-52.4	-22.7%
11	161.3	105.3	-56.0	-34.7%	247.5	199.1	-48.4	-19.5%
12	174.5	111.3	-63.3	-36.2%	253.0	220.4	-32.6	-12.9%
13	160.9	92.9	-68.0	-42.3%	252.4	188.6	-63.8	-25.3%
14	154.0	81.5	-72.5	-47.1%	241.5	203.8	-37.8	-15.6%
15	174.1	115.4	-58.8	-33.7%	248.6	223.3	-25.4	-10.2%
16	128.8	51.6	-77.1	-59.9%	220.9	163.6	-57.3	-25.9%
18	158.5	64.5	-94.0	-59.3%	244.9	168.0	-76.9	-31.4%
19	207.1	121.5	-85.6	-41.3%	254.0	222.0	-32.0	-12.6%
20	187.0	100.0	-87.0	-46.5%	253.9	206.1	-47.8	-18.8%
21	202.3	49.6	-152.6	-75.5%	254.0	137.3	-116.8	-46.0%
22	177.0	74.6	-102.4	-57.8%	252.6	178.3	-74.4	-29.4%
23	155.9	81.4	-74.5	-47.8%	238.6	197.1	-41.5	-17.4%
24	181.9	62.3	-119.6	-65.8%	254.0	162.1	-91.9	-36.2%
25	125.3	90.1	-35.1	-28.0%	225.9	209.4	-16.5	-7.3%
26	203.5	96.6	-106.9	-52.5%	253.3	207.1	-46.1	-18.2%
27	142.6	66.6	-76.0	-53.3%	234.5	159.3	-75.3	-32.1%
28	155.6	59.6	-96.0	-61.7%	234.4	153.3	-81.1	-34.6%
29	153.5	68.6	-84.9	-55.3%	240.8	153.1	-87.6	-36.4%
30	175.3	98.3	-77.0	-43.9%	251.8	207.5	-44.3	-17.6%
Avg.	160.7	94.6	-66.0	-40%	242.9	178.4	-64.6	-26.6%

B) 0.4s exposure time

Rib	0.4s exposure time							
	Terrest.	Underw.	Changes		Terrest.	Underw.	Changes	
	O	O	Diff	% Change	Y	Y	Diff	% Change
1	151.6	79.0	-72.6	-47.9%	239.1	192.5	-46.6	-19.5%
2	147.3	55.9	-91.4	-62.1%	236.9	160.1	-76.8	-32.4%
3	123.3	45.1	-78.1	-63.4%	231.6	145.5	-86.1	-37.2%
4	144.5	67.8	-76.8	-53.1%	244.6	191.0	-53.6	-21.9%
5	84.1	152.5	+68.4	81.3%	214.0	48.8	-165.3	-77.2%
6	119.8	57.1	-62.6	-52.3%	226.8	153.1	-73.6	-32.5%
7	134.4	149.5	+15.1	11.3%	233.6	57.9	-175.8	-75.2%
8	149.3	164.8	+15.5	10.4%	238.9	52.4	-186.5	-78.1%
9	144.4	66.6	-77.8	-53.9%	242.1	169.3	-72.9	-30.1%
10	94.9	51.1	-43.8	-46.1%	204.1	143.9	-60.3	-29.5%
11	141.0	78.6	-62.4	-44.2%	233.6	165.6	-68.0	-29.1%
12	141.9	84.9	-57.0	-40.2%	242.1	191.4	-50.8	-21.0%
13	139.4	66.6	-72.8	-52.2%	244.5	152.8	-91.8	-37.5%
14	131.8	68.3	-63.5	-48.2%	225.6	173.1	-52.5	-23.3%
15	156.0	87.1	-68.9	-44.2%	238.1	198.4	-39.8	-16.7%
16	104.5	33.8	-70.8	-67.7%	211.1	125.0	-86.1	-40.8%
18	143.6	44.1	-99.5	-69.3%	226.5	131.8	-94.8	-41.8%
19	194.1	95.1	-99.0	-51.0%	253.6	194.6	-59.0	-23.3%
20	167.5	73.3	-94.3	-56.3%	248.8	173.9	-74.9	-30.1%
21	190.8	37.6	-153.1	-80.3%	253.0	104.3	-148.8	-58.8%
22	161.4	49.1	-112.3	-69.6%	243.9	140.8	-103.1	-42.3%
23	131.1	56.5	-74.6	-56.9%	229.3	159.4	-69.9	-30.5%
24	160.5	40.8	-119.8	-74.6%	249.3	126.6	-122.6	-49.2%
25	111.1	69.0	-42.1	-37.9%	200.5	180.4	-20.1	-10.0%
26	190.4	79.8	-110.6	-58.1%	246.8	178.1	-68.6	-27.8%
27	114.4	47.8	-66.6	-58.3%	216.1	135.9	-80.3	-37.1%
28	135.6	41.4	-94.3	-69.5%	214.0	117.9	-96.1	-44.9%
29	133.3	46.5	-86.8	-65.1%	227.9	118.9	-109.0	-47.8%
30	151.5	75.9	-75.6	-49.9%	244.5	177.5	-67.0	-27.4%
Avg.	141.1	71.2	-69.9	-49.5%	233.1	146.9	-86.2	-37.0%

C) 1/3s exposure time

Rib	1/3s exposure time							
	Terrest.	Underw.	Changes		Terrest.	Underw.	Changes	
	O	O	Diff	% Change	Y	Y	O	O
1	137.1	66	-71.5	-52.1%	232.6	176	-56.6	-24.3%
2	131.8	49	-82.6	-62.7%	232.8	141	-92.3	-39.6%
3	106.0	37	-69.5	-65.6%	194.1	127	-67.4	-34.7%
4	123.0	55	-67.6	-55.0%	216.0	174	-42.0	-19.4%
5	64.8	128	+63.4	97.9%	163.1	40	-123.3	-75.6%
6	81.5	50	-31.1	-38.2%	197.0	133	-64.3	-32.6%
7	121.4	117	-4.9	-4.0%	225.3	47	-178.4	-79.2%
8	140.9	146	+5.0	3.5%	231.8	43	-188.8	-81.4%
9	132.3	55	-76.9	-58.1%	231.1	152	-79.5	-34.4%
10	82.3	42	-40.0	-48.6%	188.1	126	-62.4	-33.2%
11	129.8	65	-65.3	-50.3%	221.5	148	-73.5	-33.2%
12	134.3	72	-62.1	-46.3%	238.6	173	-65.3	-27.3%
13	127.9	55	-72.9	-57.0%	238.6	144	-94.3	-39.5%
14	121.5	57	-64.5	-53.1%	215.6	158	-57.8	-26.8%
15	150.5	78	-72.4	-48.1%	227.4	182	-45.6	-20.1%
16	93.1	27	-66.1	-71.0%	191.9	109	-83.4	-43.5%
18	115.0	36	-78.8	-68.5%	216.9	115	-102.0	-47.0%
19	195.4	81	-114.0	-58.3%	252.6	179	-73.4	-29.0%
20	158.8	60	-98.9	-62.3%	245.6	156	-89.6	-36.5%
21	184.0	31	-152.9	-83.1%	252.0	89	-163.5	-64.9%
22	153.9	42	-112.3	-72.9%	239.0	122	-117.0	-49.0%
23	111.4	51	-60.3	-54.1%	218.5	144	-74.1	-33.9%
24	143.0	31	-111.8	-78.1%	243.4	110	-133.4	-54.8%
25	108.4	61	-47.0	-43.4%	189.8	163	-26.8	-14.1%
26	177.0	68	-109.5	-61.9%	248.1	162	-85.9	-34.6%
27	100.5	38	-62.1	-61.8%	205.0	119	-85.8	-41.8%
28	126.4	34	-92.5	-73.2%	206.1	102	-104.6	-50.8%
29	123.8	36	-88.0	-71.1%	219.5	101	-118.9	-54.2%
30	152.5	62	-90.5	-59.3%	239.1	160	-79.4	-33.2%
Avg.	128.5	59.7	-68.9	-53.6%	221.4	130.8	-90.6	-40.9%

Appendix 33: Calculated fluorescence values of each ROI and overall average fluorescence for terrestrial photographs taken with the Crime-lite 2 and the orange filter.

A) 0.6s exposure time

Rib	Terrestrial fluorescence values, 0.6s exposure time, orange filter									Avg.
	Photograph 1			Photograph 2			Photograph 3			
	ROI 1	ROI 2	ROI 3	ROI 1	ROI 2	ROI 3	ROI 1	ROI 2	ROI 3	
1	172	174	171	172	174	171	172	174	171	172.5
2	161	168	173	161	168	173	161	168	173	166.6
3	135	139	142	135	139	141	134	138	140	137.9
4	154	156	163	154	156	163	154	156	163	157.0
5	105	112	123	105	112	123	105	111	123	112.0
6	118	127	131	119	128	132	118	127	131	125.0
7	152	160	159	152	159	159	152	160	159	156.6
8	168	168	168	168	168	168	168	168	168	168.0
9	158	165	171	158	164	171	158	164	171	163.6
10	110	125	133	111	125	133	111	125	132	121.6
11	154	164	168	154	164	168	154	164	168	161.3
12	175	175	173	175	175	173	175	175	173	174.5
13	156	164	160	158	166	161	157	165	161	160.9
14	153	157	150	154	157	150	154	157	151	154.0
15	166	178	180	166	178	181	166	178	181	174.1
16	130	127	131	130	127	130	130	125	130	128.8
18	155	163	157	155	163	157	155	163	157	158.5
19	201	211	211	201	211	211	201	210	210	207.1
20	182	190	191	181	190	191	181	190	191	187.0
21	201	201	206	201	201	206	201	201	206	202.3
22	173	179	180	173	179	180	173	179	180	177.0
23	155	157	156	155	156	156	155	157	156	155.9
24	181	183	182	181	183	182	181	182	182	181.9
25	113	130	138	112	129	136	113	131	139	125.3
26	201	207	201	201	208	202	201	207	201	203.5
27	138	150	139	138	150	140	137	149	139	142.6
28	140	165	166	139	165	166	139	165	167	155.6
29	138	153	179	138	152	179	137	152	179	153.5
30	164	178	188	164	178	188	164	178	188	175.3

B) 0.4s exposure time

Rib	Terrestrial fluorescence values, 0.4s exposure time, orange filter									Avg.
	Photograph 1			Photograph 2			Photograph 3			
	ROI 1	ROI 2	ROI 3	ROI 1	ROI 2	ROI 3	ROI 1	ROI 2	ROI 3	
1	151	154	149	151	154	149	151	154	148	151.6
2	136	148	155	139	151	159	139	151	159	147.3
3	107	129	139	107	129	140	107	128	139	123.3
4	142	143	151	141	143	150	142	144	150	144.5
5	80	85	89	80	85	89	80	85	90	84.1
6	114	120	124	116	122	126	115	121	125	119.8
7	129	138	137	129	138	137	129	138	137	134.4
8	150	148	150	150	148	150	150	148	150	149.3
9	137	145	154	138	145	154	137	145	154	144.4
10	85	98	105	85	98	105	85	98	105	94.9
11	131	144	152	131	144	151	131	144	151	141.0
12	143	144	139	143	143	138	142	143	138	141.9
13	135	143	138	136	144	139	136	144	139	139.4
14	130	135	129	130	135	129	131	135	130	131.8
15	147	161	163	147	161	163	146	160	163	156.0
16	100	106	109	100	106	109	100	106	109	104.5
18	141	149	141	140	148	140	141	149	140	143.6
19	181	201	205	181	200	204	181	200	204	194.1
20	161	171	172	161	171	173	160	171	172	167.5
21	189	189	196	189	189	196	189	189	196	190.8
22	157	164	165	157	164	164	157	163	164	161.4
23	131	132	132	130	132	131	130	131	131	131.1
24	160	162	160	160	162	160	159	161	159	160.5
25	97	118	129	95	115	125	95	115	129	111.1
26	185	196	188	186	197	190	185	196	189	190.4
27	108	124	111	109	123	110	107	123	110	114.4
28	114	147	149	116	148	150	114	147	150	135.6
29	113	133	163	113	133	163	114	134	163	133.3
30	140	152	167	140	152	167	141	153	168	151.5

C) 1/3s exposure time

Rib	Terrestrial fluorescence values, 1/3s exposure time, orange filter									Avg.
	Photograph 1			Photograph 2			Photograph 3			
	ROI 1	ROI 2	ROI 3	ROI 1	ROI 2	ROI 3	ROI 1	ROI 2	ROI 3	
1	137	139	134	137	140	134	137	139	134	137.1
2	124	133	142	124	133	142	123	133	142	131.8
3	101	109	110	101	109	110	100	108	110	106.0
4	119	121	130	120	122	131	120	121	131	123.0
5	55	68	75	55	68	75	55	67	74	64.8
6	76	83	86	76	84	87	76	84	87	81.5
7	117	125	122	118	123	122	118	126	123	121.4
8	141	140	142	141	140	142	141	140	142	140.9
9	125	133	143	125	133	142	124	133	142	132.3
10	75	86	89	74	85	90	74	85	90	82.3
11	120	131	143	120	130	143	120	131	143	129.8
12	132	132	146	132	132	136	132	132	135	134.3
13	124	133	127	124	132	127	124	132	127	127.9
14	119	123	120	120	124	122	120	124	122	121.5
15	140	156	158	140	156	158	140	156	158	150.5
16	87	96	99	87	96	98	87	95	97	93.1
18	112	119	109	114	121	111	114	120	110	115.0
19	183	203	204	183	203	204	182	201	203	195.4
20	152	163	163	152	162	163	152	163	163	158.8
21	182	182	190	182	182	190	182	182	190	184.0
22	148	157	158	148	157	158	148	157	158	153.9
23	110	113	112	110	113	112	109	112	111	111.4
24	141	144	143	141	144	143	143	145	144	143.0
25	90	114	127	90	114	126	91	115	128	108.4
26	171	183	176	172	183	176	172	183	175	177.0
27	93	111	98	92	110	98	92	110	97	100.5
28	103	139	142	103	139	142	104	139	142	126.4
29	103	124	155	103	124	155	102	124	155	123.8
30	141	156	164	142	156	164	141	156	164	152.5

Appendix 34: Calculated fluorescence values of each ROI and overall average fluorescence for terrestrial photographs taken with the Crime-lite 2 and the yellow filter.

A) 0.6s exposure time

Rib	Terrestrial fluorescence values, 0.6s exposure time, yellow filter									Avg.
	Photograph 1			Photograph 2			Photograph 3			
	ROI 1	ROI 2	ROI 3	ROI 1	ROI 2	ROI 3	ROI 1	ROI 2	ROI 3	
1	249	249	249	249	249	249	249	249	249	249.0
2	248	251	251	249	251	251	249	251	251	250.1
3	227	235	230	227	236	232	227	236	232	231.3
4	241	243	248	241	243	247	241	243	247	243.4
5	209	217	226	210	217	227	211	218	228	216.9
6	215	221	228	216	222	227	216	222	226	220.9
7	244	248	248	244	248	249	244	248	249	246.6
8	250	250	250	250	250	250	250	250	250	250.0
9	247	250	253	247	250	254	247	251	254	249.9
10	225	234	234	225	234	235	225	234	236	230.8
11	244	248	252	244	248	252	244	248	252	247.5
12	253	253	253	253	253	253	253	253	253	253.0
13	252	253	252	252	253	252	252	253	252	252.4
14	244	243	235	244	243	236	244	243	236	241.5
15	246	250	251	246	250	251	245	250	251	248.6
16	230	212	221	230	212	221	228	213	221	220.9
18	242	247	245	242	247	245	243	248	246	244.9
19	254	254	254	254	254	254	254	254	254	254.0
20	254	254	254	254	254	254	254	253	254	253.9
21	254	254	254	254	254	254	254	254	254	254.0
22	252	253	253	252	253	253	252	253	253	252.6
23	238	240	240	237	239	239	237	239	239	238.6
24	254	254	254	254	254	254	254	254	254	254.0
25	221	230	231	220	228	229	220	228	229	225.9
26	253	253	253	253	254	253	253	254	253	253.3
27	229	242	234	228	241	233	228	241	233	234.5
28	212	245	250	213	246	250	213	246	250	234.4
29	236	238	252	236	238	252	236	238	252	240.8
30	250	252	254	250	252	254	250	252	254	251.8

B) 0.4s exposure time

Rib	Terrestrial fluorescence values, 0.4s exposure time, yellow filter									Avg.
	Photograph 1			Photograph 2			Photograph 3			
	ROI 1	ROI 2	ROI 3	ROI 1	ROI 2	ROI 3	ROI 1	ROI 2	ROI 3	
1	239	239	240	239	239	239	239	239	239	239.1
2	232	238	238	233	240	239	234	241	241	236.9
3	225	235	237	225	235	236	224	236	237	231.6
4	244	244	248	243	243	247	244	244	247	244.6
5	206	217	222	206	217	222	206	216	221	214.0
6	224	226	230	224	226	230	225	229	231	226.8
7	229	236	237	229	236	237	229	236	237	233.6
8	240	239	239	239	238	238	239	239	239	238.9
9	237	244	248	237	243	248	237	243	248	242.1
10	193	208	216	193	207	216	193	207	216	204.1
11	229	235	240	228	235	240	228	234	239	233.6
12	243	241	242	243	241	242	244	241	242	242.1
13	243	246	245	243	246	244	243	246	244	244.5
14	229	228	217	229	228	217	229	228	217	225.6
15	232	241	243	232	241	243	232	241	243	238.1
16	203	216	218	202	216	218	201	215	217	211.1
18	223	230	227	223	230	226	223	230	227	226.5
19	253	254	254	253	254	254	253	254	254	253.6
20	248	250	249	247	250	249	247	250	249	248.8
21	253	253	253	253	253	253	253	253	253	253.0
22	241	245	246	241	245	246	241	246	246	243.9
23	228	230	230	228	230	230	228	230	230	229.3
24	248	250	250	248	250	250	248	250	250	249.3
25	192	205	208	191	204	207	192	205	208	200.5
26	246	248	245	247	248	246	246	248	245	246.8
27	210	226	213	209	225	212	209	225	212	216.1
28	181	231	239	181	230	239	181	230	239	214.0
29	213	230	249	213	229	246	214	229	248	227.9
30	241	245	249	241	245	249	241	245	249	244.5

C) 1/3s exposure time

Rib	Terrestrial fluorescence values, 1/3s exposure time, yellow filter									Avg.
	Photograph 1			Photograph 2			Photograph 3			
	ROI 1	ROI 2	ROI 3	ROI 1	ROI 2	ROI 3	ROI 1	ROI 2	ROI 3	
1	232	233	233	232	233	233	232	233	233	232.6
2	228	235	236	229	235	236	228	235	236	232.8
3	186	200	196	187	200	197	187	200	197	194.1
4	211	214	223	212	216	226	211	215	224	216.0
5	153	166	175	153	166	175	152	165	175	163.1
6	183	203	210	183	203	209	183	202	208	197.0
7	221	228	228	221	228	228	220	228	228	225.3
8	232	232	231	232	232	231	232	232	231	231.8
9	226	232	238	226	233	238	225	231	239	231.1
10	176	191	201	176	192	201	176	192	201	188.1
11	215	221	231	215	222	231	215	222	231	221.5
12	239	239	237	239	239	237	239	240	237	238.6
13	237	240	239	237	240	239	237	240	239	238.6
14	218	219	207	218	219	207	218	219	208	215.6
15	219	231	234	220	231	234	219	231	234	227.4
16	191	192	200	190	188	196	190	188	196	191.9
18	214	221	217	213	221	217	212	220	215	216.9
19	251	254	253	251	254	253	251	254	253	252.6
20	244	247	246	244	247	246	244	247	246	245.6
21	252	252	252	252	252	252	252	252	252	252.0
22	235	241	242	235	241	242	235	241	242	239.0
23	217	220	219	217	220	219	217	219	219	218.5
24	241	244	245	242	244	245	242	244	244	243.4
25	175	197	202	175	197	201	175	196	201	189.8
26	247	250	247	247	250	247	247	250	247	248.1
27	197	215	202	197	215	202	197	215	202	205.0
28	170	225	232	170	225	232	170	225	232	206.1
29	203	220	244	203	220	243	203	220	243	219.5
30	235	239	246	234	239	246	235	239	246	239.1

Appendix 35: Calculated fluorescence values of each ROI and overall average fluorescence for underwater photographs taken with the Crime-lite 2 and with the orange filter.

A) 0.6s exposure time

Rib	Underwater fluorescence values, 0.6s exposure time, orange filter									Avg.
	Photograph 1			Photograph 2			Photograph 3			
	ROI 1	ROI 2	ROI 3	ROI 1	ROI 2	ROI 3	ROI 1	ROI 2	ROI 3	
1	102	102	104	103	102	104	105	104	106	103.3
2	82	87	91	81	86	91	81	86	91	85.6
3	66	66	63	65	66	63	65	66	63	65.0
4	91	99	104	83	90	96	82	89	95	91.8
5	192	184	175	192	184	175	192	184	175	184.8
6	84	80	77	83	79	75	82	77	74	79.6
7	177	187	195	175	184	194	176	185	195	184.1
8	197	202	200	198	201	200	198	202	200	199.8
9	80	82	81	83	84	83	84	85	84	82.8
10	70	80	80	70	80	80	70	79	80	76.1
11	109	105	100	109	105	100	109	105	100	105.3
12	112	114	106	112	113	106	112	115	108	111.3
13	93	91	95	93	91	96	93	91	96	92.9
14	82	84	65	87	89	68	87	90	70	81.5
15	111	116	121	112	116	121	111	115	120	115.4
16	48	53	52	49	55	54	48	54	53	51.6
18	64	67	61	65	67	61	64	67	61	64.5
19	116	122	135	114	120	132	114	119	132	121.5
20	99	98	99	101	100	100	102	101	101	100.0
21	62	44	38	62	44	37	64	46	37	49.6
22	72	73	74	75	77	78	73	75	76	74.6
23	88	81	76	86	80	74	86	80	75	81.4
24	57	67	64	57	66	63	57	67	64	62.3
25	94	87	89	94	87	89	94	87	89	90.1
26	85	101	117	82	98	111	82	97	111	96.6
27	64	71	64	65	71	62	65	71	64	66.6
28	63	58	57	62	59	57	62	59	57	59.6
29	68	69	66	70	70	66	70	70	66	68.6
30	100	97	97	100	98	98	99	97	98	98.3

B) 0.4s exposure time

Rib	Underwater fluorescence values, 0.4s exposure time, orange filter									Avg.
	Photograph 1			Photograph 2			Photograph 3			
	ROI 1	ROI 2	ROI 3	ROI 1	ROI 2	ROI 3	ROI 1	ROI 2	ROI 3	
1	79	79	81	79	78	80	78	78	80	79.0
2	54	57	63	52	55	60	52	54	59	55.9
3	45	45	43	45	47	45	45	46	45	45.1
4	61	68	75	62	69	76	62	69	76	67.8
5	157	153	142	157	153	143	159	156	146	152.5
6	57	56	58	57	57	58	57	57	58	57.1
7	140	150	161	141	151	162	140	151	162	149.5
8	161	166	163	162	169	167	162	168	166	164.8
9	66	67	68	65	67	68	65	67	68	66.6
10	46	53	54	47	54	55	47	53	55	51.1
11	82	78	73	82	78	74	83	79	74	78.6
12	85	87	81	85	87	81	85	88	82	84.9
13	68	66	66	68	66	67	67	65	52	66.6
14	70	72	60	70	72	59	71	72	59	68.3
15	84	87	92	84	87	92	84	87	92	87.1
16	32	35	34	32	35	34	32	36	35	33.8
18	44	46	40	44	46	41	45	47	41	44.1
19	89	95	109	89	94	107	87	91	104	95.1
20	74	75	73	71	74	71	73	75	72	73.3
21	49	33	25	49	34	25	50	36	26	37.6
22	48	50	50	49	50	51	47	48	49	49.1
23	62	56	52	60	55	50	61	56	52	56.5
24	38	44	42	37	44	42	36	43	41	40.8
25	72	67	67	72	68	66	73	67	67	69.0
26	58	80	111	59	80	111	59	80	111	79.8
27	44	51	45	45	52	46	46	53	45	47.8
28	41	42	39	42	42	39	43	43	40	41.4
29	48	47	43	48	47	44	48	47	44	46.5
30	77	79	72	75	78	72	76	78	73	75.9

C) 1/3s exposure time

Rib	Underwater fluorescence values, 1/3s exposure time, orange filter									Avg.
	Photograph 1			Photograph 2			Photograph 3			
	ROI 1	ROI 2	ROI 3	ROI 1	ROI 2	ROI 3	ROI 1	ROI 2	ROI 3	
1	65	65	67	65	65	67	66	65	67	65.6
2	46	48	54	46	49	55	46	49	54	49.1
3	35	38	37	35	37	37	35	38	37	36.5
4	50	57	62	50	56	61	50	57	62	55.4
5	137	128	119	136	127	119	134	125	118	128.1
6	51	50	51	50	50	51	50	50	51	50.4
7	103	113	128	108	119	133	108	120	135	116.5
8	143	147	146	144	148	146	144	149	147	145.9
9	54	56	56	55	56	56	55	55	56	55.4
10	39	45	44	38	45	44	38	45	44	42.3
11	68	64	60	68	64	60	68	64	60	64.5
12	72	74	69	72	74	69	73	74	69	72.1
13	56	54	55	56	54	55	56	54	55	55.0
14	58	60	49	60	61	49	59	60	49	57.0
15	73	80	85	72	80	84	72	79	84	78.1
16	25	28	28	26	28	28	25	28	27	27.0
18	36	38	33	37	38	33	37	38	34	36.3
19	76	81	93	74	80	91	75	81	92	81.4
20	60	62	59	59	61	59	59	60	58	59.9
21	41	28	21	41	28	20	42	28	21	31.1
22	42	43	44	40	41	42	40	41	42	41.6
23	55	49	49	55	49	48	55	49	49	51.1
24	29	30	36	29	31	36	29	30	36	31.3
25	63	64	58	62	62	57	62	63	57	61.4
26	48	68	99	48	66	98	47	66	98	67.5
27	36	42	38	35	41	38	35	42	38	38.4
28	35	34	31	34	35	33	34	35	32	33.9
29	34	35	34	36	37	36	37	37	35	35.8
30	62	64	59	62	63	59	63	64	59	62.0

Appendix 36: Calculated fluorescence values of each ROI and overall average fluorescence for underwater photographs taken with the Crime-lite 2 and with the yellow filter.

A) 0.6s exposure time

Rib	Underwater fluorescence values, 0.6s exposure time, yellow filter									Avg.
	Photograph 1			Photograph 2			Photograph 3			
	ROI 1	ROI 2	ROI 3	ROI 1	ROI 2	ROI 3	ROI 1	ROI 2	ROI 3	
1	217	216	220	218	218	222	220	220	222	218.9
2	196	201	196	195	201	195	195	201	196	197.5
3	182	183	180	182	183	179	181	184	179	181.8
4	215	220	225	215	220	225	214	219	225	219.1
5	73	70	66	71	70	66	72	70	66	69.8
6	185	186	191	185	186	191	184	185	190	186.6
7	78	85	87	77	84	87	78	85	88	82.6
8	76	79	79	76	79	79	76	80	80	78.0
9	198	200	200	201	203	203	199	201	201	200.6
10	174	184	177	175	183	176	175	183	176	178.4
11	205	199	193	204	198	192	204	198	192	199.1
12	223	219	216	224	220	217	224	220	217	220.4
13	188	193	183	188	193	184	188	192	182	188.6
14	194	209	211	194	208	211	194	209	210	203.8
15	218	226	226	219	226	226	219	226	226	223.3
16	163	164	163	163	164	162	164	166	165	163.6
18	173	172	155	172	172	155	173	172	155	168.0
19	216	222	231	216	222	231	216	222	231	222.0
20	207	207	203	208	207	203	208	206	202	206.1
21	157	127	120	157	128	121	159	129	121	137.3
22	177	181	178	176	180	178	176	180	178	178.3
23	202	195	194	201	194	194	202	195	194	197.1
24	156	165	168	156	164	169	156	163	170	162.1
25	212	208	208	212	208	207	212	208	209	209.4
26	187	209	232	188	209	232	189	211	233	207.1
27	166	162	148	165	161	148	164	160	147	159.3
28	144	163	152	144	163	153	144	163	152	153.3
29	142	146	180	142	146	181	142	146	181	153.1
30	209	208	205	209	208	204	209	208	204	207.5

B) 0.4s exposure time

Rib	Underwater fluorescence values, 0.4s exposure time, yellow filter									Avg.
	Photograph 1			Photograph 2			Photograph 3			
	ROI 1	ROI 2	ROI 3	ROI 1	ROI 2	ROI 3	ROI 1	ROI 2	ROI 3	
1	191	191	195	192	192	196	192	191	196	192.5
2	157	165	159	156	164	158	157	165	159	160.1
3	146	148	143	145	147	143	145	147	143	145.5
4	186	191	197	186	192	198	186	192	199	191.0
5	51	49	45	51	49	45	51	49	45	48.8
6	156	154	151	155	153	150	154	152	149	153.1
7	54	60	62	53	59	61	54	60	62	57.9
8	53	53	51	53	54	52	51	52	51	52.4
9	167	169	170	168	170	171	168	171	172	169.3
10	141	149	140	141	149	141	141	149	141	143.9
11	172	165	157	172	165	157	172	165	158	165.6
12	196	190	186	196	191	187	195	190	186	191.4
13	152	159	145	153	158	145	153	157	146	152.8
14	162	181	182	160	178	181	161	180	182	173.1
15	190	203	203	191	203	203	191	203	203	198.4
16	127	125	123	126	125	123	126	125	123	125.0
18	138	135	116	138	136	117	138	136	117	131.8
19	184	195	212	183	194	212	183	194	211	194.6
20	174	177	171	173	176	171	173	176	171	173.9
21	122	94	88	125	95	87	127	96	88	104.3
22	139	142	141	140	142	140	140	142	141	140.8
23	165	158	155	164	158	154	164	157	153	159.4
24	119	131	132	118	131	132	119	131	133	126.6
25	184	179	178	184	179	178	183	178	178	180.4
26	156	178	209	157	179	209	158	179	208	178.1
27	140	139	124	140	140	125	139	140	124	135.9
28	110	126	118	109	126	119	109	126	119	117.9
29	110	112	142	111	113	141	110	112	142	118.9
30	179	179	173	179	178	173	180	179	173	177.5

C) 1/3s exposure time

Rib	Underwater fluorescence values, 1/3s exposure time, yellow filter									Avg.
	Photograph 1			Photograph 2			Photograph 3			
	ROI 1	ROI 2	ROI 3	ROI 1	ROI 2	ROI 3	ROI 1	ROI 2	ROI 3	
1	175	174	179	175	174	180	176	175	180	176.0
2	138	149	138	136	147	136	134	146	136	140.5
3	127	128	124	127	128	124	128	128	124	126.8
4	168	175	182	168	174	182	168	175	181	174.0
5	42	40	37	42	40	37	41	40	37	39.9
6	135	133	130	134	133	129	135	133	130	132.8
7	44	49	50	43	48	50	43	48	50	46.9
8	44	44	43	42	43	42	43	43	42	43.0
9	146	150	149	151	154	154	153	156	156	151.6
10	123	131	124	122	130	124	122	130	124	125.8
11	155	147	139	155	147	139	155	147	140	148.0
12	178	172	168	179	173	168	178	171	166	173.4
13	150	145	133	152	146	133	151	145	132	144.4
14	146	165	166	146	165	168	144	163	168	157.9
15	173	187	187	173	187	187	173	187	187	181.8
16	110	109	106	109	110	105	109	110	106	108.5
18	119	118	102	120	119	103	120	118	102	114.9
19	167	179	198	167	179	197	167	180	198	179.3
20	156	159	153	156	159	153	154	158	152	156.0
21	106	81	73	107	82	73	106	80	73	88.5
22	121	122	121	122	124	123	121	122	121	122.0
23	149	140	141	150	142	142	150	141	142	144.4
24	106	110	116	106	110	116	106	110	116	110.0
25	167	162	160	167	161	160	166	161	159	163.0
26	143	163	191	142	163	190	142	164	193	162.3
27	125	121	108	124	121	108	123	124	108	119.3
28	97	107	101	96	107	101	96	107	101	101.5
29	88	93	130	89	93	130	89	93	130	100.6
30	160	162	154	161	162	155	161	163	155	159.8

Appendix 37: Changes in average fluorescence levels exhibited by porcine bone when photographed with the Hammerhead light and the orange and filter in terrestrial and tap water contexts.

A) 0.6s exposure time

0.6s exposure time				
Rib	**Terrestrial**	**Underwater**	**Terrestrial**	**Underwater**
	Orange	**Orange**	**Diff**	**% Change**
1	185.1	81.1	-104.0	-56.2%
2	141.1	64.1	-77.0	-54.6%
3	131.5	57.1	-74.4	-56.6%
4	137.6	74.8	-62.9	-45.7%
5	107.3	40.4	-66.9	-62.4%
6	117.9	45.1	-72.8	-61.7%
7	178.6	70.9	-107.8	-60.3%
8	126.1	61.8	-64.4	-51.0%
9	141.0	61.4	-79.6	-56.5%
10	105.9	32.9	-73.0	-68.9%
11	152.9	86.6	-66.3	-43.3%
12	175.6	85.0	-90.6	-51.6%
13	146.5	51.4	-95.1	-64.9%
14	175.8	63.1	-112.6	-64.1%
15	192.8	94.1	-98.6	-51.2%
16	117.0	39.6	-77.4	-66.1%
18	130.0	48.3	-81.8	-62.9%
19	209.6	101.8	-107.9	-51.5%
20	178.4	50.5	-127.9	-71.7%
21	181.4	65.3	-116.1	-64.0%
22	181.1	53.9	-127.3	-70.3%
23	193.0	66.1	-126.9	-65.7%
24	190.4	57.1	-133.3	-70.0%
25	166.9	85.8	-81.1	-48.6%
26	207.5	89.1	-118.4	-57.0%
27	162.4	78.6	-83.8	-51.6%
28	104.4	39.1	-65.3	-62.5%
29	168.5	52.3	-116.3	-69.0%
30	171.0	67.9	-103.1	-60.3%
Average	158.2	63.6	-94.6	-59.8%

B) 0.4s exposure time

0.4s exposure time				
Rib	Terrestrial Orange	Underwater Orange	Terrestrial Diff	Underwater % Change
1	154.9	56.1	-98.8	-63.8%
2	102.5	38.1	-64.4	-62.8%
3	94.8	39.4	-55.4	-58.4%
4	104.5	52.9	-51.6	-49.4%
5	58.9	25.8	-33.1	-56.3%
6	93.6	30.8	-62.9	-67.2%
7	150.4	47.8	-102.6	-68.2%
8	94.1	42.0	-52.1	-55.4%
9	110.9	38.0	-72.9	-65.7%
10	75.8	18.1	-57.6	-76.1%
11	121.0	59.3	-61.8	-51.0%
12	151.9	59.1	-92.8	-61.1%
13	110.4	30.6	-79.8	-72.3%
14	149.8	42.4	-107.4	-71.7%
15	166.1	59.4	-106.8	-64.3%
16	83.9	24.0	-59.9	-71.4%
18	95.4	29.6	-65.8	-68.9%
19	193.0	83.5	-109.5	-56.7%
20	148.3	35.5	-112.8	-76.1%
21	150.3	45.0	-105.3	-70.0%
22	149.6	38.5	-111.1	-74.3%
23	163.6	42.3	-121.4	-74.2%
24	160.8	37.1	-123.6	-76.9%
25	138.0	55.1	-82.9	-60.1%
26	185.0	64.1	-120.9	-65.3%
27	129.4	54.8	-74.6	-57.7%
28	76.1	25.5	-50.6	-66.5%
29	135.1	36.5	-98.6	-73.0%
30	140.0	49.4	-90.6	-64.7%
Average	127.4	43.0	-84.4	-66.2%

C) 1/3s exposure time

1/3s exposure time				
Rib	Terrestrial Orange	Underwater Orange	Terrestrial Diff	Underwater % Change
1	136.9	44	-92.8	-67.8%
2	87.3	29	-58.5	-67.0%
3	81.4	31	-50.1	-61.6%
4	89.1	39	-49.8	-55.8%
5	58.4	19	-39.4	-67.5%
6	80.9	24	-56.5	-69.9%
7	132.0	39	-92.9	-70.4%
8	75.9	34	-41.9	-55.2%
9	93.5	31	-63.0	-67.4%
10	60.8	14	-46.5	-76.5%
11	100.0	49	-51.3	-51.3%
12	128.0	48	-79.6	-62.2%
13	90.3	24	-66.5	-73.7%
14	133.8	33	-100.6	-75.2%
15	150.3	50	-100.6	-67.0%
16	72.3	19	-53.5	-74.0%
18	80.1	25	-54.9	-68.5%
19	184.3	106	-78.5	-42.6%
20	127.0	31	-95.6	-75.3%
21	132.5	37	-95.9	-72.4%
22	134.1	28	-106.1	-79.1%
23	144.9	33	-111.6	-77.0%
24	143.6	29	-114.3	-79.5%
25	120.9	52	-69.0	-57.1%
26	171.8	57	-115.0	-67.0%
27	108.8	45	-64.1	-59.0%
28	63.9	19	-45.0	-70.5%
29	110.5	28	-82.5	-74.7%
30	120.4	40	-80.4	-66.8%
Average	111.0	36.1	-75.0	-67.5%

Appendix 38: Calculated fluorescence values of each ROI and overall average fluorescence for terrestrial photographs taken with the Hammerhead ALS and the orange filter.

A) 0.6s exposure time

Rib	Terrestrial fluorescence values, 0.6s exposure time, orange filter									Avg.
	Photograph 1			Photograph 2			Photograph 3			
	ROI 1	ROI 2	ROI 3	ROI 1	ROI 2	ROI 3	ROI 1	ROI 2	ROI 3	
1	185	187	185	184	186	184	184	186	184	185.0
2	141	144	139	140	143	139	140	143	139	140.9
3	125	135	138	125	134	137	124	134	137	132.1
4	130	138	150	129	138	149	129	138	149	138.9
5	105	110	110	104	109	109	103	108	107	107.2
6	113	115	127	116	117	129	113	113	125	118.7
7	174	182	181	173	182	183	173	181	183	179.1
8	120	129	132	120	128	132	120	128	132	126.8
9	131	144	152	131	143	152	132	143	151	142.1
10	105	104	111	104	103	112	104	104	113	106.7
11	157	154	146	156	154	146	156	154	146	152.1
12	184	176	163	184	175	163	184	176	163	174.2
13	145	149	144	146	149	145	145	149	144	146.2
14	179	179	162	181	180	162	182	181	163	174.3
15	199	194	184	198	193	183	198	193	183	191.7
16	112	119	123	112	118	123	111	118	122	117.6
18	123	134	133	124	134	132	125	135	133	130.3
19	204	209	219	204	209	219	204	209	218	210.6
20	171	182	185	170	182	185	170	182	185	179.1
21	192	183	164	192	182	164	192	182	164	179.4
22	181	182	181	181	181	180	181	182	181	181.1
23	193	193	195	193	191	195	193	191	194	193.1
24	188	191	193	188	191	193	188	191	193	190.7
25	167	167	167	167	167	167	166	167	167	166.9
26	194	212	222	193	212	223	192	212	223	209.2
27	166	164	156	165	163	155	166	164	156	161.7
28	103	96	121	104	98	114	103	96	117	105.8
29	152	171	189	152	171	189	153	171	189	170.8
30	170	174	170	169	173	170	169	173	170	170.9

B) 0.4s exposure time

Rib	Terrestrial fluorescence values, 0.4s exposure time, orange filter									Avg.
	Photograph 1			Photograph 2			Photograph 3			
	ROI 1	ROI 2	ROI 3	ROI 1	ROI 2	ROI 3	ROI 1	ROI 2	ROI 3	
1	154	157	154	154	157	154	153	156	152	154.6
2	99	104	102	100	105	103	102	105	104	102.7
3	91	95	98	91	97	99	90	97	100	95.3
4	96	104	117	96	105	117	96	105	117	105.9
5	58	58	58	58	58	65	58	58	64	59.4
6	87	97	99	88	97	99	86	96	98	94.1
7	146	154	152	145	154	152	146	154	150	150.3
8	89	96	99	89	96	99	89	96	99	94.7
9	101	114	121	101	114	121	101	114	121	112.0
10	72	78	84	72	72	84	72	72	84	76.7
11	124	122	115	124	122	115	124	122	115	120.3
12	156	156	144	156	152	143	156	152	143	150.9
13	110	114	109	109	113	108	108	112	107	110.0
14	152	156	136	152	156	136	153	157	137	148.3
15	174	167	154	173	167	153	174	167	154	164.8
16	89	91	68	88	90	67	88	90	67	82.0
18	93	99	94	92	99	94	93	99	95	95.3
19	186	192	205	186	192	205	186	192	206	194.4
20	140	151	154	141	152	156	141	151	156	149.1
21	164	151	130	163	150	130	164	150	130	148.0
22	149	151	150	148	151	150	148	150	149	149.6
23	165	162	169	165	162	169	160	157	166	163.9
24	159	161	164	159	161	165	157	160	163	161.0
25	139	138	138	138	138	138	138	137	137	137.9
26	164	191	209	164	191	209	162	190	209	187.7
27	133	132	123	132	131	122	132	130	122	128.6
28	74	68	90	75	69	88	75	70	90	77.7
29	120	134	159	120	134	159	120	135	159	137.8
30	140	142	137	140	142	137	140	142	136	139.6

C) 1/3s exposure time

Rib	Terrestrial fluorescence values, 1/3s exposure time, orange filter									Avg.
	Photograph 1			Photograph 2			Photograph 3			
	ROI 1	ROI 2	ROI 3	ROI 1	ROI 2	ROI 3	ROI 1	ROI 2	ROI 3	
1	136	139	136	136	138	136	136	138	135	136.7
2	86	89	86	86	89	87	86	89	88	87.3
3	78	83	85	77	83	85	77	83	85	81.8
4	81	89	101	81	90	101	81	89	101	90.4
5	58	57	61	58	57	61	58	57	60	58.6
6	76	82	85	77	83	85	77	82	85	81.3
7	127	136	133	127	136	134	127	136	135	132.3
8	71	78	81	71	78	81	70	77	80	76.3
9	85	96	103	85	96	103	84	96	103	94.6
10	59	58	70	56	59	69	56	59	69	61.7
11	104	102	92	103	103	92	103	101	92	99.1
12	137	128	115	137	128	114	137	128	114	126.4
13	90	94	89	89	92	88	88	92	88	90.0
14	140	139	119	139	138	118	139	138	118	132.0
15	158	151	138	158	151	139	157	150	138	148.9
16	76	81	57	75	79	56	75	79	56	70.4
18	120	122	112	119	121	111	119	121	111	117.3
19	78	84	79	76	83	79	78	84	79	80.0
20	176	183	199	176	183	198	176	183	199	185.9
21	119	132	134	117	131	134	118	131	134	127.8
22	144	134	114	144	134	114	143	133	114	130.4
23	133	135	135	133	135	135	133	134	135	134.2
24	144	142	149	145	142	149	145	143	149	145.3
25	141	144	148	141	143	148	141	143	147	144.0
26	122	120	121	122	120	121	121	120	120	120.8
27	146	178	200	146	178	200	147	179	200	174.9
28	108	109	103	109	111	105	111	114	106	108.4
29	60	57	79	60	58	80	60	57	78	65.4
30	95	109	133	95	111	134	94	113	134	113.1

Appendix 39: Calculated fluorescence values of each ROI and overall average fluorescence for underwater photographs taken with the Hammerhead ALS and the orange filter.

A) 0.6s exposure time

Rib	Underwater fluorescence values, 0.6s exposure time, orange filter									Avg.
	Photograph 1			Photograph 2			Photograph 3			
	ROI 1	ROI 2	ROI 3	ROI 1	ROI 2	ROI 3	ROI 1	ROI 2	ROI 3	
1	81	82	83	81	81	82	79	80	81	81.1
2	63	67	63	62	68	63	61	66	62	63.9
3	52	59	61	52	59	61	53	60	62	57.7
4	72	77	73	72	78	76	73	77	76	74.9
5	41	41	41	40	40	40	40	40	40	40.3
6	45	45	44	46	46	45	45	45	44	45.0
7	67	74	72	67	74	73	66	74	74	71.2
8	61	62	62	62	63	61	61	62	60	61.6
9	60	62	61	61	63	62	60	62	61	61.3
10	32	33	33	33	33	32	33	34	33	32.9
11	87	88	84	87	88	84	87	88	85	86.4
12	86	87	81	86	87	81	86	86	81	84.6
13	48	52	56	48	52	56	48	51	56	51.9
14	59	69	62	59	68	61	59	68	62	63.0
15	90	99	91	91	99	93	91	99	93	94.0
16	39	40	39	39	40	39	40	41	40	39.7
18	46	50	49	46	50	49	46	50	48	48.2
19	86	111	123	85	104	115	86	104	116	103.3
20	51	51	45	52	51	45	56	53	46	50.0
21	63	65	67	63	66	68	63	67	67	65.4
22	56	57	58	50	52	52	52	54	53	53.8
23	70	66	62	70	66	61	69	65	61	65.6
24	59	55	60	58	54	59	58	54	60	57.4
25	90	83	86	88	82	84	90	83	86	85.8
26	71	95	113	70	92	110	70	92	109	91.3
27	77	80	80	78	80	80	76	78	78	78.6
28	45	37	36	44	36	36	44	35	34	38.6
29	43	49	72	42	48	70	44	50	71	54.3
30	63	71	64	65	72	65	68	75	68	67.9

B) 0.4s exposure time

Rib	Underwater fluorescence values, 0.4s exposure time, orange filter									Avg.
	Photograph 1			Photograph 2			Photograph 3			
	ROI 1	ROI 2	ROI 3	ROI 1	ROI 2	ROI 3	ROI 1	ROI 2	ROI 3	
1	55	57	57	56	57	56	55	56	56	56.1
2	37	40	38	36	40	37	37	40	37	38.0
3	37	41	42	37	41	42	35	40	41	39.6
4	52	55	54	51	54	53	50	54	51	52.7
5	26	26	26	25	26	25	26	26	25	25.7
6	30	32	32	30	32	32	28	30	32	30.9
7	47	51	49	44	49	48	45	49	48	47.8
8	42	43	41	42	42	41	42	43	41	41.9
9	38	39	38	37	39	38	36	39	37	37.9
10	18	19	19	18	18	18	17	18	18	18.1
11	59	60	59	59	60	59	59	59	59	59.2
12	60	60	57	60	60	56	60	60	57	58.9
13	28	31	35	28	31	35	27	30	35	31.1
14	41	46	40	40	46	41	39	46	41	42.2
15	57	64	57	57	64	57	56	63	56	59.0
16	22	24	24	23	25	24	25	25	25	24.1
18	29	32	30	28	30	28	29	31	30	29.7
19	64	92	104	63	90	105	62	88	105	85.9
20	37	37	36	36	36	31	36	35	31	35.0
21	43	45	48	43	45	47	43	46	47	45.2
22	39	41	40	38	40	39	35	36	36	38.2
23	44	42	39	44	42	39	45	43	40	42.0
24	37	36	39	38	36	39	37	35	39	37.3
25	55	57	51	55	56	51	57	59	53	54.9
26	48	67	86	48	68	84	47	65	82	66.1
27	54	56	55	54	55	55	54	55	54	54.7
28	29	24	24	29	23	22	30	23	23	25.2
29	32	35	46	32	35	46	31	35	46	37.6
30	45	52	49	47	53	48	48	53	47	49.1

C) 1/3s exposure time

Rib	Underwater fluorescence values, 1/3s exposure time, orange filter									Avg.
	Photograph 1			Photograph 2			Photograph 3			
	ROI 1	ROI 2	ROI 3	ROI 1	ROI 2	ROI 3	ROI 1	ROI 2	ROI 3	
1	136	139	136	136	138	136	136	138	135	136.7
2	86	89	86	86	89	87	86	89	88	87.3
3	78	83	85	77	83	85	77	83	85	81.8
4	81	89	101	81	90	101	81	89	101	90.4
5	58	57	61	58	57	61	58	57	60	58.6
6	76	82	85	77	83	85	77	82	85	81.3
7	127	136	133	127	136	134	127	136	135	132.3
8	71	78	81	71	78	81	70	77	80	76.3
9	85	96	103	85	96	103	84	96	103	94.6
10	59	58	70	56	59	69	56	59	69	61.7
11	104	102	92	103	103	92	103	101	92	99.1
12	137	128	115	137	128	114	137	128	114	126.4
13	90	94	89	89	92	88	88	92	88	90.0
14	140	139	119	139	138	118	139	138	118	132.0
15	158	151	138	158	151	139	157	150	138	148.9
16	76	81	57	75	79	56	75	79	56	70.4
18	120	122	112	119	121	111	119	121	111	117.3
19	78	84	79	76	83	79	78	84	79	80.0
20	176	183	199	176	183	198	176	183	199	185.9
21	119	132	134	117	131	134	118	131	134	127.8
22	144	134	114	144	134	114	143	133	114	130.4
23	133	135	135	133	135	135	133	134	135	134.2
24	144	142	149	145	142	149	145	143	149	145.3
25	141	144	148	141	143	148	141	143	147	144.0
26	122	120	121	122	120	121	121	120	120	120.8
27	146	178	200	146	178	200	147	179	200	174.9
28	108	109	103	109	111	105	111	114	106	108.4
29	60	57	79	60	58	80	60	57	78	65.4
30	95	109	133	95	111	134	94	113	134	113.1

Appendix 40: Recorded measurements of porcine ribs (*Sus Scrofa Domesticus*) used for section B research question 1

Rib measurements				
Rib	Mass (g)	Length (mm)	Width (mm)	AVP (mm)
1	26.55	120.9	16.2	10.7
2	18.47	102.9	15.5	9.5
3	25.46	101	16.8	8.1
4	15.59	113.9	13.6	8.3
5	22.89	116.8	17.6	8.6
6	11.95	101.7	12.1	7.3
7	28.07	118.5	16.4	11.1
8	23.95	120.8	15.8	10.4
9	14.45	112.6	12.7	8.3
10	29.89	125.2	19.6	9.8
11	23.64	119.7	22.8	6.9
12	28.22	110.5	27	8.7
13	9.92	95.7	10.7	7.7
14	14	98.9	13	8.6
15	21.27	85.3	17.3	17.1
16	26.06	114.5	10.5	16.9
18	17	109.3	15.7	9
19	29.52	114.6	20.2	12.4
20	20.34	115.2	13.5	9.6
21	22.62	93.4	18.2	13.5
22	14.89	110.9	13.4	7.8
23	11.75	92.6	12.8	8.1
24	15.39	105.5	13.6	9.6
25	8.56	84.4	9.3	7.9
26	9.45	73.4	13.5	6.9
27	9	85.7	12.9	7.3
28	11.63	78.4	10.1	10.4
29	9.5	78.2	12.8	7.2
30	8.72	75.2	6.8	12.2
Average	18.23	102.61	19.87	9.65
Max	29.89	125.2	162	17.1
Min	8.56	73.4	6.8	6.9
SD	7.04	15.23	27.17	2.60
Range	21.33	51.8	155.2	10.2

Appendix 41: Graphical comparisons examining the relationship between average autofluorescence of the 29 porcine ribs (*Sus scrofa domesticus*) produced using the Crime-lite 2, in each of the deposition contexts and photography configurations, in comparison to the bone dimensions.

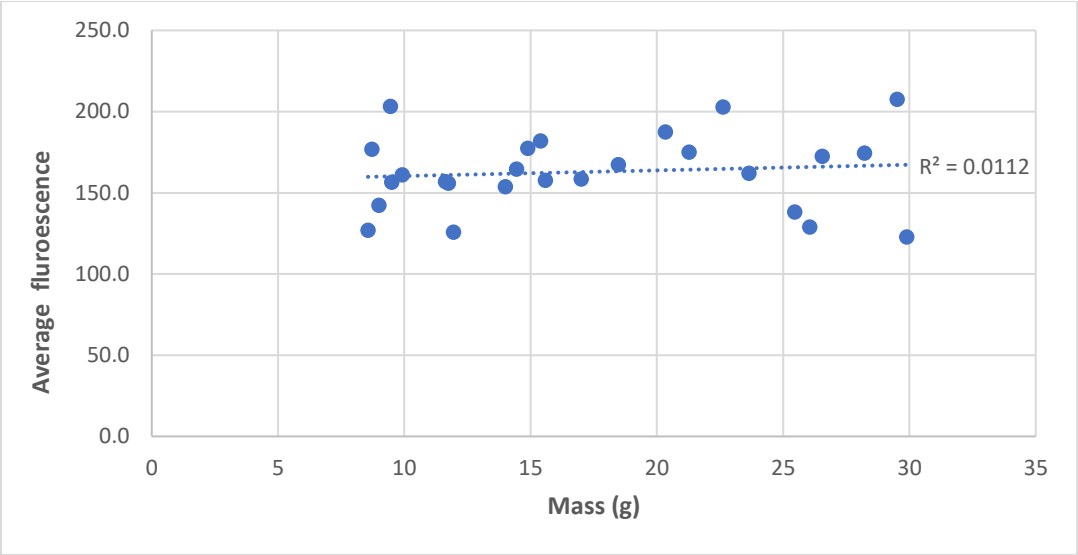

Comparison between mass and terrestrial fluorescence taken with the orange filter, 0.6s

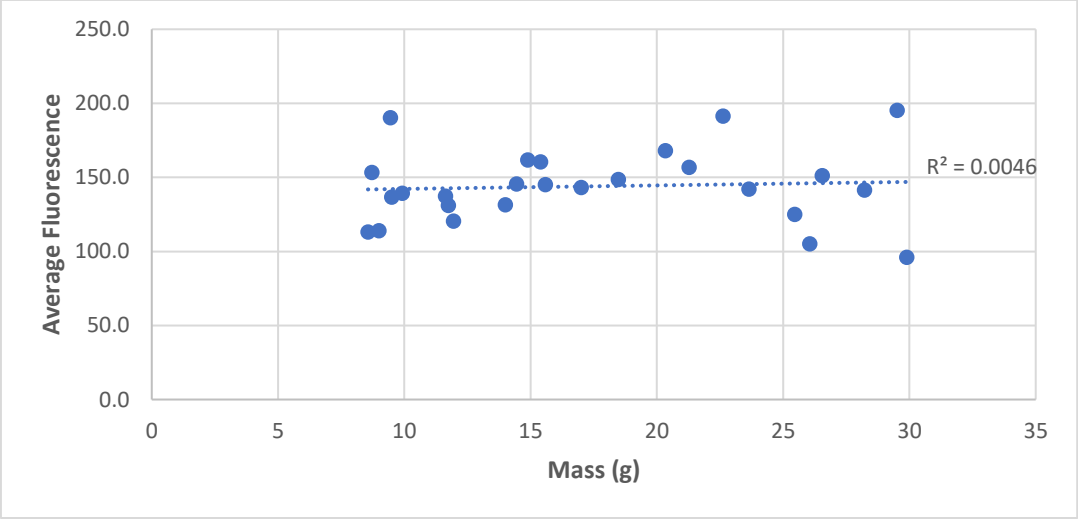

Comparison between mass and terrestrial fluorescence taken with the orange filter, 0.4s

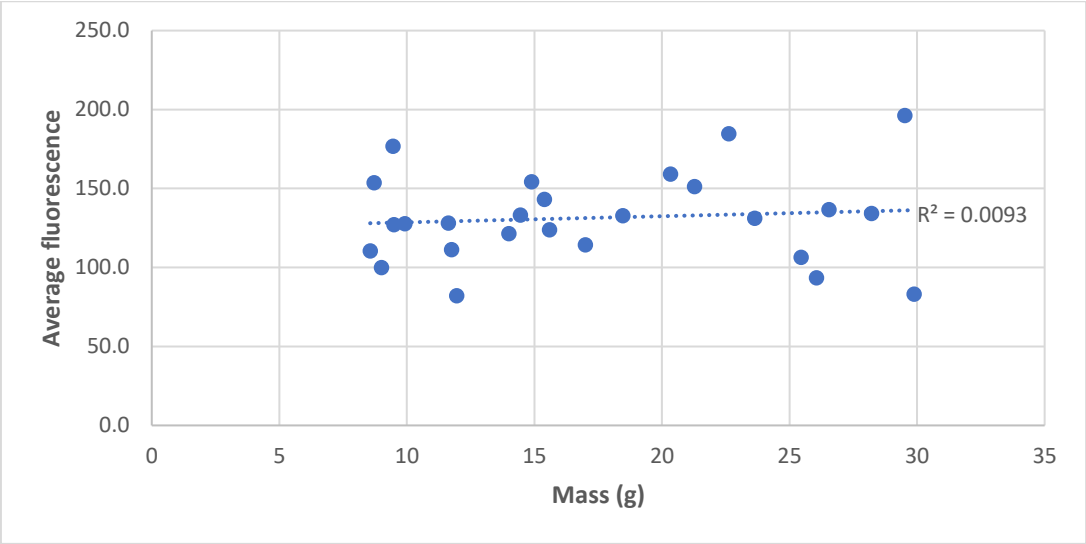

Comparison between mass and terrestrial fluorescence taken with the orange filter, 1/3s

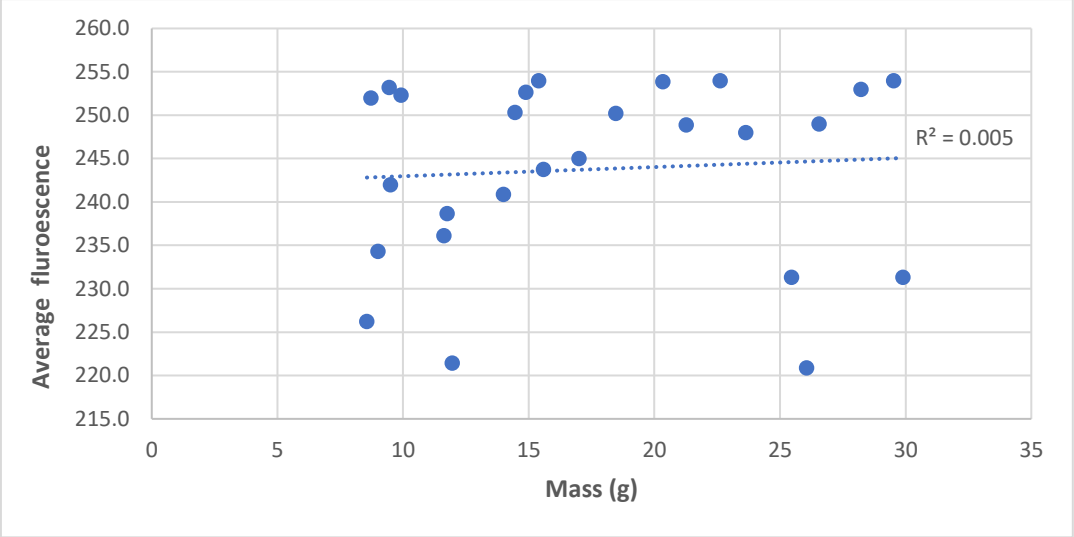

Comparison between mass and terrestrial fluorescence taken with the yellow filter, 0.6s

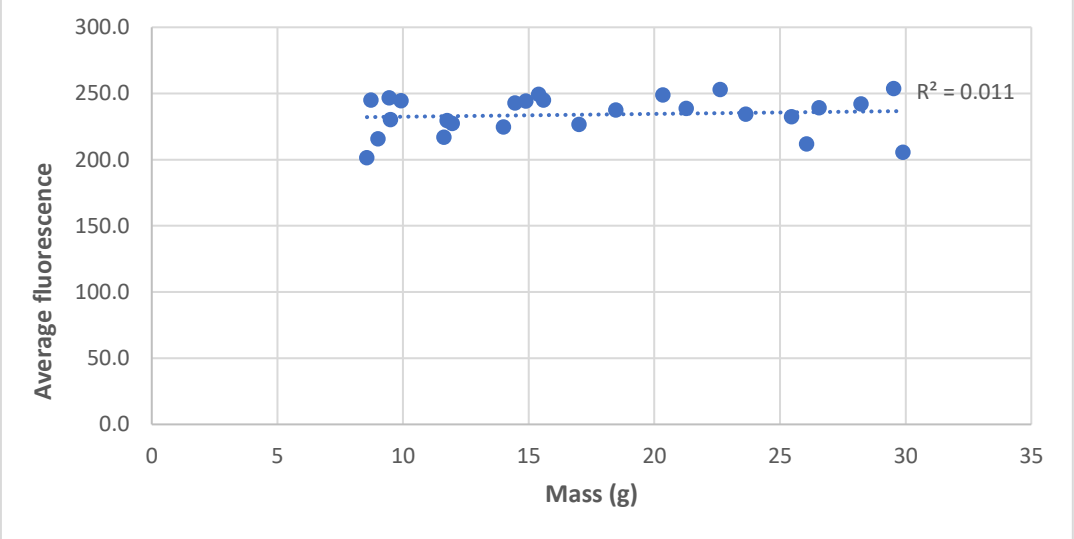

Comparison between mass and terrestrial fluorescence taken with the yellow filter, 0.4s

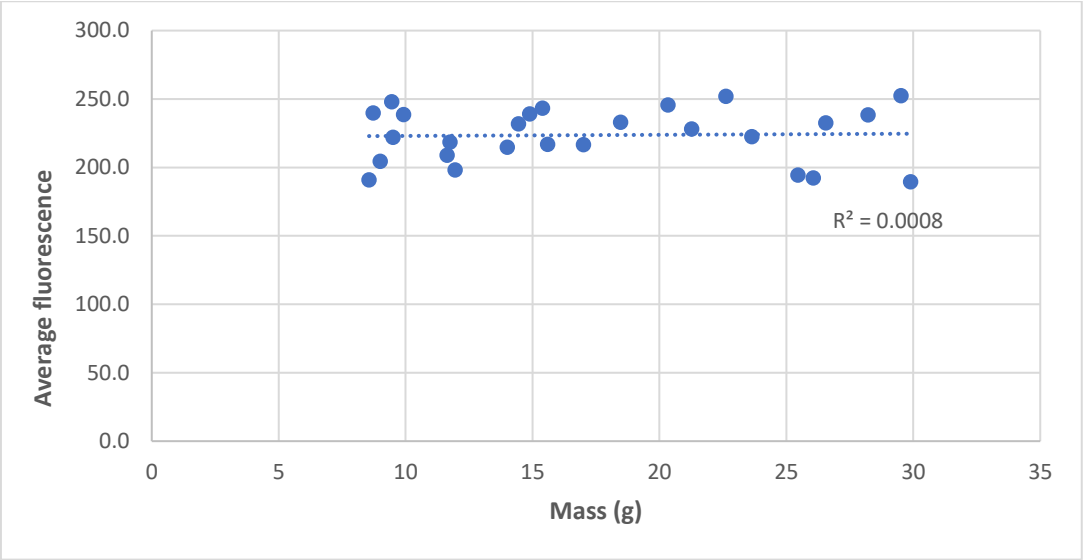

Comparison between mass and terrestrial fluorescence taken with the yellow filter, 1/3s

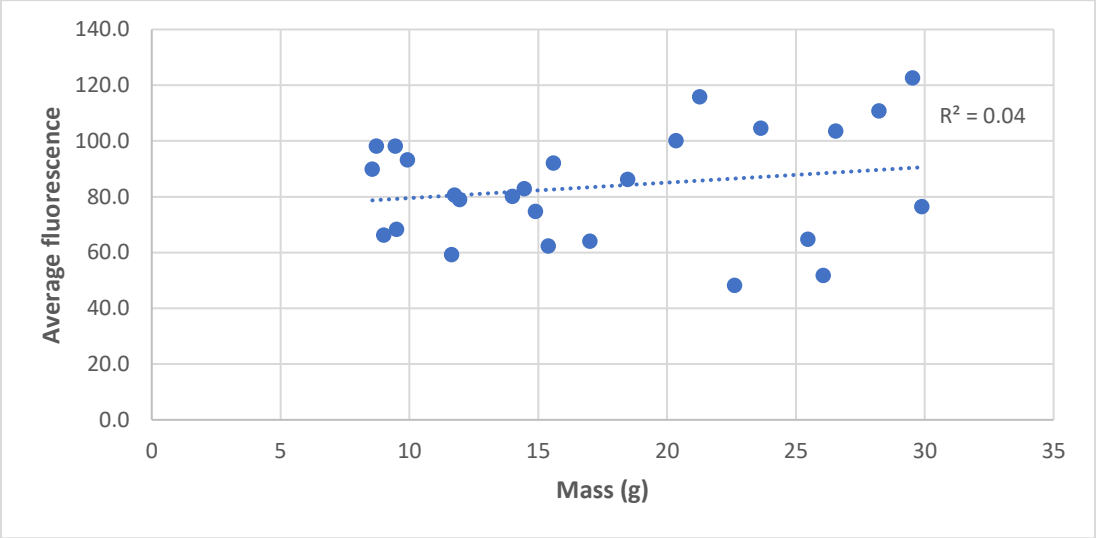

Comparison between mass and underwater fluorescence taken with the orange filter, 0.6s

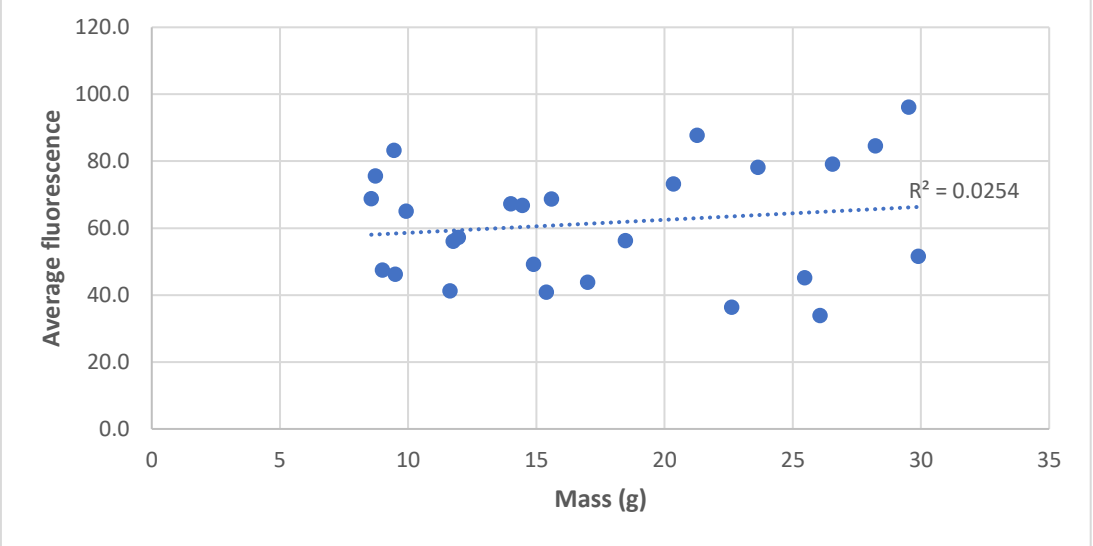

Comparison between mass and underwater fluorescence taken with the orange filter, 0.4s

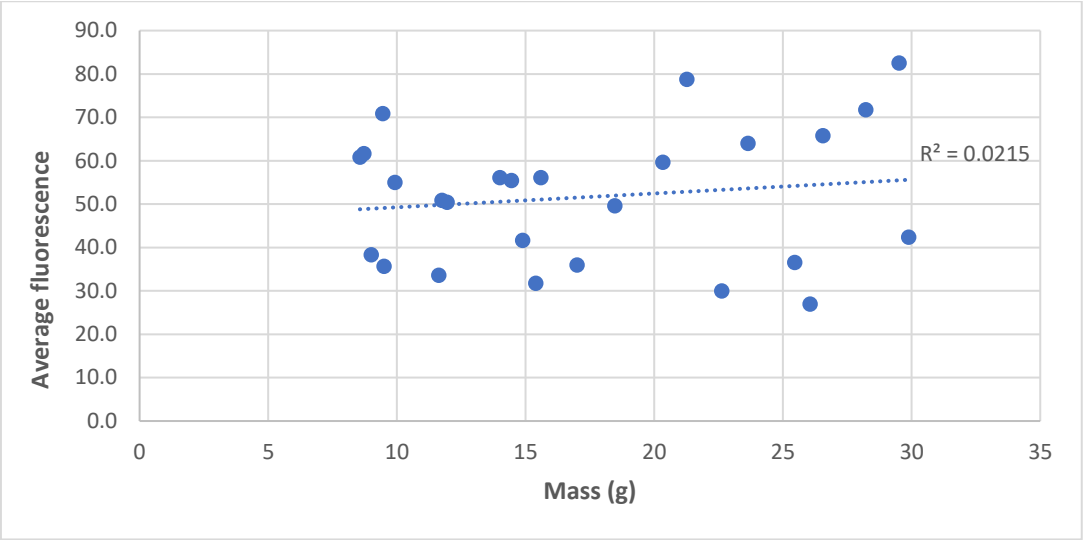

Comparison between mass and underwater fluorescence taken with the orange filter, 1/3s

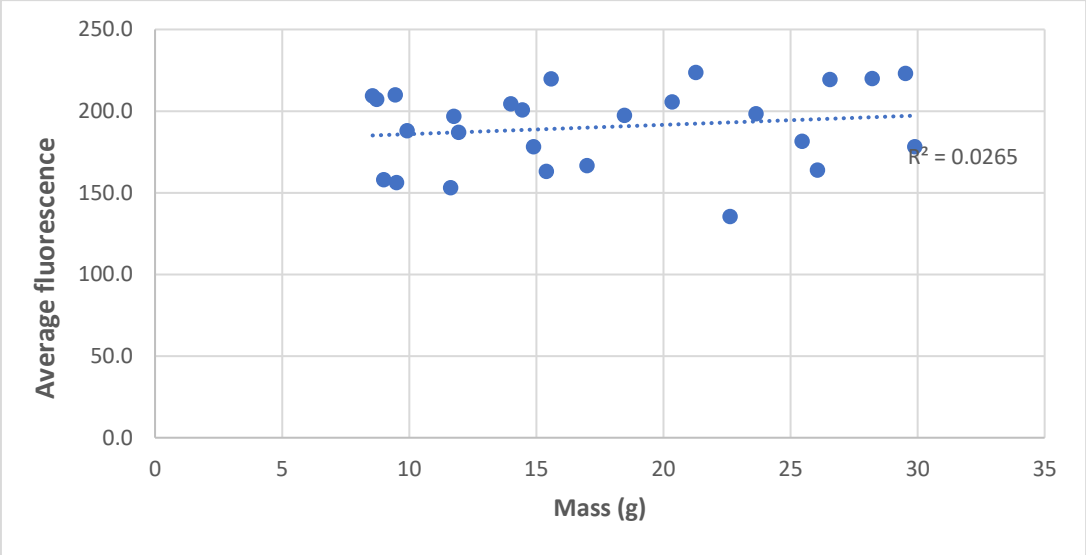

Comparison between mass and underwater fluorescence taken with the yellow filter, 0.6s

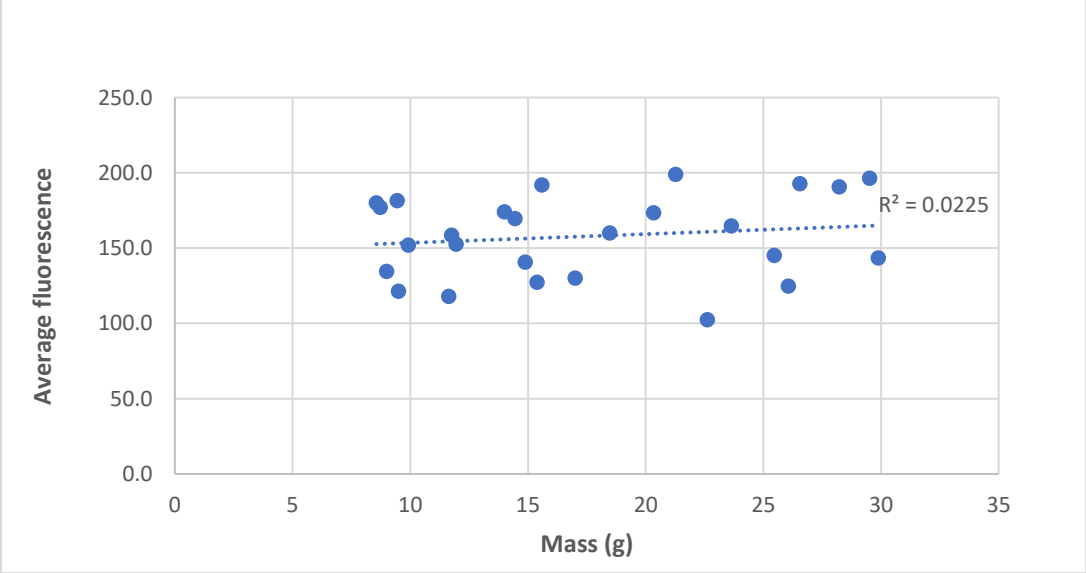

Comparison between mass and underwater fluorescence taken with the yellow filter, 0.4s

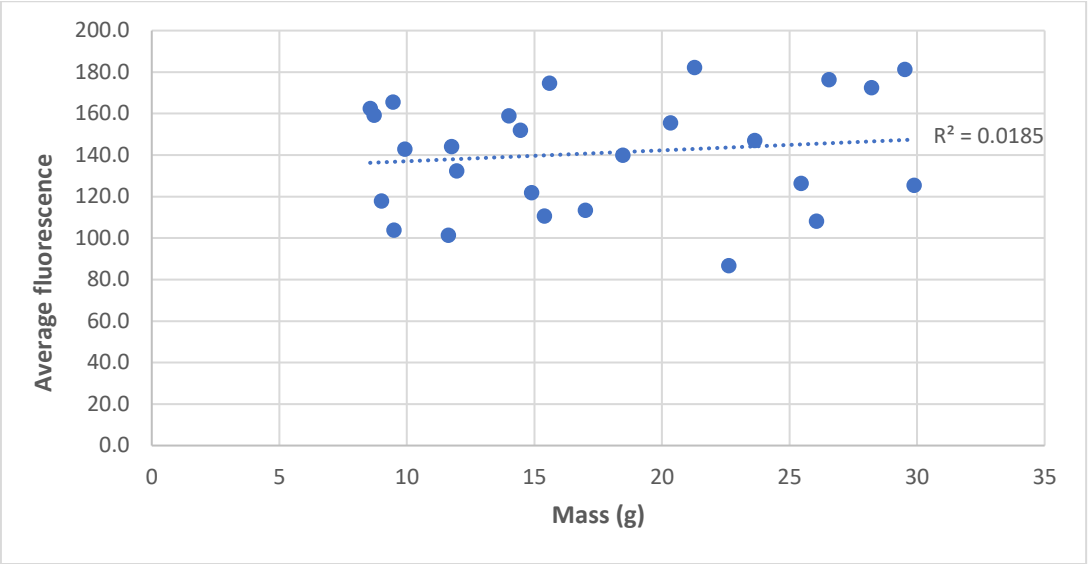

Comparison between mass and underwater fluorescence taken with the yellow filter, 1/3s

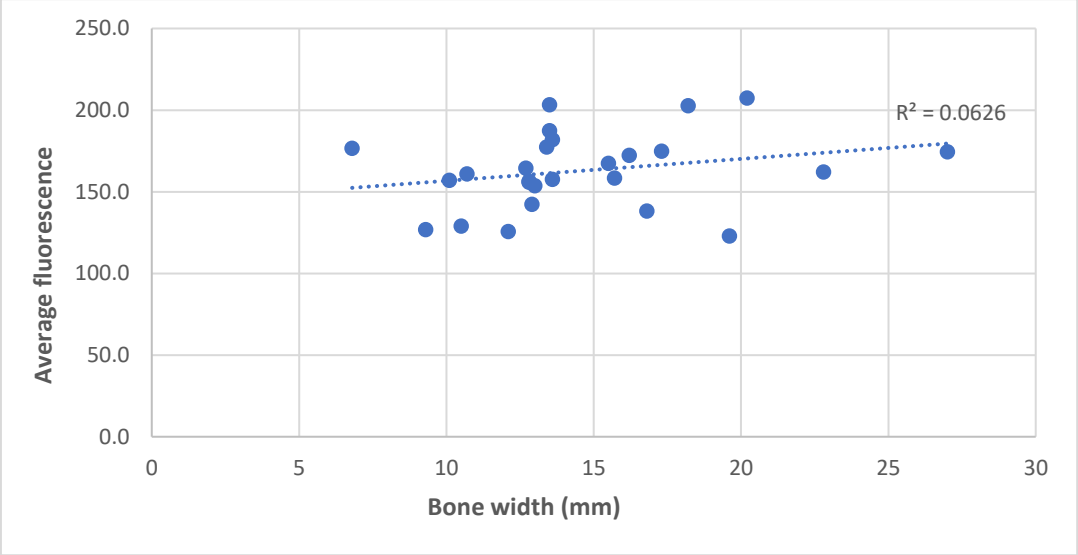

Comparison between bone width and terrestrial fluorescence taken with the orange filter, 0.6s

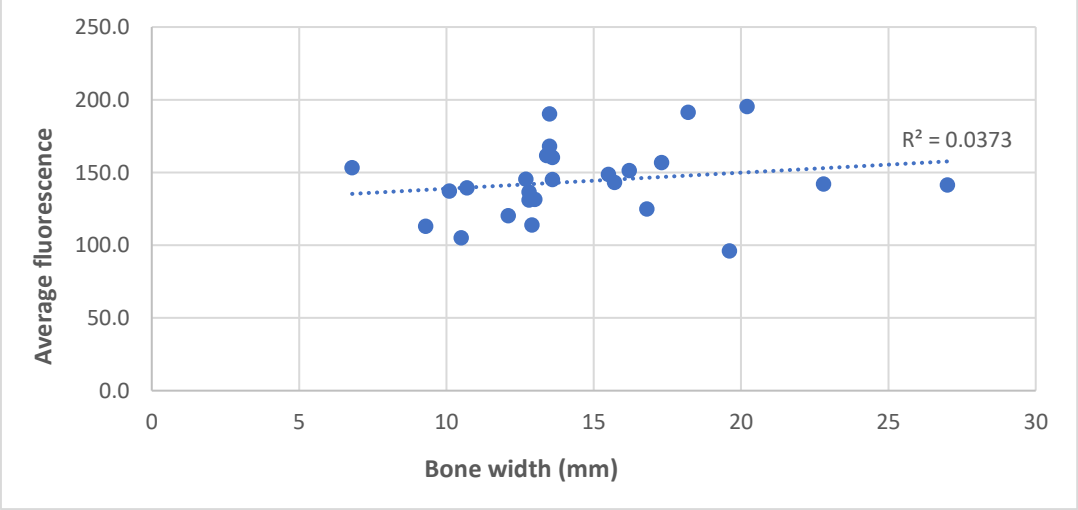

Comparison between bone width and terrestrial fluorescence taken with the orange filter, 0.4s

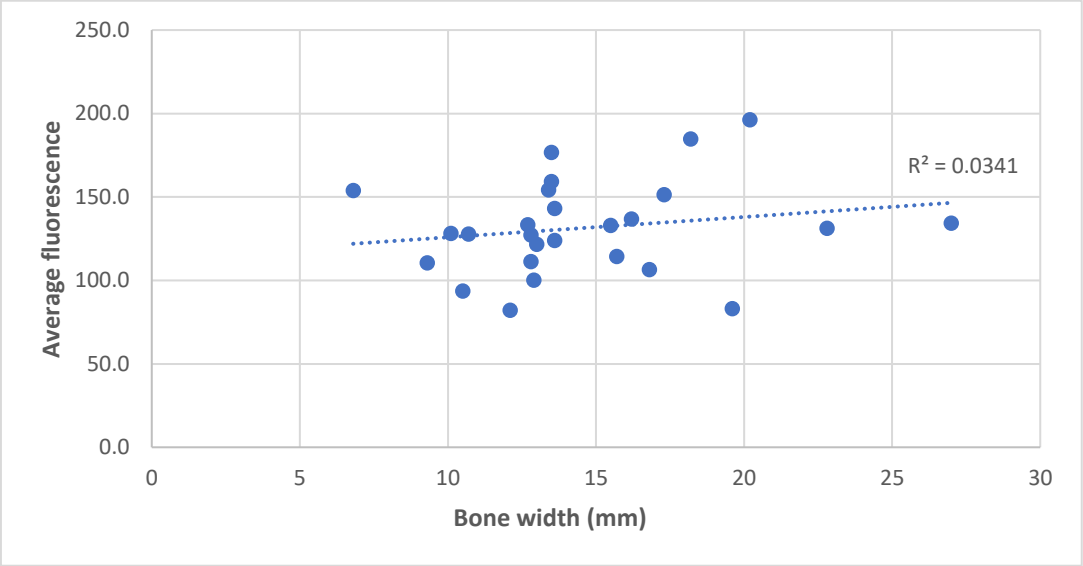

Comparison between bone width and terrestrial fluorescence taken with the orange filter, 1/3s

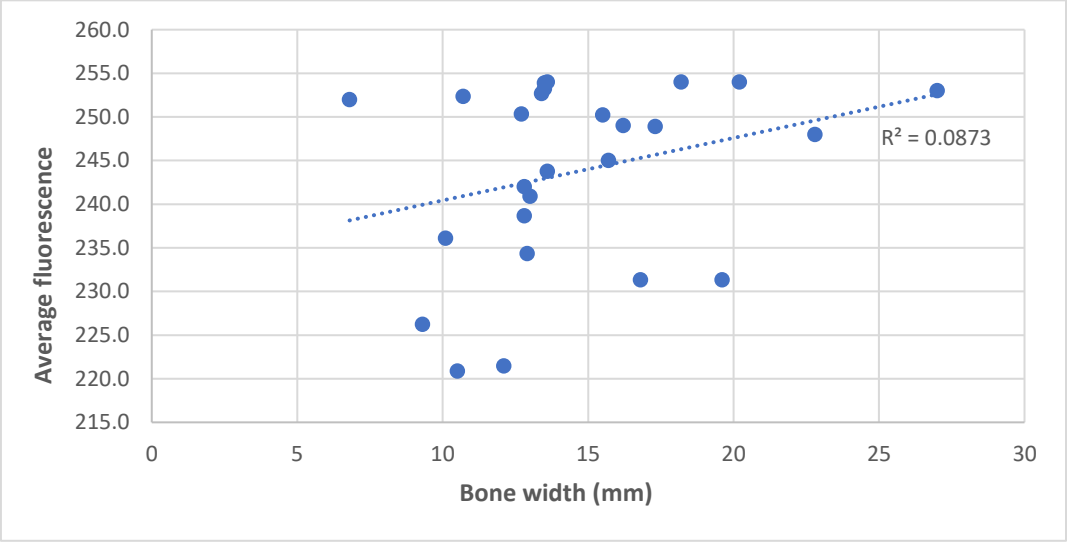

Comparison between bone width and terrestrial fluorescence taken with the yellow filter, 0.6s

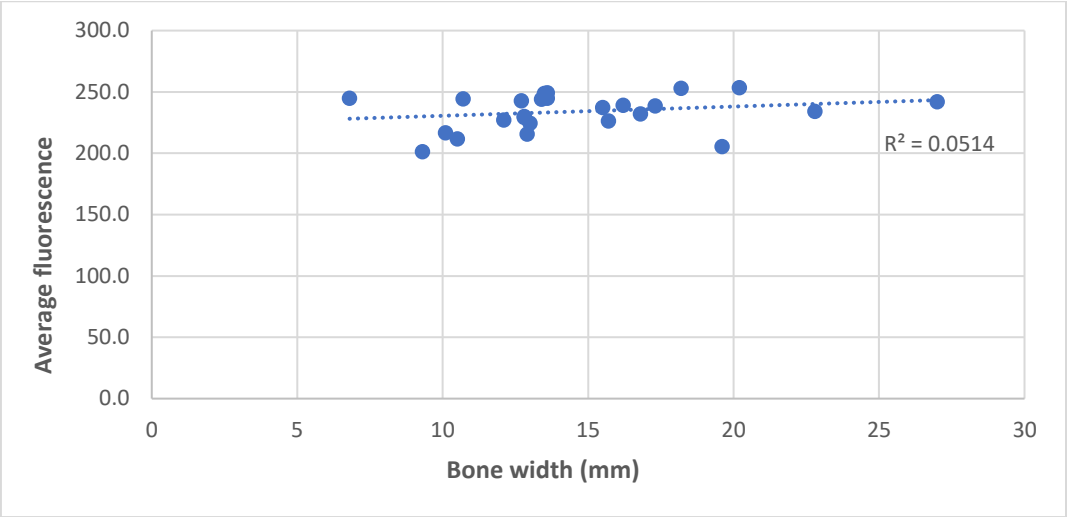

Comparison between bone width and terrestrial fluorescence taken with the yellow filter, 0.4s

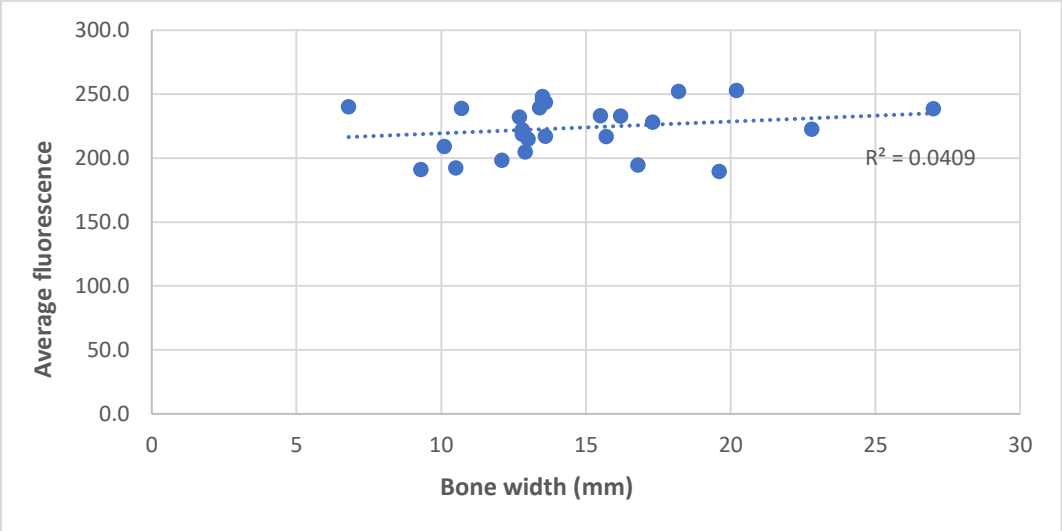

Comparison between bone width and terrestrial fluorescence taken with the yellow filter, 1/3s

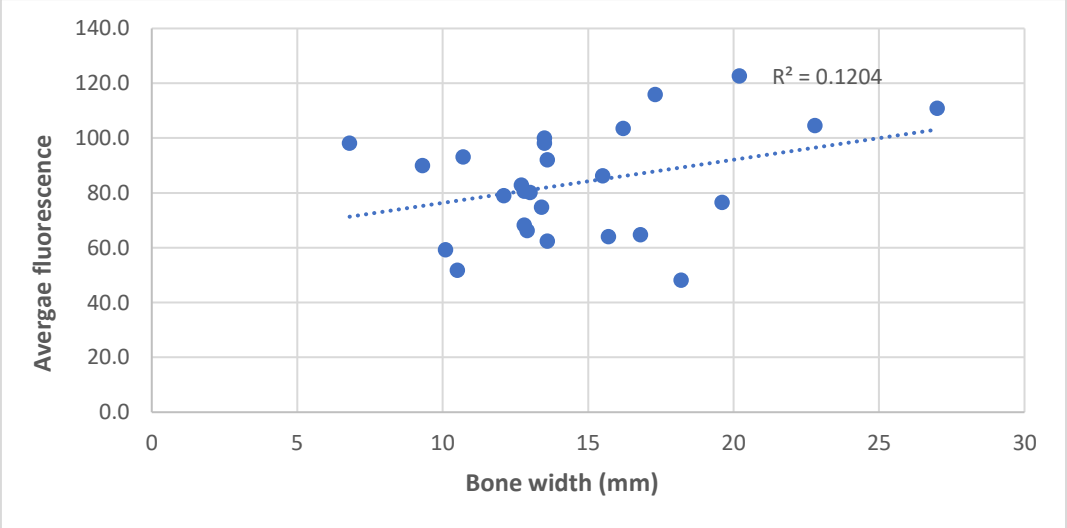

Comparison between bone width and underwater fluorescence taken with the orange filter, 0.6s

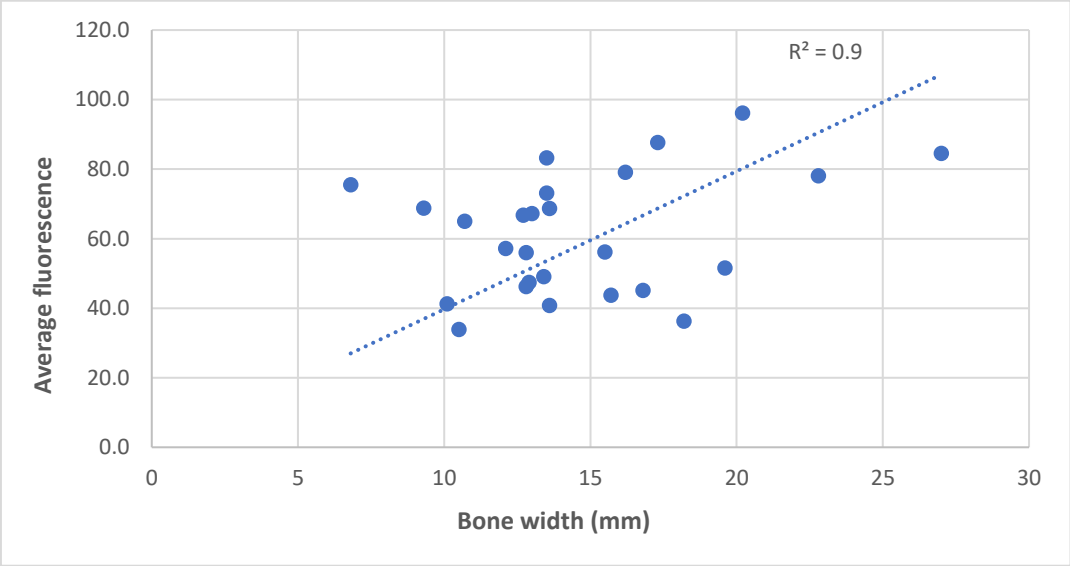

Comparison between bone width and underwater fluorescence taken with the orange filter, 0.4s

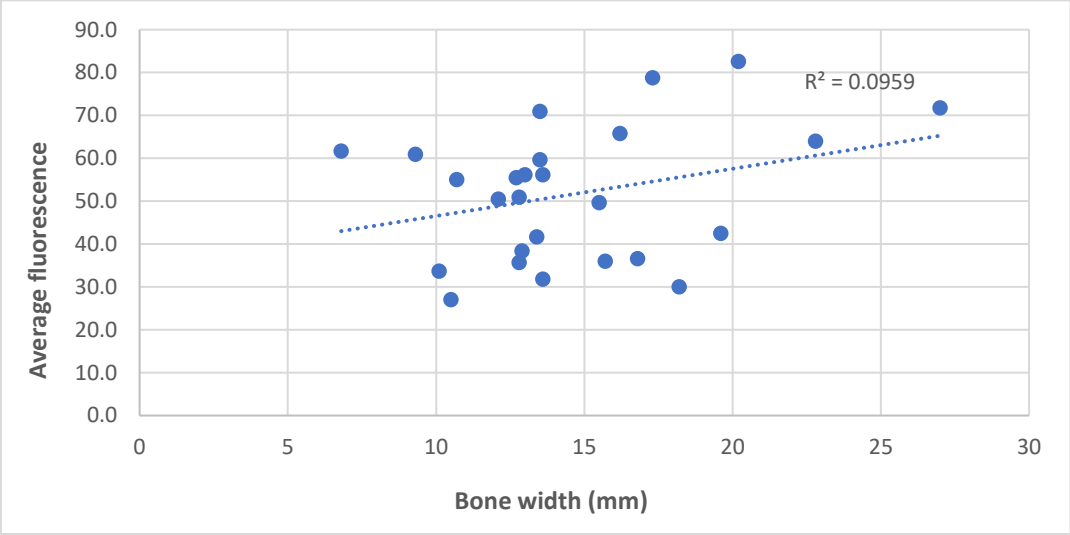

Comparison between bone width and underwater fluorescence taken with the orange filter, 1/3s

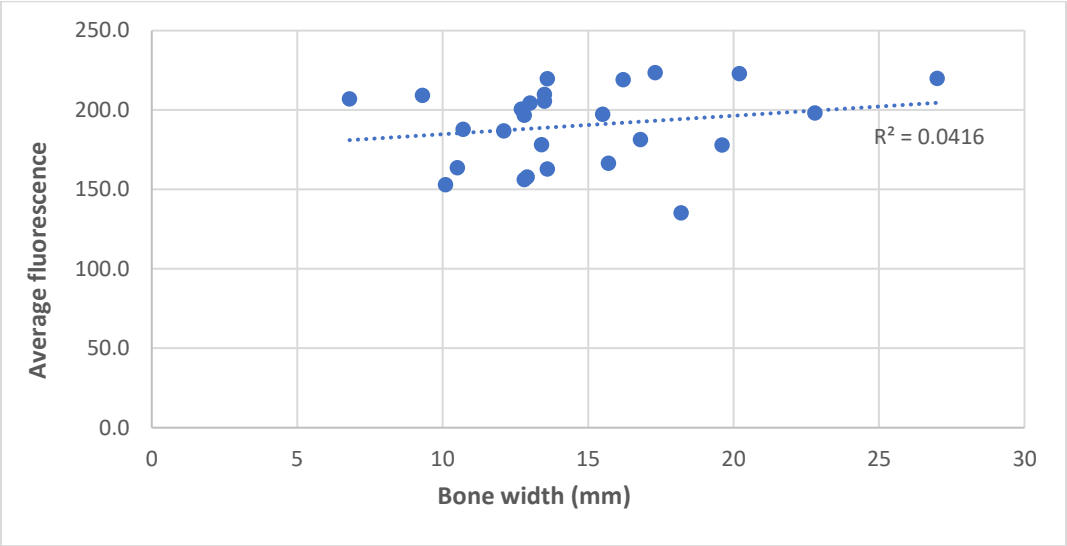

Comparison between bone width and underwater fluorescence taken with the yellow filter, 0.6s

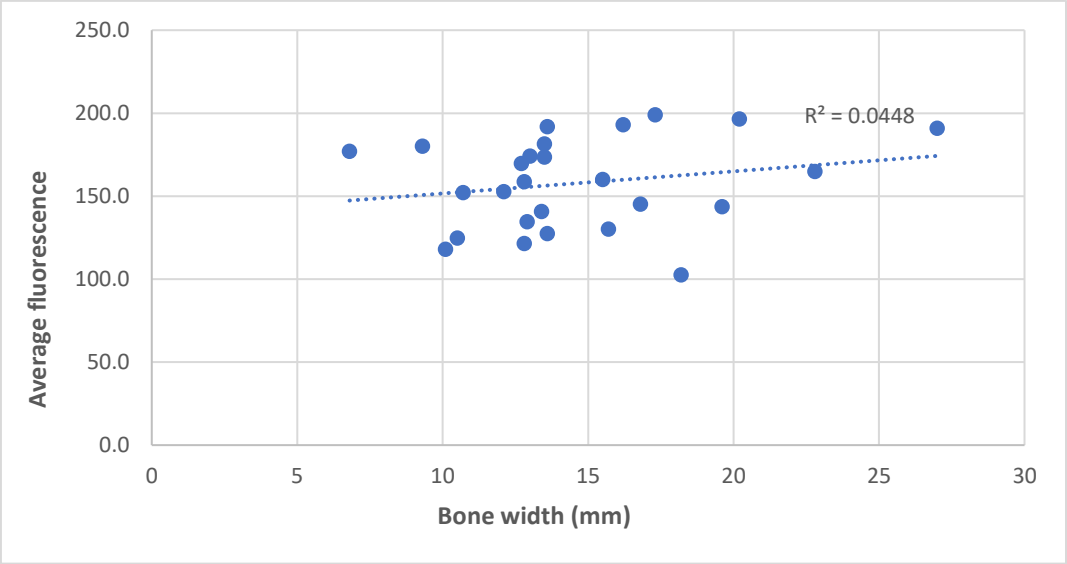

Comparison between bone width and underwater fluorescence taken with the yellow filter, 0.4s

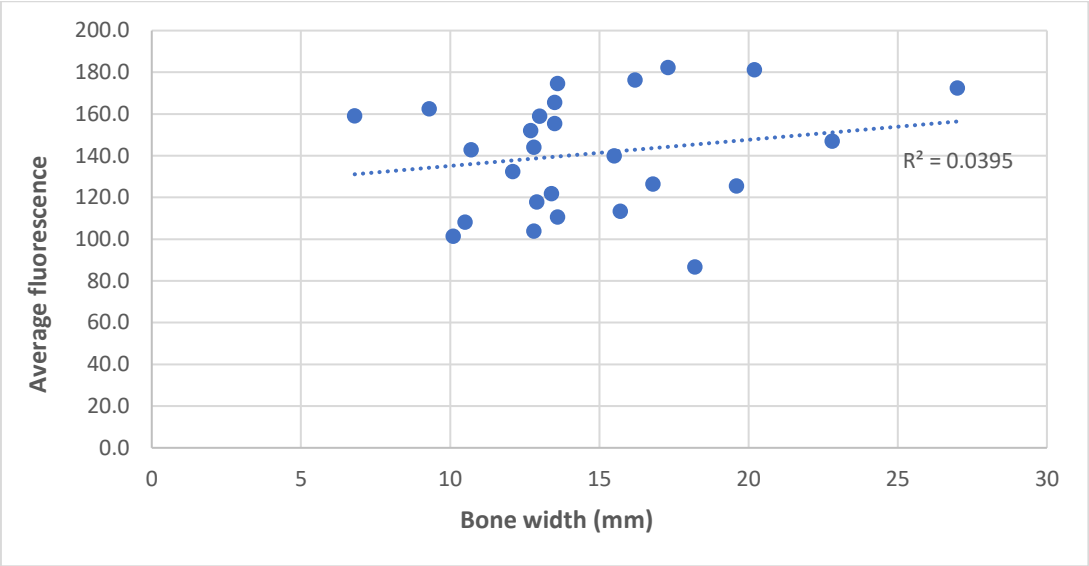

Comparison between bone width and underwater fluorescence taken with the yellow filter, 1/3s

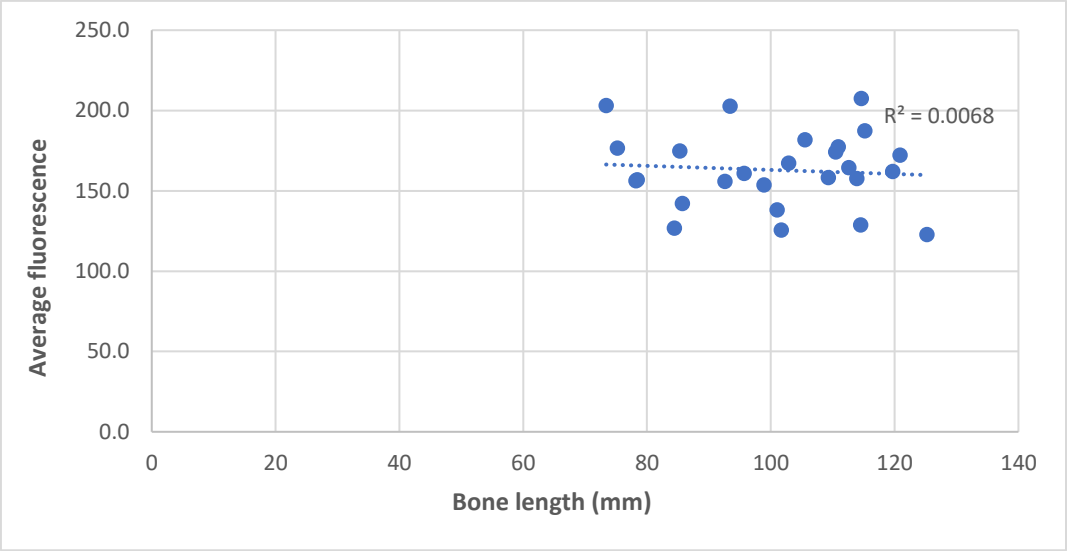

Comparison between bone length and terrestrial fluorescence taken with the orange filter, 0.6s

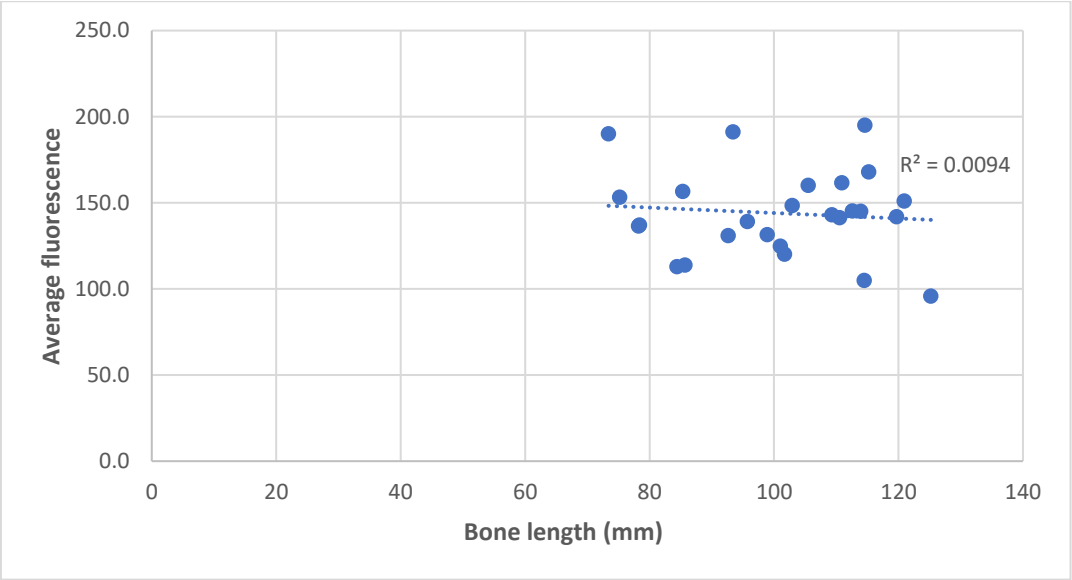

Comparison between bone length and terrestrial fluorescence taken with the orange filter, 0.4s

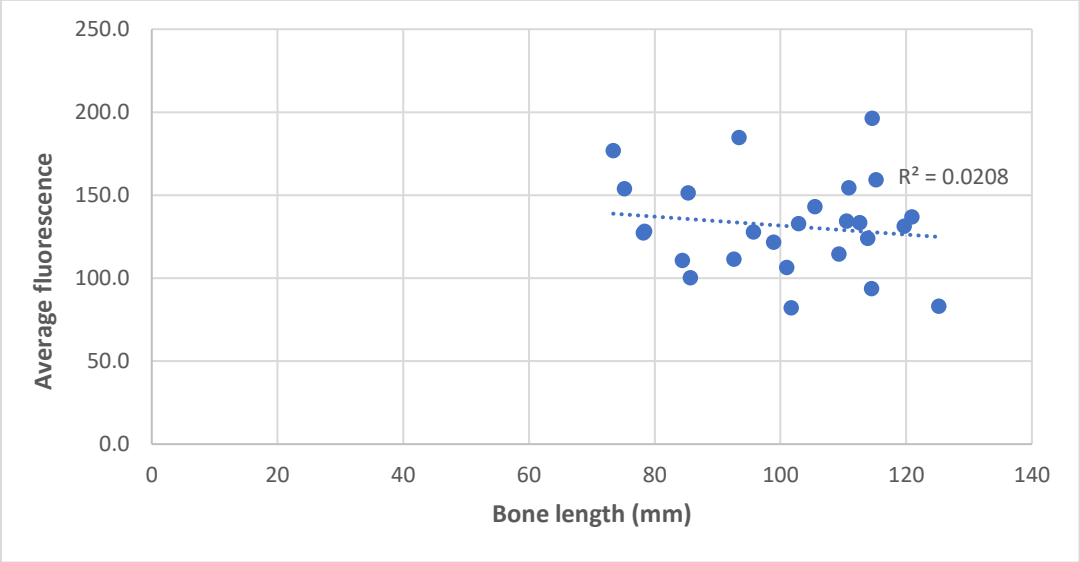

Comparison between bone length and terrestrial fluorescence taken with the orange filter, 1/3s

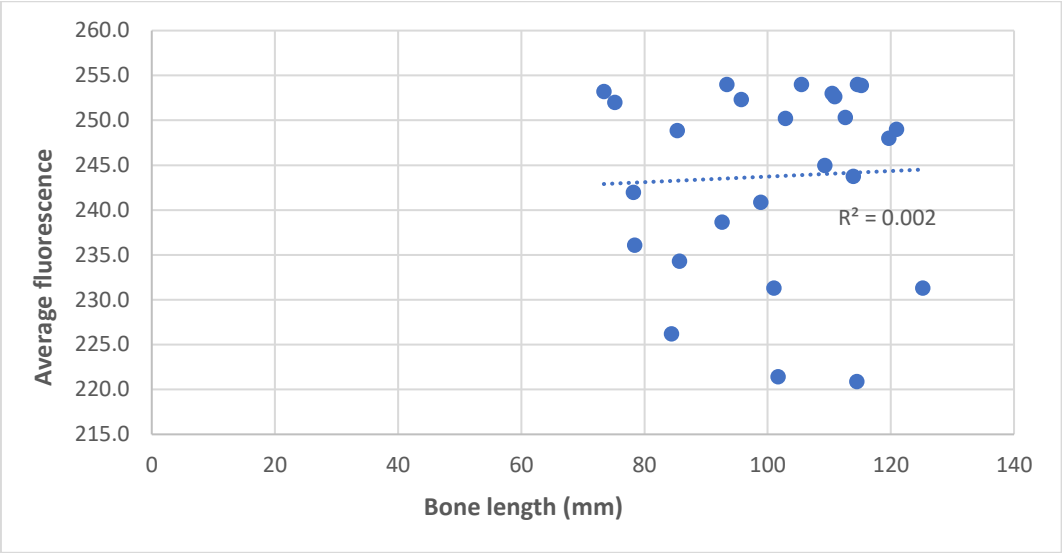

Comparison between bone length and terrestrial fluorescence taken with the yellow filter, 0.6s

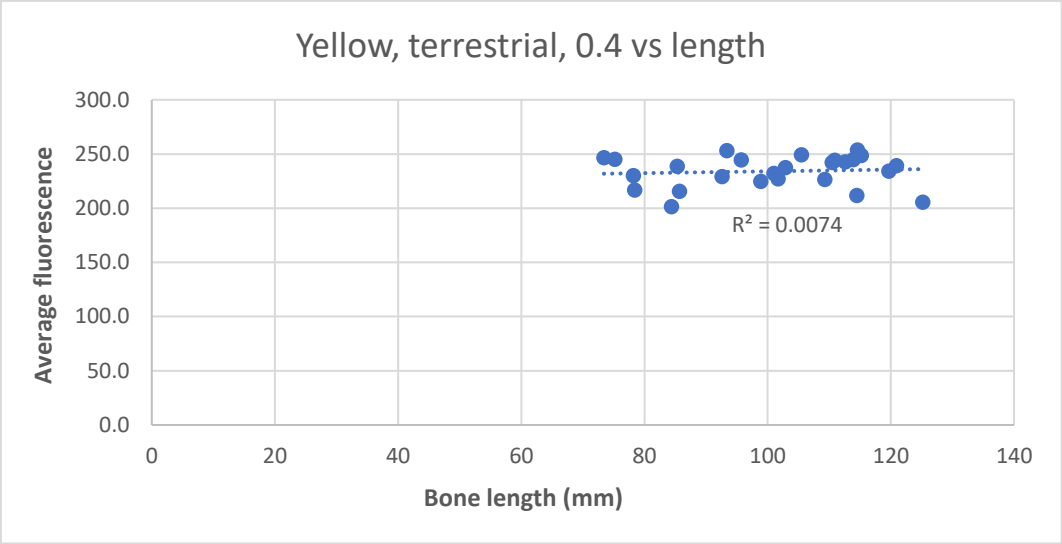

Comparison between bone length and terrestrial fluorescence taken with the yellow filter, 0.4s

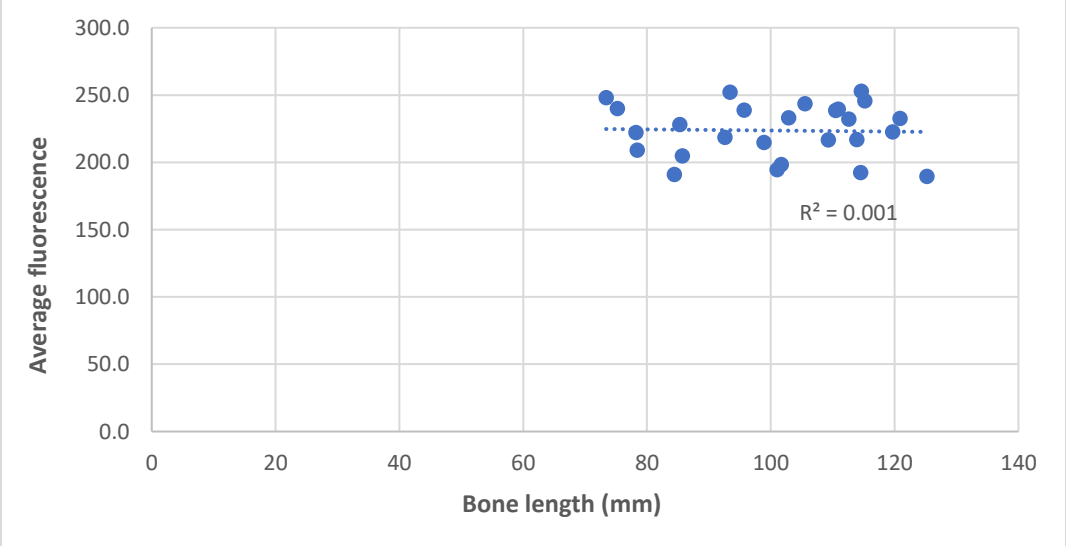

Comparison between bone length and terrestrial fluorescence taken with the yellow filter, 1/3s

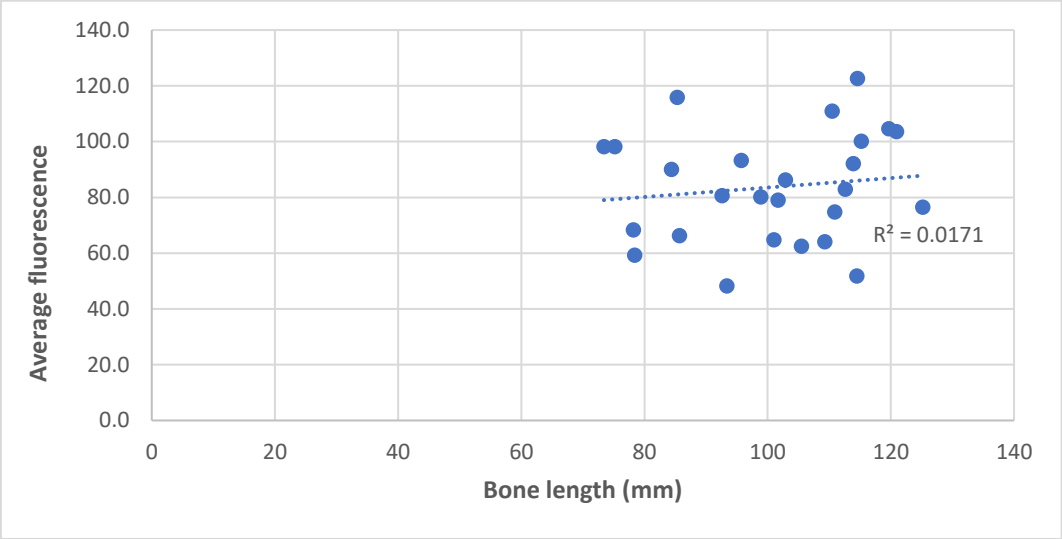

Comparison between bone length and underwater fluorescence taken with the orange filter, 0.6s

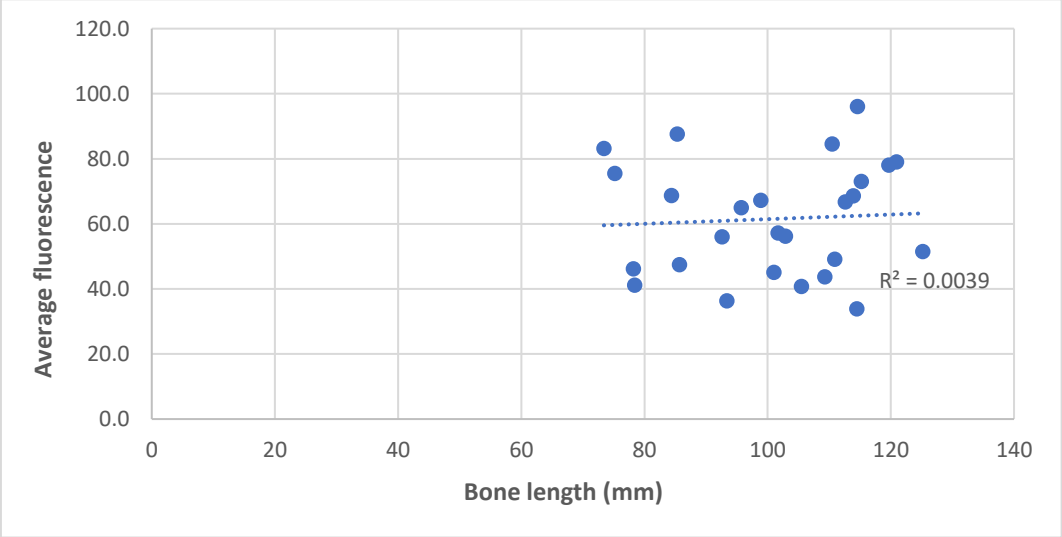

Comparison between bone length and underwater fluorescence taken with the orange filter, 0.4s

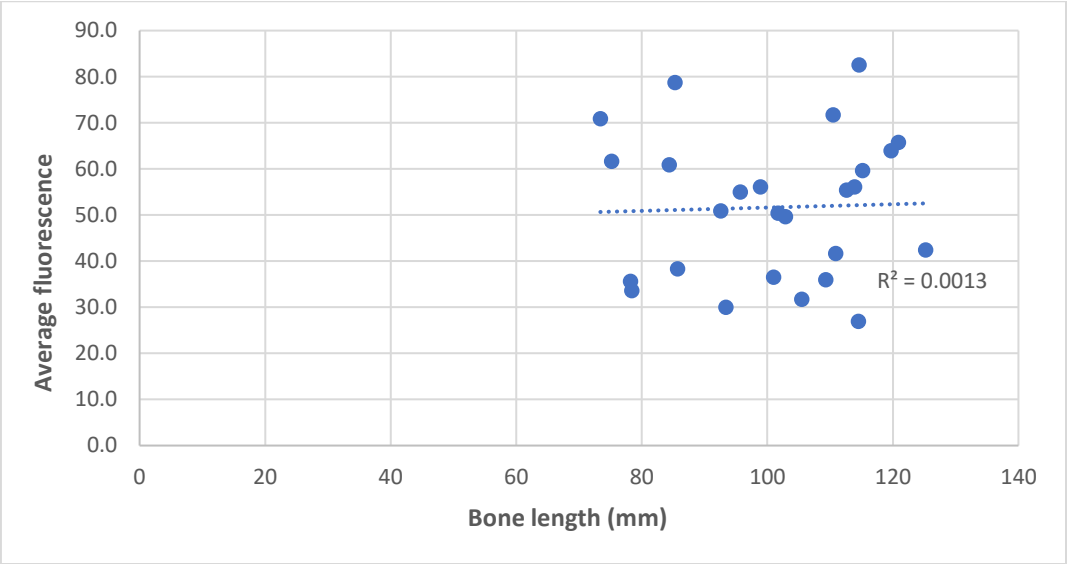

Comparison between bone length and underwater fluorescence taken with the orange filter, 1/3s

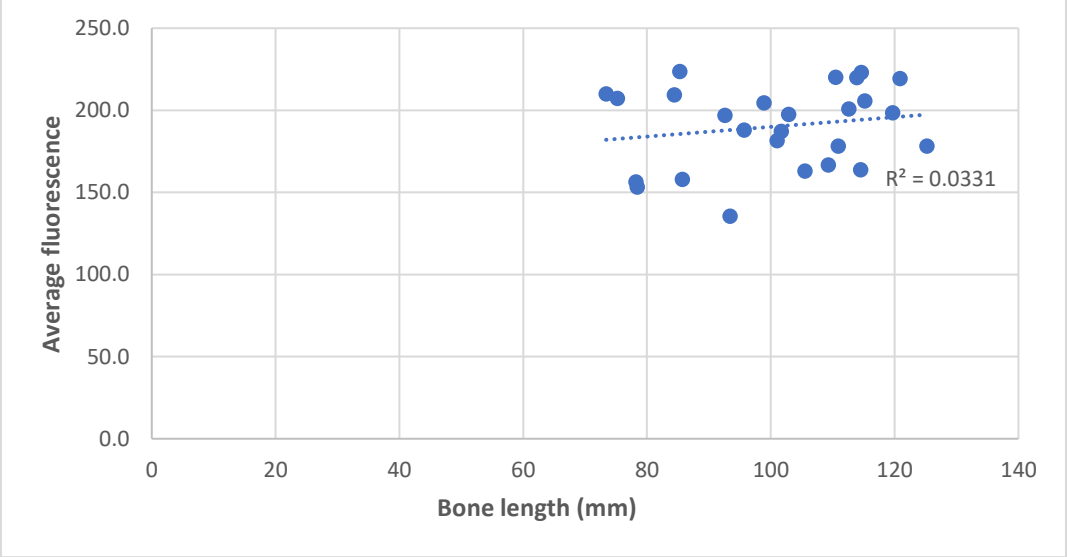

Comparison between bone length and underwater fluorescence taken with the yellow filter, 0.6s

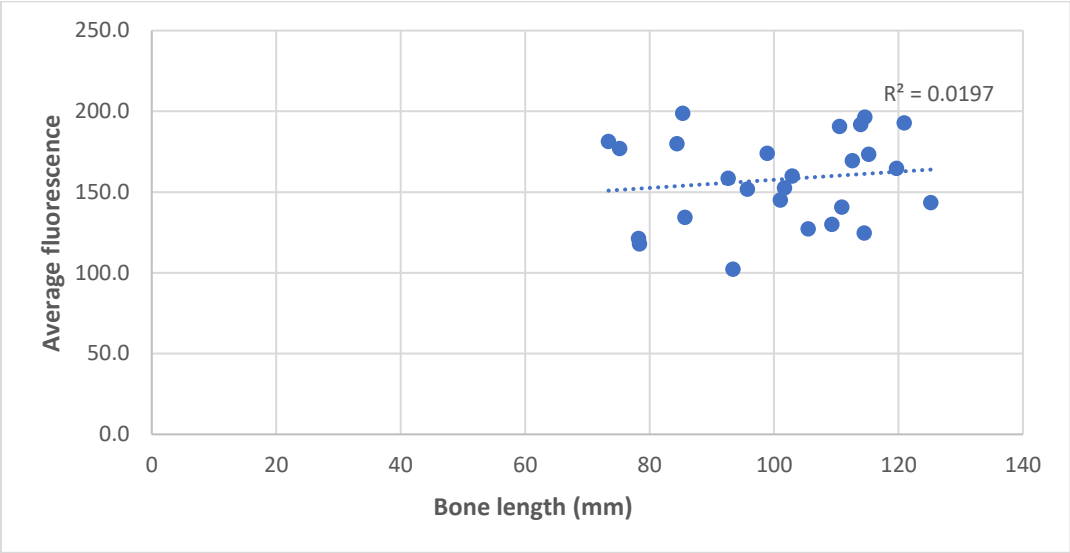

Comparison between bone length and underwater fluorescence taken with the yellow filter, 0.4s

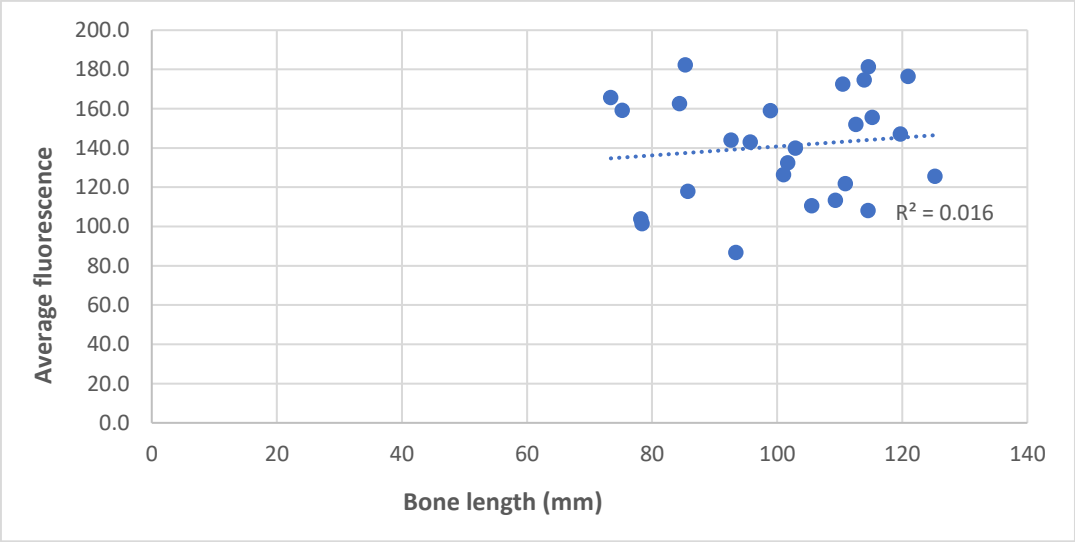

Comparison between bone length and underwater fluorescence taken with the yellow filter, 1/3s

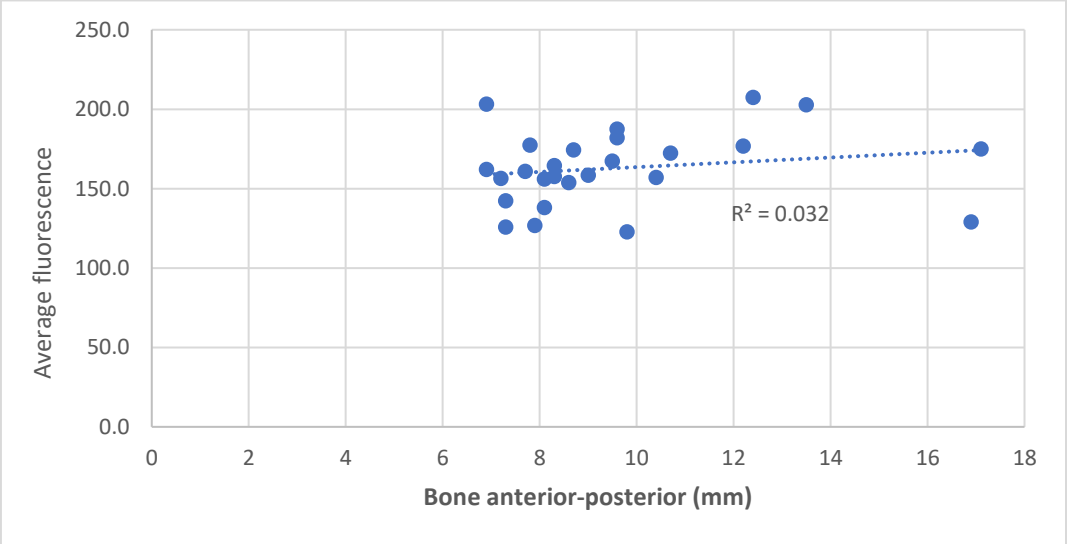

Comparison between bone anterior-posterior and terrestrial fluorescence taken with the orange filter, 0.6s

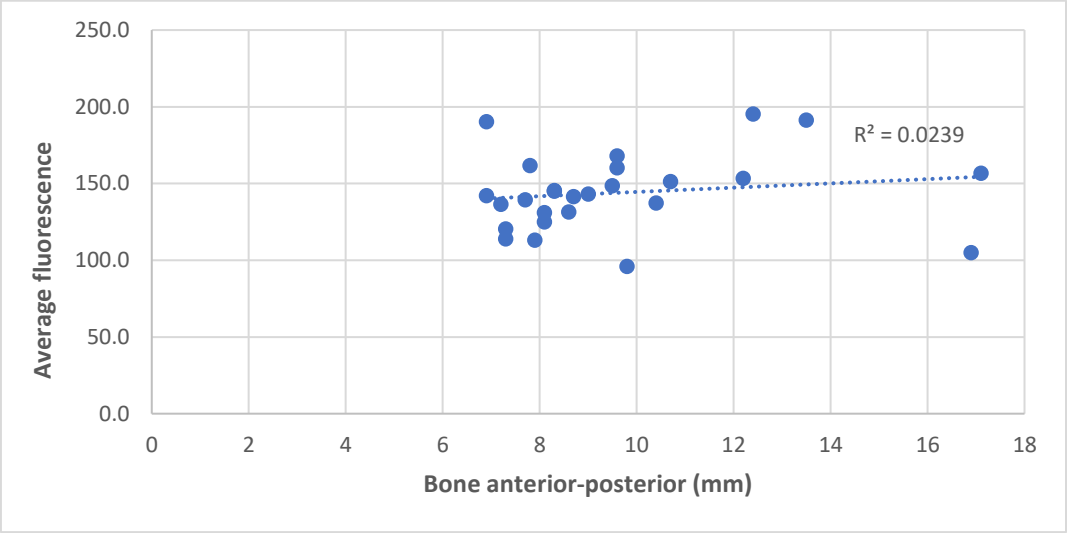

Comparison between bone anterior-posterior and terrestrial fluorescence taken with the orange filter, 0.4s

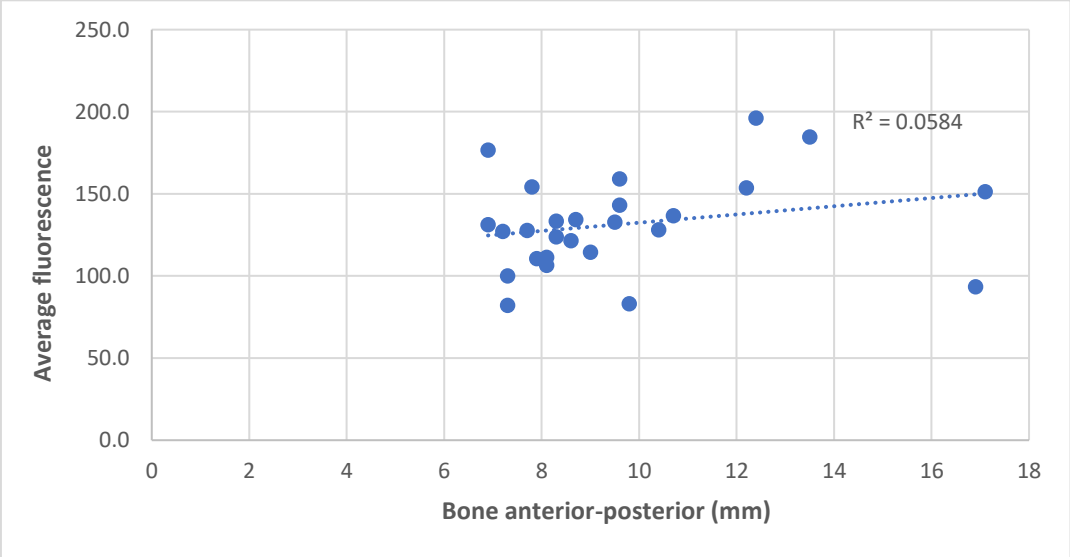

Comparison between bone anterior-posterior and terrestrial fluorescence taken with the orange filter, 1/3s

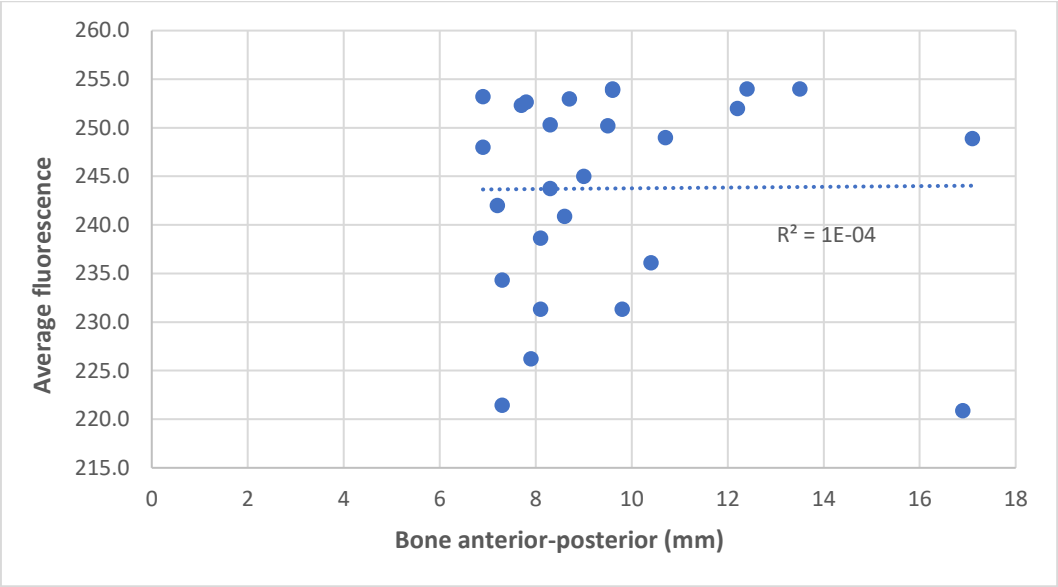

Comparison between bone anterior-posterior and terrestrial fluorescence taken with the yellow filter, 0.6s

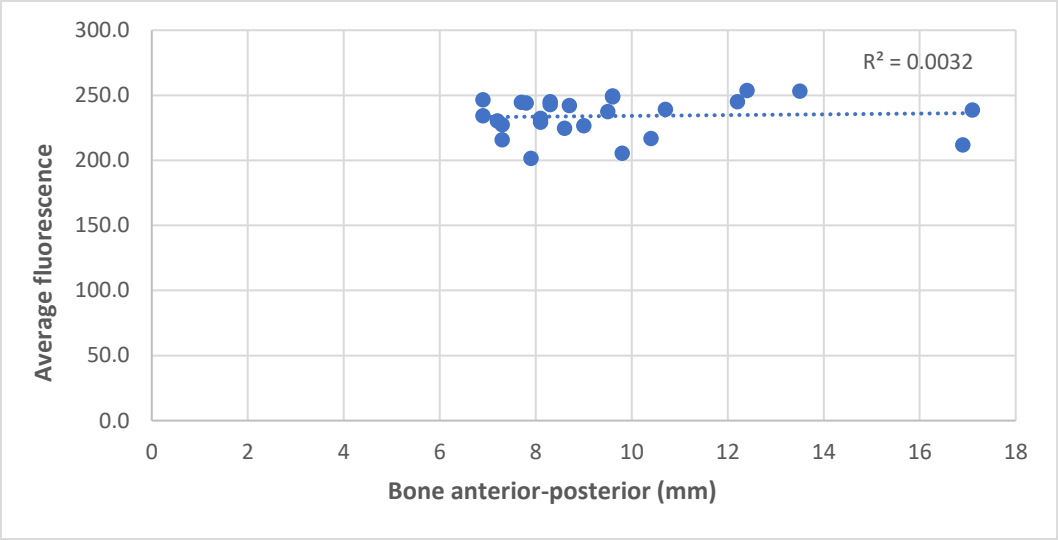

Comparison between bone anterior-posterior and terrestrial fluorescence taken with the yellow filter, 0.4s

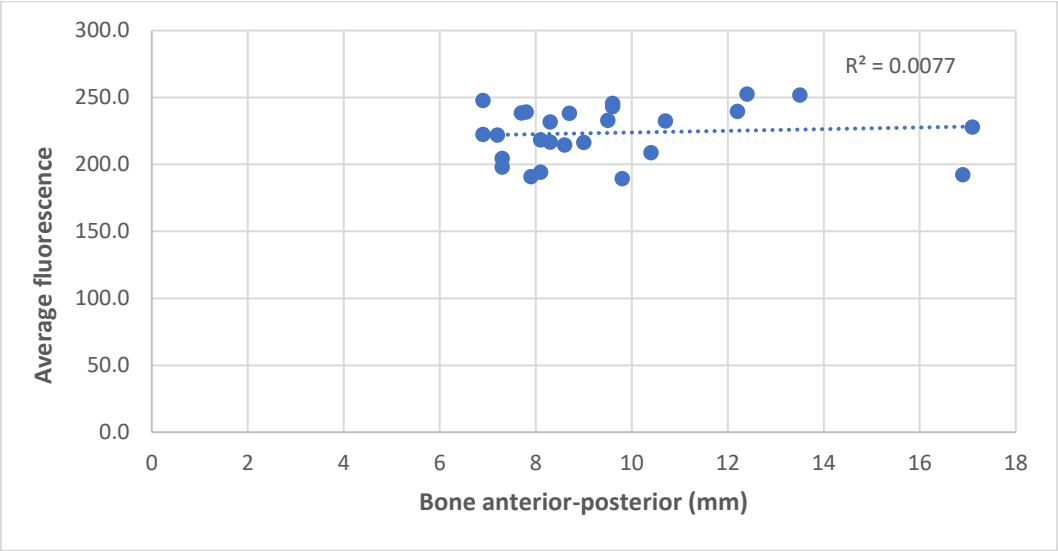

Comparison between bone anterior-posterior and terrestrial fluorescence taken with the yellow filter, 1/3s

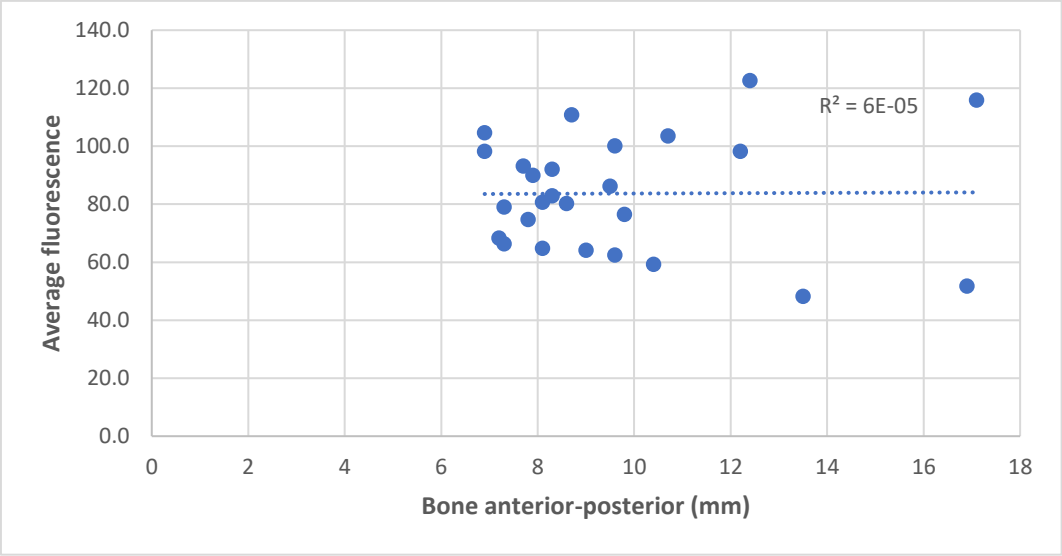

Comparison between bone anterior-posterior and underwater fluorescence taken with the orange filter, 0.6s

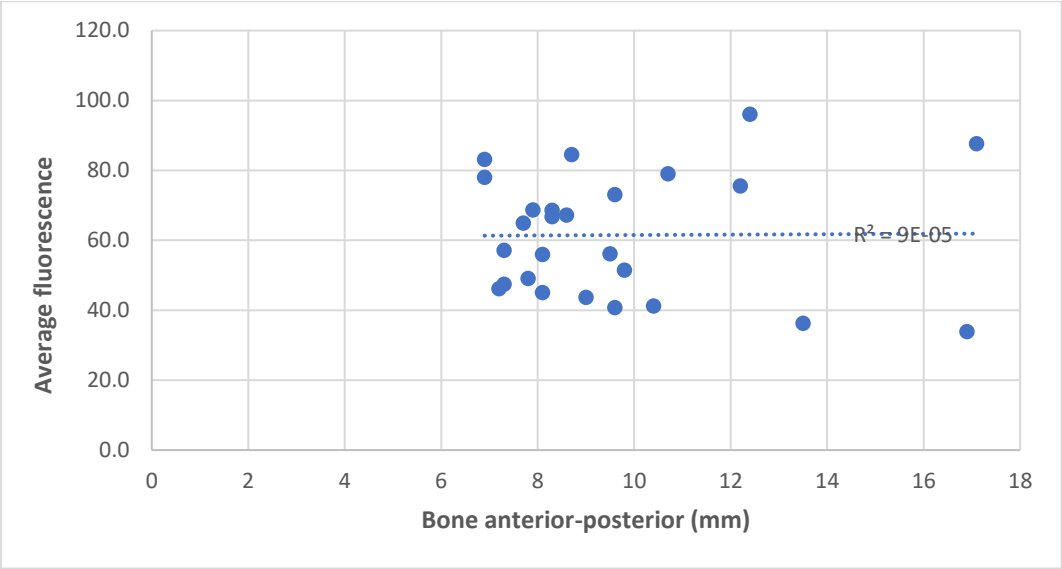

Comparison between bone anterior-posterior and underwater fluorescence taken with the orange filter, 0.4s

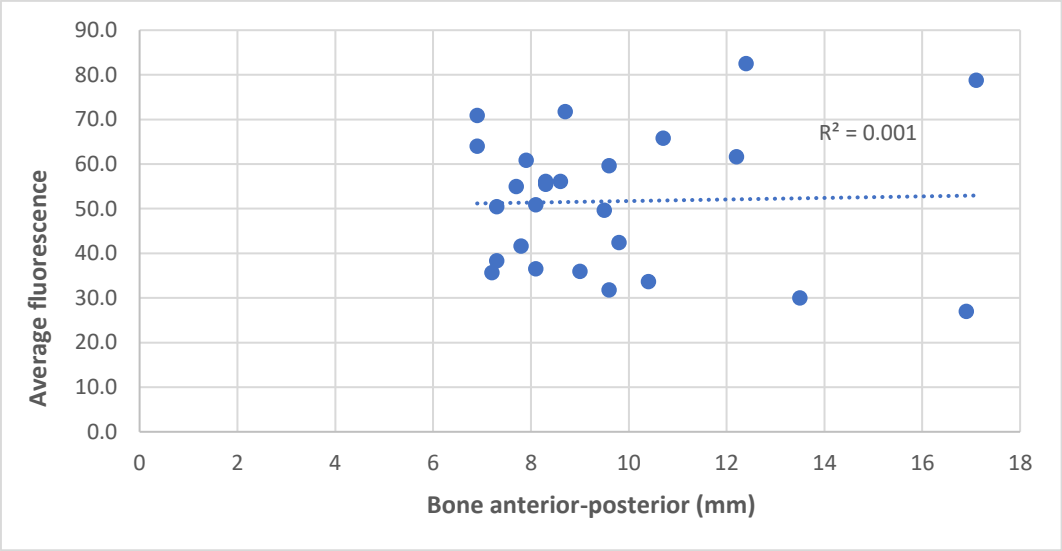

Comparison between bone anterior-posterior and underwater fluorescence taken with the orange filter, 1/3s

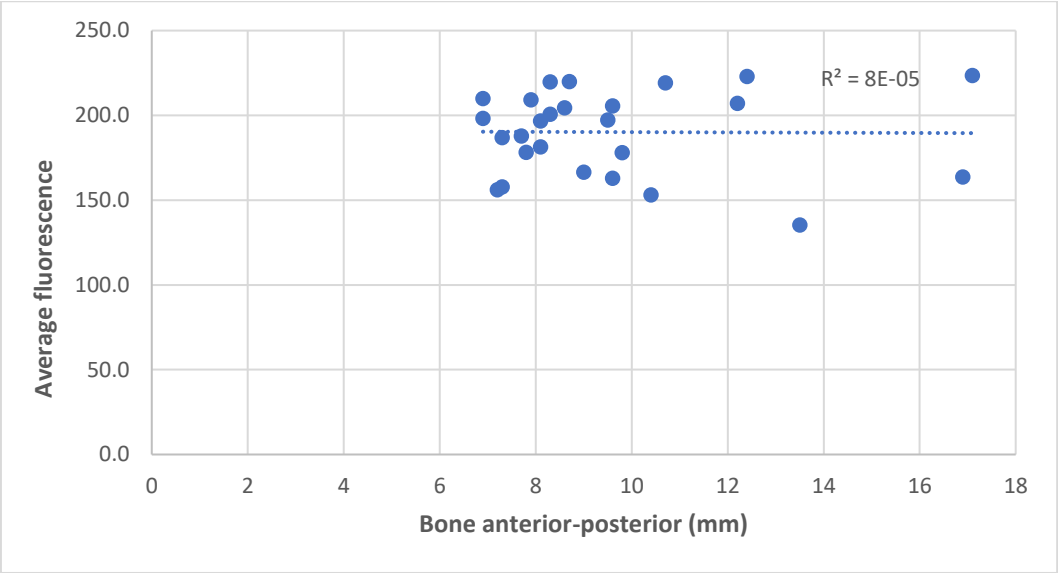

Comparison between bone anterior-posterior and underwater fluorescence taken with the yellow filter, 0.6s

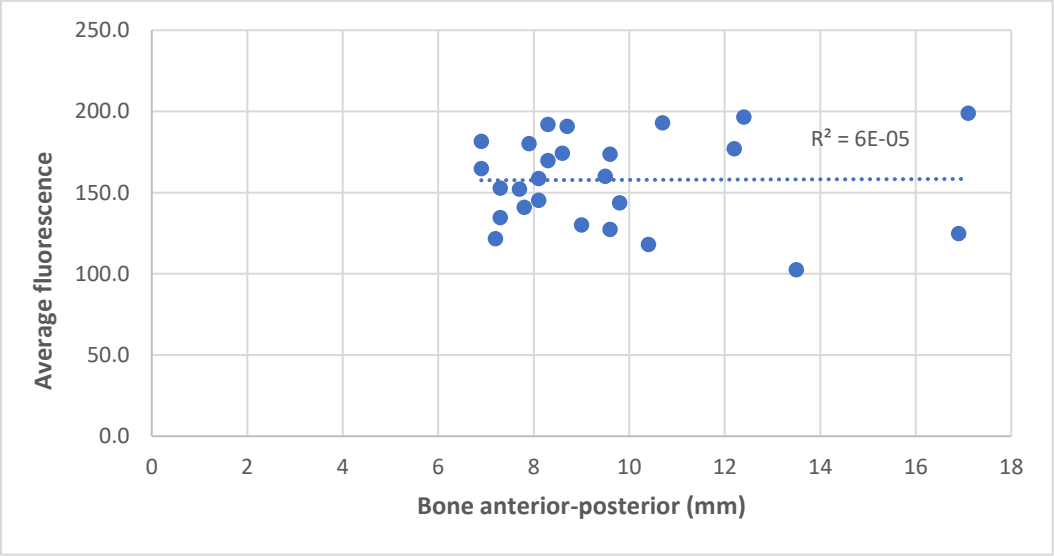

Comparison between bone anterior-posterior and underwater fluorescence taken with the yellow filter, 0.4s

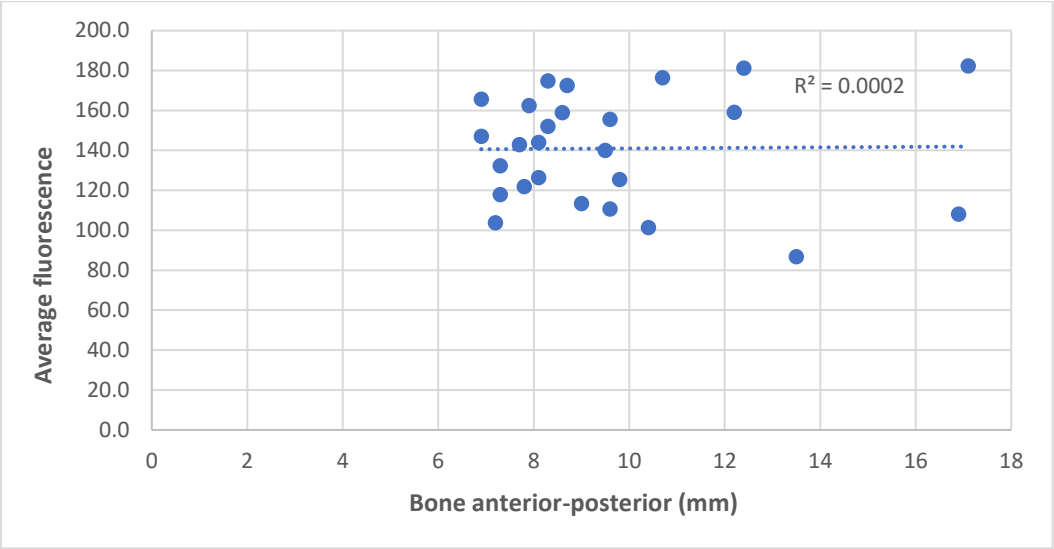

Comparison between bone anterior-posterior and underwater fluorescence taken with the yellow filter, 1/3s

Appendix 42: Graphical comparisons examining the relationship between average autofluorescence of the 29 porcine ribs (S*us scrofa domesticus*) produced using the Hammerhead ALS, in each of the deposition contexts captured using the orange filter and each of the three exposure times, compared to the bone dimensions.

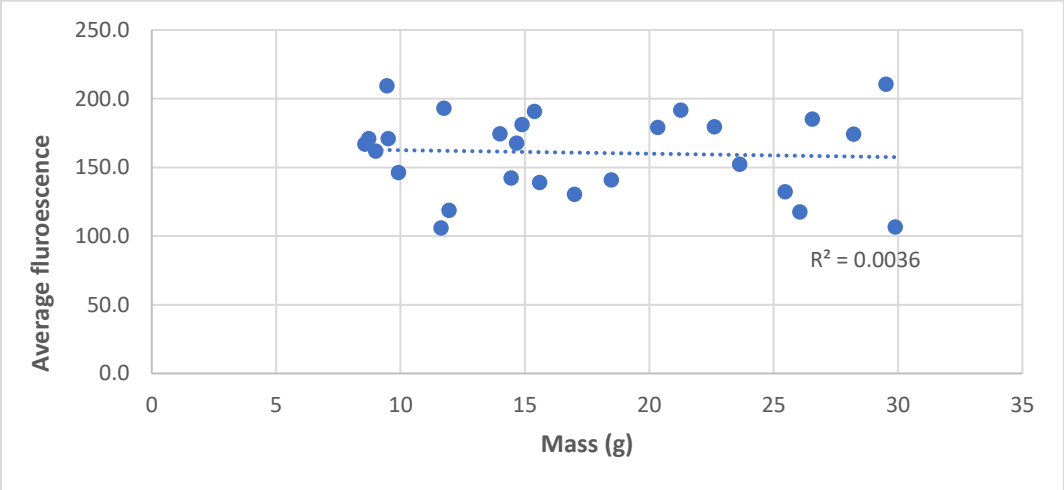

Comparison between mass and terrestrial fluorescence taken with the orange filter, 0.6s

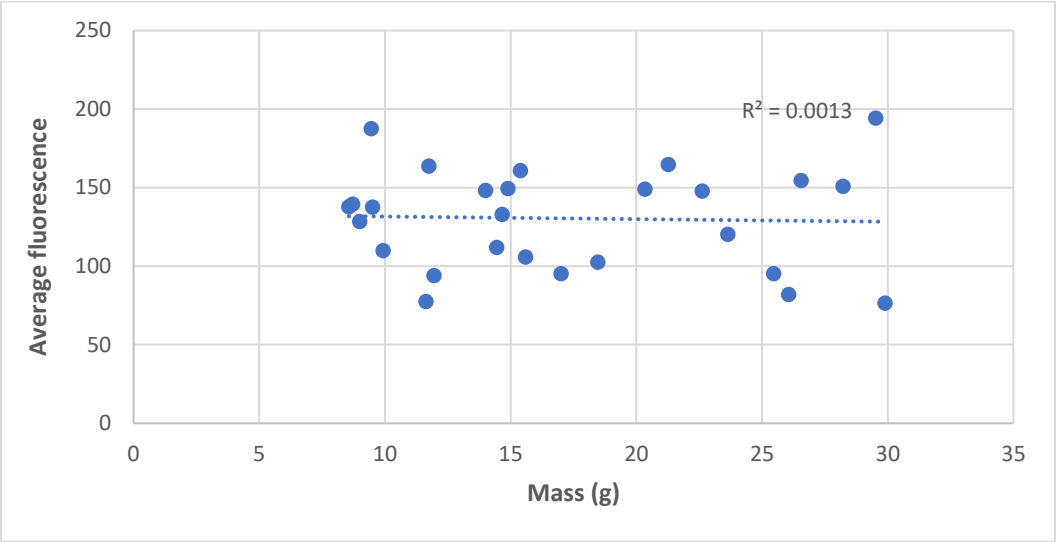

Comparison between mass and terrestrial fluorescence taken with the orange filter, 0.4s

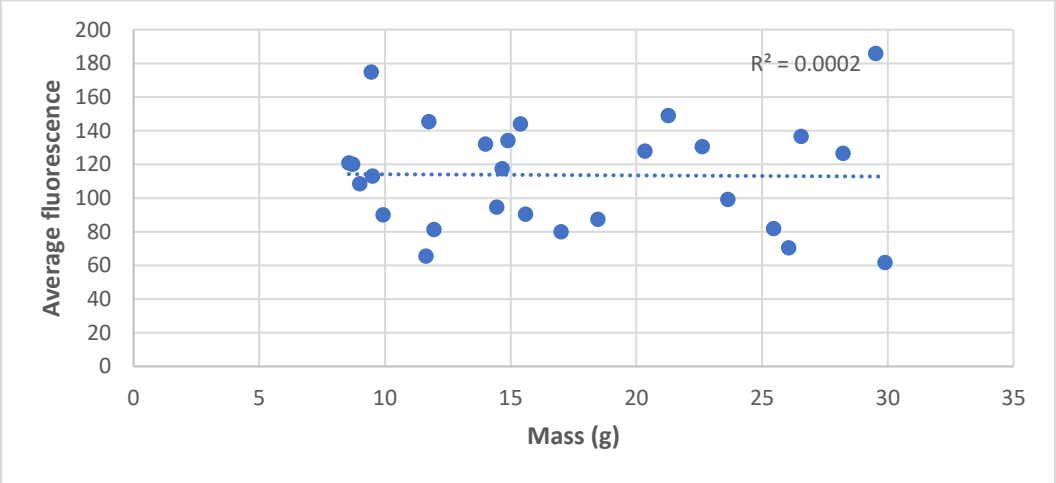

Comparison between mass and terrestrial fluorescence taken with the orange filter, 1/3s

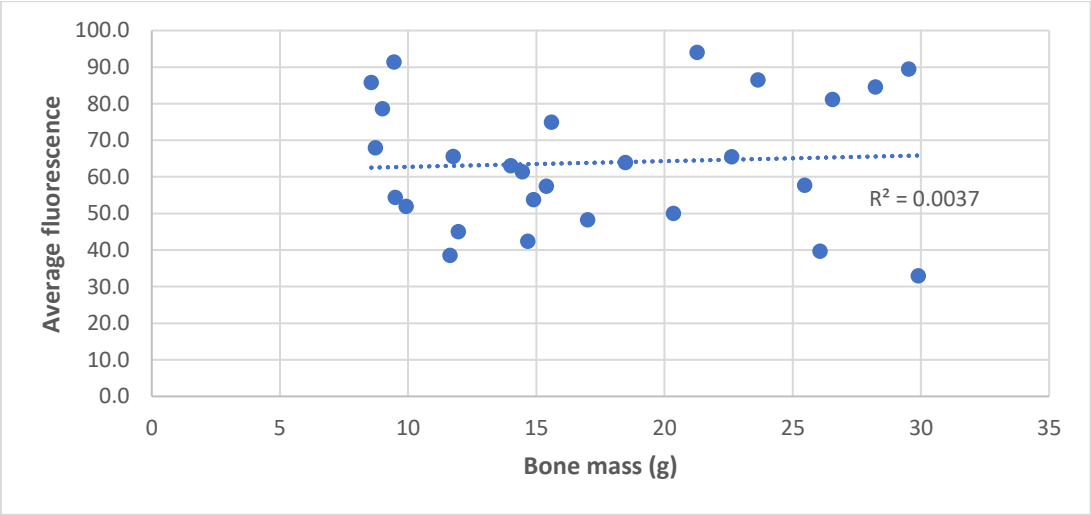

Comparison between mass and underwater fluorescence taken with the orange filter, 0.6s

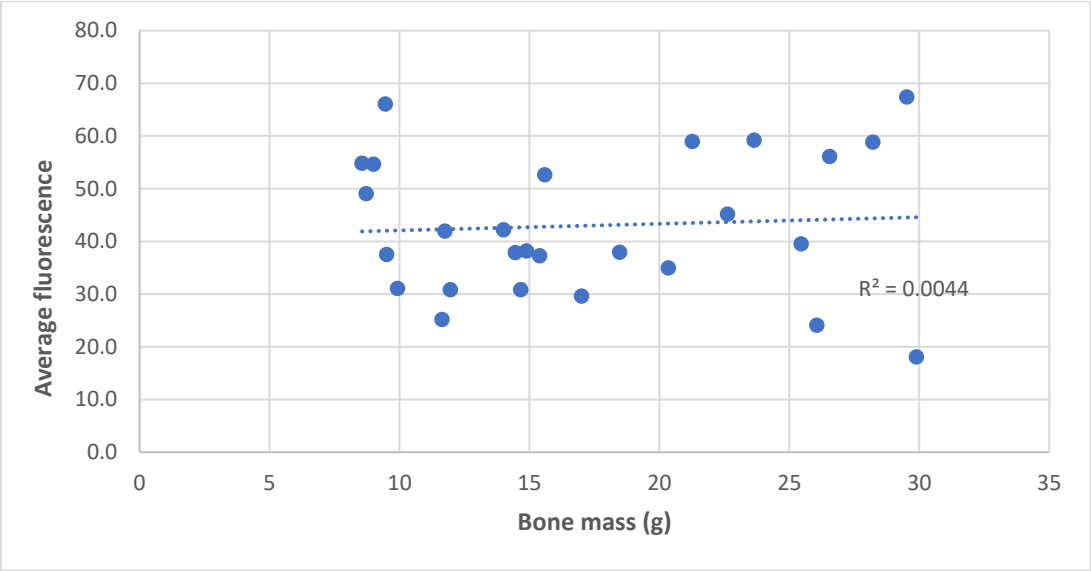

Comparison between mass and underwater fluorescence taken with the orange filter, 0.4s

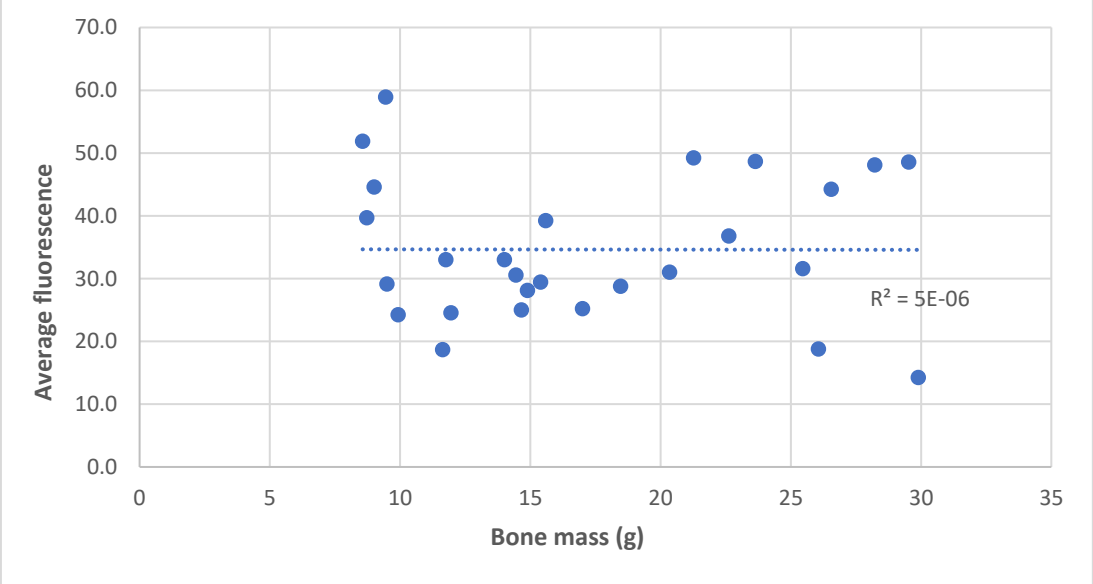

Comparison between mass and underwater fluorescence taken with the orange filter, 1/3s

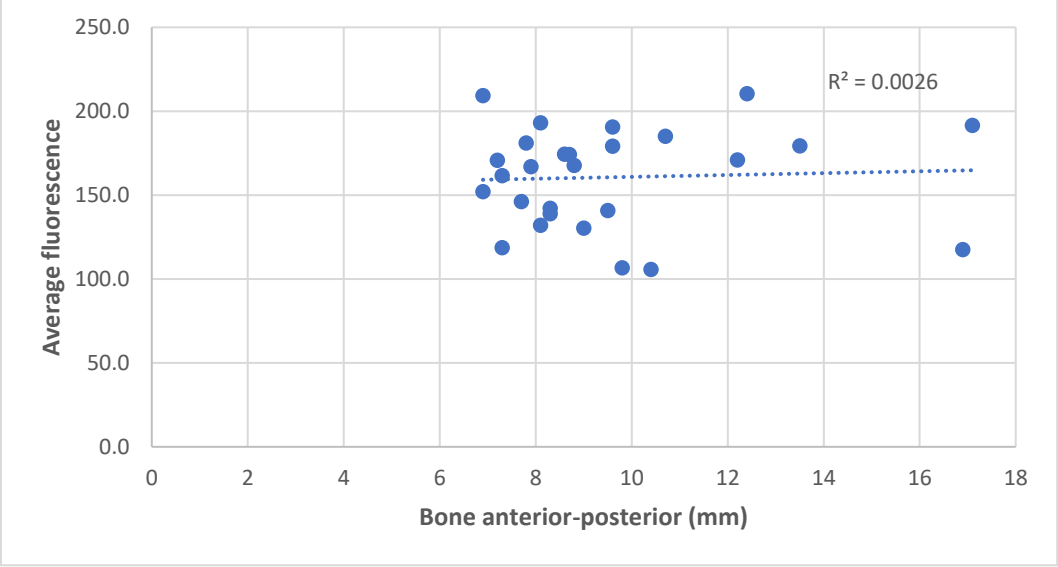

Comparison between bone anterior-posterior and terrestrial fluorescence taken with the orange filter, 0.6s

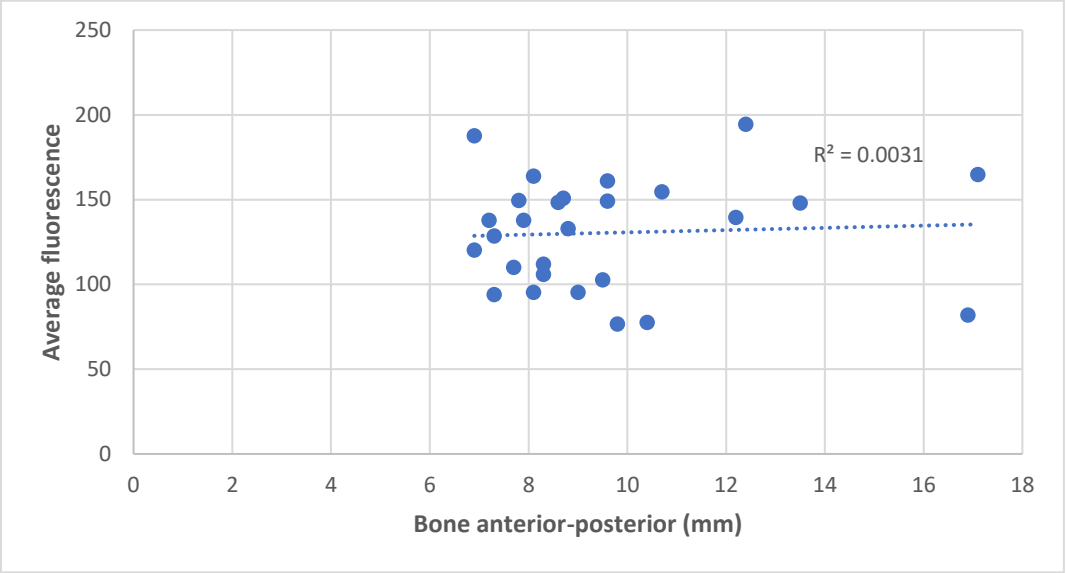

Comparison between bone anterior-posterior and terrestrial fluorescence taken with the orange filter, 0.4s

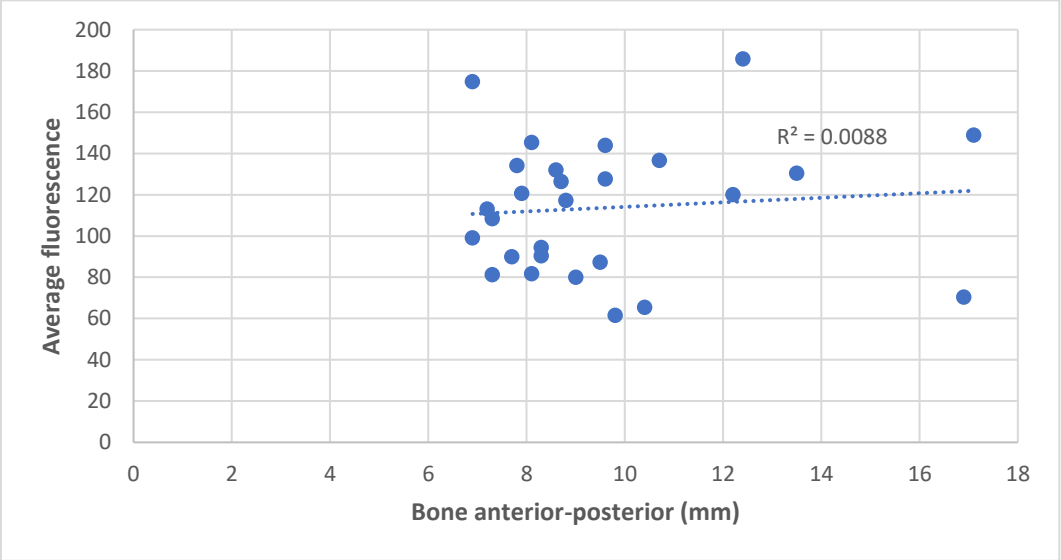

Comparison between bone anterior-posterior and terrestrial fluorescence taken with the orange filter, 1/3s

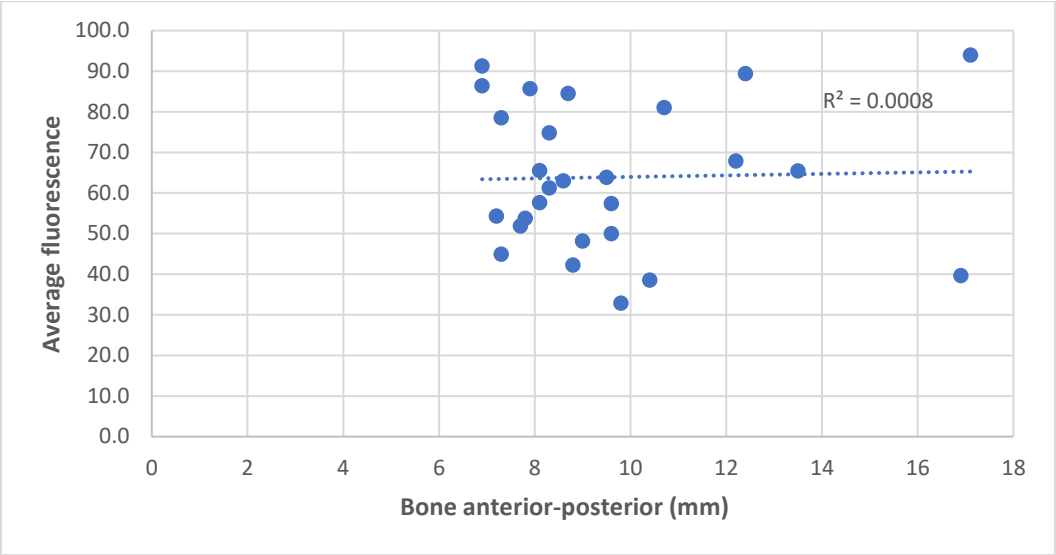

Comparison between bone anterior-posterior and underwater fluorescence taken with the orange filter, 0.6s

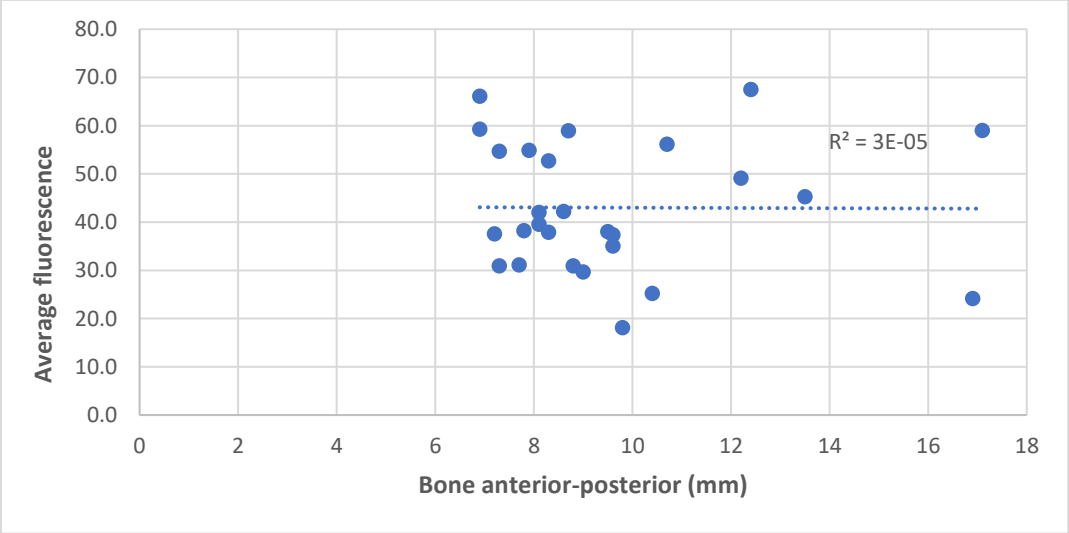

Comparison between bone anterior-posterior and underwater fluorescence taken with the orange filter, 0.4s

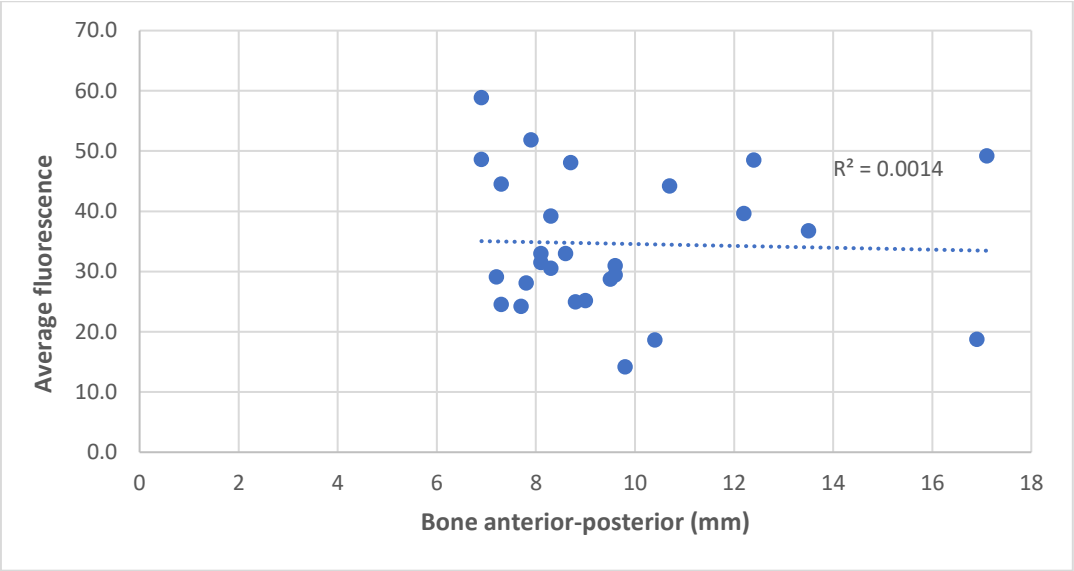

Comparison between bone anterior-posterior and underwater fluorescence taken with the orange filter, 1/3s

Appendix 43: All thermograms for the thirty porcine bones used in section B research question 1, terrestrial compared to underwater fluorescence dataset, are available on OneDrive: 43 - Thermograms for the terrestrial vs underwater dataset

Appendix 44: Graphical comparisons examining the relationship between average autofluorescence of the 29 porcine ribs (S*us scrofa domesticus*) produced using the Crime-lite 2, in each of the deposition contexts captured using the orange filter and each of the three exposure times, compared to the calculated bone collagen content.

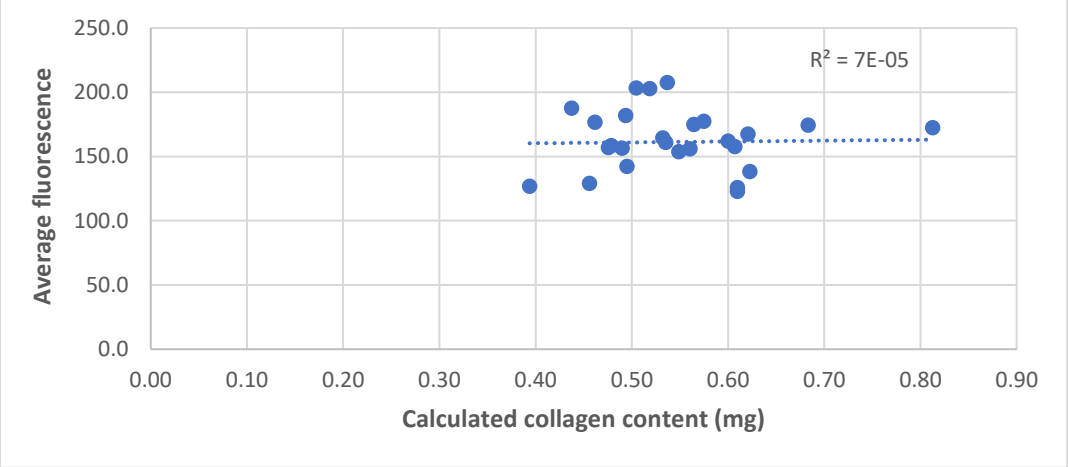

Comparison between calculated bone collagen and terrestrial autofluorescence, photographed with the orange filter at 0.6s

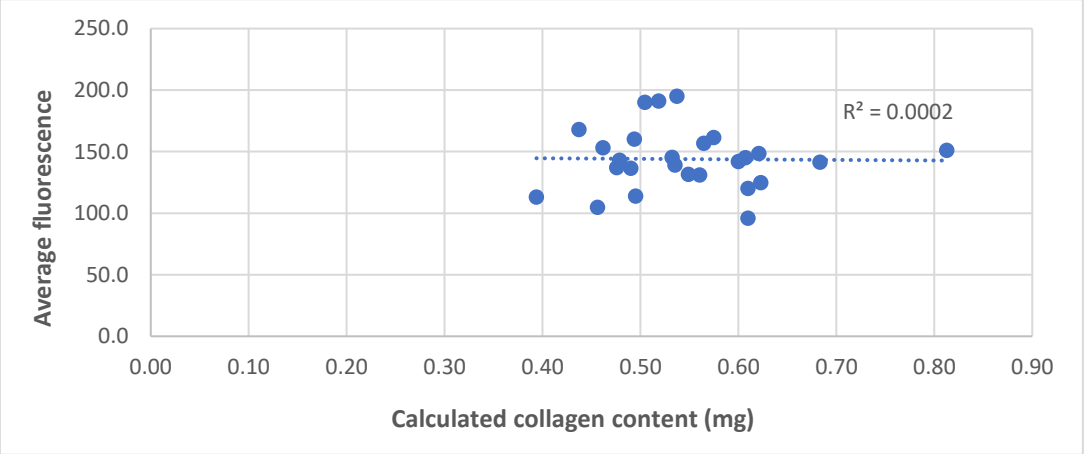

Comparison between calculated bone collagen and terrestrial autofluorescence, photographed with the orange filter at 0.4s

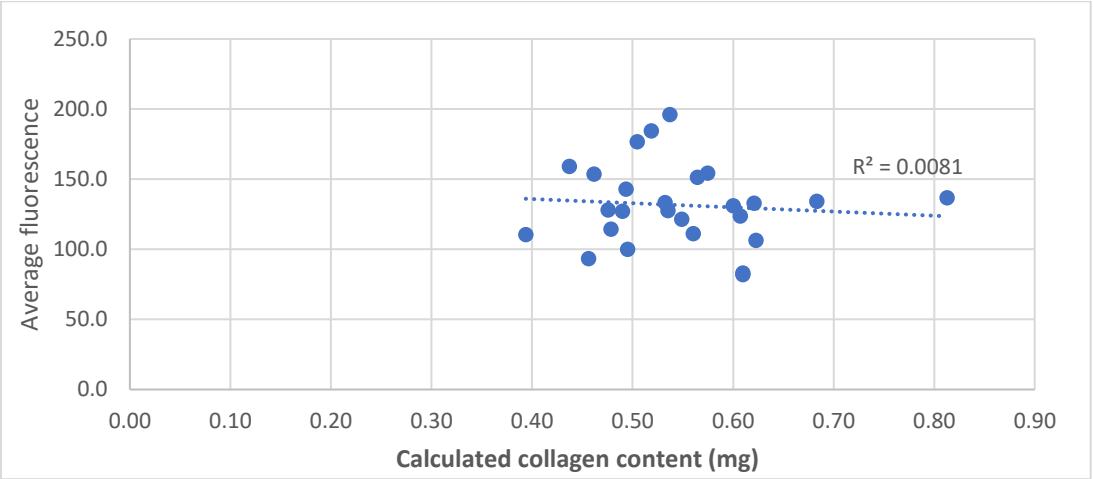

Comparison between calculated bone collagen and terrestrial autofluorescence, photographed with the orange filter at 1/3s

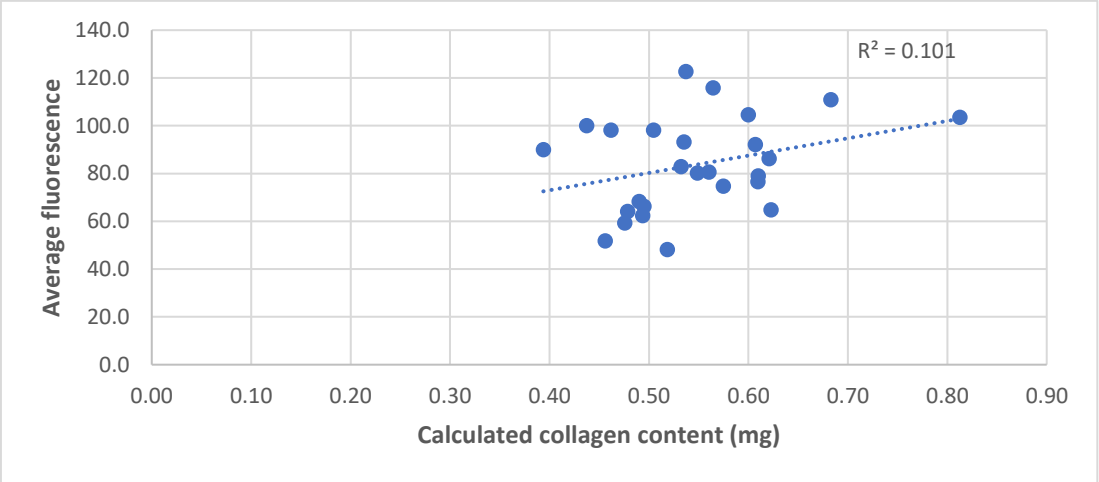

Comparison between calculated bone collagen and underwater autofluorescence, photographed with the orange filter at 0.6s

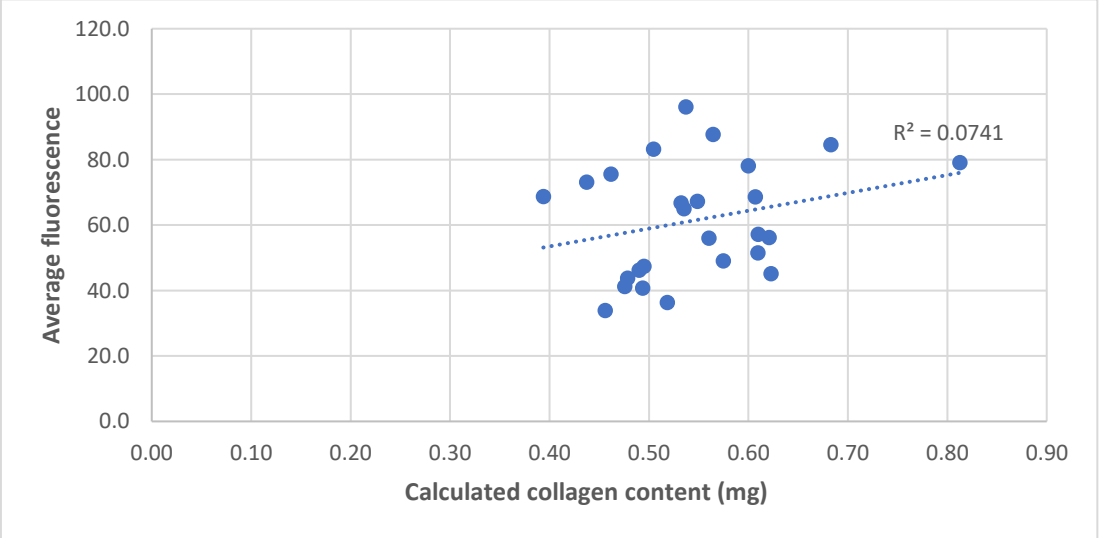

Comparison between calculated bone collagen and underwater autofluorescence, photographed with the orange filter at 0.4s

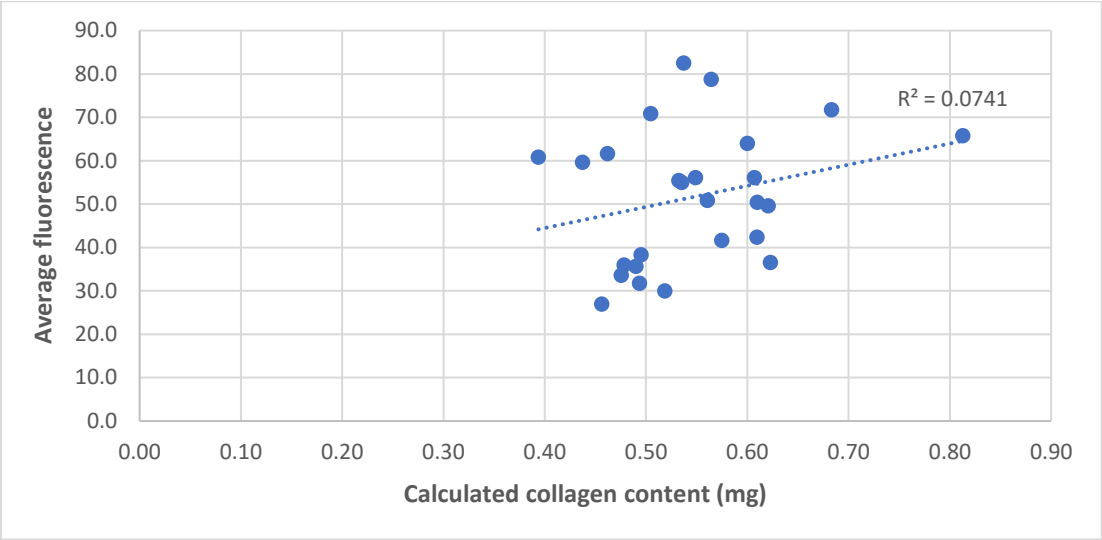

Comparison between calculated bone collagen and underwater autofluorescence, photographed with the orange filter at 1/3s

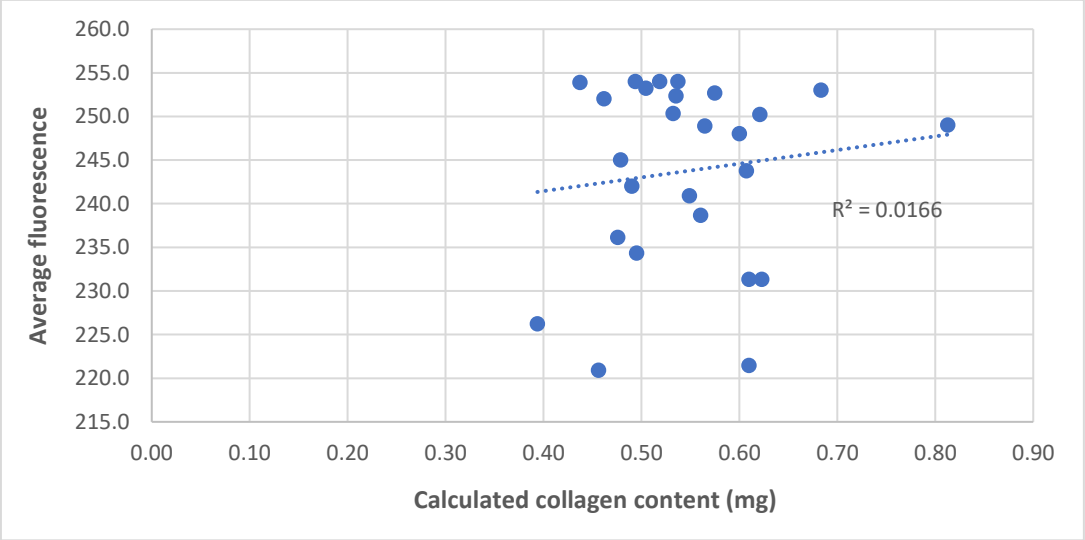

Comparison between calculated bone collagen and terrestrial autofluorescence, photographed with the yellow filter at 0.6s

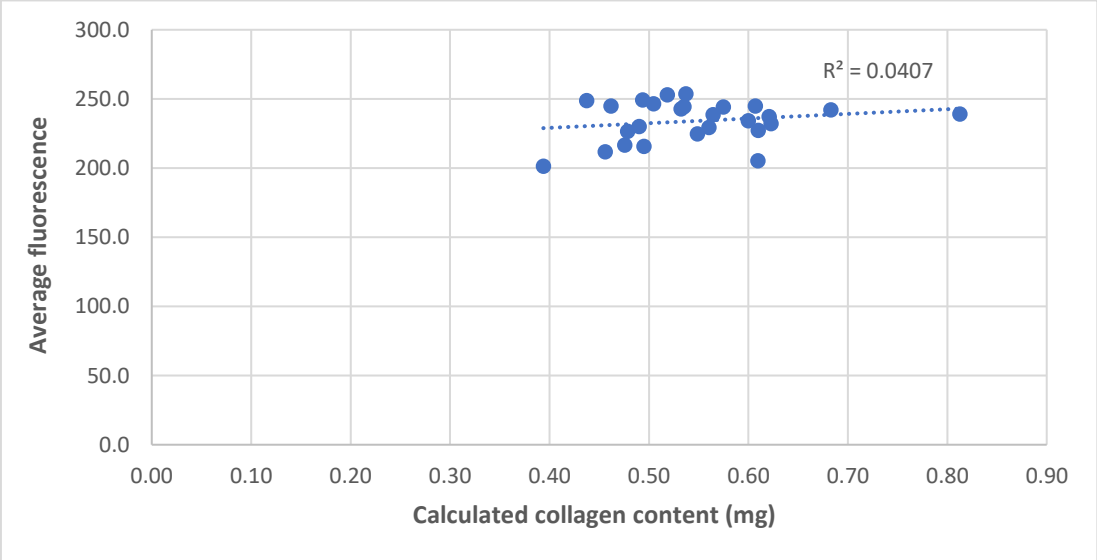

Comparison between calculated bone collagen and terrestrial autofluorescence, photographed with the yellow filter at 0.4s

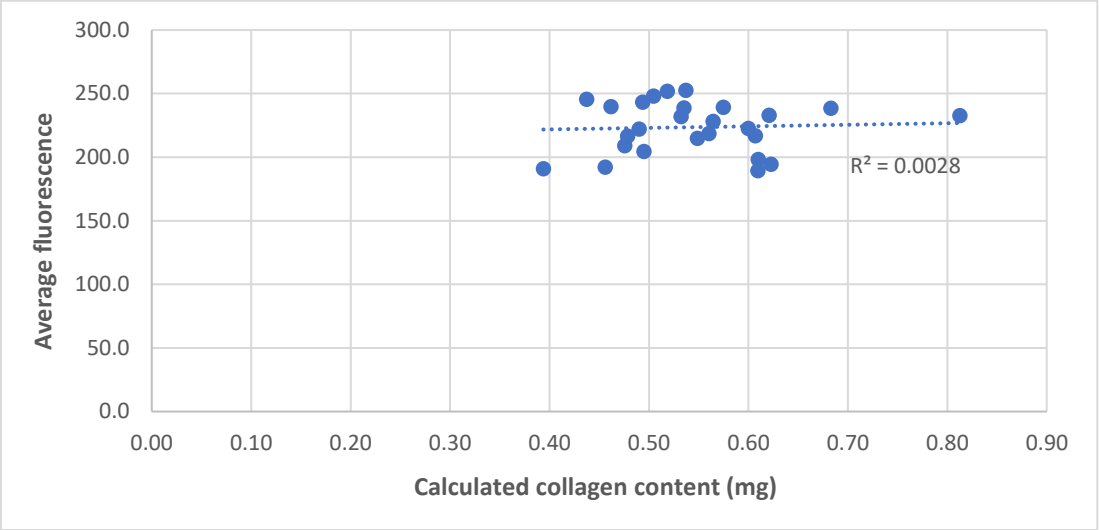

Comparison between calculated bone collagen and terrestrial autofluorescence, photographed with the yellow filter at 1/3s

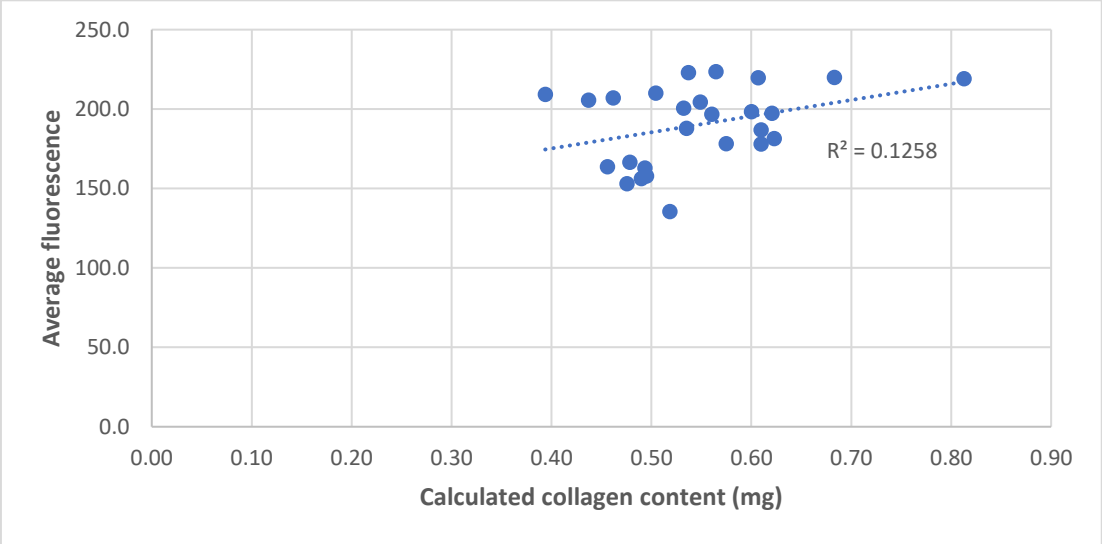

Comparison between calculated bone collagen and underwater autofluorescence, photographed with the yellow filter at 0.6s

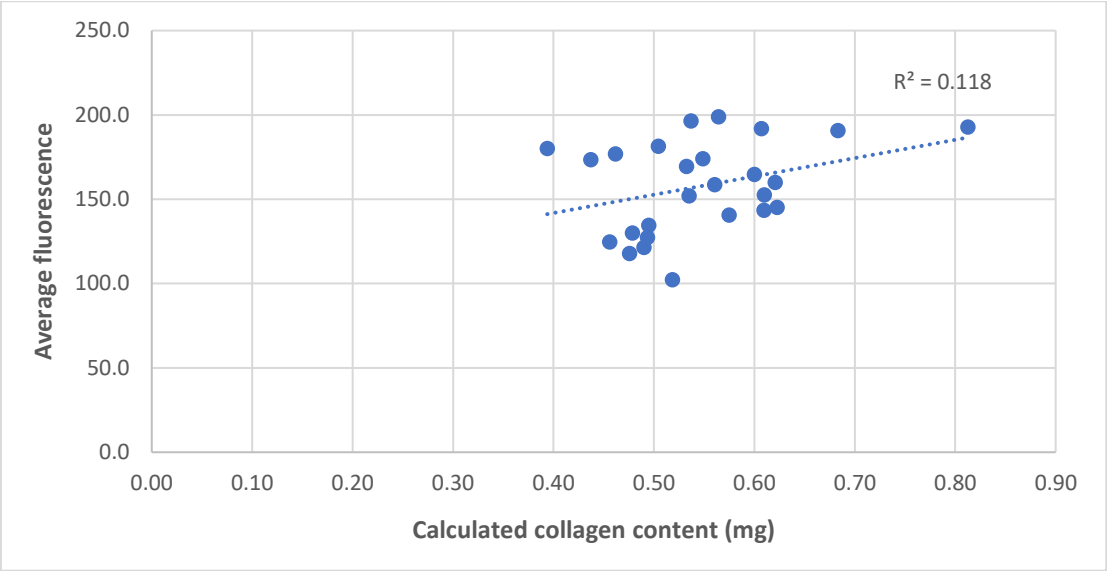

Comparison between calculated bone collagen and underwater autofluorescence, photographed with the yellow filter at 0.4s

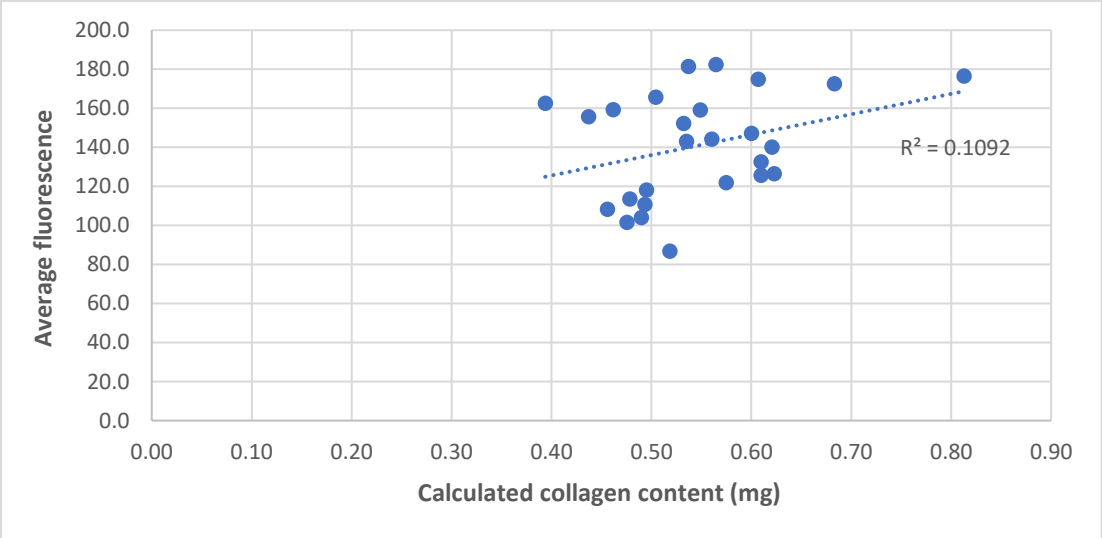

Comparison between calculated bone collagen and underwater autofluorescence, photographed with the yellow filter at 1/3s

Appendix 45: Graphical comparisons examining the relationship between average autofluorescence of the 29 porcine ribs (S*us scrofa domesticus*) produced using the Hammerhead, in each of the deposition contexts captured using the orange filter and each of the three exposure times, compared to the calculated bone collagen content.

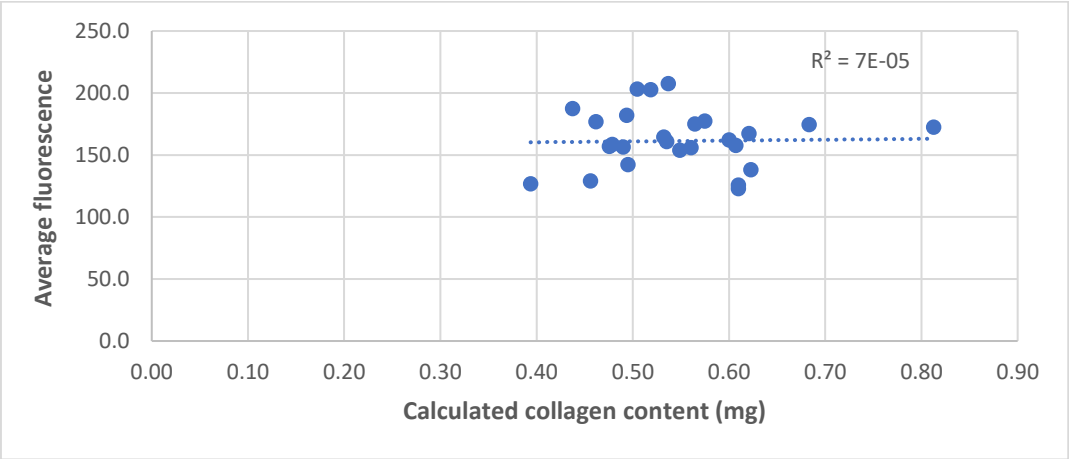

Comparison between calculated bone collagen and terrestrial autofluorescence, photographed with the orange filter at 0.6s

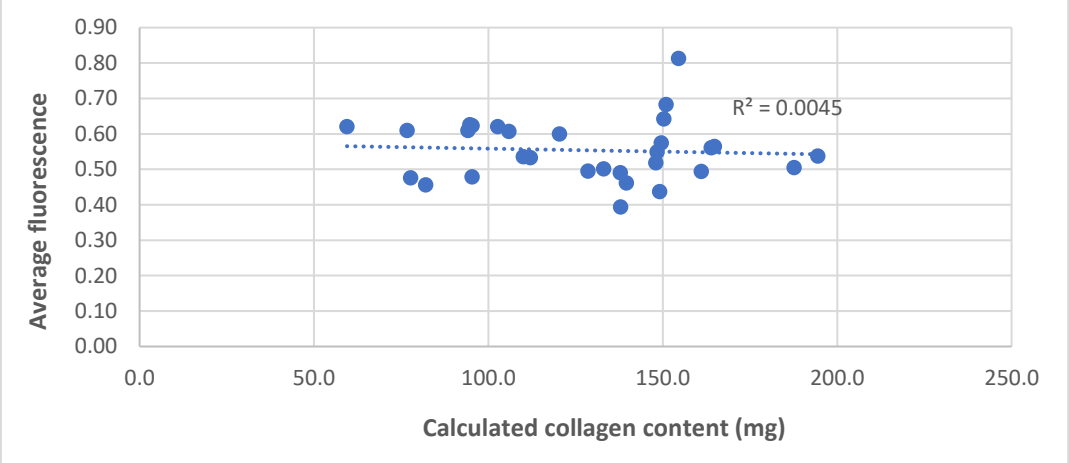

Comparison between calculated bone collagen and terrestrial autofluorescence, photographed with the orange filter at 0.4s

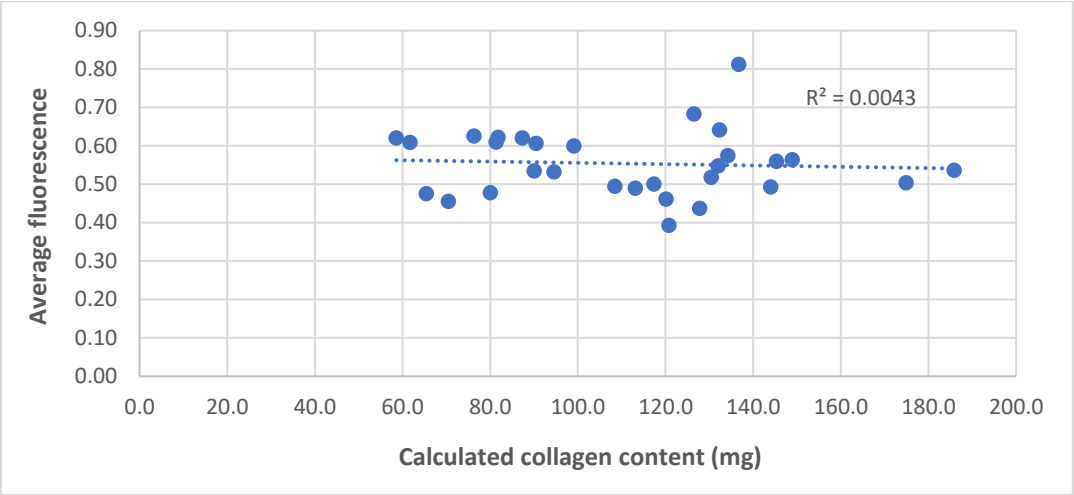

Comparison between calculated bone collagen and terrestrial autofluorescence, photographed with the orange filter at 1/3s

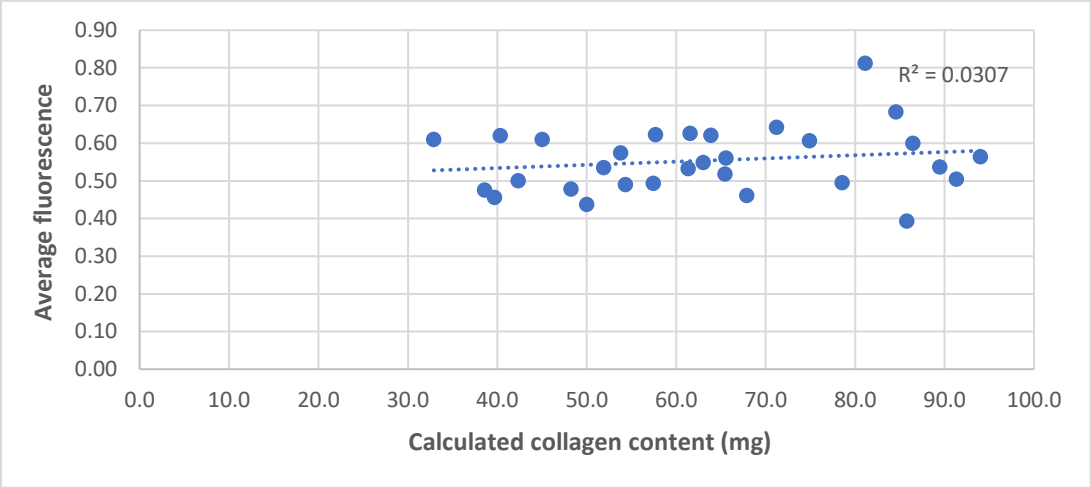

Comparison between calculated bone collagen and underwater autofluorescence, photographed with the orange filter at 0.6s

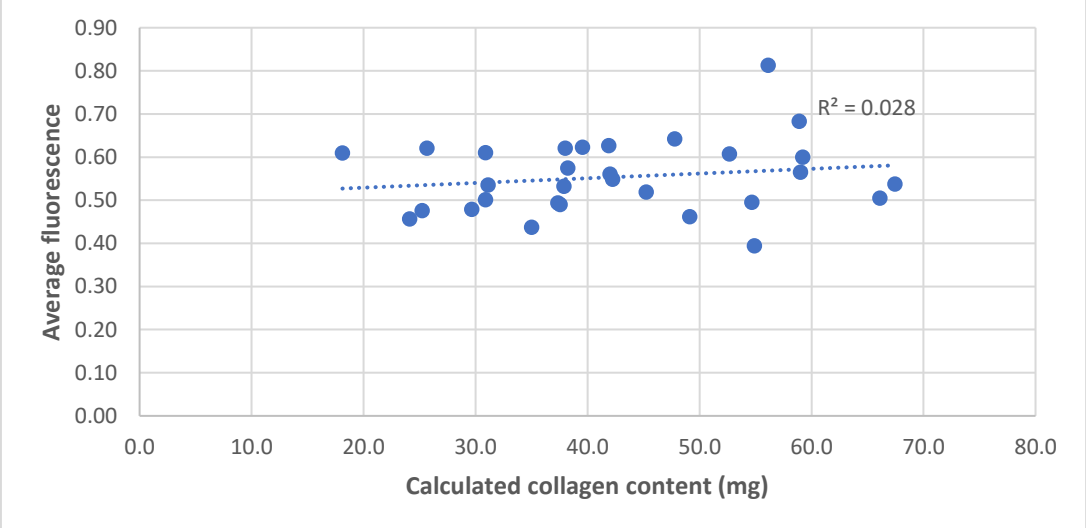

Comparison between calculated bone collagen and underwater autofluorescence, photographed with the orange filter at 0.4s

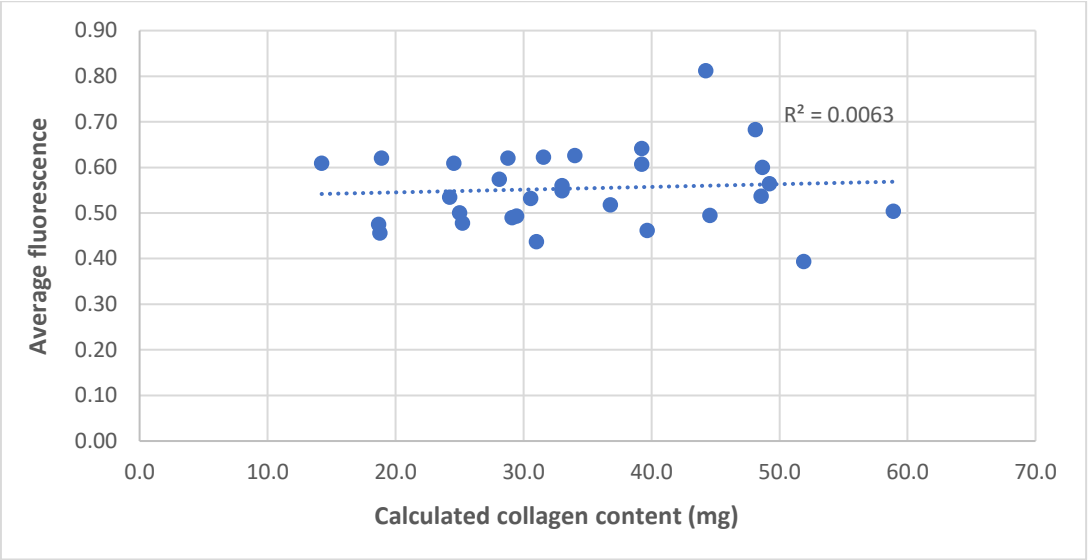

Comparison between calculated bone collagen and underwater autofluorescence, photographed with the orange filter at 1/3s

Appendix 46: Histograms performed to determine distribution of data for section B, question 1 statistical analyses.

A) Crime-lite 2 dataset

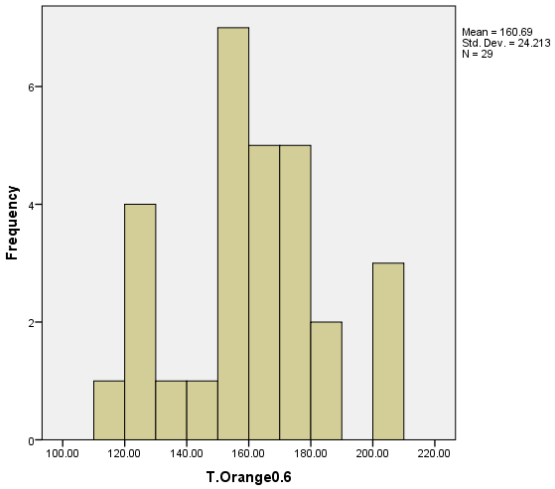

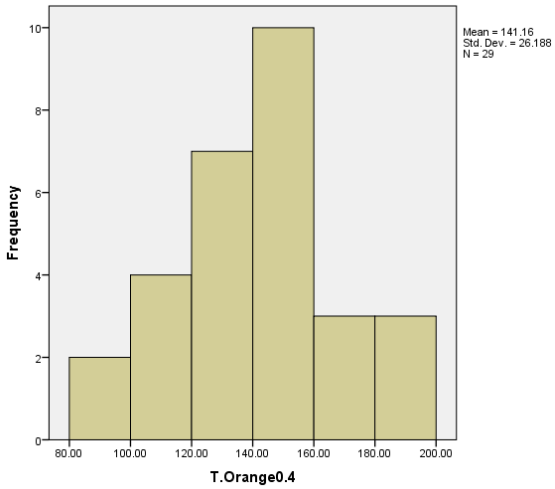

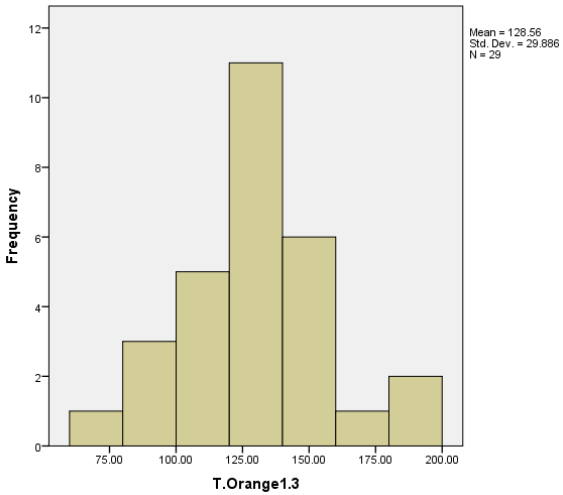

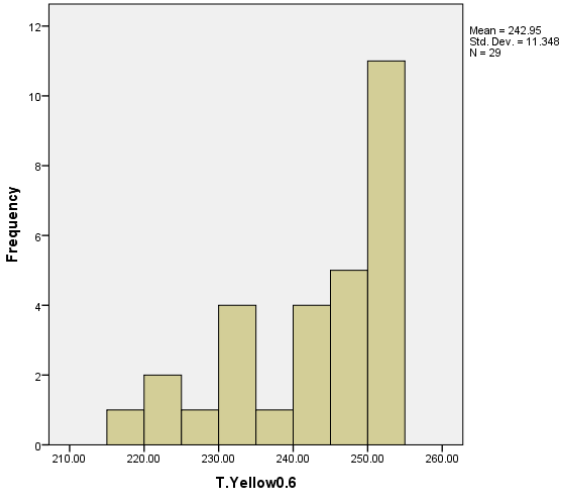
Mean = 242.95
Std. Dev. = 11.348
N = 29
Frequency
T.Yellow0.6

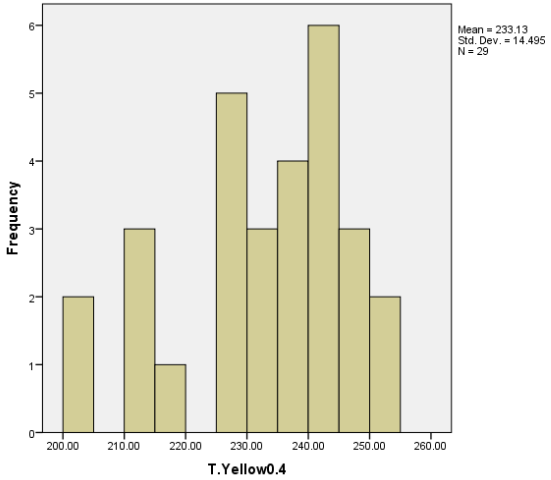
Mean = 233.13
Std. Dev. = 14.495
N = 29
Frequency
T.Yellow0.4

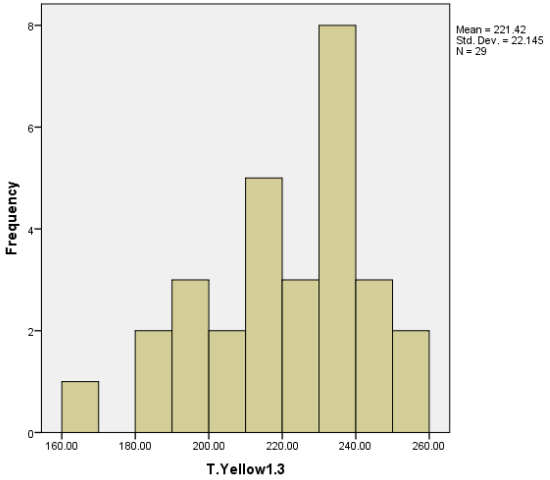
Mean = 221.42
Std. Dev. = 22.145
N = 29
Frequency
T.Yellow1.3

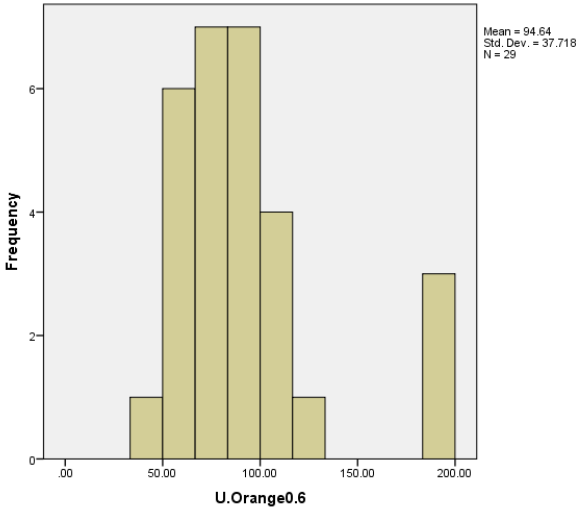
Mean = 94.64
Std. Dev. = 37.718
N = 29
Frequency
U.Orange0.6

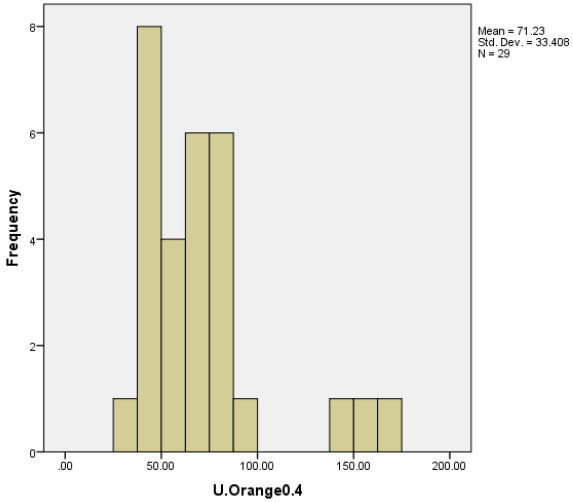
Mean = 71.23
Std. Dev. = 33.408
N = 29
Frequency
U.Orange0.4

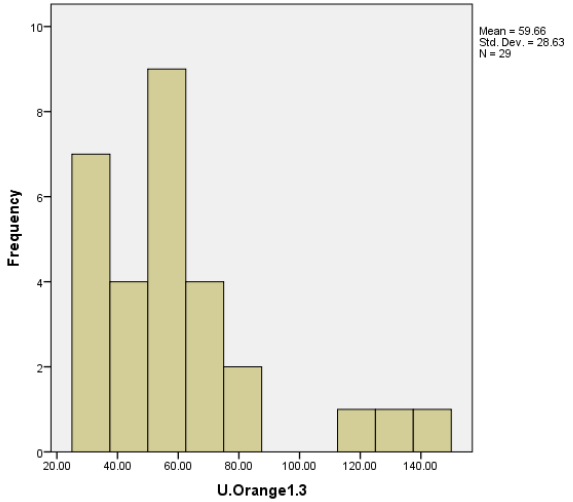
Mean = 59.66
Std. Dev. = 28.63
N = 29
Frequency
U.Orange1.3

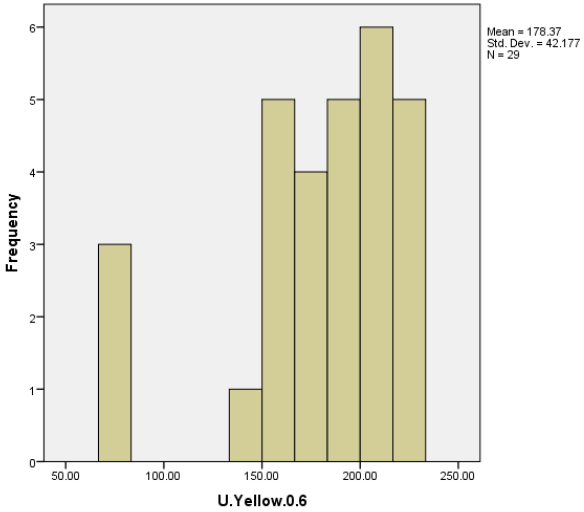

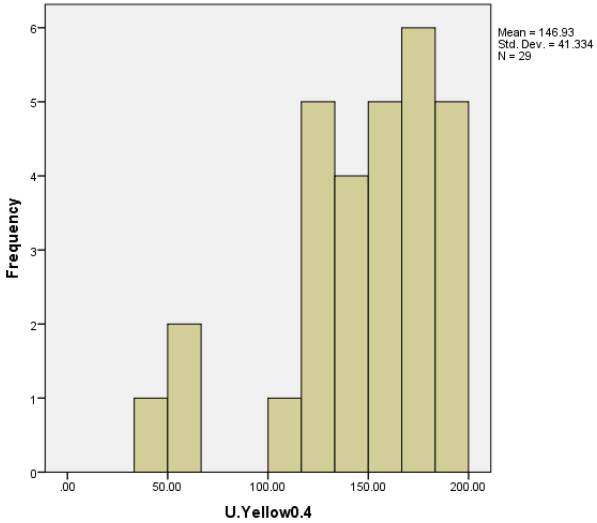

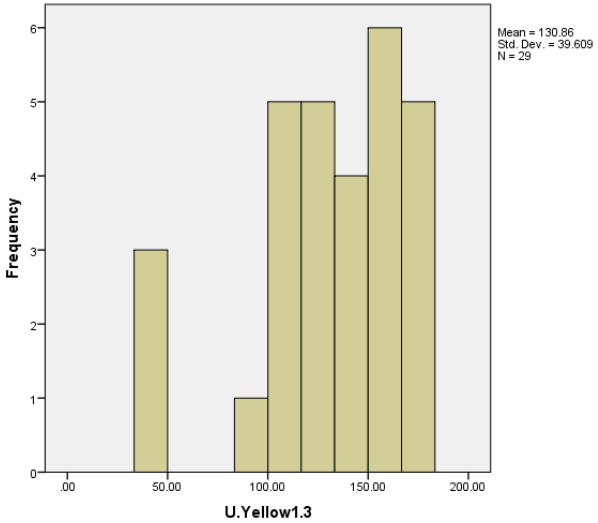

B) Hammerhead ALS dataset

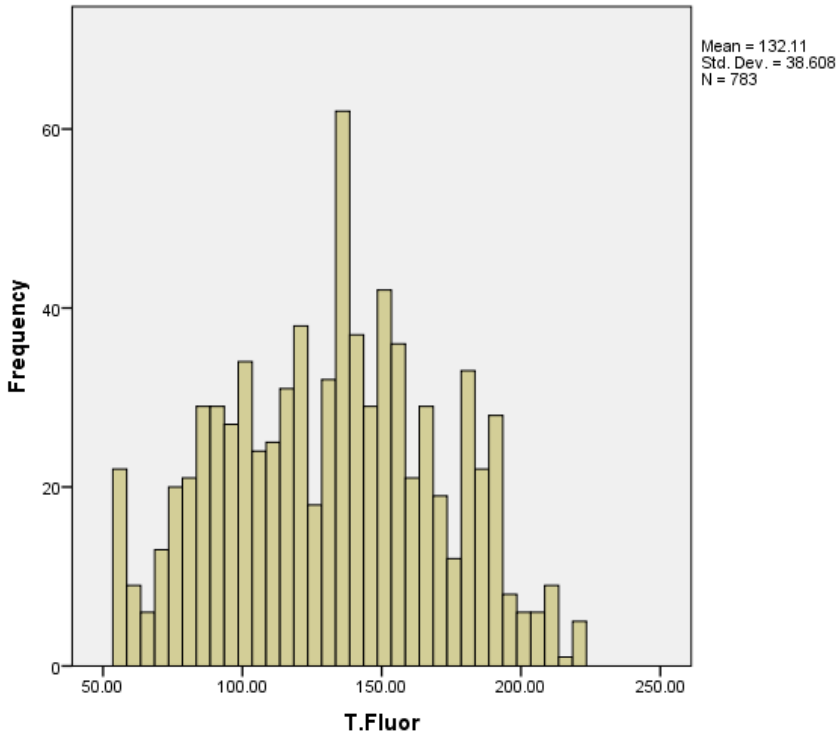
Mean = 132.11
Std. Dev. = 38.608
N = 783
Frequency
T.Fluor
0
20
40
60
50.00
100.00
150.00
200.00
250.00

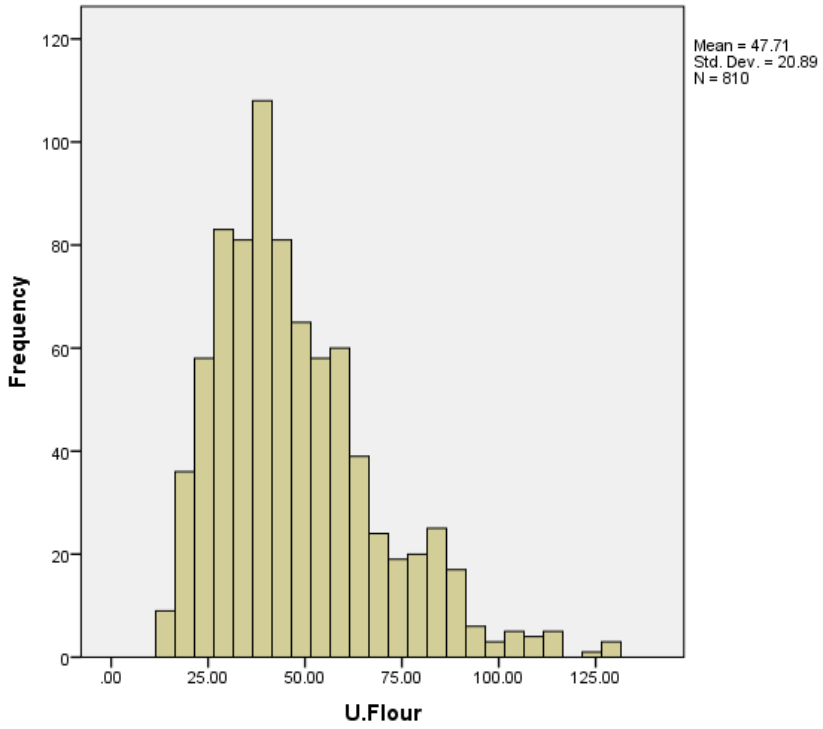
Mean = 47.71
Std. Dev. = 20.89
N = 810
Frequency
U.Flour
0
20
40
60
80
100
120
.00
25.00
50.00
75.00
100.00
125.00

C) Bone dimensions

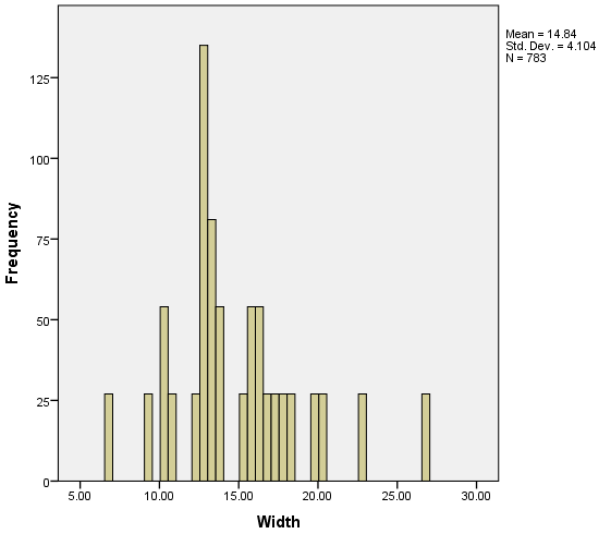

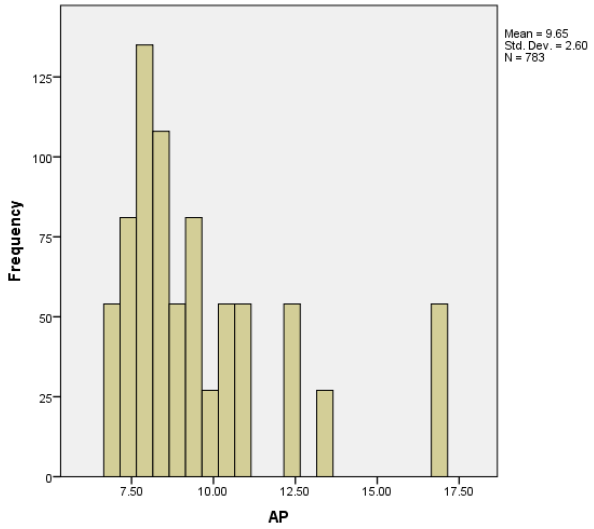

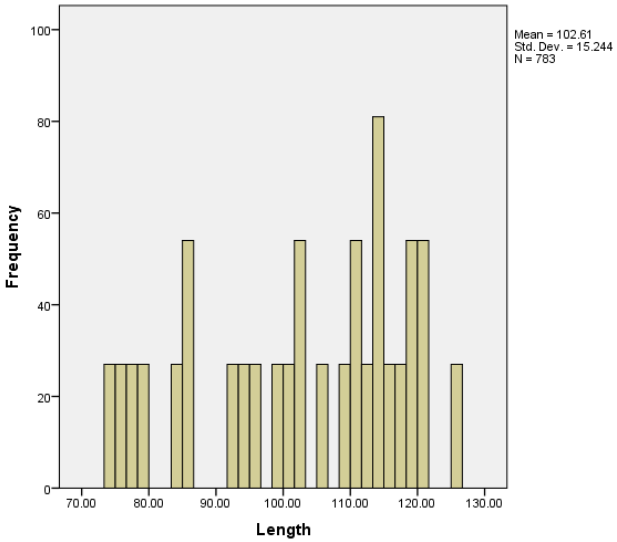

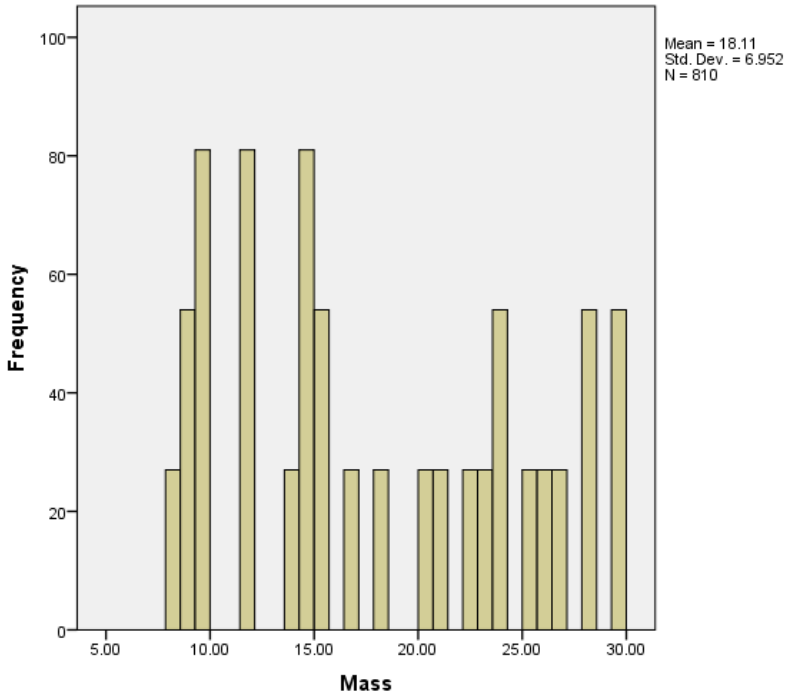
Mean = 18.11
Std. Dev. = 6.952
N = 810
Frequency
Mass
0
20
40
60
80
100
5.00
10.00
15.00
20.00
25.00
30.00

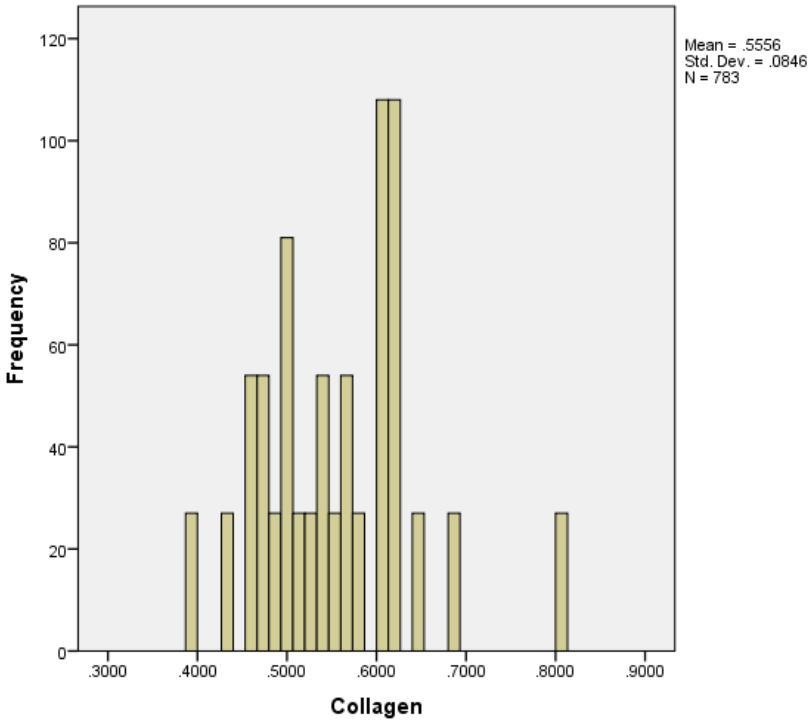
Mean = .5556
Std. Dev. = .0846
N = 783
Frequency
Collagen
0
20
40
60
80
100
120
.3000
.4000
.5000
.6000
.7000
.8000
.9000

Appendix 47: Macerated dimensions of all 54 bones used in section B, research question 2: investigating the collagen-fluorescence relationship.

Sample	Mass (g)	Length (mm)	Width (mm)	A/P (mm)
1	20.59	78	18.1	13.9
2	11.23	75.4	16.6	9.3
3	8.92	98.7	11.3	7.9
4	14.91	118.8	14.6	9.3
5	15.51	75.1	20.1	10.9
6	9	86.3	11.2	9.6
7	18.31	76	24.3	8.9
8	5.52	63.4	10.1	7
9	18.39	133.8	12.5	10.6
10	6.68	105.9	10.8	6.9
11	9	67.3	15.6	8.2
12	7.77	80.9	12.6	7.1
13	10.64	66.8	16.1	9.9
14	18.67	68	17.3	15.3
15	15.68	63.7	17.1	14.1
16	9.24	89.7	12.7	7.8
17	8.79	83.3	13.4	7.5
18	7.29	67.3	12.3	8.4
19	16.32	115.9	15	9.4
20	18.75	85	19.9	12.2
21	10.15	91.6	11.1	10.5
22	8.03	82	13.9	6.6
23	11.29	93.4	12.1	9.8
24	24	71.5	22.1	16.2
25	7.36	73.5	13.6	7.1
26	11.42	109.9	10.8	9.7
27	7.27	59.1	14.4	9.2
28	21.07	67.4	26.5	13.8
29	6.16	61.4	12.2	8.2
30	15.22	69.7	23.7	10.8
31	12.74	88.4	17.1	8.8
32	8.7	83.8	13.2	7.9
33	10.91	86.7	15.7	8.6
34	10.86	101.6	12.8	7.8
35	5.16	64.2	11.9	5.5
36	17.27	72.9	23.2	12.3
37	7.75	70.8	12.9	6.8
38	9.57	84.7	13.9	8.9
39	14.15	117.3	12.8	9
40	10.18	98	12.4	9.3
41	6.94	83.7	11.7	7.6
42	11.26	105.5	11.8	8.2

43	16.8	75	12.1	13.2
44	20.16	97.1	22.3	10.9
45	5.28	55.8	12.2	6.5
46	9.54	69.1	14.8	8.2
47	10.95	88.9	14.4	7.6
48	7.93	80.7	11.4	8.2
49	15.04	79.5	20.1	10.3
50	6.9	75.4	11.9	6.9
51	18	67.2	18.3	13.5
52	7.82	72.4	12.3	7
53	6.71	65.3	12.9	7.2
54	14.69	63.2	20	12.6
Average	11.82	81.96	15.08	9.42
Min	5.2	55.8	10.1	5.5
Max	24.0	133.8	26.5	16.2
Range	18.8	78.0	16.4	10.7
S.D.	4.7	17.0	4.0	2.4

Appendix 48: Visual tables of summarised terrestrial fluorescence results for all 54 porcine ribs examined in section B, research question 2: investigating the collagen-fluorescence relationship.

Rib	Natural	0.6	0.4	1/3
1				
2		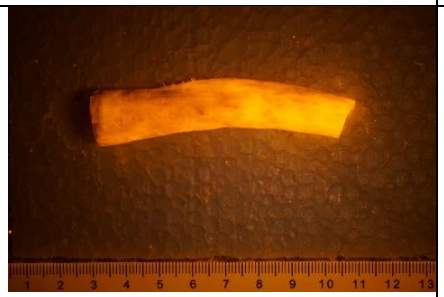	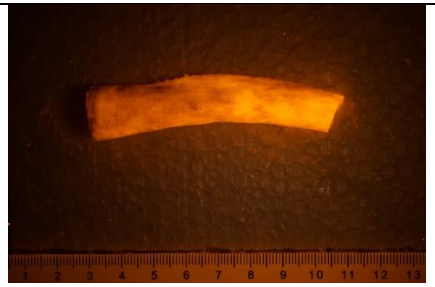	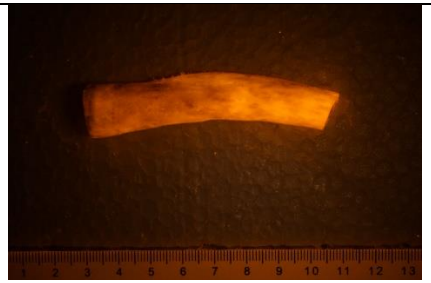

3		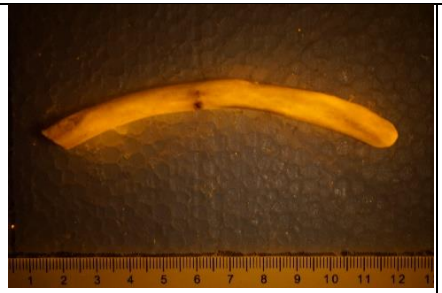		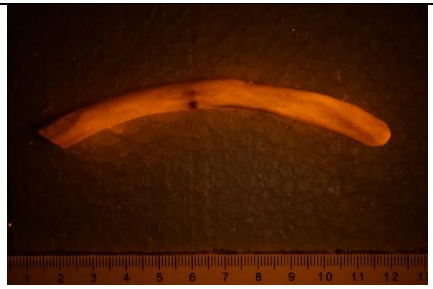
4		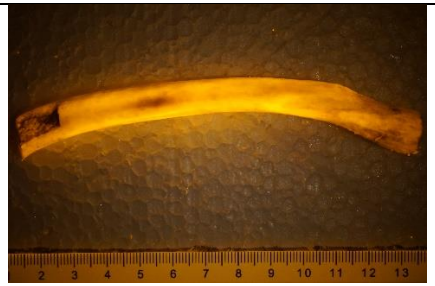	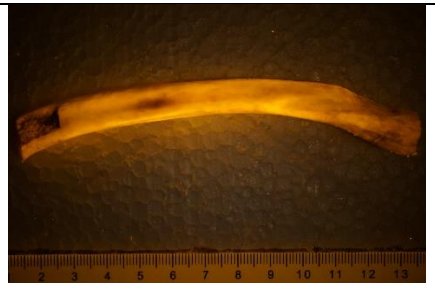	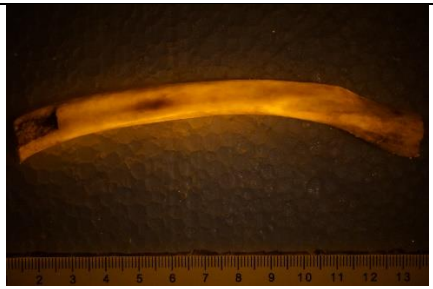
5		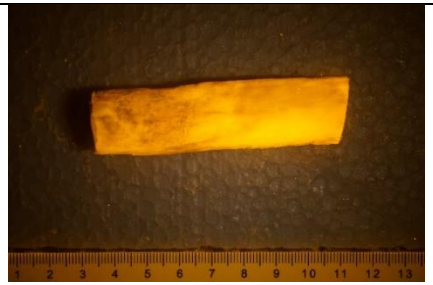	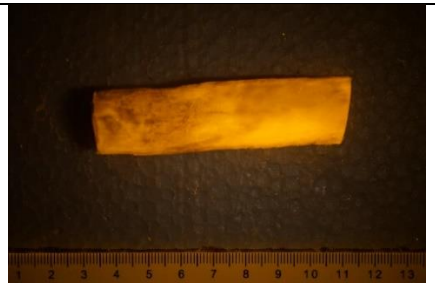	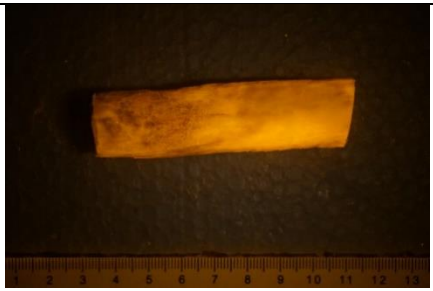

6				
7				
8				

9		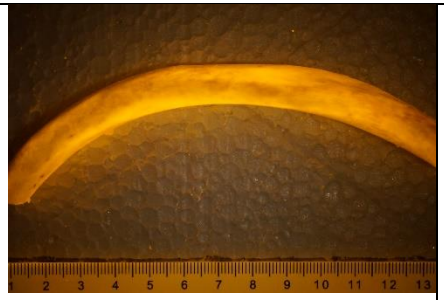	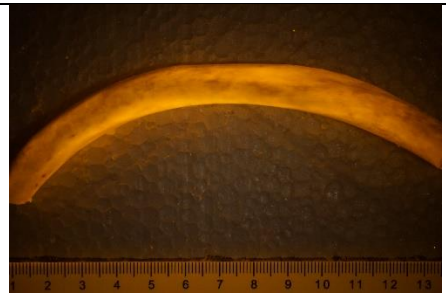	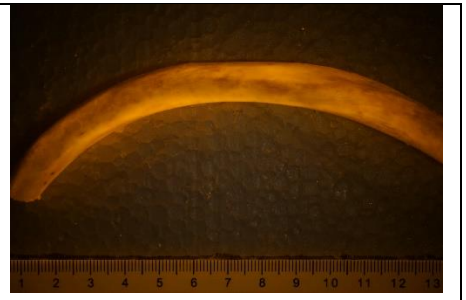
10		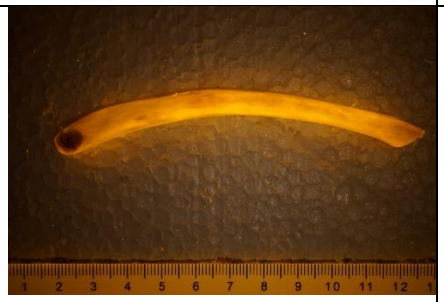	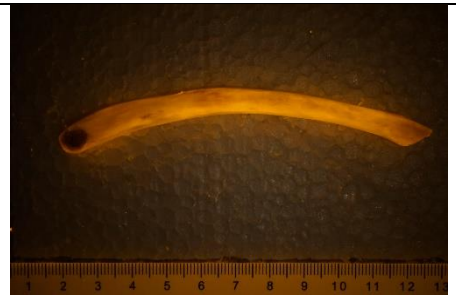	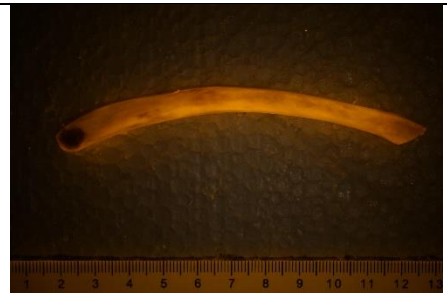
11		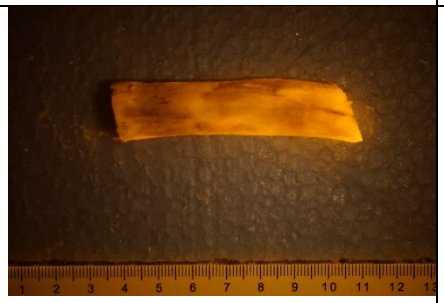		

12		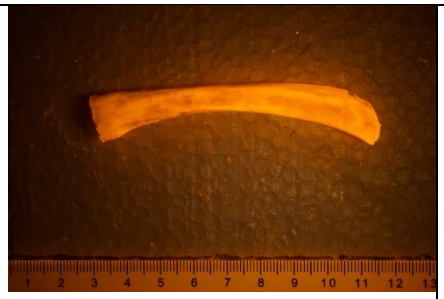		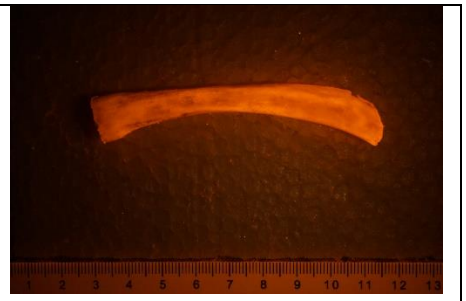
13				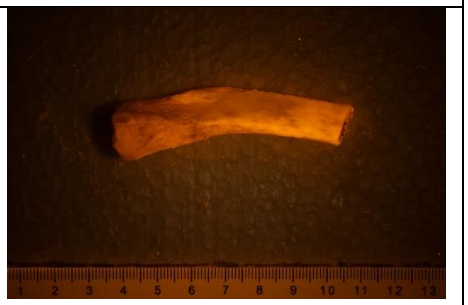
14		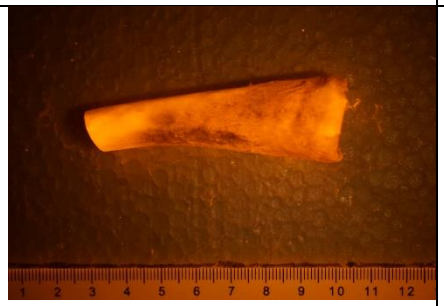	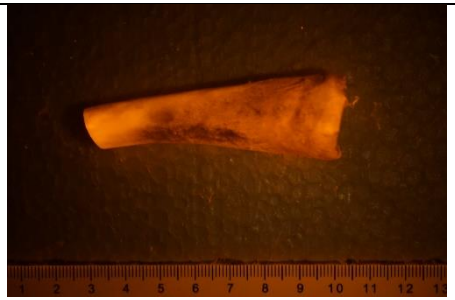	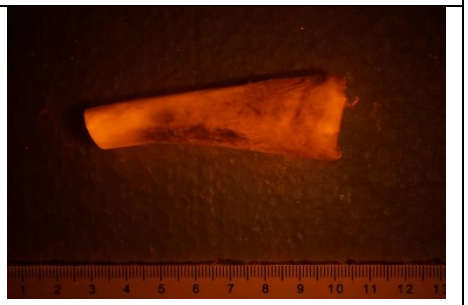

15				
16		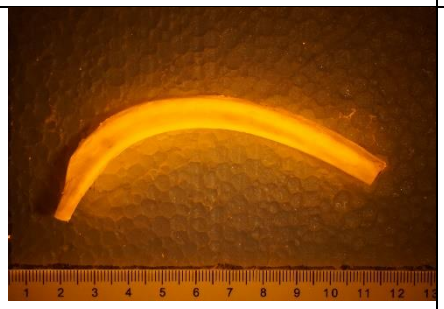	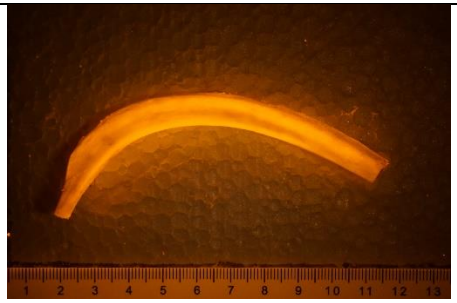	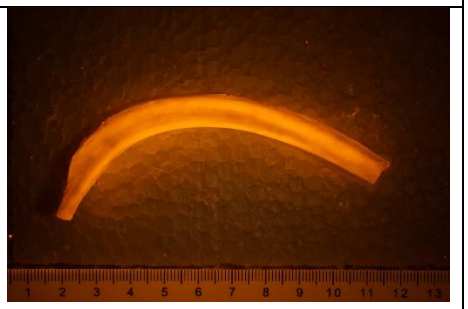
17				

18		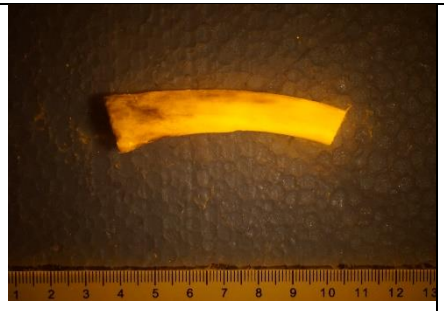	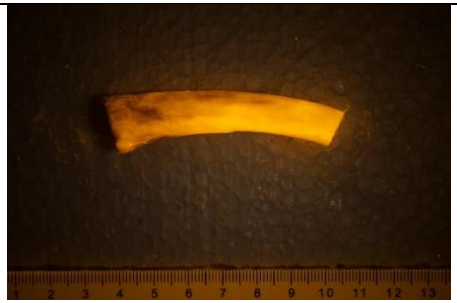	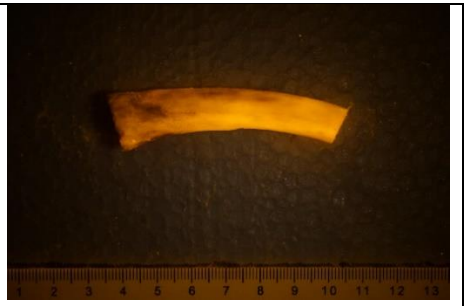
19		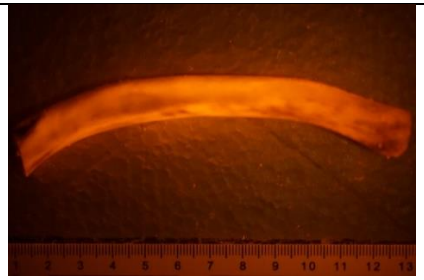	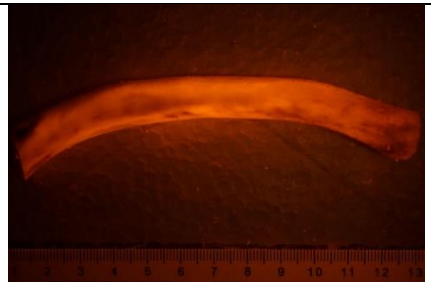	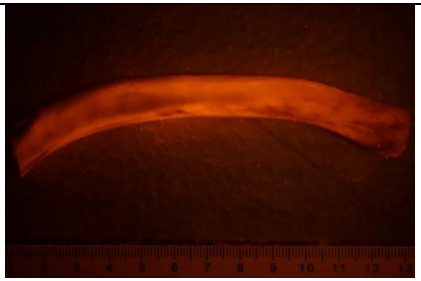
20				

21		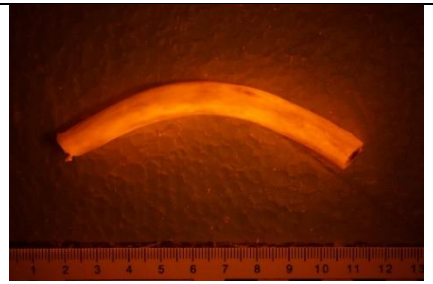	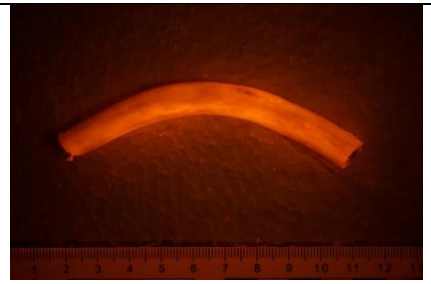	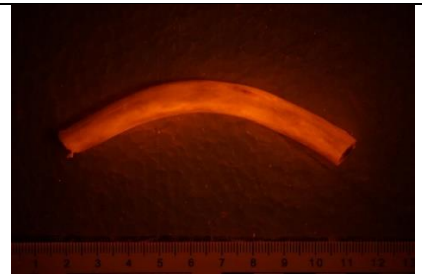
22	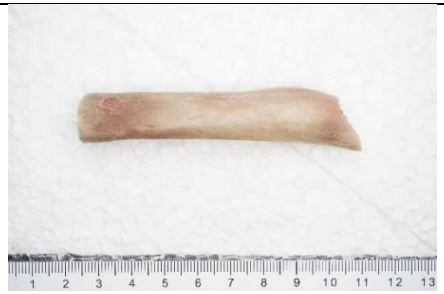	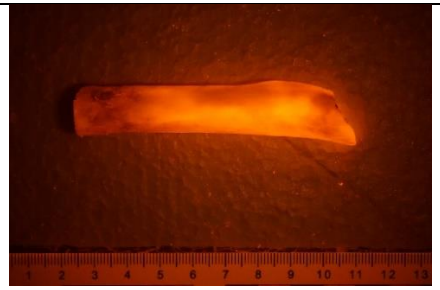	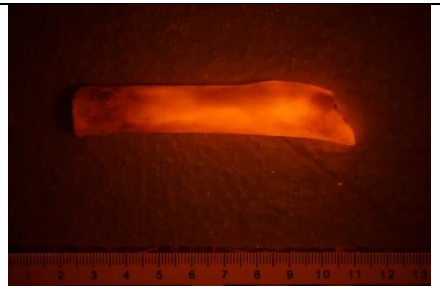	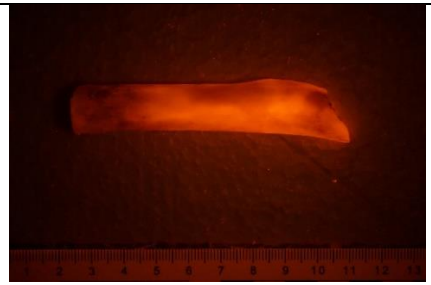
23		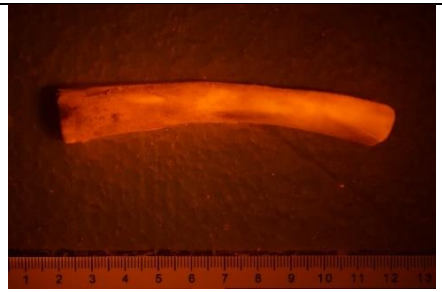	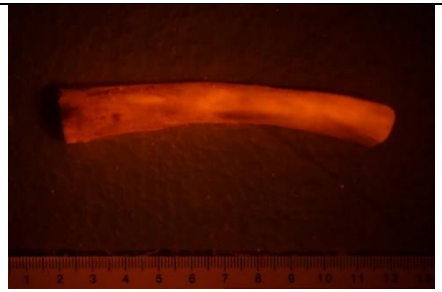	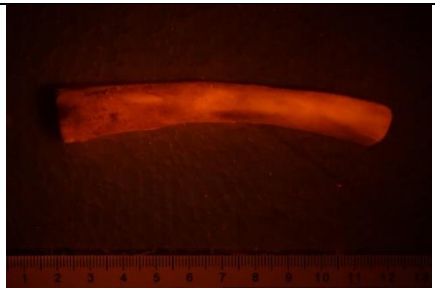

24		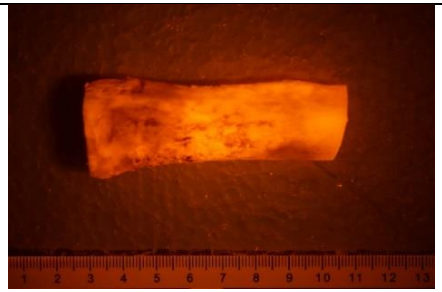	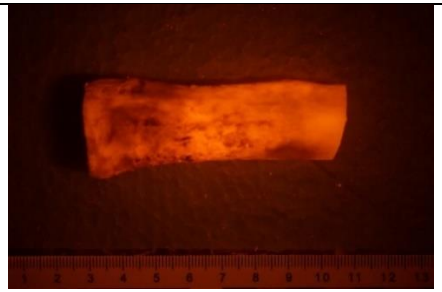	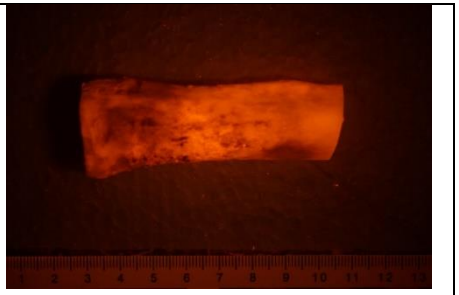
25		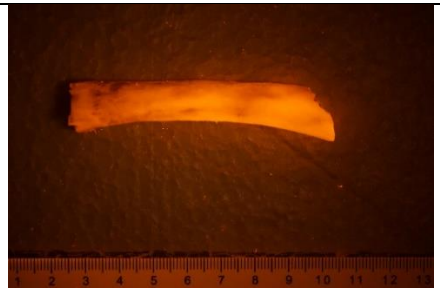	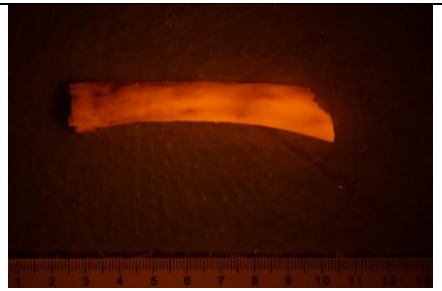	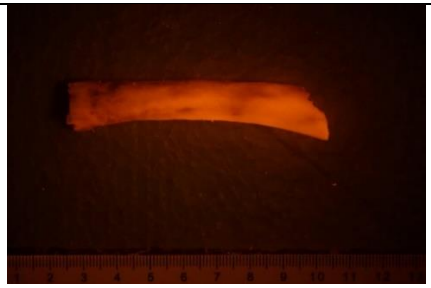
26		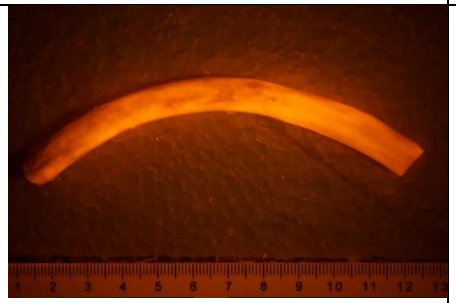	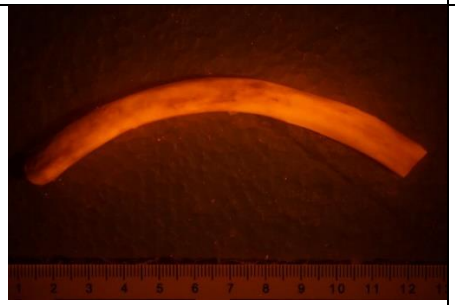	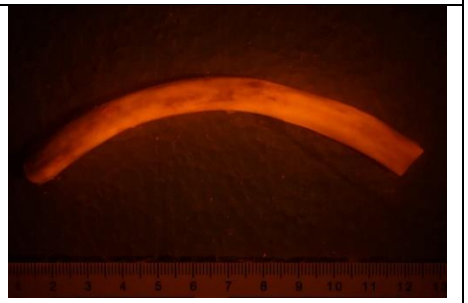

27	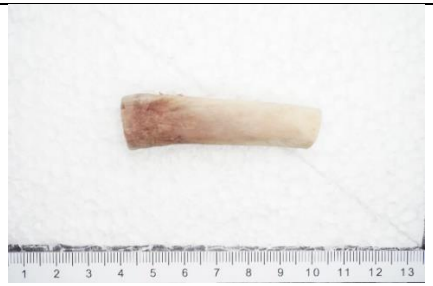			
28		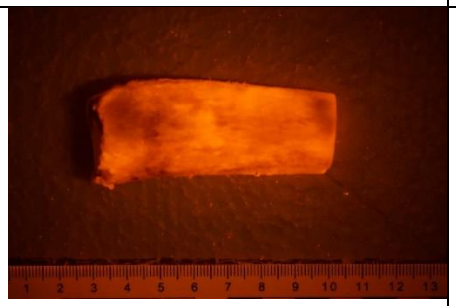	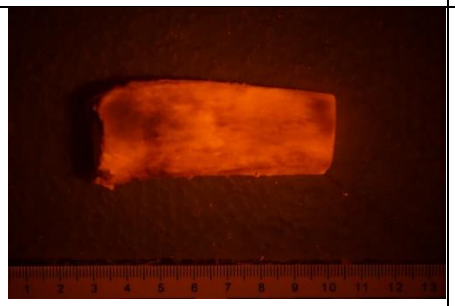	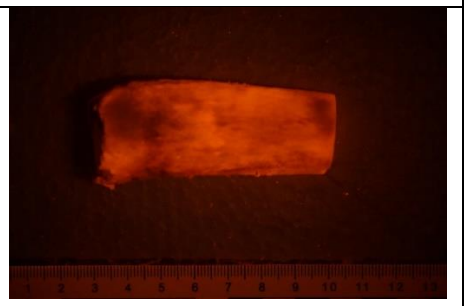
29			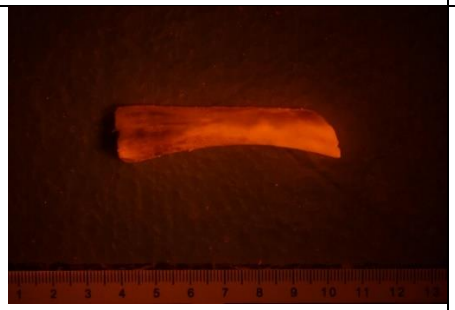	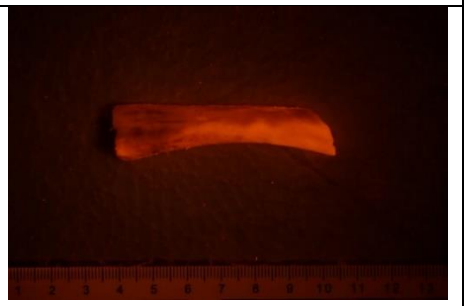

30	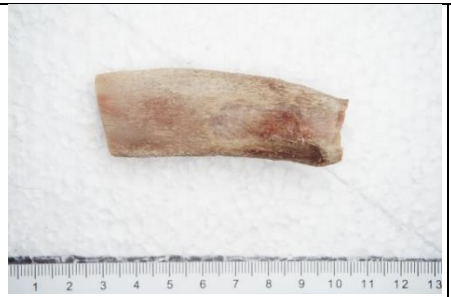	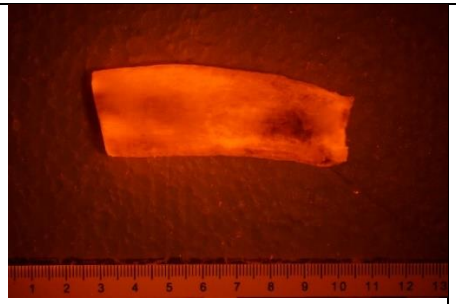	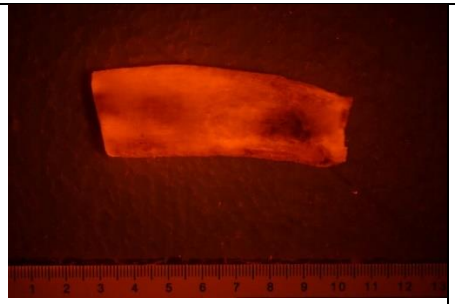	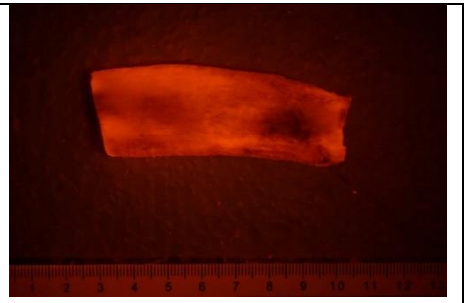
31				
32			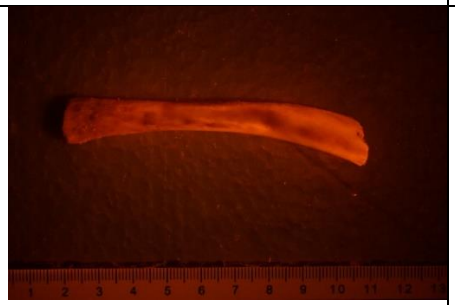	

33		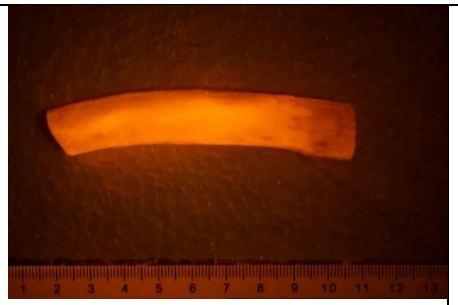	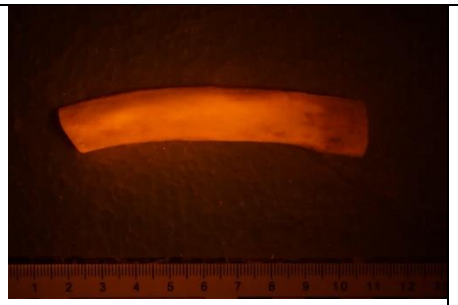	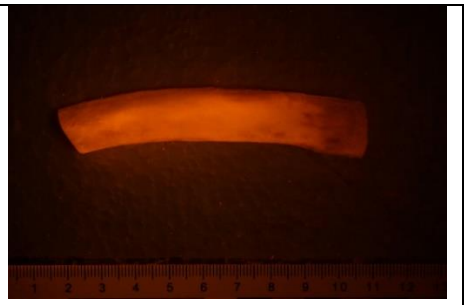
34		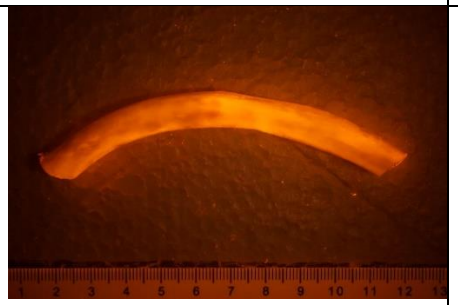	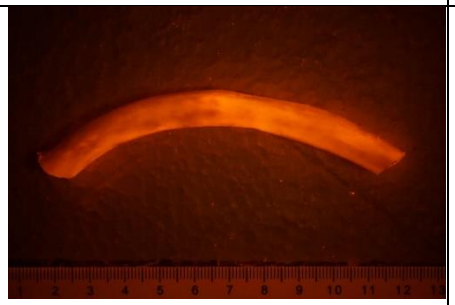	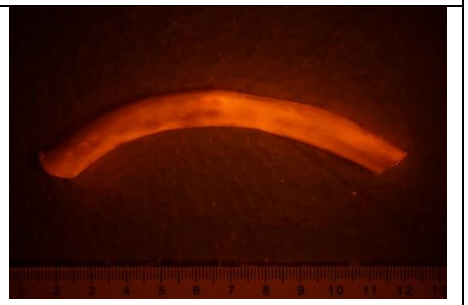
35		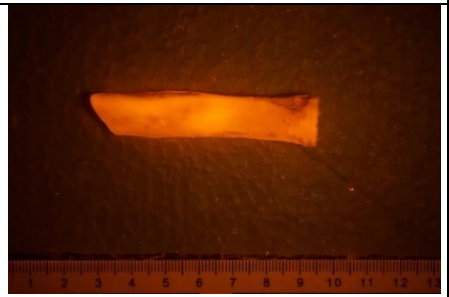	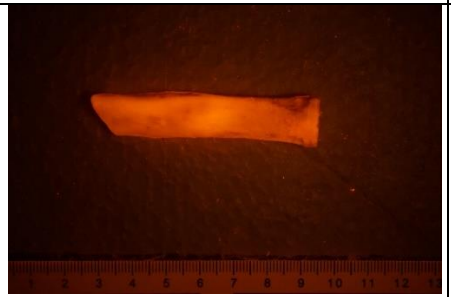	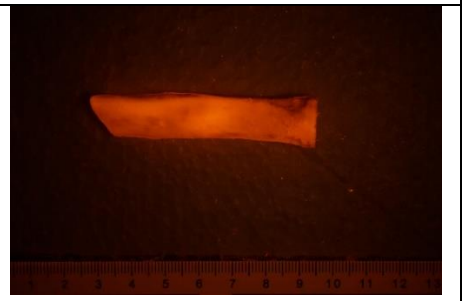

36		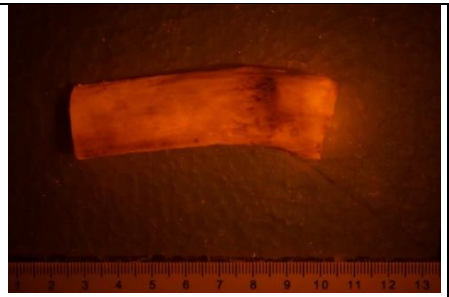	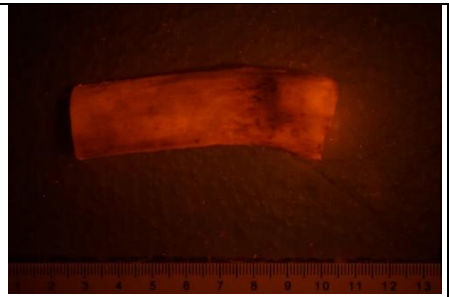	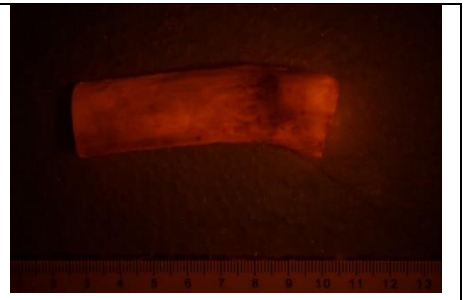
37		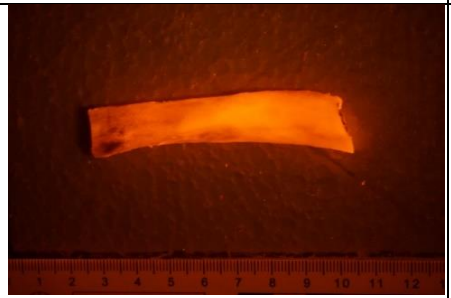	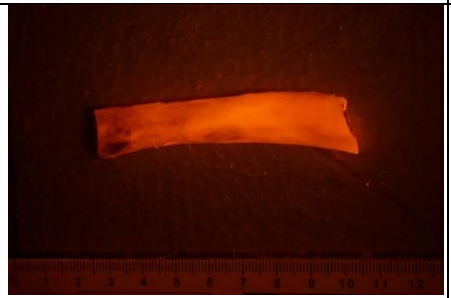	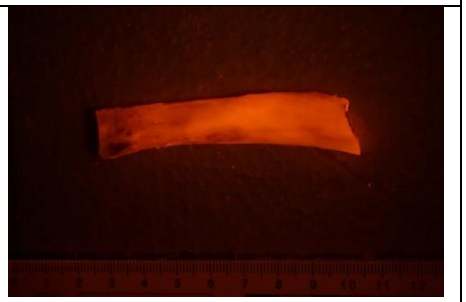
38		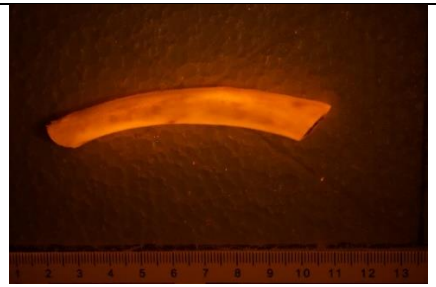	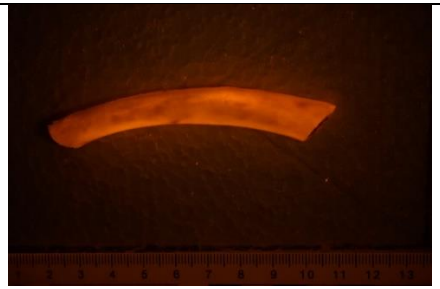	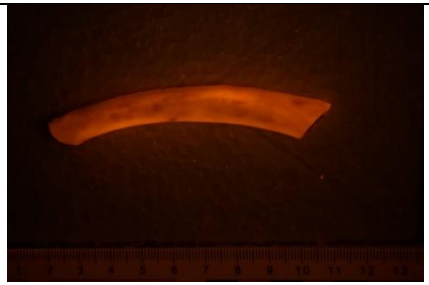

39		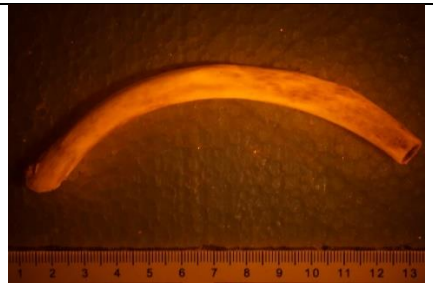	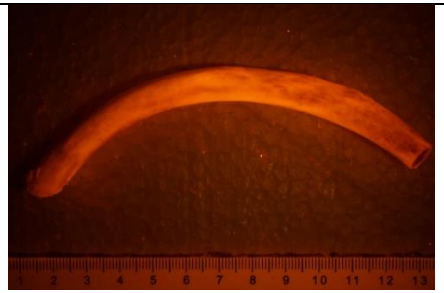	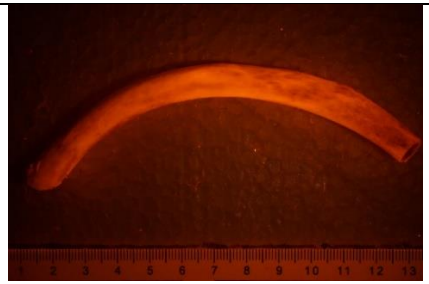
40		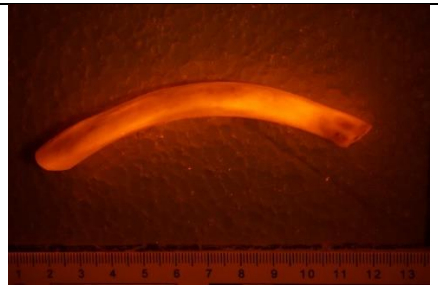	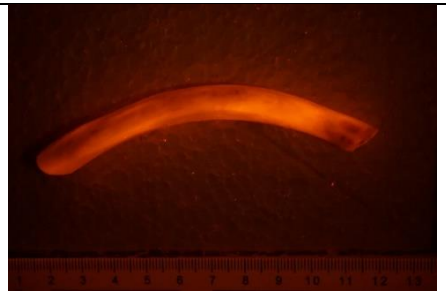	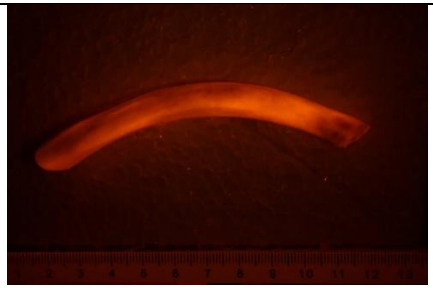
41				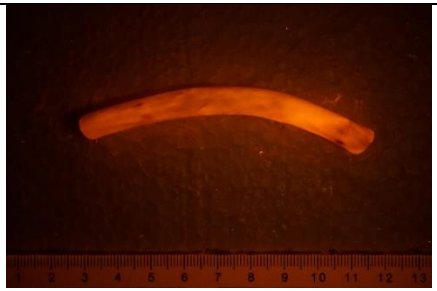

42		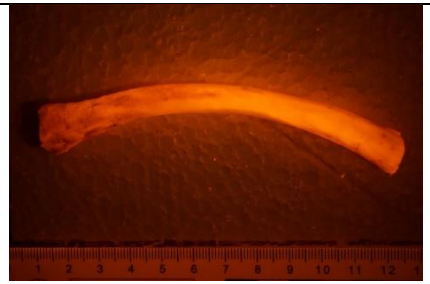	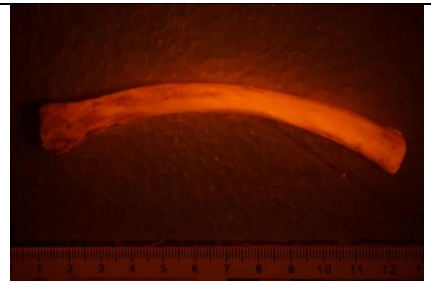	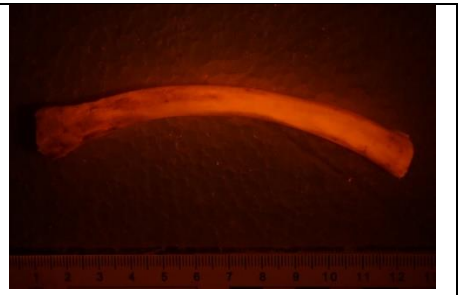
43		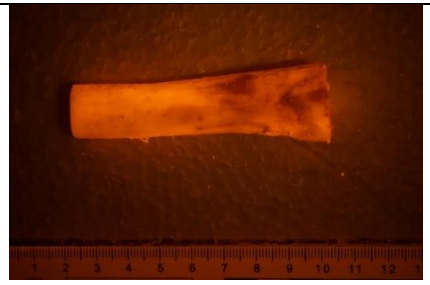	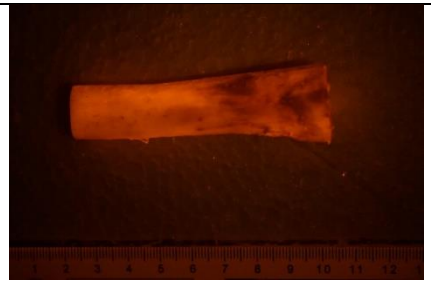	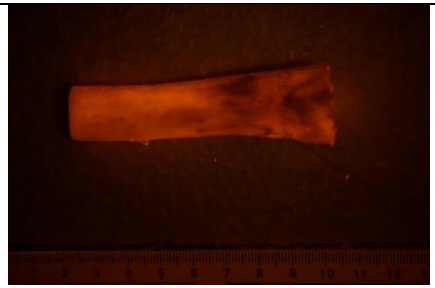
44		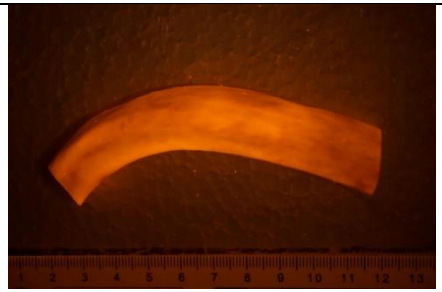	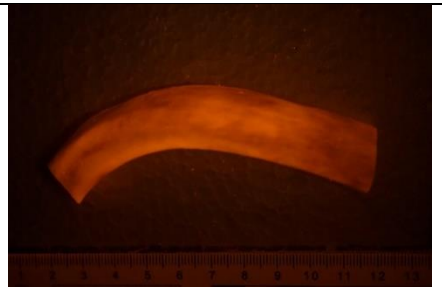	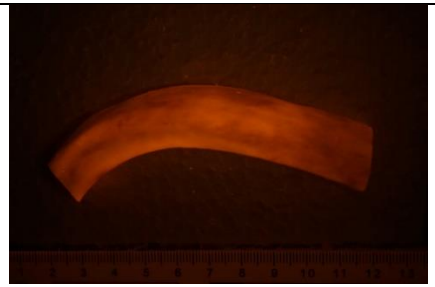

45		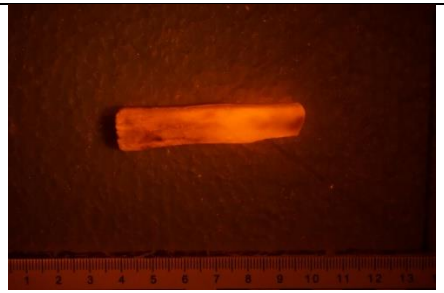		
46				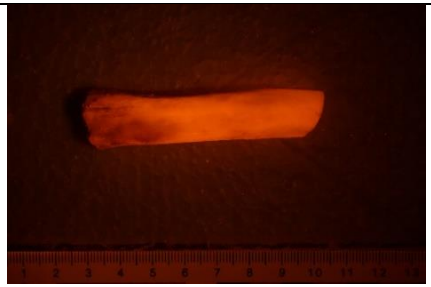
47			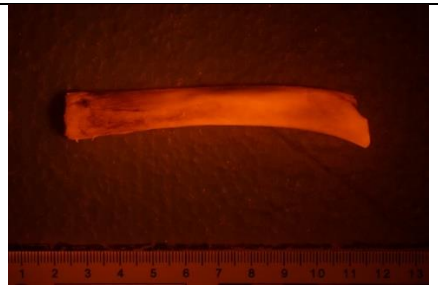	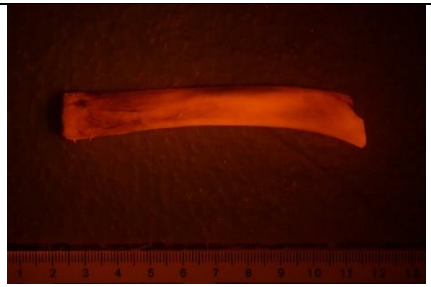

48		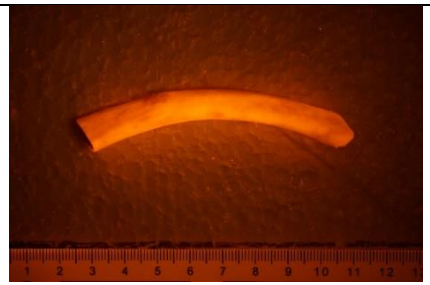	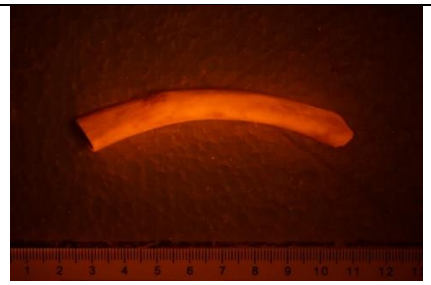	
49		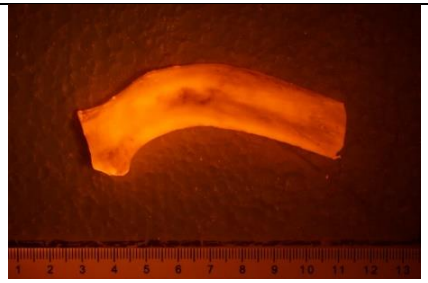	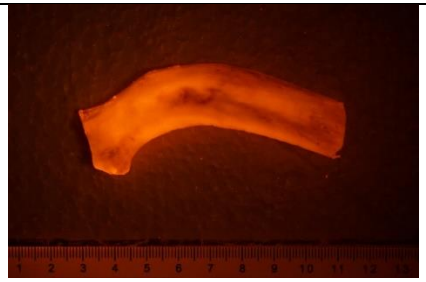	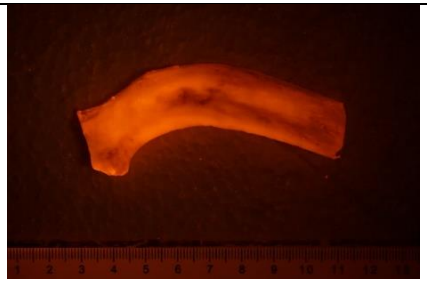
50		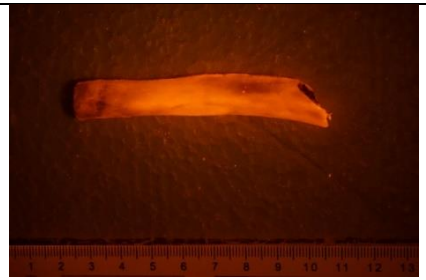	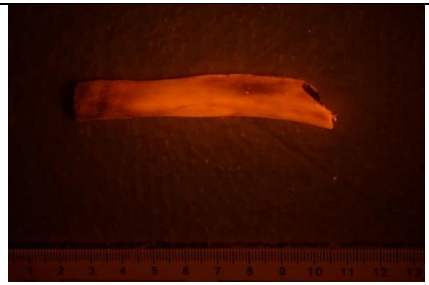	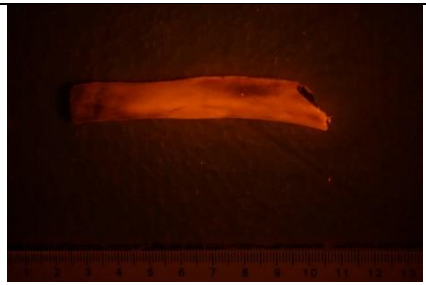

51		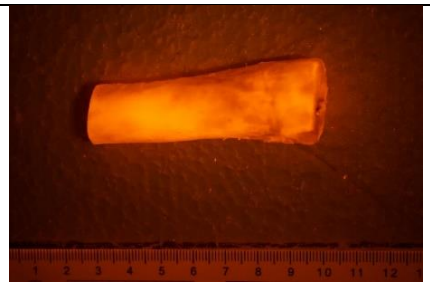		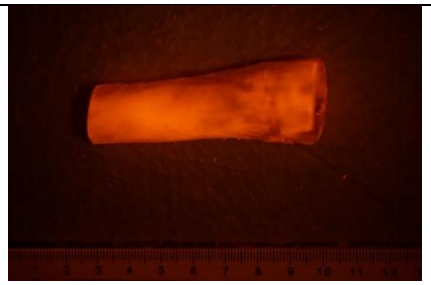
52		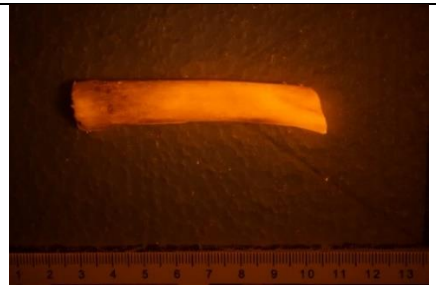	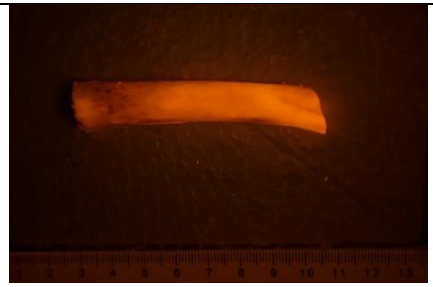	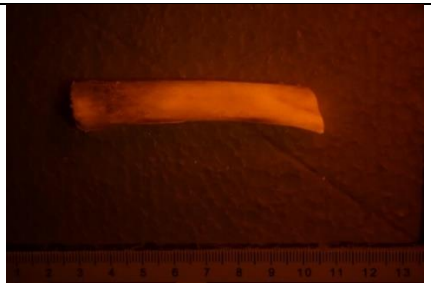
53				

54				

Appendix 49: Visual tables of summarised underwater fluorescence results for all 54 porcine ribs examined in section B, research question 2: investigating the collagen-fluorescence relationship.

Rib	Natural	0.6	0.4	1/3
1				
2			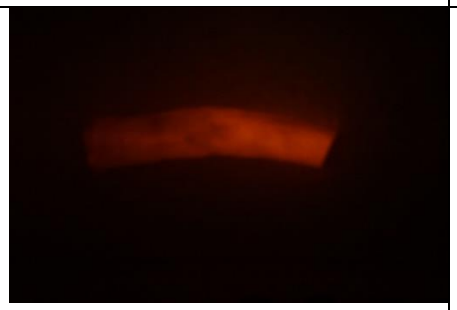	

3		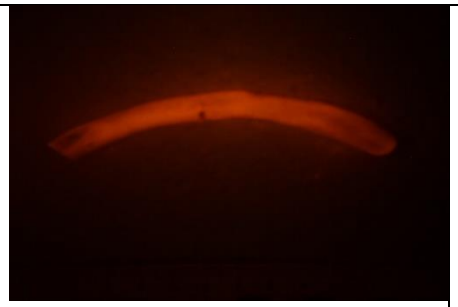	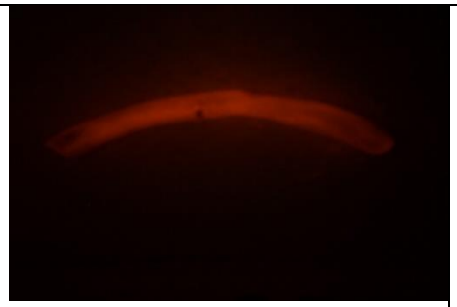	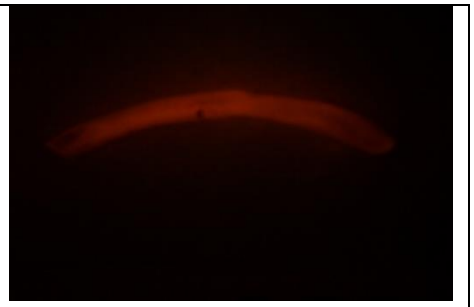
4				
5			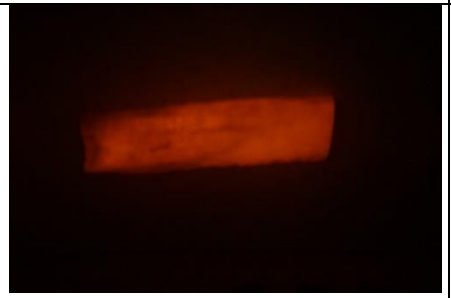	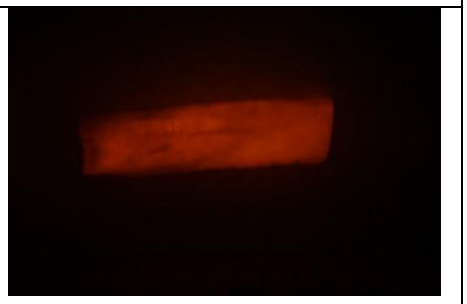

6			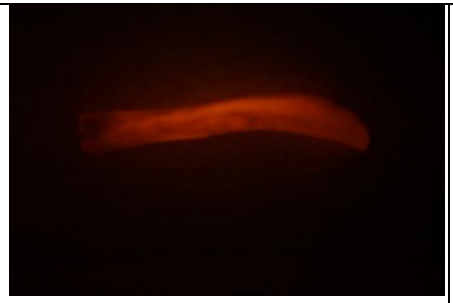	
7		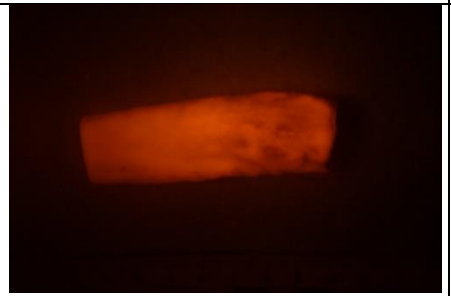	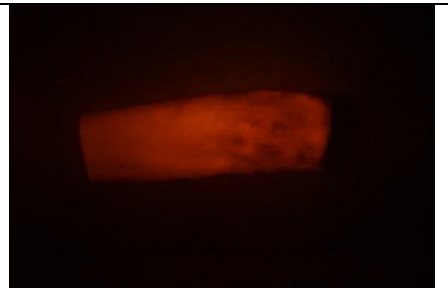	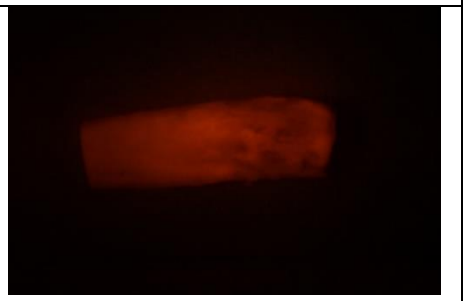
8			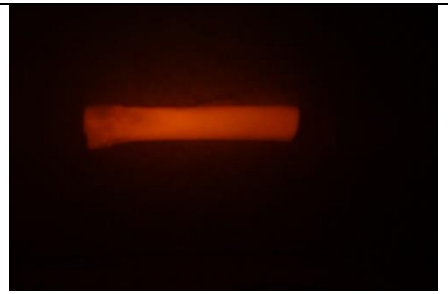	

9		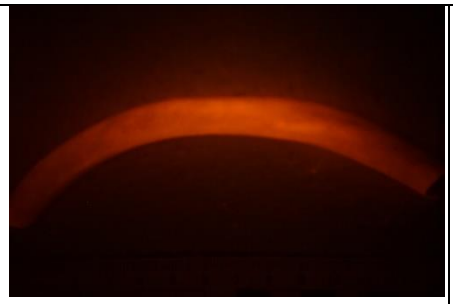		
10		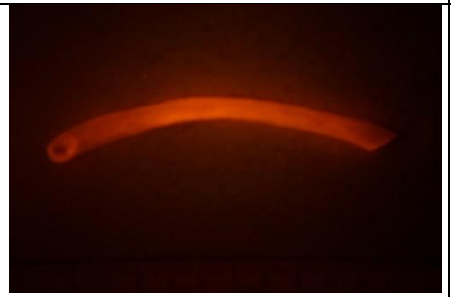	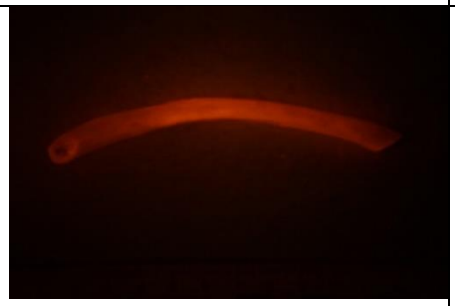	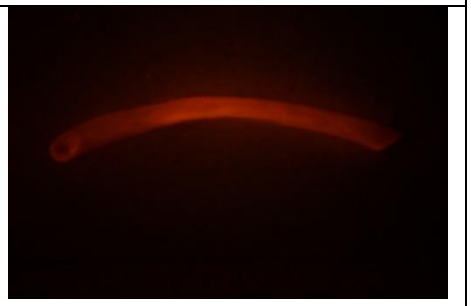
11				

12				
13		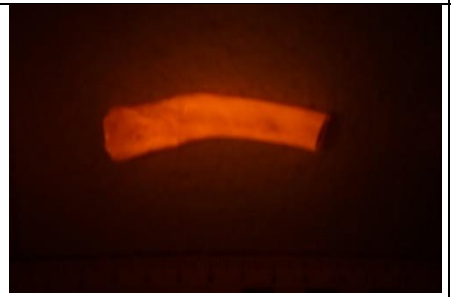	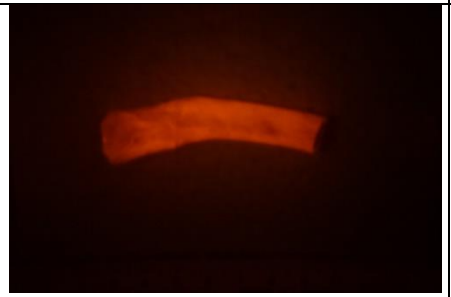	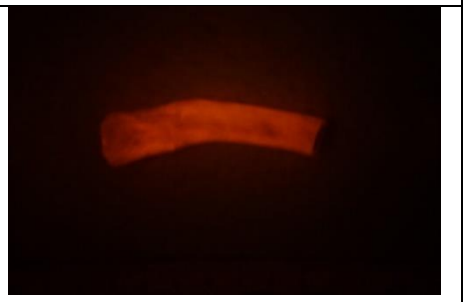
14		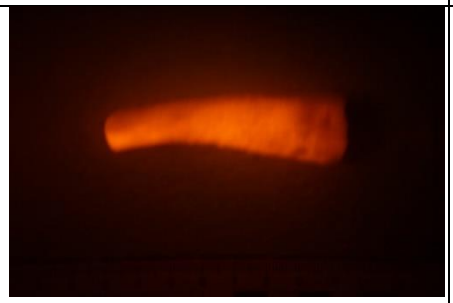		

15			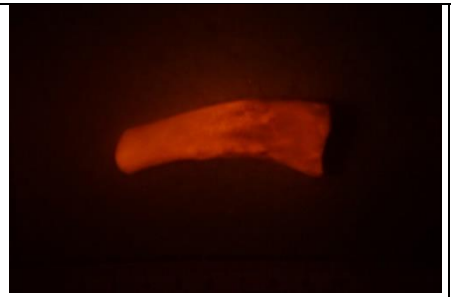	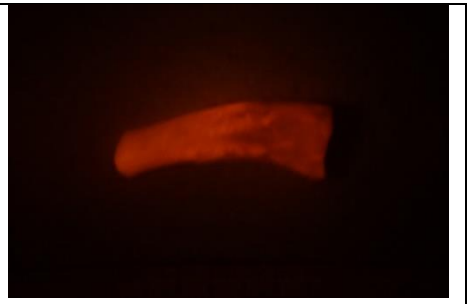
16		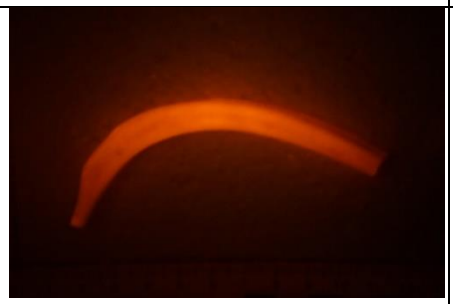		
17				

18			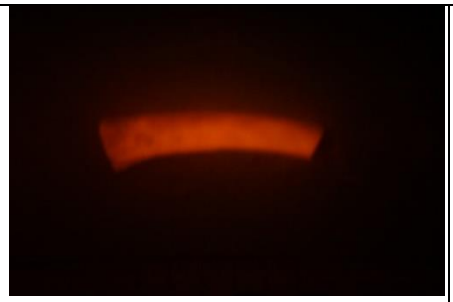	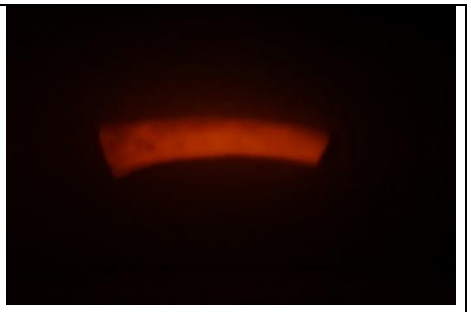
19		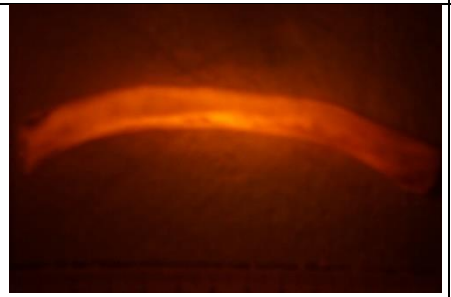	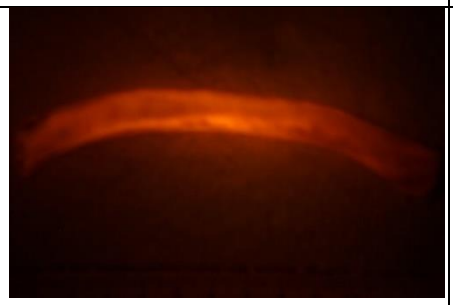	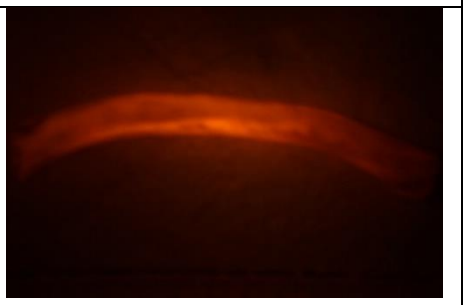
20		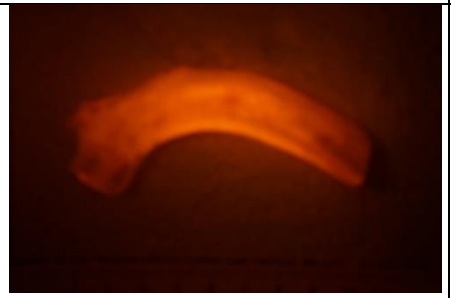	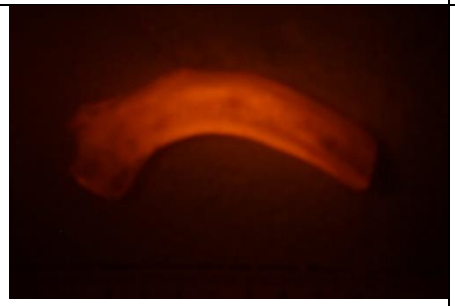	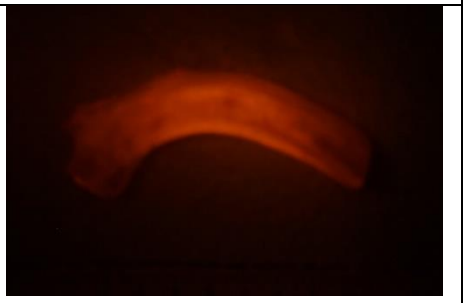

21		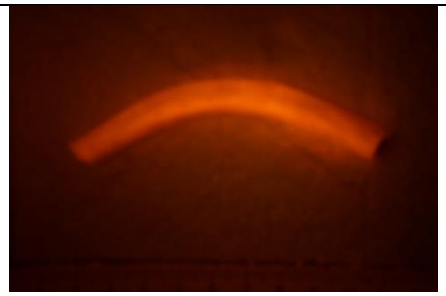		
22				
23				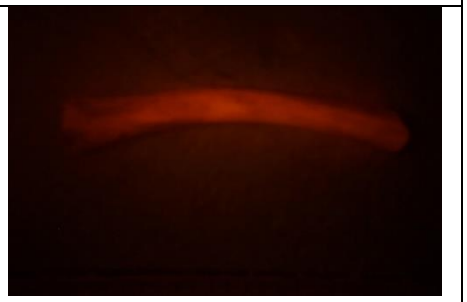

24				
25				
26				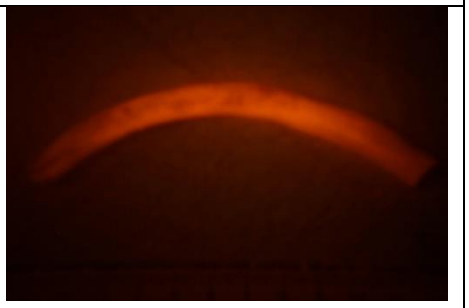

27	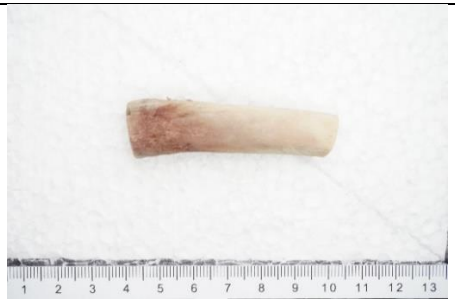			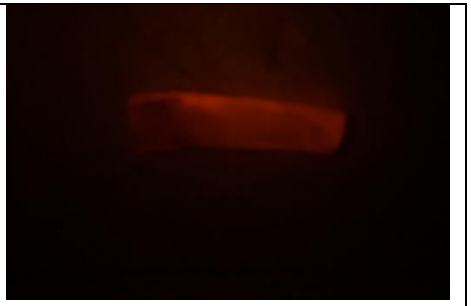
28		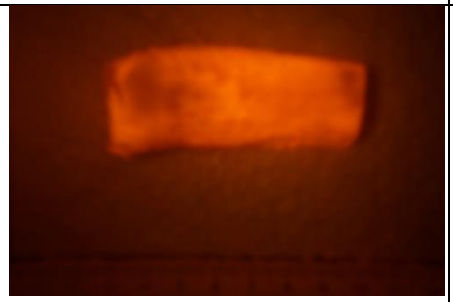		
29	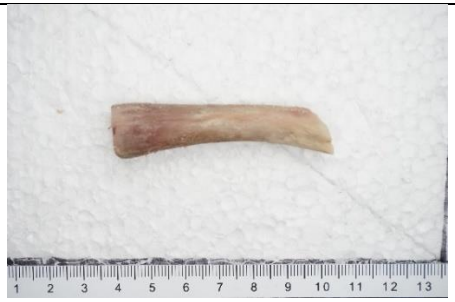			

30	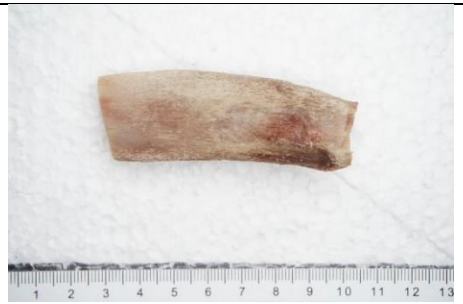	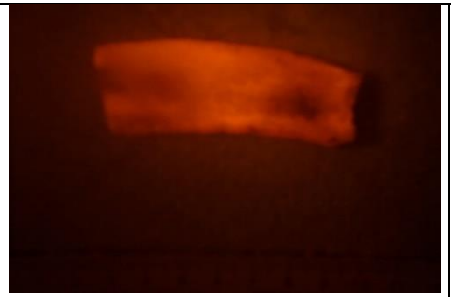	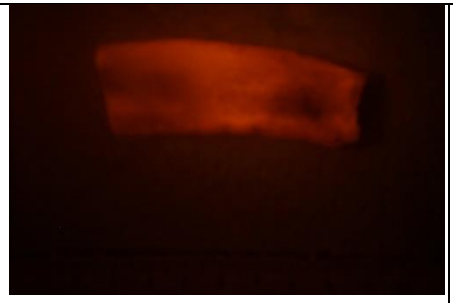	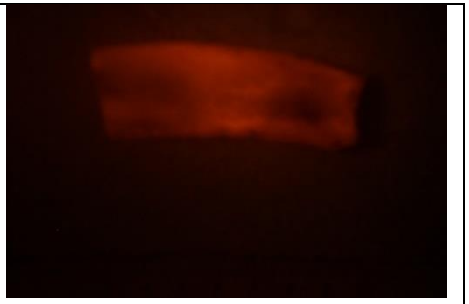
31		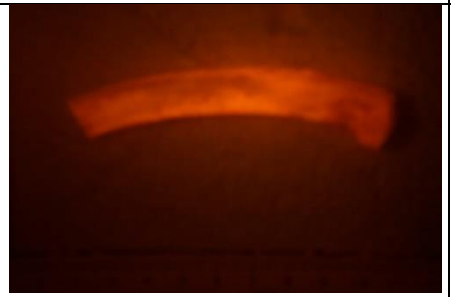		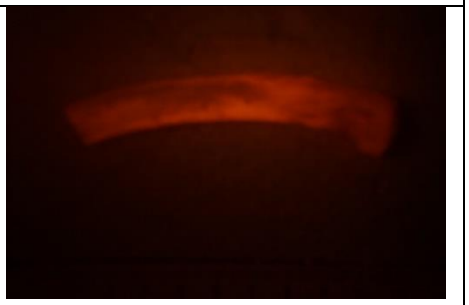
32				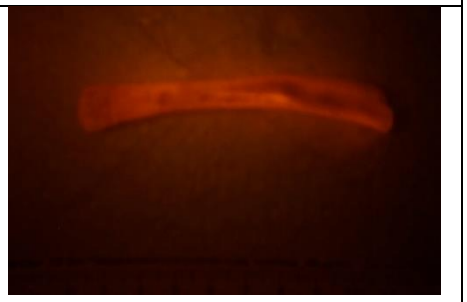

33		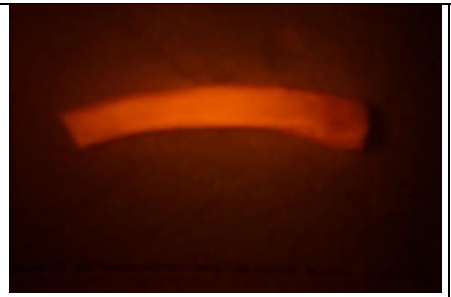	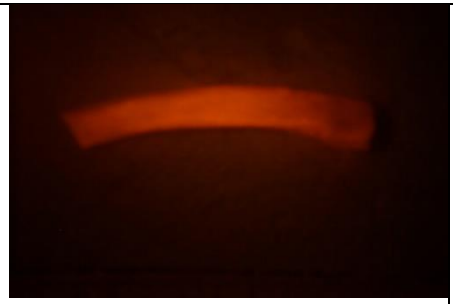	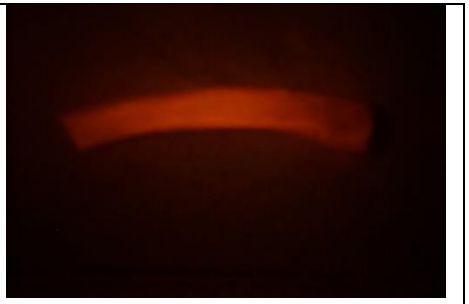
34				
35				

36		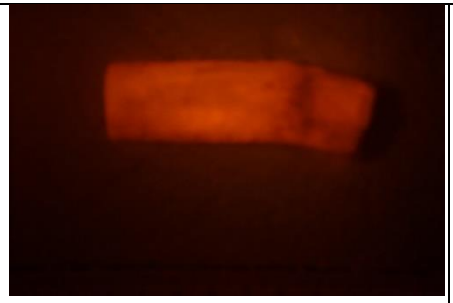		
37				
38		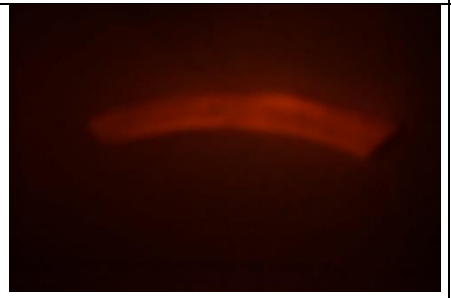		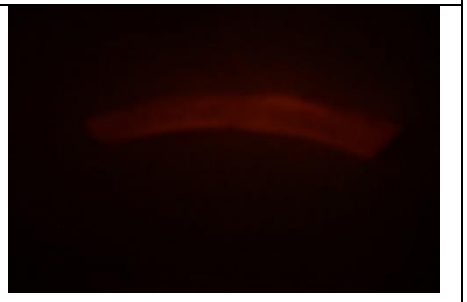

39				
40				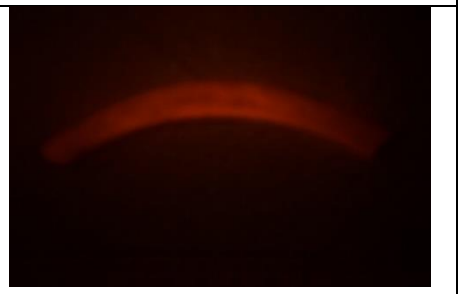
41		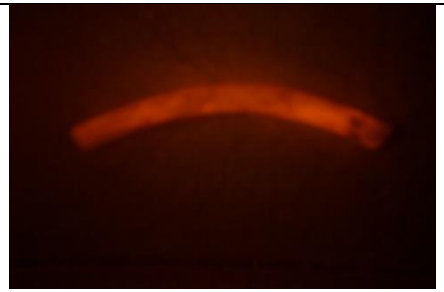	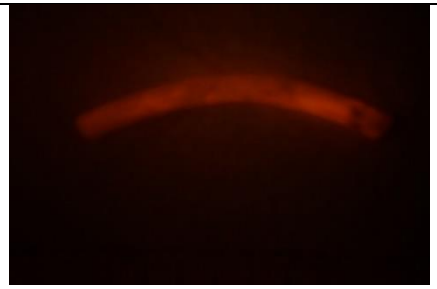	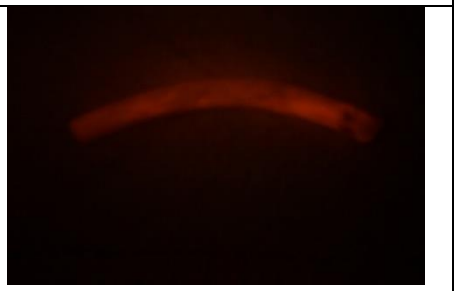

42				
43				
44				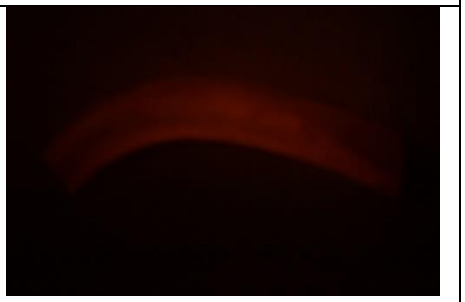

45				
46				
47		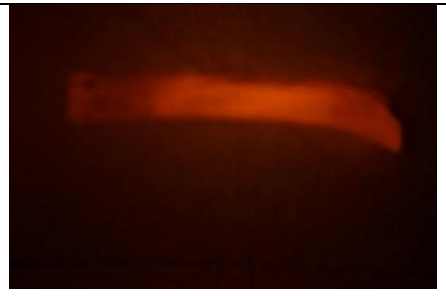		

48		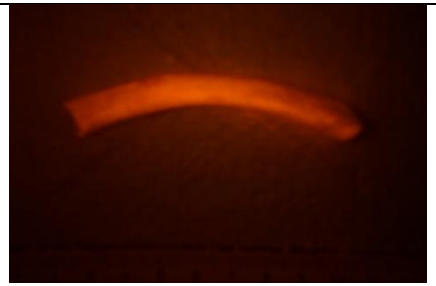	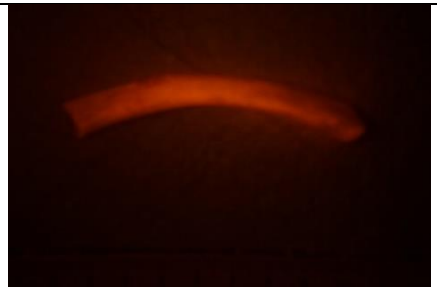	
49		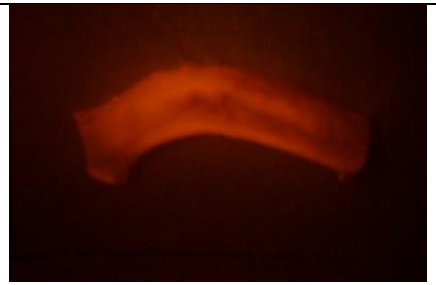		
50				

51				
52				
53				

54			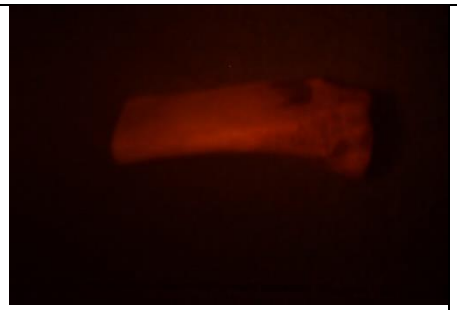	

Appendix 50: All terrestrial fluorescence and OFC processed photographs for the 54 macerated porcine bones for section B, question 2: Collagen-fluorescence relationship are available on OneDrive: 50 - All terrestrial fluorescence and OFC processed images for section B, question 2, collagen-fluorescence relationship

Appendix 51: All submerged fluorescence and OFC processed photographs for the 54 macerated porcine bones for section B, question 2: Collagen-fluorescence relationship are available on OneDrive: 51 - All submerged fluorescence and OFC processed images for section B, research question 2, collagen-fluorescence relationship

Appendix 52: All terrestrial fluorescence values for the 54 macerated porcine bones used in section B research question 2, investigating the collagen-fluorescence relationship.

A) 0.6s exposure time

Rib	0.6s Exposure time									Avg.
	Photograph 1			Photograph 2			Photograph 3			
	ROI 1	ROI 2	ROI 3	ROI 1	ROI 2	ROI 3	ROI 1	ROI 2	ROI 3	
1	173	176	179	174	177	180	175	177	180	176.8
2	147	156	180	147	156	181	146	157	180	161.1
3	127	142	147	127	141	145	126	141	145	137.9
4	184	185	183	183	185	182	183	185	182	183.6
5	180	189	180	180	189	180	179	189	179	182.8
6	170	180	188	172	181	189	172	180	188	180.0
7	154	150	139	153	149	137	153	149	137	146.8
8	186	189	190	184	188	190	183	187	189	187.3
9	157	166	168	157	166	168	158	166	167	163.7
10	158	173	167	158	173	167	159	173	166	166.0
11	105	115	128	105	115	128	105	115	129	116.1
12	143	149	160	144	149	160	144	151	162	151.3
13	125	128	129	124	127	128	124	126	127	126.4
14	125	114	105	126	114	106	125	114	105	114.9
15	74	76	106	74	76	106	73	76	106	85.2
16	174	177	166	174	177	166	174	176	166	172.2
17	171	182	163	171	182	163	170	182	163	171.9
18	167	177	171	168	177	171	167	177	170	171.7
19	143	142	142	142	142	142	142	142	142	142.1
20	149	138	142	149	137	142	149	136	142	142.7
21	138	135	145	138	136	145	136	135	144	139.1
22	125	112	116	125	112	115	124	111	115	117.2
23	122	138	126	122	138	126	122	138	126	128.7
24	145	152	142	145	152	142	144	152	142	146.2
25	140	151	137	140	151	137	139	150	136	142.3
26	138	128	139	138	128	139	138	127	138	134.8
27	132	141	153	131	141	152	131	141	152	141.6
28	135	138	126	135	138	127	134	138	128	133.2
29	112	122	121	113	122	121	113	122	121	118.6
30	114	116	114	114	116	114	114	116	114	114.7
31	91	101	103	89	99	101	89	100	102	97.2
32	78	78	79	78	78	79	78	78	79	78.3
33	139	148	144	134	144	140	134	144	139	140.7
34	126	150	155	125	150	155	126	151	156	143.8
35	146	157	142	146	157	141	146	157	142	148.2
36	88	96	86	88	95	87	88	95	87	90.0
37	144	150	151	144	150	150	142	148	150	147.7
38	113	131	136	114	131	137	114	131	137	127.1
39	147	146	139	146	145	138	146	144	137	143.1

40	120	131	145	120	131	144	120	131	144	131.8
41	134	143	151	134	143	152	134	143	151	142.8
42	127	141	149	127	141	149	127	141	149	139.0
43	133	113	80	133	113	79	133	113	78	108.3
44	123	134	132	123	133	132	123	133	131	129.3
45	109	120	141	109	120	140	109	120	140	123.1
46	157	158	153	157	158	152	157	157	152	155.7
47	112	119	126	112	118	125	113	119	126	118.9
48	129	125	115	130	126	116	133	129	118	124.6
49	102	108	117	103	108	117	102	107	117	109.0
50	134	129	120	135	130	121	135	130	121	128.3
51	138	138	122	137	137	121	137	137	121	132.0
52	148	150	149	148	150	149	148	150	149	149.0
53	87	100	111	87	99	110	90	102	113	99.9
54	98	93	84	98	93	84	96	91	82	91.0
Average	134.00	138.81	138.56	133.89	138.59	138.30	133.74	138.52	138.19	136.95

B) 0.4s exposure time

Rib	0.4s Exposure time									Avg.
	Photograph 1			Photograph 2			Photograph 3			
	ROI 1	ROI 2	ROI 3	ROI 1	ROI 2	ROI 3	ROI 1	ROI 2	ROI 3	
1	148	152	157	149	153	158	149	153	158	153.0
2	117	132	158	117	132	158	117	135	157	135.9
3	98	110	115	99	110	115	95	107	111	106.7
4	153	154		152	154	151	152	154	151	152.6
5	147	162	149	148	162	150	147	162	149	152.9
6	145	153	163	145	153	163	144	153	163	153.6
7	121	116	105	121	116	105	121	116	104	113.9
8	156	159	160	156	160	160	156	159	160	158.4
9	125	134	135	124	133	135	124	133	136	131.0
10	125	142	136	125	142	136	124	141	133	133.8
11	75	84	97	74	83	95	74	83	94	84.3
12	114	120	132	114	121	133	113	120	131	122.0
13	94	93	93	94	92	92	93	92	92	92.8
14	92	82	74	93	83	75	93	83	75	83.3
15	53	57	83	53	59	84	52	56	81	64.2
16	152	146	137	153	155	144	153	155	144	148.8
17	138	151	131	138	151	132	138	151	131	140.1
18	133	147	137	134	147	137	134	148	138	139.4
19	113	112	112	113	112	112	113	112	112	112.3
20	118	105	111	117	104	110	117	105	110	110.8
21	108	107	115	108	107	115	108	107	115	110.0
22	98	86	89	98	86	90	97	85	89	90.9
23	94	109	99	94	109	99	94	109	99	100.7
24	118	126	114	118	126	114	118	126	114	119.3
25	110	121	108	110	121	108	110	121	108	113.0
26	110	100	110	110	99	110	109	99	109	106.2
27	103	112	124	102	111	123	102	111	123	112.3
28	106	110	99	106	110	99	106	110	99	105.0
29	85	94	93	85	93	92	86	94	93	90.6
30	90	92	89	90	92	89	89	92	89	90.2
31	69	81	83	69	81	83	69	80	83	77.6
32	55	55	55	55	55	55	54	55	55	54.9
33	116	121	111	115	120	110	114	119	109	115.0
34	101	127	132	102	128	133	102	127	133	120.6
35	118	132	115	118	131	114	119	131	114	121.3
36	63	69	61	63	69	61	63	69	61	64.3
37	116	123	125	116	122	124	115	121	124	120.7
38	83	99	107	83	99	106	83	99	107	96.2
39	120	118	112	119	118	111	119	118	111	116.2
40	89	99	112	90	100	113	89	99	112	100.3
41	107	115	123	106	114	122	106	114	122	114.3
42	99	112	121	99	112	120	100	113	120	110.7

43	103	84	54	103	83	53	102	83	53	79.8
44	92	102	99	91	101	99	91	101	99	97.2
45	82	93	112	82	93	111	82	93	112	95.6
46	131	131	125	131	131	125	131	131	125	129.0
47	86	90	98	86	91	98	86	91	98	91.6
48	101	97	88	102	97	88	100	95	86	94.9
49	78	82	91	78	82	92	78	82	91	83.8
50	106	105	100	106	105	100	106	105	100	103.7
51	106	106	92	106	106	92	107	106	92	101.4
52	116	118	117	116	118	117	116	118	117	117.0
53	100	108	114	101	109	114	100	108	114	107.6
54	70	66	59	70	65	58	70	65	58	64.6
Average	106.41	111.13	110.02	106.43	111.22	110.80	106.11	111.02	110.44	109.37

C) 1/3s exposure time

Rib	1/3s Exposure time									Avg.
	Photograph 1			Photograph 2			Photograph 3			
	ROI 1	ROI 2	ROI 3	ROI 1	ROI 2	ROI 3	ROI 1	ROI 2	ROI 3	
1	136	141	145	136	141	145	136	140	144	140.4
2	102	121	143	102	121	143	102	119	143	121.8
3	88	98	103	87	97	101	88	99	103	96.0
4	135	137	134	135	137	134	136	137	134	135.4
5	132	146	133	130	146	133	130	145	133	136.4
6	122	134	145	122	134	145	121	134	144	133.4
7	107	103	93	106	103	93	106	102	91	100.4
8	139	142	143	138	142	143	136	141	142	140.7
9	107	112	113	107	112	114	107	112	113	110.8
10	108	122	116	108	122	116	107	122	116	115.2
11	66	75	86	65	74	85	64	73	85	74.8
12	104	111	121	103	110	121	103	110	121	111.6
13	86	87	87	85	86	86	86	87	86	86.2
14	82	74	65	82	74	66	82	74	66	73.9
15	51	47	72	51	48	73	50	46	71	56.6
16	145	146	138	144	146	138	144	146	137	142.7
17	122	133	114	123	134	114	123	133	114	123.3
18	126	140	132	124	138	131	126	140	132	132.1
19	98	97	97	98	97	97	98	97	97	97.3
20	102	92	96	102	91	96	102	91	96	96.4
21	93	91	100	93	91	100	93	91	100	94.7
22	84	74	78	84	74	78	84	74	78	78.7
23	79	95	85	80	95	85	80	95	85	86.6
24	106	111	100	106	111	100	105	111	100	105.6
25	95	105	92	95	105	93	95	105	92	97.4
26	94	85	95	94	85	95	94	84	95	91.2
27	89	97	110	89	97	110	89	97	109	98.6
28	92	95	85	92	95	85	93	95	85	90.8
29	71	79	78	72	79	78	72	79	78	76.2
30	77	78	75	76	78	74	76	78	74	76.2
31	56	66	69	56	66	69	56	66	69	63.7
32	45	46	45	45	45	45	44	45	45	45.0
33	96	102	91	99	104	94	98	103	93	97.8
34	89	114	119	89	114	119	89	113	120	107.3
35	105	114	96	105	114	96	105	113	96	104.9
36	52	57	50	52	57	50	53	58	51	53.3
37	99	103	108	98	103	108	97	101	106	102.6
38	69	84	92	70	84	92	70	84	91	81.8
39	110	108	104	110	108	104	108	107	103	106.9
40	77	87	100	77	88	101	77	88	101	88.4
41	91	99	106	90	98	105	90	98	105	98.0

42	88	99	106	87	98	105	87	98	105	97.0
43	86	68	42	86	68	42	86	66	40	64.9
44	77	85	83	77	86	83	77	85	83	81.8
45	69	79	97	68	78	97	68	78	97	81.2
46	115	115	110	115	115	110	114	115	109	113.1
47	71	76	82	71	76	82	71	77	83	76.6
48	97	93	82	96	92	82	96	92	85	90.6
49	67	71	80	67	71	80	67	71	80	72.7
50	93	89	82	93	90	83	93	90	83	88.4
51	93	94	79	93	93	79	93	93	79	88.4
52	103	104	104	102	104	104	102	104	103	103.3
53	87	96	102	87	96	103	87	96	103	95.2
54	57	53	47	57	53	47	58	53	47	52.4
Average	93.15	97.59	97.22	92.94	97.48	97.26	92.85	97.24	97.06	95.87

Appendix 53: All underwater fluorescence values for the 54 macerated porcine bones used in section B research question 2, investigating the collagen-fluorescence relationship.

A) 0.6s exposure time

Rib	0.6s Exposure time									Avg.
	Photograph 1			Photograph 2			Photograph 3			
	ROI 1	ROI 2	ROI 3	ROI 1	ROI 2	ROI 3	ROI 1	ROI 2	ROI 3	
1	129	135	135	129	135	135	129	135	135	133.0
2	138	144	157	138	145	158	137	145	157	146.6
3	77	91	88	77	91	89	75	89	87	84.9
4	92	87	79	92	87	79	91	86	79	85.8
5	124	136	129	124	136	128	123	136	128	129.3
6	132	123	115	131	123	115	131	123	114	123.0
7	134	136	132	133	135	133	133	135	134	133.9
8	152	148	143	153	149	143	151	147	142	147.6
9	121	120	120	122	120	120	121	119	120	120.3
10	90	93	86	90	92	85	88	91	84	88.8
11	77	78	78	77	78	78	77	78	77	77.6
12	62	60	54	61	59	53	60	58	52	57.7
13	78	92	96	79	93	96	79	93	97	89.2
14	125	122	118	124	122	119	124	122	119	121.7
15	78	63	66	79	62	66	78	62	68	69.1
16	126	134	135	130	141	141	128	138	139	134.7
17	105	104	95	102	101	93	102	102	94	99.8
18	118	131	130	117	131	131	117	130	130	126.1
19	109	117	126	109	118	126	109	118	126	117.6
20	122	122	115	121	121	115	120	121	114	119.0
21	109	114	120	109	114	120	109	114	119	114.2
22	150	148	147	149	147	146	146	145	144	146.9
23	96	106	101	96	106	102	95	106	102	101.1
24	117	131	110	115	130	110	115	129	110	118.6
25	119	126	135	123	129	137	127	133	139	129.8
26	138	136	145	131	131	144	129	133	144	136.8
27	57	64	64	56	64	63	56	63	63	61.1
28	121	132	123	120	132	123	118	132	122	124.8
29	104	105	105	105	105	106	104	105	106	105.0
30	87	95	93	83	92	92	84	93	93	90.2
31	102	116	114	102	116	113	102	115	113	110.3
32	106	107	111	104	105	109	104	105	109	106.7
33	117	116	106	118	116	106	118	116	107	113.3
34	111	117	118	114	120	120	113	119	119	116.8
35	153	158	151	154	158	151	153	158	150	154.0
36	88	87	84	88	87	84	87	86	84	86.1

37	69	69	75	68	71	75	68	70	75	71.1
38	45	47	54	44	46	52	43	44	49	47.1
39	84	88	88	84	87	88	84	87	87	86.3
40	88	89	91	87	88	90	87	87	89	88.4
41	70	71	71	70	72	71	69	70	70	70.4
42	64	64	60	65	65	62	64	65	61	63.3
43	84	77	75	83	75	74	83	76	74	77.9
44	46	52	57	46	52	57	46	51	56	51.4
45	86	103	110	87	103	110	86	102	109	99.6
46	108	108	104	106	107	103	106	107	103	105.8
47	79	87	95	79	87	94	78	86	93	86.4
48	101	97	98	100	97	98	102	98	99	98.9
49	75	70	64	75	69	63	74	69	63	69.1
50	68	67	63	68	67	63	68	66	61	65.7
51	126	122	104	126	123	106	126	122	106	117.9
52	84	89	89	80	87	87	80	87	87	85.6
53	63	79	75	63	79	75	63	79	75	72.3
54	69	71	68	63	66	62	63	66	62	65.6
Average	99.50	102.67	101.20	99.06	102.44	101.09	98.57	102.07	100.72	100.81

B) 0.4s exposure time

Rib	0.4s Exposure time									Avg.
	Photograph 1			Photograph 2			Photograph 3			
	ROI 1	ROI 2	ROI 3	ROI 1	ROI 2	ROI 3	ROI 1	ROI 2	ROI 3	
1	99	104	105	98	104	105	97	104	105	102.3
2	114	122	132	113	122	131	113	122	131	122.2
3	53	68	64	51	65	63	51	64	63	60.2
4	65	60	54	65	61	54	65	61	54	59.9
5	94	103	94	94	103	93	94	103	93	96.8
6	100	92	84	99	91	84	97	90	84	91.2
7	103	104	102	103	103	101	103	103	101	102.6
8	123	118	112	121	116	110	119	114	109	115.8
9	93	91	94	93	91	93	92	90	93	92.2
10	75	78	70	75	78	72	74	76	70	74.2
11	51	52	52	51	52	51	51	51	51	51.3
12	41	40	35	39	38	34	41	39	36	38.1
13	56	69	70	55	68	70	56	69	69	64.7
14	97	94	91	98	93	91	95	93	91	93.7
15	50	39	42	48	39	41	49	39	42	43.2
16	97	107	109	97	107	110	96	108	111	104.7
17	74	73	68	75	75	69	78	80	71	73.7
18	77	88	89	80	90	92	73	82	86	84.1
19	81	90	98	81	91	98	81	91	100	90.1
20	93	93	88	91	91	86	92	92	87	90.3
21	82	88	91	82	88	91	82	88	91	87.0
22	109	110	110	109	110	110	110	110	110	109.8
23	71	80	72	71	80	73	69	79	75	74.4
24	91	104	85	91	104	85	90	103	85	93.1
25	102	106	110	100	104	110	96	102	108	104.2
26	100	100	112	100	100	113	99	100	113	104.1
27	36	41	41	35	41	40	35	41	41	39.0
28	86	101	92	87	100	92	87	100	92	93.0
29	134	133	133	134	133	133	133	133	134	133.3
30	60	66	65	55	65	65	55	64	65	62.2
31	71	84	83	71	84	83	70	84	82	79.1
32	74	76	79	73	75	78	73	74	77	75.4
33	90	89	80	89	88	80	89	88	79	85.8
34	89	94	94	89	95	94	90	95	94	92.7
35	125	131	121	124	130	120	124	130	118	124.8
36	60	60	58	60	61	59	62	61	60	60.1
37	45	47	50	45	47	50	45	47	50	47.3
38	29	30	34	29	30	34	29	30	34	31.0
39	58	61	62	57	60	61	56	60	61	59.6
40	60	60	62	60	60	62	60	60	62	60.7
41	42	42	42	40	40	40	42	42	42	41.3

42	44	47	45	43	46	44	44	45	43	44.6
43	55	52	44	55	52	44	55	51	43	50.1
44	31	34	38	31	34	38	31	34	38	34.3
45	56	65	77	55	65	78	54	64	78	65.8
46	79	79	74	79	79	74	78	78	73	77.0
47	53	57	62	53	57	63	52	55	61	57.0
48	75	75	75	71	68	69	70	67	69	71.0
49	50	46	42	51	47	42	52	48	42	46.7
50	45	44	40	45	44	40	45	44	40	43.0
51	98	93	76	97	92	75	97	93	76	88.6
52	55	62	63	55	61	62	53	60	61	59.1
53	41	53	51	41	53	50	40	53	50	48.0
54	41	43	38	41	43	39	40	42	38	40.6
Average	73.57	76.63	75.07	73.06	76.19	74.80	72.67	75.85	74.67	74.72

C) 1/3s exposure time

Rib	1/3s Exposure time									Avg.
	Photograph 1			Photograph 2			Photograph 3			
	ROI 1	ROI 2	ROI 3	ROI 1	ROI 2	ROI 3	ROI 1	ROI 2	ROI 3	
1	84	89	89	83	89	89	83	88	89	87.0
2	95	103	111	95	102	111	96	103	112	103.1
3	42	52	51	42	53	51	42	52	51	48.4
4	52	48	43	52	48	43	52	48	43	47.7
5	80	88	79	80	89	79	80	89	79	82.6
6	86	77	69	85	77	70	84	76	70	77.1
7	88	88	83	88	89	84	88	88	84	86.7
8	104	99	94	107	101	96	107	102	96	100.7
9	82	80	80	81	80	80	81	80	80	80.4
10	61	61	55	58	59	53	58	59	53	57.4
11	41	42	41	42	42	42	41	42	42	41.7
12	33	33	30	33	33	30	32	32	29	31.7
13	44	55	56	45	55	56	45	55	56	51.9
14	78	80	79	74	79	80	76	78	79	78.1
15	41	32	35	40	32	35	39	31	33	35.3
16	84	94	96	83	93	95	84	94	96	91.0
17	64	72	61	65	72	62	64	71	61	65.8
18	59	68	70	58	66	69	59	67	71	65.2
19	68	74	78	62	67	74	62	67	74	69.6
20	77	77	72	77	77	72	78	77	73	75.6
21	69	73	78	68	72	77	67	72	77	72.6
22	108	100	97	106	100	96	105	99	96	100.8
23	56	65	62	56	65	62	55	64	62	60.8
24	78	92	74	79	92	73	79	92	73	81.3
25	84	89	94	84	88	94	79	84	91	87.4
26	90	88	98	90	87	97	92	89	97	92.0
27	30	35	34	30	34	34	30	34	34	32.8
28	74	86	78	73	86	78	74	86	78	79.2
29	90	91	92	89	90	91	89	90	91	90.3
30	49	54	53	47	53	53	45	52	52	50.9
31	59	70	68	58	70	67	59	71	68	65.6
32	64	65	69	65	66	70	64	65	69	66.3
33	75	74	66	75	74	66	75	74	66	71.7
34	83	89	86	83	89	86	81	87	85	85.4
35	109	114	104	109	114	105	109	113	105	109.1
36	45	47	47	45	47	47	45	47	47	46.3
37	36	36	39	35	35	38	33	31	34	35.2
38	23	25	28	22	23	26	22	23	26	24.2
39	47	49	49	46	48	50	46	48	49	48.0
40	49	48	50	49	50	51	48	49	50	49.3
41	36	36	36	35	34	35	33	33	34	34.7

42	36	36	35	36	36	35	37	37	36	36.0
43	44	41	35	45	42	35	45	41	36	40.4
44	23	26	29	23	25	29	23	25	29	25.8
45	47	57	69	45	54	67	44	53	65	55.7
46	62	61	57	64	63	58	63	63	58	61.0
47	42	47	53	43	47	54	42	47	53	47.6
48	62	59	59	61	59	59	58	56	55	58.7
49	41	38	34	41	38	33	41	38	34	37.6
50	34	34	32	35	35	32	35	35	33	33.9
51	82	77	61	82	78	62	82	77	60	73.4
52	41	48	52	40	47	49	40	48	49	46.0
53	43	40	36	43	40	35	43	40	36	39.6
54	33	34	30	34	35	31	32	34	31	32.7
Average	61.24	63.63	62.15	60.85	63.31	61.96	60.48	62.89	61.67	62.02

Appendix 54: All thermograms for the 54 macerated porcine bones used in section B research question 2, investigating the collagen-fluorescence relationship are available on OneDrive: 54 - Thermograms for section B, question 2, Collagen-fluorescence relationship

Appendix 55: Calculated collagen data for the 54 macerated porcine bones used in section B research question 2, investigating the collagen-fluorescence relationship.

Rib	Total organic content (mg)	Calculated collagen content (90%) (mg)
1	0.7294	0.66
2	0.5357	0.48
3	0.6179	0.56
4	0.5849	0.53
5	0.6407	0.58
6	0.6068	0.55
7	0.5847	0.53
8	0.5640	0.51
9	0.5557	0.50
10	0.7355	0.66
11	0.5430	0.49
12	0.6307	0.57
13	0.5961	0.54
14	0.6272	0.56
15	0.8874	0.80
16	0.6841	0.62
17	0.5392	0.49
18	0.5769	0.52
19	0.5423	0.49
20	0.5693	0.51
21	0.4973	0.45
22	0.5676	0.51
23	0.5760	0.52

24	0.3817	0.34
25	0.5352	0.48
26	0.5642	0.51
27	0.5504	0.50
28	0.7647	0.69
29	0.5744	0.52
30	0.5780	0.52
31	0.6100	0.55
32	0.5729	0.52
33	0.5717	0.51
34	0.6075	0.55
35	0.6193	0.56
36	0.5816	0.52
37	0.5966	0.54
38	0.5597	0.50
39	0.5495	0.49
40	0.5653	0.51
41	0.5606	0.50
42	0.5277	0.47
43	0.5414	0.49
44	0.4338	0.39
45	0.5374	0.48
46	0.4926	0.44
47	0.5754	0.52
48	0.5655	0.51
49	0.6182	0.56
50	0.5645	0.51
51	0.8873	0.80
52	0.5748	0.52
53	0.5331	0.48
54	0.5343	0.48
Average	0.59	0.53

Appendix 56: All comparison charts for the average underwater fluorescence values compared to the bone dimensions, section B, question 2: Collagen-fluorescence relationship.

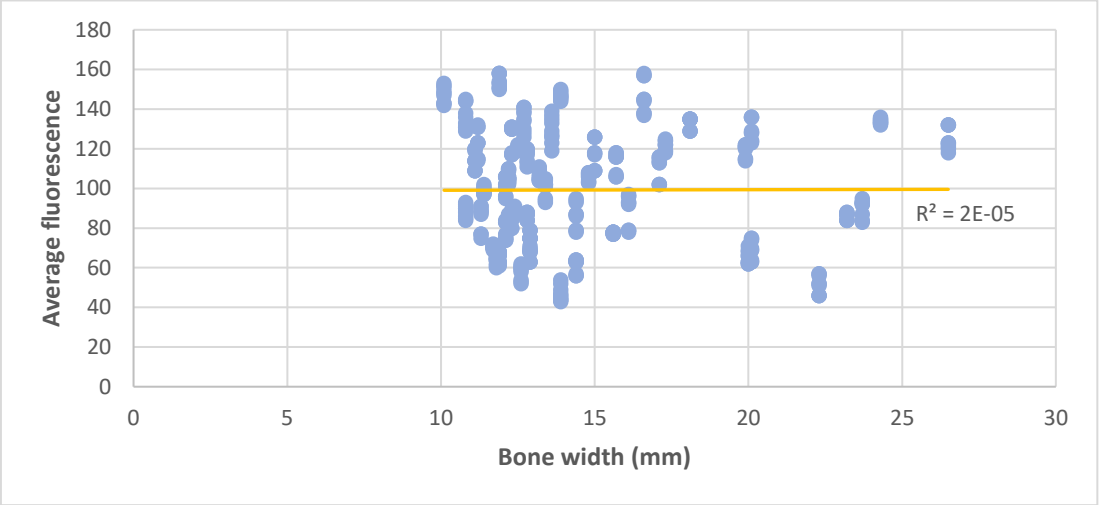

Comparison between bone width and underwater autofluorescence, photographed with the orange filter at 0.6s

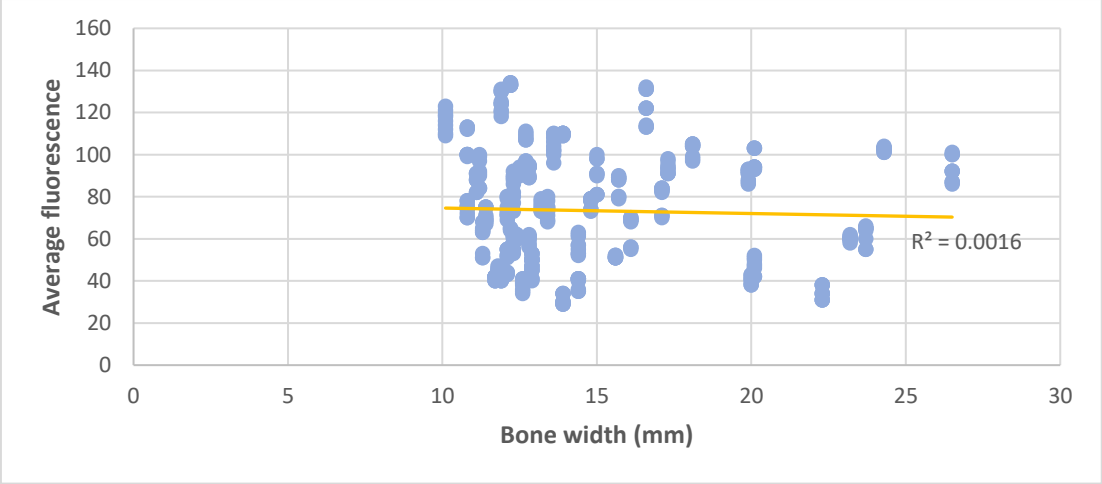

Comparison between bone width and underwater autofluorescence, photographed with the orange filter at 0.4s

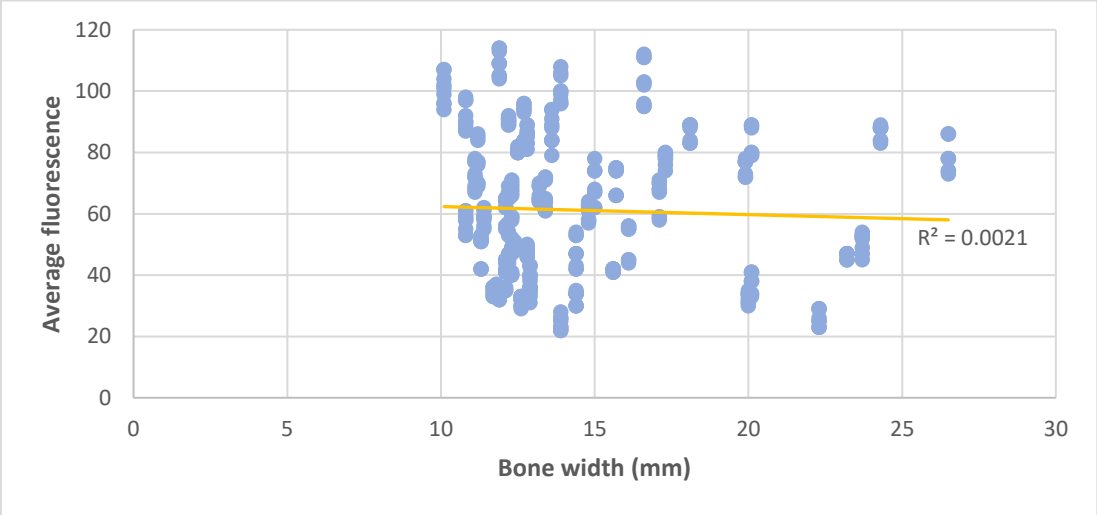

Comparison between bone collagen and underwater autofluorescence, photographed with the orange filter at 1/3s

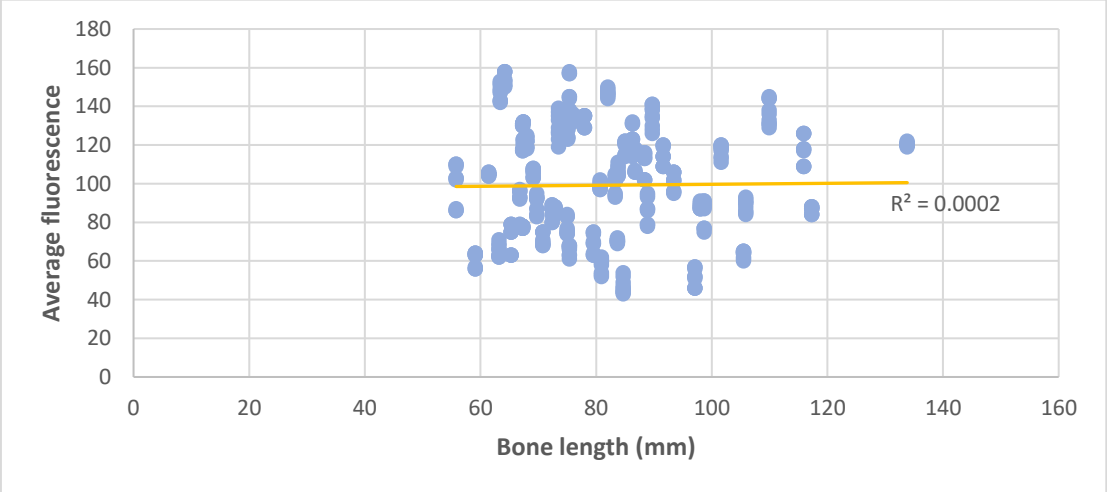

Comparison between bone length and underwater autofluorescence, photographed with the orange filter at 0.6s

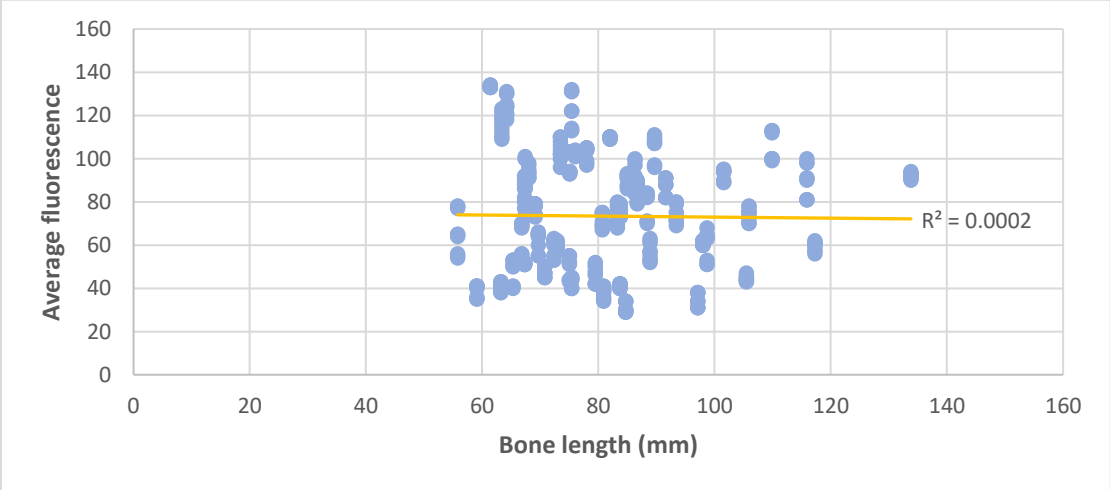

Comparison between bone length and underwater autofluorescence, photographed with the orange filter at 0.4s

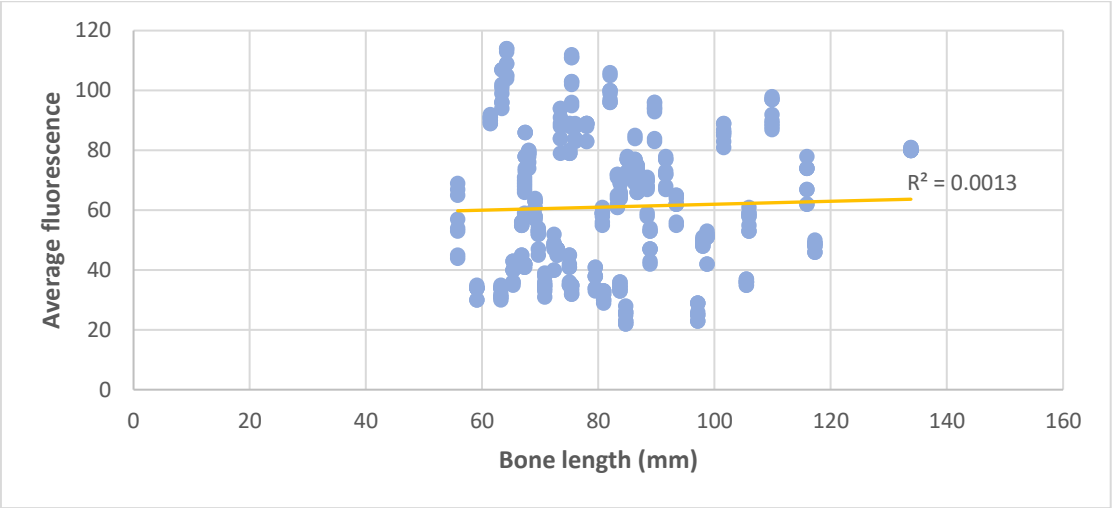

Comparison between bone length and underwater autofluorescence, photographed with the orange filter at 1/3s

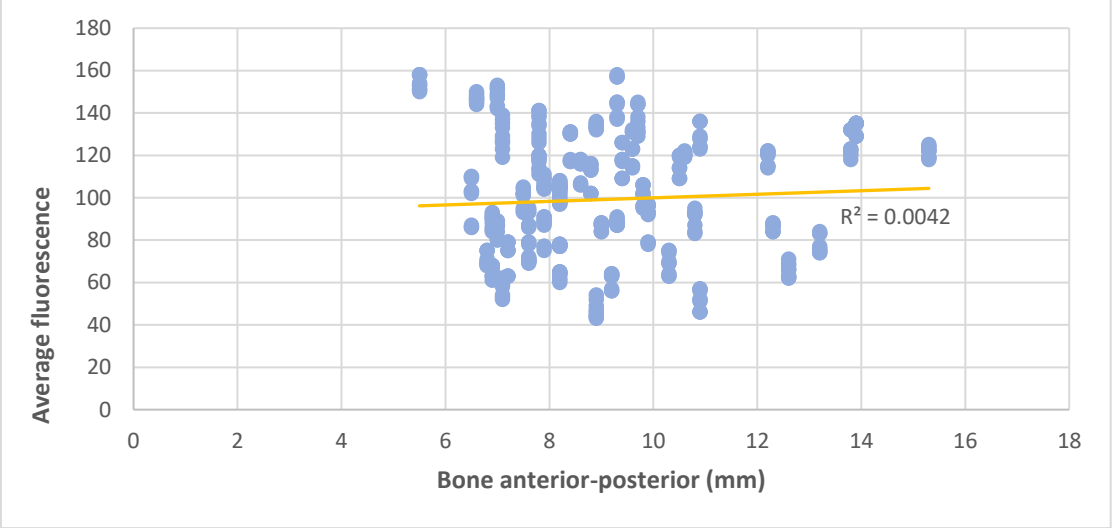

Comparison between bone A/P and underwater autofluorescence, photographed with the orange filter at 0.6s

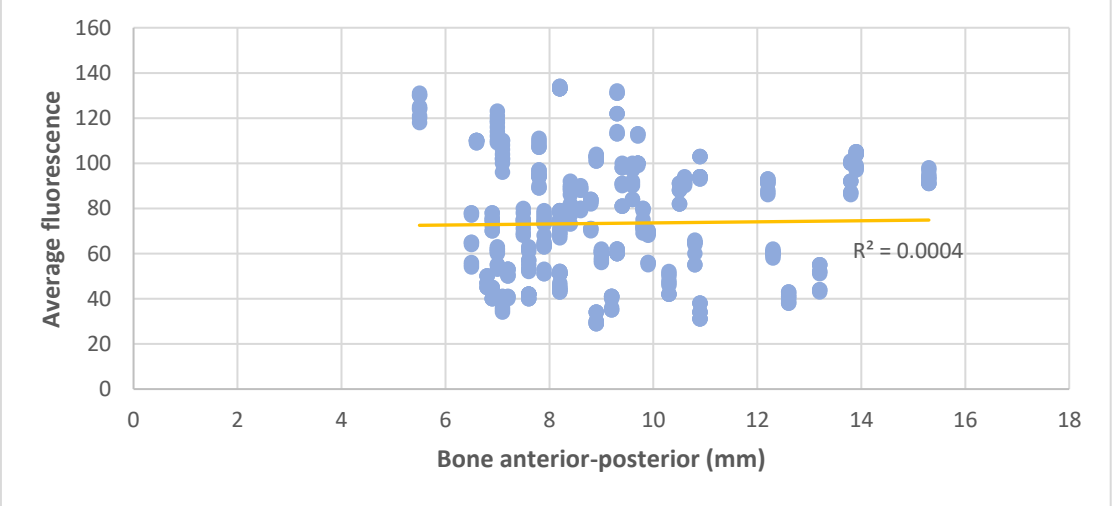

Comparison between bone A/P and underwater autofluorescence, photographed with the orange filter at 0.4s

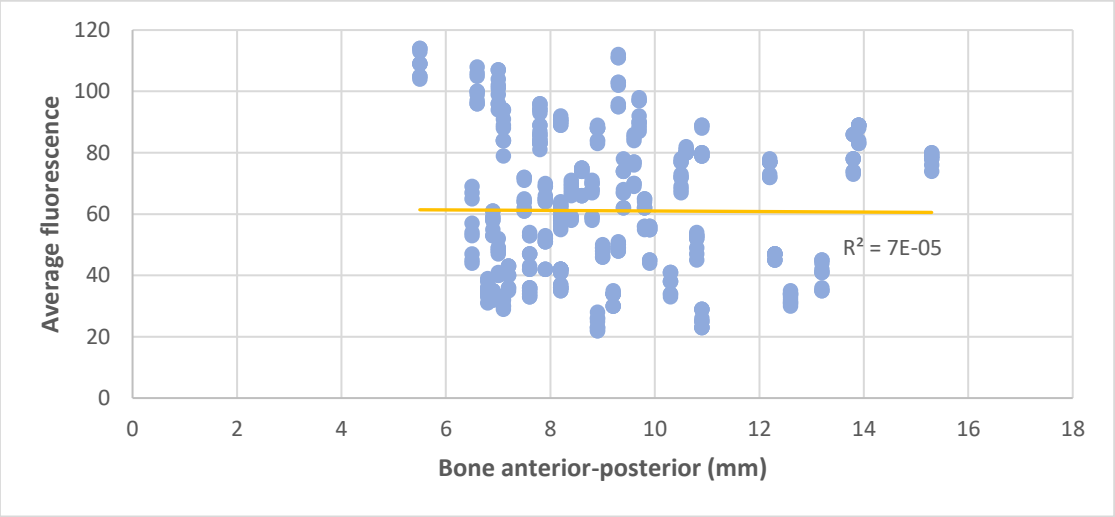

Comparison between bone A/P and underwater autofluorescence, photographed with the orange filter at 1/3s

Appendix 57: All comparison charts for the average terrestrial fluorescence values compared to the bone dimensions, section B, question 2: Collagen-fluorescence relationship.

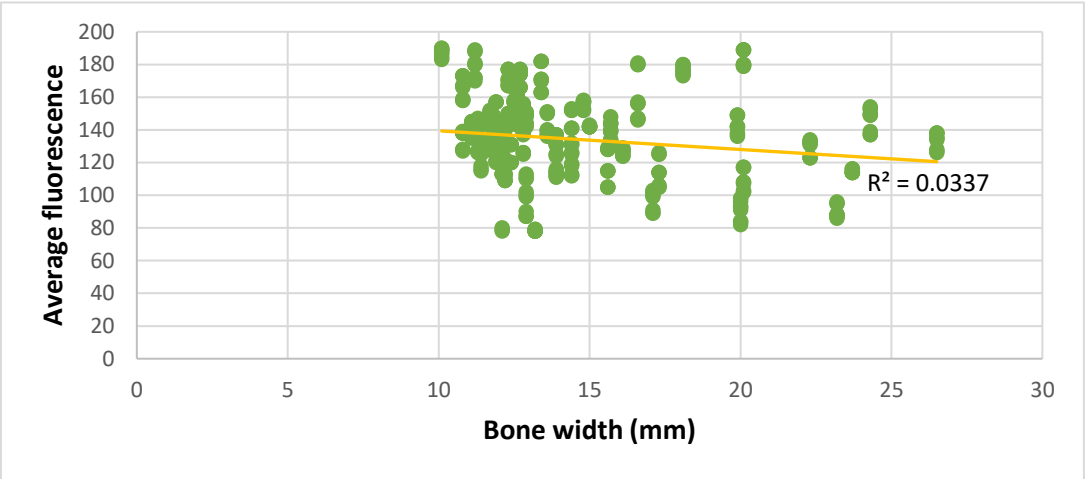

Comparison between bone width and terrestrial autofluorescence, photographed with the orange filter at 0.6s

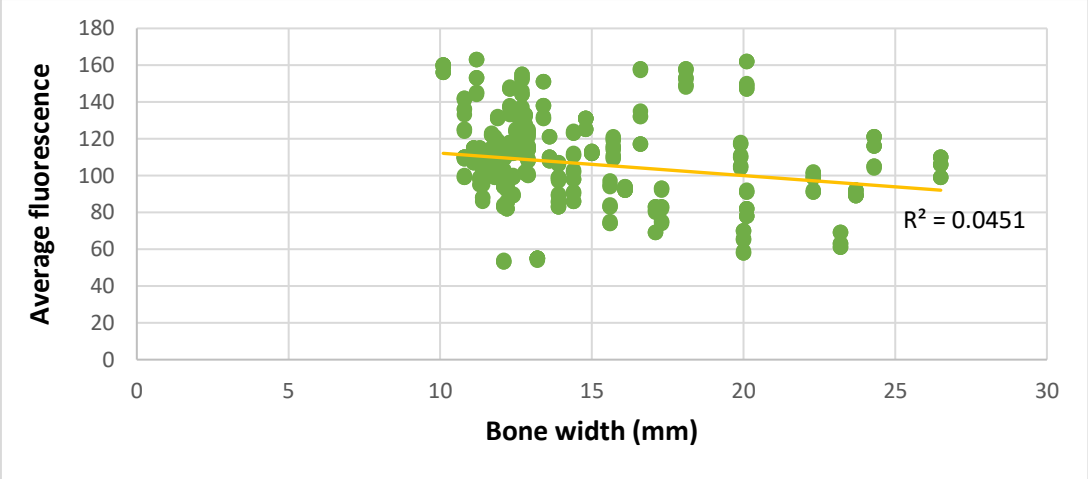

Comparison between bone width and terrestrial autofluorescence, photographed with the orange filter at 0.4s

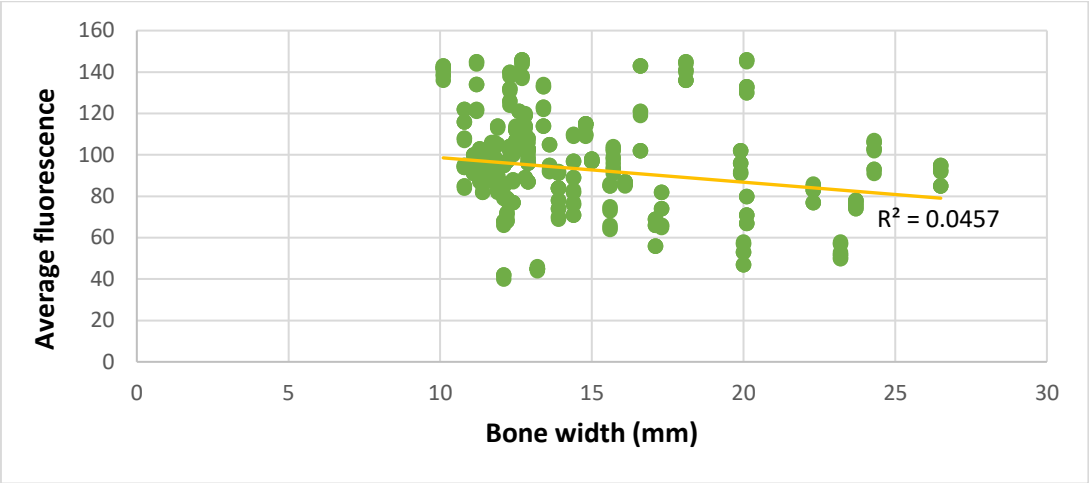

Comparison between and terrestrial autofluorescence, photographed with the orange filter at 1/3s

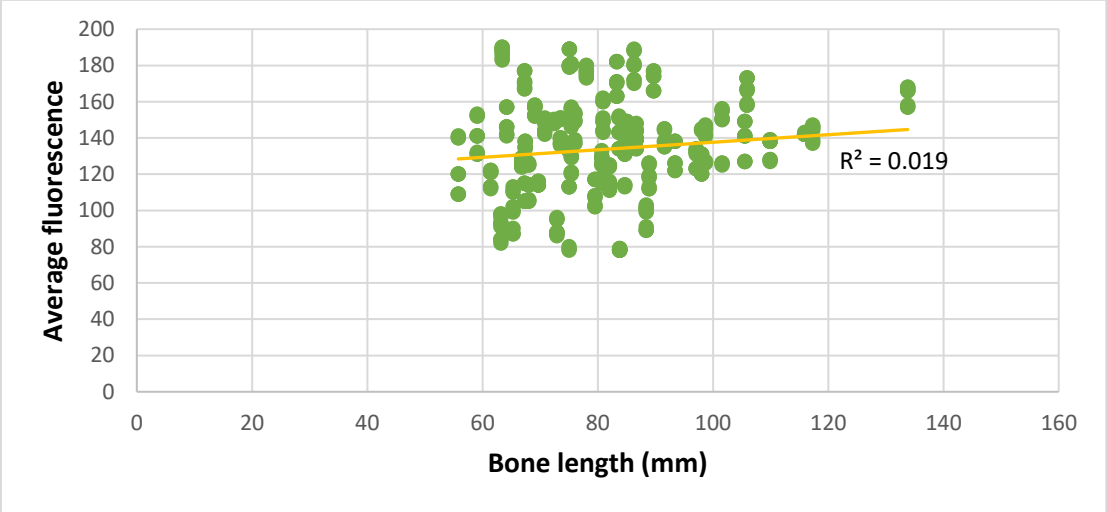

Comparison between bone length and terrestrial autofluorescence, photographed with the orange filter at 0.6s

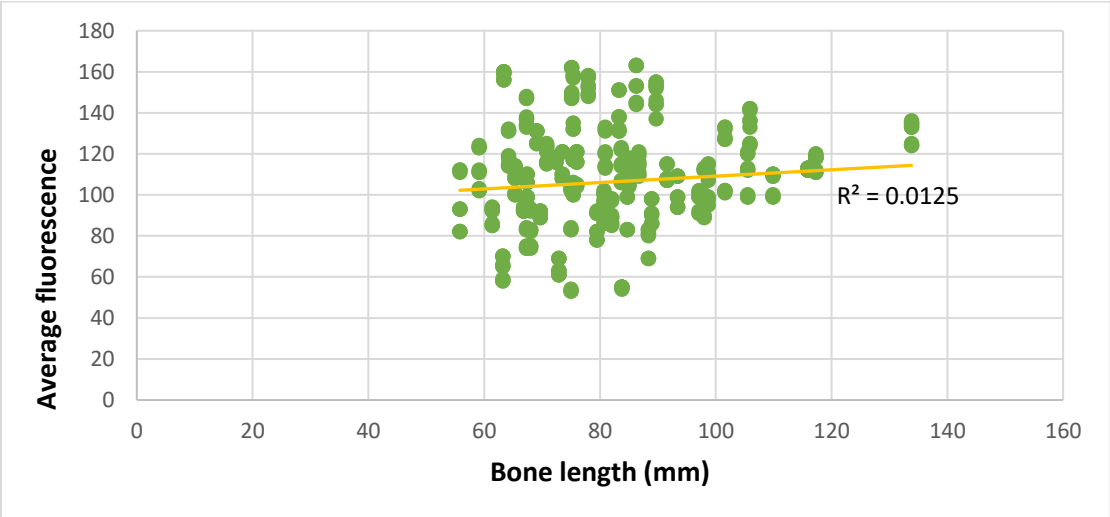

Comparison between bone length and terrestrial autofluorescence, photographed with the orange filter at 0.4s

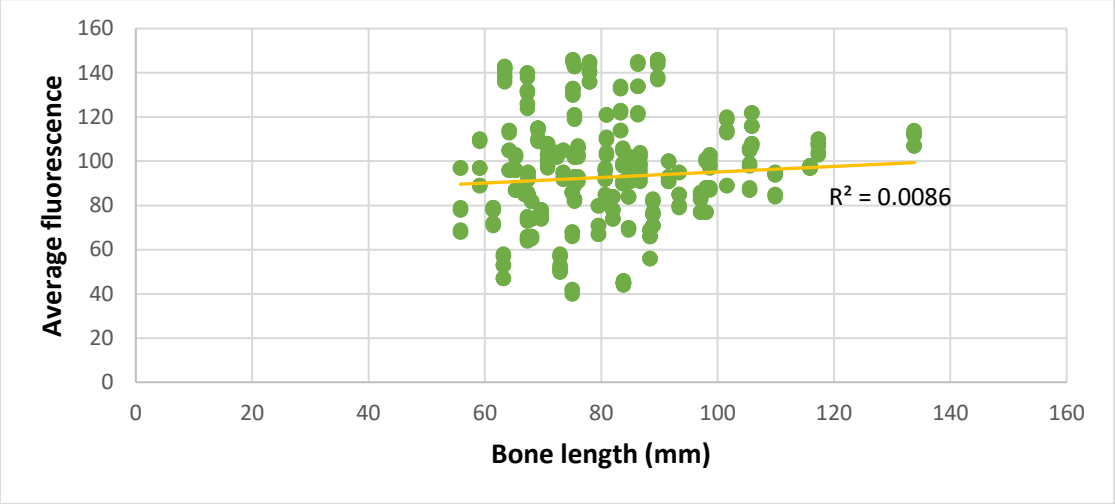

Comparison between bone length and terrestrial autofluorescence, photographed with the orange filter at 1/3s

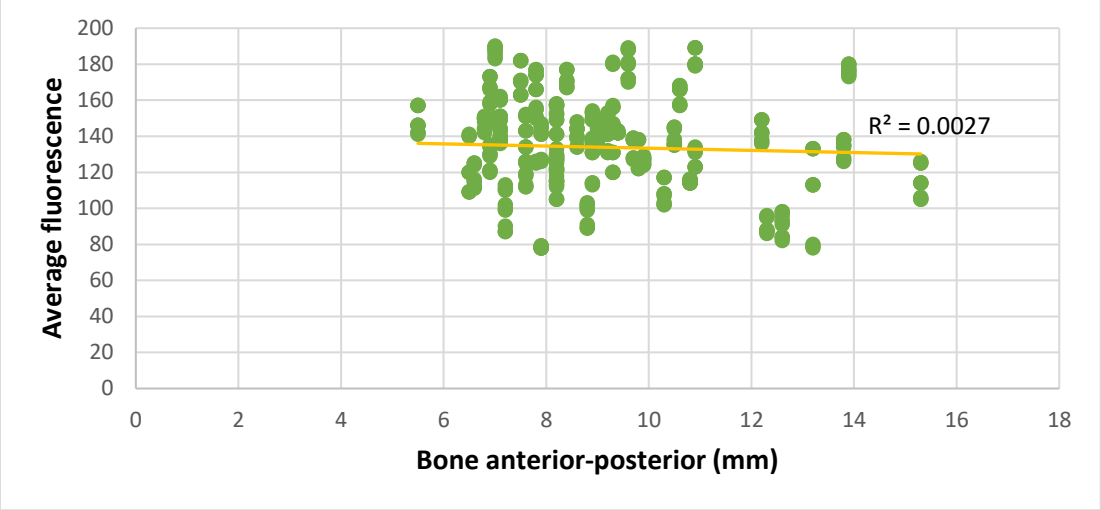

Comparison between bone A/P and terrestrial autofluorescence, photographed with the orange filter at 0.6s

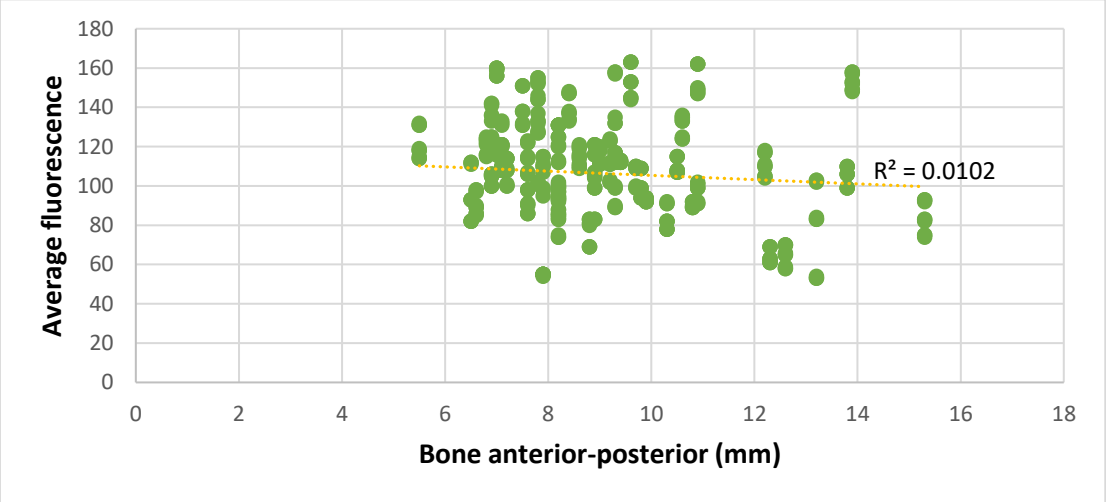

Comparison between bone A/P and terrestrial autofluorescence, photographed with the orange filter at 0.4s

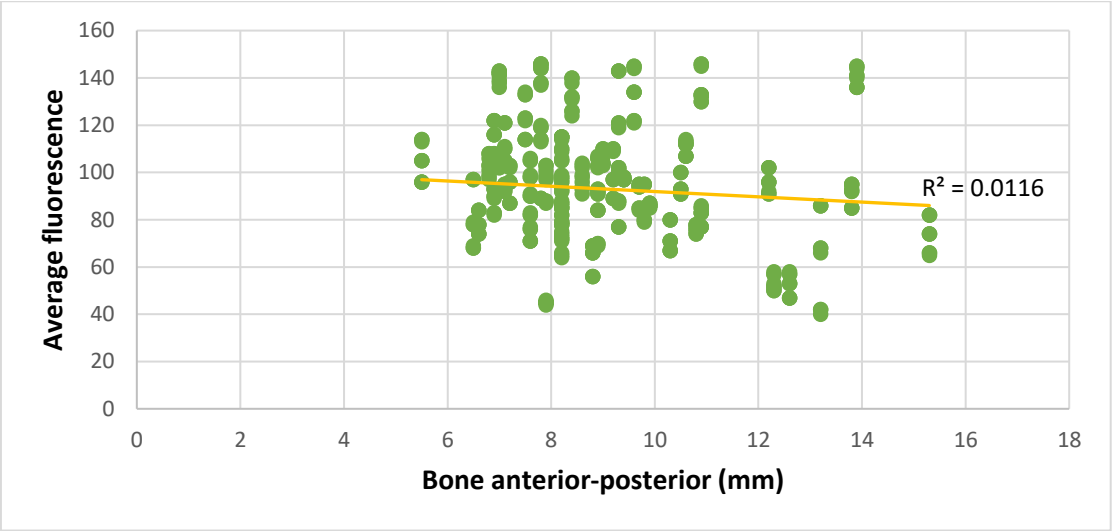

Comparison between bone A/P and terrestrial autofluorescence, photographed with the orange filter at 1/3s

Appendix 58: Histograms performed to determine the normality of data for section B, question 2: Collagen-fluorescence relationship statistical analyses.

A) Calculated collagen and bone mass.

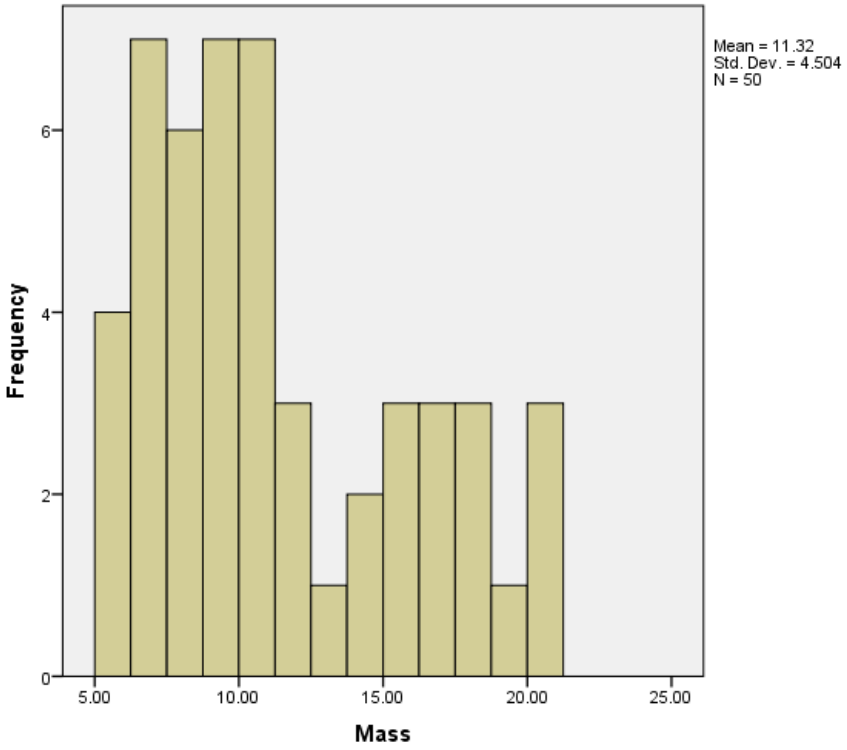

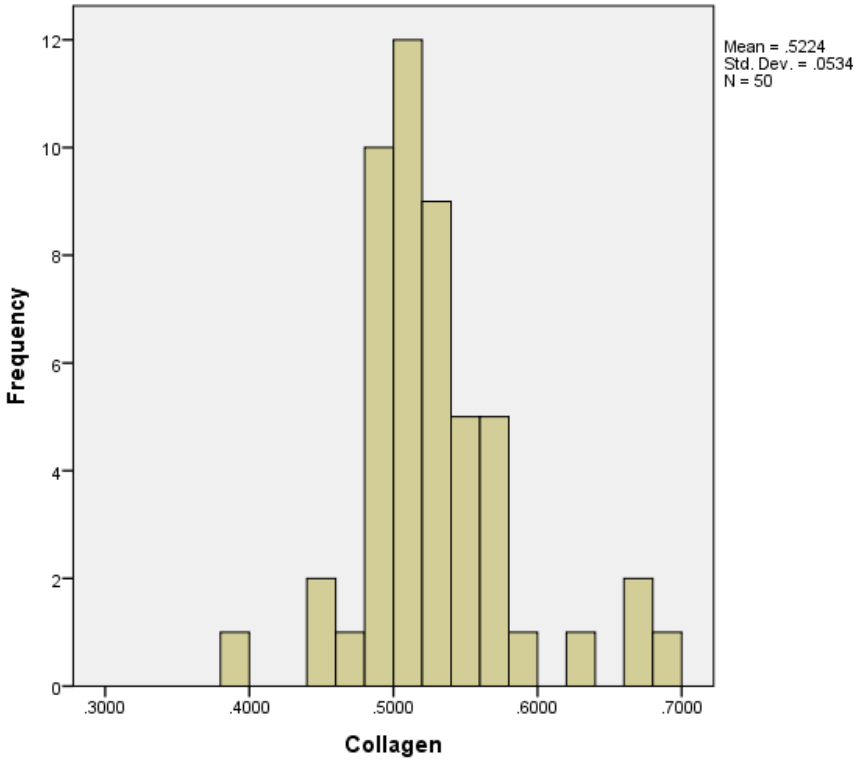

B) Terrestrial fluorescence data

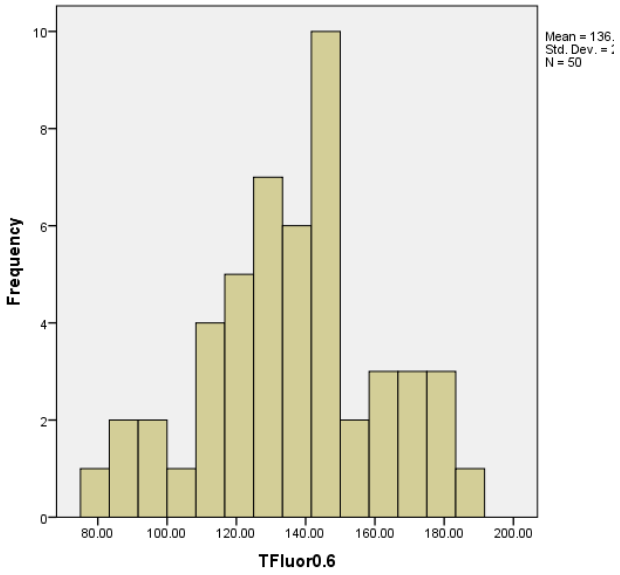

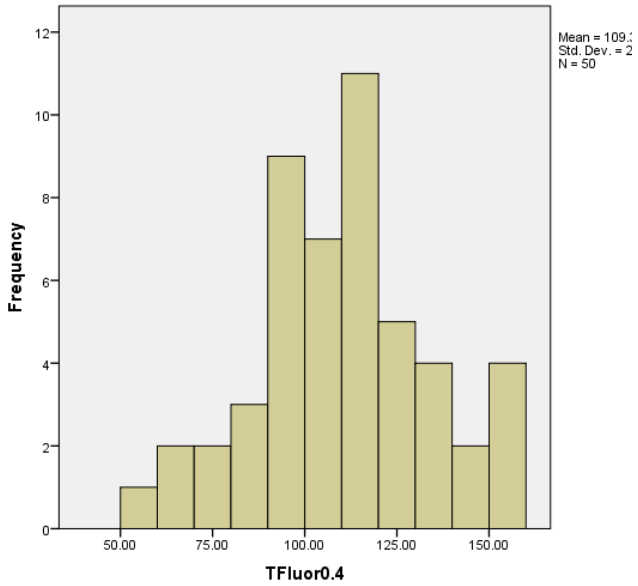

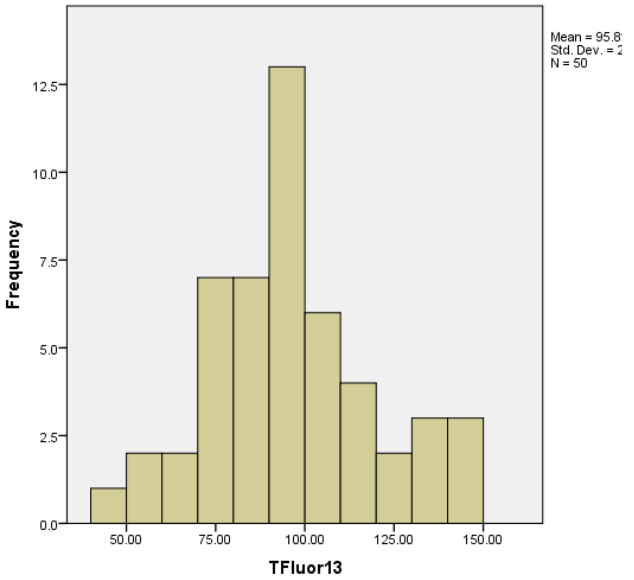

C) Underwater fluorescence data

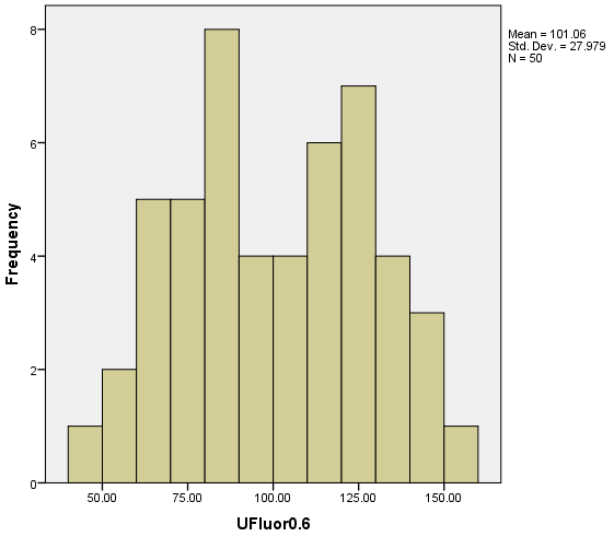

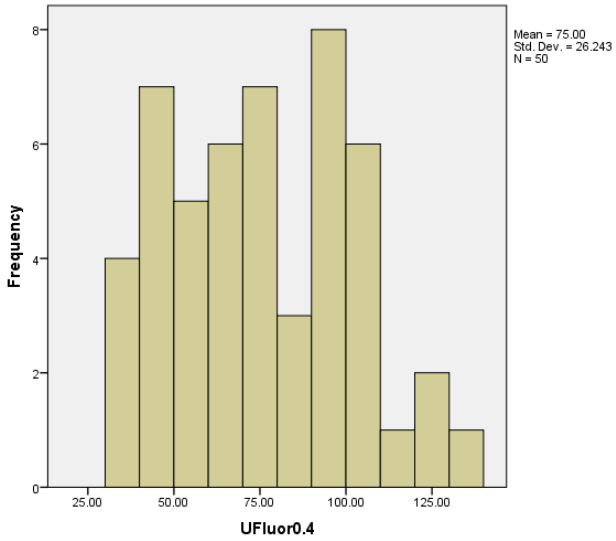

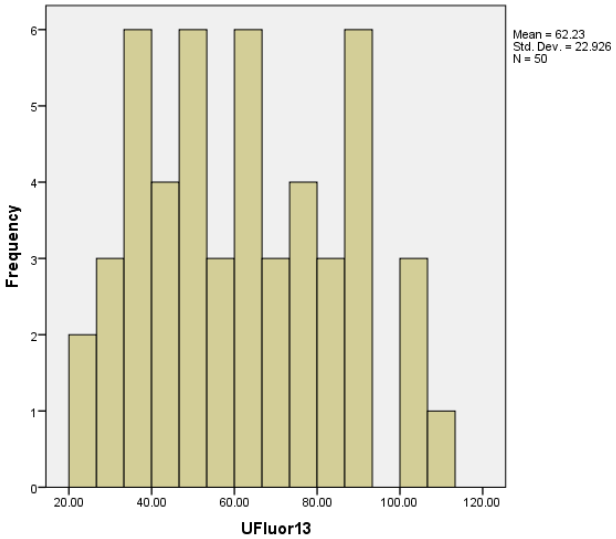

Appendix 59: All quantified fluorescence values for each ROI across all three photographs (1/3s exposure time) for each of the 27 non-bone control items examined in section B, question 3: differentiation and controls.

A) Hammerhead, terrestrial fluorescence, orange filter.

No.	Specimen	Photograph 1				Photograph 2				Photograph 3			
		ROI 1	ROI 2	ROI 3	Avg.	ROI 1	ROI 2	ROI 3	Avg.	ROI 1	ROI 2	ROI 3	Avg.
1	Stick 1: 130 x 15mm	159	159	140	99.7	159	159	140	152.7	159	159	140	152.7
2	Stick 2: 117 x 18mm	75	67	65	44.0	75	68	64	69.0	75	67	65	69.0
3	Tree bark	140	153	154	102.3	140	153	154	149.0	140	153	153	148.7
4	Driftwood: 100 x 18mm	99	94	87	60.3	99	95	89	94.3	101	95	89	95.0
5	Blue mussel (Mytilus edulis)	27	21	18	13.0	27	21	18	22.0	27	21	18	22.0
6	Great scallop shell (Pecten maximus)	72	75	78	51.0	71	75	78	74.7	72	75	78	75.0
7	Queen scallop shell (Aequipecten opercularis)	134	124	122	82.0	134	124	122	126.7	134	124	122	126.7
8	Shield limpet (Lottia pelta)	135	127	72	66.3	135	129	73	112.3	134	127	72	111.0
9	Cockle shell (Cerastoderma edule)	168	174	152	108.7	168	174	152	164.7	168	174	152	164.7
10	Oyster shell (Ostrea edulis)	75	54	34	29.3	75	54	34	54.3	75	54	34	54.3
11	Freshwater mussel shell (Margaritifera margaritifera)	173	163	159	107.3	173	163	158	164.7	173	163	159	165.0
12	Stone 1 Yellow/orange: 44 x 31mm	119	105	88	64.3	119	105	88	104.0	119	106	88	104.3
13	Stone 2 white: 48 x 39mm	118	113	94	69.0	118	114	94	108.7	118	114	94	108.7
14	Stone 3 pale grey: 50 x 32mm	26	26	26	17.3	26	26	27	26.3	26	26	26	26.0
15	Stone 4 dark grey: 80 x 50mm	17	14	12	8.7	17	15	13	15.0	17	14	13	14.7
16	Stone 5 grey: 59 x 29mm	33	34	32	22.0	33	34	32	33.0	33	34	32	33.0
17	Ceramic fragment 1 white, crackle glaze: 63 x 47mm	62	55	46	33.7	63	55	47	55.0	63	56	47	55.3
18	Ceramic fragment 2 yellow/brown stoneware: 61 x 55mm	28	26	23	16.3	28	26	23	25.7	28	26	23	25.7

19	Ceramic fragment 3 red/orange: 52 x 22mm	29	27	23	16.7	29	27	24	26.7	29	27	23	26.3
20	Sea glass 1: Translucent, colourless 41 x 23mm	78	77	73	50.0	78	77	73	76.0	78	77	73	76.0
21	Sea glass 2: Frosted, colourless 33 x 26mm	76	77	74	50.3	76	77	75	76.0	76	76	74	75.3
22	Fresh Leaf	40	36	35	23.7	39	36	34	36.3	39	36	34	36.3
23	Old leaf	139	143	142	95.0	139	144	142	141.7	139	144	142	141.7
24	Sea glass 3: Pale green sea glass 38.5 x 35.3mm	144	143	141	94.7	144	143	141	142.7	144	143	141	142.7
25	Sea glass 4: Frosted dark brown 31.1 x 18.6mm	29	30	29	19.7	29	30	29	29.3	29	29	28	28.7
26	Sea glass 5: Frosted dark green 28.7 x 24.8mm	29	27	26	17.7	28	27	26	27.0	28	27	26	27.0
27	Sea glass 6: Translucent light brown 20.4 x 17.3mm	25	24	29	17.7	25	24	30	26.3	25	24	30	26.3

B) Hammerhead, underwater

No.	Specimen	Photograph 1				Photograph 2				Photograph 3			
		ROI 1	ROI 2	ROI 3	Avg.	ROI 1	ROI 2	ROI 3	Avg.	ROI 1	ROI 2	ROI 3	Avg.
1	Stick 1: 130 x 15mm	107	107	83	63.3	107	107	82	98.7	107	106	82	98.3
4	Driftwood: 100 x 18mm	37	31	26	19.0	36	31	26	31.0	37	31	26	31.3
5	Blue mussel (Mytilus edulis)	7	6	4	3.3	7	6	4	5.7	7	6	4	5.7
6	Great scallop shell (Pecten maximus)	20	23	25	16.0	18	23	25	22.0	19	23	24	22.0
7	Queen scallop shell (Aequipecten opercularis)	37	35	34	23.0	36	35	34	35.0	36	35	34	35.0
8	Shield limpet (Lottia pelta)	49	62	36	32.7	49	61	36	48.7	49	62	37	49.3
9	Cockle shell (Cerastoderma edule)	75	85	64	49.7	76	85	64	75.0	78	85	62	75.0
10	Oyster shell (Ostrea edulis)	41	35	30	21.7	41	34	30	35.0	40	34	30	34.7
11	Freshwater mussel shell (Margaritifera margaritifera)	83	85	81	55.3	83	85	81	83.0	83	85	81	83.0
12	Stone 1 Yellow/orange: 44 x 31mm	42	37	26	21.0	41	37	25	34.3	40	38	25	34.3
13	Stone 2 white: 48 x 39mm	44	37	32	23.0	44	37	32	37.7	43	37	32	37.3
14	Stone 3 pale grey: 50 x 32mm	6	6	6	4.0	6	6	6	6.0	6	5	5	5.3
15	Stone 4 dark grey: 80 x 50mm	6	5	4	3.0	6	5	4	5.0	6	5	4	5.0
16	Stone 5 grey: 59 x 29mm	12	12	11	7.7	12	12	11	11.7	12	12	11	11.7
17	Ceramic fragment 1 white, crackle glaze: 63 x 47mm	29	25	20	15.0	29	24	20	24.3	29	25	20	24.7
18	Ceramic fragment 2 yellow/brown stoneware: 61 x 55mm	10	10	9	6.3	10	10	9	9.7	11	11	10	10.7
19	Ceramic fragment 3 red/orange: 52 x 22mm	8	8	7	5.0	8	8	7	7.7	8	8	7	7.7
20	Sea glass 1: Translucent, colourless 41 x 23mm	27	26	25	17.0	27	26	25	26.0	26	26	25	25.7
21	Sea glass 2: Frosted, colourless 33 x 26mm	24	26	25	17.0	23	25	24	24.0	24	25	24	24.3
24	Sea glass 3: Pale green sea glass 38.5 x 35.3mm	27	27	26	17.7	27	26	26	26.3	27	26	25	26.0
25	Sea glass 4: Frosted dark brown 31.1 x 18.6mm	7	6	5	3.7	7	6	6	6.3	7	6	6	6.3
26	Sea glass 5: Frosted dark green 28.7 x 24.8mm	7	6	6	4.0	7	7	7	7.0	7	7	7	7.0
27	Sea glass 6: Translucent light brown 20.4 x 17.3mm	8	7	10	5.7	7	7	9	7.7	8	7	9	8.0

C) Crime-lite 2, orange filter

No.	Specimen	ROI 1	ROI 2	ROI 3	Avg.	ROI 1	ROI 2	ROI 3	Avg.	ROI 1	ROI 2	ROI 3	Avg.
1	Stick 1: 130 x 15mm	147	174	169	114.3	146	174	169	163.0	147	174	169	163.3
2	Stick 2: 117 x 18mm	92	93	78	57.0	91	93	78	87.3	90	93	78	87.0
3	Tree bark	162	162	165	109.0	161	162	165	162.7	161	162	165	162.7
4	Driftwood: 100 x 18mm	175	169	162	110.3	176	170	162	169.3	175	169	162	168.7
5	Blue mussel (Mytilus edulis)	37	18	37	18.3	37	18	36	30.3	37	18	36	30.3
6	Great scallop shell (Pecten maximus)	95	99	105	68.0	96	99	105	100.0	96	99	105	100.0
7	Queen scallop shell (Aequipecten opercularis)	156	139	144	94.3	156	139	144	146.3	156	139	144	146.3
8	Sheild limpet (Lottia pelta)	132	139	108	82.3	133	140	108	127.0	132	139	108	126.3
9	Cockle shell (Cerastoderma edule)	201	211	210	140.3	202	211	210	207.7	201	211	210	207.3
10	Oyster shell (Ostrea edulis)	145	95	94	63.0	145	95	94	111.3	145	95	93	111.0
11	Freshwater mussel shell (Margaritifera margaritifera)	195	196	192	129.3	194	196	192	194.0	194	196	192	194.0
12	Stone 1 Yellow/orange: 44 x 31mm	151	116	127	81.0	152	115	128	131.7	153	116	127	132.0
13	Stone 2 white: 48 x 39mm	163	165	156	107.0	163	165	156	161.3	163	165	156	161.3
14	Stone 3 pale grey: 50 x 32mm	19	19	23	14.0	19	19	23	20.3	19	20	23	20.7
15	Stone 4 dark grey: 80 x 50mm	38	37	32	23.0	39	37	33	36.3	39	38	33	36.7
16	Stone 5 grey: 59 x 29mm	59	57	55	37.3	59	57	54	56.7	58	56	54	56.0
17	Ceramic fragment 1 white, crackle glaze: 63 x 47mm	62	55	46	33.7	63	55	47	55.0	63	55	47	55.0
18	Ceramic fragment 2 yellow/brown stoneware: 61 x 55mm	16	15	15	10.0	16	15	15	15.3	16	15	15	15.3
19	Ceramic fragment 3 red/orange: 52 x 22mm	29	27	23	16.7	29	27	24	26.7	29	27	23	26.3
20	Sea glass 1: Translucent, colourless 41 x 23mm	137	139	136	91.7	137	139	136	137.3	137	139	136	137.3
21	Sea glass 2: Frosted, colourless 33 x 26mm	134	134	129	87.7	134	134	129	132.3	134	133	129	132.0
22	Fresh Leaf	84	77	72	49.7	84	77	72	77.7	85	77	72	78.0
23	Old leaf	158	159	153	104.0	158	159	153	156.7	158	159	153	156.7
24	Sea glass 3: Pale green sea glass 38.5 x 35.3mm	117	117	115	77.3	117	117	115	116.3	118	117	115	116.7
25	Sea glass 4: Frosted dark brown 31.1 x 18.6mm	28	30	31	20.3	28	30	30	29.3	28	30	31	29.7

26	Sea glass 5: Frosted dark green 28.7 x 24.8mm	26	25	25	16.7	25	24	24	24.3	25	24	24	24.3
27	Sea glass 6: Translucent light brown 20.4 x 17.3mm	32	18	17	11.7	32	18	17	22.3	32	18	17	22.3

D) Crime-lite 2, yellow filter

No.	Specimen	ROI 1	ROI 2	ROI 3	Avg.	ROI 1	ROI 2	ROI 3	Avg.	ROI 1	ROI 2	ROI 3	Avg.
1	Stick 1: 130 x 15mm	248	249	241	163.3	248	249	241	246.0	249	249	241	246.3
2	Stick 2: 117 x 18mm	189	191	170	120.3	189	191	170	183.3	189	191	170	183.3
3	Tree bark	244	246	246	164.0	244	246	246	245.3	244	246	246	245.3
4	Driftwood: 100 x 18mm	244	244	239	161.0	244	244	239	242.3	244	244	239	242.3
5	Blue mussel (Mytilus edulis)	116	90	68	52.7	116	90	68	91.3	116	89	67	90.7
6	Great scallop shell (Pecten maximus)	211	213	216	143.0	211	213	216	213.3	211	212	215	212.7
7	Queen scallop shell (Aequipecten opercularis)	255	254	254	169.3	254	254	254	254.0	255	254	254	254.3
8	Sheild limpet (Lottia pelta)	225	231	216	149.0	226	231	216	224.3	225	231	216	224.0
9	Cockle shell (Cerastoderma edule)	253	254	254	169.3	253	254	254	253.7	253	254	254	253.7
10	Oyster shell (Ostrea edulis)	240	197	212	136.3	242	197	210	216.3	238	197	213	216.0
11	Freshwater mussel shell (Margaritifera margaritifera)	253	254	253	169.0	254	254	253	253.7	253	254	253	253.3
12	Stone 1 Yellow/orange: 44 x 31mm	234	243	203	148.7	234	243	203	226.7	234	243	203	226.7
13	Stone 2 white: 48 x 39mm	250	250	247	165.7	250	250	247	249.0	250	250	247	249.0
14	Stone 3 pale grey: 50 x 32mm	83	88	84	57.3	83	88	85	85.3	83	88	84	85.0
15	Stone 4 dark grey: 80 x 50mm	93	83	73	52.0	92	83	73	82.7	92	83	73	82.7
16	Stone 5 grey: 59 x 29mm	161	158	152	103.3	161	157	152	156.7	161	157	152	156.7
17	Ceramic fragment 1 white, crackle glaze: 63 x 47mm	254	253	249	167.3	254	253	249	252.0	254	253	249	252.0
18	Ceramic fragment 2 yellow/brown stoneware: 61 x 55mm	254	252	250	167.3	254	252	250	252.0	254	253	250	252.3
19	Ceramic fragment 3 red/orange: 52 x 22mm	230	221	205	142.0	229	220	205	218.0	229	220	205	218.0
20	Sea glass 1: Translucent, colourless 41 x 23mm	243	243	241	161.3	243	243	241	242.3	243	243	241	242.3
21	Sea glass 2: Frosted, colourless 33 x 26mm	241	241	239	160.0	241	241	239	240.3	241	241	239	240.3
23	Old leaf	245	244	242	162.0	245	244	242	243.7	245	244	242	243.7
24	Sea glass 3: Pale green sea glass 38.5 x 35.3mm	234	233	230	154.3	234	233	230	232.3	234	233	230	232.3
25	Sea glass 4: Frosted dark brown 31.1 x 18.6mm	104	91	97	62.7	104	90	97	97.0	104	91	97	97.3
26	Sea glass 5: Frosted dark green 28.7 x 24.8mm	72	70	71	47.0	72	70	71	71.0	72	70	71	71.0

27	Sea glass 6: Translucent light brown 20.4 x 17.3mm	101	53	71	41.3	100	54	71	75.0	101	54	71	75.3

Appendix 60: All terrestrial fluorescence and OFC processed photographs for the 27 non-bone control items examined in section B, question 3: differentiation and controls, are available on OneDrive: 60 - Hammerhead fluorescence and OFC processed images of non-bone controls

Appendix 61: All submerged fluorescence and OFC processed photographs for the 27 non-bone control items examined in section B, question 3: differentiation and controls, are available on OneDrive: 61 - Crime-lite 2 fluorescence and OFC processed images of non-bone controls

Appendix 62: All fluorescence and OFC processed photographs for the porcine collagen powder and epoxy resin controls examined in section B, question 3: differentiation and controls, are available on OneDrive: 62 - Fluorescence and OFC processed photographs for the porcine collagen powder and epoxy resin control blocks

Appendix 63: All quantified fluorescence values for each ROI across all three photographs (1/3s exposure time) for porcine collagen powder and epoxy resin control blocks examined in section B, question 3: differentiation and controls.

Terrestrial												
Specimen	F1	F2	F3	Avg.	F1	F2	F3	Avg.	F1	F2	F3	Avg.
Collagen powder	239	242	244	241.7	239	242	243	241.3	239	242	243	241.3
	215	218	221	218.0	215	218	221	218.0	215	218	221	218.0
	208	210	212	140.7	208	210	212	210.0	208	210	212	210.0
Resin only (oval)	196	192	192	193.3	196	192	192	128.0	196	192	192	193.3
	145	140	140	93.3	145	140	140	141.7	145	140	140	141.7
	78	74	75	49.7	78	74	75	75.7	78	74	75	75.7
Resin only (square)	199	191	188	192.7	200	191	188	193.0	200	191	188	193.0
	151	140	136	92.0	150	140	136	142.0	150	140	136	142.0
	84	75	71	48.7	84	75	72	77.0	84	75	71	76.7
Underwater												
Specimen	F1	F2	F3	Avg.	F1	F2	F3	Avg.	F1	F2	F3	Avg.
Collagen powder	203	205	204	204.0	203	205	205	204.3	203	205	205	204.3
	183	186	185	123.7	183	186	185	184.7	183	186	185	184.7
	136	142	140	94.0	138	143	140	140.3	139	143	140	140.7
Resin only (oval)	84	80	70	78.0	85	81	71	50.7	85	80	71	78.7
	40	38	32	23.3	39	37	32	36.0	39	37	32	36.0
	21	19	15	11.3	20	19	15	18.0	21	20	16	19.0
Resin only (square)	88	84	74	82.0	88	83	74	81.7	85	84	74	81.0
	41	39	34	24.3	42	40	35	39.0	42	40	35	39.0
	22	20	17	12.3	22	20	17	19.7	21	20	17	19.3

Appendix 64: Technical data sheet for the calcined bone ash powder purchased from PotClays Ltd (https://www.potclays.co.uk/)

Potclays Ltd. Albion Works, Brickkiln Lane,
Etruria, Stoke-on-Trent, ST4 7BP ENGLAND
+44(0)1782 219816 | sales@potclays.co.uk
potclays.co.uk
VAT Reg. GB 279384016

POTCLAYS LIMITED

TECHNICAL DATA SHEET

BONE ASH (DRY-GROUND)

PRODUCT CODE 3412

- Calcined, ground animal bones used as a flux in bone china and some glazes.
- Produces very high whiteness and translucency.
- The essential constituent used to produce translucency in bone china bodies.
- A secondary flux in glazes and occasionally used as an opacifier.

Typical XRF Analysis (% by wt)

as determined by an independent UKAS accredited laboratory:

Silica (SiO_2)	0.52
Titania (TiO_2)	<0.03
Alumina (AL_2O_3)	0.39
Ferric Oxide (Fe_2O_3)	<0.03
Lime (CaO)	53.59
Magnesia (MgO)	1.18
Potash (K_2O)	0.05
Soda (Na_2O)	0.93
Phosphorus Pentoxide (P_2O_5)	41.40
Lead Oxide (PbO)	<0.03
Barium Oxide (BaO)	<0.03
Loss of Ignition at 1200°C	1.11

Date 03/12/2020

Appendix 65: All terrestrial fluorescence and OFC processed photographs for the six demineralised bone controls examined in section B, question 3: differentiation and controls, are available on OneDrive: 65 - All terrestrial fluorescence and OFC processed images for the demineralised bone controls

Appendix 66: All submerged fluorescence and OFC processed photographs for the six demineralised bone controls examined in section B, question 3: differentiation and controls, are available on OneDrive: 66 - All submerged fluorescence and OFC processed images for the demineralised bone controls

Appendix 67: Terrestrial and aquatic fluorescence values for each photograph and ROI for each demineralised bone control examined in section B, question 3: differentiation and controls.

Terrestrial												
Rib	Photograph 1				Photograph 2				Photograph 2			
	ROI 1	ROI 2	ROI 3	Av.	ROI 1	ROI 2	ROI 3	Av.	ROI 1	ROI 2	ROI 3	Av.
1	195	191	191	192.3	195	191	191	192.3	195	191	191	192.3
2	153	156	151	153.3	153	156	151	153.3	153	156	151	153.3
3	193	180	187	186.7	193	180	187	186.7	193	180	187	186.7
4	176	182	197	185.0	176	182	197	185.0	176	182	197	185.0
5	198	203	206	202.3	198	203	206	202.3	198	203	206	202.3
6	204	201	200	201.7	204	201	200	201.7	204	201	200	201.7
Underwater												
1	102	90	82	91.3	101	90	82	91.0	101	89	81	90.3
2	79	75	84	79.3	80	75	85	80.0	79	76	84	79.7
3	84	72	66	74.0	84	72	66	74.0	84	73	66	74.3
4	66	66	76	69.3	66	66	75	69.0	66	65	75	68.7
5	95	101	97	97.7	93	100	97	96.7	90	97	95	94.0
6	101	86	77	88.0	102	86	77	88.3	102	86	77	88.3

Appendix 68: Observed bone modifications, assigned Munsell colour readings, and the estimated percentage coverage for the six deproteinised porcine ribs examined in section B, question 3: differentiation and controls

No.	Munsell colour			% coverage		Description of visual modifications
	S.E.	D	V.E.	Ant.	Post.	
1	7.5 YR 5/4	7.5 YR 3/1	7.5 YR 2.5/1	90	70	**Anterior:** Mostly charred, small patches of beige/brown, evidence of patina along inferior margin. **Posterior**: Extensive charring with cracks.
2	7.5 YR 6/2	7.5 YR 6/3	7.5 YR 6/4	15	80	**Anterior**: Brownish/cream colour, dry surface texture. Small cracks, very mild patina towards sternal epiphysis. **Posterior**: Extensive charring, loss of approx. 60% of cortical bone, exposure of trabecular. Delamination and flaking at vertebral epiphysis.
3	5 YR 4/2	5 YR 6/2	5 YR 2/1	45	20	**Anterior:** Charring to vertebral epiphysis, small areas of retained tissue. Patches of greyish discolouration to diaphysis, fraying and small cracks to towards sternal end. **Posterior:** Extensive longitudinal fractures but little colour change other than small patch of charring to vertebral end, and greyish discolouration on the central/sternal epiphysis.
4	7.5 YR 5/2	7.5 YR 5/3	7.5 YR 7/2	30	65	**Anterior:** Delamination, obvious porosity, and calcination to the vertebral end. Small patches of charring and brown colour to the shaft and sternal end. **Posterior:** Extensive crazing, and longitudinal fractures from the sternal end. Patches of calcination towards sternal aspect, and orange/white patches indicating where the rib was in contact with the grill.
5	7.5 YR 6/1	7.5 YR 2.5/1	7.5 YR 2.5/1	100	85	**Anterior:** Totally charred, patches of calcination to the vertebral end and extensive crazing. Loss of approx. 50% of cortical bone, exposing charred trabecular underneath. **Posterior:** Charring to vertebral end, patch of calcination towards sternal end. Brown/orange colouration on diaphysis with small amount of cracking/patina.
6	7.5 YR 2.5/1	7.5 YR 2.5/1	7.5 YR 2.5/1	100	50	**Anterior:** Totally charred, moderate delamination along the shaft, small patches of cortical bone loss to the sternal end. **Posterior:** 50% charring, towards vertebral end. Central/sternal regions brownish/beige with small patches of bluish/grey. A section of cortical bone has become separated from the main rib at the sternal end.

Appendix 69: All fluorescence values for each photograph and ROI for each demineralised bone control examined in section B, question 3: differentiation and controls.

Rib	ROI 1	ROI 2	ROI 3	Avg.	ROI 1	ROI 2	ROI 3	Avg.	ROI 1	ROI 2	ROI 3	Avg.
1	19	18	13	16.7	19	18	13	16.7	21	19	13	17.7
2	208	208	209	208.3	208	208	209	208.3	209	208	209	208.7
3	145	111	91	115.7	145	110	90	115.0	145	110	90	115.0
4	96	119	187	134.0	95	120	187	134.0	94	122	187	134.3
5	19	15	12	15.3	20	14	12	15.3	20	13	12	15.0
6	9	9	8	8.7	10	9	8	9.0	9	9	7	8.3

Appendix 70: All fluorescence and OFC processed photographs for the six deproteinised bone controls examined in section B, question 3: differentiation and controls, are available on OneDrive: 70 - All fluorescence and OFC processed photographs for the six deproteinised bone controls

Appendix 71: All fluorescence values for each photograph and ROI for the bone ash control examined in section B, question 3: differentiation and controls.

Specimen	ROI 1	ROI 2	ROI 3	Avg.	ROI 1	ROI 2	ROI 3	Avg.	ROI 1	ROI 2	ROI 3	Avg.
Embedded bone ash	64	62	57	39.7	64	62	57	61.0	64	61	56	60.3
Bone ash powder	89	90	83	57.7	89	90	83	87.3	89	90	83	87.3

Appendix 72: All fluorescence and OFC processed photographs for the bone ash controls examined in section B, question 3: differentiation and controls, are available on OneDrive: 72 - All fluorescence and OFC processed images for the bone ash controls

Appendix 73: Section B, question 4, maceration temperature monitoring for the preparation of the porcine bones.

Set 1 (5 ribs)	
Ambient temp: 17.9°C	Starting temp: 79.6°C
Interval (mins)	Temperature (°C)
30	81.9
60	86.4
90	84.6

Set 2 (5 ribs)	
Ambient temp: 14.1°C	Starting temp: 81.1°C
Interval (mins)	Temperature (°C)
30	85.5
60	91.1
90	84.8

Set 3 (4 ribs)	
Ambient temp: 17.3°C	Starting temp: 79.3°C
Interval (mins)	Temperature (°C)
30	83.6
60	87.8
90	88.5

Set 4 (4 ribs)	
Ambient temp: 17.7°C	Starting temp: 80.3°C
Interval (mins)	Temperature (°C)
30	84.4
60	87.6
90	86.4

Set 5 (5 ribs)	
Ambient temp: 15.9°C	Starting temp: 80.8°C
Interval (mins)	Temperature (°C)
30	84.1
60	88.2
90	88.7

Set 6 (5 ribs)	
Ambient temp: 16.2°C	Starting temp: 80.4°C
Interval (mins)	Temperature (°C)
30	80.9
60	84
90	85.4

Set 7 (4 ribs)	
Ambient temp: 16.4°C	Starting temp: 81°C
Interval (mins)	Temperature (°C)
30	83.9
60	85.4
90	86.2

Set 8 (4 ribs)	
Ambient temp: 16.5°C	Starting temp: 79.8°C
Interval (mins)	Temperature (°C)
30	84.3
60	87.8
90	88.1

Set 9 (5 ribs)	
Ambient temp: 18.1°C	Starting temp: 81.3°C
Interval (mins)	Temperature (°C)
30	85.3
60	89.8
90	89.3

Set 10 (5 ribs)	
Ambient temp: 18.1°C	Starting temp: 79.3°C
Interval (mins)	Temperature (°C)
30	84.8
60	81.1
90	84.6

Set 11 (4 ribs)	
Ambient temp: 18.6°C	Starting temp: 79.8°C
Interval (mins)	Temperature (°C)
30	83.4
60	88.3
90	87.3

Set 12 (4 ribs)	
Ambient temp: 17.8°C	Starting temp: 81.6°C
Interval (mins)	Temperature (°C)
30	86.2
60	88.3
90	84.5

Appendix 74: All pre- and post-maceration (hot water 80°C) thermograms for the six porcine bones selected from the dataset in section B research question 4, investigating the impact of the aquatic environment are available on OneDrive: 74 - Pre and post maceration thermograms for the six porcine ribs selected from section B question 4

Appendix 75: Temperature data for section B, question 4: Impact of the taphonomic environment is available on OneDrive: 75 - Temperature data for section B, question 4 - the impact of aquatic taphonomic environment

Appendix 76: All post-submersion fluorescence and OFC processed photographs for the 54 porcine ribs in section B, question 4: Impact of the aquatic taphonomic environment, are available on OneDrive:

Appendix 77: Visual tables of summarised post-submersion fluorescence results for all 54 porcine ribs examined in section B, research question 4: Impact of the aquatic taphonomic environment. The day 0 visual tables are available in appendix 48 & 49 as the data was previously used in question 2.

A) 2-months - terrestrial

Rib	Natural	Exposure time (s)		
		0.6	0.4	1/3
1				
2				
3		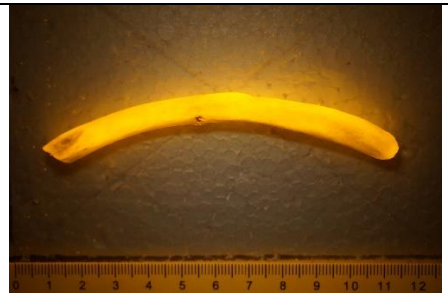		

4		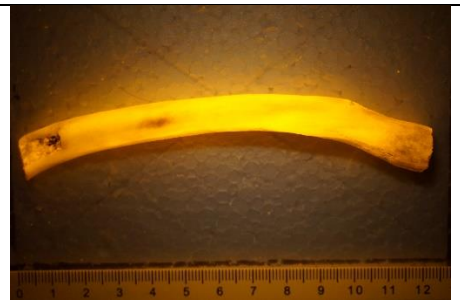	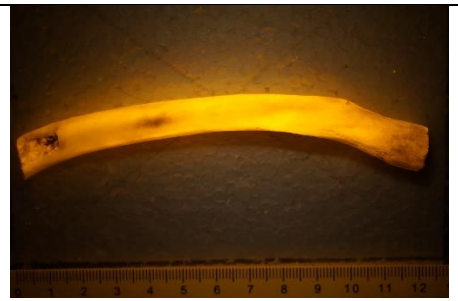	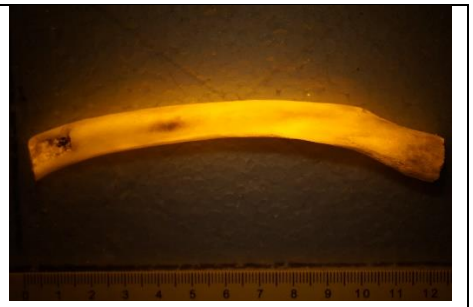
5		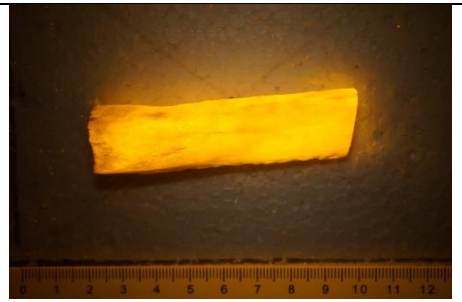		
6				

7		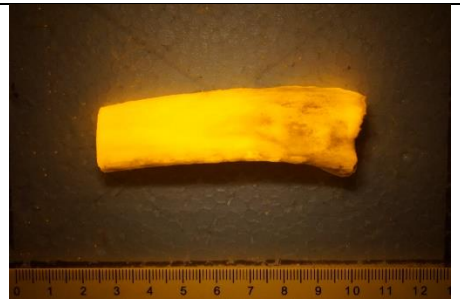		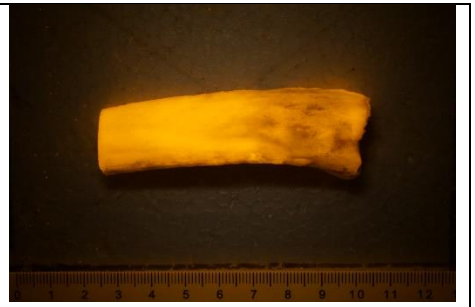
8		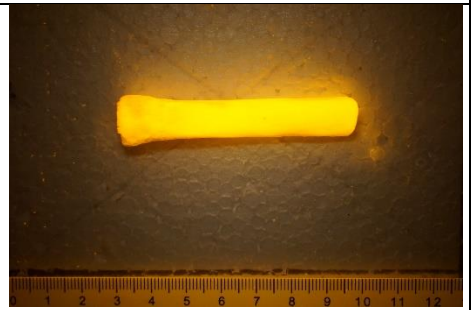		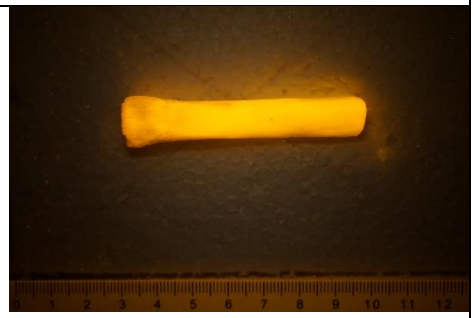
9		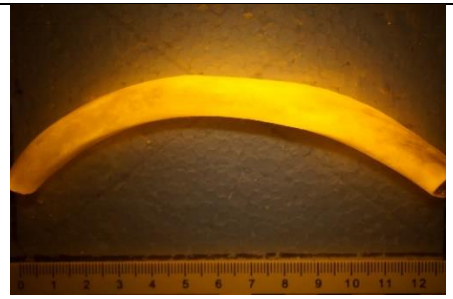	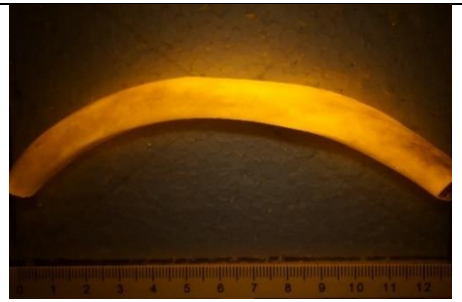	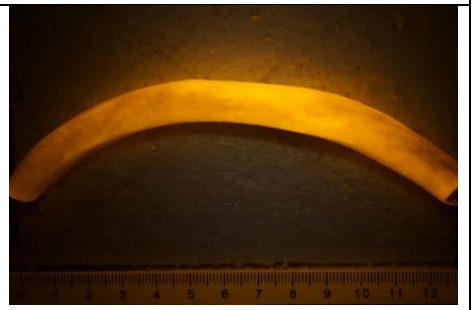

10		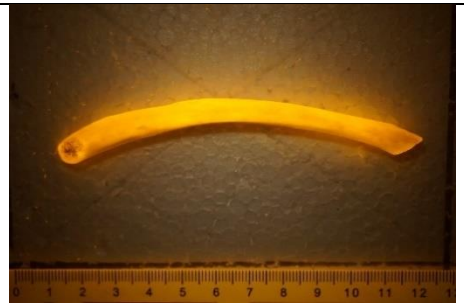		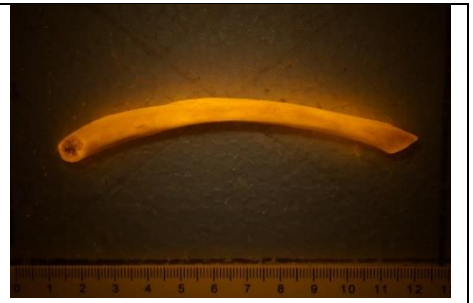
11	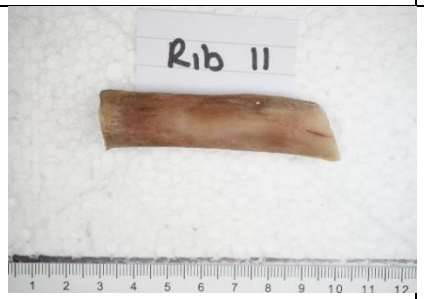		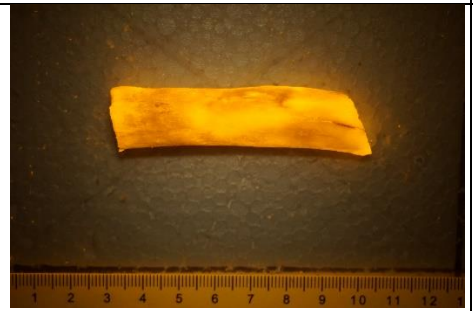	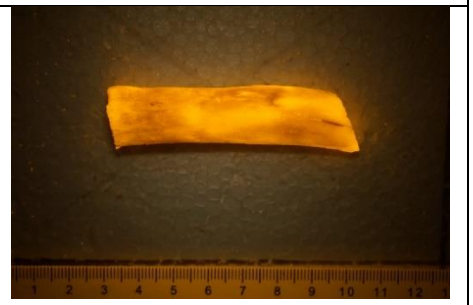
12		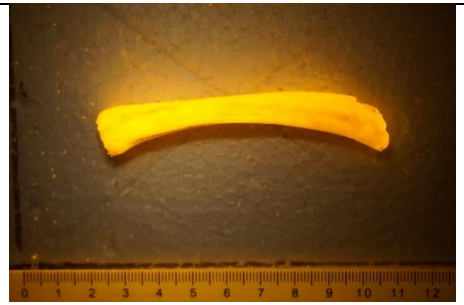	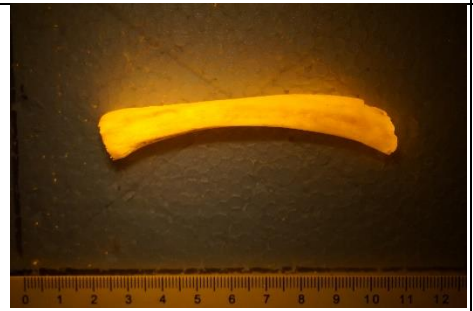	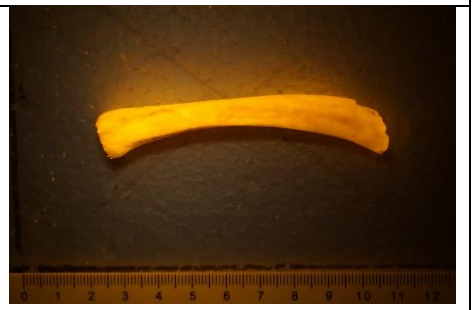

13		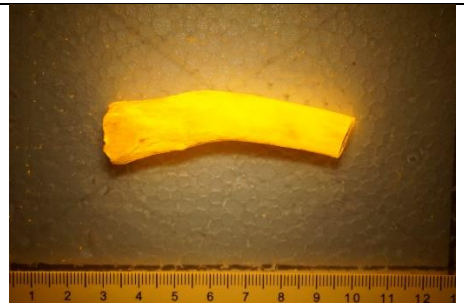	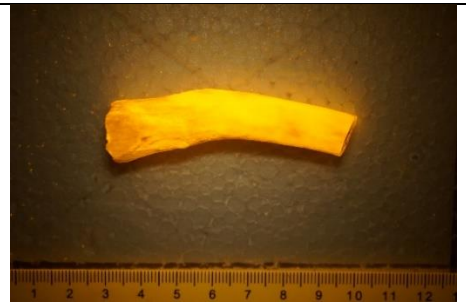	
14		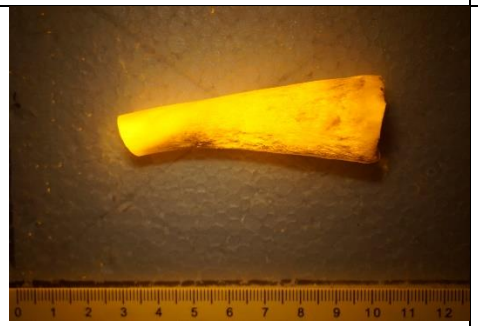		
15		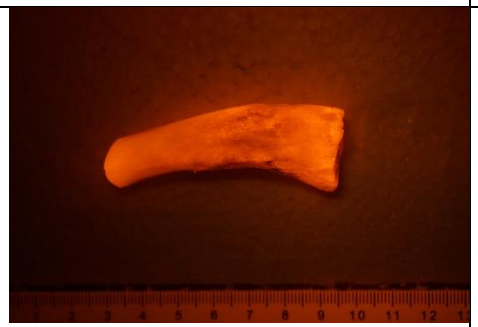		

16		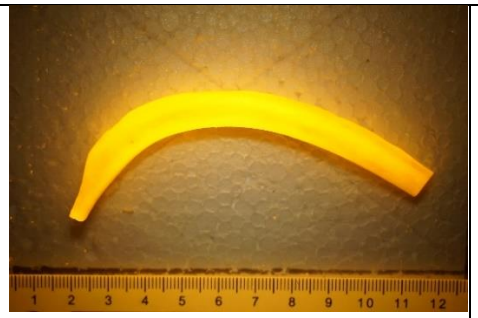		
17				
18				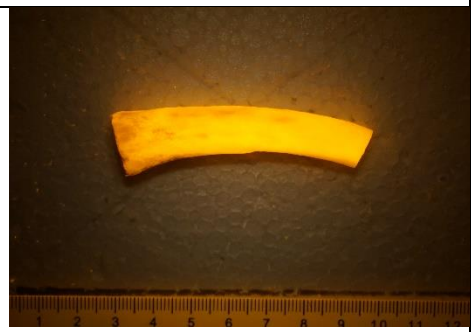

B) 2 months - submerged

Rib	Natural	Exposure time (s)		
		0.6	0.4	1/3
1				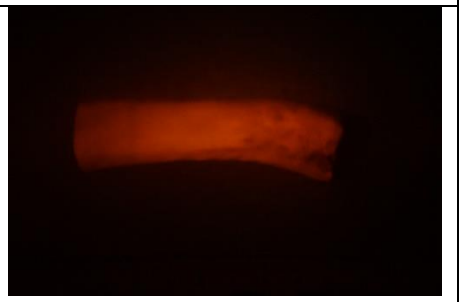
2			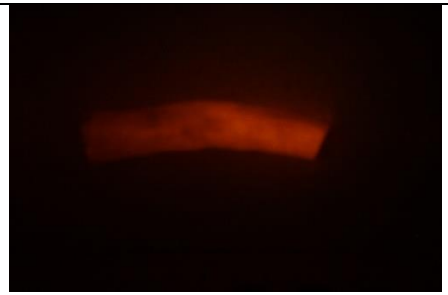	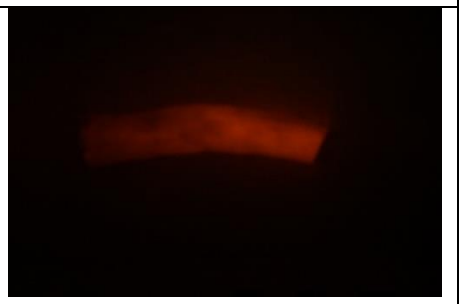

3		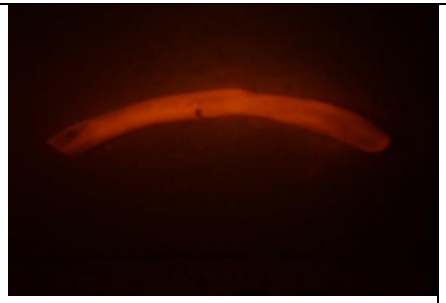	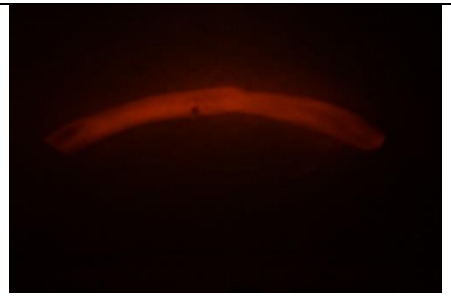	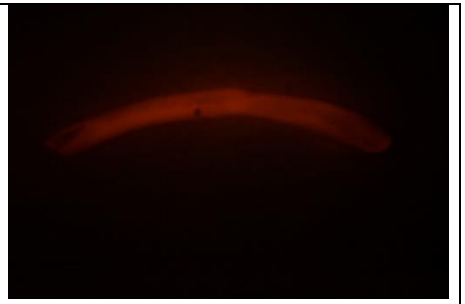
4		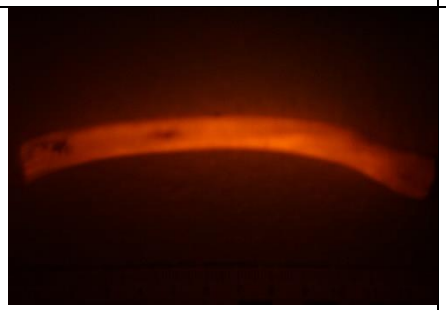		
5				

6			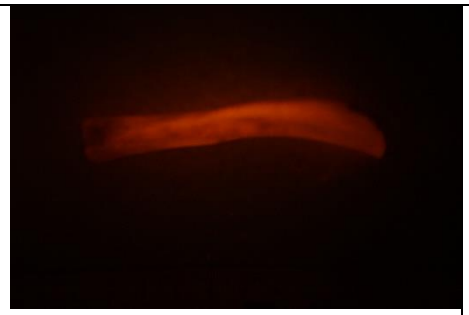	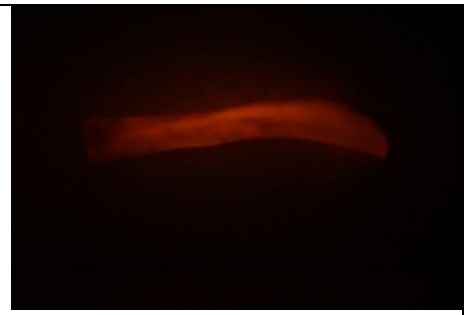
7		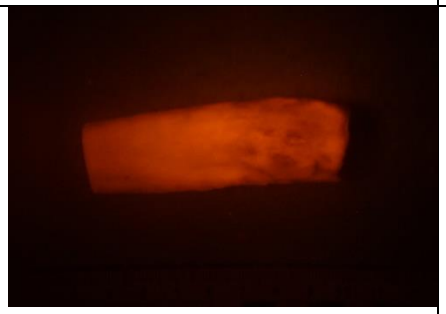	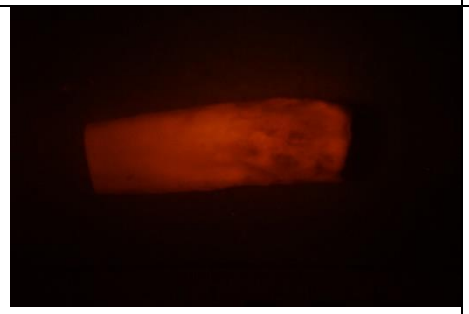	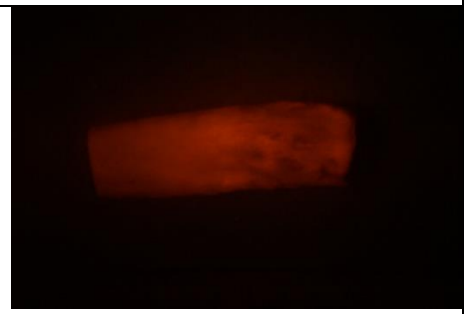
8		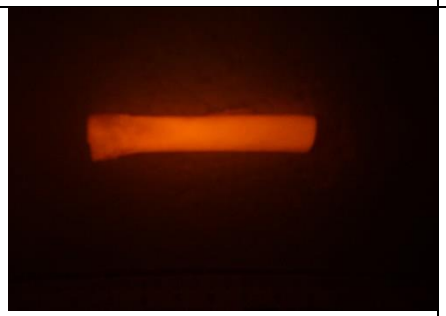		

9				
10		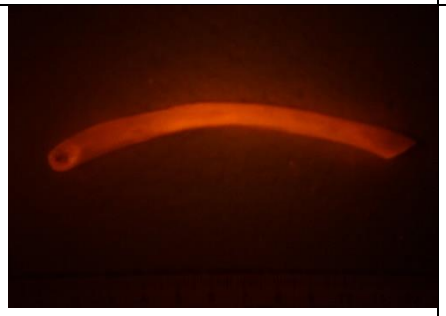	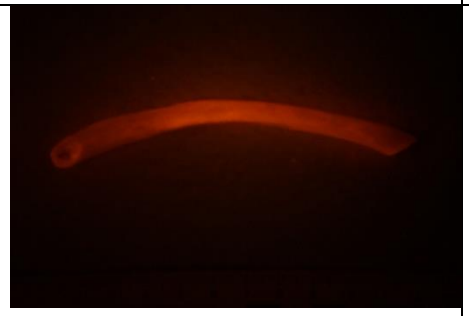	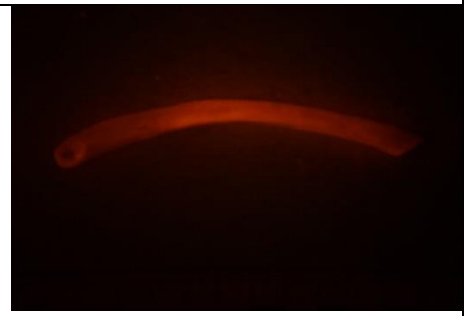
11	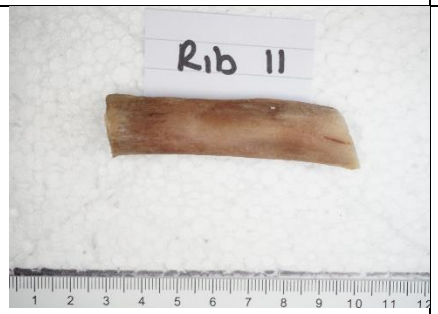			

12				
13				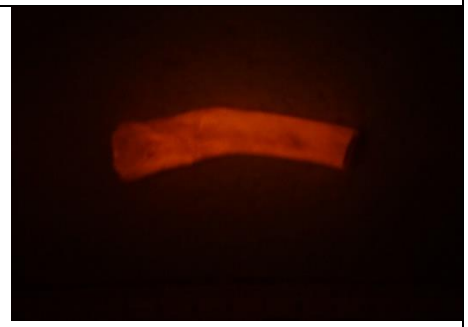
14				

15			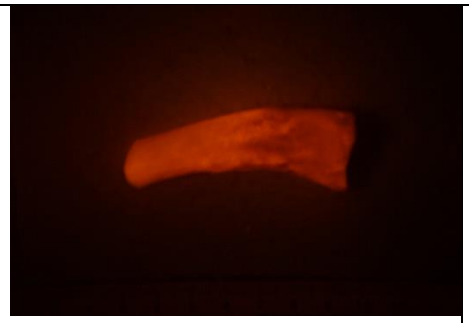	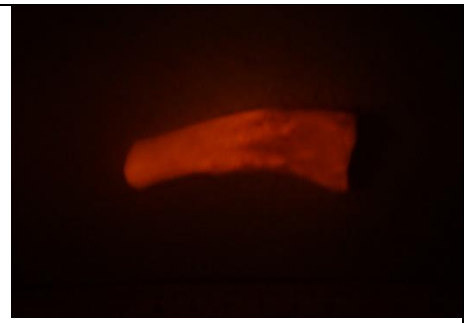
16				
17				

18		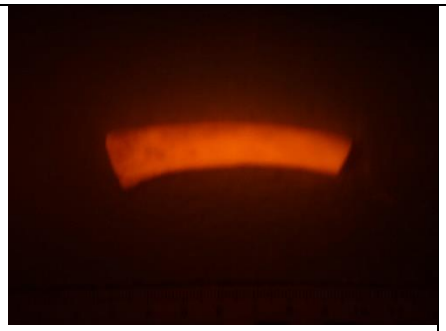	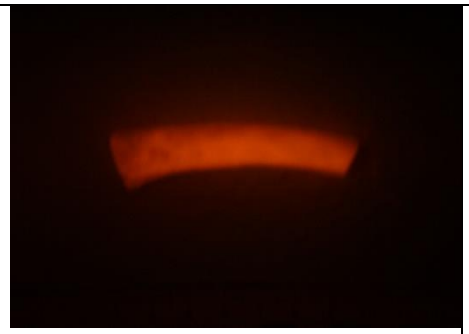	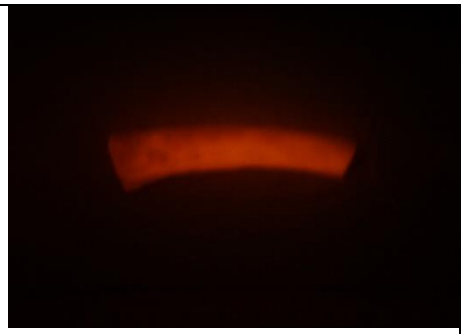

C) 4-months - terrestrial

Rib	Natural	Exposure time (s)		
		0.6	0.4	1/3
1		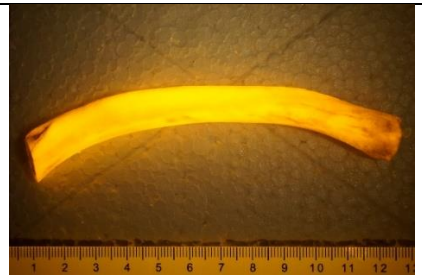	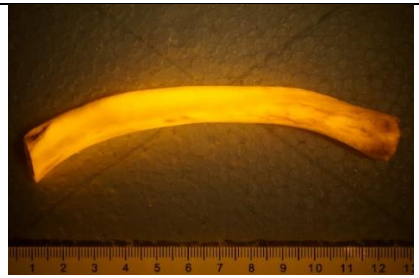	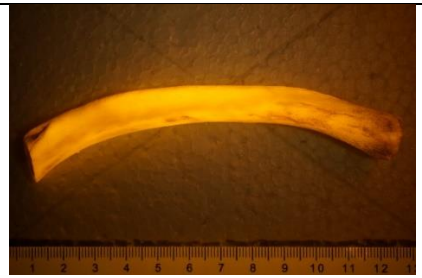
2				
3				

4				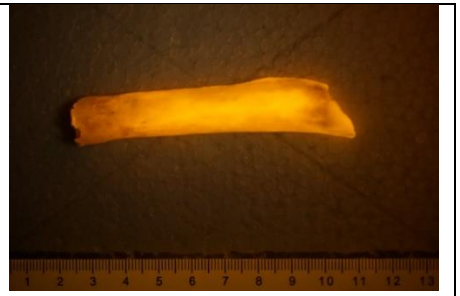
5		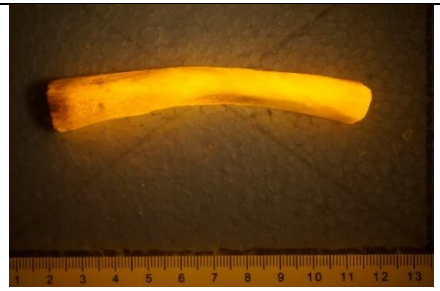		
6				

7				
8		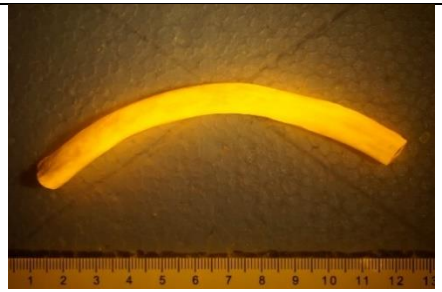	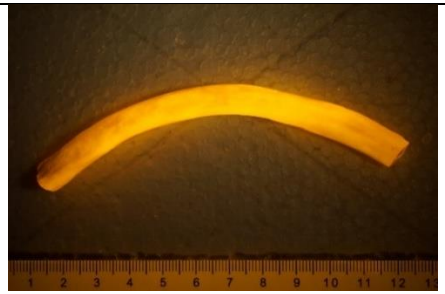	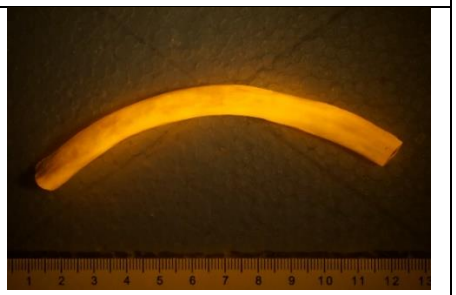
9		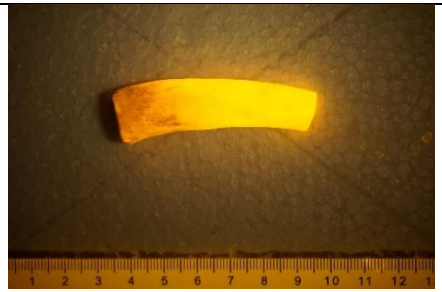	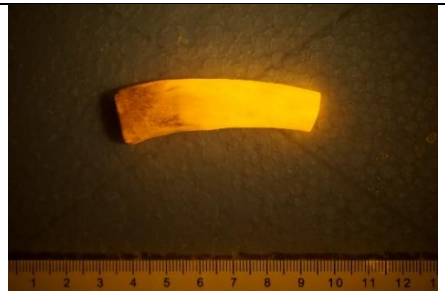	

10			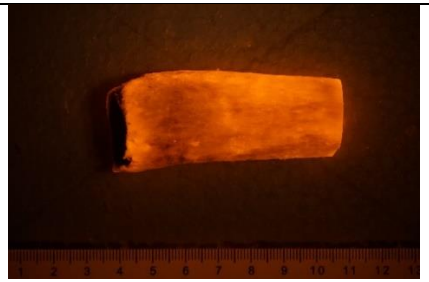	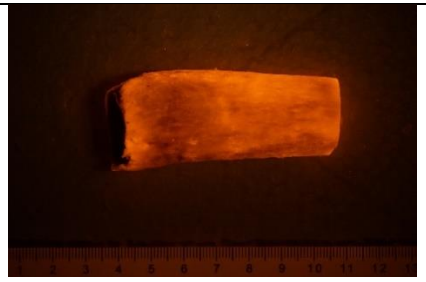
11		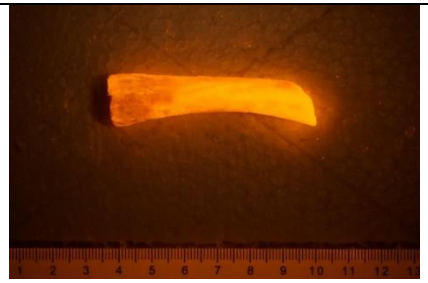	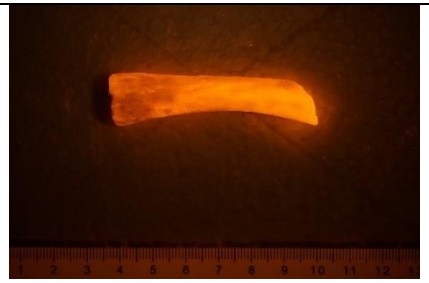	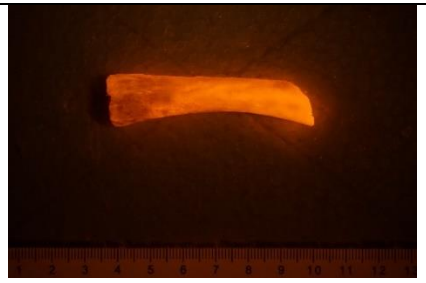
12		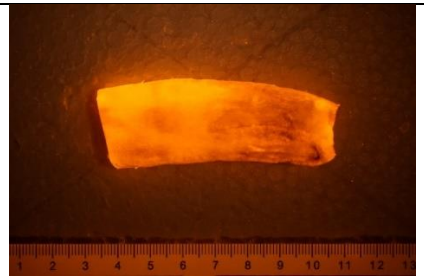	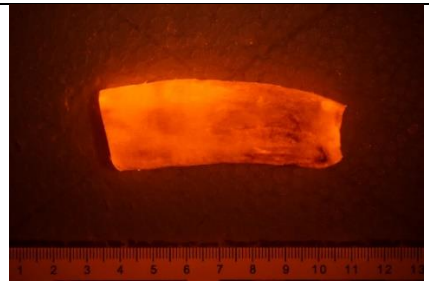	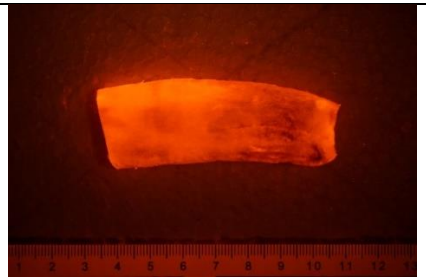

13		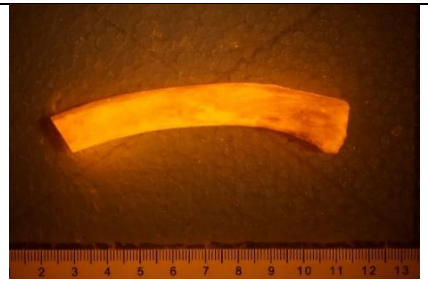	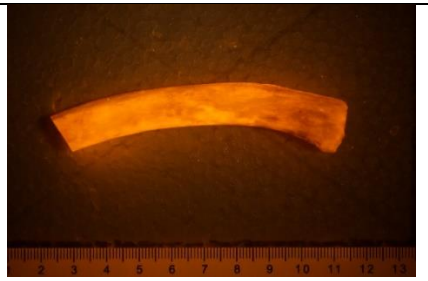	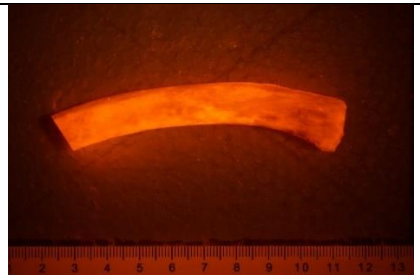
14				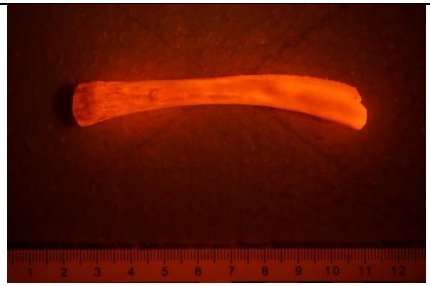
15		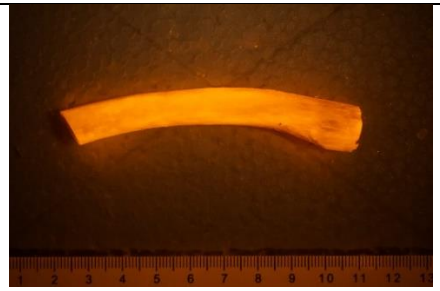	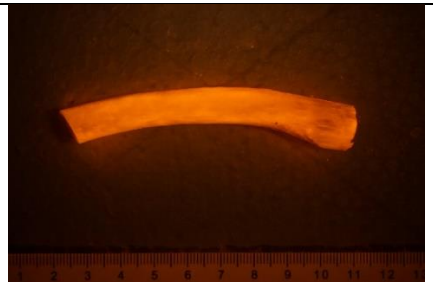	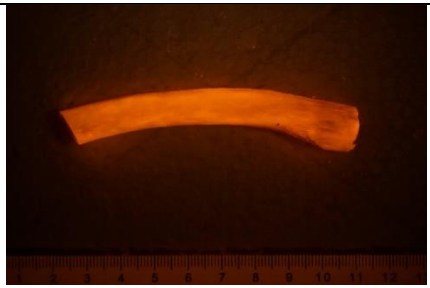

16		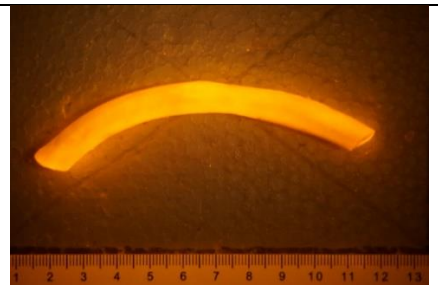	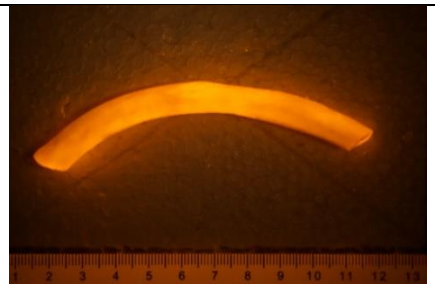	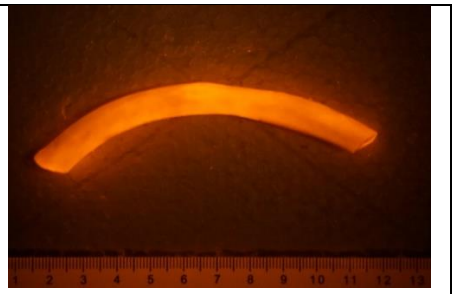
17		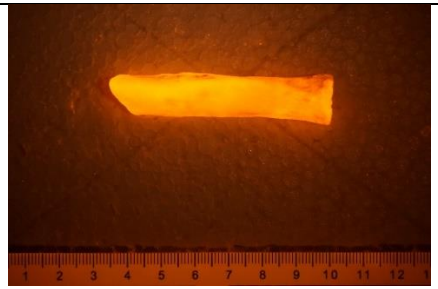	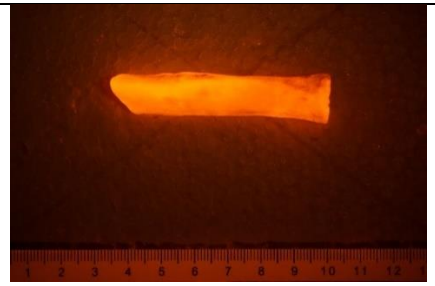	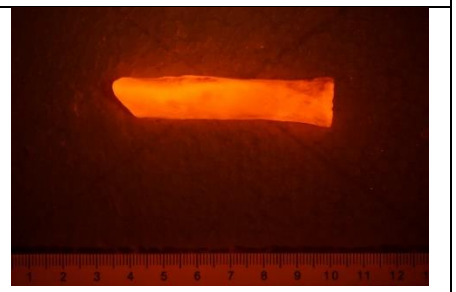
18		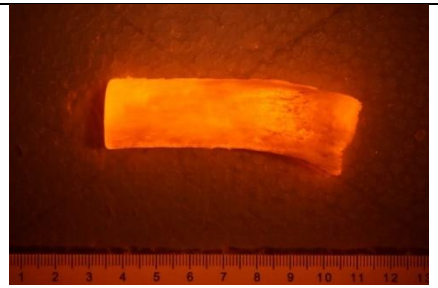	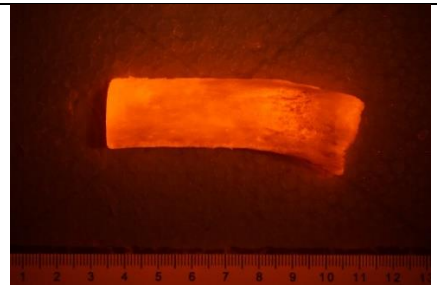	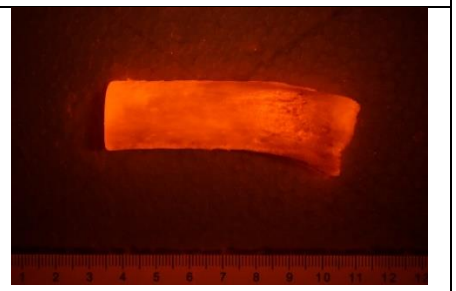

D) 4 month – submerged.

Rib	Natural	Exposure times (s)		
		0.6	0.4	1/3
1		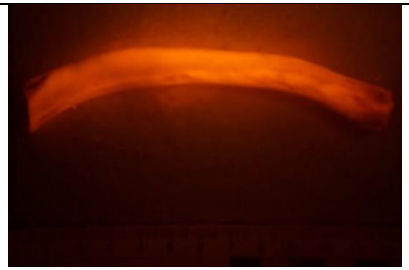	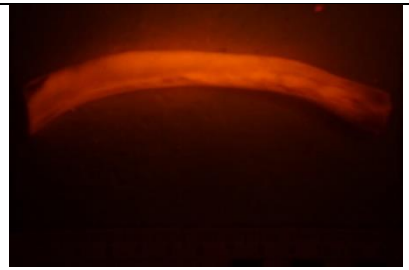	
2		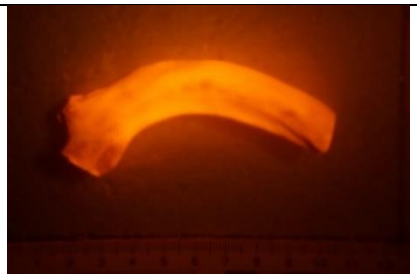		
3				

4		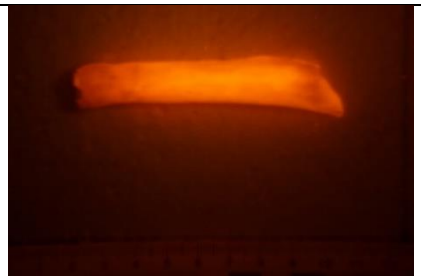		
5		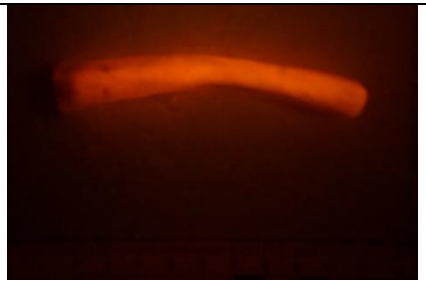	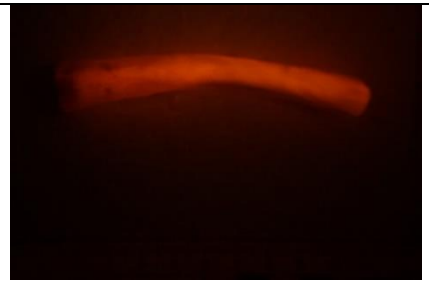	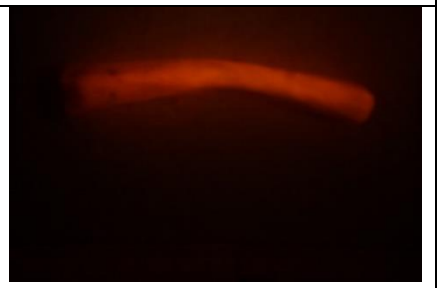
6		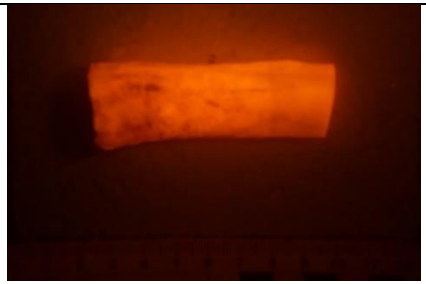		

7		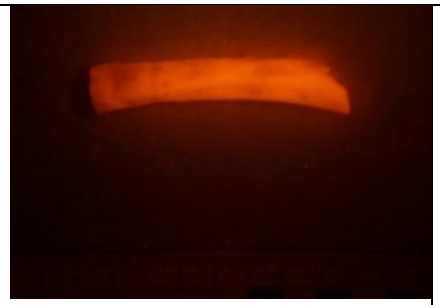		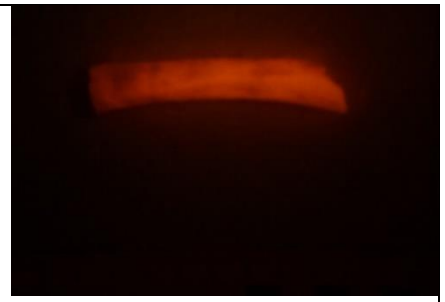
8				
9				

10			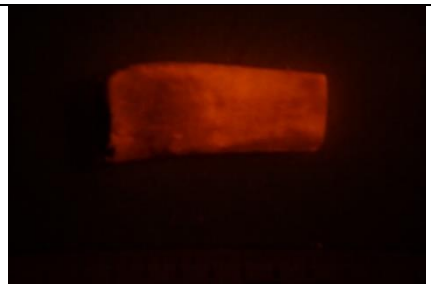	
11				
12		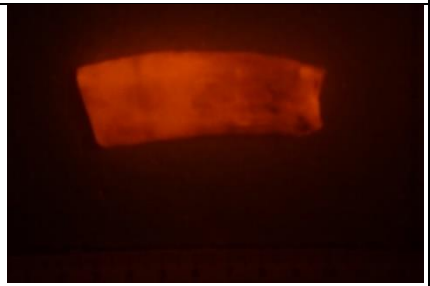	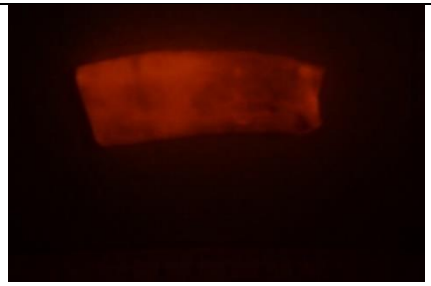	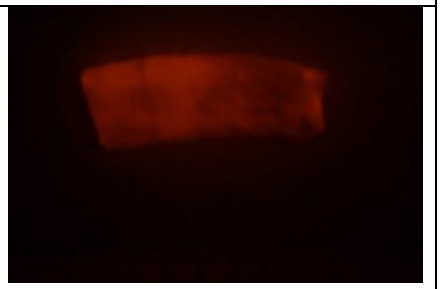

13		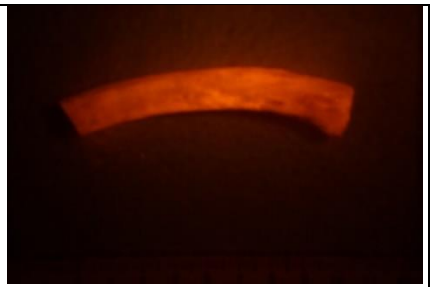		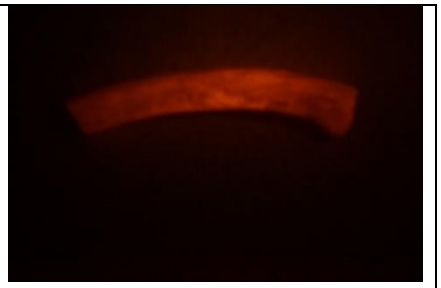
14		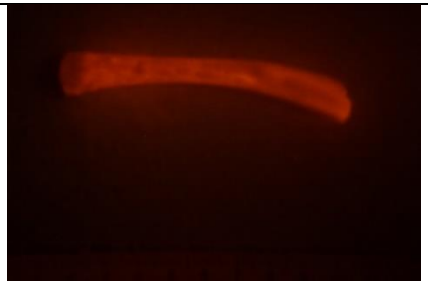	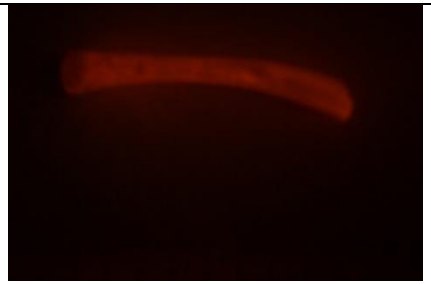	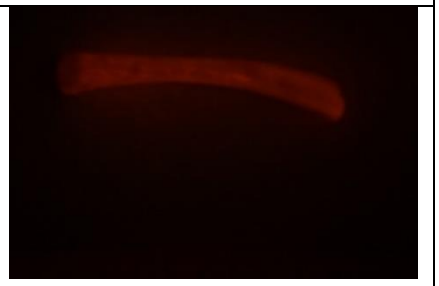
15		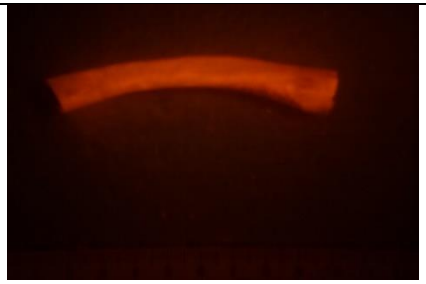	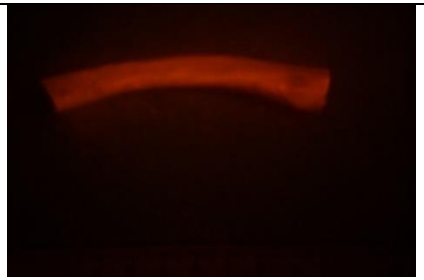	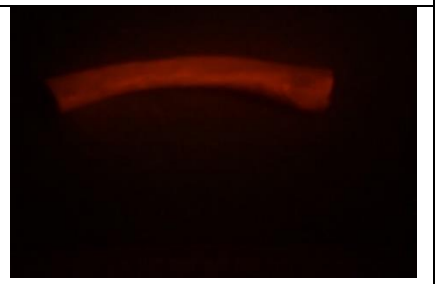

16		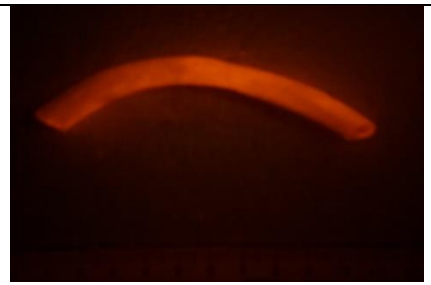	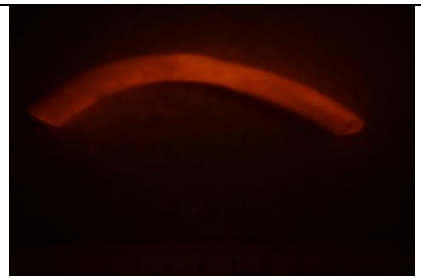	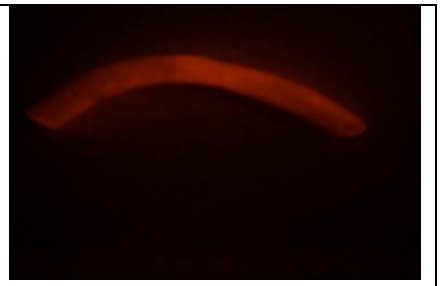
17				
18		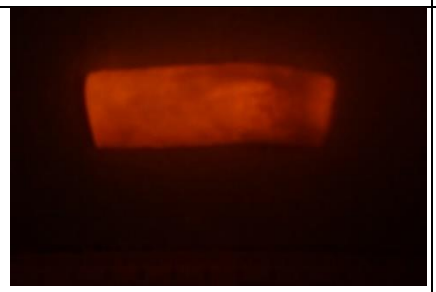	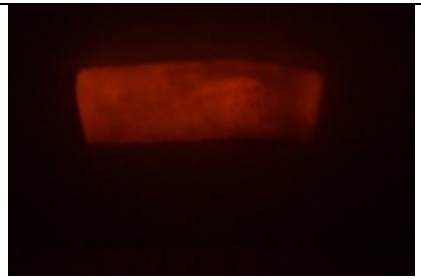	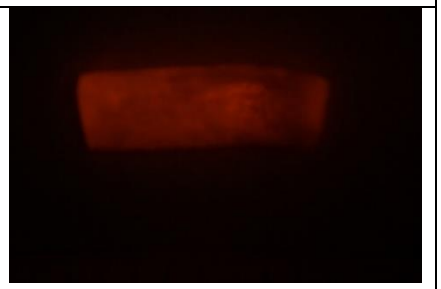

E) 6-month terrestrial

Rib	Natural	Exposure time (s)		
		0.6	0.4	1/3
1		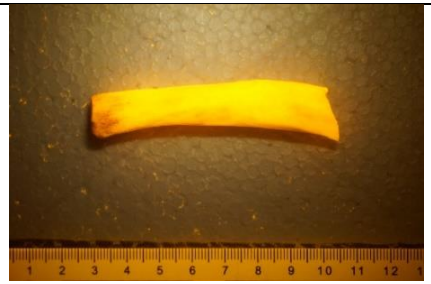		
2			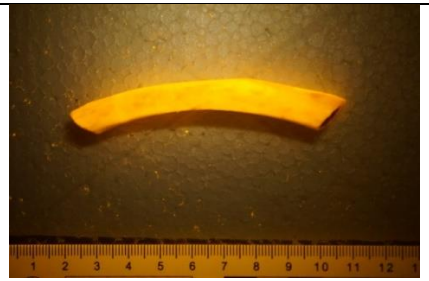	

3		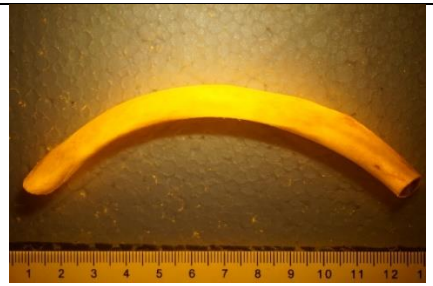	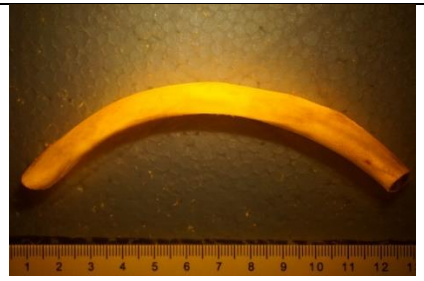	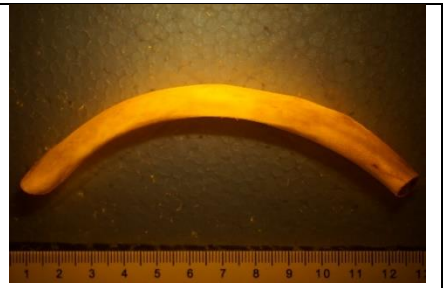
4				
5				

6		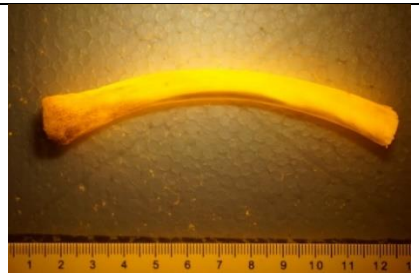	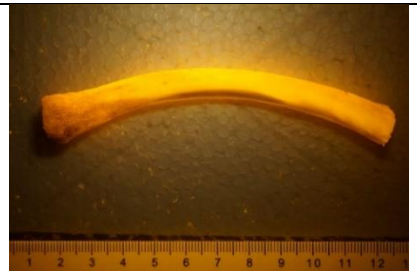	
7		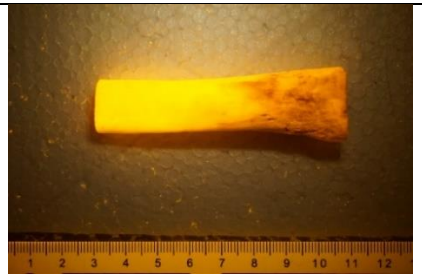		
8			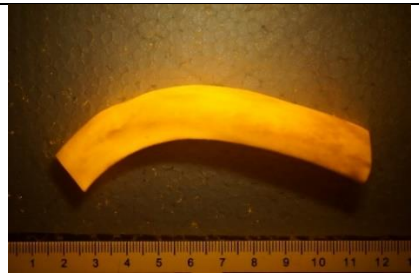	

9			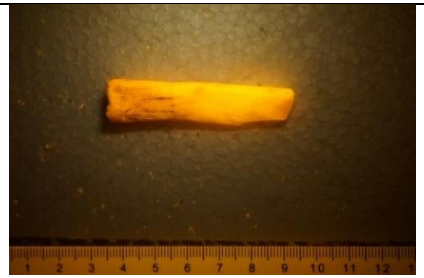	
10		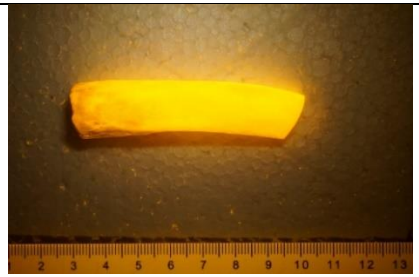		
11				

12				
13				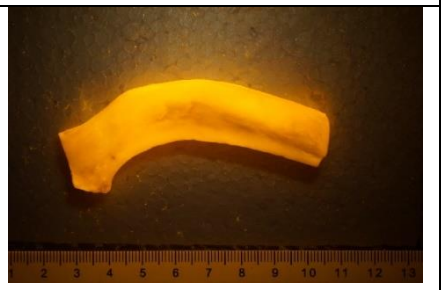
14				

15		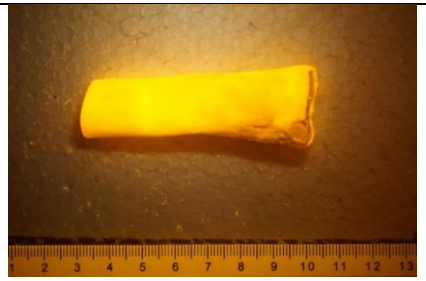		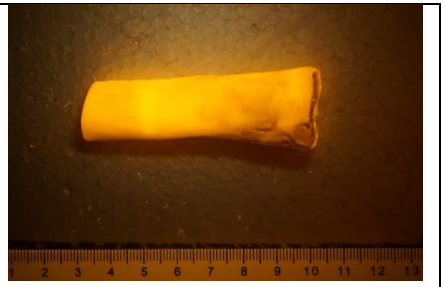
16		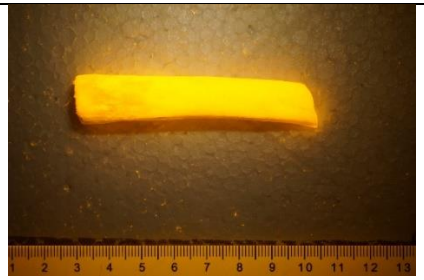	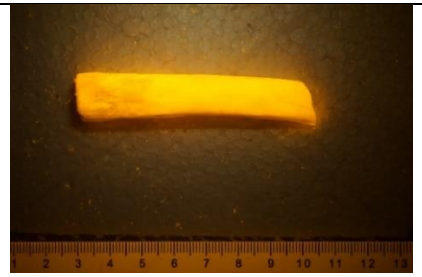	
17		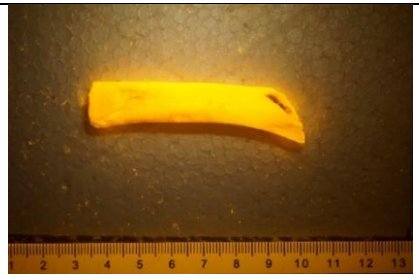	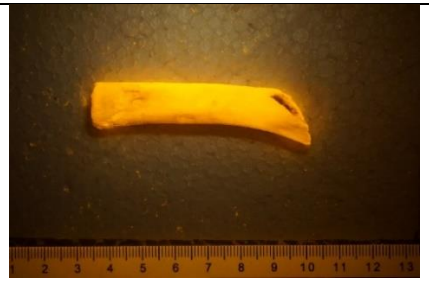	

18		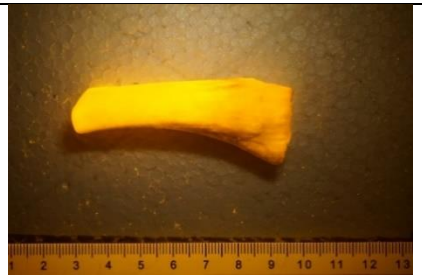		

F) 6 - months - submerged

Rib	Natural	Exposure time (s)		
		0.6	0.4	1/3
1				
2				
3				

4		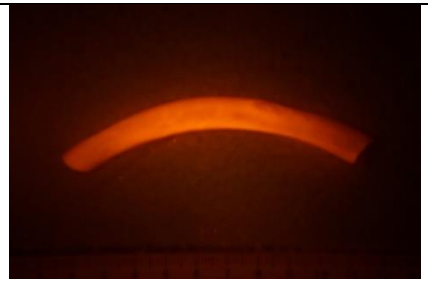		
5				
6				

7				
8				
9				

10		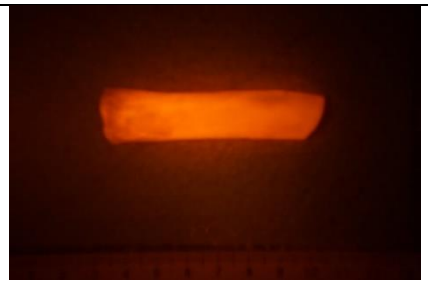		
11				
12		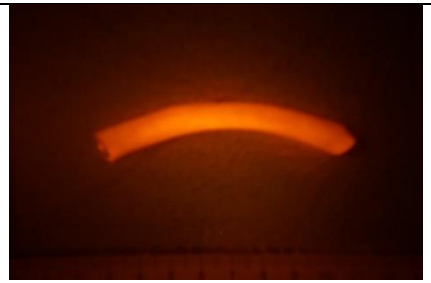		

13		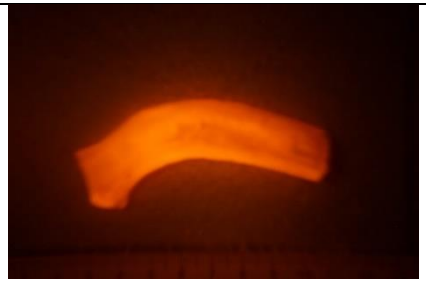		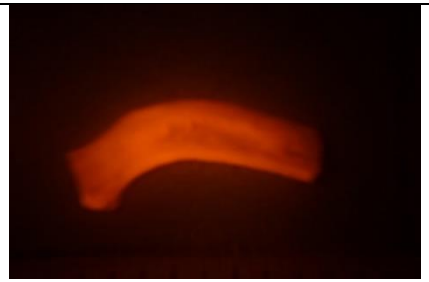
14		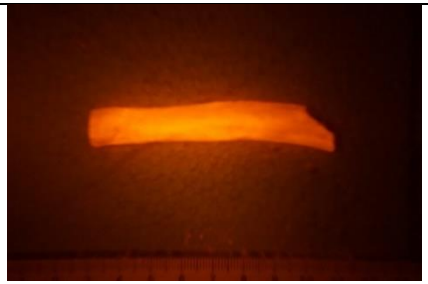		
15				

16		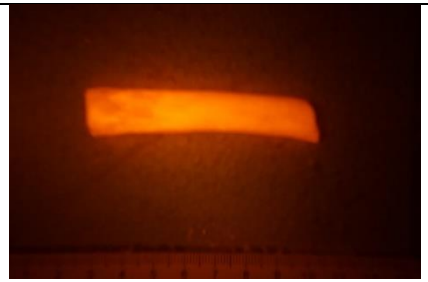		
17				
18				

Appendix 78: All thermograms for section B, question 4: Impact of the aquatic taphonomic environment, are available on OneDrive: 78 - Thermograms for section B, question 4, Impact of the aquatic taphonomic environment

Appendix 79: Histograms performed to determine the normality of the post-submersion data for section B, question 4: Impact of the aquatic taphonomic environment, statistical analyses.

A) 2-month.

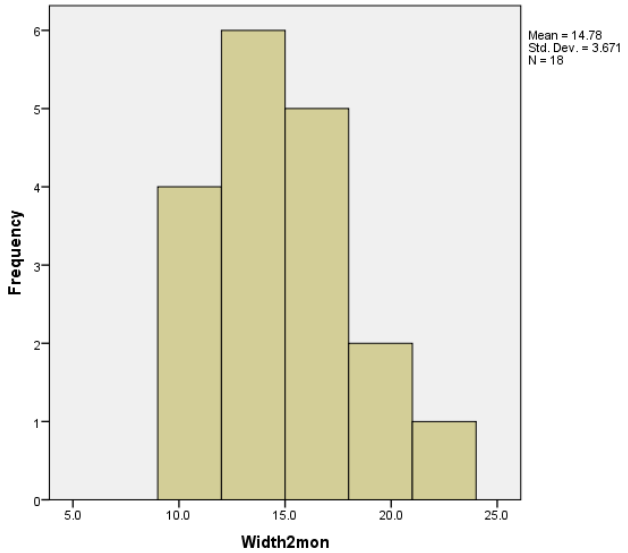

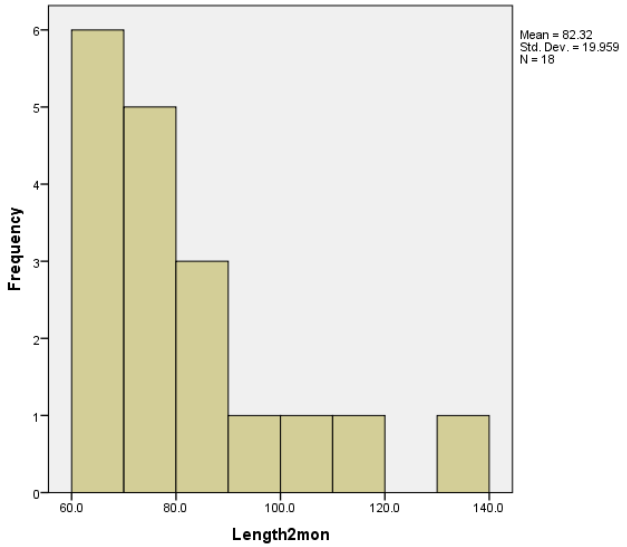

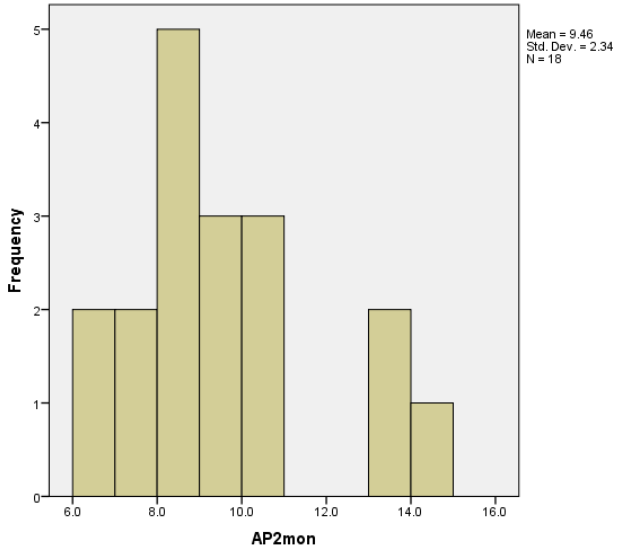
Mean = 9.46
Std. Dev. = 2.34
N = 18
Frequency
AP2mon

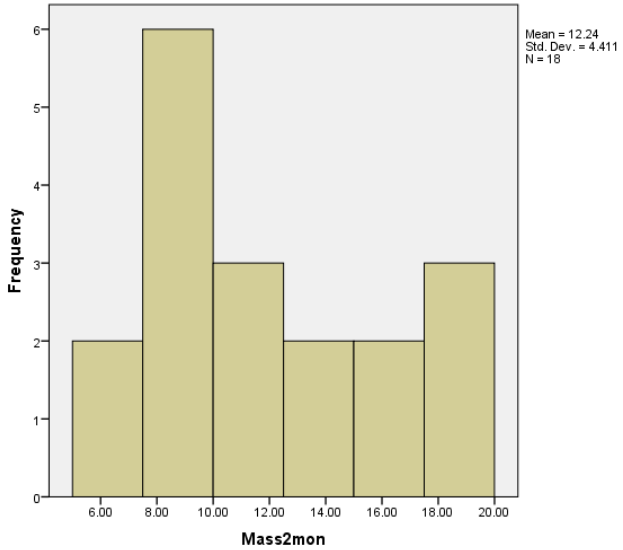
Mean = 12.24
Std. Dev. = 4.411
N = 18
Frequency
Mass2mon

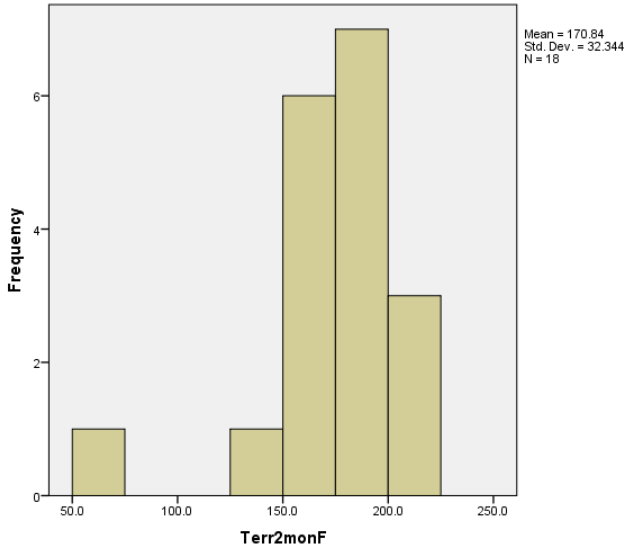
Mean = 170.84
Std. Dev. = 32.344
N = 18
Frequency
Terr2monF

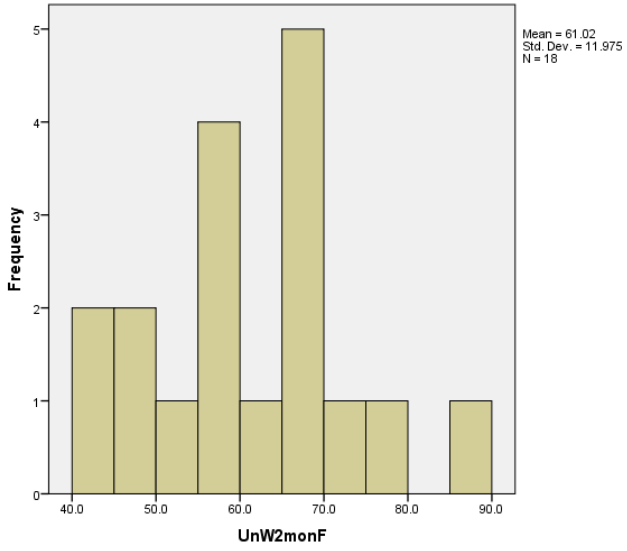
Mean = 61.02
Std. Dev. = 11.975
N = 18
Frequency
UnW2monF

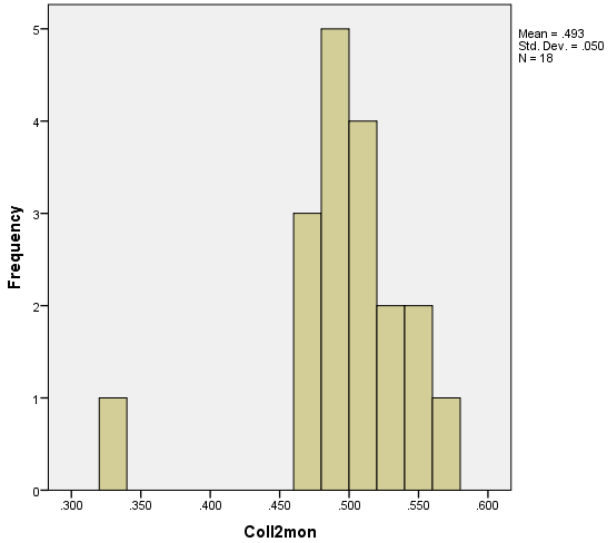
Mean = .493
Std. Dev. = .050
N = 18
Frequency
0
1
2
3
4
5
.300
.350
.400
.450
.500
.550
.600
Coll2mon

B) 6-month

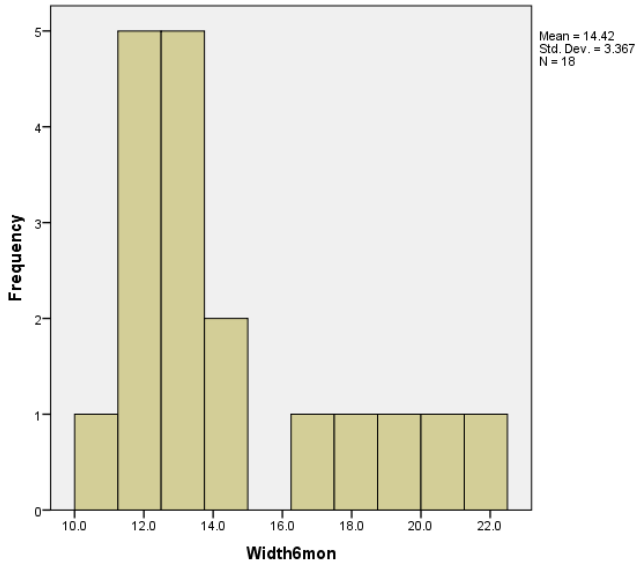
Mean = 14.42
Std. Dev. = 3.367
N = 18
Frequency
Width6mon
10.0
12.0
14.0
16.0
18.0
20.0
22.0

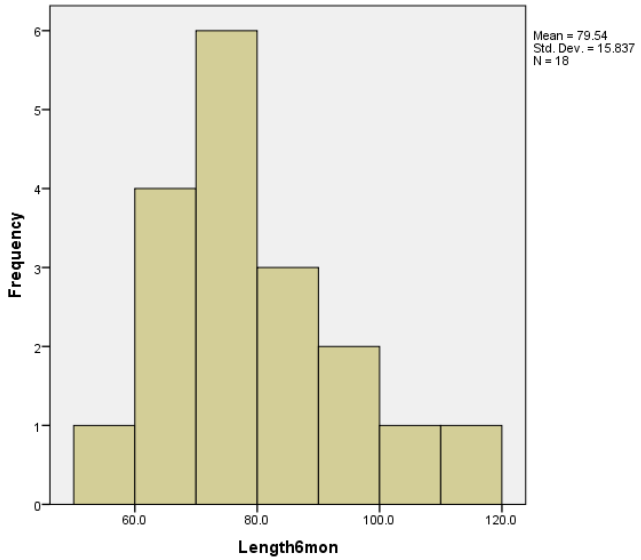
Mean = 79.54
Std. Dev. = 15.837
N = 18
Frequency
Length6mon
60.0
80.0
100.0
120.0

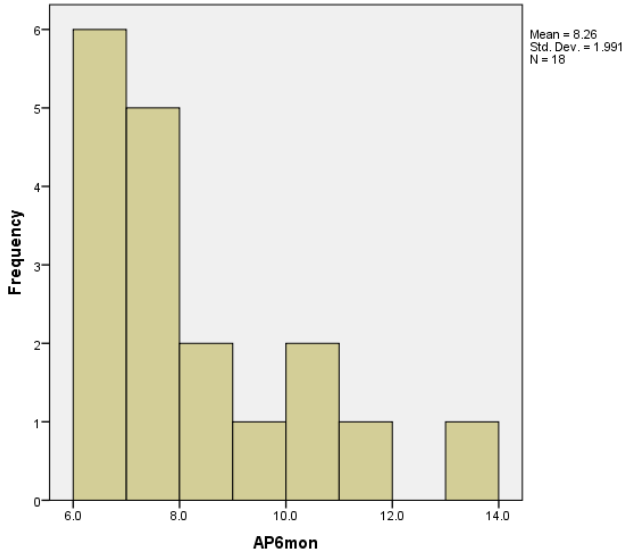
Mean = 8.26
Std. Dev. = 1.991
N = 18
Frequency
AP6mon

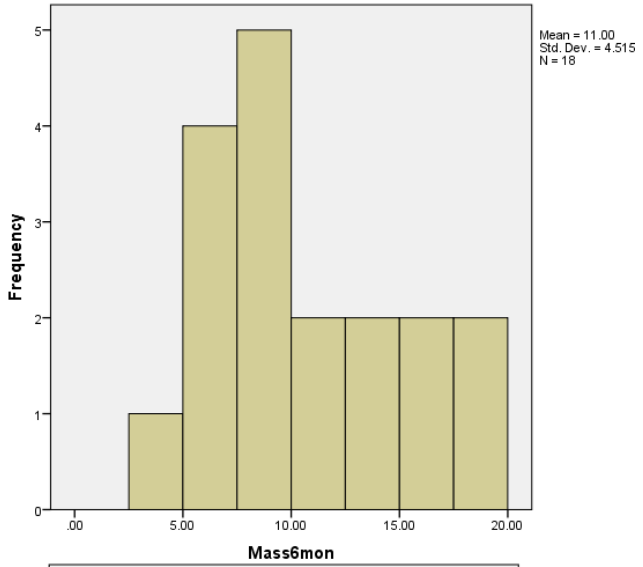
Mean = 11.00
Std. Dev. = 4.515
N = 18
Frequency
Mass6mon

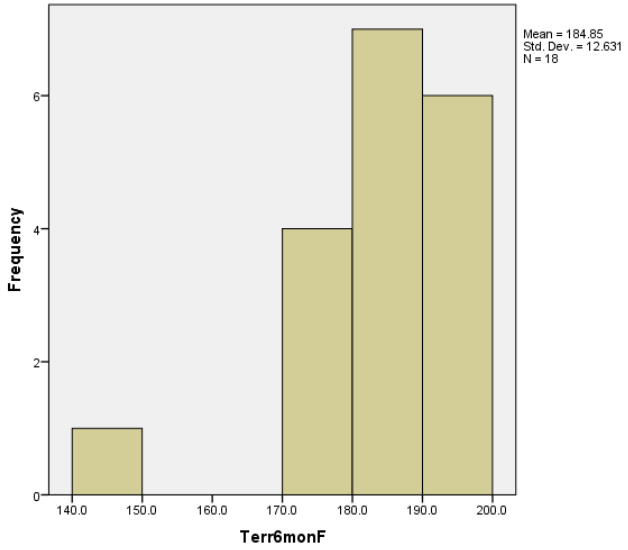
Mean = 184.85
Std. Dev. = 12.631
N = 18
Frequency
Terr6monF

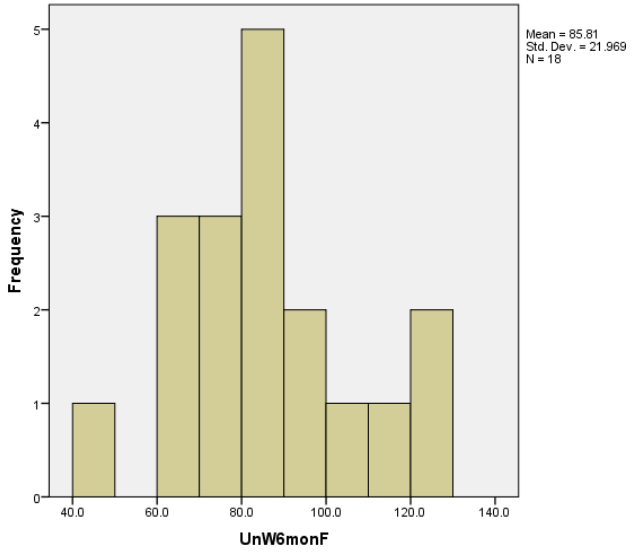
Mean = 85.81
Std. Dev. = 21.969
N = 18
Frequency
UnW6monF

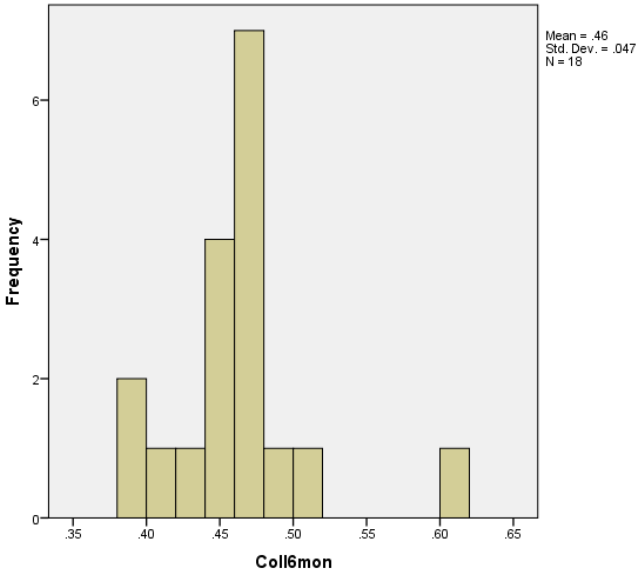
Mean = .46
Std. Dev. = .047
N = 18
Frequency
0
2
4
6
.35
.40
.45
.50
.55
.60
.65
Coll6mon

Appendix 80: Histograms performed to determine the normality of the post-submersion data for section B, question 4: Impact of the aquatic taphonomic environment, for each tap water and saltwater dataset.

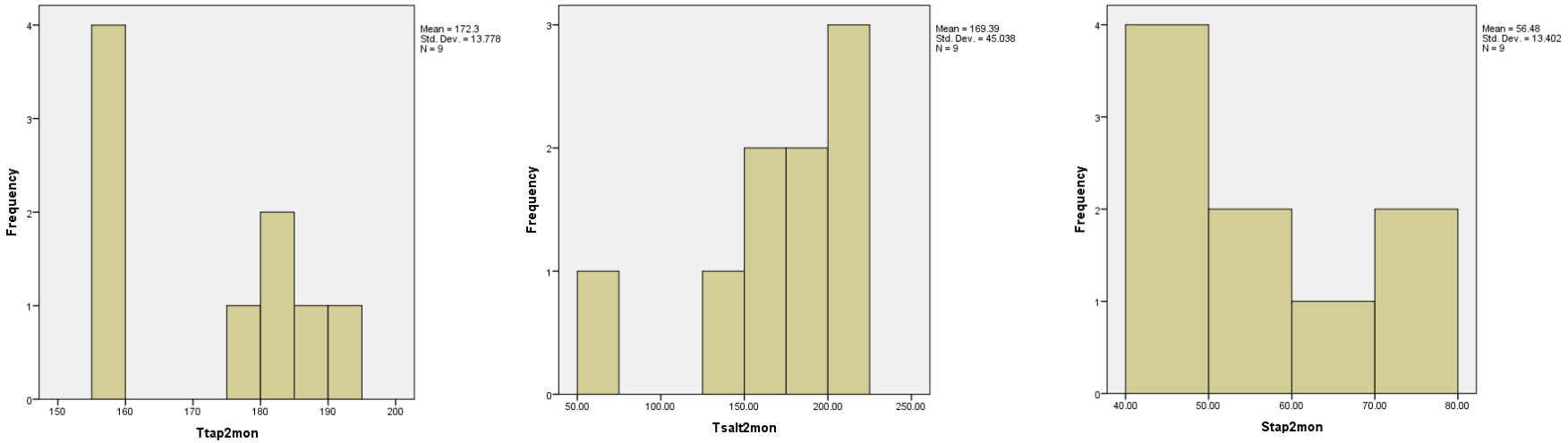

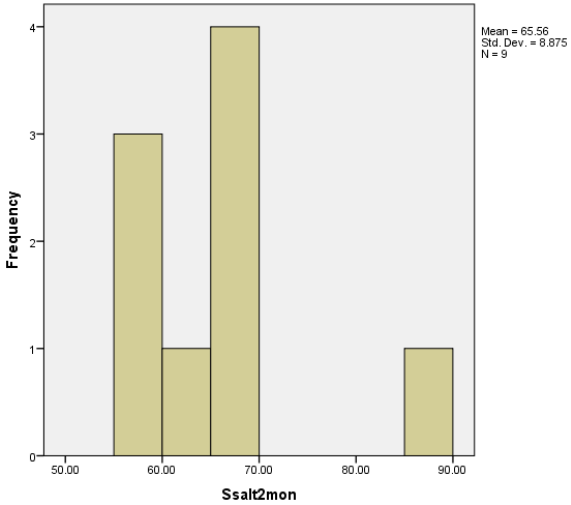
Mean = 65.56
Std. Dev. = 8.875
N = 9
Frequency
Ssalt2mon

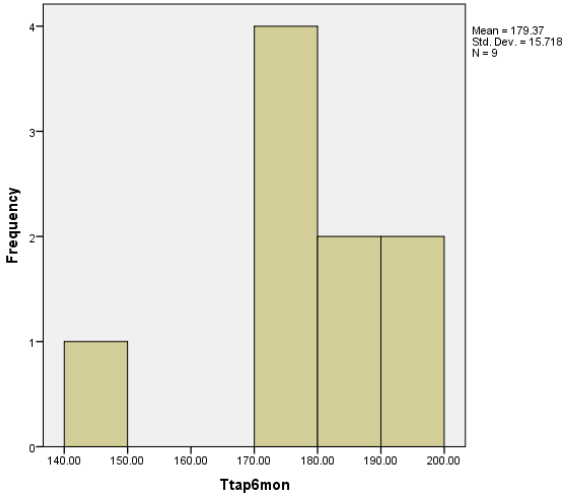
Mean = 179.37
Std. Dev. = 15.718
N = 9
Frequency
Ttap6mon

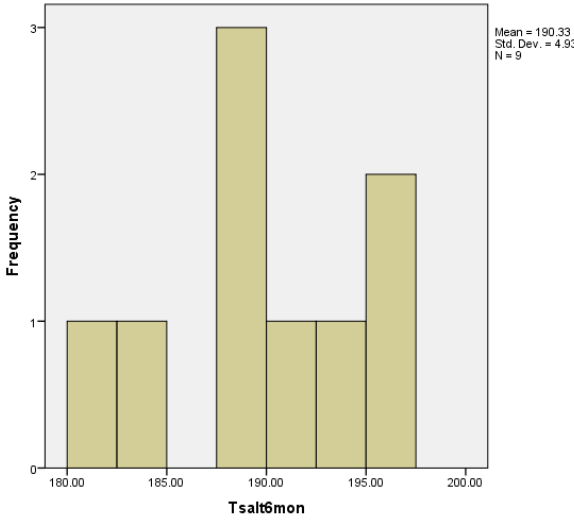
Mean = 190.33
Std. Dev. = 4.93
N = 9
Frequency
Tsalt6mon

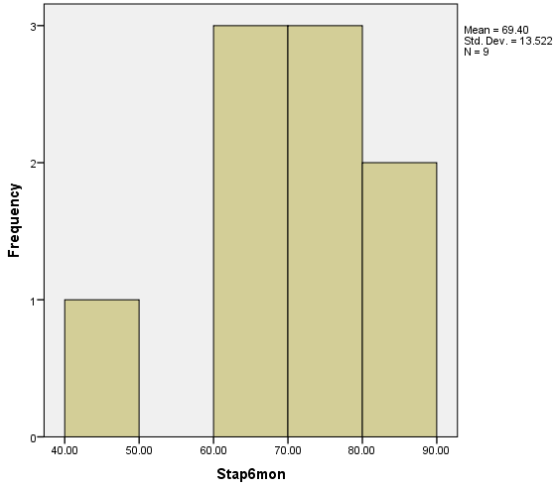
Mean = 69.40
Std. Dev. = 13.522
N = 9
Frequency
Stap6mon

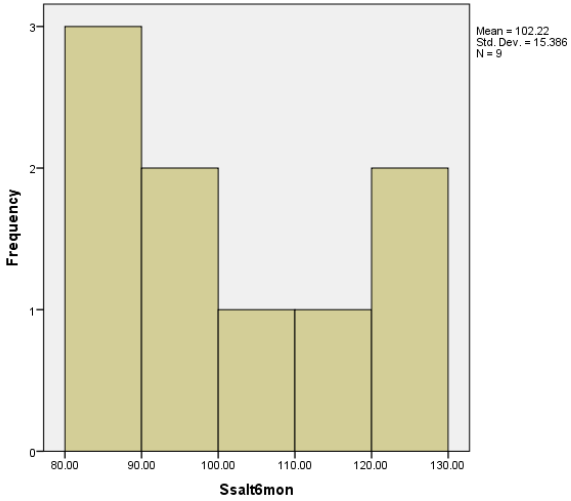
Mean = 102.22
Std. Dev. = 15.386
N = 9
Frequency
Ssalt6mon